The Transcriptomic Profiling of Human Colorectal Precancerous Lesions

Dissertation

zur

Erlangung der naturwissenschaftlichen Doktorwürde

(Dr. sc. nat.)

vorgelegt der

Mathematisch-naturwissenschaftlichen Fakultät

der

Universität Zürich

von

Elisa Cattaneo

aus

Italien

Promotionskomitee

Prof. Dr. Josef Jiricny (Vorsitz)

Prof. Dr. François Verrey

Dr. Giancarlo Marra (Leitung der Dissertation)

Zürich, 2010

Dedicated to my aunt Maria

TABLE OF CONTENT

1. SUMMARY

Colorectal tumorigenesis is one of the best known processes of cellular transformation in human beings. Its characterization has moved ahead by leaps and bounds during the last three decades, thanks to major advances in the fields of endoscopy, histology and molecular biology. The carcinogenic process in the colon starts when genetic or epigenetic alterations appear and accumulate in the cells of epithelial crypts. In most cases, the transformation process begins with qualitative, quantitative, and spatial subversion of the Wnt signaling pathway, the physiological regulator of epithelial homeostasis. Other crucial alterations affect key genes involved in different signal transduction pathways, apoptosis, and DNA repair such as mismatch repair. These events, which seem to appear at specific stages of tumor progression, eventually lead to malignant and invasive neoplastic lesions.

Colorectal cancer was assumed for many years to be a homogenous condition, but recently it turned out to include several distinct clinical, histological, and molecular phenotypes. Such heterogeneity can also be recognized in the lesions believed to be its precursors. Advances in the fields of endoscopy and pathology have provided us with a more accurate classification of preinvasive lesions, which better reflects their relevance in colorectal tumorigenesis. Precancerous colorectal lesions have been thus reclassified into different categories based on their morphological and histological appearance. Macroscopically, they are divided into *polypoid* (pedunculated and sessile) and *nonpolypoid* (slightly elevated, completely flat or depressed) lesions. Histologically, they can present classical adenomatous features or a peculiar architecture characterized by infolding of the glandular epithelium (also called serration). Serrated lesions display some molecular alterations usually non detected in adenomas, and they are believed to progress into colorectal cancer by means of a new pathway of tumorigenesis, namely the serrated pathway. The distinction of precancerous colorectal lesions based on their morphology, and the belief that they represent different entities, were the central themes driving the design of this study. In an attempt to identify genes and pathways whose dysregulation might play crucial roles in the transformation

process, we performed a comprehensive transcriptomic analysis of nonpolypoid and polypoid colorectal precancerous lesions. Our study represents the first gene expression analysis of a large collection of the two types of precancerous lesions. Furthermore, it was carried out using the Affymetrix exon array platform that allowed us to investigate the expression level of all transcripts of the human genome with unprecedented sensitivity.

The in-depth analysis of our transcriptomics data revealed that the two types of precancerous lesions could be easily segregated into different clusters using several unsupervised and supervised analytical tools. A prominent prevalence of expression changes in genes involved in cell cycle related networks was observed in the polypoid group of lesions, suggesting that a profound dysregulation of the cell cycle is crucial for propulsion of cell proliferation in these lesions. In contrast, nonpolypoid lesions were characterized by an overrepresentation of expression changes in genes involved in growth factor signaling pathways, apoptosis and cell adhesion, suggesting that these lesions might exploit activation of cell survival pathways and avoidance of apoptosis for their progression. We have identified a list of genes whose expression changes are more specifically associated with the polypoid or the nonpolypoid phenotype. These changes will be complemented by additional data from other -omics studies (a metabolomics study is in progress in our laboratory) in order to investigate the differences between polypoid and nonpolypoid lesions within a systems biology framework.

The data analysis also showed that the transcriptome of nonpolypoid lesions was less dramatically subverted than that of the polypoid lesions (in comparison with normal mucosa samples). In a large proportion of changes, the up- or downregulation of transcript levels followed a normal mucosa → nonpolypoid → polypoid sequence, although expression values in nonpolypoid lesions were always closer to that of the cognate, precancerous group of samples. Certain biological processes, such as Wnt signaling, cytoskeleton remodelling and immune response, were similarly dysregulated in the two groups of lesions. In addition, supervised analyses identified the *diameter of the lesions* and *degree of cytological dysplasia* as the two most relevant clinical variables associated with specific patterns of gene

expression, as was the case also for polypoid lesions in a previous study conducted in our laboratory.

In conclusion, although nonpolypoid lesions appear to explore different pathways of transformation, they also share many similarities with polypoid lesions. This was expected, since both precancerous lesions arise and grow in the same organ and are likely forced to overcome a series of similar selection pressures. At this stage of our investigation, we could only suggest that it is wise to apply the same level of clinical surveillance to both types of precancerous lesions.

One gene transcript whose expression changes were dramatic in all the precancerous lesions was *TMIGD1* (*transmembrane and immunoglobulin domain containing 1*). In comparison with the transcript levels in the corresponding normal mucosa samples, *TMIGD1* was found to be 19 and 66 (log_2 values) times less expressed in nonpolypoid and polypoid lesions respectively, and even more -152 fold - in adenocarcinomas. This striking phenomenon and the originality of the finding (probes for the analysis of the expression level of this gene were not present in the microarray platforms used in previous studies), along with the fact that its biological function is presently unknown, prompted us to invest time in a better characterization of its expression profile (mRNA as well as its protein product).

We could fully confirm the microarray data by analyzing the studied samples with real-time quantitative RT-PCR. In addition, we extended this analysis to other tissues and we found that the expression of the *TMIGD1* mRNA was higher in the lower gastrointestinal tract and kidney. The stable expression of the full length *TMIGD1* cDNA in *TMIGD1*-deficient SW480 colon cancer cells showed that this protein is expressed in the cytoplasm. An accumulation of TMIGD1 was evident in the perinuclear compartment (likely associated with the rough endoplasmic reticulum, but also localization in mitochondria should be considered), however the entire cytoplasm and the cell membrane were also stained. The fiber-like pattern of staining suggests that TMIGD1 might be associated also with the cytoskeleton.

In immunohistochemical studies, the expression of TMIGD1 was limited to the upper portion of the intestinal epithelial crypts (where differentiated cells are

located), while it was absent in the proliferative compartment. In the villi of the terminal ileum and in renal tubules, TMIGD1 was markedly localized in the brush border. As expected, its expression decreased dramatically in nonpolypoid and polypoid lesions, as well as in adenocarcinomas. Interestingly, the staining for TMIGD1 was correlated with the degree of cellular differentiation and its expression was completely lost in poorly differentiated neoplasms. *TMIGD1* might therefore be a novel marker of epithelial differentiation in the lower gastrointestinal tract and in the kidney. The effects of its downregulation during the transformation process in the colorectum remain to be elucidated.

2. ZUSAMMENFASSUNG

Die Entstehung von Darmkrebs beim Menschen ist einer der am besten verstandenen Abläufe der zellulären Entartung. Das Verständnis dieses Prozesses ist in den letzten drei Jahrzehnten sprunghaft angestiegen, nicht zuletzt durch die Fortschritte auf den Gebieten der Endoskopie, der Histologie und der Molekularbiologie. Der kanzerogene Prozess beginnt, wenn genetische oder epigenetische Veränderungen in den Zellen der Krypten des Darmepithels auftreten und sich anhäufen. In den meisten Fällen geht diese Transformation mit einer qualitativen, quantitativen und räumlichen Zerstörung des Wnt-Signalweges, dem physiologischen Regulator der zellulären Homeostasis, einher. Weitere wichtige Veränderungen betreffen Schlüsselgene, welche in verschiedenen Signalwegen, dem programmierten Zelltod und DNA-Reparaturwegen, z.B. der postreplikativen Fehlpaarungsreparatur, eine wichtige Rolle spielen. Diese Ereignisse scheinen bestimmte Abschnitte der Krebsentwicklung zu kennzeichnen und führen möglicherweise zu dem Entstehen bösartiger und invasiver Tumore.

Im Falle des Darmkrebses nahm man lange Zeit an, dass es sich um ein relativ einheitliches Krankheitsbild handele. In neuere Studien wurden jedoch unterschiedliche klinische, histologische und molekulare Krankheitsbilder festgestellt. Diese Unterschiede können auch schon in Vorläuferstadien der Tumore beobachtet werden. Fortschritte in der Endoskopie und Pathologie ermöglichen heutzutage eine bessere Klassifizierung der prä-invasiven Läsionen wodurch sich genauere Rückschlüsse auf die weitere Entartung schließen lassen. Daher hat man die Vorläuferstadien des Darmkrebses, basierend auf dem morphologischen und histologischen Erscheinungsbild, neu gruppiert. Makroskopisch unterscheidet man polypöse (gestielt und festsitzend) und nicht-polypöse (leicht erhöhte, flache oder eingedrückte) Läsionen. Histologisch gesehen kommen klassische adenomähnliche Formen vor oder Formen die durch eine seltsame Einstülpung des Drüsenepithels (auch gezahnt genannt) gekennzeichnet sind. Gezahnte Läsionen weisen einige molekulare Veränderungen auf, die normalerweise nicht in Adenomen beobachtet werden. Man geht davon aus, dass sich diese über einen neuartigen Weg zu

Darmkrebs ausweiten können, den so genannten „gezahnten“ Weg. Die Unterscheidung von präkanzerösen Läsionen mittels ihrer Morphologie und die Annahme, dass diese verschiedene Einheiten darstellen, war das zentrale Leitmotiv für die Aufnahme dieser Studie. In dem Versuch Gene und Signalwege zu identifizieren, deren Deregulation ein wichtige Rolle in der Krebsentstehung spielt, haben wir eine umfassende Transkriptions-Analyse von nicht-polypösen und polypösen Läsionen, die als Darmkrebsvorläufer angesehen werden können, durchgeführt. Unsere Studie ist daher die erste Genexpressionsanalyse mit einer großen Anzahl dieser beiden unterschiedlichen Arten von präkanzerösen Läsionen. Darüber hinaus haben wir unsere Analyse mir der Affymetrix exon array Plattform durchgeführt, die es uns erlaubt die Expressionsniveaus aller Transkripte des menschlichen Genoms in nie da gewesener Genauigkeit zu untersuchen.

Die Analyse unserer Daten durch ungeordnete und geordnete Methoden zeigte, dass sich beide Arten der präkanzerösen Läsionen leicht in zwei unterschiedliche Gruppen aufteilen lassen. In der Gruppe der polypösen Läsionen zeigten Gene, welche mit dem Zellzyklus assoziiert sind, ein verändertes Expressionsmuster. Dies legt nahe, dass eine massive Deregulation des Zellzyklus für die Proliferation der Zellen bei dieser Art der Läsion von Nöten ist. Im Gegensatz dazu werden die nicht-polypösen Läsionen dadurch gekennzeichnet, dass sie eine Überexpression von Genen aufweisen, welche in Signalwegen von Wachstumsfaktoren, dem programmierten Zelltod oder der Zelladhäsion ein Rolle spielen. Dies lässt darauf schließen, dass eine Aktivierung von Signalwegen nötig ist, die das Überleben der Zellen fördern und den Zelltod unterdrücken. Wir konnten eine Liste von Genen erstellen, deren veränderte Expression mit dem polypösen oder nicht-polypösen Erscheinungsbild der Läsionen assoziiert ist. Diese Änderungen werden durch Daten von anderen „-omics“-Studien (eine Metabolomics-Studie wird zurzeit in unserem Labor durchgeführt) vervollständigt. Dadurch erhoffen wir uns, die Unterschiede zwischen polypösen und nicht-polpöyen Läsionen in einem systembiologischen Rahmenwerk studieren zu können.

Die Analyse unserer Daten zeigt zudem, dass das Transkriptom der nicht-polypösen Läsionen weniger „zerrüttet“ war als das der polypösen Läsionen (im

Vergleich zu den Proben der normalen Schleimhaut). Die meisten Veränderungen der Hoch- oder Runterregulierung der Transkripte folgten einem ähnlichen Muster: normale Schleimhaut → nicht polypöse Läsion → polypöse Läsion (wobei die Werte der nicht-polypösen Läsionen immer näher an den Werten ihrer verwandten Gruppe, der polypösen Läsionen, lagen). Bestimmte biologische Prozesse, wie der Wnt -Signalweg, der Aufbau der Zytoskeletts und die Immunantwort, waren in beiden Gruppen gleichermaßen verändert. Zusätzlich stellten wir mittels „überwachten" multivarianten Analysen fest, dass die zwei klinisch relevanten Variablen (Durchmesser der Läsionen und Grad der zytologischen Entartung) mit einem bestimmten Muster der Genexpression assoziiert sind, wie es auch in einer früheren Studie aus unserem Labor mit polypösen Läsionen der Fall war. Zusammengefasst lässt sich sagen, dass nicht-polypöse und polypöse Läsionen vielen Gemeinsamkeiten aufweisen, obwohl die nicht-polypösen Läsionen einen anderen Weg der malignen Entartung einschlagen. Dies war in sofern nicht verwunderlich, als dass die präkanzerösen Läsionen im selben Organ entstehen und daher sehr wahrscheinlich ist, dass für ihre maligne Transformation ähnliche Hürden überwunden werden müssen. Folglich lässt sich durch unsere Studie schließen, dass es sinnvoll wäre, bei beiden Arten der präkanzerösen Läsionen die gleichen klinischen Beobachtungen einzuleiten.

Ein Transkript, dessen Expression sich in allen prä-kanzerogenen Läsionen sehr drastisch verändert ist *TMIGD1*(transmembrane and immunoglobulin domain containing 1). Im Vergleich zu den Transkriptionsniveaus in den entsprechenden Proben der normalen Schleimhaut, wurde *TMIGD1* in nicht-polypösen Läsionen und polypösen Läsionen 19-fach bzw. 66-fach geringer exprimiert ($\log_2$ Werte) und in Adenokarzinomen sogar 152-fach. Diese beachtliche Tatsache und die Originalität unserer Ergebnisse (in unserer Analyse wurde die Expression dieses Genes im Gegensatz zu früheren Microarrays durch spezifische Sonden für abgedeckt), und die Tatsache, dass die biologische Funktion bisher nicht bekannt ist, veranlassten uns dazu, eine bessere Charakterisierung des Expressionsprofils zu beginnen (sowohl auf mRNA-als auch auf Proteinniveau).

Wir konnten die Daten der Microarray Analyse durch eine quantitative RT-PCR bestätigen. Zudem haben wir die Expression in weiteren Geweben untersucht und festgestellt, dass die Expression der *TMIGD1* mRNA im unteren Margen-Darm-Trakt und in der Niere erhöht ist. Die stabile Expression der kompletten *TMIGD1* cDNA in der *TMIGD1*-defizienten Krebszelllinie SW480 zeigte, dass das Protein im Zytoplasma exprimiert wird. Wir stellten sowohl eine perinukleäre Ansammlung des Proteins (sehr wahrscheinlich handelt es sich um eine Assoziation mit dem rauen endoplasmatischen Retikulum, jedoch sollte ein Lokalisation in den Mitochondrien nicht ausser Acht gelassen werden) als auch eine Lokalisation im gesamten Zytoplasma und an der Zellmembran fest. Die faserartige Färbung legt eine Assoziation von TMIGD1 mit dem Zytoskelett nahe.

Durch immunohistochemische Analysen konnten wir zeigen, dass die Expression von TMIGD1 auf dem oberen Abschnitt der intestinalen-epithelialen Krypten beschränkt war (hier befinden sich differenzierte Zellen), wobei die Expression in den zellteilungs-aktiven Bereichen fehlte. In den Zotten des terminalen Ileums und in den Nierengefäßen lokalisierte TMIGD1 eindeutig im Bürstensaum. Wir zu erwarten war, war die Expression in nicht-polypösen und polypösen Läsion als auch in den Adenokarzinomen dramatisch reduziert. Interessanterweise zeigte die Färbung für TMIGD1 eine Korrelation zwischen dem Grad der zellulären Differenzierung, wobei die Expression in schwach differenzierten gänzlich Neoplasma fehlte. Daher könnte TMIGD1 ein neuer Marker für die epitheliale Differenzierung im unteren Margen-Darm-Traks und in der Niere angesehen werden. Die Auswirkungen der Runterregulierung während der zellulären Entartung während Darmkrebsentwicklung werden Gegenstand weiterer Untersuchungen sein.

3. INTRODUCTION

3.1 Colorectal cancer

Colorectal carcinoma (CRC) represents one of the main causes of mortality and morbidity, especially in Western countries, with the highest rates observed in North America, Western Europe, Australia, and the lowest rates in Africa and Asia. Nowadays, however, there is a slight decrease in the incidence of colorectal cancer as a result of effective intervention and life style changes in western countries, while in developing countries, the economic development and the adoption of western life-styles have led to an increased of it. Based on cancer incidence rates estimated in the United States, colorectal cancer is the fourth most frequent cancer in humans (after prostate, breast and lung cancers).[1] Wide geographic variation in colorectal cancer incidence and mortality rates are believed to be due, partially, to life style (i.e. obesity, consumption of red meat, inverse relation with physical activity and consumption of fruits and vegetables) and environmental factors.

Colorectal cancer is actually a multifactorial disease whose development constitutes a good example of the complex interaction between genetic and environmental causes. Its pathogenesis is tightly related to the age factor, showing a bimodal incidence with a first peak in correspondence to the fourth-fifth decade and an exponential growth after the age of fifty.

Although high-penetrance mutations in several genes have been identified in most of the hereditary syndromes predisposing to colorectal cancer, in the large majority of cases, the etiology still remains elusive. Colorectal cancer is traditionally divided into sporadic (80%), that means not familial, and familial (i.e. hereditary) cases (20%).

3.2 Basic anatomy and physiology of the large intestine

To better understand what is and how CRC develops it is important to have a brief introduction about the anatomy and the physiology of the large intestine.

A brief introduction will be also done about the intestinal cell renewal mechanism because its (de)regulation is closely linked to cancer onset.

Around 200 cells per crypt are generated every day in the intestine. This complicated and precise mechanism needs to be strictly controlled to preserve a correct equilibrium. This equilibrium is called homeostasis and it is maintained by, at least, three different coordinated processes: cell proliferation[2], cell migration[3], and anoikis. The intestinal cell proliferation is not individually driven by each cell type but controlled by the crypt niche, meaning that the two clearly defined proliferative and differentiated compartments are strictly preserved while the cells travel beside the crypt-villi axes[4]. While the location of four to six stem cells[5, 6], at the crypt bottom in the large intestine seems to be clear, their position in the small intestine is less obvious; they have been placed immediately above the Paneth cells[7, 8], or mixed with Paneth cells at the very bottom of the crypts[9]. The intestinal stem cells are characterized by preservation of an undifferentiated phenotype, permanent production of all different cell lineages, self-maintenance and renewal abilities, and regeneration capability after damage.

The epithelium layer is subjected to a constant cell migration towards the villi or the surface epithelium. There are only two cell types that escape this effect: Paneth cells and stem cells. Finally, the process called anoikis, is the cell shedding at the top of the villi, in the small intestine, or at the surface of the epithelium, in the large intestine, by which the cells lose contact with the cellular matrix and undergo apoptosis.

Large intestine anatomy and physiology[10-14]

The lower gastrointestinal tract is constituted of the small and large intestine. The large intestine or colon extends from the end of the ileum (i.e., terminal part of the small intestine) to the anus. It is divided into: caecum, colon, rectum and anus. The large intestine is long 1.2 to 1.8 meters and its calibre is greater than that of the small intestine. The first part of the large intestine is the caecum, small segment connecting the terminal part of the ileum to the ascending colon through the ileocecal valve.

The colon is the part of the intestine located between the ceacum and the rectum. It is composed of several distinct segments: the ascending, the transversum and the descending. The colon from the caecum to the mid transverse colon (splenic flexure) is also known as proximal colon , while the remaining part is known as the left colon. The first part of the colon is the *ascending colon*. The ascending colon expands from the caecum to the hepatic flexure (the turn of the colon by the liver). The *transverse colon* extends from the hepatic flexure to the splenic flexure (the turn of the colon by the spleen).

The *descending colon* is the part of the colon from the splenic flexure to the beginning of the sigmoid colon. The *sigmoid colon* is the last part of the large intestine before the rectum. Its diameter is approximately 2.5 cm, being the narrowest portion of the colon. Next to the sigmoid colon appears the rectum, the final straight portion of the intestine, of about 12 to 15 cm in length, which ends in the anus.

The structure of the colon wall reflects that of the entire gastrointestinal (GI) tract. Four concentric layers surrounding the inner cavity, the lumen, can be distinguished: mucosa, submucosa, muscularis propria, and serosa. The innermost layer of the colon, surrounding the lumen, is the mucosa. The normal colorectal mucosa is constituted by 3 main elements: epithelium of the surface and crypts, lamina propria and muscolaris mucosae, the latter separates the mucosa from the deeper submucosa. The intestine contains a complex, rapidly proliferating, and perpetually differentiating *epithelium*. The epithelium constitutes the major barrier between the intestinal lumen and the lamina propria and regulates fluxes between

these two compartments. Epithelial cell migration and differentiation occurs continuously, and the process of cellular renewal takes approximately three to five days. Shedding cells are removed from the crypts by a process known as *anoikis*, in which altered cellular adhesion results in apoptosis. The epithelial layer of the human colon is made up of a single sheet of columnar epithelial cells, which form finger-like invaginations into the underlying connective tissue of the lamina propria to form the basic functional unit of the intestine, the crypt. The base of the crypts is believed to hold the stem cell population, within the stem cell niche, formed by the stem cells themselves and mesenchymal cells that surround the crypt base.

There are four major terminally differentiated epithelial cell types present in the colon: the colonocytes or absorptive cells, responsible for ions and water absorption, the mucus-secreting goblet cells, which synthesize, store and secrete mucin, peptide hormone-secreting cells and Paneth cells, which secrete antibacterial proteins (lysozyme and defensins).

The lamina propria extends between crypts and reaches the muscularis mucosae; it contains a variety of cells, including fibroblasts lymphocytes, plasma cells, eosinophils, macrophages and mast cells, which are arranged among strands of collagen tissue. Colonic mucosa contains also well formed gut associated lymphoid tissue which is responsible for local defence against harmful agents originating in the gut lumen.

The muscularis mucosae is a thin layer of smooth muscle which separates the epithelium and lamina propria from the submucosa.

The submucosa is a loose connective tissue layer containing numerous arteries as well as venous and lymphatic plexuses that support the mucosa, and muscularis mucosae. It also joins the mucosa to the bulk of underlying smooth muscle. The muscularis propria consists of a circular inner muscular layer and a longitudinal outer muscular layer condensed into three bands, the teniae coli.

The serosa is a mesothelial cell layer overlying loose connective tissue coated in mucus to prevent friction damage from the intestine rubbing against other tissues.

The colon has different functions: to lubricate waste products, to absorb remaining fluids (added to the food during digestion), salts and vitamins, and to store waste products until excretion. It has no digestive function (no digestive enzymes are secreted). By the time the chyme has reached the colon, almost all nutrients and 90% of the water have been absorbed by the body in the small intestine. At this point some electrolytes like sodium, magnesium, and chloride are left as well as indigestible carbohydrates known as dietary fiber. As the chyme moves through the large intestine, most of the remaining water is removed, while the chyme is mixed with mucus and bacteria known as gut flora, and becomes feces. The bacteria break down some of the fiber for their own nourishment and create acetate, propionate, and butyrate as waste products, which in turn are used by the cell lining of the colon for nourishment. A part of these and other metabolic functions, the gut flora also plays important protective and structural roles.

3.3 Pathways to colorectal cancer

3.3.1 On the way to cancer

Preinvasive lesions of the human colorectum are small areas of tissue that alter the surface contour of the gut mucosa. They are conventionally referred to as "polyps" which indicates growth protruding into the intestinal lumen, and this is indeed a fair description of most premalignant colorectal lesions.

It is nowadays accepted that there are also others, which are only slightly raised above the mucosal surface, or flat, or even depressed. Standard colonoscopy is performed to identify and resect these benign lesions in the belief that some of them will progress to cancer. **Figure 1** illustrates the conventional pathway by which this progression is thought to occur. The first step is the development of early morphologic changes in discrete clusters of epithelial crypts. In aberrant crypt foci (ACFs) the aberrant crypts are usually larger than normal and have thicker epithelial lining and dilated or slit-like openings that are raised slightly above the

adjacent mucosa. ACFs are classified histologically as dysplastic and nondysplastic. Apart from their size nondysplastic crypts are not remarkably abnormal, and their proliferative compartments are confined to the lower portion of the glands , as they should be. However, they often display signs of hyperplasia and infolding of the epithelium into the crypt lumen, a phenomenon referred to as *serration*, which is discussed on greater details below. Dysplastic crypts in contrast, present signs of cellular atypia (mucin depletion, nuclear enlargement, stratification and loss of polarity) and upward expansion of the proliferative compartment toward the mouth of the crypts. ACFs are encountered much more frequently in colons harboring adenomatous polyps or adenocarcinomas (80%-100% of all cases), and 20%-50% of these show signs of dyplasia[15]. The view of ACFs as probable precursors of preinvasive colorectal neoplasms is supported by findings of identical molecular changes in both types of lesions. Indeed, although they are more common features of premalignant neoplasms, mutations involving the *KRAS* or *BRAF* oncogenes or the adenomatous polyposis coli (*APC*) tumor suppressor gene, nuclear accumulation of β-catenin, aberrant DNA methylation, and low-level genomic instability have also been reported in some ACFs. The weight that should be assigned to ACFs - their presence, number and type – in planning surveillance colonoscopy is currently unclear, but the increasing use of magnifying chromoendoscopy is expected to provide important information on this question.

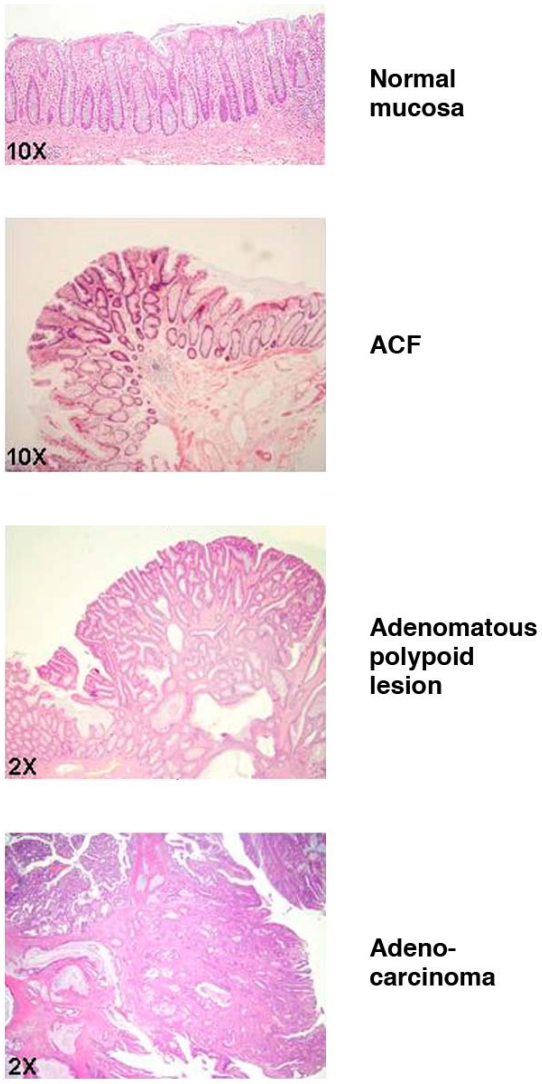

Figure 1. A simplified 4-stage model of the transformation of normal colorectal mucosa into adenocarcinoma.

The figure shows the histologic features of the four stages of the adenoma-carcinoma pathway to colorectal cancer. In order, from top to bottom: normal mucosa; aberrant crypt focus (ACF); tubulo-villous adenoma with epithelial dysplasia and invasive adenocarcinoma. The dysplastic ACF came from the colon of a patient with colon cancer (H&E staining, 25x magnification). The photomicrogram shows approximately 12 of the 50 or so aberrant crypts included in the ACF, which is slightly raised above (≈ 500 μm) the surface of the gut mucosa. Compared with the surrounding normal crypts (right, upper corner), the aberrant crypts are larger and longer with initial signs of branching and infolding of the epithelium. The epithelial lining presents low-grade dysplasia (mild mucin depletion, hyperchromatic nuclei, initial signs of nuclear enlargement, occasional areas of stratification). In the lower left corner, the crypt lumens are enlarged – a frequent finding at the borders of ACFs. The adenomatous polypoid lesion shows a prevalent tubular growth pattern with some villous projections. The degree of dysplasia varies from low-grade (left half of the lesion) to high-grade (right half, superficial). In the lower left corner is present a portion of normal mucosa of the stalk. Adenocarcinoma: irregular branching of glands showing atypical epithelium. They are surrounded by stroma composed of dense fibrous tissue comprising spindle cells in a collagenuos and inflammatory background (desmoplastic reaction). (Magnification: Normal mucosa, 10 X; ACF, 10X; Adenoma, 2X; Adenocarcinoma, 10X)

Preinvasive neoplasms – the next stage – are also a frequent finding. They are identified in a roughly one third of all asymptomatic adults undergoing standard colonoscopy, but, some may regress on their own, and only a fraction will be transformed in cancer. The progression process generally involves increases in size and in the degree of cellular atypia. Lesions over 1 cm in diameter with high degree of dysplasia (referred to as *advance adenomas*) are the ones farthest along on the road toward malignancy. (The term *adenoma* is used hereafter to refer to neoplasms – regardless of their macroscopic appearance – that display epithelial dysplasia). Several lines of evidence indicate that some of these preinvasive lesions will indeed give rise to colorectal cancers. For one thing, the frequency of these benign neoplasms and that of colorectal cancers both increase with age, but the age/prevalence curve for the former is shifted to the left by ~10 years. The regional distribution of cancers within the colon also parallels that of large adenomas. In addition, the expected incidence of colorectal cancer is substantially reduced by colonoscopy with polypectomy (even though 10-20% of all premaligant lesions, mainly those with diameter < 5 mm, are likely to be missed on standard endoscopy[16]). And finally, there is the impressive frequency at which preinvasive adenocarcinomas are detected within an advanced adenoma, especially those displaying villous growth patterns and particularly severe dysplasia. About half of all the adenocarcinomas are elevated above the surrounding mucosa, and in the other half growth occurs at or below the surface of the normal tissue, so it seems that both polypoid and nonpolypoid benign lesions give rise to cancer.

3.3.2 Breaking convention: The contribution of modern endoscopy and histology

For decades, all preinvasive colorectal lesions were referred to as polyps. Preneoplastic growth that did not protrude into the gut lumen was first detected in the eighties by Japanese endoscopists[17]. Once these nonprojecting lesions were recognized, they were reported with increasing frequency in other countries as well,

where they represented 10-40% of all the preinvasive neoplasms encountered during screening colonoscopy[18]. Since then, attempts have been made to reclassify preinvasive lesions of the digestive tract.

A newer, more precise terminology refers to all protruding lesions as ***polypoid*** and sub-classifies them as *pedunculated* (attached with a pedicle or stalk) or *sessile* (attached by a broad base).

At the other end of the spectrum are the ***nonpolypoid*** lesions. They are still widely referred to as "flat" although most are actually slightly elevated (< 2.5 mm above the surface of the gut mucosa); those that are completely flat or slightly depressed are rare, but even when they are small, they are generally farther along on the road to cancer[19]. The more accurate endoscopic classification of preinvasive colorectal lesions led to some important observations.

While true polypoid lesions were more frequently detected in the left colon (from the splenic flexure to the rectum), nonpolypoid lesions were more common in the right colon (from the caecum to the splenic flexure).

Even more important was the discovery that, while most of the latter lesions had classic adenomatous features, others presented a peculiar histologic pattern characterized by infolding of the glandular epithelium. As noted earlier, this phenomenon is referred to as *serration*, because it produces a saw-toothed (or serrated) pattern in longitudinally sectioned crypts[20] (**Figure 2**). Serrated crypt architecture proved to be typical of lesions that were then (and sometimes still are) being referred to as *hyperplastic polyps*.

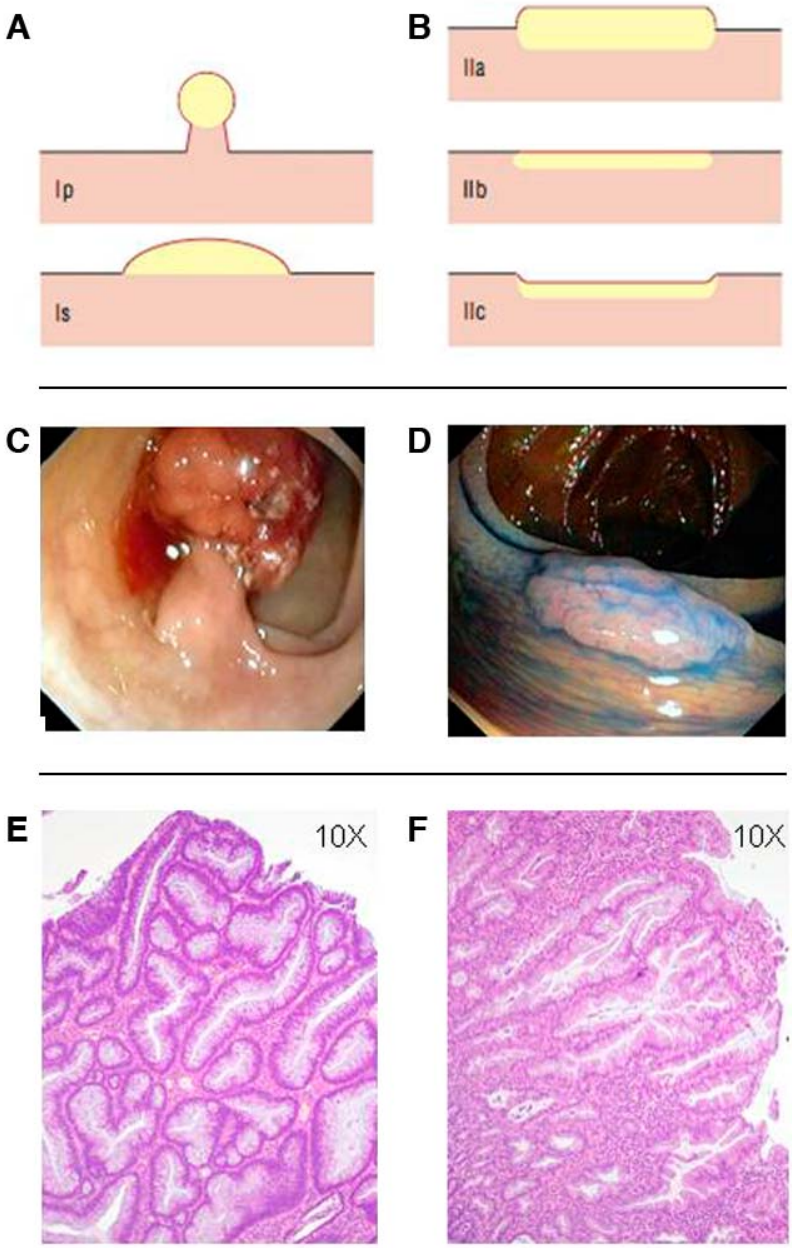

Figure 2. Polypoid and nonpolypoid preinvasive lesions of the colorectum.

A and **B**, Types of tumor growth associated with the development of colorectal neoplasia (Paris classification). Polypoid (**A**) lesions can be pedunculated *(Type Ip*) or sessile (*Type Is*); most nonpolypoid (**B**) lesions are slightly elevated (*Type IIa*), but some are completely flat (*Type IIb*) or depressed (*Type IIc*). Mixed growth patterns can also be found. The endoscopic appearances of polypoid (pedunculated) and nonpolypoid (slightly elevated) lesions are shown in panel **C** and **D**, respectively. Histological examination shows conventional adenomatous features (tubular proliferation with low-grade epithelial dysplasia) in a pedunculated polyp (**E**; magnification, 10X) and the serrated pattern (irregular shape of the crypts with serration of glandular lumens) in a nonpolypoid lesion (**F**; magnification, 10X). Either of these histological patterns can be found in polypoid and nonpolypoid lesions.

They had long been considered innocuous with a negligible risk for progression to cancer, mainly because, in spite of their architectural abnormalities, they showed no clear signs of epithelial dysplasia. The term *hyperplastic polyp* is gradually being abandoned in favour to nondysplastic serrated polyp (although in both cases, the term "polyp" is a misnomer since many of these lesions are nonpolypoid). It is also becoming increasingly clear that this category includes morphologically and molecularly distinct subsets with different propensities for malignant transformation.

Three major histologic subtypes have been identified thus far[21]. Goblet-cell serrated polyp (GCSPs) have the fewest architectural anomalies, and it is generally agreed that they are unlikely to progress to cancer. These lesions are found primarily in the left colon and most are small rectal lesions. They contain enlarged, nonbranching crypts displaying little or no epithelial infolding. Their main abnormality consists in an increased goblet cell/columnar cell ratio that affects the entire length of the glands.

Microvesicular serrated polyps (MVSPs) are more common than GCSPs. They are found throughout the colon, although their frequency is also highest in the left colon and rectum. The crypts are elongated and funnel-shaped, but the proliferative compartment is normally confined to the bottom of the gland. The upper crypts contain numerous microvacuolated columnar cells. The upper 2/3 of the crypt (and less commonly the crypt base as well) typically presents epithelial serration.

The third subset comprises lesions that are still widely referred to as *sessile serrated adenomas* (SSAs). The term is imprecise: first, because the group includes both sessile polyps and nonpolypoid lesions, and second, because the dysplasia that is the hallmark of an adenoma is absent in these lesions. SSAa are generally found in the right colon. They are characterized by L-shaped or inverted-T shaped crypts lined with infolded epithelium from base to mouth. The proliferative compartment is sometimes expanded, but as noted, there is no real cytologic dysplasia. Histologic and molecular findings suggest that SSAs evolve from MVSPs and that some do eventually become dysplastic. But at this point, they are usually referred to as

serrated adenomas (SAs). The histologic definition of this term is still matter of debate among pathologists so their diagnosis displays substantial interobserver variation. Because cellular dysplasia is an essential feature of SAs, some are likely to be classified as conventional adenomas. Mixed lesions containing serrated areas interspersed with areas displaying conventional adenomatous changes can also be found[22].

In a recent study[23], 65% of the premalignant lesions resected during standard colonoscopy were conventional adenomas. The other 35% displayed serrated architecture and were generally classified as "hyperplastic polyps". Most of the latter were MVSPs or GCSPs (30%), a few were SSAs (~4%), and less than 2% were dysplastic. Similar figures (60% conventional adenomas, ~40% serrated lesions) emerged from another study based on magnifying chromoendoscopy[24]. 9% of all lesions removed in this study were SSAs, and 2.4% were dysplastic (SAs).
Therefore alongside the conventional adenoma-carcinoma pathway illustrated in figure 1, there seems to be a second, less frequent route, the serrated pathway, which also leads to the development of colorectal adenocarcinoma (**Figure 3**).

There is evidence of its existence at both ends of the transformation process. Serrated crypt morphology has, in fact, been described in some nondysplastic ACFs[25], and ~10% of all colorectal cancers have predominantly serrated histologic patterns (the serrated adenocarcinomas)[26] or contain peripheral remnants of serrated adenoma[27]. The mixed (serrated and conventionally adenomatous) histology observed in some preinvasive lesions suggest that the two pathways have somehow intersected or merged during tumorigenesis.

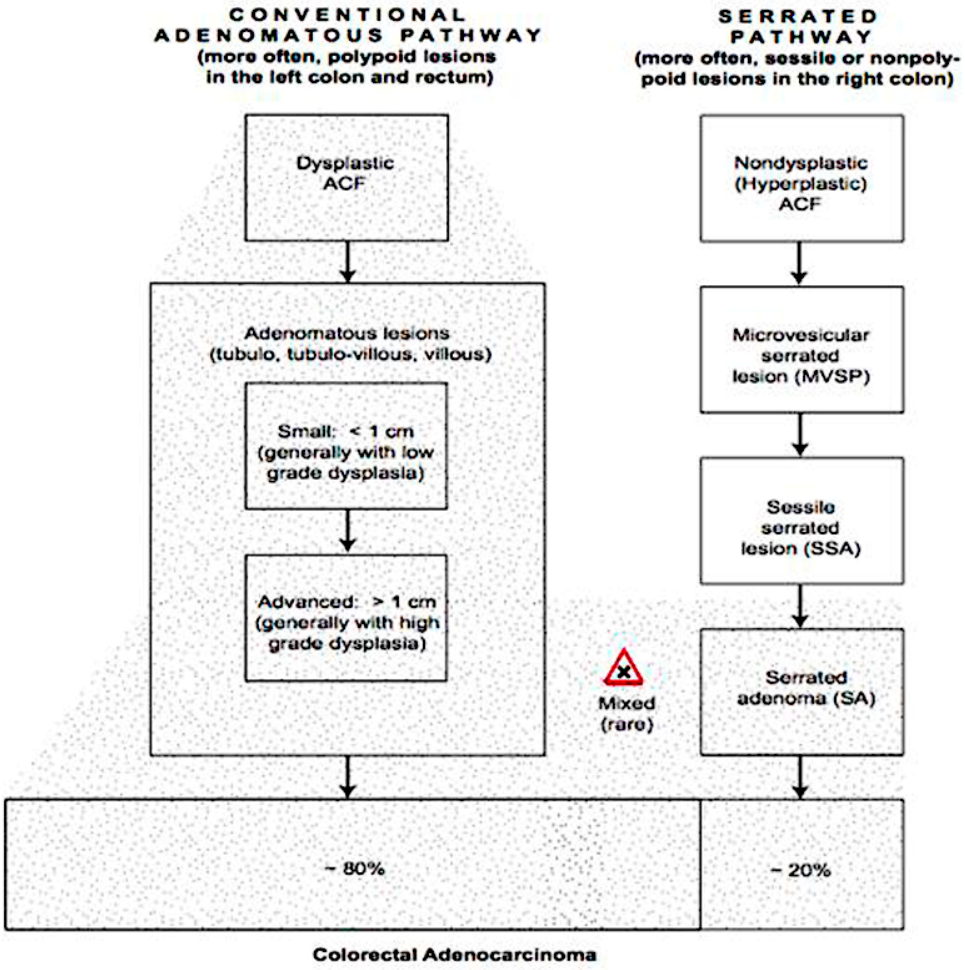

Figure 3. The best characterized pathways to colorectal adenocarcinoma.

The conventional adenomatous pathway is the most common route to adenocarcinoma. The cancers that arise through this pathway can be located anywhere in the colorectum, but they are more frequent in the left colon and rectum. Progressively severe cellular and architectural dysplasia (shaded region) is the hallmark of this pathway. It can already be found in the earliest-stage lesions, such as ACFs. The putative stations in the "less traveled" serrated pathway are shown on the right. Architectural abnormalities are an early feature of this pathway, whereas cellular dysplasia appears late (details in the text). Among the lesions that develop through this pathway, those most likely to develop into cancer are located in the right colon.

In summary, 2 out of 3 preinvasive colorectal lesions discovered at endoscopy are classic adenomas with tubular and/or villous architecture and some degree of dysplasia. The third will present a serrated histological pattern, in rare cases combined with dysplastic changes. The classic adenomas are usually pedunculated (or less frequently, sessile) polyps but around 1/3 are nonpolypoid[23,

[24, 28]. Among serrated lesions, polypoid and nonpolypoid patterns are more or less equally represented. Small serrated polyps (<5 mm in diameter) with microvesicular or goblet-cell features are likely to be encountered in the left colon and rectum. Larger MVSPs (which are usually sessile polyps or nonpolypoid lesions) and SSAs are more frequently found in the right colon. As for the dysplastic serrated lesions (SA), over two thirds are polypoid, and most are located in the left colon[29]. However , there is compelling molecular evidence that their less common, right colon counterparts are far more important: these proximal SAs seem to be the ones that evolve along the serrated pathway, presumably giving rise to 20% of adenocarcinomas found in the colorectum.

Advances in the fields of endoscopy and pathology have provided us with more accurate classification of preinasive lesions that better reflects their relevance in colorectal tumorigenesis.

3.3.3 Convention-breaking findings from molecular biology

The availability of tissue samples of preinvasive lesions removed during endoscopy or surgery fuelled attempts to identify the crucial molecular events that allow these lesions to form and progress toward cancer. In general, increases in lesion size are paralleled by increasingly bizarre architectural and cytologic atypia, and the larger lesions (polypoid or nonpolypoid) are the ones most likely to become malignant.

Interestingly, molecular alterations considered highly relevant to the transformation process in the colon are often found in some but not all premalignant lesions, and when they are present, their prevalence frequently correlates poorly with the size or severity of lesions. Some well known examples are oncogene mutations (*KRAS* and *BRAF*) ad more extensive genetic or epigenetic alterations, such as microsatellite instability or the methylator phenotype. The fact that some of these changes appear to be mutually exclusive suggest that

precancerous cells can be transformed into invasive cancer cells by different sequences of mutations.

Nevertheless, there does seem to be a common denominator in the onset and progression of most, if not all, precancerous lesions of the colorectum: aberrant activation of the Wnt signaling cascade.

Canonical Wnt signaling is a crucial driver of epithelial-cell division within the lower third of the intestinal crypt, which represents one of the simplest self renewing biological entities in mammals[30] (more details in the chapter in the Appendix). Constitutive Wnt signaling leads to an expansion of the proliferative compartment of the crypt, destroying the equilibrium between proliferation and differentiation, and this loss generally coincides with the development of precancerous lesions. In virtually all colorectal tumors (preinvasive and invasive) this inappropriate signaling reflects abnormal stabilization of β-catenin, and in 60%-80%, the cause is homozygous mutation of the well known tumor suppressor gene *APC*[31-34], which presumably occurs in the progenitor stem cells at the crypt base[35, 36]. *APC* mutation is therefore a frequent event in the initial stages of colon tumorigenesis, but it is not the only cause of the altered stability and distribution of β-catenin that characterizes colorectal tumors. Wnt signaling can also be constitutively activated by somatic changes affecting other crucial pathway components. They can be genetic[37-39] or epigenetic[40].

Many human tumors develop and evolve as a result of the deregulation of multiple signaling pathways, and this is undoubtedly true of colorectal tumors as well, but colorectal tumorigenesis also seems to be characterized by the selection of repeated alterations (or hits) involving the Wnt pathway. These observations suggest that Wnt signaling dysregulation itself may be modulated during transformation to meet the specific needs of the tumor at various points in its journey. The quality of the dysregulated signaling also changes when one pathway component instead of another is altered. For instance, compared with tumors bearing β-catenin mutations, those with abnormal APC function are thought to be more prone to DNA ploidy changes, because APC is also involved in mitotic spindle formation and chromosome segregation, processes that are essential for the

maintenance of chromosomal stability[41]. Low-level chromosomal instability has in fact been detected in adenomatous polyps and in dysplastic ACFs of patients with APC mutations[42, 43], although no genomic imbalances were found when a small series of adenomas with biallelic *APC* mutations were recently subjected to comparative genomic hybridization analysis[44].

The RAS/RAF/MEK/ERK cascade is another signaling pathway that is frequently dysregulated in colorectal carcinogenesis, and it, too, transforms extracellular signals into transcriptional regulation.

The MAPK/ERK cascade is a classical "survival" pathway, in that it promotes cell proliferation and prevents apoptosis. Two of its gene components, *KRAS* and *BRAF*, are known oncogenes that often present gain-of-function mutations in preinvasive colorectal lesions. The hyperactive mutant kinases they encode ($KRAS^{G12D}$ and $BRAF^{V600E}$, for example) maintain a state of chronically activated "survival signaling" in premalignant cells.

Loss of this normal homeostatic equilibrium seems to be associated with a substantial increase in DNA replication stress. Unlike the proliferating cells of normal colorectal crypts, premalignant epithelial cells with oncogene-activated survival signaling display classic examples of cellular responses to DNA damage, including phosphorylation of checkpoint kinase CHK2 and the histone H2AX, or signs, of telomere attrition[45, 46]. These events halt the cells at specific stage of the cell cycle so that the DNA damage can be repaired. This checkpoint repair system is probably one of several mechanisms that put a brake on the progression of tumorigenesis and allow lesions to remain in the preinvasive stage for years (**Figure 4**).

BRAF and *KRAS* oncogene mutations are early mutually exclusive events that can already be detected in ACFs[25]. The former is more frequent in serrated ACFs, and the latter is more common in ACFs that lack serration. Interestingly enough, this difference is maintained as transformation progresses. In fact, *BRAF* mutations are found in over 2/3 of all MVSPs, SSAs, and dysplastic SAs, and they are also present in ~15% of all adenocarcinomas, mainly those right-colon cancers that

develop along the serrated pathway. *KRAS* mutations are detected in 30-40% of conventional adenomas and in ~1/3 of all adenocarcinomas[27, 47] (**Figure 4**).

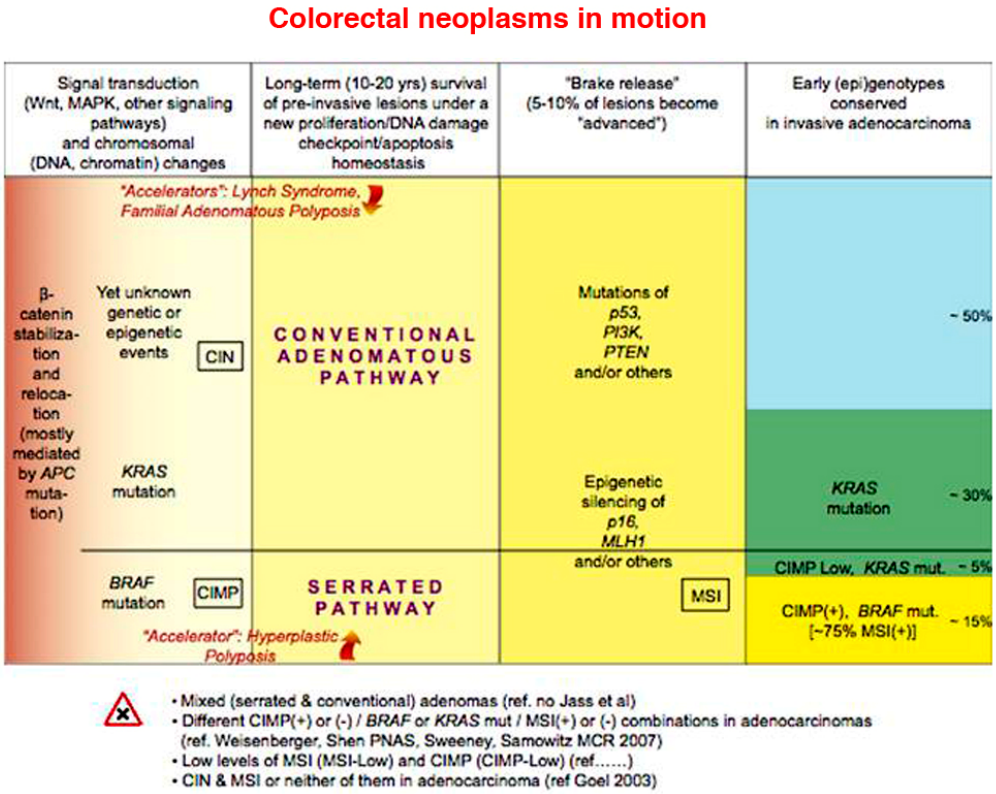

Figure 4. Molecular pathways and crossroads in colorectal transformation.

The conventional adenomatous pathway and the serrated pathway are currently the best characterized stepwise models of colorectal carcinogenesis. In both, dysregulation of Wnt signaling (β-catenin stabilization and nuclear translocation) is an early event. It can be caused by different (epi)mutations. (In the conventional adenomatous pathway, the most frequent cause is *APC* mutation). Other early events have also been documented, including mutations affecting components of the MAPK/ERK cascades (i.e., *KRAS* or *BRAF* mutations, which are mutually exclusive) and chromosomal changes, like CIN (lower-level compared to that seen in advanced adenocarcinomas) or CIMP. And there are undoubtedly others that have yet to be discovered. They account for roughly half of all adenocarcinomas, i.e., those with no evidence of the early alterations listed above (far right column – light blue segment). Mutations involving "survival signaling" cascades (e.g., MAPK/ERK) alter the normal homeostatic equilibrium between proliferation, checkpoint repair of DNA damage, and apoptosis, allowing preinvasive lesions to survive for years. Additional mutations are necessary to allow the tumor to move on into the advanced stage, where malignancy is imminent. The nature of these "brake-releasing" events differs, depending on which pathway the tumor is moving along. Crossroad warning sign: Accelerators: Colon cancer predisposition syndromes - each represents high-speed transformation along one of the pathways shown in this figure: the adenomatous pathway in Lynch syndrome and familial adenomatous polyposis; the serrated pathway in hyperplastic polyposis. The information reported in this figure is based on rates of detection of a dozen or so genetic and epigenetic alterations in preinvasive colorectal lesions and their persistence in advanced adenocarcinomas. The relative frequency of a given alteration or combination of alterations can vary considerably from study to study owing to differences in inclusion criteria (i.e., types of lesion studied), in the number and type of molecular changes investigated, and in the method(s) employed to detect these changes. Abbreviations: CIN (chromosomal instability); CIMP (CpG island methylator phenotype); MIN: microsatellite instability.

While activating mutation of *KRAS* or *BRAF* seems to be an early event in the process of colorectal transformation, 50-60% of all adenocarcinomas show no sign of either mutation. If, as it seems, oncogene activation of survival signaling allows preinvasive lesions to avoid cell death for many years, it seems reasonable to expect that benign lesions without *KRAS* or *BRAF* mutation would have mutations/alterations involving other oncogenes. To date, however, none have been identified.

The end of this more or less lengthy preinvasive stage and the onset of true malignancy is believed to be caused by the addition of one or more new genetic or epigenetic alterations.

The "brake-releasing" events are nonrandom, but they may differ, depending on the nature of the preinvasive neoplasm. Some lesions are set in motion by mutation of the tumor suppressor gene *TP53*, which is often altered in advance colorectal tumors; in others, the crucial event affects another survival signaling pathway (e.g., mutation of *PIK3CA* or *PTEN* in the PTEN/PI3K/AKT/mTOR pathway)[48] or another Wnt signaling protein; and in others, the brake-releasing hit targets a gene needed for genomic stability (the DNA mismatch repair gene, *MLH1*, for example).

The type of event(s) necessary to provoke the transition to invasiveness seems to be dictated at least in part by the original genetic feature of premalignant lesion. (somatic *MLH1* silencing, for instance, seems to be the most common trigger for progression of *BRAF*-mutated serrated lesions).

The serrated pathway shown in figure 4 generates colorectal neoplasms that are phenotypically distinct from those that develop through the conventional, APC-driven, adenoma-carcinoma sequence.

BRAF-mutated, serrated lesions give rise to sporadic MLH1-deficient cancers of the right colon, which are more frequent in women and occur later than other sporadic colon cancers (peak prevalence between the ages of 70 and 80 years). A frequent feature of these neoplasm is the CpG islands methylator phenotype (CIMP), which is characterized by a nonrandom transcriptional silencing of several cancer-

relevant gene promoters, like those of *p16* and *MLH1*[27, 49-56]. Relatively rare in conventional adenomas, the CIMP is found in 70%-80% of all dysplastic serrated lesions of the right colon, and it is closely associated with *BRAF* mutations. The basis of this association is unknown, and it is also unclear why CIMP-positive tumors prefer the right colon of women. The latter aspect presumably highlights roles played by hormonal and environmental factors (including cigarette smoking[57] and hypoxia[58, 59]).

High-throughput sequencing technology and system biology studies (based on genomics, transcriptomics, and proteomics, and other more specific – omics) will certainly improve mutation detection, providing us with a more precise picture of the colorectal oncogenetic tree[60, 61] than the one represented in figure 4.

3.3.4 Fast track transformation models: inherited syndromes

The adenomatous and serrated pathways of colorectal transformation can be discerned within three inherited syndromes (*familial adenomatous polyposis, Lynch syndrome* and *hyperplastic polyposis*) that are major risk factors for the development of colon cancer. In this section, after a general overview of familial and sporadic colon cancer, major emphasis will be put in the hyperplastic polyposis syndrome, as a model of the serrated pathway of transformation. (For details on inherited syndromes refers to chapters: Cattaneo *et al*. "Pathways and crossroads to colorectal cancer". In *Advances in understanding the basic pathogenesis and clinical management of pre-invasive disease*. Edited by Fitzegerald R., 2009, in press and Sabates-Bellver et al., Getting familiar with familial colon cancer. Chapter in the Falk Symposium 158 book "*Intestinal Inflammation and Colorectal Cancer*", 2007-A reprints are included in the Appendix)

The estimated risk of developing colorectal cancer is approximately one out of 18 persons in Western countries (USA; Europe). This ~5% lifetime probability of

developing colorectal cancer increases to 10-15% in individuals with one first-degree relative affected by CRC[62].

The percentage increases considerably if more than one relative are affected by CRC or other cancers often diagnosed in familial aggregations of CRC. The cumulative lifetime probability reaches 60-100% in carriers of a mutation in a highly penetrant allele, such as in one of the DNA mismatch repair (MMR) genes[63] in hereditary non-polyposis colon cancer (HNPCC, also known as Lynch syndrome) or in the *adenomatous polypoisis coli* (*APC*) gene in familial adenomatous polyposis (FAP)[64]. MMR-defective HNPCC represents the most frequent CRC predisposition syndrome of known aetiology, and adenocarcinomas of MMR(-) HNPCC account for ~3% of all cancers in the colon. FAP is responsible for ~0.5% of all CRC, and additional ~0.5% arise in the colorectum of individuals affected by one of the hamartomatous polyposis syndromes or by hyperplastic polyposis, whose underlying genetic alterations are the subject of intense research.

A genetic susceptibility underlines an additional 15% of all CRC[65], also referred to as familial or hereditary, but the underlying genetic disorder is unknown. In this large portion of familial colon cancers the cumulative lifetime risk is very variable, ranging from very high in familial aggregations that are clinically indistinguishable from HNPCC, but not associated with MMR defects, to conditions with only a slightly higher predisposition to CRC as compared to the general population.

At this latter end of the spectrum lies a blurred border between familial and non-familial (hereafter called sporadic) CRC. In this group lie many apparently sporadic cases that could be familial (i.e., in small families where only one case has been detected so far, in cases of poor diagnosis or where medical records are incomplete, in families where a *de novo* mutation arose for the first time, non-paternity, etc), or apparently familial that could be sporadic (i.e., two sporadic CRC in the same family).

Thus, the challenge for the years to come is to unravel novel high-penetrance presisposition alleles responsible for familial aggregations of CRC clinically similar to HNPCC but with intact MMR, and low penetrance alleles responsible for the

remainder of familial CRC. Theoretically, all the remaining sporadic CRC might also be associated with very low penetrance mutations or polymorphisms whose degree of penetrance may be modulated by environmental factors, mainly dietary ones. Importantly, the genetic alterations detected in rare inherited syndromes can have roles also in the initiation and progression of a large portion of sporadic cases when these alterations occur somatically, as for those in *APC* or the MMR gene *MLH1*.

The discovery rate in the field of cancer genetics has dramatically increased due to the implementation of genomics, with which an enormous number of identified genetic variants and their combinations can be used in studies aimed at verifying their associations with the predisposition to CRC.

3.3.5 Hyperplastic polyposis

The paradigm of "fast-track transformation" along the serrated pathway is the syndrome known as *hyperplastic polyposis* (HP), a rare (and underdiagnosed) condition that is often associated with *BRAF*^{V600E} and the CIMP. HP is diagnosed when there are[66]:i) at least five histologically diagnosed hyperplastic polyps proximal to the sigmoid colon, including two with diameter exceeding 10 mm; ii) any number of hyperplastic polyps proximal to the sigmoid colon plus first-degree kinship with a patient known to have HP; or iii) over 30 hyperplastic polyps distributed throughout the colon. HP presents with a variety of preinvasive lesions, which include not only hyperplastic polyps but also larger SSAs and even classical adenomas.

The syndrome is now known to confer an increased risk for malignant transformation, although the reported magnitude of this risk varies to some extent from study to study[67-69]. HP-related colorectal cancers show a predilection for the proximal colon, and their onset occur roughly 10 years earlier than that of sporadic colorectal cancers and about two decades later than those related to the Lynch syndrome.

Fewer than 150 cases of HP have been reported to date, and the picture that is emerging is that of a heterogeneous entity. Some authors have suggested[70] that there are actually two different phenotypes. They advocate reserving the term "hyperplastic polyposis" for cases characterized by multiple, small, pancolonic hyperplastic polyps and using "serrated adenomatous polyposis" when there are smaller numbers of relatively large, proximal, hyperplastic polyps with features of SSA. Familial aggregations has been documented in relatively few cases. When present, it seems to reflect dominant transmission of an unidentified genetic predisposition to CIMP, which frequently leads to somatic methylation of the *MLH1* promoter[71, 72].

Compared with patients harboring sporadic serrated lesions, those with HP have a significantly higher frequency of methylated alleles in the normal colon mucosa[73, 74], and this finding is also consistent with the possibility of genetically determined CIMP:

Serrated adenomatous polyposis is likely to be diagnosed with increasing frequency thanks to the introduction of innovative colonoscopy technologies and greater awareness of these lesions among pathologists. If its inherited nature is confirmed, it might some day provide a model for the identification of the initial molecular alterations that trigger the serrated pathway of colorectal carcinogenesis.

4. MATERIALS and METHODS

Tumor samples

All the precancerous colorectal lesions (polypoid and nonpolypoid) included in the study were obtained during colonoscopy. Polypoid lesions and matched normal mucosa were collected during a previous study[61] at the Gastroenterology Unit of the Belcolle Hospital (Viterbo, Italy).

Nonpolypoid lesions and matched normal mucosa were collected in the Gastroenterology Units of three different hospitals: Istituto Ospedaliero Fondazione Poliambulanza, Brescia; Istituto Clinico Humanitas, Milano and Ospedale A. Maresca, Torre del Greco, Italy.

Tissue sampling and RNA extraction (see below) were carried out similarly in both groups of precancerous lesions.

Patients with documented hereditary syndromes (Lynch syndrome, familial polyposis and hyperplastic polyposis) were not included in the study.

The tissues were collected prospectively with informed patient consent and the approval of the local Human Research Ethics Committee.

Chromoendoscopy[75], the intravital staining of the gastrointestinal mucosa, was performed during all the colonoscopies for the collection of nonpolypoid lesions as it provides additional diagnostic information regarding the epithelial morphology and pathophysiology. The technique consists in stain-spraying the mucosal surface to enhance the characteristics of both normal and abnormal gastrointestinal mucosa. Chromoendoscopy in the colon pursues the following aims: screening for polyp and nonpolypoid or depressed neoplasia, and differentiating between hyperplastic and adenomatous lesions.

Nonpolypoid lesions were collected only from the proximal segment of the colon (caecum, ascending, hepatic flexure and transversum) and their macroscopic appearance was classified according to the Paris Endoscopic Classification[76]. This classification distinguishes polypoid (or protruding) lesions from nonpolypoid (or

non-protruding) lesions: in the former type, the height of the lesion is more than one third of its diameter, whereas the latter type is defined as every irregularity of the mucosal layer whose height is less than one third of its diameter. The distinction between a sessile lesion and a slightly elevated lesion is based on the extent of the elevation from the adjacent mucosa (the cut-off limit is 2.5 mm in the columnar epithelium). In agreement with this classification, lesions morphologically defined slightly elevated (IIa), completely flat (IIb), depressed (IIc) or mixed (i.e IIa-IIc) were considered for the collection of nonpolypoid lesions in the study.

Immediately after removal, a small sample of epithelial tissue (30 mg) was cut from the surface of each lesion to reduce contamination with sub-mucosal, non-epithelial tissue (**Figure 5**). We excluded lesions of less than 1 cm of diameter to ensure that this sampling procedure would not interfere with the histological diagnosis. The approach used allowed us to obtain specimens with a high percentage of epithelial cells without resorting to microdissection, which could diminish quantity and quality of the extracted RNA. For each lesion, four biopsies of normal mucosa from the same colonic segment ($\geq$ 2 cm from the site of the lesion) were collected in order to compare the transcriptome of the neoplasia with that of the corresponding normal colonic mucosa. The lesional samples and the normal mucosal biopsies were immersed in *RNAlater* (Ambion, Huntington, UK) for subsequent microarray analysis, and the remainder of the lesion was submitted for pathological analysis.

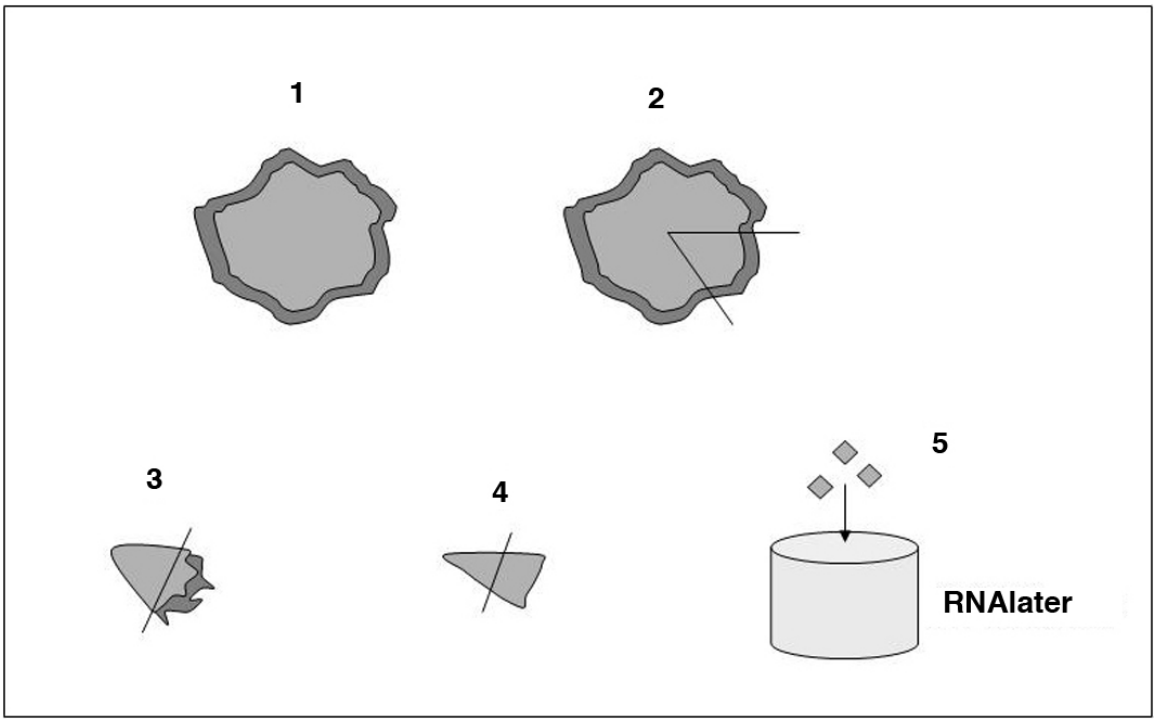

Figure 5. Sampling procedure from nonpolypoid lesions for RNA extraction.

Immediately after endoscopic excision, the tissue sample was immersed in *RNAlater* solution (1). A portion of the lesion was then cut by an expert pathologist (2), and the necrotic areas (from the endoscopic cauterization) removed (3). The tissue section was further divided into small pieces to allow fast penetration of the *RNAlater* solution (4 and 5). A total of ~20 mg of tissue was thus stored at 4ºC for one night, and at -20ºC till RNA was extracted

Total RNA was extracted (RNeasy Mini Kit, Qiagen, Valencia, CA) from homogenized tissue and its integrity was verified by capillary gel electrophoresis (Experion System, BioRad). Only RNAs with a ribosomal ratio 28S/18S between 1.5 and 2.2 were further processed for microarray analysis (**Figure 6**).

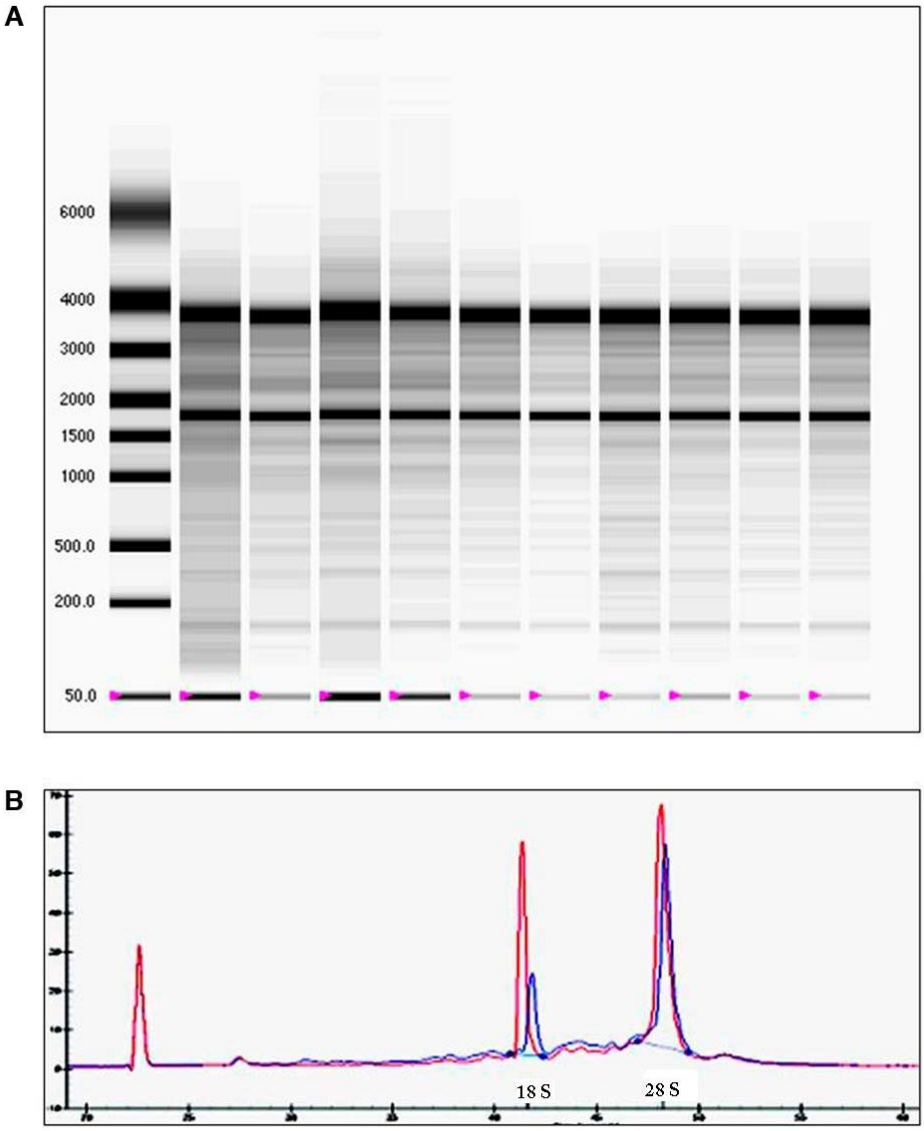

Figure 6. Evaluation of RNA integrity and efficiency of rRNA reduction.

The degree of RNA degradation was assed by the Experion system and RNA StdSens analysis kit (BioRad). Ratio of the two large ribosomal RNA molecules (28S/18S rRNA) provides a measure of RNA degradation since the 28S rRNA is more susceptible to degradation than the 18S rRNA fragment. Intact eukaryotic RNA samples generally have a 28S/18S ribosomal RNA ratio of 2.0-2.2.The Experion software automatically determines the 28S/18SrRNA ratio and provides a visual assessment of degradation in electropherograms or virtual gel images. In panel A, a gel-like image of high quality RNA extracted from nonpolypoid lesions is shown.The 18S and 28S ribosomal RNA bands are clearly visible, with 28S/18S ratio between 1.8-2.0. the electropherogram in panel B shows the 28S and 18S rRNA peaks before (*red*) and after (*blue*) the process of ribosomal reduction. This analysis was performed to verify the efficiency of this step (see sample preparation in Figure 7)

Microarray analysis

Two µg of total RNA were processed as follows (**Figure 7**). The ribosomal RNA was first removed with RiboMinus Human Transcriptome Isolation kit (Invitrogen), in order to significantly reduce the 28S and 18S ribosomal subunits population from the total RNA sample. This step minimizes the background and thereby increases the array detection sensitivity and specificity. Double-stranded cDNA was synthesized with random hexamers tagged with a T7 promoter sequence using the Whole Transcript Sense Target Labeling kit (Affymetrix, Santa Clara, CA, USA). The cDNA was subsequently amplified by T7 RNA polymerase to produce several copies of antisense cRNA. In a second cycle of cDNA synthesis, random hexamers were used to prime reverse the transcription of the cRNA and to produce single stranded DNA in a sense orientation. The sense cDNA was then fragmented by uracil DNA glycosylase (UDG) and apurinic/apyrimidic endonuclease 1 (APE1), and biotin-labelled with terminal deoxynucleotidyl transferase (TdT) using the GeneChip WT Terminal labeling kit (Affymetrix). The size of fragmented cDNA was finally determined using Bioanalyzer (Agilent, Santa Clara, CA, USA). All the samples with optimal fragment size in the range of 50-200 bps were further processed.

Hybridization was performed using 5 µg of biotinylated, fragmented cDNA (i.e. target), which was applied to the GeneChip Human Exon 1.0 ST array (Affymetrix). Incubation was performed at 45°C for 16 hours. Following hybridization, the non-specifically bound material was removed by washing in the Affymetrix Fluidics Station 450 (protocol FS450_0001, and using reagents from the GeneChip Hybridization, Wash and Stain kit of Affymetrix), and detection of specifically-bound target was performed by scanning the array in the Affymetrix GeneChip Scanner 3000 7G.

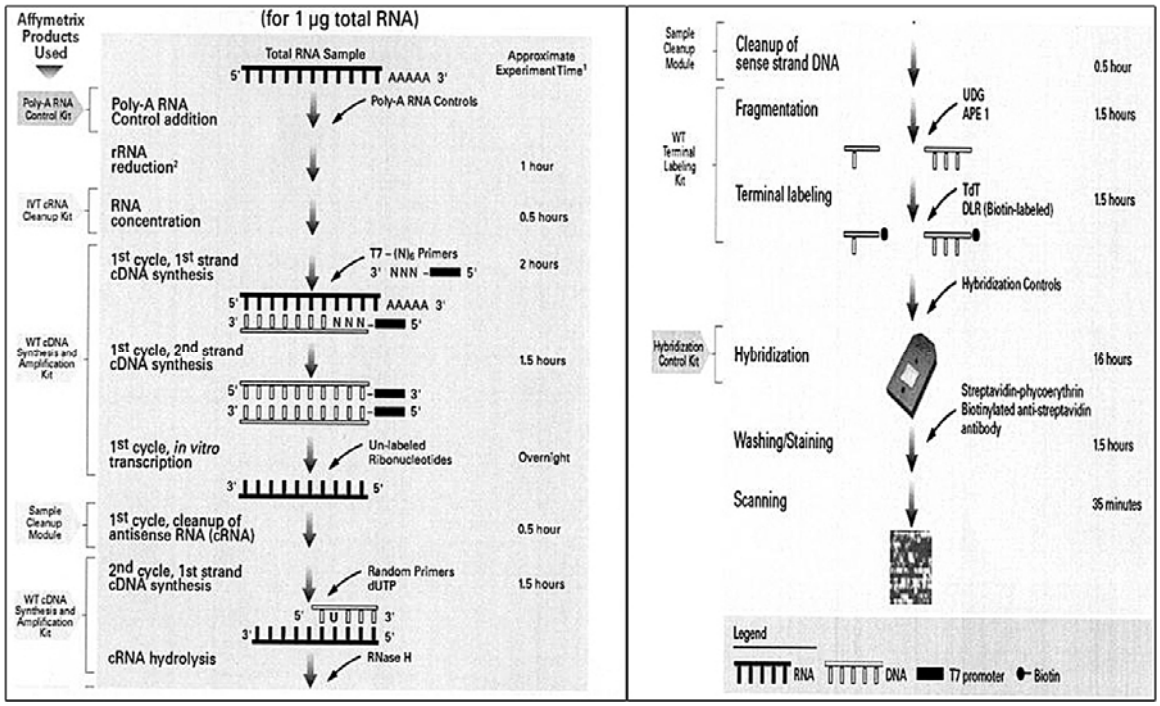

Figure 7. The complete Exon array workflow

Scheme of the standard steps of exon microarray sample preparation. Total RNA was subjected to ribosomal RNA reduction, then it was reverse transcribed to cDNA by random hexamers tagged with a T7 promoter. cDNA was amplified by a T7 RNA Polymerase in order to obtain many copies of cRNA. cRNA was subsequently subjected to a second cDNA synthesis to produce single stranded DNA in a sense orientation. The sense strand DNA was fragmented by UDG and APE1 and then biotin-labeled by TdT. Fragmented DNA was hybridized to the GeneChip Human Exon 1.0 ST array. Following hybridization, the non-specifically bound material was removed by washing and detection of specifically-bound targets was performed by scanning the array in the Affymetrix GeneChip Scanner 3000 7G.

Cell intensities (.CEL files) were captured by the Affymetrix GeneChip Operating Software (GCOS) and Affymetrix Expression Console Software (version1.0) was used to perform quality assessments. CEL files were finally analyzed in the Partek Genomics Suite software (Partek Inc., St.Louis, MO).

Array design

The GeneChip Human Exon 1.0 ST array was designed by Affymetrix to be as inclusive as possible at the exon level, deriving from annotations ranging from empirically determined, highly curated mRNA sequences to ab-initio computational predictions[77]. The Exon array contains approximately 5.4 million *probes*, grouped into 1.4 million *probe sets* interrogating over 1 million *exon clusters* (i.e., usually corresponding to one exon).

A probe set is a set of synthetic oligonucleotide probes, usually four in number, on Exon array that interrogate gene expression from one exon. The exon cluster is a group of one or more probe sets that cover a contigous stretch of putatively transcribed genomic sequence, tipically corresponding to an exon within a transcript. The transcript cluster is a group of one or more exon clusters covering a region of the genome reflecting all the exonic transcription evidence known for the region and corresponding to a known or putative gene (**Figure 8**).

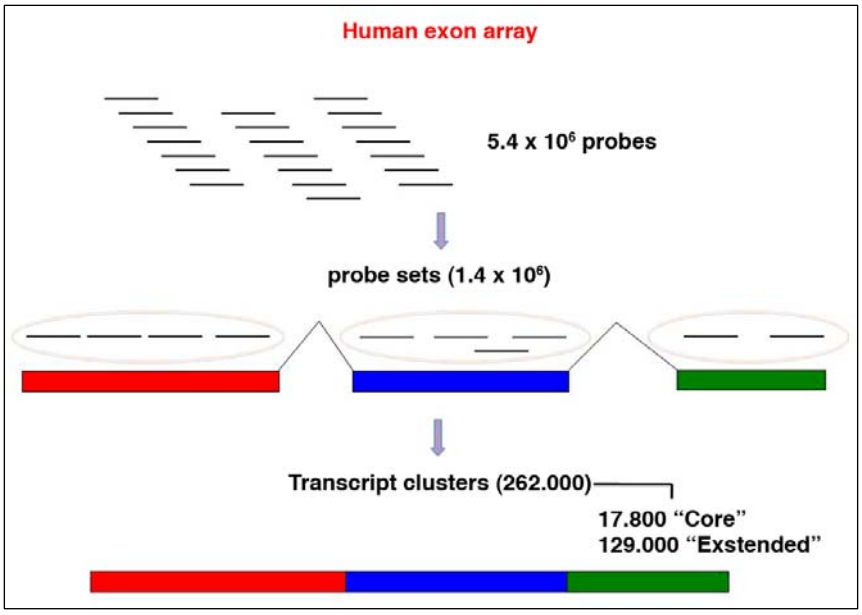

Figure 8.Human Exon array design

The human Exon Array was designed to target all the annotated and predicted exons in humans. To this aim, 5.4 million of probes were designed. Four probes form a unit called *probe set* which recognizes an exon in most of the cases. 1.4 million of probe sets can virtually be resembled into over 262.000 *transcript clusters* according to a range of annotation source. Well annotated probe sets encompass the *core set* of 17.800 transcript clusters. Predicted and well annotated probe sets form the *extended set* of 129.000 transcript clusters.

Differently from the previous generation of Affymetrix arrays, the Exon array does not include a paired mismatch feature for each perfect match feature; surrogate mismatch intensities are derived from 25,000 pooled "anti-genomic" background probes with the same GC content as each perfect match feature. Anti-genomic sequences are not present in the human, rat or mouse genome.

The Exon array probe sets are classified based on the level of annotational confidence[77]:

1. "Core" (17,800 transcript clusters): RefSeq and full length GenBank mRNAs;
2. "Extended" (129,000 transcript clusters): core probe sets and cDNA transcripts, syntenic rat and mouse mRNA, Ensemble, microRNA, Mitomap, Vegagene and VegaPseudogene annotations;
3. "Full" (262,000 transcript clusters): core and extended probe sets and ab-initio predictions from Geneid, Genscan, GENSCAN Suboptimal, Exoniphy, RNAgene, SGpGene and TWINSCAN.

The transcriptomic analysis was performed in a data set encompassing all core probe sets (228,871 sets for 17,881 transcript clusters) with the addition of the well annotated probe sets unique for the extended set (74,732 sets for 5,887 transcript clusters). The analysis was therefore not restricted to the core set, but was extended to all the well-annotated transcripts (303,603 probe sets) with the aim to increase the chance of discovering additional and novel transcript level changes associated with tumor development.

Pre-processing of raw data and analysis

The Partek Genomics Suite software was mainly used for data pre-processing, while BioConductor (an open source software packages) was employed for the statistical analysis. The tissue data set composed of 84 samples (42 lesions each matched with the corresponding normal mucosa) was subjected to background adjustments and normalization in order to remove biases of non-biological origin.

Much of the variation in intensity levels can arise from technical rather than biological causes. Non biological sources of variation can be introduced during sample preparation, array manufacture, hybridization and in the measurement process. Therefore, it is really important to normalize data, as much as possible, in order to remove the technical variation while still retaining the informative biological variation.

The background noise was detected by the "Detection above Background" (DABG) algorithm[78]. The DABG score can be calculated for each probe sets by matching perfect match probes to members of the background pool with the same GC content and measuring the relative distance between the two.

Only after background correction it is possible to perform the expression summary. The expression summary is the process by which the values for each individual probe in a probe set are summarized to generate a single value for that probe set. There are many different techniques used to perform the expression summary, even if they all perform some kind of weighted average.

The normalization was carried out using the "quantile normalization" algorithm for both the exon and the gene (transcript clusters) levels, and it was performed within each array and also between arrays. The robust multichip analysis (RMA)[79] algorithm, was used to estimate exon signal based on probe intensities. Since RMA does not use mismatch probes, after normalization (by default, quantile), data are fitted to a global model of expression and probe affinities. The model is based on the hypothesis that the intensity measured for a perfect match spot depends on three things: the amount of material available to bind to the spot, the stickiness of the probe and a measurement error. RMA works by estimating, for each probe sets, a value for the probe and the chip effects that would result in the pattern of perfect match values observed in the data. This process of "model fitting" is performed using an algorithm called median polish, a fast numeric technique used for estimating model parameters.

The library files used were: HuEx-1_0-st-v2.all.ps, HuEx-1_0-st-v2.r2.control.ps, HuEx-1_0-st-v2.r2.dt1.hg18.core.ps, HuEx-1_0-st-v2.r2.dt1.hg18.extended.mps, HuEx-1_0-st-v2.r2.dt1.hg18.full.mps, HuEx-1_0-st-

v2.r2.genomic.bgp, HuEx-1_0-st-v2.r2.pgf, HuEx-1_0-st-v2.r2.qcc, HuEx-1_0-st-v2.r2.antigenomic.bgp, and HuEx-1_0-st-v2.r2.unmapped-transcripts.ps.

Expression data were subjected to three multivariate analyses[80]: Principal Component Analysis (PCA), Between Group Analysis (BGA) based on Correspondence Analysis (CoA), which are dimension reduction methods, and hierarchical clustering, an agglomerative approach.

Reduction methods simplify the data set, ideally in ways that impart additional information about its structure and they are considered unsupervised (PCA) meaning that the reduction is derived solely from the data rather than reflecting any a priori knowledge or classification scheme. Each of these approaches project the data into a new multidimensional space based on linear combination of variables that retain a large amount of the original data variation.

Much like PCA, correspondence analysis displays a low-dimensional projection of the data into a plane. CoA attempts to separate dissimilar objects from each other (i.e., samples dispersion), while similar objects are clustered together resulting in small distances. Furthermore, CoA represents variables in a high dimensional space as vectors and it does so for two variables simultaneously, thus revealing associations between them.

Between Group Analysis is a multiple discriminant approach (supervised) that can be safely used with any combination of numbers of genes and samples. It is often the case, especially when dealing with microarray data, that the number of variables (genes) far exceeds the number of cases (arrays) and thus filtering and pre-selection of genes is required. A feature of BGA is that it can be used when the number of variables exceeds the number of cases. In our analysis, BGA was used in combination with CoA. When combined with CoA, BGA is especially powerful as it allows us to examine the correspondence between the grouped samples and those genes which most facilitate the discrimination of these groupings.

For the identification of pattern in gene expression data a hierarchical cluster analysis was performed. There are various hierarchical clustering algorithms that differ in the manner in which distances are calculated between the growing clusters and the remaining members of the data set. In our analysis, we performed

agglomerative technique, namely hierarchical clustering in which single expression profiles are joined to form groups, which are further joined until the process has been carried to completion, forming a single hierarchical tree.

A further analysis performed was the redundancy analysis (RDA). RDA expresses how much of the variance in one set of variables (independent variables) can be explained by the others (dependent variables). The proportion of the total variance in the dependent variables that can be explained by a linear combination of the independent variable is termed redundancy. This analysis was used to deduce which variable among those considered in the study had the capability to segregate the plotted objects (i.e. samples).

BGA based on $\log_2$ ratio expression values was used to reveal the association between independent variables (tissue type, histology type, size diameter of lesions and degree of dysplasia) and expression profile patterns.

Analysis of variance (ANOVA) was used to identify genes differentially expressed in nonpolypoid and polypoid lesions versus normal mucosa. Benjamini-Hochberg multiple testing correction was applied with a false discovery rate of 0.001(step down method).

Gene ontology analysis was performed by using a GeneGo MetaCore software. The list of differentially expressed genes (*p value* <0.05) outcoming from the pairwise comparisons (nonpolypoid lesions *vs* normal mucosa and polypoid lesions *vs* normal mucosa) were applied for the analysis. The main interest was to identify differentially affected pathways and processes between the two groups. Thus, Enrichment analysis consisted of matching gene IDs of possible targets (i.e.,differentially expressed genes in nonpolypoid and polypoid lesions vs normal mucosa) for the “common”, and “unique” sets with gene IDs in functional ontologies in MetaCore. The lower *p*-value means higher relevance of the entity (i.e.,pathway, process) to the data set, which shows in higher rating for the entity.

For each entity are specified the objects (i.e.,genes) that are common and unique to the two experiments (nonpolypoid vs normal mucosa and polypoid versus normal mucosa).

Human colon cancer cell lines and *TMIGD1* cloning and expression

The human colorectal cancer cell line SW480 was obtained by the American Type Culture Collection (ATCC). The Gateway Technology from Invitrogen was used for the cloning of *TMIGD1*. The *TMIGD1* full length cDNA was initially cloned into an "entry" vector and transformed into a T1-Phage Resistant *E.coli*. The *TMIGD1* from the entry vector clone was then recombined via an *attL-attR* reaction into a "destination" vector, the pcDNA 3.2/V5-DEST (Invitrogen). To facilitate both cloning and characterization of the cloned genes in their host, the destination vector contains a CcdB gene in between the recombination sites. The bactericidal toxin CcdB, encoded by the F plasmid ccd (control of cell division or death) locus, belongs to a recently discovered programmed cell death system and it targets the bacterial gyrase. When its action is not prevented by the CcdA antidote, CcdB causes cell death. In a gateway vector system, CcdB is inactivated by the insertion of a foreign DNA fragment. The introduction of an insert into cloning sites located within the 5'end of a fused CcdB results in the sole recovery of E.Coli bearing vectors with an insert. The recombination reaction was transformed into *E. coli* and the expression vector selected with Neomycin 0.4mg/ml (G-418, Geneticin Sulphate, 11811-031 Gibco, UK).

SW480 cells cultured in Leibovit's L-15 medium (GIBCO, Invitrogen), supplemented with 10% fetal bovine serum, 10,000 U/ml penicillin and 10,000 µg/ml streptomycin were stably transfected for 24 hours using the Lipofectamine 2000 (Invitrogen) reagent, in compliance with the manufacturer's protocol. Subclones stably expressing *TMIGD1* were derived from the bulk culture of SW480. All cells were maintained at 37°C in a 5% CO_2 humidified atmosphere.

Real time RT-PCR

One-step real-time retro transcription poly chain reaction (real time RT-PCR) was performed with the Roche LightCycler 480 System using the LightCycler 480 SYBR Green I Master kit (Roche, Basel, Switzerland) in compliance with the manufacturer's instructions.

The RNA extracted from precancerous lesions and normal mucosa was first converted to cDNA by using Transcriptor First Strand cDNA syntesis kit (Roche, Basel, Switzerland). 0.5 µM of each oligonucleotide primer (Microsynth, Balgach, Switzerland) and 100 ng of cDNA were mixed in 20 µl of standard reaction volume. Primer sequences and RT-PCR reaction conditions are available on request.

The *Ct* is the cycle that corresponds to the beginning of the log-phase amplification; one cycle difference in Ct corresponds to a ~2-fold change in RNA concentration. A relative quantification analysis was done by comparing the levels of two different target sequences in a single sample (*e.g.*, target gene of interest and *GAPDH*), with the final result being the ratio of these targets. For comparison purposes the second gene is a reference gene that is found in constant copy numbers under all test conditions. This reference gene provides a basis for normalizing sample-to-sample differences. A relative quantification analysis compares two ratios:

- the ratio of a target DNA sequence to a reference DNA sequence in an unknown sample;
- the ratio of the same two sequences in a standard sample called "calibrator". The calibrator is a positive sample with a stable ratio of target-to-reference and is used to normalize all samples within one run.

All the experiments were performed in duplicate, and the specificity of each amplification product was verified by agarose gel electrophoresis.

Mutational analysis of *KRAS* and *BRAF* genes

Analysis of *KRAS* and *BRAF* point mutations in exons 2 and 15, respectively. Exon 2 includes codons 12 and 13 of *KRAS* and exon 15 codon 600 of *BRAF*. *KRAS* exon 2 was PCR-amplified from tumor DNA as a 173 bp fragment using the primers 5'-AAGGCCTGCTGAAAATGACTG-3' (forward) and 5'-CAAAGAATGGTCCTGCACCAG-3' (reverse), while the exon 15 of *BRAF* gene was amplified as 103 bp fragment using the primers 5'-GAAGACCTCACAGTAAAAATAG-3'(sense) and 5'-TCCACAAAATGGATCCAGAC-3' (antisense).

PCR products were purified by ExoSAP-IT® kit (USB Corporation, Clevelend, Ohio) at 37°C for 45 min and subsequently at 80°C for 15 min.

Mutations were then assessed by ABI PRISM SNaPshot Multiplex Kit (Applied Biosystems, Foster City, CA, USA) at the relevant nucleotides, (i.e. c.34, c.35 c.37, c.38 and c.1799 of *KRAS* and *BRAF*, respectively) using single base extension SNaPshot primers listed in the Table 1. The multiplex SNaPshot reaction was performed in a final volume of 10μl , containing 1 μl of each PCR product, 2 μl of the SNaPshot Multiplex Ready Reaction Mix, 1 μl of 5x sequencing buffer of Big Dye V3.1 Terminator Kit and SNaPshot primers at a concentration of 0.01-0.06 μM.

Cycling conditions were carried out according to the recommendation of the kit manufacturer and SNaPshot products were subsequently purified by treatment with 2 U of shrimp alkaline phosphatase (USB Corporation, Cleveland, Ohio) at 37°C for 45 min. After heat inactivation of the enzyme at the 80°C for 15 min, the fluorescently labeled products were separated using a 7 min run on ABI Prism 3130 DNA sequencer and data were analyzed using GeneMapper Analysis Software version (Applied Biosystems).

Table 1.

KRAS and *BRAF*- single base extension SNaPshot primers

Gene	Codon	Nucleotide	Primer orientation	Primer sequence (5'→3')	Primer length
KRAS	12	c.34	forward	AACTTGTGGTAGTTGGAGCT	20
KRAS	12	c.34	reverse	ct$(gact)_2$CACTCTTGCCTACGCCAC	28
KRAS	12	c.35	forward	$(gact)_4$ACTTGTGGTAGTTGGAGCTG	36
KRAS	12	c.35	reverse	$(gact)_6$GCACTCTTGCCTACGCCA	42
KRAS	13	c.37	forward	$(gact)_7$TTGTGGTAGTTGGAGCTGGT	48
KRAS	13	c.37	reverse	act$(gact)_8$AAGGCACTCTTGCCTACGC	54
KRAS	13	c.38	forward	t$(gact)_{10}$GTGGTAGTTGGAGCTGGTG	60
KRAS	13	c.38	reverse	act $(gact)_{11}$CAAGGCACTCTTGCCTACG	66
BRAF	600	c.1799	forward	act$(gact)_{12}$GTGATTTTGGTCTAGCTACAG	72
BRAF	600	c.1799	reverse	ct$(gact)_{14}$ACCCACTCCATCGAGATTTC	78

Immunohistochemistry

Normal, precancerous and cancerous colorectal samples were obtained from the Department of Pathology of the Istituto Ospedaliero Fondazione Poliambulanza, Brescia. Ten μm serial sections from paraffin blocks were mounted on silanised slides, then deparaffinised and rehydrated.

The antigen retrieval was carried out by heating the section in a pressure cooker at 120°C for 2 min in 10 mM citrate-buffered solution (pH 6.0). DAKO peroxidase blocking reagent and goat serum were sequentially used to suppress non-specific staining due respectively to endogenous peroxidase activity and nonspecific binding of antibodies. Incubation with primary antibodies was performed as follow: anti-hMSH2: 24 hours at 4°C with Ab NA27 (Calbiochem); anti-hMSH6: 24 hours at 4°C (pH 9.0) with BD610919 (BD PharMingen); anti-hMLH1: 24 hour at 4°C with BD551091 (BD PharMingen); anti-hPMS2: 24 hours at 4°C with BD556415 (BD PharMingen); anti-TMIGD1: 24 hour at 4°C with HPA021946 (Sigma); anti-ß-catenin: 24 hour at 4°C with ab6301 (Abcam).

After washing, anti-mouse (anti-rabbit for TMIGD1) secondary antibodies conjugated to peroxidase labeled polymer (DAKO EnVision+ kit) were applied for 30 min at RT, and the peroxidase activity was developed by incubation with 3, 3' diaminobenzidine (DAB) chromogen solution (DAKO). The sections were then counterstained slightly with haematoxylin.

Tissue microarrays were kindly provided by Dr. Holger Moch of the pathology Department of the University of Zurich.

Immunocytochemistry

Glass cover-slips seeded with parental SW480 cells and stably transfected SW480 cells expressing *TMIGD1* were washed twice with ice cold PBS and fixed in 50% ethanol / 50% methanol for 15 min at RT. Fixed cells were permeabilized with 0.25% Triton X-100 for 10 min, blocked with goat serum (X0907, DAKO) for 30 min and then incubated 24 hours with anti-TMIGD1 (1:50; HPA021946, Sigma). After being washed three times with PBS, the cells were incubated with the secondary antibody (labelled polymer-HRP anti-rabbit, DakoCytomation EnVision+ System-HRP; K4010) for 30 min and then washed again three times with PBS. The cells were finally incubated for 10 min with DAB (3,3-diaminobenzidine tetrahydrochloride), quickly washed with PBS and then mounted in mounting medium (EUKITT, O.Kindler, GmbH, Germany). The cells were analyzed by light microscopy.

Immunofluorescence

Cells were seeded on glass cover-slips and grown to 70% of confluence, then fixed in 3% Formaldehyde from PFA dissolved in PBS pH 7.4, for 10 min at RT. After being washed, the cells were incubated in 0.1% SDS in PBS pH 7.4 for 5 min (antigen retrieval treatment) and then subjected to blocking in 2% BSA/PBS/0.02% Triton-

X-100 for 30 min at RT. Incubation with primary anti-TMIGD1 antibody was performed at RT for 1 hour. After being washed three times with PBS, cells were incubated with a secondary antibody (FITC conjugated anti-rabbit 1:500, anti-actin 1:500 and DAPI 1:1000) for 1 hour at RT. Lastly, cells were washed with PBS and mount with VectaSchield mounting medium (H-1000, VectaSchield Laboratories, CA, USA). Images were captured using a fluorescence microscope (Olympus BioSystems GmbH, Germany).

Preparation of total protein extracts

Total protein extraction from cell monolayer (triple-detergent lysis buffer)

About 8 x10^6 cells were washed twice with PBS. After adding 500 µl of lysis buffer (50 mM TrisCl pH 8.0, 150 mM NaCl , 0.02% Sodium azide, 0.1% SDS, 1% Triton X-100, 1% Sodium deoxycholate, 2 mM EDTA, 1mM PMSF, 1X *Complete* EDTA-free, 30 mM DTT), the cells were collected by scraping, homogeneized by mixing with a 18 G needle and a 2ml syringe and the suspension gently rocked on an orbital shaker at 4°C for 20-40 min. The completion of the cell lysis was verified under the microscope with trypan blue staining. The lysate was centrifuged in an Eppendorf microfuge for 15 min at 14,000 *xg* and the supernatant was collected, snap frozen in small aliquots in liquid nitrogen, and stored at - 80°C.

Membrane protein extraction from cell monolayer

About 16 x 10^6 cells were washed three times with PBS. After adding 1 ml of lysis buffer (300 mM Mannitol, 20 mM Hepes-Tris pH 7.4, 2 mM EDTA, H2O, 1mM PMSF, 1X *Complete* EDTA-free), the cells were collected by scraping. The cells suspension was homogeneized by mixing with a 25G needle and a 2-ml syringe. Cell lysis was verified under the microscope with trypan blue staining. The lysate was subjected to a first step of centrifugation (100 *xg* , 4°C, for 10 min) in order to eliminate cell debris. The supernatant was then transferred into a plastic

ultracentrifuge tube (12ml PA, PKG 50, 03699, Thermo Scientific,USA) and an ultracentrifugation (41,000 rpm) was performed at 4°C for 45 min. The supernatant was discarded, the membrane pellet homogeneized and then resuspended in a proper amount of resuspension buffer (300 mM Mannitol, 20 mM Hepes-Tris pH 7.4, 2 mM EDTA, H2O, , 0.1% Triton X-100, 0.5% Na-deoxycholate, 1mM PMSF, 1X *Complete* EDTA-free). The membrane suspension was collected and snap frozen in liquid nitrogen and stored at -80°C.

*Crypts isolation for protein extraction (*adapted from Fujimoto K. et al., *Gastroenterology* 2002;123:1941) [81]

Colonic crypts were isolated from 2 pieces of colonic tissue, surgically obtained from patients undergoing anesthesia for colonic resection. The specimens were taken from a morphologically normal zone, and their size was approximately of 1 x 5 cm. The specimens were collected immediately after resection and washed in PBS. The tissue was then transferred to a tube containing 3mM EDTA and 0.5mM DTT in sterile PBS and incubated at RT for 75 min. After being washed with PBS, colonic crypts were vigorously shaken in a PBS solution for 30 sec in order to lift the mucosa from the submucosa. The shaking step was repeated three times and each time the PBS containing crypts was collected in a microfuge. The gross morphology of the suspension of isolated crypts was assessed by light microscopy. Crypt architecture was well preserved in most of the crypts. The crypts containing PBS was then centrifuged (400 rpm) for 5 min, PBS was removed and crypts were subjected to a lysis with the triple-detergent buffer described above.
Proteins were extracted in compliance with the above mentioned protocol (*Protein extraction from cell monolayer; triple-detergent lysis buffer*).
Protein concentration in any type of extract was calculated with the Bradford method[82].

Concentration of proteins present in cell culture medium

Cells (two T175 flasks) were first washed with PBS to remove the presence of the culture medium and then incubated for 8 hours with fetal bovin serum free medium. After 8 hours, the medium was collected and spin down to remove any particles in regular 60 ml Falcon tubes. Protease inhibitors were added (1mM PMSF and 1X *Complete* EDTA-free).

Filters of Amicon Ultra-15 centrifugal filter units columns (Millipore, MA,USA) were first washed twice with PBS and then the Amicon colums were centrifuged for 5 min at 3000 *xg* in a swinging bucket rotor. Clarified cell culture medium was added on the top of the Amicon filters and centrifuged for 5 min, at 3000 *xg* at 4°C. The centrifugation step was repeated till obtained a decent amount of concentrated sample (usually 200-800 ul, final concentration). The concentrated suspension was collected and snaps frozen in liquid nitrogen and stored at -80°C.

Western Blot

Seventy µg of total proteins from each sample were loaded on a 12% SDS PAGE and transferred to Hybond-P PVDF membranes (Amersham Pharmacia Biotech, Little Chalfont, UK) according to standard protocols.
The blots were first blocked in TBS-T (20 mM Tris-HCl pH 7.4, 150 mM
NaCl, 0.1 % Tween-20) containing 5% non-fat dry milk for 1 hour at 37 °C , and then incubated with the following primary antibodies for 2 hours at RT: anti TMIGD1(Rabbit polyclonal,1:300; HPA021946, Sigma), anti-MSH6 (Mouse monoclonal,1:2000; 610918, BD Transduct Laboratories)

After being washed three times with TBS-T, the blots were incubated with a horseradish peroxidase (HRP)-coupled secondary antibody for 1 hour at RT. Following another three wash steps, immunoreactive proteins were detected using enhanced chemiluminescence (ECL, Amersham Pharmacia Biotech, Little Chalfont, UK).

5. RESULTS

Aim of the study

The main goal of this study was to identify biomarkers of colorectal tumorigenesis through the molecular analysis of different types of early neoplastic lesions of the human large intestine. Preneoplastic lesions of the colon are heterogeneous, they display distinct clinical, histological and molecular phenotypes. Polypoid lesions with classical adenomatous histology have been the subject of innumerable studies, whereas nonpolypoid lesions remain still poorly investigated. The study was thus focused on the identification of biological differences between the two groups. To this aim, we performed a powerful analysis of the gene expression profile of nonpolypoid lesions and compared it with that of polypoid ones, the ultimate goal being the identification of genes and pathways whose dysregulation might play a crucial role in different pathways of colorectal tumorigenesis.

Results

A portion of nonpolypoid lesions, which are macroscopically distinguishable from polypoid lesions (see Paris classification in *Materials and Methods*), are believed to develop through a nonadenomatous pathway of carcinogenesis, namely the serrated pathway (see *Introduction*). Furthermore, sessile serrated adenomas, a histologic subgroup of the serrated family of lesions, likely represent the precursors of MMR(-) sporadic colorectal cancers, especially if located in the proximal colon (caecum, ascending, and transversum). Twenty five nonpolypoid lesions (type *IIa*, *IIb*, *IIc* or mixed), each with matched normal mucosa, were thus prospectively collected from the proximal colon of 21 patients. Seventeen polypoid lesions (type *Ip*) from 17 patients, each with matched normal mucosa, were also collected prospectively, but from any tracts of the colorectum (**Table 2**). As mentioned in *Materials and Methods*, this latter group represents the most frequent precancerous lesions of the colorectum which are generally more frequently detected in the distal colon.

Table 2.

Characteristics of the 37 patients with nonpolypoid or polypoid precancerous lesions included in the study

Patient	Age	Sex	Colon segment involved	Maximum lesion diameter (mm)	Paris classification #	Pit pattern classification º	Microscopic appearance	Highest degree of dysplasia in the lesion ▪	No. lesions at study colonoscopy ∞
AM(1) *	75	F	T	70	IIa-IIb	3S-3L	VA	HGD	7
AM(2) *			T	20	IIa	3S-3L	VA	HGD	
BG(1) *	72	F	C	30	IIa	4	TA	LGD	9
BG(2) *			T	20	IIa	3S-3L	TA	LGD	
GG	75	F	T	40	IIa-IIc	3S-3L	TA	HGD	1
CE	73	F	A	40	IIa-IIc	2-3L	SA (mixed) ≠	HGD	1
BE	44	M	HF	35	IIa	3S-3L	TA	LGD	2
BR	79	F	A	20	IIa	4	TA	LGD	1
GM	67	F	A	20	IIa	3L	TA	LGD	1
MGF	48	M	HF	15	IIa	3L	TA	LGD	1
ML	69	F	A	40	IIa	3L	TVA	LGD	1
SG	83	M	A	25	IIa	3L	TA	LGD	4
ZP	66	M	C	25	IIa	3L	TA	HGD	2
AR	79	M	A	35	IIa-IIc	5N	TVA	HGD	2
OO(1) *	54	F	C	45	IIa	3L	TVA	LGD	16
OO(2) *			A	12	IIa	3L	TA	LGD	
BGP	74	F	C	50	IIa	3L	TVA	LGD	1
SG	62	F	A	15	IIa	3S-3L	SA (mixed)	LGD	1
RM	52	F	T	15	IIa	2	SSA ≠	no dysplasia	1
MC(1) *	54	F	C	50	IIa	2-3L	TA	HGD	2
MC(2) *			A	20	IIa	2-3L	TA	LGD	
BM	72	M	A	25	IIa	3S-3L	TA	LGD	1
GV(2) *	79	M	A	25	IIa	3L	VA	LGD	3
BC	47	M	A	20-25	IIa-IIc	3S-3L	MVSP ≠	no dysplasia	3
DDR	66	M	A	12	II a	3L	MVSP	no dysplasia	1
RA	64	F	A	15	Ip	na	TA	LGD	2
SD	56	M	A	15	Ip	na	TA	LGD	2
NF	79	M	A	20	Ip	na	TVA	LGD	3
PF	27	M	A	15	Ip	na	TVA	HGD	3
PG	40	F	S	30	Ip	na	TVA	LGD	51[1]
MA	83	M	S	12	Ip	na	TVA	LGD	3
MM	50	M	S	30	Ip	na	TVA	HGD	3
SA	74	F	S	20	Ip	na	TVA	LGD	1
GN	69	M	R	40	Ip	na	TA	LGD	3
BA	69	M	S	30	Ip	na	TA	LGD	7
PF	56	M	S	30	Ip	na	TA	LGD	3
MR	58	F	D	20	Ip	na	TA	LGD	3
SMA	52	F	S	30	Ip	na	TA	LGD	3
PL	69	F	S	15	Ip	na	TVA	LGD	3
BG	58	F	A	15	Ip	na	TVA	LGD	1
GV(1) *	79	M	T	30	Ip	na	VA	LGD	3
WE	73	M	A	30	Ip	na	TVA	HGD	1

Abbreviations: M, male; F, female; C, caecum; A, ascending colon; HF, hepatic flexure; T, transversum; D, descending colon; S, sigma; R, rectum; na, Pit pattern not reported by the endoscopist; TA, tubular adenoma; TVA, tubulovillous adenoma; VA, villous adenoma; MVSP, microvesicular serrated polyp; SA, serrated adenoma; SSA, sessile serrated adenoma; LGD, low-grade dysplasia; HGD, high-grade dysplasia.

Macroscopic appearance of neoplastic lesions was classified according to Paris Endoscopic Classification. The Paris Endoscopic Classification of Superficial Neoplastic Lesions. Gastrointest Endosc 2003;58(suppl.):S3-S27

º Morphological analysis of colonic crypt patterns according to Kudo's classification. Kudo S, Rubio CA, Teixeira CR, et al. Pit pattern in colorectal neoplasia:endoscopic magnifying view. Endoscopy 2001;33;367-7

▪ Low-grade versus high-grade dysplasia as defined by the WHO classification of tumors of the digestive system, editorial and consensus conference in Lyon, France, November 6-9, 1999.IARC

≠ Serrated adenomas carrying *BRAF* mutation, glutamic acid for valin substitution at codon 600 (V600E)

*****Two lesions from these patients were analyzed

¹ Patient suspected of attenuated familial polyposis. The mutational analysis of *APC* and *MYH* genes is currently not available

The mean age of onset of the studied lesions was 66.1 ± 11.8 years in the nonpolypoid group of patients (57% females and 43% males). In contrast, patients carrying polypoid lesions (average age of onset: 62.1 ± 14.7) were more frequently males (58.8%). The lower age of onset in this latter group is in part attributable to the presence in this group of an exceptionally young individual (27 years old) who was reported having neither a positive family history for colorectal cancer nor a germ line mutation in genes which are associated with predisposition to this cancer.

Eighty percent (20/25) of the nonpolypoid lesions presented adenomatous histology (tubular, villous, or tubulovillous subtypes), while the remaining 20% showed serrated histology (2 microvesicular serrated polyps, 2 serrated adenomas and 1 sessile serrated adenoma). All 17 polypoid lesions were classical adenomas, as expected.

The degree of dysplasia (as defined by the WHO classification of tumors of the digestive system), was *low* in most of the lesions belonging to both groups (60% of nonpolypoid lesions and 82% of polypoid) and *high* in 28% of nonpolypoid and 17.6% of polypoid lesions. Only few nonpolypoid lesions (2 microvesicular serrated polyps and 1 sessile serrated adenoma) did not show dysplasia. The size (diameter) of the lesions had a range spanning from 15 to 70 mm. All lesions were divided in

four classes based on their diameter size (10-20 mm; 21-30 mm; 31-40 mm; >40 mm).

The total number of synchronous lesions was ≤4 in most of the patients (33/37), and 4 to 16 in three patients. Only one patient carried 51 synchronous adenomas and was thus suspected of *attenuated familial polyposis* (mutational analysis of *APC* and *MYH* in the germ line DNA is in progress).

Mutational analysis of *KRAS* (codon 12 and 13) and *BRAF* (exon 15) genes in the group of nonpolypoid lesions detected 12 lesions (48%) with mutations in the former gene (2 Gly12Cys; 6 Gly12Asp, 2 Gly12Val and 2 Gly12Ala) and an additional 3 lesions (12%) with the $BRAF^{V600E}$ mutation. The 3 cases mutated in *BRAF* were serrated (**Supplementary Table 1**).

Immunohistochemistry analysis was performed to detect the expression of the mismatch repair protein MLH1. This protein resulted expressed in all the nonpolypoid lesions (**Supplementary Table 1**). As expected, all the polypoid lesions also expressed MLH1 (data not shown).

Multivariate analysis of exon array data

Microarray analysis of 303,603 probe sets (core and well-annotated extended probe sets) revealed expression levels above background for 23,768 transcript clusters in at least one of the two main groups of tissues (42 normal mucosa samples and corresponding 42 precancerous lesions).

For the analysis of the microarray data three multivariate approaches, Principal Component Analysis (PCA), Between Group Analysis (BGA) based on Correspondence Analysis (CoA), and Hierarchical Clustering Analysis (HCA) were used to detect clusters of samples with similar expression profile and differentially expressed genes. While HCA is a commonly known tool in the field of microarray data analysis, it is worth to mention here that PCA and CoA are dimension-reduction or ordination methods which project the original data into a new low dimensional space. The dimensions of the low dimensional space are derived composite

variables or components as well as the orthogonal axes of this new space. The objects (i.e. *tissue samples*) are ordered along these derived axes. The distance between objects in the low dimensional space represents their dissimilarity in respect of the original variables, i.e. the dissimilarity in respect of their gene expression profiles. PCA, BGA as well as HCA showed not only different gene expression profiles for precancerous lesions and the matched normal mucosa samples, but also for the two lesions subtypes *nonpolypoid* and *polypoid*.

As depicted in the PCA score plot (**Figure 9**), the first three principal components (PC1, PC2 and PC3) represent 50.3% of the total variance of the original data set. PC1 (36% of the total variance, i.e. the first principal component accounts for as much as possible of the variability in the original data) reflected the inter-individual (i.e. patient-to-patient) variability. (The patient-to-patient variability issue will be further discussed in the next paragraph.) The second axis (PC2 representing the 10.3% of the total variance) is orthogonal to the first and captures the maximum of the remaining variance. PC2 was correlated with the factors responsible of the segregation of the objects -- and hence of the expression changes -- among the 3 tissue types, whereas PC3 did not have any obvious biological interpretation. Based on the ordination of the samples along the first 3 PCA axes it was concluded that patient-to-patient variability explained the largest proportion (36%) and tissue type the second largest proportion (10.3%) of the total gene expression variance. More than 50% of the total variance is due to other factors and remains unexplained after PCA. However, the absence of singularized samples (far away from any clusters) as well as the high proportion of variance explained by the PCA axes 1 and 2 (as compared to a randomized PCA model which explains no more than 17% and 8% of the total variance by the first two axes) confirmed both the quality (homogeneity) of the original data as well as the reliability of the derived PCA model.

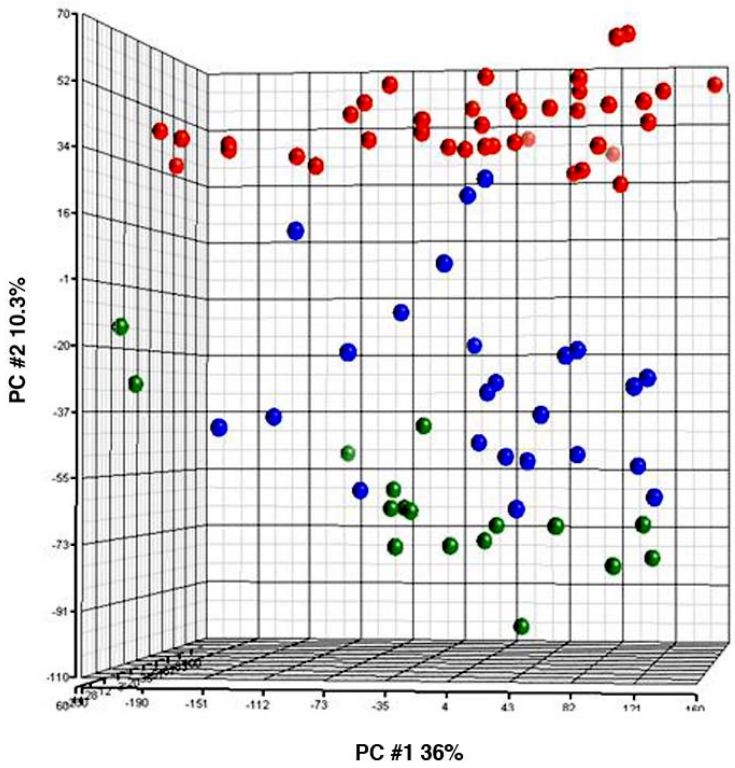

Figure 9. **Principal Component Analysis (PCA)of log_2 expression intensity values**

PCA score plot of the RMA (i.e Robust Multi Array) preprocessed intensity values of all 84 specimens (*red dots*, normal mucosa; *blue dots*, nonpolypoid lesions; *green dots*, polypoid lesions). The first 3 principal components (PCs) explain 50.3% of the total variance. PC1 captures 36% of the total variance and reflects the inter-individual variability. PC2 explains 10.3 % of the total variance and is associated with the variable "tissue type" (normal mucosa *vs* precancerous lesions). PC3 accounts for 4.07% of the total variance and has not been associate with any specific variables yet.

HCA was applied to describe in detail the relations (similarities and dissimilarities) between the samples scored with the eigenvector analysis. To reduce the confounding effect of patient-to-patient variability, the clustering of the samples was based on the expression level of only 6,862 transcript clusters showing significant differential expression between normal mucosa and lesions [*p* value <0.01, FDR of 0.01 (step-up method[83, 84])]. Two main clusters, that of precancerous lesions and that of normal mucosa samples (with the exception of 2 neoplastic samples, a microvesicular serrated polyp and a sessile serrated adenoma, which clustered with the samples of normal mucosa) could be identified (**Figure 10**). The interpretation of the dendrogram, in which the distance along the tree from one

element to the next represents their relative degree of similarity, indicates that the group of precancerous lesions presents higher variability than the group of the normal tissue. Two homogeneous clusters and one mixed could be identified within the group of precancerous lesions. The two homogeneous clusters, including 34 precancerous lesions, were represented by 21 nonpolypoid lesions (*blue* branches) and 15 polypoid lesions (*green* branches). A mixed cluster of 4 nonpolypoid and 2 polypoid lesions could be observed at the left end of the lesions dendrogram.

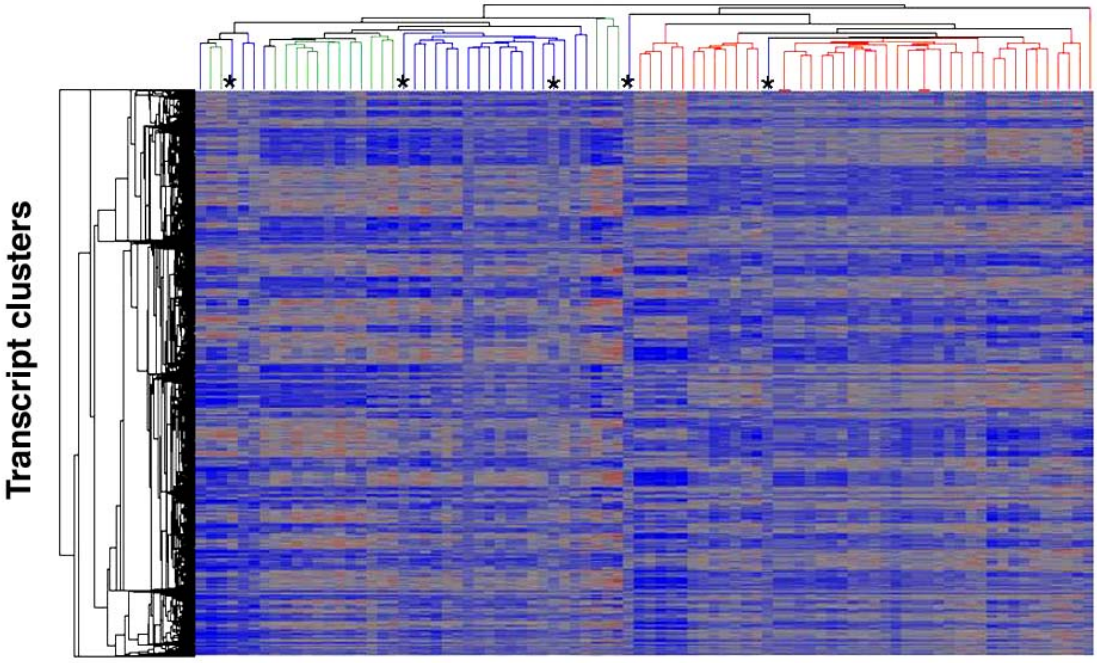

Figure 10. **Hierarchical Clustering Analysis of log_2 expression intensity values**

The 84 tissue samples represented on the horizontal axis include 42 normal mucosa (*red branches*) and 42 precancerous lesions, grouped in nonpolypoid lesions (*blue branches*) and polypoid lesions (*green branches*). On the vertical axis, 6,862 transcript clusters with differential expression in the tissue types are displayed (*p* value <0.01; FDR 0.01). Each transcript cluster is color coded to indicate the level of expression of the gene relative to its median expression level across the entire tissue sample set (*blue*, low; *red*, high).
In the precancerous lesions branch, sub branches representing individual samples and small groups merge at higher levels than those of the normal mucosa branch, reflecting lower level similarity (i.e. higher variability among the precancerous lesions).
Lesions characterized by serrated histology are marked by an asterisk.

In order to find the association between the most important discriminating variable, *tissue type*, with other dependent variables (i.e. genes), a between group analysis (CoA based) was accomplished. BGA, in fact, attempts not only to separate dissimilar objects from each other based on a multivariate profile, but it is also an exploratory method for the study of associations between the multivariate set of profile variables and a co-variables assumed to be independent or explanatory variable. In **Figure 11 A,** a map of the samples score showed the efficiency of CoA in distinguishing between normal mucosa samples and precancerous lesions. There was however, a very strong influence of the patient-to-patient variability reflected in the samples dispersion (i.e. distances among samples scores) within each of the three ellipses. In **Figure 11 B,** on axis 1 the genes were plotted that most contributed to the discrimination between these groupings (i.e. normal mucosa, nonpolypoid and polypoid lesions). On axis 2 there are plotted genes that have different expression in nonpolypoid and polypoid lesions, respectively.

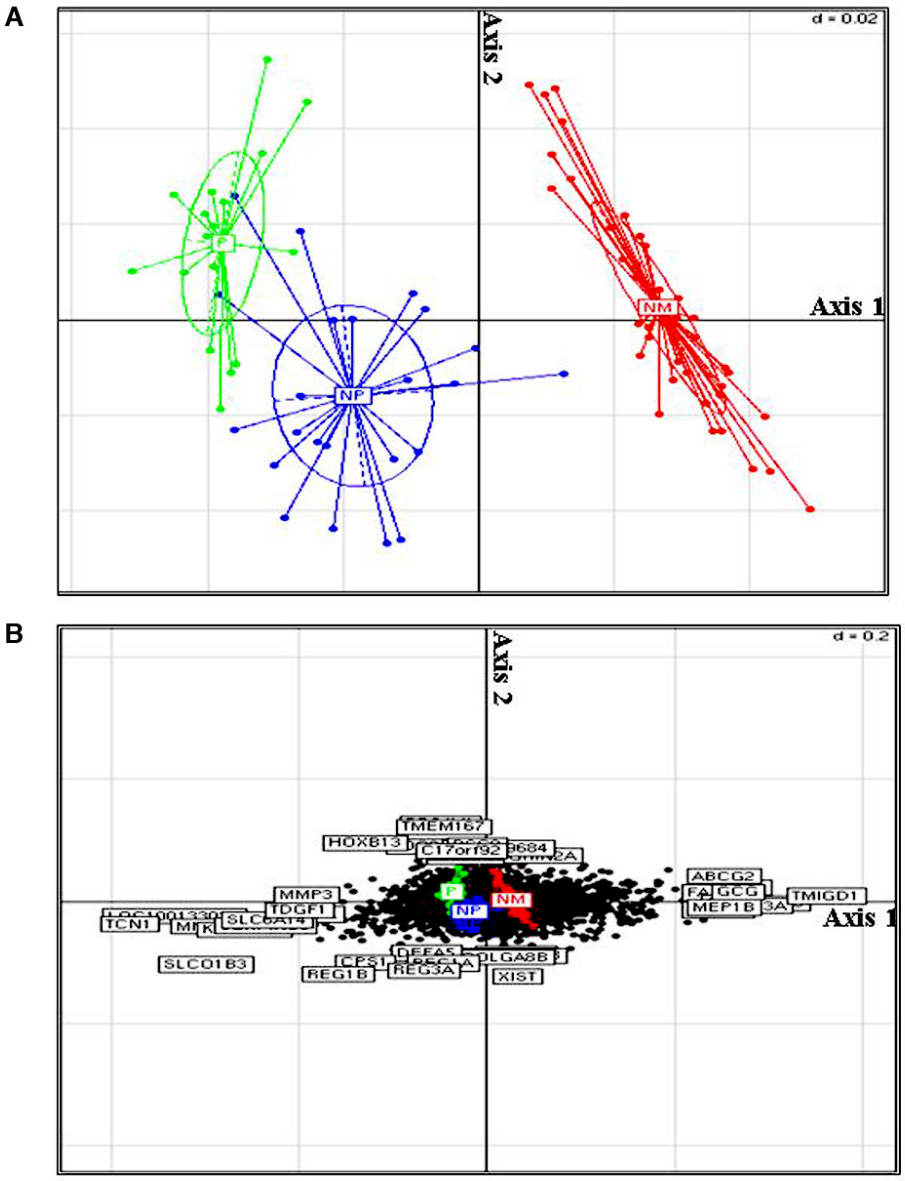

Figure 11. Between Group Analysis (BGA) based on Correspondence Analysis (CoA) of log_2 expression intensity values

CoA based, Between Group Analysis, of RMA preprocessed intensity values of all 84 specimens (*red dots*, normal mucosa; *blue dots*, nonpolypoid lesions; *green dots*; polypoid lesions).
Panel **A**: the map of the sample scores on the first two axes shows that CoA efficiently discriminated between normal mucosa samples and precancerous lesions, nonpolypoid and polypoid, respectively. The dispersion of objects (i.e. samples) along axis 2 is indicative of high inter-individual (patient-to-patient) variability. Axis 1 is a discriminating component, clearly associated with the tissue type variable (i.e., normal mucosa *vs* precancerous lesions).
Panel **B**: plot of the genes that most contributed to the discrimination between these groups (i.e. normal mucosa, nonpolypoid and polypoid lesions). At the ends of axis 1, the genes contributing to the segregation between normal tissue and all the precancerous lesions (nonpolypoid and polypoid) are plotted. On axis 2, the genes that have different expression in nonpolypoid and polypoid lesions respectively, are plotted.

Despite the efficient discrimination of the objects in both PCA and BGA analyses, samples scores, as already mentioned, were still much influenced by the major variance represented by the inter-individual variability. Patient-to-patient variability is commonly observed in such studies due to the high level of genetic and epigenetic variation among individuals in the general population. Single nucleotide polymorphisms, copy-number variants, alternative splicing, post-transcriptional and post-translational modifications, and epigenetic modifications account for the phenotypic plasticity that allows individuals to proceed along the evolutionary path. Phenotypic variation is also modulated by environmental influences. Thus, in order to identify the variables contributing to the gene expression changes we have detected, the noise of the patient-to-patient variability was reduced by using the $\log_2$ ratio expression values (that is, the expression level of any given transcript in each lesion relatively to its basal level in the corresponding normal mucosa).

The first approach performed to identify and classify the variables able to explain a proportion of the total variance in the data set, was a redundancy analysis (RDA), a constrained form of multivariate analysis, based on the PCA of a set of independent (explanatory) variables and a set of dependent variables (explained). Here, the clinical descriptors were seen as independent variables and the gene expression as a dependent variable set that can be predicted from the clinical variables. The result of RDA is a PCA model which is constrained to optimize the "prediction" of the gene expressions from the clinical variables. The relations between samples and the two variable sets are finally visualized in a series of plots, in particular, here, by a correlation circle for the clinical variables and a score plot for the samples. In a correlation circle (**Figure 12**), the position of the uniformly scaled variables on the surface of a multidimensional sphere is shown as a projection on a plane defined by a pair of relevant ordination axes (RDA axes 1 and 2 or 1 and 3). The circle of correlation shows the proximity of the variables inside a unit circle and is therefore useful to evaluate the affinities and the antagonisms between the variables. In Figure 12, the two correlation circles showed how clinical and pathological variables contributed to explain the total variance in the data set.

The vectors approaching the circumference (vector length ≈1) are those well represented in the new coordinates system. In the correlation circle A, the RDA axes plotted are axes 1 and 2. The *tissue type* variable has the longest vectors (~ 1) and thus this is the variable explaining the major proportion of the total variance in the data set, followed by the others as *histology type* (adenomatous *vs* serrated histology), *degree of dysplasia* (no dysplasia *vs* low and high degree of dysplasia), and *diameter* of the lesions. In the circle B of Figure 4, axes 1 and 3 were plotted. Here, the scenario is slightly different due to the added variance in agreement with the increase in axes number. The reversed order of the variables relevance in the plane of RDA axes 1 and 3 (*diameter*, *histology type*, *degree of dysplasia* and *tissue type)* corroborated the ranking of the variables inferred from the correlation circle in the plane of the RDA axes 1, 2, and highlighted the relevance of the variable *diameter* in the first three dimensions of the reduced ordination space.

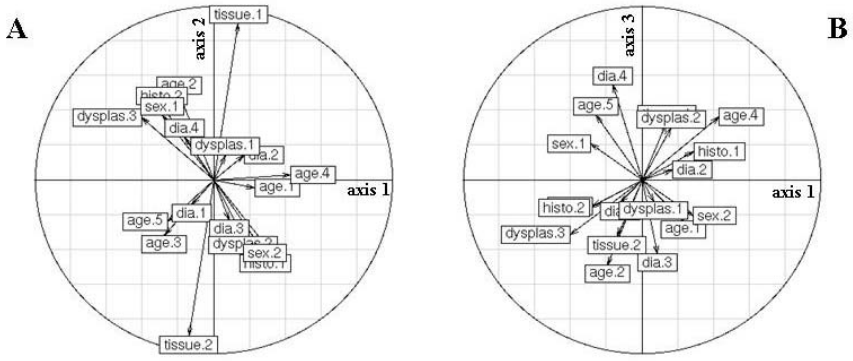

Figure 12. Correlation circles for clinical descriptors (variables) based on Redundancy Analysis (RDA) of log_2 ratio expression intensity values

A. Correlation circle in the dimensions of the RDA axes 1 and 2. Each clinical/pathological variable is represented by a vector. Vectors whose length approaches the radius of the circle (i.e. length approximately equal to 1) are the best represented variables in the new coordinate system. Vectors pointing in the same or opposite directions represent positively or negatively correlated variables, respectively. The order of the variables' relevance, inferred from the length of the vectors, was identified as: *tissue type*, *histologic type*, *degree of dysplasia* and *diameter* of lesions.
B. Correlation circle in the dimensions of the RDA axes 1 and 3. The reversed order of the variables' relevance (*diameter*, *histologic type*, *degree of dysplasia* and *tissue type*) in the plane of RDA axes 1 and 3 corroborates the ranking of the variables inferred from the correlation circle in the plane of the RDA axes 1 and 2, as well as the relevance of the variable *diameter* in the first three dimensions of the reduced ordination space.

Taking in consideration both correlation circles, the classification of the variables, in order of their relevance, was elaborated as follow: *tissue type*, *histology type*, *diameter* of the lesions, and *degree of dysplasia*. Score plots with distribution ellipses for each of these four variables were drawn (**Figure 13**) in order to visualize their capacity to segregate the samples (log_2 ratio expression values were used in all the score plots). All 42 precancerous samples were plotted in three-dimensional view on the axes 1, 2 and 3 by two perpendicular planes. The *tissue type* variable, as shown before with PCA and BGA analyses, was confirmed to be the variable that more efficiently segregated the samples along axis 1. In contrast, the ellipses of the other three variables displayed a certain degree of overlapping.

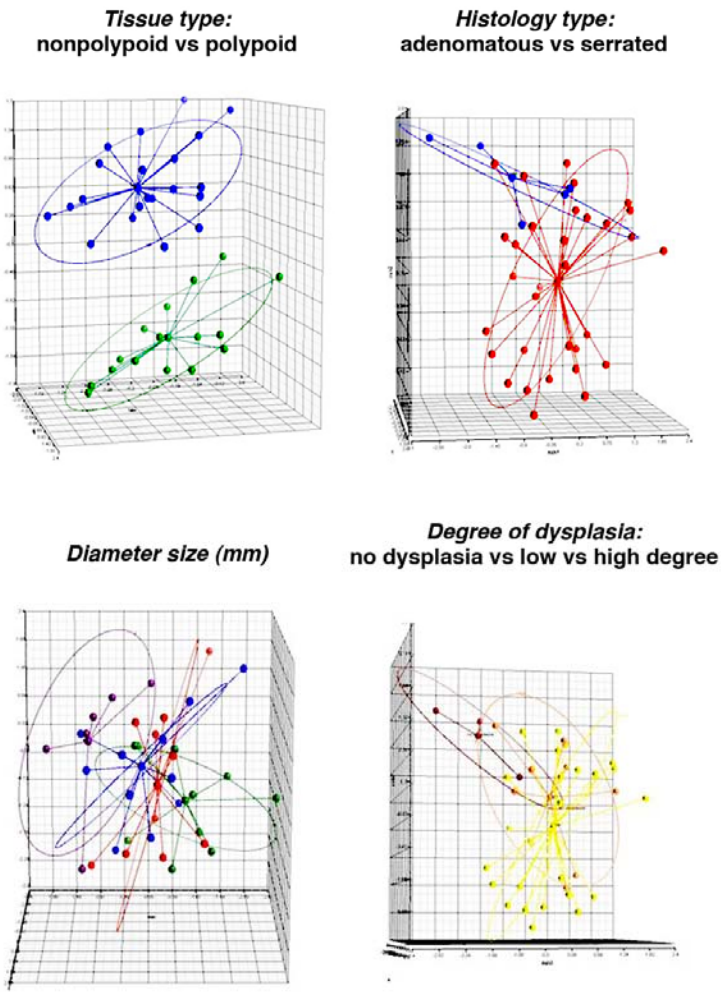

Figure 13. Sample score plots based on the Redundancy Analysis (RDA) of log_2 ratio expression intensity values

Score plots with samples grouped by the variables considered as relevant in the correlation circles shown in Figure 12. For each variable, *tissue type*, *histologic type*, *diameter size* and *degree of dysplasia*, the same scaled log_2 ratio expression values of all (nonpolypoid and polypoid) lesions are plotted. Score plots are visualized in the planes of the BGA axes 1 and 2 as well as 1 and 3, i.e. representing the 3D view on the axes 1, 2 and 3 by two perpendicular planes. *Tissue type* is the only variable able to fully segregate the samples in clear clusters.

The variables identified as relevant in the previous analyses, *tissue type*, *histology type*, *diameter* and *degree of dysplasia,* were the grouping factors evaluated in the following BGA analyses. For each variable (**Figures 14** and **15**), the map of the sample scores and the top genes that most discriminate the groups assigned to the variable tested were depicted. The lists of the discriminating genes for each variable are provided in the **Supplementary table 2** (Appendix).

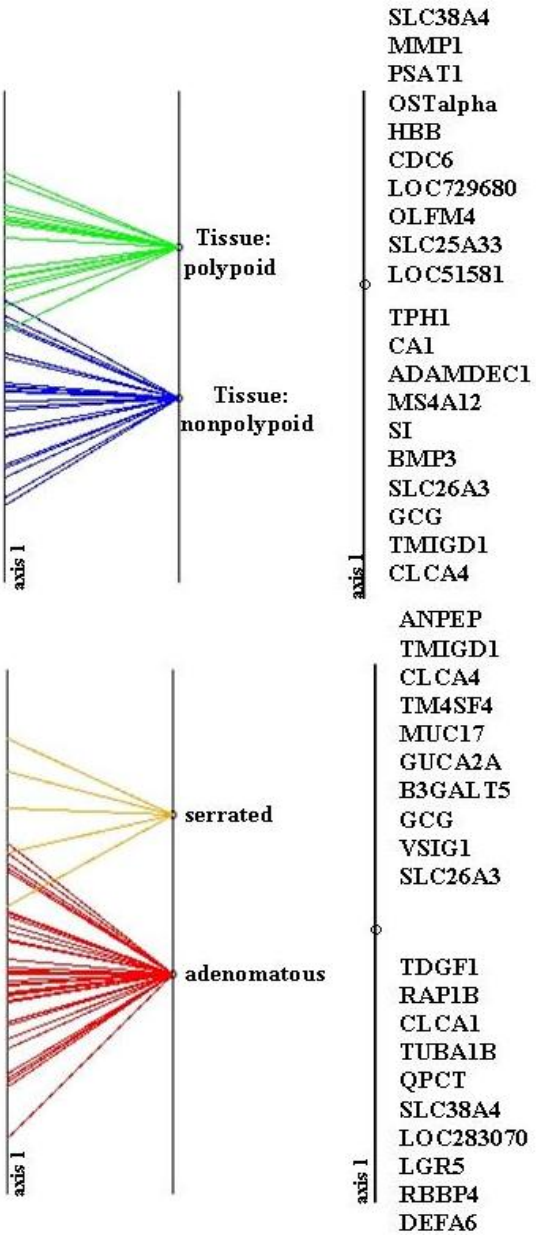

Figure 14. Between Group Analysis (BGA) of log_2 ratio expression intensity values with the variables, *tissue type* (nonpolypoid *versus* polypoid), or *histologic type* (adenomatous *versus* serrated), as grouping factors (i.e.,supervised for tissue type or histologic type, respectively).

For grouping factors with two levels, only the scores on the first BGA axis are meaningful. For this reason the results of BGA for tissue and histologic type are visualized in 1 dimension graph showing the BGA axis 1 scores only.
Panel **A**: 1D plot of BGA scores using *tissue type* as grouping factor. Samples are displayed on the axis 1 as lines,(*green* lines, polypoid lesions, *blue* lines, nonpolypoid lesions).
Top genes contributing most to the segregation of the polypoid and nonpolypoid samples are plotted as well on axis 1.
Panel **B**: 1D plot of BGA scores using *histologic type* as grouping factor. Samples are displayed on the axis 1 as lines [*orange* lines, serrated lesions, *red* lines, adenomatous lesions). Top genes contributing most to the segregation of serrated and adenomatous lesions are plotted as well on axis 1.

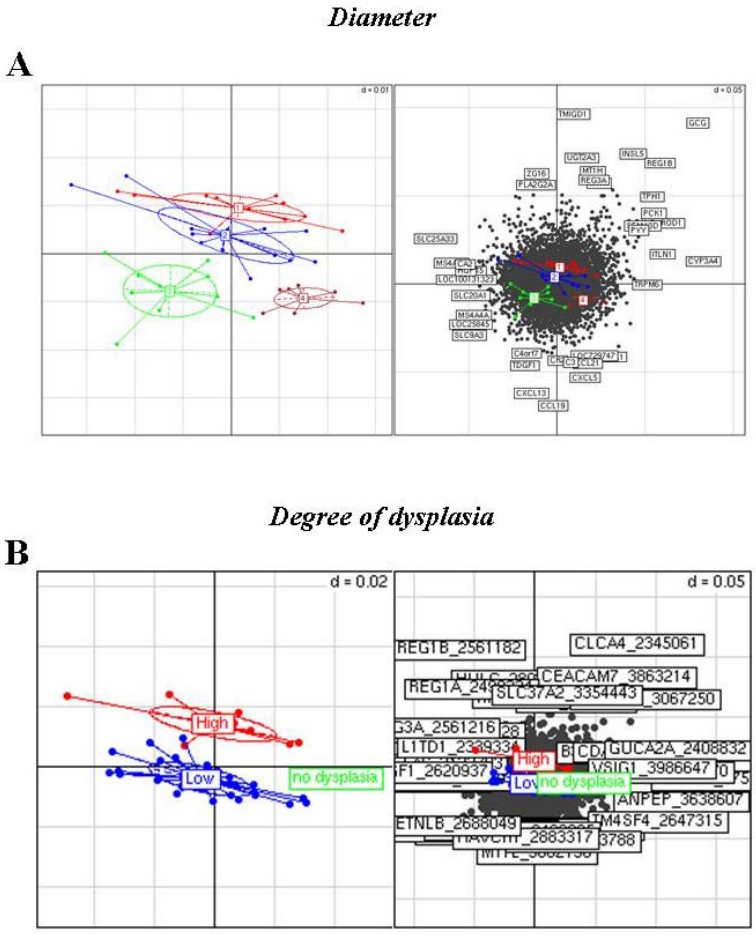

Figure 15. Between Group Analysis (BGA) of log_2 ratio expression intensity values with the variables *diameter* and *degree of dysplasia*, as grouping factors (i.e, supervised for diameter or degree of dysplasia, respectively).

For grouping factors with more than two levels, the scores on the first 2 BGA axes could be meaningful. For this reason, the results of BGA for *diameter* and *degree of dysplasia* are visualized in a biplot with BGA axes 1 and 2.
Panel **A**: the 2D map of the samples score on axes 1 and 2 showed the groupings based on adenoma size classes. Each of the four size-related groups is delimited by an ellipse with a labelled centroid. The ellipses representing the lesions with diameter < 30mm (*red* and *blue* ellipses) are well separated form those (*green* and *purple* ellipses) representing lesions with diameter >30 mm, along the axis 2. Next to the map, along axis 2, the top genes contributing to the segregation of lesions with diameter > or < of 30 mm are plotted.
Panel **B**: the 2D map of the samples score on axes 1 and 2 shows the groupings based on the degree of dysplasia (no dysplasia, low degree of dysplasia and high degree of dysplasia). Along axis 2, the ellipse representing the lesions with high degree of dysplasia (*red* ellipse) is well separated from the ellipse representing lesions with low and no dysplasia (*blue* and *green* ellipses). Next to the map, along axis 1 are plotted the genes contributing to the segregation of the samples based on the presence of dysplasia (no dysplasia group *vs* low and high dysplasia groups). Along axis 2, the genes contributing to the segregation of the samples based on the degree of dysplasia (low dysplasia group *vs* high dysplasia group) are plotted.

Being the *tissue type* the variable that explained much of the variance in the data set, we then performed the ANOVA (analysis of variance) to assign *p*-values to gene transcripts based on their ability to distinguish between tissue groups. The hypothesis tested was that, under the assumption that sample populations are normally distributed and have a homogeneous variance, there is no difference between gene-expression levels across conditions. Three independent groups were tested: nonpolypoid lesions, polypoid lesions, and normal mucosa. Among 23,768 expressed transcript clusters, 9,859 displayed significant changes (*tissue type p* value <0.05) in precancerous lesions. To highlight the most significant changes, we generated a list of 2,293 genes (*tissue type p* value < 0.001, and a FDR (step down method) value of 0.001) (**Supplementary Table 3** in Appendix). By setting specific contrasts in the ANOVA model, *p* values and $\log_2$ fold change for each pairwise comparison (nonpolypoid lesions *vs* normal mucosa, and polypoid lesions *vs* normal mucosa) were additionally generated and reported in Supplementary Table 3.

After an in-depth evaluation of the gene lists generated by ANOVA and BGA and the analysis of dot plots of hundreds of single transcripts, it emerged that, in a large proportion of them, the expression levels in nonpolypoid lesions occupied an intermediate position between those detected in the normal mucosa and in polypoid lesions (examples in Figures 29 and 30). However, the expression levels in the two groups of lesions were, almost invariably, closer and well separated from those found in the corresponding samples of normal mucosa. From these data, it emerged that the transcriptomes of nonpolypoid and polypoid lesions are rather similar, at least qualitatively. However, a gene ontology enrichment analysis allowed highlighting the dissimilarities between the two groups of precancerous lesions by revealing the main dysregulated pathways and processes in each group of lesions.

Two lists of significant genes (*p* value < 0.05) obtained by the pairwise comparisons "nonpolypoid *vs* normal mucosa" and "polypoid *vs* normal mucosa", were uploaded in the MetaCore software and used to reveal the first 10 most statistically significant GeneGo *pathways maps*, *processes* and *metabolic networks* in both groups (**Supplementary Table 4**, Appendix). As illustrated in **Figure 16**, the number of the objects falling in a given *pathway* for each of the two comparisons

were visualized as colored bar (*orange*, nonpolypoid; *blue*, polypoid), while the common objects were depicted as *blue-striped* bars. Several pathways of *cell cycle regulation* were affected much more frequently in the group of polypoid lesions, whereas *oxidative phosphorylation* and *IGF1 signalling pathway* appeared to be more specifically involved in the neoplastic process of nonpolypoid lesions. The category of *process networks* (**Figure 17**) displayed a similar scenario: Processes related to cell cycle regulation (*cell cycle S phase; cell cycle core; cell cycle G2-M*) were overrepresented in the group of polypoid lesions. In contrast, a different scenario was observed as for the *metabolic networks* category (**Figure 18**), where almost all the first 10 categories were similarly dysregulated in both groups, except for the pentose phosphate pathway (metabolic networks 4, 5, and 6 in the figure 18) that was more severely affected in polypoid lesions.

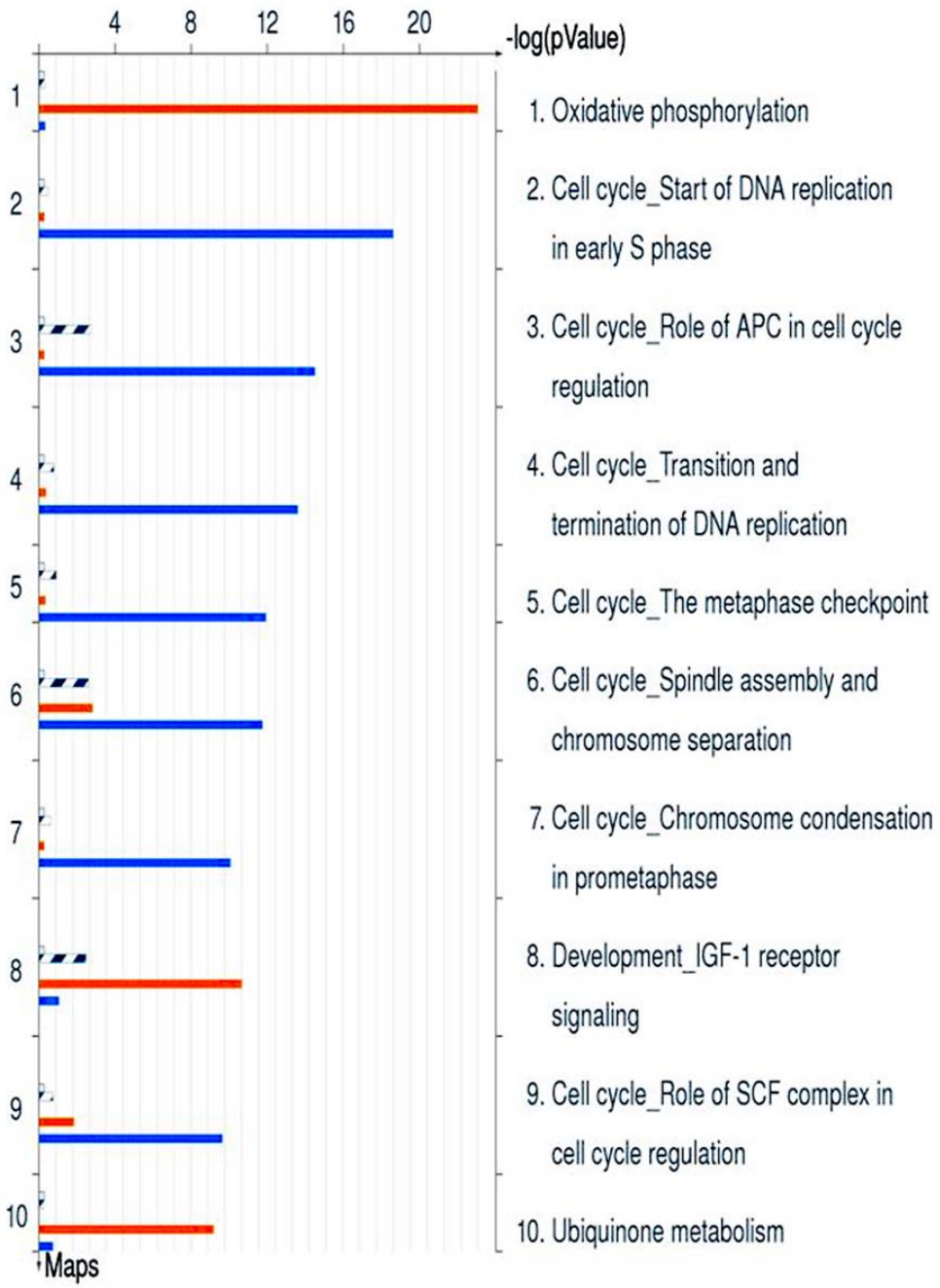

Figure 16. GeneGo Metacore differentially affected pathways

Bar graph showing the first 10 statistical differentially regulated GeneGo *pathway maps* between nonpolypoid (*orange*, bars) and polypoid lesions (*blue*, bars). The length of the horizontal orange and blue bars is proportional to the number of uniquely differentially expressed genes (classified as components of a given pathway map) in nonpolypoid and polypoid lesions, respectively (compared with normal mucosa). Striped blue bars are indicative of commonly dysregulated genes in both groups of lesions.

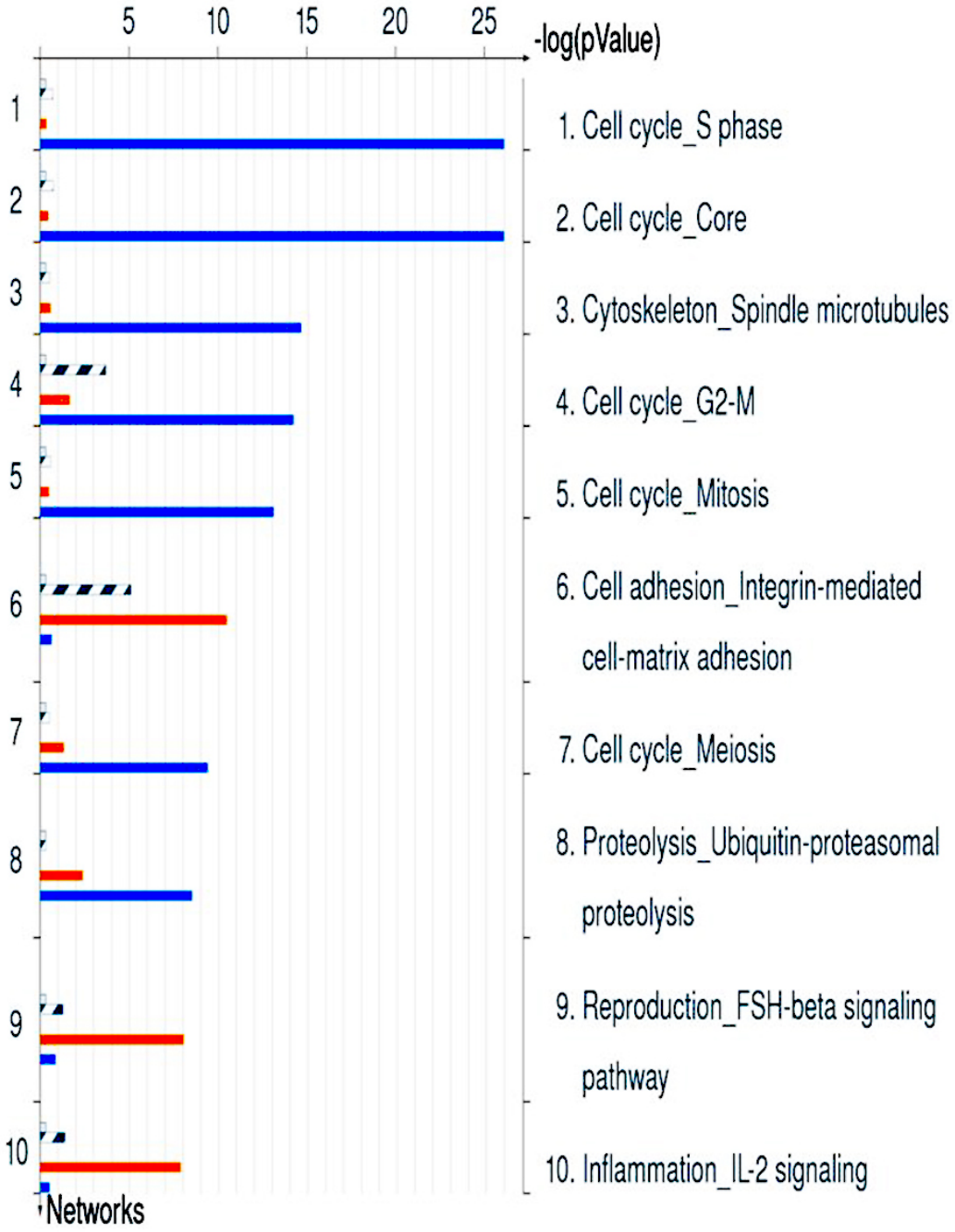

Figure 17. GeneGo differentially affected process networks

Bar graph showing the first 10 statistical differentially regulated process networks between nonpolypoid (*orange*, bars) and polypoid lesions (*blue*, bars). The length of the horizontal orange and blue bars is proportional to the number of uniquely differentially expressed genes (classified as components of a given process network) in nonpolypoid and polypoid lesions, respectively (compared with normal mucosa). Striped blue bars are indicative of commonly dysregulated genes in both groups of lesions.

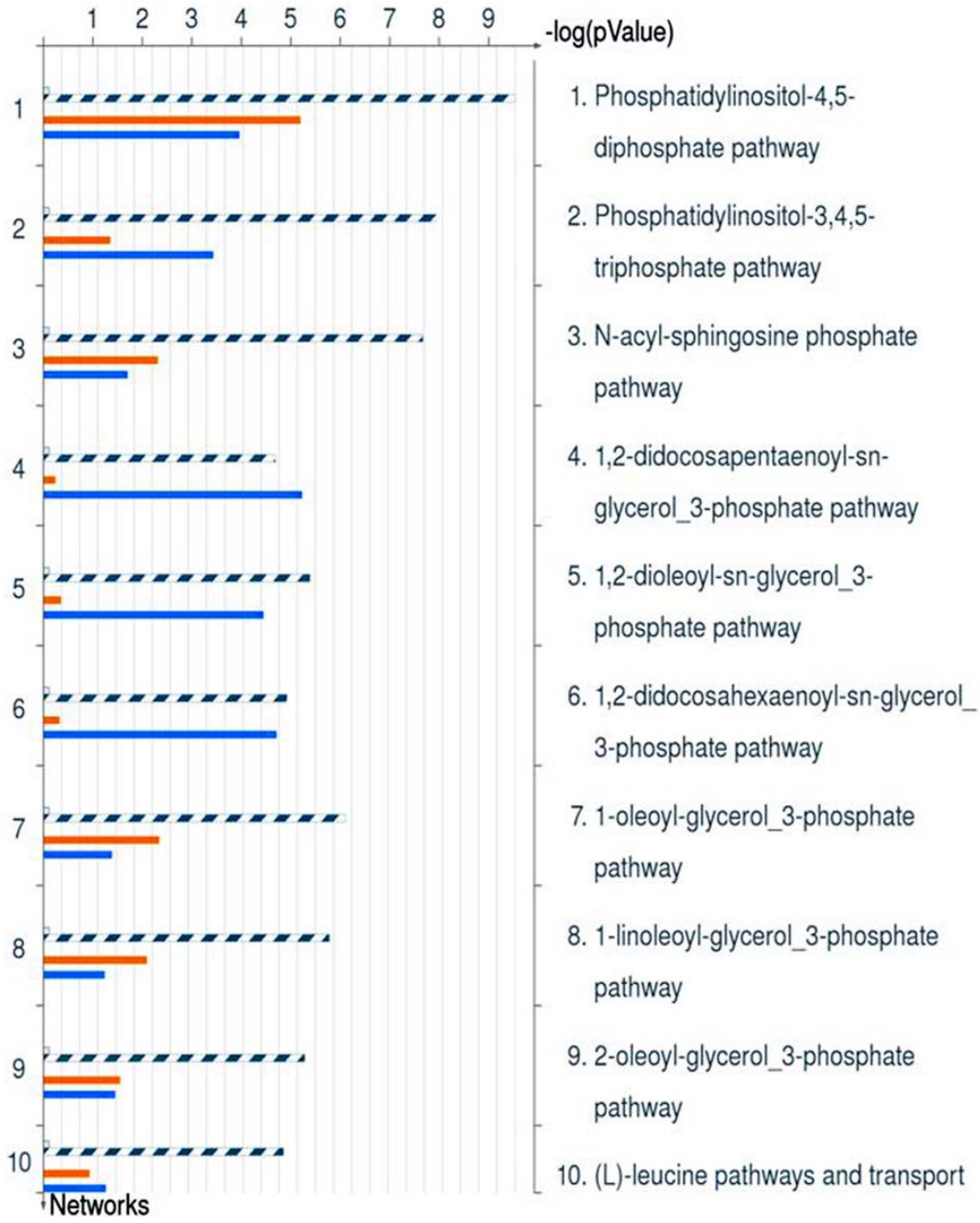

Figure 18. GeneGo differentially affected metabolic networks

Bar graph showing the first 10 statistical differentially regulated metabolic networks between nonpolypoid (*orange*, bars) and polypoid lesions (*blue*, bars). The length of the horizontal orange and blue bars is proportional to the number of uniquely differentially expressed genes (classified as components of a given metabolic network) in nonpolypoid and polypoid lesions, respectively (compared with normal mucosa). Striped blue bars are indicative of commonly dysregulated genes in both groups of lesions.

Among the genes whose expression profile clearly showed the normal mucosa → nonpolypoid → polypoid sequence showed in Figure 29, *TMIGD1* was of particular interest. This gene expression change was detected in the lists of discriminating genes associated with all the clinical and pathologic variables investigated, and often it was one of the top genes in these lists. As illustrated in the score plot (**Figure 19**), *TMIGD1* mRNA normalized intensity values were found to be markedly diminished in nonpolypoid and polypoid lesions, compared to the transcript levels in the corresponding normal mucosa samples. The dramatic down-regulation in the expression of *TMIGD1* in colorectal neoplasms and the originality of this finding (probes for the analysis of the expression level of this gene were not present in the microarray platforms used in our and other previous studies), along with the fact that its biological function is unknown, prompt us to invest time for a better characterization of the expression profile of this messanger RNA and its protein product.

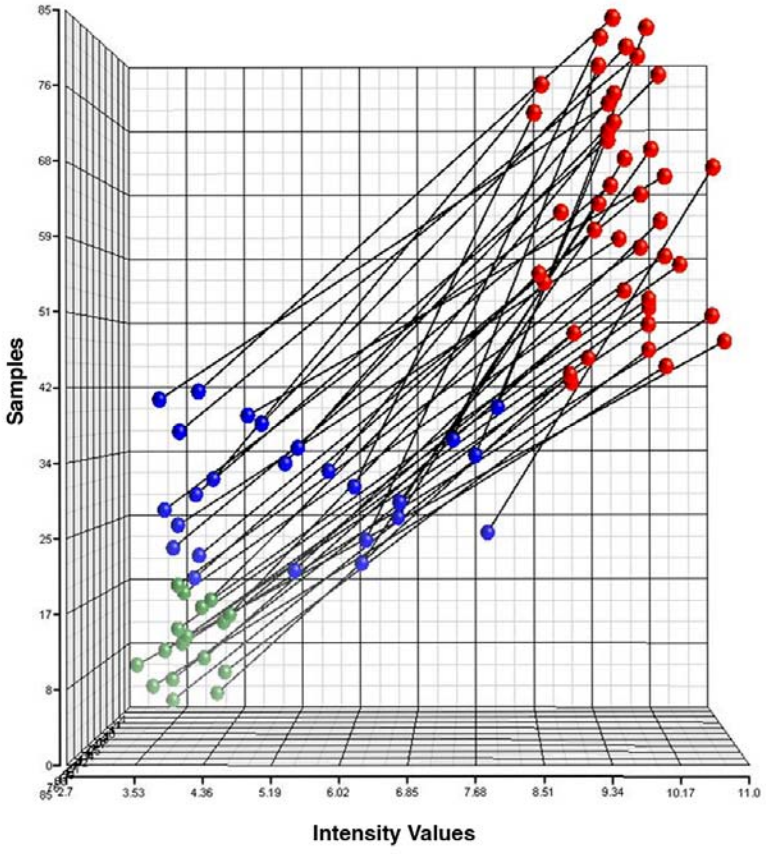

Figure 19. *TMIGD1* score plot of log_2 expression intensity values

Score plot of *TMIGD1* RMA preprocessed log_2 intensity values for each sample.
Axis 1: *TMIGD1* mRNA intensity values; Axis 2: the 84 samples.
TMIGD1 mRNA is highly expressed in samples of normal mucosa (*red* dots) but it is progressively downregulated in nonpolypoid (*blue* dots) and polypoid lesions (*green* dots).

TMIGD1, *transmembrane and immunoglobulin domain containing 1*, is a gene encoding a predicted membrane protein, whose function is unknown. The gene (NCBI GeneID 388364; National Center for Biotechnology Information; data bank accession code NM_206832), is located on human chromosome 17 (17q11.2) and contains seven exons. The coding cDNA contains 789 nucleotides and encodes a functional protein of 262 aminoacids. Putative *TMIGD1* orthologs were found in *Pan Troglodytes* (99.49 % nucleic (n) acid and 98.85% amino acid (aa) similarity), *Canis Familiaris* (85.44% n and 75.86% aa), *Bos Taurus* (83.91% n and 78.16% aa), and *Rattus Norvegicus* (81.8% n and 75.4% aa).

In an *in silico* analysis conducted by our collaborator Dr. Janusz M. Bujnicki, TMIGD1 was found to contain three main domains (a transmembrane domain, an immunoglobulin C-2 type, and an immunoglobulin like domain), and a structure that is similar to that of members of the large Ig-CAM family of adhesion molecules (a tentative structure of the protein is shown in **Figure 20**). Beside the two Ig-like domains located at the center, there are also two hydrophobic helices at the ends. The orientation between these four elements is still completely arbitrary. The helices are predicted to be transmembrane and hypothesized to be necessary for the protein anchorage to the membrane; however the N-terminal helix is actually predicted as a signal peptide.

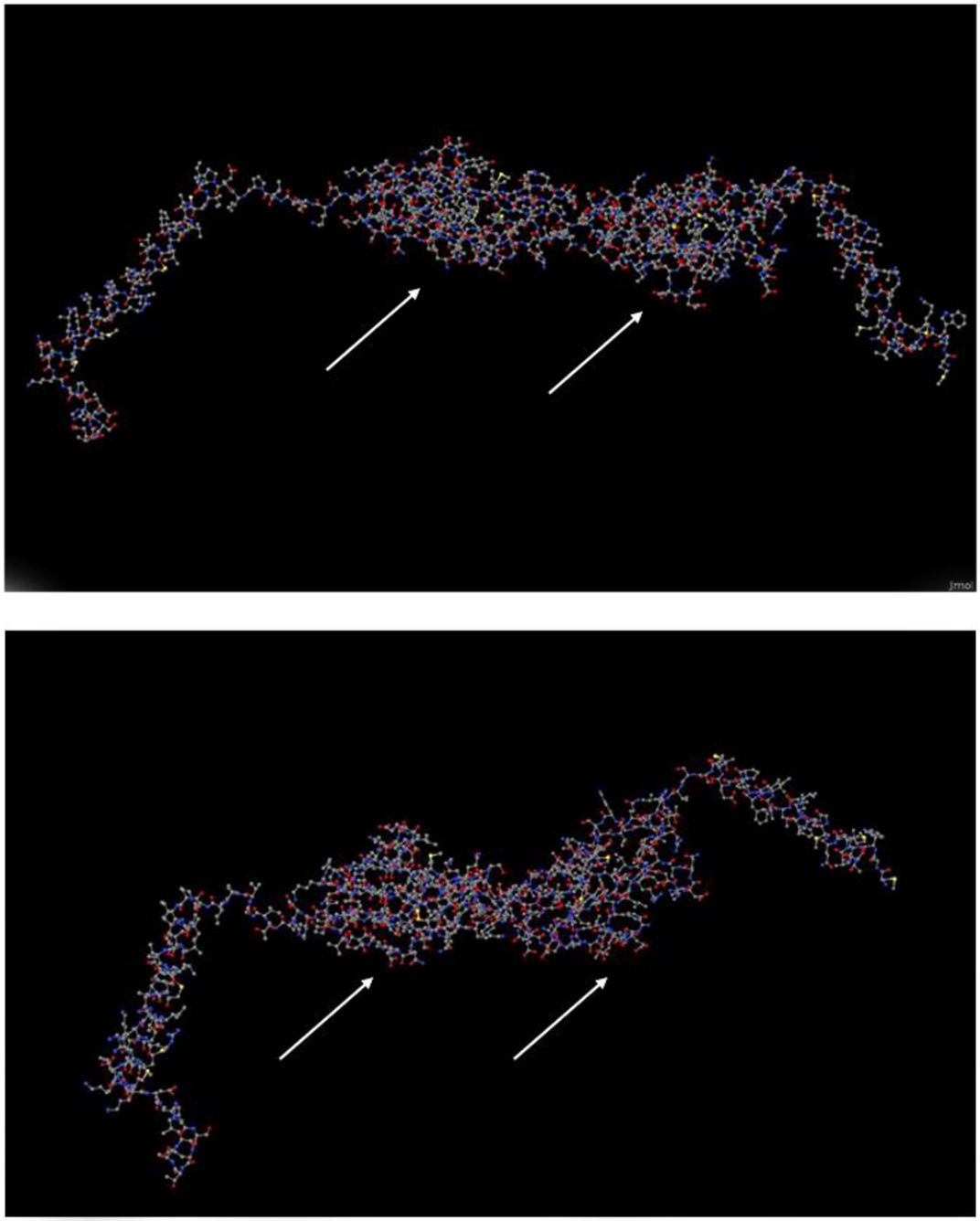

Figure 20. Predicted structure of the TMIGD1 protein based on in silico analysis.

Predicted structural model of the TMIGD1 protein: two Ig-like domains (white arrows for reference) are located in the center of the predicted structure, whereas two hydrophobic helices are at the ends. The helices are predicted to be trans-membrane. Both helices could help keeping the protein attached to the membrane, although the N-terminal helix is predicted as a signaling peptide. The orientation among these four elements remains still completely arbitrary.

Based on the gene expression profiles of the two groups of colonic precancerous lesions (nonpolypoid and polypoid) and their matched normal mucosa, *TMIGD1* was found to be markedly down regulated in all samples (-19 fold in nonpolypoid, and -66.3 fold in polypoid lesions).

To check whether *TMIGD1* down regulation was maintained during tumor progression, transcriptomic analysis was performed also in a few advanced colorectal cancer samples. Six colon adenocarcinomas (3 MMR proficient and 3 MMR deficient) and four matched normal mucosa were analyzed with the Human Exon Array. Multivariate analysis showed that *TMIGD1* was 125 fold downregulated in the 6 cancers (**Figure 21**).

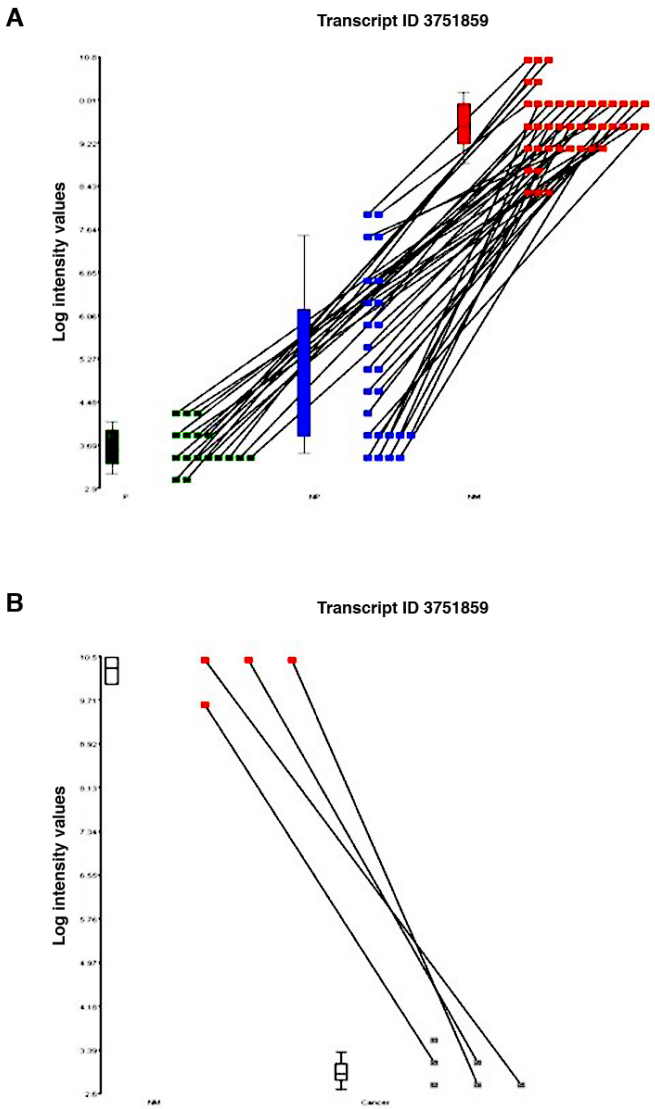

Figure 21. *TMIGD1* mRNA log_2 expression intensity values in colorectal precancerous lesions and cancers.

Panel **A**. Y axis: log_2 expression intensity values of *TMIGD1* mRNA detected in nonpolypoid (*blue* squares) and polypoid (*green* squares) lesions, with the Human Exon array. Matched normal mucosa (*red*, squares) are grouped all together (the black lines indicate the correspondence between the lesion and its matched normal mucosa). X axis: samples divided in the three groups: polypoid, nonpolypoid and normal mucosa.
For the three groups, the boxes indicate the distribution of *TMIGD1* expression values, while the whiskers represent the shifting from the normal distribution.

Panel **B**. Y axis: log_2 expression intensity values of *TMIGD1* mRNA detected with the Human Exon array in six colon cancers (*grey,* squares) and four matched normal mucosa (*red*, squares).
X axis: samples divided in 2 groups, normal mucosa and colorectal cancer.
For the two groups, the boxes indicate the distribution of *TMIGD1* expression values, while the whiskers represent the shifting from the normal distribution.

These findings were fully confirmed by real time quantitative RT-PCR analysis of mRNA extracted from samples used for the microarray study (**Figure 22**). Real time RT-PCR data also showed that *TMIGD1* mRNA is equally represented in all colon segments (caecum, ascending, transversum, descending and rectum), and is also highly expressed in the terminal ileum(**Figure 23**).

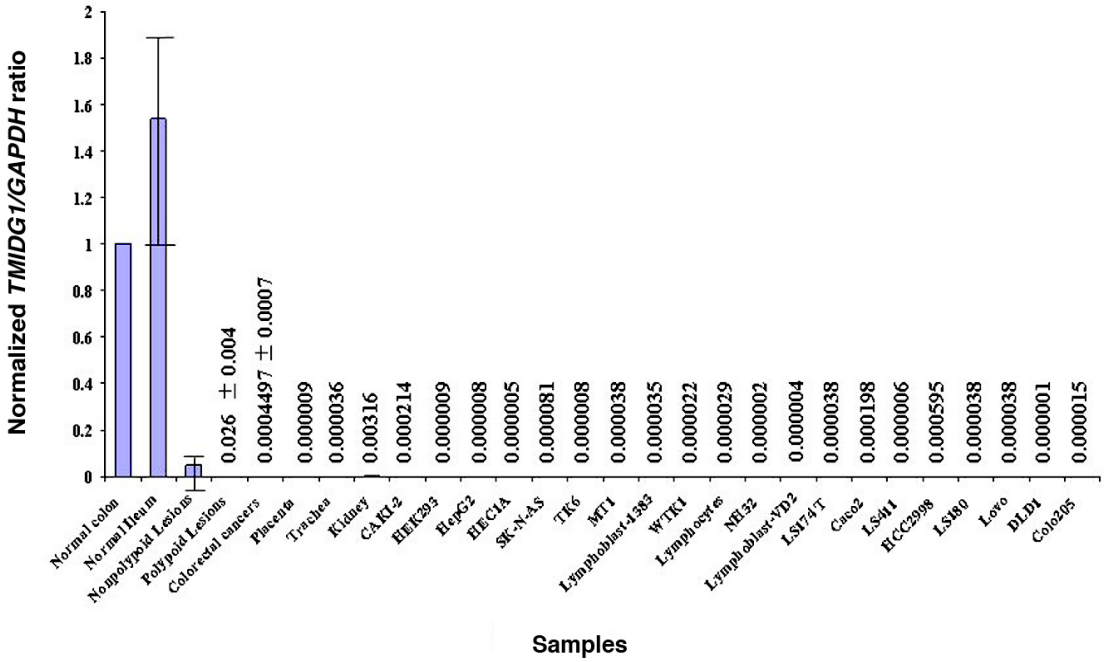

Figure 22. **Analysis of *TMIGD1* mRNA expression in tissues and cell lines.**

Microarray data generated with the Affymetrix Exon array platform were validated by quantitative real time RT-PCR. The *TMIGD1* mRNA levels in normal colonic mucosa, precancerous neoplasms (nonpolypoid and polypoid), and colon tumors were consistent with the microarray data.
The graphic shows only tissues and cell lines where *TMIGD1* was found to be expressed or slightly expressed. [Several normal tissues (spleen, esophagus, liver, bladder, brain, cervix, heart, lung, ovary, prostate, skeletal muscle, thymus and thyroid) did not express *TMIGD1*, as well as several cancer cell lines (SW480, Colo741, HT29, HT29M6, CO115, CO115 treated with 5-AZA deoxycytidine, Sw48, CX1, SW837, HCT116, SW620, Vaco481, SW403, LnCaP, MCF7, Hela, Beas2B, U2OS, 293T, A2780, LAN-1, Sk-N-SH)].
mRNA levels were detected by amplification of the coding region of *TMIGD1* and the control housekeeping gene *GAPDH*. Relative quantification analysis compares the levels of two different targets (target gene of interest and housekeeping gene) in a single sample and expresses the final result as a ratio of these targets.
Y axis: normalized ratio: $[\text{conc.target/conc.reference}]_{\text{sample}}$: $[\text{conc.target/conc.reference}]_{\text{calibrator}}$.
The calibrator is a positive sample with a stable ratio of target to reference and is used to normalize all samples within one run. X axis: samples

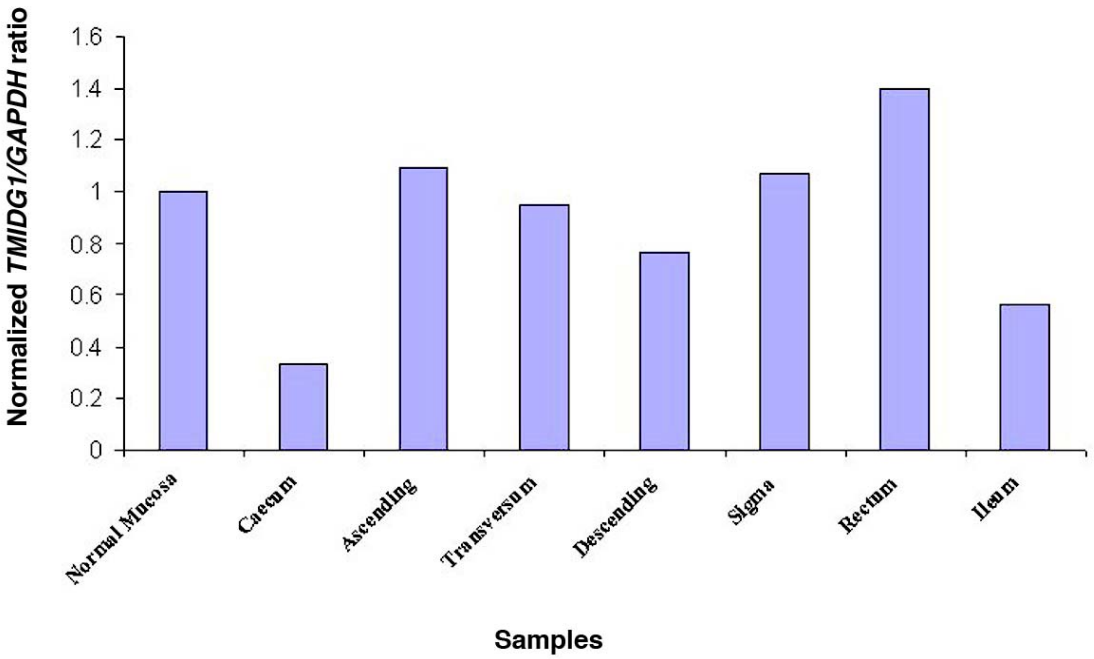

Figure 23. *TMIGD1* mRNA expression in different colon segments and in the small intestine

Real time RT-PCR amplification of the coding region of *TMIGD1* and the control housekeeping gene *GAPDH*, in colonic samples and ileum (terminal ileum). Except for the caecum segment, where *TMIGD1* expression is relatively lower, *TMIGD1* expression is equally represented in the remaining segments.
Relative quantification analysis compares the levels of two different targets (target gene of interest and housekeeping gene) in a single sample and expresses the final result as a ratio of these targets.
Y axis: normalized ratio: $[\text{conc.target/conc.reference}]_{\text{sample}}$: $[\text{conc.target/conc.reference}]_{\text{calibrator}}$.
The calibrator is a positive sample with a stable ratio of target to reference and is used to normalize all samples within one run. X axis: samples.

In order to detect the *TMIGD1* pattern of expression in extra-colonic tissues, several healthy tissues and cancer cell lines were also evaluated by real time quantitative RT-PCR. Three additional normal tissues (placenta, trachea and kidney) and only few cancer cell lines (colon cancer cell line HCC2998 and kidney cancer cell line CAKI-2) showed expression of this gene although at much lower level than in the normal colonic mucosa. (Total RNAs extracted from the different tissues were purchased from Ambion. The quality of the RNA was checked and found to be optimal, but information is not available on the precise region of a given organ that was actually sampled) (Figure 22)

Since *TMIGD1* mRNA was poorly expressed in almost all our cell lines, a DNA vector (pcDNA 3.2/V5-DEST) for the mammalian expression of *TMIGD1* was generated using the Gateway cloning system (Invitrogen), and used to stably transfect the human SW480 colorectal cancer cell line (see *Materials* and *Methods*). As a negative control, the same cell line was stably transfected with the same vector without the *TMIGD1* cDNA. The stably transfected SW480 cell line (bulk culture expressing *TMIGD1*) and single-cell clones were isolated by neomycin resistance and their RNA analyzed by real time RT-PCR for the expression of *TMIGD1*. Both, SW480 bulk culture and some of the clones (n°4 and n°8 clones in particular) were highly expressing *TMIGD1* mRNA (**Figure 24, A**).

TMIGD1 expression was subsequently estimated at the protein level by Western blot analysis (**Figure 24, B**). The samples so far tested were the colonic normal mucosa (protein extracts from isolated colonic crypts, see *Materials and Methods),* SW480 bulk culture expressing *TMIGD1* and its derived clones. Two protein extracts for each sample were prepared, total membrane protein extract (TME) and total extract (TE) with the aim to investigate how TMIGD1 was distributed in the cellular compartments. Western blot analysis, in agreement with real time RT-PCR data, showed a clear, sharp band corresponding to the expressed protein, in the normal colonic mucosa and in SW480 cells transfected with *TMIGD1*cDNA (bulk culture and clones) (Figure 24, A and B). As expected, SW480 transfected with the empty vector was negative. Protein enrichment was observed in all the total membrane protein extracts, supporting the prediction of membrane localization of TMIGD1. However, the protein was also clearly present in extracts from the cytoplasmic compartment. To verify whether the protein was secreted in the extracellular compartment, supernatant from each of the SW480 transfected cell lines was collected and tested by Western blot. There was no detection of TMIGD1 in any of the three supernatants, SW480 expressing *TMIGD1*, SW480 clone 8 and SW480 empty vector, respectively (**Figure 24 B**).

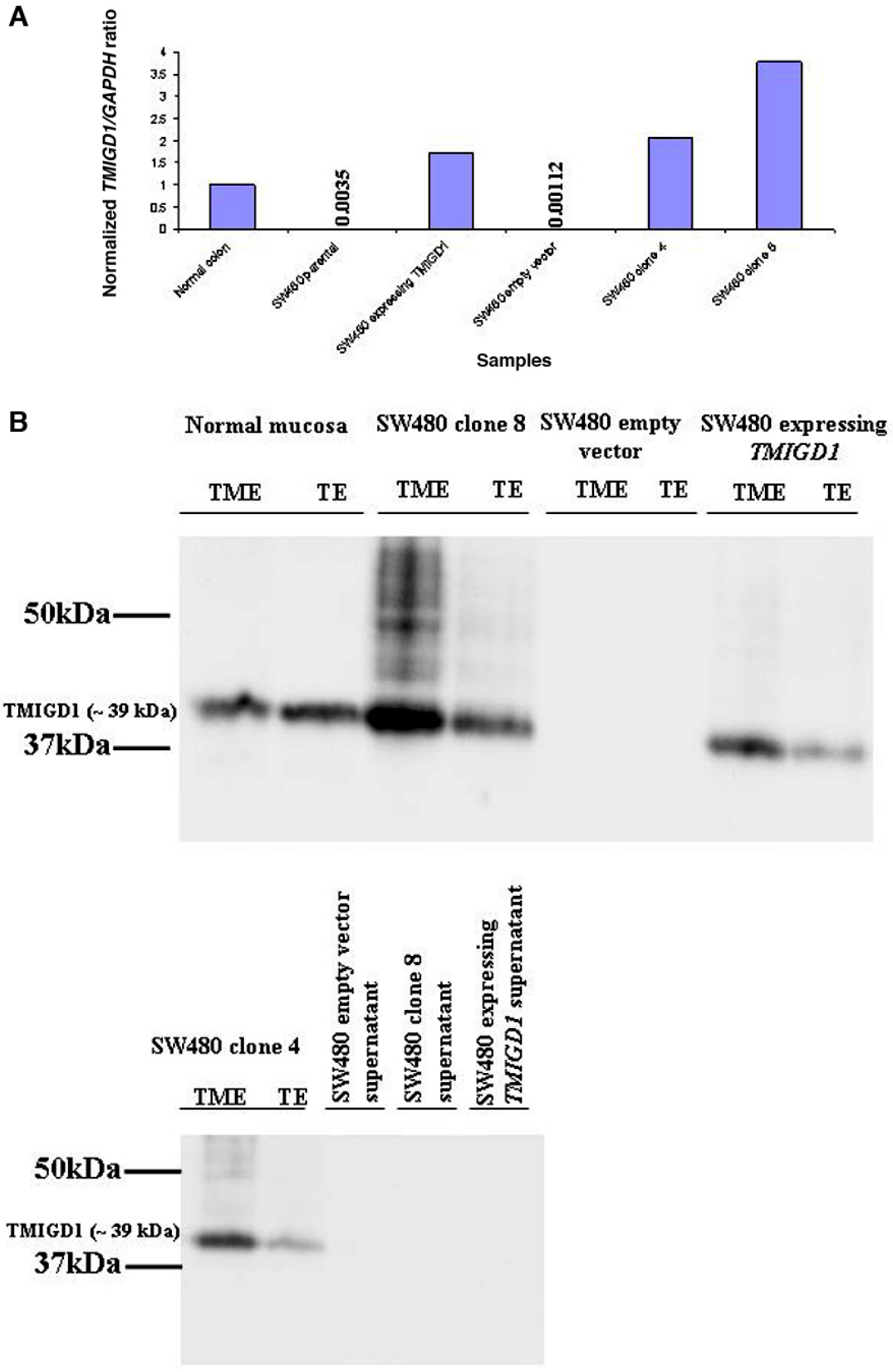
A
Normalized TMIGD1/GAPDH ratio
4
3.5
3
2.5
2
1.5
1
0.5
0
0.0035
0.00112
Normal colon
SW480 parental
SW480 expressing TMIGD1
SW480 empty vector
SW480 clone 4
SW480 clone 8
Samples
B
Normal mucosa
SW480 clone 8
SW480 empty vector
SW480 expressing TMIGD1
TME
TE
TME
TE
TME
TE
TME
TE
50kDa
TMIGD1 (~ 39 kDa)
37kDa
SW480 clone 4
SW480 empty vector supernatant
SW480 clone 8 supernatant
SW480 expressing TMIGD1 supernatant
TME
TE
50kDa
TMIGD1 (~ 39 kDa)
37kDa

Figure 24. *TMIGD1* mRNA and protein expression in SW480 colon cancer cells stably transfected with pcDNA 3.2/V5-DEST vector carrying the full length *TMIGD1* cDNA

Panel **A**: Real time RT-PCR amplification of the coding region of *TMIGD1* and the control housekeeping gene *GAPDH* in SW480 parental colorectal cell line and SW480 colon cancer cells stably transfected with pcDNA 3.2/V5-DEST vector carrying the full length *TMIGD1* cDNA (bulk culture and derivative clones 8 and 4). Negative control: SW480 transfected with the empty DEST vector. Relative quantification analysis compares the levels of two different targets (target gene of interest and housekeeping gene) in a single sample and expresses the final result as a ratio of these targets.
Y axis: normalized ratio: $[\text{conc.target/conc.reference}]_{\text{sample}}$: $[\text{conc.target/conc.reference}]_{\text{calibrator}}$.
The calibrator is a positive sample with a stable ratio of target to reference and is used to normalize all samples within one run. X axis: samples.
Panel **B**: Western blot analysis confirming, at the protein level, the RT-PCR data shown in panel A. Samples: normal colonic mucosa, SW480 colorectal cell line stably expressing *TMIGD1* (bulk culture and its derivative clones 4 and 8), supernatant from cell culture medium of SW480 stably expressing *TMIGD1* (bulk culture and clone 8). Negative control: SW480 cell line transfected with empty DEST vector. TME, total membrane protein extract; TE, total protein extract. The ~39 kDa band corresponds to TMIGD1 protein of 262 aminoacids.

To gain further insights into the protein localization in the cell, three additional approaches were used: Immunocytochemistry (ICC), immunohistochemistry (IHC), and immunofluoresce (IF). In studies with SW480 cell lines, a specific membrane and cytoplasmic staining was detected in about 5% of the cells with both ICC (**Figure 25**) and IF (**Figure 26**) (details on staining patterns in the figure legends). In immunofluorescence analysis, cells were double stained for actin (red stain), a protein localized in the cytoskeleton, and for nucleic acids [4'-6-Diamidino-2-phenylindole (DAPI), blue stain]. No co-localization between actin and TMIGD1 was observed. Furthermore, it could be excluded the presence of the protein at the nuclear level.

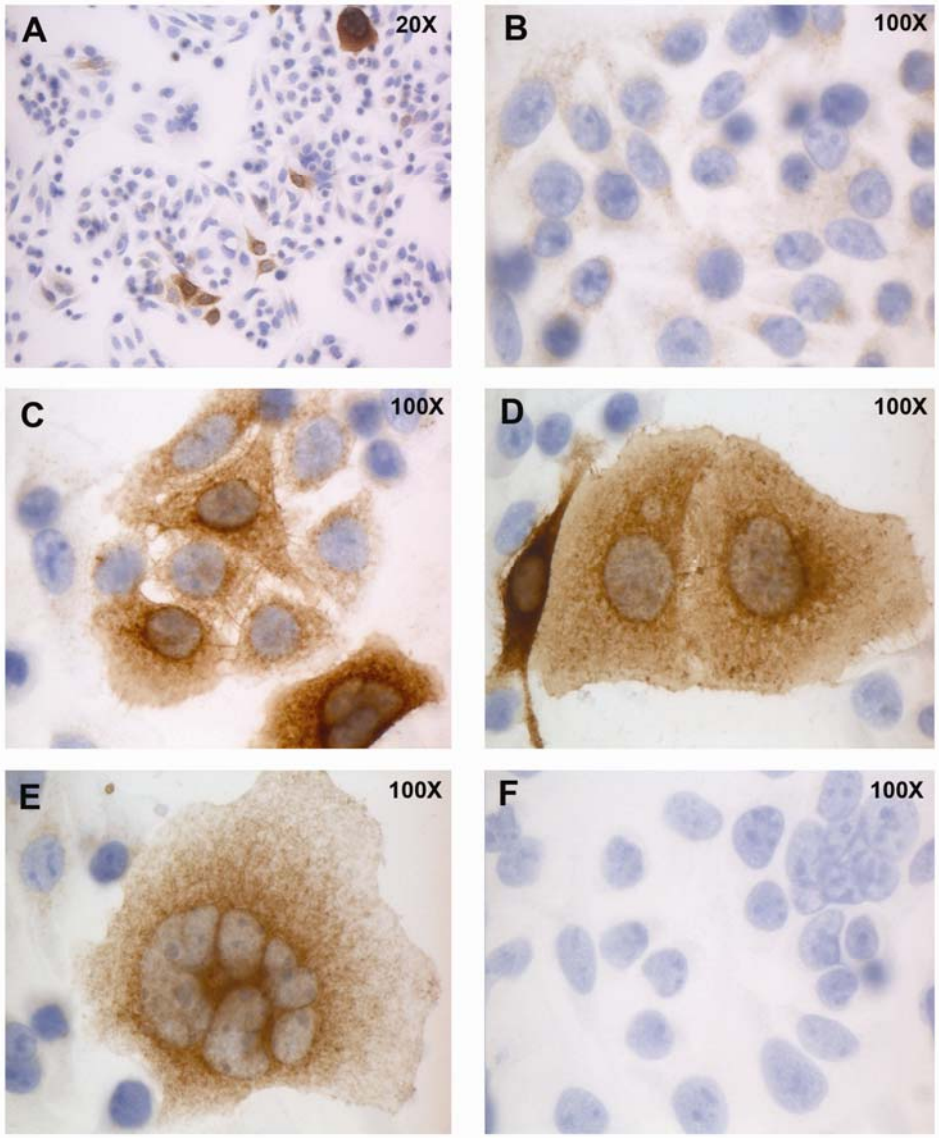

Figure 25. Expression of TMIGD1 in SW480 colon cancer cells stably transfected with pcDNA 3.2/V5-DEST carrying the full length *TMIGD1* cDNA

(Immunocytochemistry performed on the selected *clone 8*). **A**. A portion of cells are strongly positive for TMIGD1, whereas most of them show low expression that can be appreciated in panel **B** or even no staining. In panels **C**, **D**, and **E**, the intra-cytoplasmic distribution of TMIGD1 can be easily detected: An accumulation of TMIGD1 appears in the perinuclear compartment (likely associated with the rough endoplasmic reticulum), however the entire cytoplasm and the cell membrane are also stained. The fiber-like pattern of staining suggests that TMIGD1 might be associated also with the cytoskeleton. **D**. Negative control: SW480 cells stably transfected with the empty vector pcDNA 3.2/V5-DEST.

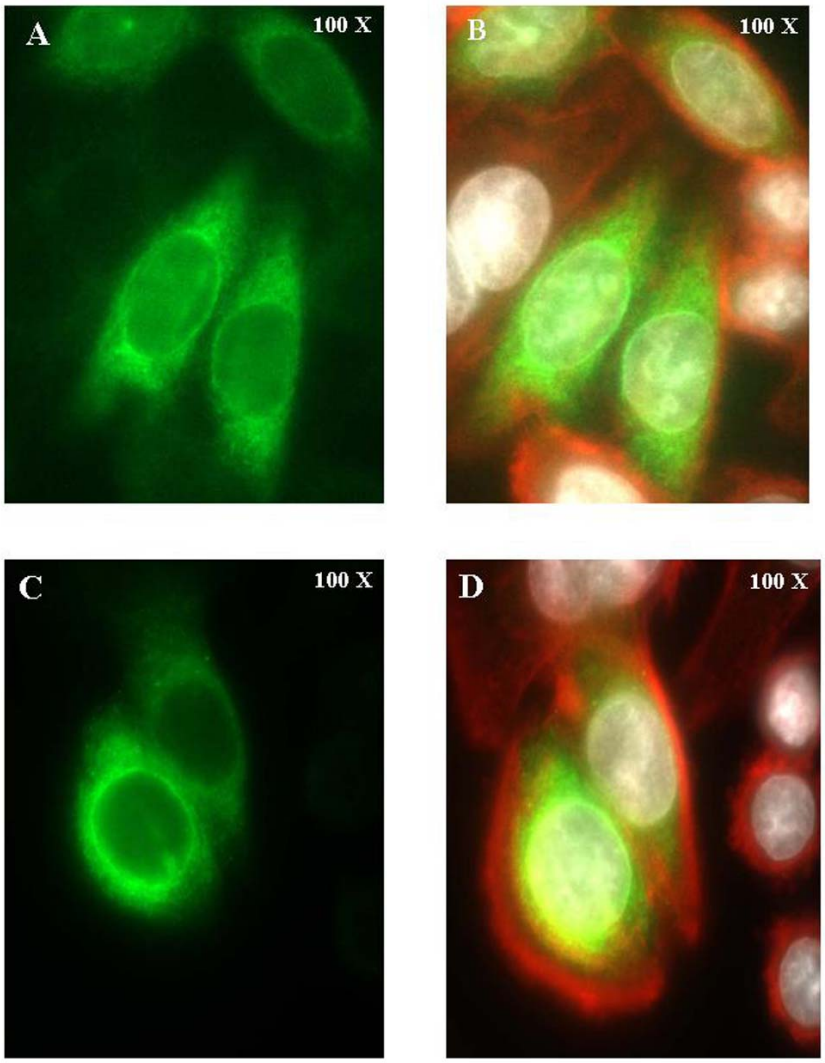

Figure 26. **Expression of TMIGD1 in SW480 colon cancer cells stably transfected with pcDNA 3.2/V5 DEST vector carrying the full length *TMIGD1* cDNA**

(immunofluorescence on the selected *clone 8*). Cellular proteins were stained with the specific primary antibody followed by the detection with the fluorochrome-conjugated secondary antibodies: TMIGD1 *green*, actin *red* and 4'-6-Diamidino-2-phenylindole (DAPI, *blue* stain) for the nucleus. A portion of cells are strongly positive for TMIGD1, whereas some of them show low expression that can be appreciated in panel **B** and **D** or even no staining.
A and **B.** SW480 epithelial-type cells **C** and **D.** SW480 round-type cells.
In all four panels, the intra-cytoplasmic distribution of TMIGD1 could be easily detected and nuclear staining excluded. TMIGD1 appears to concentrate at the perinuclear compartment (likely associated with the rough endoplasmic reticulum). The absence of co-localization between TMIGD1 and actin (panel B and D) indicates that TMIGD1 protein does not localize at the level of the cytoskeleton.

In tissue samples, IHC showed that the epithelium of the normal colorectal mucosa expresses TMIGD1 (**Figure 27**). The staining was cytoplasmic and present in the upper 2/3 of the colonic crypts where mostly differentiated cells are located. TMIGD1 was not detected in the lower portion of the crypts which represents the stem and proliferating cells compartment. Precancerous lesions showed a weaker TMIGD1 staining than that observed in the normal mucosa, while cancers were negative or slightly positive. The immunostaining reflected thus the trend observed in the transcriptomics studies.

TMIGD1 was also markedly expressed in the villi of the ileum (compartment with differentiated cells), but it was absent in the Lieberkühn crypts (proliferative compartment) (**Figure 28**). In this epithelium, the expression of TMIGD1 was very strong in the apical membrane of absorptive cells (i.e. in the brush border).

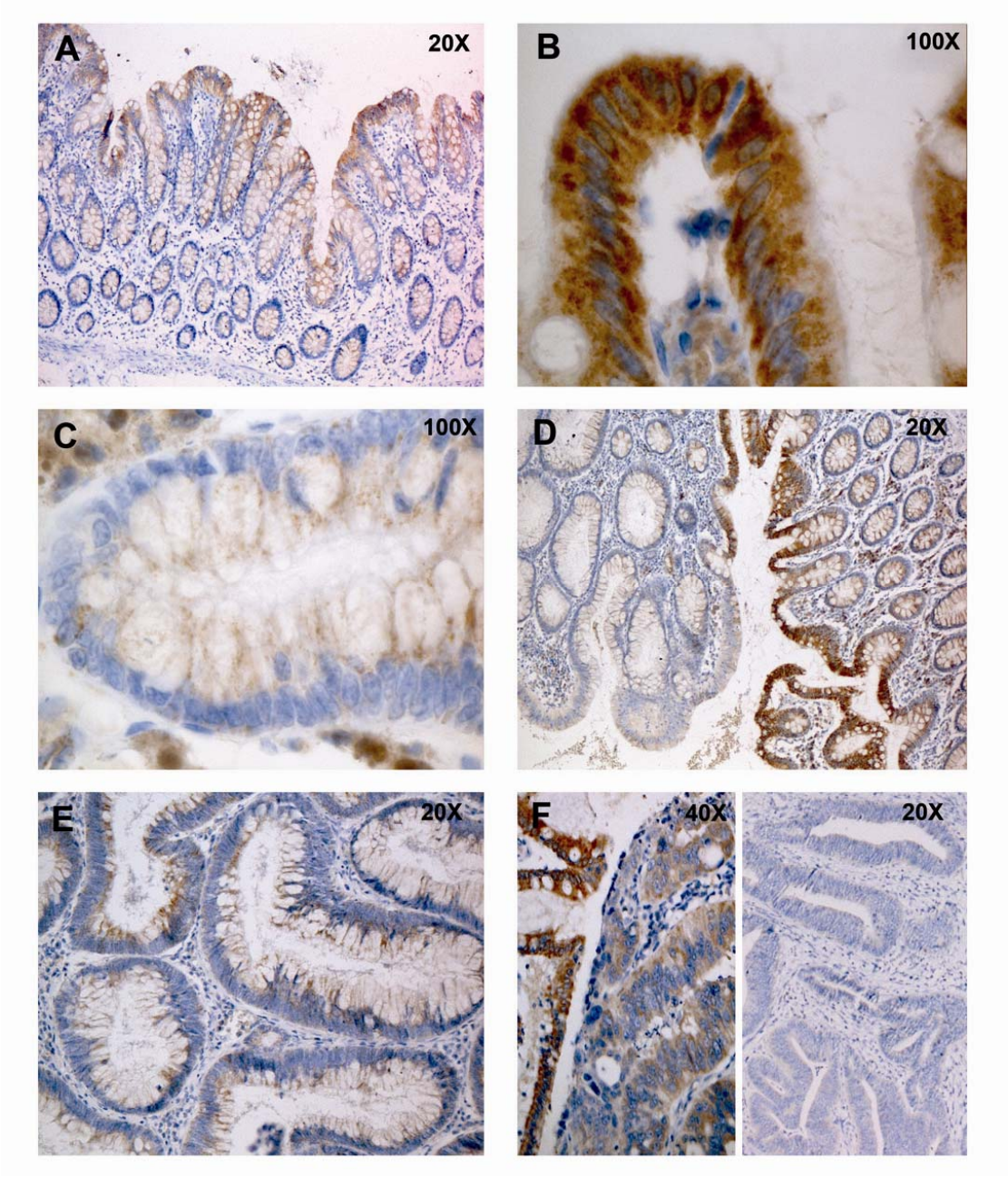

Figure 27. Expression of TMIGD1 in normal and neoplastic colonic tissues

(Immunohistochemistry). **A.** Normal colonic mucosa showing the expression of TMIGD1 limited to the upper portion of the epithelial crypts where differentiated cells are located. A higher magnification of the top of a crypt in panel **B** shows markedly positive superficial cells: As expected, the staining of TMIGD1 is cytoplasmic. Panel **C** shows that the expression of TMIGD1 is very low in the lower crypt where the proliferative compartment resides. **D**. Marked decrease of the TMIGD1 expression in a nonpolypoid lesion (15359 Brescia) in the left half of the picture (compare with the staining of the corresponding normal mucosa in the right part of the picture). **E**. Polypoid, adenomatous lesion (628 Brescia) also showing a dramatically decreased expression of TMIGD1. **F**. Two colon cancers, one (on the left) is a well differentiated adenocarcinoma which shows residual expression of TMIGD1, whereas the second (on the right) poorly differentiated cancer shows complete loss of expression.

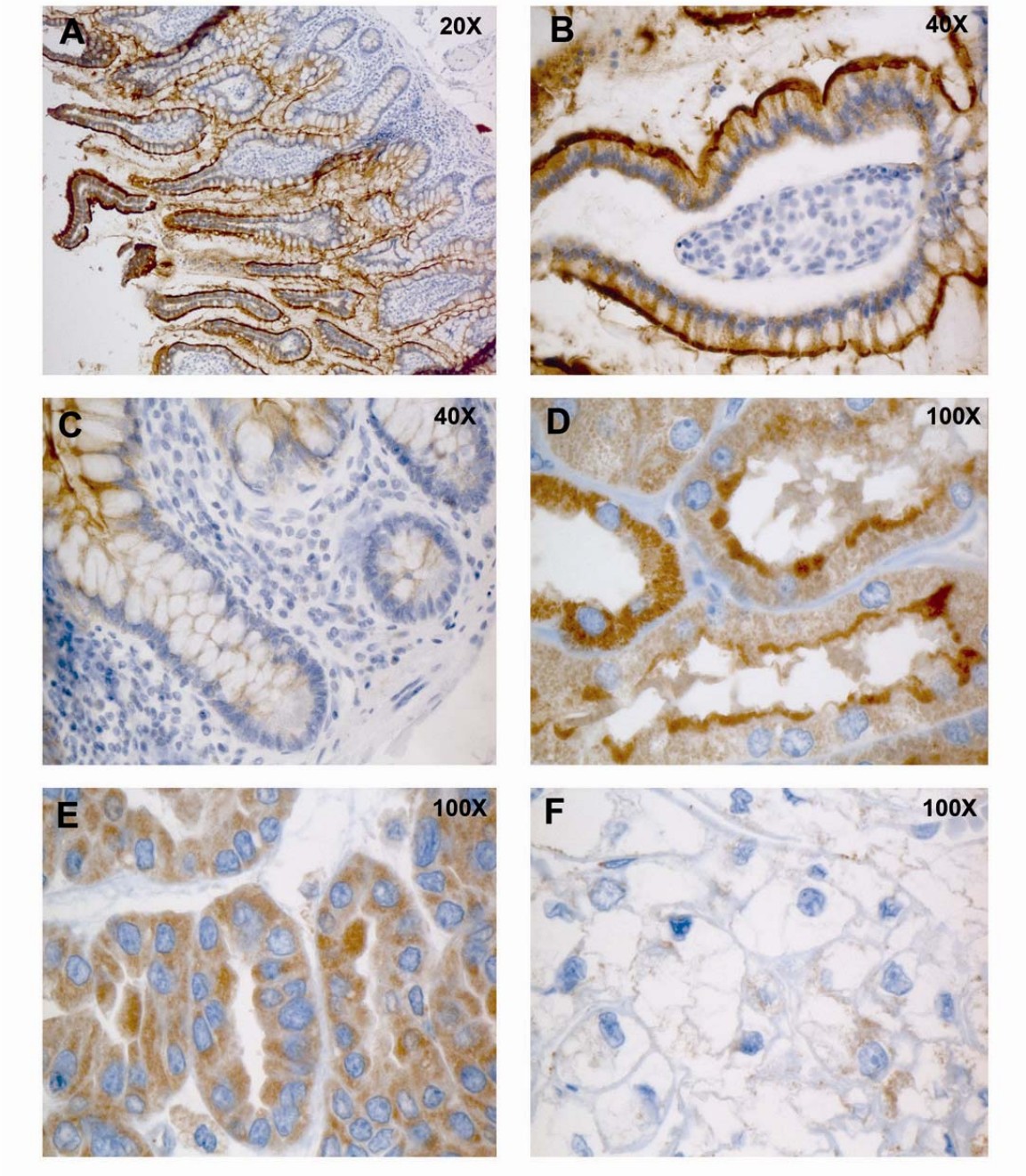

Figure 28. Immunohistochemical expression of TMIGD1 in terminal ileum and kidney.

TMIGD1 is expressed in the villi of the terminal ileum (**A**), where is markedly localized in the brush border (**B**). Its expression is almost absent in the proliferative crypt compartment (**C**). Among a series of other organs analyzed, tubuli of the normal kidney showed the highest expression (**D**) and a strong localization in the brush border. The expression of TMIGD1 was preserved in a papillary renal carcinoma (**E**), but was very low in clear cell renal carcinomas (an example in panel **F**).

6. DISCUSSION

Colorectal tumorigenesis is one of the most explored and understood processes of cellular transformation in humans. Decades of in-depth investigation emphasized the complexity and the heterogeneous nature of colorectal cancer, which is indeed characterized by several distinct clinical, histological and molecular phenotypes. Due to the diverse nature of this disease, its pathological features and the underlying molecular mechanisms are being continually refined.

A parallel heterogeneity can be observed in the lesions believed to represent the precursors of colorectal cancers. Until recently, two major forms of precancerous lesions were recognized: the adenoma and the hyperplastic polyp. The role of the adenoma in colorectal cancer development was clearly established when in 1988 Volgestein *et al*[47] introduced the concept of a multistep model of carcinogenesis, by characterizing the genetic events occurring in progressive pathological stages (i.e., from adenomas of different size to cancer). On the other hand, hyperplastic polyps have been conceived as innocuous lesions that, although often observed in colons of patients with colorectal cancer, were thought to have no malignant potential of their own.

Evidence that adenoma might not represent the only precursor of colorectal cancer began to emerge in the nineties, when Longacre & Fenoglio-Preiser [85] demonstrated the existence of a group of polyps showing mixed, both hyperplastic and adenomatous histologic features. These lesions were termed *serrated adenomas*, and the authors believed that they represent a variant of villous or tubulovillous adenoma. Only later, with the study of Torlakovic & Snover[86], lesions with serrated histology were proposed to be a variant of hyperplastic polyps. These lesions display characteristic molecular alterations not observed in colorectal adenomas, and they might progress to colorectal cancer by means of a new pathway of tumorigenesis, namely the *serrated pathway*. (For a detailed description of the histological and molecular features of this heterogenous group of lesions, as well as of their current nomenclature, see *Introduction* and Figure 3 of. Cattaneo *et al*.

"Pathways and crossroads to colorectal cancer". In *Advances in understanding the basic pathogenesis and clinical management of pre-invasive disease*. Edited by Fitzegerald R., 2009, in press - A reprint is included in the Appendix).

A second level of complexity derives from the macroscopic classification of precancerous lesions in the colorectum. For decades, all the preinvasive colorectal lesions were referred to as polyps that are lesions protruding into the gut lumen. Preneoplastic growths that did not protrude into the lumen were first detected in the eighties by Japanese endoscopists[17]. Ongoing improvement of the endoscopic techniques (i.e. chromoendoscopy and high magnification colonoscopy) allowed the identification of such lesions also in other countries. The newer and more precise terminology[76] (see *Introduction*) refers to all protruding lesions as polypoid and sub-classify them as pedunculated (attached with a stalk to the mucosa) or sessile (attached to a mucosa by a broad base). The counterpart is represented by nonpolypoid lesions still widely referred to as "flat", although most are actually slightly elevated (however, less than 2.5 mm above the surface of the gut mucosa). Those that are completely flat or slightly depressed are much rarer (see Figure 2).

The distinction of preinvasive colorectal lesions based on their morphology, and the belief that they represent different entities, were the pivotal aspects being considered in planning this study. The sample series collected for the study has been extensively described in both *Material & Methods* and *Results* (see also Table 2). However, few additional aspects should be here discussed. Although nonpolypoid lesions were collected solely from the proximal segment of the colon (the objective being to enrich for lesions presumably proceeding through the serrated pathway, as previously discussed), only 5 (20%) of them presented serrated histological features [2 microvesicular serrated lesions (MVSP), 1 sessile serrated lesion (SSA), and 2 serrated adenomas (SA)]. This frequency is similar to that reported by Carr *et al*.[23], who described a prevalence of 65% of conventional adenomas among precancerous lesions resected during standard colonoscopy. The other 35% displayed serrated architecture. More specifically among serrated lesions, 30% were MVSP, 4% were SSA, and less than 2% were SA. Similar figures (~60% conventional adenomas, ~40% serrated lesions) emerged from another

study[24] based on magnifying chromoendoscopy. Nine percent of all lesions removed in this study were SSA, and 2.4% were SA. Since the inter-observer agreement among pathologists in the classification of serrated lesions is rather low[87], all our lesions were analyzed by two pathologists with long experience in gastrointestinal pathology. The histological diagnosis reported in Table 2 reflects the final agreement between the two pathologists. The molecular analysis helped us complement the histological diagnosis. The two microvesicular serrated lesions and the sessile serrated adenoma were indeed found to carry the *BRAF*^{V600E} mutation, known to be associated with these histological subtypes (see *Introduction*). Evidence of this association was recently published by Carr *et al*[23], who showed that, within the group of serrated lesions, sessile serrated adenomas and microvesicular serrated lesions were significantly more likely to harbour a *BRAF*^{V600E} mutation. *BRAF* and *KRAS* oncogene mutations are early and mutually exclusive events that can even be detected in aberrant crypt foci[25 71, 88-90]. *BRAF* mutations are found in over two thirds of all MVSPs, SSAs, and dysplastic SAs, and they are also present in ~15% of all adenocarcinomas, mainly those in the proximal colon which develop along the serrated pathway. *KRAS* mutations are in contrast detected in 30-40% of conventional adenomas and in ~1/3 of all adenocarcinomas[27]. A similar prevalence of *KRAS* mutations (48%) was also reported in our nonpolypoid cases (see Supplementary Table 1, Appendix)

The last aspect to be commented about the molecular feature of the nonpolypoid lesions is that the expression of MLH1 was retained in all of them, although a portion of such lesions, especially those located in the proximal colon, are believed to represent the precursor of MLH1 deficient, sporadic colon cancers (see *Introduction* and Cattaneo *et al*., "Pathways and crossroads to colorectal cancer". In *Advances in understanding the basic pathogenesis and clinical management of pre-invasive disease*. Edited by Fitzegerald R., 2009, in press - A reprint is included in the Appendix). These results, in agreement with those reported by Sawyer *et al*[91], confirm that the gain-of-function *BRAF* mutation precedes the epigenetic silencing of *MLH1*. The late acquisition of this epigenetic event during tumor progression, and the consequent increase of mutation rate due to MMR deficiency, would lead to

the accumulation of mutations in target genes involved in the control of cellular homeostasis. This step might fuel the transition from a premalignant to a malignant status.

While the gene expression profile of polypoid lesions have been extensively studied over the past years[92-95], that of nonpolypoid lesions still remain poorly investigated. A single microarray study has compared the gene expression profile of these two types of precancerous lesions[96]. Eighteen "flat-type" adenomas and eighteen "protruded-type" adenomas were analyzed with a gene expression platform including only 550 genes. Nevertheless, the two groups could be divided into two major clusters by hierarchical clustering analysis, and therefore they were characterized by different expression profiles. Among 550 genes, the transcript level of 32 was found to differ significantly between the two groups. Only one gene from this list, *MUCIN 3*, was found to be differentially expressed also between our two groups of precancerous lesions. However, it should be considered that the two studies differ markedly as for both the selection of samples and the type of microarray platform.

Our study represents the first gene expression analysis of a large collection of precancerous lesions, carried out with a microarray platform that allows investigating the expression level of all the transcripts of the human genome. The Exon array used in our study differs from the previous Affymetrix arrays (i.e. U133Plus2.0) in terms of number, placement, and annotational confidence of oligonucleotide probes. Actually three major changes define the Exon array design: 1) the feature size has been reduced to allow for more probes on the array; 2) as for the background, no matching MM (mismatch) probes are used for every PM (perfect match) probe, but alternatively antigenomic background probes that are not matched to any putative transcript region; 3) human Exon probes are designed to interrogate the entire length of a gene, while probes in the U133Plus2.0 array hybridize mostly with the 3' end of genes. Exon probes are designed for each exon and can be used altogether to summarize the expression level of a gene[97]. Since we have previously used different Affymetrix arrays, we could test the performance of

Exon arrays relative to that of 3'-based arrays. We confirmed the results that have been published by others[97], who found that, in a comparison between Exon and U133Plus2.0 arrays, the former offers greater sensitivity and specificity and may allow more accurate quantitative measurement of the level of gene expression. However, the high degree of correspondence seen in a second study[98] between Exon and U133Plus2.0 arrays for probe sets with consistent signal strength and mapping to the same genomic region, provides strong evidence supporting the reliability of Exon arrays, not only for probe sets that can be successfully mapped to the existing arrays, but also for the many thousands of additional probe sets that provide the full coverage of the transcriptome.

Although the Exon array provided us with such a high resolution, we limited our analysis to a group of 23,768 thousands *annotated* genes (17,881 "core" transcript clusters plus 5,887 from the "extended" group) for two reasons. First, we intended to limit our analysis to changes in the expression of genes with known function (even if only partially) and/or likely encoding proteins or regulatory RNA molecules. (The inclusion of tens of thousand unannotated transcript clusters from putatively noncoding genomic regions might have reduced the discriminatory power of expression changes in annotated genes between groups.) Second, we tried to reduce the complexity of our data set due to the rather complicated analytical tools that are presently available for Exon array data (such as the Partek Genomic Suite we have used).

The first hint that polypoid and nonpolypoid lesions could have been distinguished based on their expression profile came from the unsupervised analyses we performed (see Figures *9,10,11*). From this analysis, we could also infer that, although the two types of lesions were segregated in different clusters, they were also sharing a large proportion of the gene expression changes (in comparison with the normal mucosa). An in-depth evaluation of the multivariate analyses, as well as of dot plots of single-gene intensity values, revealed that the transcriptome of nonpolypoid lesions, although more similar to that of polypoid lesions, was somehow closer to that of normal mucosa samples. Examples of dot plots emphasizing this phenomenon are reported in **Figure 29**, where an expression

change found to be significantly upregulated in both lesional groups, and another whose upregulation was significant only for the polypoid group, are shown. Of the 2,432 genes found to be significantly dysregulated in precancerous lesions (*p* value <0.001, FDR of 0.001, step-down method), 1,429 were so in the polypoid group and 1,003 in the nonpolypoid group (683 were concomitantly dysregulated in both groups) (see Venn diagram in **Figure 30**). The lower number of genes differentially expressed only in nonpolypoid lesions (320 genes, compared with the 746 genes only dysregulated in polypoid lesions), as well as the fact that genes dysregulated in nonpolypoid lesions were often (68%) dysregulated also in polypoid lesions (compared with 48% of those dysregulated in polypoid lesions), corroborated our observation that up- or downregulations of transcript levels often followed a *normal mucosa* → *nonpolypoid* → *polypoid* sequence (although expression values in nonpolypoid lesions were always closer to that of the cognate, precancerous group of samples).

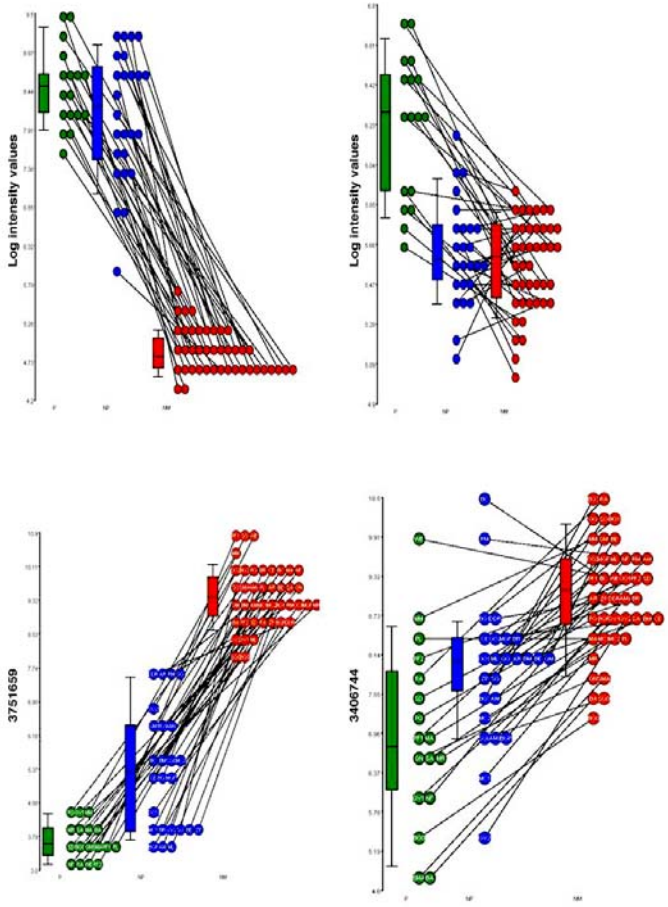

Figure 29. Example of score plots of the expression level of four genes in the three groups of tissues

Example of four score plots showing the general transcriptomic trend observed in the analysis: up- or downregulated genes often follow a *normal mucosa* → *nonpolypoid* → *polypoid* sequence.
The 2 plots in the upper panel show respectively genes found to be significantly upregulated in both groups of lesions, and another whose upregulation was significant only in the polypoid group,
The 2 plots in the lower panel show respectively genes found to be significantly downregulated in both groups of lesions, and another whose downregulation was significant only in the polypoid group. Each dot plots has on the Y axis the log2 expression intensity values and in the X axis the samples groups polypoid (*green* dots), nonpolypoid (*blue* dots) and normal mucosa (*red*, dots).

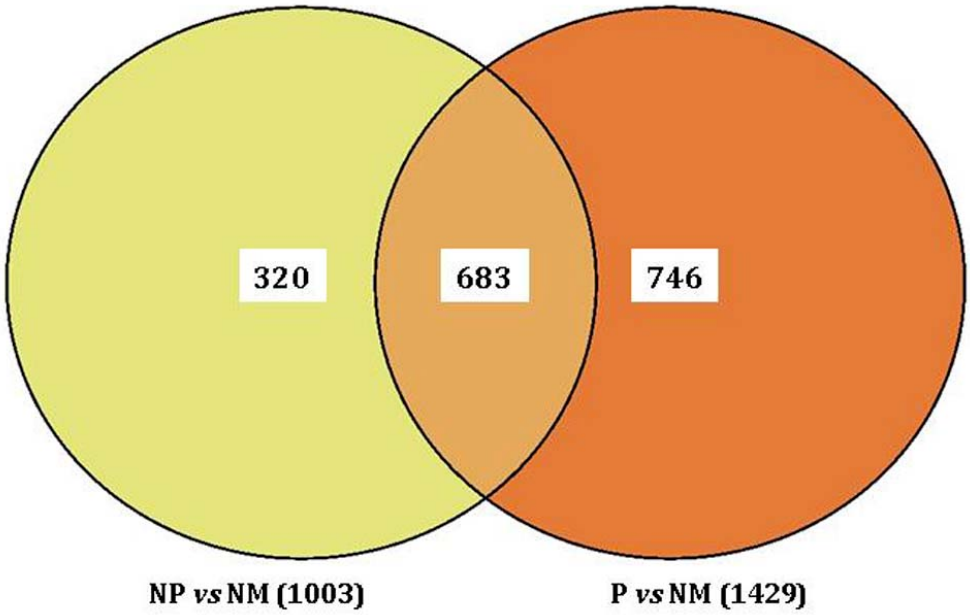

Figure 30. Venn Diagramm illustration of the number of genes differentially and commonly dysregulated in precancerous lesions (compared with normal mucosa).

Intersection of gene lists generated by a pairwise comparison between precancerous lesions and normal mucosa [nonpolypoid (NP) *vs* normal mucosa (NM) and polypoid (P) *vs* normal mucosa (NM)].
2,432 genes were significantly dysregulated in precancerous lesions (*p* value <0.001, FDR of 0.001, step-down method): 1,429 of which in the polypoid group and 1,003 in the nonpolypoid group (683 were concomitantly dysregulated in both groups). The lower number of genes differentially expressed only in nonpolypoid lesions (320 genes, compared with the 746 genes only dysregulated only in polypoid lesions), as well as the fact that genes dysregulated in nonpolypoid lesions were often (68%) dysregulated also in polypoid lesions (compared with 48% of those dysregulated in polypoid lesions), corroborates the observation that up- or downregulations of transcript levels often followed a *normal mucosa → nonpolypoid → polypoid* sequence.

Constrained analysis allowed us to identify, among the clinical and pathological variables considered in the study, those able to explain most of the variation in the original data set. These variables were then classified based on their capacity to segregate the plotted objects (i.e. samples). The most relevant variable was undoubtedly the *tissue type*, accounting for nonpolypoid and polypoid lesions segregation, followed by *histology type* (adenomatous vs serrated), *diameter of the lesions* and the *degree of cytologic dysplasia*. The same variables were subjected to a between group analysis and found to be associated with different gene expression patterns.

From the data discussed so far, it might emerge that nonpolypoid and polypoid lesions do not differ strikingly, in biological terms based on the transcriptome. To certain extent, this was expected, since both precancerous lesions arise and grow in the same organ, likely forced to overcome a series of similar selection pressures in order to advance along the transformation process. However, the Gene Ontology analysis demonstrated that the two types of lesions are far from being identical. By using dedicated software (GeneGO MetaCore), we could pinpoint the *biological pathways* and *process networks* that are most significantly and differentially involved in the pathogenesis of each of the two groups of lesions. The cut-offs we selected for this kind of analysis were a *p* value of 0.05 and an FDR of 0.05 (step-up method) in order to include a large number of gene expression changes in the analysis and thus increase its sensitivity. The lists generated included differentially expressed genes in nonpolypoid or polypoid lesions versus their matched normal mucosa. Differences between the groups of lesions were computed by counting, for each pathway/process, the number of genes found in common and unique for each experiment. The pathways and processes likely involved in the transformation process in each group were identified based on how many genes of those representing each category actually showed a significant expression change (see Figures 16, 17, 18 and Supplementary Table 4 of Appendix*)*.

A striking preponderance of *cell-cycle* related process networks was observed in the polypoid group of lesions (first three statistically significant process networks, Supplementary Table 4 of Appendix). Among the genes involved in these processes, important cell-cycle regulators such as *BUB1, CCNA2, CDC2, CDC14A, CDC6, DSCC1,* and *MCM7*, were up- or downregulated (log fold change higher than 1.7 or lower than -1.7) exclusively in polypoid lesions. The prevalence of cell-cycle processes in polypoid lesions was also confirmed when we examined the biological pathways that were differentially affected between the two groups of lesions. Figure 16 clearly illustrates the overrepresentation of cell-cycle related genes in polypoid lesions. The length of the horizontal blue bars in this figure, which is proportional to the number of uniquely differentially expressed genes in polypoid lesions (compared with normal mucosa samples), was far longer than that of orange

bars (i.e. uniquely differentially expressed genes in nonpolypoid lesions) or striped bars (i.e. commonly dysregulated genes in both groups). Much of the molecular circuitry that enables normal cells to respond to antigrowth signals is associated with the cell-cycle regulation, specifically the components governing the transit of the cell through the G1 phase, which was the most over-represented cell-cycle subcategory in our polypoid lesions. It could be hypothesized therefore that in these lesions the cell-cycle regulation is likely the most important mechanism being severely affected, leading thus to higher proliferation rates. This abnormal function might be preponderant, in polypoid lesions, to many other capabilities usually acquired by transforming cells, such as self sufficiency in growth signals, insensitivity to antigrowth signals, or apoptosis evasion.

In contrast, the differentially affected process networks in nonpolypoid lesions were *cell adhesion_integrin mediated cell matrix adhesion* and two signaling processes, the *reproduction_FSH-beta signaling pathway* and the *inflammation_IL-2 signaling*. We argued thus that nonpolypoid lesions might be characterized by a greater number of dysregulated signaling pathways compared with polypoid lesions. Indeed, among the differentially affected biological pathways (Figure 16), *development_IGF-1 receptor signaling* was found to be more involved in nonpolypoid than polypoid lesions. *IGF-1* receptor signaling pathway is known to confer survival signals advantage to tumor cells[99, 100]. Finally, it was surprising that the *oxidative phosphorylation* pathway was peculiar to nonpolypoid lesions, and that most of the genes involved in this pathway were downregulated in these lesions. Alterations in oxidative phosphorylation resulting from mitochondrial dysfunction have long been hypothesized to be involved in tumorigenesis [101, 102]. Although we relied only on transcritptomic data, we could hypothesize that, downregulation of most of the genes involved in the oxidative phosphorylation, should impair this cellular function. Defects in oxidative phosphorylation have been recently correlated to induction of apoptosis resistance[103]. Severe inhibition of the respiratory chain can suppress the activation of the proapoptotic Bcl-2 proteins Bax and Bak, either of which serves as a near obligate mediator of mitochondrial membrane permeabilization[104].

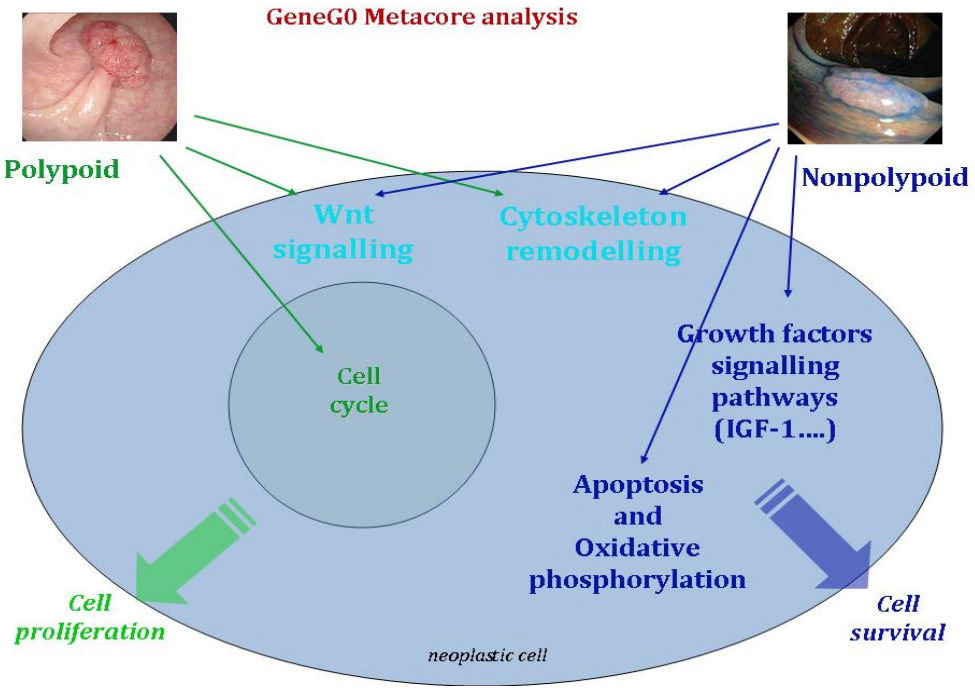

Figure 31. GeneGo MetaCore analysis of the transcriptome of precancerous lesions.

The GeneGo MetaCore analysis highlighted the pathways/process networks significantly represented and differentially affected in the two groups of precancerous lesions, nonpolypoid and polypoid.
The Wnt signaling and the cytoskeleton remodeling were found to be dysregulated in both types of lesions. Cell cycle regulation pathways and processes were overrepresented only in polypoid lesions while growth factors signaling pathways (e.g.IGF-1 signaling) were overrepresented in nonpolypoid lesions, as well as the oxidative phosphorylation pathway.
This analysis pointed out that the propulsion of cell proliferation is achieved differently in the two types of lesions. While polypoid lesions appear to take advantages of a profound dysregulation of the cell cycle, nonpolypoid lesions seem to benefit from modifications in cell survival pathways, presumably through an activation of growth factors signaling pathways and an attenuation of apoptosis.

Therefore, it was tempting to speculate that the two types of lesions differ in how propulsion of cell proliferation is achieved. While polypoid lesions take advantages of a profound dysregulation of the cell cycle, nonpolypoid lesions seem to benefit from modifications in cell survival pathways, presumably through an activation of growth factor signaling pathways and an attenuation of apoptosis (**Figure.31**). A mechanism of apoptosis evasion was also proposed for serrated lesions by Jass J. *et al.*[105] based on the observation that inhibition of anoikis might be the underlying mechanism common to all lesions showing epithelial serration.

Based on their hypothesis, the inhibition of apoptosis could be due either to an epigenetic mechanism in response to tissue injury or to a "neoplasia-like" mechanism involving a mutation of a proto-oncogene as *BRAF* or *KRAS*[106, 107].

Figure 31 also shows the biological processes that are commonly dysregulated in both types of lesions, such as the Wnt signalling and cytoskeleton remodeling. The pathways that were most represented in both groups of lesions were indeed *cytoskeleton remodeling*, *TGF-β, WNT signaling pathway* and *immune response* (Supplementary Table 4). Wnt and TGF- *β* signalling are known to be abnormally dysregulated in the vast majority of colorectal neoplasms[108].

We also analyzed the gene expression changes that might affect the metabolism (Figure 18 and Supplementary Table 4). Briefly, while pathways leading to lipid synthesis were equally represented in both groups, 3 pathways involved in a process of glucose turnover that produces NADPH as reducing equivalents and pentoses as essential part of nucleotides, were more represented in the group of nonpolypoid lesions. Tumor cells must increase their cellular biomass prior to cell division, therefore metabolic changes are necessary to provide tumor cells with sufficient substrates for the biosynthetic machinery. Some of the glycolytic intermediates feed the pentose phosphate pathway leading to the synthesis of ribose-5-phosphate. Oncogenes and tumor suppressor gene products play an important role in diverting glycolytic metabolites into the branches of the penthose phosphate pathway[104, 109]. This observation leads us to speculate that nonpolypoid and polypoid lesions might also differ markedly in their metabolism. However, we believe that the study of the cell metabolism requires the integration of transcriptomics data with the metabolomics ones. In this respect, a project on the metabolome of colorectal neoplasms is in progress in our laboratory.

TMIGD1

We have recently initiated a project for the functional characterization of TMIGD1, a protein with unknown function whose corresponding mRNA was found dramatically downregulated in both nonpolypoid and polypoid lesions. By immunocyto- and immunohistochemistry studies the protein was found to be

expressed in the cytoplasm and the membrane compartment of cells. In the colonic normal mucosa TMIGD1 was expressed in the upper 2/3 of the crypts, were differentiated absorptive cells are located. Interestingly, in the proliferative compartment of the crypts TMIGD1 was completely absent. Similar pattern of expression was observed in the small intestine (terminal ileum) were expression of TMIGD1 was strictly limited to the brush border. The Lieberkühn crypts, which represent the proliferative compartment, did not express the protein. These evidences and the fact that TMIGD1 expression is lost progressively in the process of epithelial cell transformation (from benign neoplasia to cancer), encouraged us to hypothesize TMIGD1 as marker of epithelial differentiation.

We have also been successful to re-express *TMIGD1* in a colon cancer cell line, SW480, devoid of this protein (Figure 24). Interestingly, only a small portion of stably-transfected SW480 cells strongly express TMIGD1, whereas its expression is low or absent in the majority of cells. This finding was associated with a strong immunodetection signal in Western blot. One possibility is that these cells may select for loss of expression of this protein during cellular expansion. This silencing process, whatever its underlying mechanism might be, could be related to our hypothesis that *TMIGD1* may be a marker of cellular differentiation. Therefore, a highly proliferating cancer cell line like SW480 might take advantage by switching off its expression. However, we have seen that the small percentage of *TMIGD1*-positive cells was an early phenotype, present already after few passages of the stably-transfected cells, and it was unchanged after more than 1 month of cellular expansion.

SW480 cell line is known to be constituted of two distinct subpopulations[110], which were designated E-type (i.e. epithelial) and R-type (i.e. round) (**Figure 32**). The majority of SW480 E-type cells, is characterized by adhesive growth to plastic plates and typical cuboidal shape of cells forming epithelial colonies. The less abundant R type cells have rounded morphology, tend to grow as piled up on each other and they are loosely attached to the plate. SW480 cells harbor most of the genetic abnormalities that characterize advanced colon cancers such as activation of *KRAS* oncogene, *CMYC* amplification, deletion of chromosome 18, and mutation of

APC and *p53* tumor suppressor genes. In addition, these cells are defective for E-cadherin and express high levels of nuclear ß-catenin, transforming growth factor and epidermal growth factor receptors[111]. Compared to E-type, isolated R-type cells display decreased doubling time, loss of contact inhibition, less adhesiveness to culture plates and anchorage-independent growth in soft agar, and a much more aneuploid karyotype. All these findings suggest that the R-type cells represent a more malignant variant of the E-type cells.

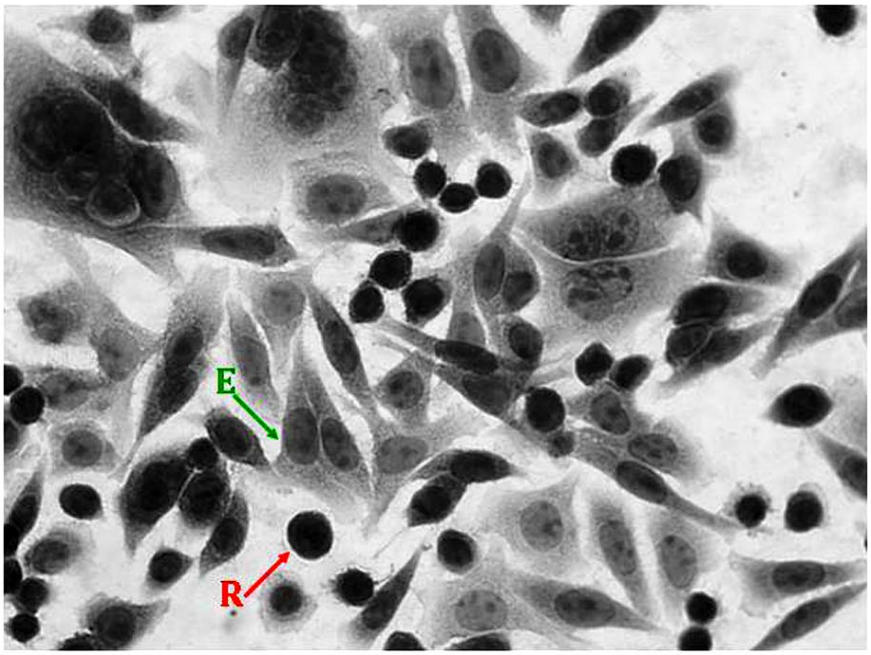

Figure 32. Two distinct subpopulation of the SW480 colorectal cell line

Two subpopulations characterize SW480 colorectal cancercells: Epithelial (E) type cells (green arrow for reference) and Round (R) type cells (red arrow for reference). SW480 E-type cells represent the majority and are characterized by adhesive growth to plastic plates and typical cuboidal shape of cells forming epithelial colonies.
The R type cells, less abundant, have rounded morphology, tend to grow as piled up on each other and they are loosely attached to the plate.

In our ICC experiments, we have seen that our transfected cell line shows a 70% of E-type cells and a 30% of R-type cells (higher percentage compare to data reported in the literature), and that both types of cells are stained (Figure 25) for TMIGD1. More specifically, TMIGD1 was present in the 6.29% of the E-type cells

and in the 2.17% of the R-type cells. E-type cells were characterized by an intense and sharp perinuclear staining with a tendency to temper in a surrounding cytoplasm (Figure 26 A, B), whereas R-type cells, being characterized by a large nucleus and narrow cytoplasm, showed a slightly modified pattern of staining that was mainly concentrated at the plasma membrane and/or widespread in the cytoplasm (Figure 26 C, D). The fact that TMIGD1 was more expressed in E-type cells supported our hypothesis of *TMIGD1* might be a marker of cellular differentiation.

7. PERSPECTIVES

Our data represent the first comprehensive transcriptomics analysis of nonpolypoid and polypoid precancerous colorectal lesions accomplished with the Affymetrix Exon array platform. The results reported in this dissertation regard the expression level of the annotated transcript clusters (corresponding to approximately 23,000 genes). The gene expression analysis will be soon extended to all the predicted exons (an additional 2.5 thousands transcript clusters). This work should reveal additional gene expression changes (including those of noncoding RNAs) that might be exploited for diagnostic, prognostic and therapeutic applications. The Exon array should also allow us to investigate the frequency of alternative splicing events in different tissues. A first attempt to analyze this phenomenon has been made by our collaborators (Drs. Susanne Pedersen, Lawrence LaPointe, Clinical Genomics Pty Ltd , Australia). This analysis has highlighted that exon level gene chip analysis is complicated due to data size, annotations differences between Ensembl and Affymetrix-based databases, and a lack of established bioinformatics tools for these very large data sets. Given the difficulties so far encountered, the analysis will be repeated once more appropriate analytical tools will be available.

A long-term objective is to integrate our transcriptomics data with those that will be generated in a metabolomics study recently initiated in our group. These data, along with other -omics data available in public databases, will ultimately help us to generate a reliable computer replica of different types of colorectal neoplasms.

The functional characterization of *TMIGD1* is another priority in our group. The establishment of an SW480 clone in which the expression of *TMIGD1* will be induced by doxycycline is in progress. This perfectly isogenic cellular system will be an invaluable tool for the analysis of the biological roles of *TMIGD1*. The functional changes resulting from the inducible expression of *TMIGD1* will be monitored with cell proliferation and cell viability assays, as well as methods for analyzing cell migration and invasion.

8. REFERENCES

1. Jemal A, Siegel R, Ward E, Murray T, Xu J, Smigal C, Thun MJ. Cancer statistics, 2006. CA Cancer J Clin 2006;56:106-30.
2. Hermiston ML, Wong MH, Gordon JI. Forced expression of E-cadherin in the mouse intestinal epithelium slows cell migration and provides evidence for nonautonomous regulation of cell fate in a self-renewing system. Genes Dev 1996;10:985-96.
3. Heath JP. Epithelial cell migration in the intestine. Cell Biol Int 1996;20:139-46.
4. Potten CS, Loeffler M. Stem cells: attributes, cycles, spirals, pitfalls and uncertainties. Lessons for and from the crypt. Development 1990;110:1001-20.
5. Marshman E, Booth C, Potten CS. The intestinal epithelial stem cell. Bioessays 2002;24:91-8.
6. Potten CS. Stem cells in gastrointestinal epithelium: numbers, characteristics and death. Philos Trans R Soc Lond B Biol Sci 1998;353:821-30.
7. Bach SP, Renehan AG, Potten CS. Stem cells: the intestinal stem cell as a paradigm. Carcinogenesis 2000;21:469-76.
8. Booth C, Potten CS. Gut instincts: thoughts on intestinal epithelial stem cells. J Clin Invest 2000;105:1493-9.
9. Bjerknes M, Cheng H. Clonal analysis of mouse intestinal epithelial progenitors. Gastroenterology 1999;116:7-14.
10. Raven Press book L. Physiology of the gastrointestinal tract. 1987.
11. Wilkins LW. Text book of Gastroenterology. 1999.
12. Crosnier C, Stamataki D, Lewis J. Organizing cell renewal in the intestine: stem cells, signals and combinatorial control. Nat Rev Genet 2006;7:349-59.
13. Humphries A, Wright NA. Colonic crypt organization and tumorigenesis. Nat Rev Cancer 2008;8:415-24.
14. Ponz de Leon M, Di Gregorio C. Pathology of colorectal cancer. Dig Liver Dis 2001;33:372-88.
15. Takayama T, Katsuki S, Takahashi Y, Ohi M, Nojiri S, Sakamaki S, Kato J, Kogawa K, Miyake H, Niitsu Y. Aberrant crypt foci of the colon as precursors of adenoma and cancer. N Engl J Med 1998;339:1277-84.
16. Winawer SJ. The multidisciplinary management of gastrointestinal cancer. Colorectal cancer screening. Best Pract Res Clin Gastroenterol 2007;21:1031-48.
17. Muto T, Kamiya J, Sawada T, Konishi F, Sugihara K, Kubota Y, Adachi M, Agawa S, Saito Y, Morioka Y, et al. Small "flat adenoma" of the large bowel with special reference to its clinicopathologic features. Dis Colon Rectum 1985;28:847-51.
18. Kudo S, Lambert R, Allen JI, Fujii H, Fujii T, Kashida H, Matsuda T, Mori M, Saito H, Shimoda T, Tanaka S, Watanabe H, Sung JJ, Feld AD, Inadomi JM,

O'Brien MJ, Lieberman DA, Ransohoff DF, Soetikno RM, Triadafilopoulos G, Zauber A, Teixeira CR, Rey JF, Jaramillo E, Rubio CA, Van Gossum A, Jung M, Vieth M, Jass JR, Hurlstone PD. Nonpolypoid neoplastic lesions of the colorectal mucosa. Gastrointest Endosc 2008;68:S3-47.

19. Update on the paris classification of superficial neoplastic lesions in the digestive tract. Endoscopy 2005;37:570-8.
20. Snover DC, Jass JR, Fenoglio-Preiser C, Batts KP. Serrated polyps of the large intestine: a morphologic and molecular review of an evolving concept. Am J Clin Pathol 2005;124:380-91.
21. O'Brien MJ. Hyperplastic and serrated polyps of the colorectum. Gastroenterol Clin North Am 2007;36:947-68, viii.
22. Jass JR, Baker K, Zlobec I, Higuchi T, Barker M, Buchanan D, Young J. Advanced colorectal polyps with the molecular and morphological features of serrated polyps and adenomas: concept of a 'fusion' pathway to colorectal cancer. Histopathology 2006;49:121-31.
23. Carr NJ, Mahajan H, Tan KL, Hawkins NJ, Ward RL. Serrated and non-serrated polyps of the colorectum: their prevalence in an unselected case series and correlation of BRAF mutation analysis with the diagnosis of sessile serrated adenoma. J Clin Pathol 2009;62:516-8.
24. Spring KJ, Zhao ZZ, Karamatic R, Walsh MD, Whitehall VL, Pike T, Simms LA, Young J, James M, Montgomery GW, Appleyard M, Hewett D, Togashi K, Jass JR, Leggett BA. High prevalence of sessile serrated adenomas with BRAF mutations: a prospective study of patients undergoing colonoscopy. Gastroenterology 2006;131:1400-7.
25. Rosenberg DW, Yang S, Pleau DC, Greenspan EJ, Stevens RG, Rajan TV, Heinen CD, Levine J, Zhou Y, O'Brien MJ. Mutations in BRAF and KRAS differentially distinguish serrated versus non-serrated hyperplastic aberrant crypt foci in humans. Cancer Res 2007;67:3551-4.
26. Makinen MJ. Colorectal serrated adenocarcinoma. Histopathology 2007;50:131-50.
27. O'Brien MJ, Yang S, Mack C, Xu H, Huang CS, Mulcahy E, Amorosino M, Farraye FA. Comparison of microsatellite instability, CpG island methylation phenotype, BRAF and KRAS status in serrated polyps and traditional adenomas indicates separate pathways to distinct colorectal carcinoma end points. Am J Surg Pathol 2006;30:1491-501.
28. Hurlstone DP, Cross SS, Adam I, Shorthouse AJ, Brown S, Sanders DS, Lobo AJ. A prospective clinicopathological and endoscopic evaluation of flat and depressed colorectal lesions in the United Kingdom. Am J Gastroenterol 2003;98:2543-9.
29. Oka S, Tanaka S, Hiyama T, Ito M, Kitadai Y, Yoshihara M, Haruma K, Chayama K. Clinicopathologic and endoscopic features of colorectal serrated adenoma: differences between polypoid and superficial types. Gastrointest Endosc 2004;59:213-9.
30. Clevers H. Wnt/beta-catenin signaling in development and disease. Cell 2006;127:469-80.

31. Groden J, Thliveris A, Samowitz W, Carlson M, Gelbert L, Albertsen H, Joslyn G, Stevens J, Spirio L, Robertson M, et al. Identification and characterization of the familial adenomatous polyposis coli gene. Cell 1991;66:589-600.
32. Iwamoto M, Ahnen DJ, Franklin WA, Maltzman TH. Expression of beta-catenin and full-length APC protein in normal and neoplastic colonic tissues. Carcinogenesis 2000;21:1935-40.
33. Powell SM, Zilz N, Beazer-Barclay Y, Bryan TM, Hamilton SR, Thibodeau SN, Vogelstein B, Kinzler KW. APC mutations occur early during colorectal tumorigenesis. Nature 1992;359:235-7.
34. Su LK, Kinzler KW, Vogelstein B, Preisinger AC, Moser AR, Luongo C, Gould KA, Dove WF. Multiple intestinal neoplasia caused by a mutation in the murine homolog of the APC gene. Science 1992;256:668-70.
35. Barker N, Ridgway RA, van Es JH, van de Wetering M, Begthel H, van den Born M, Danenberg E, Clarke AR, Sansom OJ, Clevers H. Crypt stem cells as the cells-of-origin of intestinal cancer. Nature 2009;457:608-11.
36. Zhu L, Gibson P, Currle DS, Tong Y, Richardson RJ, Bayazitov IT, Poppleton H, Zakharenko S, Ellison DW, Gilbertson RJ. Prominin 1 marks intestinal stem cells that are susceptible to neoplastic transformation. Nature 2009;457:603-7.
37. Ilyas M, Tomlinson IP, Rowan A, Pignatelli M, Bodmer WF. Beta-catenin mutations in cell lines established from human colorectal cancers. Proc Natl Acad Sci U S A 1997;94:10330-4.
38. Morin PJ, Sparks AB, Korinek V, Barker N, Clevers H, Vogelstein B, Kinzler KW. Activation of beta-catenin-Tcf signaling in colon cancer by mutations in beta-catenin or APC. Science 1997;275:1787-90.
39. Samowitz WS, Powers MD, Spirio LN, Nollet F, van Roy F, Slattery ML. Beta-catenin mutations are more frequent in small colorectal adenomas than in larger adenomas and invasive carcinomas. Cancer Res 1999;59:1442-4.
40. Suzuki H, Watkins DN, Jair KW, Schuebel KE, Markowitz SD, Chen WD, Pretlow TP, Yang B, Akiyama Y, Van Engeland M, Toyota M, Tokino T, Hinoda Y, Imai K, Herman JG, Baylin SB. Epigenetic inactivation of SFRP genes allows constitutive WNT signaling in colorectal cancer. Nat Genet 2004;36:417-22.
41. Alberici P, Fodde R. The role of the APC tumor suppressor in chromosomal instability. Genome Dyn 2006;1:149-70.
42. Cardoso J, Molenaar L, de Menezes RX, van Leerdam M, Rosenberg C, Moslein G, Sampson J, Morreau H, Boer JM, Fodde R. Chromosomal instability in MYH- and APC-mutant adenomatous polyps. Cancer Res 2006;66:2514-9.
43. Luo L, Li B, Pretlow TP. DNA alterations in human aberrant crypt foci and colon cancers by random primed polymerase chain reaction. Cancer Res 2003;63:6166-9.
44. Sieber OM, Heinimann K, Gorman P, Lamlum H, Crabtree M, Simpson CA, Davies D, Neale K, Hodgson SV, Roylance RR, Phillips RK, Bodmer WF, Tomlinson IP. Analysis of chromosomal instability in human colorectal adenomas with two mutational hits at APC. Proc Natl Acad Sci U S A 2002;99:16910-5.

45. Bartkova J, Rezaei N, Liontos M, Karakaidos P, Kletsas D, Issaeva N, Vassiliou LV, Kolettas E, Niforou K, Zoumpourlis VC, Takaoka M, Nakagawa H, Tort F, Fugger K, Johansson F, Sehested M, Andersen CL, Dyrskjot L, Orntoft T, Lukas J, Kittas C, Helleday T, Halazonetis TD, Bartek J, Gorgoulis VG. Oncogene-induced senescence is part of the tumorigenesis barrier imposed by DNA damage checkpoints. Nature 2006;444:633-7.
46. Raynaud CM, Jang SJ, Nuciforo P, Lantuejoul S, Brambilla E, Mounier N, Olaussen KA, Andre F, Morat L, Sabatier L, Soria JC. Telomere shortening is correlated with the DNA damage response and telomeric protein down-regulation in colorectal preneoplastic lesions. Ann Oncol 2008;19:1875-81.
47. Vogelstein B, Fearon ER, Hamilton SR, Kern SE, Preisinger AC, Leppert M, Nakamura Y, White R, Smits AM, Bos JL. Genetic alterations during colorectal-tumor development. N Engl J Med 1988;319:525-32.
48. Wood LD, Parsons DW, Jones S, Lin J, Sjoblom T, Leary RJ, Shen D, Boca SM, Barber T, Ptak J, Silliman N, Szabo S, Dezso Z, Ustyanksky V, Nikolskaya T, Nikolsky Y, Karchin R, Wilson PA, Kaminker JS, Zhang Z, Croshaw R, Willis J, Dawson D, Shipitsin M, Willson JK, Sukumar S, Polyak K, Park BH, Pethiyagoda CL, Pant PV, Ballinger DG, Sparks AB, Hartigan J, Smith DR, Suh E, Papadopoulos N, Buckhaults P, Markowitz SD, Parmigiani G, Kinzler KW, Velculescu VE, Vogelstein B. The genomic landscapes of human breast and colorectal cancers. Science 2007;318:1108-13.
49. Chan TL, Zhao W, Leung SY, Yuen ST. BRAF and KRAS mutations in colorectal hyperplastic polyps and serrated adenomas. Cancer Res 2003;63:4878-81.
50. Goel A, Nagasaka T, Arnold CN, Inoue T, Hamilton C, Niedzwiecki D, Compton C, Mayer RJ, Goldberg R, Bertagnolli MM, Boland CR. The CpG island methylator phenotype and chromosomal instability are inversely correlated in sporadic colorectal cancer. Gastroenterology 2007;132:127-38.
51. Kambara T, Simms LA, Whitehall VL, Spring KJ, Wynter CV, Walsh MD, Barker MA, Arnold S, McGivern A, Matsubara N, Tanaka N, Higuchi T, Young J, Jass JR, Leggett BA. BRAF mutation is associated with DNA methylation in serrated polyps and cancers of the colorectum. Gut 2004;53:1137-44.
52. Menigatti M, Truninger K, Gebbers JO, Marbet U, Marra G, Schar P. Normal colorectal mucosa exhibits sex- and segment-specific susceptibility to DNA methylation at the hMLH1 and MGMT promoters. Oncogene 2009;28:899-909.
53. Nosho K, Irahara N, Shima K, Kure S, Kirkner GJ, Schernhammer ES, Hazra A, Hunter DJ, Quackenbush J, Spiegelman D, Giovannucci EL, Fuchs CS, Ogino S. Comprehensive biostatistical analysis of CpG island methylator phenotype in colorectal cancer using a large population-based sample. PLoS One 2008;3:e3698.
54. O'Brien MJ, Yang S, Clebanoff JL, Mulcahy E, Farraye FA, Amorosino M, Swan N. Hyperplastic (serrated) polyps of the colorectum: relationship of CpG island methylator phenotype and K-ras mutation to location and histologic subtype. Am J Surg Pathol 2004;28:423-34.

55. Toyota M, Ahuja N, Ohe-Toyota M, Herman JG, Baylin SB, Issa JP. CpG island methylator phenotype in colorectal cancer. Proc Natl Acad Sci U S A 1999;96:8681-6.
56. Weisenberger DJ, Siegmund KD, Campan M, Young J, Long TI, Faasse MA, Kang GH, Widschwendter M, Weener D, Buchanan D, Koh H, Simms L, Barker M, Leggett B, Levine J, Kim M, French AJ, Thibodeau SN, Jass J, Haile R, Laird PW. CpG island methylator phenotype underlies sporadic microsatellite instability and is tightly associated with BRAF mutation in colorectal cancer. Nat Genet 2006;38:787-93.
57. Samowitz WS, Albertsen H, Sweeney C, Herrick J, Caan BJ, Anderson KE, Wolff RK, Slattery ML. Association of smoking, CpG island methylator phenotype, and V600E BRAF mutations in colon cancer. J Natl Cancer Inst 2006;98:1731-8.
58. Laiho P, Kokko A, Vanharanta S, Salovaara R, Sammalkorpi H, Jarvinen H, Mecklin JP, Karttunen TJ, Tuppurainen K, Davalos V, Schwartz S, Jr., Arango D, Makinen MJ, Aaltonen LA. Serrated carcinomas form a subclass of colorectal cancer with distinct molecular basis. Oncogene 2007;26:312-20.
59. Lee SH, Kim J, Kim WH, Lee YM. Hypoxic silencing of tumor suppressor RUNX3 by histone modification in gastric cancer cells. Oncogene 2009;28:184-94.
60. di Pietro M, Sabates Bellver J, Menigatti M, Bannwart F, Schnider A, Russell A, Truninger K, Jiricny J, Marra G. Defective DNA mismatch repair determines a characteristic transcriptional profile in proximal colon cancers. Gastroenterology 2005;129:1047-59.
61. Sabates-Bellver J, Van der Flier LG, de Palo M, Cattaneo E, Maake C, Rehrauer H, Laczko E, Kurowski MA, Bujnicki JM, Menigatti M, Luz J, Ranalli TV, Gomes V, Pastorelli A, Faggiani R, Anti M, Jiricny J, Clevers H, Marra G. Transcriptome profile of human colorectal adenomas. Mol Cancer Res 2007;5:1263-75.
62. Fuchs CS, Giovannucci EL, Colditz GA, Hunter DJ, Speizer FE, Willett WC. A prospective study of family history and the risk of colorectal cancer. N Engl J Med 1994;331:1669-74.
63. Hendriks YM, de Jong AE, Morreau H, Tops CM, Vasen HF, Wijnen JT, Breuning MH, Brocker-Vriends AH. Diagnostic approach and management of Lynch syndrome (hereditary nonpolyposis colorectal carcinoma): a guide for clinicians. CA Cancer J Clin 2006;56:213-25.
64. Bussey H. Familial Polyposis Coli. Baltimore:Johns Hopkins University Press 1975.
65. Cannon-Albright LA, Skolnick MH, Bishop DT, Lee RG, Burt RW. Common inheritance of susceptibility to colonic adenomatous polyps and associated colorectal cancers. N Engl J Med 1988;319:533-7.
66. Burt RW. World Health Organization classification of tumors.Pathology & genetics. Tumors of the digestive system. 2000:135-136.
67. Ferrandez A, Samowitz W, DiSario JA, Burt RW. Phenotypic characteristics and risk of cancer development in hyperplastic polyposis: case series and literature review. Am J Gastroenterol 2004;99:2012-8.

68. Jass JR. Familial colorectal cancer: pathology and molecular characteristics. Lancet Oncol 2000;1:220-6.
69. Lage P, Cravo M, Sousa R, Chaves P, Salazar M, Fonseca R, Claro I, Suspiro A, Rodrigues P, Raposo H, Fidalgo P, Nobre-Leitao C. Management of Portuguese patients with hyperplastic polyposis and screening of at-risk first-degree relatives: a contribution for future guidelines based on a clinical study. Am J Gastroenterol 2004;99:1779-84.
70. Torlakovic E, Snover DC. Sessile serrated adenoma: a brief history and current status. Crit Rev Oncog 2006;12:27-39.
71. Beach R, Chan AO, Wu TT, White JA, Morris JS, Lunagomez S, Broaddus RR, Issa JP, Hamilton SR, Rashid A. BRAF mutations in aberrant crypt foci and hyperplastic polyposis. Am J Pathol 2005;166:1069-75.
72. Jass JR. Colorectal polyposes: from phenotype to diagnosis. Pathol Res Pract 2008;204:431-47.
73. Minoo P, Baker K, Goswami R, Chong G, Foulkes WD, Ruszkiewicz AR, Barker M, Buchanan D, Young J, Jass JR. Extensive DNA methylation in normal colorectal mucosa in hyperplastic polyposis. Gut 2006;55:1467-74.
74. Young J, Jass JR. The case for a genetic predisposition to serrated neoplasia in the colorectum: hypothesis and review of the literature. Cancer Epidemiol Biomarkers Prev 2006;15:1778-84.
75. Peitz U, Malfertheiner P. Chromoendoscopy: from a research tool to clinical progress. Dig Dis 2002;20:111-9.
76. The Paris endoscopic classification of superficial neoplastic lesions: esophagus, stomach, and colon: November 30 to December 1, 2002. Gastrointest Endosc 2003;58:S3-43.
77. Affymetrix. Exon Array probe annotations. http://www.affymetrix.com/support/technical/whitepapers/exon_probeset_trans_clust_whitepaper.pdf.
78. Affymetrix Exon array background correction. Affymetrix Whitepaper. available: http://www.affymetrix.com/support/technical/whitepapers/exon_background_correction_whitepaper.pdf. Accessed 10 December 2007. 2005.
79. Irizarry RA, Hobbs B, Collin F, Beazer-Barclay YD, Antonellis KJ, Scherf U, Speed TP. Exploration, normalization, and summaries of high density oligonucleotide array probe level data. Biostatistics 2003;4:249-64.
80. Quinn G.P. KMJ. Experimental Design and Data Analysis for Biologists. Cambridge University Press 2006.
81. Fujimoto K, Beauchamp RD, Whitehead RH. Identification and isolation of candidate human colonic clonogenic cells based on cell surface integrin expression. Gastroenterology 2002;123:1941-8.
82. Bradford. Anal. Biochem, 1976;72:248.
83. Benjamini Y, Hochberg, Y. On the adaptive control of the false discovery rate in multiple testing with independent statistics. J. Behav. Educ. Statist 1999.
84. Benjamini Y, Hochberg, Y. Controlling the false discovery rate { a new and powerful approach to multiple testing. J. Roy. Statist. Soc. Ser. 1995.

85. Longacre TA, Fenoglio-Preiser CM. Mixed hyperplastic adenomatous polyps/serrated adenomas. A distinct form of colorectal neoplasia. Am J Surg Pathol 1990;14:524-37.
86. Torlakovic E, Snover DC. Serrated adenomatous polyposis in humans. Gastroenterology 1996;110:748-55.
87. Farris AB, Misdraji J, Srivastava A, Muzikansky A, Deshpande V, Lauwers GY, Mino-Kenudson M. Sessile serrated adenoma: challenging discrimination from other serrated colonic polyps. Am J Surg Pathol 2008;32:30-5.
88. Davies H, Bignell GR, Cox C, Stephens P, Edkins S, Clegg S, Teague J, Woffendin H, Garnett MJ, Bottomley W, Davis N, Dicks E, Ewing R, Floyd Y, Gray K, Hall S, Hawes R, Hughes J, Kosmidou V, Menzies A, Mould C, Parker A, Stevens C, Watt S, Hooper S, Wilson R, Jayatilake H, Gusterson BA, Cooper C, Shipley J, Hargrave D, Pritchard-Jones K, Maitland N, Chenevix-Trench G, Riggins GJ, Bigner DD, Palmieri G, Cossu A, Flanagan A, Nicholson A, Ho JW, Leung SY, Yuen ST, Weber BL, Seigler HF, Darrow TL, Paterson H, Marais R, Marshall CJ, Wooster R, Stratton MR, Futreal PA. Mutations of the BRAF gene in human cancer. Nature 2002;417:949-54.
89. Rajagopalan H, Bardelli A, Lengauer C, Kinzler KW, Vogelstein B, Velculescu VE. Tumorigenesis: RAF/RAS oncogenes and mismatch-repair status. Nature 2002;418:934.
90. Sandmeier D, Benhattar J, Martin P, Bouzourene H. Serrated polyps of the large intestine: a molecular study comparing sessile serrated adenomas and hyperplastic polyps. Histopathology 2009;55:206-13.
91. Sawyer EJ, Cerar A, Hanby AM, Gorman P, Arends M, Talbot IC, Tomlinson IP. Molecular characteristics of serrated adenomas of the colorectum. Gut 2002;51:200-6.
92. Notterman DA, Alon U, Sierk AJ, Levine AJ. Transcriptional gene expression profiles of colorectal adenoma, adenocarcinoma, and normal tissue examined by oligonucleotide arrays. Cancer Res 2001;61:3124-30.
93. Agrawal D, Chen T, Irby R, Quackenbush J, Chambers AF, Szabo M, Cantor A, Coppola D, Yeatman TJ. Osteopontin identified as lead marker of colon cancer progression, using pooled sample expression profiling. J Natl Cancer Inst 2002;94:513-21.
94. Lin YM, Furukawa Y, Tsunoda T, Yue CT, Yang KC, Nakamura Y. Molecular diagnosis of colorectal tumors by expression profiles of 50 genes expressed differentially in adenomas and carcinomas. Oncogene 2002;21:4120-8.
95. Williams NS, Gaynor RB, Scoggin S, Verma U, Gokaslan T, Simmang C, Fleming J, Tavana D, Frenkel E, Becerra C. Identification and validation of genes involved in the pathogenesis of colorectal cancer using cDNA microarrays and RNA interference. Clin Cancer Res 2003;9:931-46.
96. Nosho K, Yamamoto H, Adachi Y, Endo T, Hinoda Y, Imai K. Gene expression profiling of colorectal adenomas and early invasive carcinomas by cDNA array analysis. Br J Cancer 2005;92:1193-200.
97. Robinson MD, Speed TP. A comparison of Affymetrix gene expression arrays. BMC Bioinformatics 2007;8:449.

98. Okoniewski MJ, Hey Y, Pepper SD, Miller CJ. High correspondence between Affymetrix exon and standard expression arrays. Biotechniques 2007;42:181-5.
99. Hanahan D, Weinberg RA. The hallmarks of cancer. Cell 2000;100:57-70.
100. Samani AA, Yakar S, LeRoith D, Brodt P. The role of the IGF system in cancer growth and metastasis: overview and recent insights. Endocr Rev 2007;28:20-47.
101. Vander Heiden MG, Cantley LC, Thompson CB. Understanding the Warburg effect: the metabolic requirements of cell proliferation. Science 2009;324:1029-33.
102. Pathania D, Millard M, Neamati N. Opportunities in discovery and delivery of anticancer drugs targeting mitochondria and cancer cell metabolism. Adv Drug Deliv Rev 2009.
103. Tomiyama A, Serizawa S, Tachibana K, Sakurada K, Samejima H, Kuchino Y, Kitanaka C. Critical role for mitochondrial oxidative phosphorylation in the activation of tumor suppressors Bax and Bak. J Natl Cancer Inst 2006;98:1462-73.
104. Kroemer G, Pouyssegur J. Tumor cell metabolism: cancer's Achilles' heel. Cancer Cell 2008;13:472-82.
105. Higuchi T, Jass JR. My approach to serrated polyps of the colorectum. J Clin Pathol 2004;57:682-6.
106. Cardone MH, Roy N, Stennicke HR, Salvesen GS, Franke TF, Stanbridge E, Frisch S, Reed JC. Regulation of cell death protease caspase-9 by phosphorylation. Science 1998;282:1318-21.
107. Datta SR, Dudek H, Tao X, Masters S, Fu H, Gotoh Y, Greenberg ME. Akt phosphorylation of BAD couples survival signals to the cell-intrinsic death machinery. Cell 1997;91:231-41.
108. Elliott RL, Blobe GC. Role of transforming growth factor Beta in human cancer. J Clin Oncol 2005;23:2078-93.
109. DeBerardinis RJ, Lum JJ, Hatzivassiliou G, Thompson CB. The biology of cancer: metabolic reprogramming fuels cell growth and proliferation. Cell Metab 2008;7:11-20.
110. Tomita N, Jiang W, Hibshoosh H, Warburton D, Kahn SM, Weinstein IB. Isolation and characterization of a highly malignant variant of the SW480 human colon cancer cell line. Cancer Res 1992;52:6840-7.
111. Palmer HG, Gonzalez-Sancho JM, Espada J, Berciano MT, Puig I, Baulida J, Quintanilla M, Cano A, de Herreros AG, Lafarga M, Munoz A. Vitamin D(3) promotes the differentiation of colon carcinoma cells by the induction of E-cadherin and the inhibition of beta-catenin signaling. J Cell Biol 2001;154:369-87.

9. ACKNOWLEDGEMENTS

I would like to especially thank Prof. Jiricny for giving me the possibility of doing the PhD in his Institute and for the stimulating and optimistic discussions about translational research!
A very special thank to his wife, Anne, for being such a good English teacher and for making me always so comfortable since the beginning.

I would like to thank "the boss", Dr. Marra, for his extraordinary patience in teaching, and for showing me always enthusiasm and dedication to the field of research.

I would like to thank Prof. Verrey for his constant interest in my project and for his helpful advices. I would like also to thank some of his lab members, in particular Simone and Raphael for spending time teaching me many techniques and for being such a nice people with me.

I would like to thank and recognize the contribution to this work done by all our collaborators.

A special thank to all my lab mates, in particular to Jacob and Emiljia for all their help (especially at the beginning!) and constant support. Emanuele, Amit and Mirco for scientific support but mostly for creating a relaxing and joyful atmosphere in the lab.

Thank to all technical assistants in the institute: Conny, Christine, Christiane, Ester, Christoph, Malika, Farah, and Peter Binz, for their efficient work.
A special thank to Ippa for being always helpful and smiling.

Thank to the members of the FGCZ, especially Andrea for the microarray technical assistance and Endre for being so patient in explaining the unknown (to me!) world of statistics, mathematics and bioinformatics.

My sincere gratitude to all the members of the institute, in particular, to my friends Dennis and Medini for the fruitful scientific discussions (came along with good beer(s)!), Silvi, Esther and Isabella for their special friendship in and out of the lab!

A special GRAZIE to my best friend Paolo for being always present in all these years and able to suggest me at the right moment, the right thing to do.
GRAZIE to all my friends in Italy…but especially to Miri & family, Cri, French and Andre.

GRAZIE to my parents and especially to my brothers, Marco, Andrea and Francesco who have contributed to reach this further goal.

10. CURRICULUM VITAE

SURNAME: CATTANEO

NAME: Elisa

DATE of BIRTH: May 26, 1978

PLACE of BIRTH: Como, Italy

NATIONALITY: Italian

EDUCATION:		DEGREE:
1992-1997	Liceo Scientifico "Paolo Giovio" Como	Maturita' Scientifica
1997-2004	Universita' degli Studi di Milano Facoltà di Medicina e Chirurgia	M.D.
2005	General Practioner Internership	Licensure: July 2005 (Licenced to practice in Italy)

CLINICAL TRAINING

2003-2005:
Attending student, Dept. of Gastroenterology, Istituto Clinico Humanitas, Milan.
In-patient evaluation focused on basic training in Internal Medicine.

RESEARCH TRAINING

2004-2005:
Istituto Clinico Humanitas, Milan. Mentor: Dr. Alberto Malesci. Tutor: Dr. Luigi Laghi. "*Prevalence of K-RAS mutations in sporadic and hereditary colorectal cancers with mismatch repair defects".*

Since September 2005:
MD/Ph.D. student at the Institute of Molecular Cancer Research, University of Zurich
Director: Prof. J.Jiricny; Tutor: Dr. G.Marra
Research project: "*The transcriptomic profiling of human colorectal precancerous lesions*".

PUBLICATIONS

1) Sabates-Bellver J., Cattaneo E., Heinimann K., Jiricny J., and Marra G.
"Getting familiar with familial colon cancer." Chapter in the Falk Symposium 158 book "Intestinal Inflammation and colorectal Cancer", 2007

2) Sabates-Bellver J.,Laurens G. Van der Flier, Mariagrazia de Palo, Elisa Cattaneo, Caroline Maake, Hubert Rehrauer, Endre Laczko, Michal A. Kurowski, Janusz M. Bujnicki, Mirco Menigatti, Judith Luz, Teresa V. Ranalli, Vito Gomes, Alfredo Pastorelli, Roberto Faggiani, Marcello Anti, Josef Jiricny, Hans Clevers, and Giancarlo Marra.
"Transcriptome profiling of human colorectal adenomas identifies a novel biomarker of ephitelial transformation". *Molecular Cancer Research 2007*, 5: 1263-75.

3) Luigi Laghi, Paolo Bianchi, Andrea Zecchini, Elisa Cattaneo, Jacob Sabates-Bellver, Katia Villa, Alessandro Repici, Massimo Roncalli, Giancarlo Marra, Alberto Malesci.
"Expression of Twist1 in colo-rectal tumors correlates with malignant transformation, local invasion and metastases at diagnosis" (submitted for the American Gastroenterological Association meeting, May 2007).

4) Elisa Cattaneo, Endre Laczko, J. Sabates-Bellver, Alberto Malesci, Luigi Laghi and G. Marra.
"The SPDEF transcription factor is a putative determinant of the mucinous phenotype in colorectal cancer" (submitted for the Digestive Disease Week meeting, May 2009)

5) E. Cattaneo, E. Laczko, F. Buffoli, F. Zorzi, M.A. Bianco, L. Laghi, J. Sabates-Bellver, J. Jiricny, and G. Marra.
"The transcriptome of nonpolypoid colorectal lesions" (submitted for the Charles Rodolphe Brupbacher Symposium, February 2009).

6) Elisa Cattaneo, Michael Baudis, Federico Buffoli, Maria Antonia Bianco, Fausto Zorzi, , and Giancarlo Marra. "Pathways and crossroads to colorectal cancer". In *Advances in understanding the basic pathogenesis and clinical management of pre-invasive disease*. Edited by Fitzegerald R., 2009, in press

11. APPENDIXES

11.1 Supplementary data

Supplementary Table 1.

Molecular characteristics of 25 nonpolypoid lesions included in the study

Patient	Microscopic appearance	Highest degree of dysplasia in the lesion ▪	hMLH1 IHC	*BRAF*status (exon 15)	*KRas* status (exon 2:codons 12 and 13)
AM(1) *	VA	HGD	POS	wt	Gly12Cys
AM(2) *	VA	HGD	POS	wt	wt
BG(1) *	TA	LGD	POS	wt	Gly12Val
BG(2) *	TA	LGD	POS	wt	Gly13Asp
GG	TA	HGD	POS	wt	wt
CE	SA (mixed)	HGD	POS	mut (V600E)	wt
BE	TA	LGD	POS	wt	wt
BR	TA	LGD	POS	wt	Gly12Val
GM	TA	LGD	POS	wt	Gly12Asp
MGF	TA	LGD	POS	wt	Gly12Asp
ML	TVA	LGD	POS	wt	Gly12Asp
SG	TA	LGD	POS	wt	Gly13Asp
ZP	TA	HGD	POS	wt	wt
AR	TVA	HGD	POS	wt	wt
OO(1) *	TVA	LGD	POS	wt	Gly12Cys
OO(2) *	TA	LGD	POS	wt	wt
BGP	TVA	LGD	POS	wt	Gly12Ala
SG	SA (mixed)	LGD	POS	wt	wt
RM	SSA	no dysplasia	POS	mut (V600E)	wt
MC(1) *	TA	HGD	POS	wt	wt
MC(2) *	TA	LGD	POS	wt	wt
BM	TA	LGD	POS	wt	Gly12Ala
GV(2) *	VA	LGD	POS	wt	wt
BC	MVSP	no dysplasia	POS	mut (V600E)	wt
DDR	MVSP	no dysplasia	POS	wt	Gly12Asp

Abbreviations: IHC, immunohistochemistry;TA, tubular adenoma; TVA, tubulovillous adenoma; VA, villous adenoma; MVSP, microvesicular serrated polyp; SA, serrated adenoma; SSA, sessile serrated adenoma; LGD, low-grade dysplasia; HGD, high-grade dysplasia. POS, positive; wt, wild-type; mut, mutated; Gly, glycine; Cys, cysteine; Val, valine;Asp, aspartate; Ala, alanine; V600E, valine to glutamate substitution at codon 600.

▪ Low-grade versus high-grade dysplasia as defined by the WHO classification of tumors of the digestive system, editorial and consensus conference in Lyon, France, November 6-9, 1999.IARC

*****Two lesions from these patients were analyzed

Supplememtary table 2.

Selection (top hundred) of genes whose expression displays significant association with variables as *tissue type* (nonpolypoid *vs* polypoid), *histology type* (adenomatous *vs* serrated), *diameter size* (small *vs* large), and *degree* of *dysplasia* (no dysplasia *vs* low and high). Genes ranking based on their highest positive or negative score on between group analysis axes 1 or 2.

	Tissue type (nonpolypoid *vs* polypoid)				**Histology type (adenomatous vs serrated)**			
	highest positive score on axis 1		**highest negative score on axis 1**		**highest positive score on axis 1**		**highest negative score on axis 1**	
	Transcript ID	Gene Symbol	Transcript ID	Gene Symbol	Transcript ID	Gene Symbol	Transcript ID	Gene Symbol
1	3452417	SLC38A4	2345061	CLCA4	3638607	ANPEP	2620937	TDGF1
2	3388807	MMP1	3751859	TMIGD1	3751859	TMIGD1	3421118	RAP1B
3	3175971	PSAT1	2584113	GCG	2345061	CLCA4	2345023	CLCA1
4	2659393	OSTalpha	3067250	SLC26A3	2647315	TM4SF4	3453732	TUBA1B
5	3360401	HBB	2733483	BMP3	3016070	MUC17	2477438	QPCT
6	3720896	CDC6	2703750	SI	2408832	GUCA2A	3452417	SLC38A4
7	3504369	LOC729680	3332424	MS4A12	3921490	B3GALT5	3235663	LOC283070
8	3490892	OLFM4	3090294	ADAMDEC1	2584113	GCG	3422144	LGR5
9	2319340	SLC25A33	3142967	CA1	3986647	VSIG1	2849592	RBBP4
10	4036196		3365203	TPH1	3067250	SLC26A3	3122703	DEFA6
11	2761829	FGFBP1	3928415	CLDN8	2703750	SI	3255284	C10orf99
12	3129149	PBK	2417008	INSL5	2324084	CDA	3856612	ZNF43
13	3504367	LOC729680	2531908	B3GNT7	3933559	TFF1	2561216	REG3A
14	3690154	NETO2	3210013	TRPM6	2898986	SLC17A4	3540074	AKAP5
15	3388830	MMP3	3890640	PCK1	3655621	ZG16	3490892	OLFM4
16	3401786	C12orf5	3165025	RP11-145E5.4	2751009	ANXA10	2507928	HNMT
17	3783788	MEP1B	3237282	FAM23A	2794408	HPGD	2505419	NOC2L
18	2833691	KCTD16	2408832	GUCA2A	2584018	DPP4	3183206	SLC44A1
19	3843677	NAG18	3063501	CYP3A4	3596147	GCNT3	2565935	ANKRD36B
20	3292694	DNA2	2730746	SLC4A4	3461883	PTPRR	2941972	C6orf105
21	3258966	CYP2C18	3204285	CCL19	2570193	MALL	3137875	GGH
22	3670663	CENPN	2732508	CXCL13	2777276	ABCG2	3023803	
23	3168508	MELK	3549092	CHGA	2974592	VNN1	2872958	MGC32805
24	3541383	ARG2	2709750	SST	3063501	CYP3A4	3875908	PLCB4
25	2327373	LOC100129624	2779231	ADH1B	2412624	RAB3B	2880422	SPINK1
26	3852565	ASF1B	3204301	CCL21	2514304	DHRS9	3249978	STOX1
27	3058944	HGF	2855285	SEPP1	3598267	OSTbeta	2339334	L1TD1
28	2333136	CDC20	2898986	SLC17A4	2633737	GPR128	3181417	ANP32B
29	2575949	TUBA3E	3932397	C21orf88	3114512	FER1L6	3540079	AKAP5
30	3166815	SPINK4	2440413	ITLN1	3142967	CA1	2561182	REG1B
31	3248289	CDC2	3059667	SEMA3D	3218077	ALDOB	3392091	FAM55D
32	3880827	GINS1	2835300	SLC26A2	2602304	TM4SF20	4013422	PGAM4
33	3128731	PNMA2	3921490	B3GALT5	3421824	C12orf28	2402991	CHCHD3

34	2378937	DTL	3662150	MT1M	2730746	SLC4A4	3767480	AXIN2
35	2469252	RRM2	3758775	PYY	3090294	ADAMDEC1	3210616	PRUNE2
36	3011838	STEAP1	3863214	CEACAM7	3758775	PYY	2319340	SLC25A33
37	3104758	RPSA	3982612	GPR174	3028164	LOC100124692	3389353	CASP1
38	3607510	FANCI	3237280	FAM23A	3734517	OTOP2	3504369	LOC729680
39	3249533	AKR1B10	3105600	CA2	2842624	PCDH24	2847967	SEMA5A
40	3629103	KIAA0101	3323748	TMEM16E	3321361	SPON1	3498476	UNQ1829
41	3527514	NP	2945882	CMAH	2844888	BTNL3	3253438	RPS24
42	3703885	SLC7A5	2432336	LOC727820	3114477	FER1L6	3299467	ANKRD22
43	3388785	MMP10	2598261	FN1	3405748	EMP1	2704996	SKIL
44	2339334	L1TD1	2700244	CP	3863214	CEACAM7	3401786	C12orf5
45	3485074	RFC3	3593931	GLDN	3365203	TPH1	3169331	ALDH1B1
46	3944129	HMOX1	3333899	RARRES3	2909263	MEP1A	3292590	PBLD
47	3725572	B4GALNT2	3960174	LGALS2	3549092	CHGA	2726542	FLJ21511
48	3527785	SLC39A2	2854088	LIFR	2559637	NAT8B	2783715	MAD2L1
49	3331903	FAM111B	3522327	SLC15A1	3165025	RP11-145E5.4	3521816	OXGR1
50	2783715	MAD2L1	3662201	MT1H	2899012	SLC17A4	2375893	SNRPE
51	2354433	HSD3B2	3652902	SCNN1B	3783788	MEP1B	3351525	LOC100131323
52	3721926	TUBG1	2584018	DPP4	3316600	MUC2	2688049	RETNLB
53	2527253	IGFBP2	2772088	UGT2B17	3160658	SLC1A1	3195971	CBWD1
54	3747399	KRT14	2372858	RGS2	2662435	CIDECP	3369249	APIP
55	3324447	FIBIN	3848039	C3	2372858	RGS2	2951078	RPL35
56	3797543	FLJ38028	2377283	CR2	3114443	FER1L6	3690154	NETO2
57	2388219	EXO1	3443868	CD69	3475324	RHOF	3135567	LYPLA1
58	2354634	PHGDH	2940202	F13A1	2775909	PLAC8	2828135	LYRM7
59	3696666	NQO1	3681488	PLA2G10	3443226	MFAP5	3975431	RPSA
60	3800245	TERF1	3321361	SPON1	2498911	SULT1C2	3512948	C13orf18
61	3516443	FLJ25694	2374126	NR5A2	3756566	KRT20	2651835	GPR160
62	3587457	ARHGAP11A	2779271	ADH1C	2590491	NEUROD1	3124972	KIAA0484
63	2548699	CYP1B1	2373336	CFH	3105600	CA2	2457691	TLR5
64	3703112	GINS2	3761538	HOXB13	3980614	GDPD2	3409317	REP15
65	2673085	CDC25A	2356425	PDZK1	3890640	PCK1	2781592	RBMXP4
66	3772158	TK1	3592304	SLC28A2	3376512	HRASLS2	4042278	MMP23A
67	3122984	SPAG11B	3617574	GOLGA8B	3693141	PLLP	3807487	RPL17
68	3318052		2372781	RGS1	3175274	PCSK5	2435005	SELENBP1
69	2500919	SLC20A1	3450655	CPNE8	3448088	BHLHB3	3314040	BNIP3
70	3357397	GLB1L2	2925590	TMEM200A	2717481	MGC10981	3977646	GSPT2
71	3377423	CDCA5	3332465	MS4A8B	3028184	LOC100124692	3315675	IFITM1
72	3936913	CDC45L	2865390	EDIL3	2496907	IL1R2	2842561	HIGD2A
73	3023803		3811000	RNF152	2733483	BMP3	3076489	MRPS33
74	3689880	RAB43	2400027	PLA2G2A	4054128	LOC100132488	3348911	SDHD
75	2540157	ODC1	2974592	VNN1	2997674	LOC641963	2999664	LOC222070
76	3299469	ANKRD22	3598267	OSTbeta	3028120	LOC93432	4014029	RPS6KA6
77	3216671	CTSL2	3031517	GIMAP7	2409820	BEST4	3360401	HBB
78	3186123	ORM1	3142217	PAG1	2359492	SPRR1A	2649609	MLF1
79	3474831	OASL	2373842	PTPRC	2996970	LOC401324	2785685	LOC646187
80	3590086	RAD51	3655621	ZG16	3811000	RNF152	3986623	LOC286440
81	3178583	CKS2	2565935	ANKRD36B	4016319	NXF3	3711806	MEIS3P1
82	2997376	ANLN	2337740	PRKAA2	2709750	SST	3399623	THYN1
83	2947073	HIST1H1B	2806468	IL7R	2671936	SLC6A20	3666873	NFAT5

84	3477610		3351300	CD3G	3522912	ZIC5	3981735	LOC554203
85	3228545	OBP2B	3587553	GREM1	3332424	MS4A12	2860666	TAF9
86	3080280	XRCC2	3729419	CA4	3142217	PAG1	3304970	SH3PXD2A
87	3593575	SLC27A2	2554018	EFEMP1	2401251	HTR1D	3519840	SLITRK6
88	3758317	BRCA1	3061438	SAMD9	3907556	FLJ40606	3388673	MMP7
89	3122703	DEFA6	2635741	CD96	2501204	IL1RN	3733065	MAP2K6
90	3886223	MYBL2	3061484	LOC253012	3933550	TFF2	2780388	CXXC4
91	3145107	CCNE2	2480585	RHOQ	3729419	CA4	3540076	AKAP5
92	3761608	LOC100128010	2590491	NEUROD1	2332481	GUCA2B	2431031	HMGCS2
93	3200648	ADFP	2870964	EPB41L4A	2381903	RP11-452F19.2	3345415	SFRS2B
94	2367015	FMO2	2937144	SMOC2	3808745	CCDC68	3701779	HSPC105
95	3658980	GPT2	2777276	ABCG2	3274898	TUBAL3	2530713	CCL20
96	3808678	SNRPG	3114022	ZHX2	3761034	ATAD4	3003143	MRPS17
97	2953570	TREM1	3351280	CD3E	3932397	C21orf88	3955483	bA9F11.1
98	2900091	HIST1H2AL	2647073	CPB1	3592304	SLC28A2	3635159	ST20
99	2729821	TMPRSS11E	2601648	DOCK10	2955638	CLIC5	2877159	HNRNPA0
100	3881443	TPX2	2887309	DUSP1	3995331	CSAG1	3115418	POU5F1

	Diameter (lesions with diameter < 30mm vs lesions with diameter >30mm)				**Degree of dysplasia: no dysplasia vs low and high dysplasia**			
	highest positive score on axis 2		**highest negative score on axis 2**		**highest positive score on axis 1**		**highest negative score on axis 1**	
	Transcript ID	Gene Symbol	Transcript ID	Gene Symbol	Transcript ID	Gene Symbol	Transcript ID	Gene Symbol
1	3751859	TMIGD1	3204285	CCL19	3751859	TMIGD1	2345023	CLCA1
2	2584113	GCG	2732508	CXCL13	3638607	ANPEP	2620937	TDGF1
3	2417008	INSL5	2773369	CXCL5	2408832	GUCA2A	2561216	REG3A
4	2772167	UGT2A3	2620937	TDGF1	3016070	MUC17	3122703	DEFA6
5	2561182	REG1B	3204301	CCL21	2647315	TM4SF4	2565935	ANKRD36B
6	3662201	MT1H	3848039	C3	3986647	VSIG1	2688049	RETNLB
7	3655621	ZG16	2377283	CR2	3067250	SLC26A3	2849592	RBBP4
8	2561216	REG3A	3709744	NDEL1	2345061	CLCA4	2561182	REG1B
9	3662247	MT1X	3851230	LOC729747	3921490	B3GALT5	3122828	DEFA5
10	2400027	PLA2G2A	2730303	C4orf7	2324084	CDA	2339334	L1TD1
11	3928415	CLDN8	3173479	FOXD4L3	2584113	GCG	3711806	MEIS3P1
12	2830861	EGR1	3360724	OR56A1	2898986	SLC17A4	3210616	PRUNE2
13	2815018	RPL7L1	3201300	IFNA6	3933559	TFF1	3422144	LGR5
14	3917582	KRTAP6-3	3203636	SUGT1P	2751009	ANXA10	2319340	SLC25A33
15	3114443	FER1L6	3477993	LOC100134058	3655621	ZG16	2880422	SPINK1
16	3544525	FOS	3789769	ONECUT2	2514304	DHRS9	3452417	SLC38A4
17	2656379		3617574	GOLGA8B	3596147	GCNT3	2507928	HNMT
18	3365203	TPH1	3512948	C13orf18	2412624	RAB3B	2490324	REG1A
19	2731542	AREG	3527290	OR4N2	3598267	OSTbeta	4037778	DMBT1
20	2501835	DPP10	2367881	GAS5	3863214	CEACAM7	3490892	OLFM4
21	2409820	BEST4	2756238	LOC100129466	2570193	MALL	3856612	ZNF43
22	3114512	FER1L6	3358946	CTSD	3090294	ADAMDEC1	2351809	LOC100130383
23	3114477	FER1L6	2861093	FLJ40092	3105600	CA2	3351525	LOC100131323
24	3991889	FAM127A	3909768		2974592	VNN1	3875908	PLCB4

25	2898934	SCGN	3026216	CHRM2	3376512	HRASLS2	3150281	SAMD12
26	2490324	REG1A	3756319	CCR7	3461883	PTPRR	3409317	REP15
27	3662150	MT1M	3370855	LOC399884	2794408	HPGD	3137875	GGH
28	2531908	B3GNT7	2810627	LOC401188	3332424	MS4A12	2382667	DNAH14
29	2783493	FABP2	2443450	SELL	2332481	GUCA2B	3392091	FAM55D
30	3376512	HRASLS2	3564350	FLJ45671	3405748	EMP1	3767480	AXIN2
31	3124972	KIAA0484	2781138	LEF1	2372858	RGS2	3421118	RAP1B
32	3681488	PLA2G10	2439303		3142967	CA1	3540074	AKAP5
33	3314040	BNIP3	3318443	TRIM22	3218077	ALDOB	3975431	RPSA
34	2525989	CPS1	2345061	CLCA4	2498911	SULT1C2	3540076	AKAP5
35	3016070	MUC17	3768295	LOC100131307	2844888	BTNL3	3570774	PDZD11
36	2650357	ARL14	3512275	LOC400128	2777276	ABCG2	4014029	RPS6KA6
37	3890640	PCK1	3422144	LGR5	2496907	IL1R2	2872958	MGC32805
38	2572274	LOC389023	3982741	WBP11	2730746	SLC4A4	2477438	QPCT
39	3549757	SERPINA3	3558912	LOC728755	2703750	SI	2827525	SLC12A2
40	3443226	MFAP5	3336400	RBM14	2899012	SLC17A4	2432412	PDE4DIP
41	2436524	TPM3	3084347	DEFB109	3475324	RHOF	3401920	GALNT8
42	3067250	SLC26A3	3578152	TCL1A	3421824	C12orf28	3235663	LOC283070
43	3182396	LOC100129070	3621002	LOC100129835	3718191	CCL8	4042278	MMP23A
44	4022447	GPC3	2845362	SLC9A3	2359352	LCE2D	3208355	CBWD3
45	3933559	TFF1	3688019	LOC647086	3028164	LOC100124692	4055661	MAOA
46	3061484	LOC253012	3921599	PCP4	2514926	EIF2S2	3249978	STOX1
47	2779271	ADH1C	3197418	LOC100128701	3890640	PCK1	2815018	RPL7L1
48	3960174	LGALS2	3436744	TMEM132B	3443226	MFAP5	2941972	C6orf105
49	3692999	MT1G	2759201	LOC100129623	2835119	LOC728264	2651835	GPR160
50	4031664	RBMY2FP	3230440	RP11-216L13.5	3114512	FER1L6	3807487	RPL17
51	3662106	MT1DP	3167301	WDR40A	2773972	CXCL11	3986623	LOC286440
52	2408832	GUCA2A	3679801	GRIN2A	2401251	HTR1D	2457691	TLR5
53	3019939	FOXP2	2849592	RBBP4	2662435	CIDECP	2868044	PCSK1
54	3258625	GPR120	4015538	HNRPA1P5	2584018	DPP4	3827572	
55	3662130	MT1L	2457919	LOC441124	3063501	CYP3A4	3535425	TXNDC1
56	3902379	LOC100130623	3331129	OR5AK2	2709750	SST	2847967	SEMA5A
57	3592304	SLC28A2	2737596	BANK1	3886773	SEMG1	3061484	LOC253012
58	3453732	TUBA1B	3953600	KLHL22	3693141	PLLP	3851493	ZNF799
59	3332465	MS4A8B	2602477	LOC100132934	3165025	RP11-145E5.4	3023803	
60	2703750	SI	3756703	KRTAP2-1	3894545	SDCBP2	3416907	ITGA7
61	3522327	SLC15A1	3273846	LOC642422	3522912	ZIC5	2471351	LOC284952
62	3386217	CHORDC1	2440258	SLAMF6	3204285	CCL19	3840125	ZNF766
63	4043381	S100A1	3104489	STMN2	3549092	CHGA	3210497	PRUNE2
64	2975014	SGK1	2731916	LOC100129865	3142217	PAG1	2461717	TOMM20
65	2359352	LCE2D	3401786	C12orf5	2671936	SLC6A20	3519840	SLITRK6
66	3274898	TUBAL3	3752584	ARGFXP2	2559637	NAT8B	3169331	ALDH1B1
67	2590491	NEUROD1	2348992	VCAM1	2842624	PCDH24	2338397	LOC391044
68	2647073	CPB1	3619157		2602304	TM4SF20	2389062	FAM36A
69	3906886	LOC149703	4039195	HERC2P7	3175274	PCSK5	2946714	HIST1H2BK
70	3984136		3756591	KRT23	2955638	CLIC5	3105430	LRRCC1
71	2761829	FGFBP1	2327162	LOC729973	3653677	AQP8	2405358	KIAA0509
72	2733498	BMP3	2523874	ICOS	2733483	BMP3	3513752	CAB39L
73	2745065	LOC646484	3399655	LOC729860	2501204	IL1RN	3580769	CKB
74	2951655	FKBP5	2878973	LOC729080	3756566	KRT20	3255284	C10orf99

75	2411569	SLC5A9	3172884	LOC100132139	3932397	C21orf88	3136294	
76	3662158	MT1JP	3372728	LOC340970	3028184	LOC100124692	4010017	RP11-167P23.2
77	3249043	REEP3	3281429	LOC729432	3758775	PYY	2585933	SPC25
78	2721087	GBA3	4051214	LOC100128670	2775909	PLAC8	2860666	TAF9
79	2429235	AMPD1	3939952	DKFZP434P211	2409820	BEST4	3724432	LRRC37A2
80	2582124	NR4A2	2345849	LOC400759	2717481	MGC10981	3369249	APIP
81	3059667	SEMA3D	3208327	LOC100133034	2940202	F13A1	3230440	RP11-216L13.5
82	3579712	LOC100130955	2455191	LOC284669	3204301	CCL21	3777958	RAB12
83	2709750	SST	2391813	SLC35E2	2845362	SLC9A3	2520429	MYO1B
84	3937967	FLJ26056	3583541	LOC283767	3811000	RNF152	2402991	CHCHD3
85	2354433	HSD3B2	3558375	GZMB	2656379		2430975	LOC644237
86	3868726	KLKP1	2379665	PROX1	2633737	GPR128	3717250	NF1
87	3039671	SOSTDC1	3838385	CD37	3587553	GREM1	3401786	C12orf5
88	3025433	AKR1B10	2326463	CD52	3980614	GDPD2	2783473	LOC401152
89	2878273	HBEGF	3761164	SKAP1	3928415	CLDN8	3479289	PXMP2
90	3900857	C20orf56	3339066	KRTAP5-10	2939782		3181417	ANP32B
91	3593931	GLDN	3657747	LOC100129631	2384558	TMEM78	3292694	DNA2
92	2841165	LOC100129026	2892316	LOC285771	2898934	SCGN	2736224	ATOH1
93	2799030	SLC6A19	3452417	SLC38A4	3907190	SLPI	2562603	LOC90784
94	3106961	LOC286144	3340404	SPCS2	3734517	OTOP2	3060182	ABCB1
95	3322201	LOC441453	3281311	C10orf115	3448088	BHLHB3	3333425	SCGB1D2
96	3122828	DEFA5	3982612	GPR174	4016319	NXF3	2353283	VANGL1
97	3715614	SLC13A2	3981829	LOC554203	2859387	HTR1A	2697490	CEP70
98	3981701	TSIX	3961910	LOC100129648	3200031	BNC2	2425447	DPH5
99	3974019	TSPAN7	2945741	C6orf32	3321361	SPON1	2997097	
100	3734322	KIF19	3388673	MMP7	2835125	LOC728264	3388673	MMP7

Supplementary Table 3.

Genes with markedly altered expression in precancerous lesions (statistical significance was assessed by one -way ANOVA using *Tissue type p*.v <0.001 and FDR step down method of 0.001). P-values and $\log_2$ fold changes (FC) for pairwise comparisons, nonpolypoid *vs* normal mucosa (NP*vs*NM) and polypoid *vs* normal mucosa (P*vs*NM) were calculated. [p-values significancy assessed by one-way ANOVA test (*p*v<0.001) and FDR, step down method of 0.001].

Affymetrix Transcript ID	Gene_assignment	Gene Symbol	*Tissue type p*-value	*p*-v (NP vs. NM)	Log FC (NP vs. NM)	*p*-v (P vs. NM)	Log FC (P vs. NM)
3326635	NM_000610 // CD44 // CD44 molecule (Indian blood group) // 11p13 // 960 /// NM_0	CD44	2.02E-27	2.16E-23	2.97091	6.75E-22	3.32588
3604147	NM_018689 // KIAA1199 // KIAA1199 // 15q24 // 57214 /// ENST00000356249 // KIAA1	KIAA1199	1.65E-26	3.03E-22	9.47069	2.44E-21	13.1131
3697746	NM_015020 // PHLPPL // PH domain and leucine rich repeat protein phosphatase-lik	PHLPPL	3.96E-26	1.04E-21	-2.91885	3.63E-21	-3.5068
2733483	NM_001201 // BMP3 // bone morphogenetic protein 3 // 4q21 // 651 /// ENST0000028	BMP3	4.00E-26	6.75E-18	-4.81337	6.04E-24	-16.7064
3751859	NM_206832 // TMIGD1 // transmembrane and immunoglobulin domain containing 1 // 1	TMIGD1	1.76E-25	1.75E-19	-18.959	5.44E-22	-66.3636
3729419	NM_000717 // CA4 // carbonic anhydrase IV // 17q23 // 762 /// ENST00000300900 //	CA4	2.89E-24	3.27E-19	-5.5067	4.03E-20	-8.9876
3165025	NR_003529 // RP11-145E5.4 // antisense noncoding RNA in the INK4 locus // 9p21.3	RP11-145E5.4	3.75E-24	1.07E-15	-3.15355	3.05E-22	-8.62233
3719210	NM_024308 // MGC4172 // short-chain dehydrogenase/reductase // 17q12 // 79154 //	MGC4172	3.76E-24	5.57E-20	-3.47596	3.84E-19	-4.17803
3921933	NM_012105 // BACE2 // beta-site APP-cleaving enzyme 2 // 21q22.3 // 25825 /// NM	BACE2	3.83E-24	1.74E-18	1.91813	1.59E-20	2.46748
3774906	NM_003004 // SECTM1 // secreted and transmembrane 1 // 17q25 // 6398 /// ENST000	SECTM1	1.17E-23	2.83E-18	-2.9147	7.18E-20	-4.22882
2408832	NM_033553 // GUCA2A // guanylate cyclase activator 2A (guanylin) // 1p35-p34 //	GUCA2A	1.37E-23	2.57E-18	-9.85327	1.02E-19	-21.0042
2777276	NM_004827 // ABCG2 // ATP-binding cassette, sub-family G (WHITE), member 2 // 4q	ABCG2	2.10E-23	9.28E-19	-7.08986	5.57E-19	-11.1396
2456687	NM_018713 // SLC30A10 // solute carrier family 30, member 10 // 1q41 // 55532 //	SLC30A10	2.71E-23	8.16E-20	-6.44879	1.41E-17	-7.00735
2409820	NM_153274 // BEST4 // bestrophin 4 // 1p33-p32.3 // 266675 /// ENST00000372207 /	BEST4	1.04E-22	5.00E-18	-4.7066	2.07E-18	-6.87213
3469319	NM_018171 // APPL2 // adaptor protein, phosphotyrosine interaction, PH domain an	APPL2	1.73E-22	2.31E-17	-1.83577	1.26E-18	-2.23045
3666366	NM_001793 // CDH3 // cadherin 3, type 1, P-cadherin (placental) // 16q22.1 // 10	CDH3	3.22E-22	6.97E-19	4.78051	1.73E-16	5.01246
3764399	NM_017763 // RNF43 // ring finger protein 43 // 17q22 // 54894 /// ENST000003762	RNF43	3.51E-22	1.30E-18	2.87397	9.42E-17	3.08975
3454892	NM_007210 // GALNT6 // UDP-N-acetyl-alpha-D-galactosamine:polypeptide N-acetylga	GALNT6	3.72E-22	3.38E-18	2.66274	3.43E-17	3.03189
3734517	NM_178160 // OTOP2 // otopetrin 2 // 17q25.1 // 92736 /// ENST00000331427 // OTO	OTOP2	5.99E-22	3.24E-17	-5.16622	8.26E-18	-7.954
2908423	NM_001078177 // SLC29A1 // solute carrier family 29 (nucleoside transporters), m	SLC29A1	6.15E-22	2.67E-18	2.39115	1.23E-16	2.56919
2898986	NM_005495 // SLC17A4 // solute carrier family 17 (sodium phosphate), member 4 //	SLC17A4	7.74E-22	8.16E-15	-3.46903	2.06E-19	-7.94106
3598267	NM_178859 // OSTbeta // organic solute transporter beta // 15q22.31 // 123264 //	OSTbeta	9.49E-22	2.81E-17	-7.95725	2.18E-17	-12.6067
3653677	NM_001169 // AQP8 // aquaporin 8 // 16p12 // 343 /// ENST00000219660 // AQP8 //	AQP8	9.62E-22	6.26E-18	-12.7823	1.11E-16	-17.0548
3816778	NM_002067 // GNA11 // guanine nucleotide binding protein (G protein), alpha 11 (	GNA11	1.23E-21	8.54E-19	-2.0249	2.56E-15	-1.96021
2835848	NM_078483 // SLC36A1 // solute carrier family 36 (proton/amino acid symporter),	SLC36A1	1.36E-21	1.00E-15	-1.75779	1.94E-18	-2.28137
3280573	NM_006393 // NEBL // nebulette // 10p12 // 10529 /// NM_213569 // NEBL // nebule	NEBL	1.64E-21	4.15E-19	5.09268	1.59E-14	4.20095
2710599	NM_021101 // CLDN1 // claudin 1 // 3q28-q29 // 9076 /// ENST00000295522 // CLDN1	CLDN1	1.81E-21	2.64E-18	4.74487	1.21E-15	4.8107

2520069	NM_001042521 // MGC13057 // hypothetical protein MGC13057 // 2q32.2 // 84281 ///	MGC13057	2.15E-21	4.50E-17	-2.63313	6.16E-17	-3.19984
3791782	NM_002639 // SERPINB5 // serpin peptidase inhibitor, clade B (ovalbumin), member	SERPINB5	2.26E-21	5.39E-19	6.47402	2.29E-14	5.15621
3767480	NM_004655 // AXIN2 // axin 2 // 17q23-q24 // 8313 /// ENST00000307078 // AXIN2 /	AXIN2	2.30E-21	6.66E-17	3.64005	4.69E-17	4.87107
3142217	NM_018440 // PAG1 // phosphoprotein associated with glycosphingolipid microdomai	PAG1	2.68E-21	5.47E-14	-2.25257	4.18E-19	-4.09289
2862696	NM_003633 // ENC1 // ectodermal-neural cortex (with BTB-like domain) // 5q12-q13	ENC1	2.88E-21	7.27E-17	2.37842	6.48E-17	2.87009
3549092	NM_001275 // CHGA // chromogranin A (parathyroid secretory protein 1) // 14q32 /	CHGA	3.49E-21	6.28E-14	-3.31257	5.65E-19	-7.9226
3220384	NM_057159 // LPAR1 // lysophosphatidic acid receptor 1 // 9q31.3 // 1902 /// NM_	LPAR1	3.64E-21	1.21E-14	-1.88395	1.61E-18	-2.73665
2815220	NM_173490 // TMEM171 // transmembrane protein 171 // 5q13.2 // 134285 /// ENST00	TMEM171	4.43E-21	1.21E-17	-2.60159	1.11E-15	-2.74937
3201488	NM_078487 // CDKN2B // cyclin-dependent kinase inhibitor 2B (p15, inhibits CDK4)	CDKN2B	5.45E-21	5.01E-15	-2.01277	5.42E-18	-2.83972
3592755	NM_153618 // SEMA6D // sema domain, transmembrane domain (TM), and cytoplasmic d	SEMA6D	5.90E-21	5.62E-15	-2.76674	5.66E-18	-4.58128
3891447	NM_207032 // EDN3 // endothelin 3 // 20q13.2-q13.3 // 1908 /// NM_207034 // EDN3	EDN3	7.90E-21	4.13E-13	-1.98888	6.51E-19	-3.52459
2894573	NM_145649 // GCNT2 // glucosaminyl (N-acetyl) transferase 2, I-branching enzyme	GCNT2	8.16E-21	3.05E-17	-3.31505	1.24E-15	-3.66376
2494709	NM_020184 // CNNM4 // cyclin M4 // 2p12-p11.2 // 26504 /// ENST00000377075 // CN	CNNM4	8.57E-21	2.17E-16	-1.66642	1.61E-16	-1.86809
3883013	NM_021202 // TP53INP2 // tumor protein p53 inducible nuclear protein 2 // 20q11.	TP53INP2	8.95E-21	5.23E-16	-1.96408	7.55E-17	-2.38257
3622176	NM_014080 // DUOX2 // dual oxidase 2 // 15q15.3 // 50506 /// ENST00000389039 //	DUOX2	1.05E-20	7.19E-19	9.26465	7.30E-13	5.79995
3175274	NM_006200 // PCSK5 // proprotein convertase subtilisin/kexin type 5 // 9q21.3 //	PCSK5	1.06E-20	1.12E-14	-2.7632	8.69E-18	-4.63863
3741875	NM_015113 // ZZEF1 // zinc finger, ZZ-type with EF-hand domain 1 // 17p13.2 // 2	ZZEF1	1.30E-20	3.35E-15	-1.60916	2.96E-17	-1.94756
2923868	NM_181794 // PKIB // protein kinase (cAMP-dependent, catalytic) inhibitor beta /	PKIB	1.33E-20	6.29E-17	-2.3143	1.40E-15	-2.52327
2360257	NM_000565 // IL6R // interleukin 6 receptor // 1q21 // 3570 /// NM_181359 // IL6	IL6R	1.39E-20	8.47E-17	-2.16291	1.08E-15	-2.37665
3677913	NM_001116 // ADCY9 // adenylate cyclase 9 // 16p13.3 // 115 /// ENST00000294016	ADCY9	1.47E-20	6.24E-16	-1.54728	1.54E-16	-1.73747
2730746	NM_001098484 // SLC4A4 // solute carrier family 4, sodium bicarbonate cotranspor	SLC4A4	1.52E-20	1.29E-13	-3.67611	3.10E-18	-8.95996
3653098	NM_022097 // CHP2 // calcineurin B homologous protein 2 // 16p12.1 // 63928 ///	CHP2	1.53E-20	8.06E-17	-3.56768	1.39E-15	-4.11255
3883064	NM_018677 // ACSS2 // acyl-CoA synthetase short-chain family member 2 // 20q11.2	ACSS2	1.73E-20	2.79E-17	-2.0013	6.53E-15	-2.03768
3090294	NM_014479 // ADAMDEC1 // ADAM-like, decysin 1 // 8p21.2 // 27299 /// ENST0000025	ADAMDEC1	1.74E-20	5.03E-12	-3.33561	5.71E-19	-11.1878
2332481	NM_007102 // GUCA2B // guanylate cyclase activator 2B (uroguanylin) // 1p34-p33	GUCA2B	2.06E-20	4.31E-16	-4.90869	4.00E-16	-6.91611
3936442	NM_001127649 // PEX26 // peroxisomal biogenesis factor 26 // 22q11.21 // 55670 /	PEX26	2.24E-20	7.91E-17	-1.7826	2.99E-15	-1.87216
3664924	NM_005182 // CA7 // carbonic anhydrase VII // 16q22.1 // 766 /// NM_001014435 //	CA7	2.26E-20	9.27E-16	-3.45957	2.26E-16	-4.81441
3388673	NM_002423 // MMP7 // matrix metallopeptidase 7 (matrilysin, uterine) // 11q21-q2	MMP7	2.40E-20	2.33E-16	8.40838	1.01E-15	11.8027
3654669	NM_177528 // SULT1A2 // sulfotransferase family, cytosolic, 1A, phenol-preferrin	SULT1A2	2.41E-20	1.26E-15	-2.41724	1.91E-16	-3.10827
2773872	NM_014435 // NAAA // N-acylethanolamine acid amidase // 4q21.1 // 27163 /// NM_0	NAAA	2.41E-20	2.23E-14	-1.62938	1.92E-17	-2.0872
2765865	NM_001085400 // RELL1 // RELT-like 1 // 4p14 // 768211 /// NM_001085399 // RELL1	RELL1	2.48E-20	8.50E-16	-1.75761	2.90E-16	-2.02761
3887117	NM_001127695 // CTSA // cathepsin A // 20q13.1 // 5476 /// NM_000308 // CTSA //	CTSA	2.52E-20	2.31E-16	-1.63626	1.11E-15	-1.76647
3894545	NM_080489 // SDCBP2 // syndecan binding protein (syntenin) 2 // 20p13 // 27111 /	SDCBP2	2.67E-20	4.25E-16	-2.66247	6.54E-16	-3.22801
3456081	NM_000966 // RARG // retinoic acid receptor, gamma // 12q13 // 5916 /// NM_00104	RARG	2.82E-20	7.78E-17	1.67517	4.88E-15	1.73472
3569814	NM_001102 // ACTN1 // actinin, alpha 1 // 14q24.1-q24.2|14q24|14q22-q24 // 87 //	ACTN1	2.98E-20	1.27E-14	1.56834	4.04E-17	1.91857
2334476	NM_015112 // MAST2 // microtubule associated serine/threonine kinase 2 // 1p34.1	MAST2	3.74E-20	2.03E-15	-1.46897	2.66E-16	-1.64291
3190190	NM_005564 // LCN2 // lipocalin 2 // 9q34 // 3934 /// ENST00000373017 // LCN2 //	LCN2	3.79E-20	3.40E-16	5.01332	1.58E-15	6.4521
3896621	NM_017671 // FERMT1 // fermitin family homolog 1 (Drosophila) // 20p12.3 // 5561	FERMT1	4.63E-20	4.47E-16	2.3922	1.73E-15	2.75792
3020343	NM_001127500 // MET // met proto-oncogene (hepatocyte growth factor receptor) //	MET	5.18E-20	1.22E-16	2.83635	9.60E-15	3.01721
2398820	NM_007365 // PADI2 // peptidyl arginine deiminase, type II // 1p36.13 // 11240 /	PADI2	5.69E-20	8.89E-16	-1.93303	1.23E-15	-2.20615
2828520	NM_003060 // SLC22A5 // solute carrier family 22 (organic cation/carnitine trans	SLC22A5	6.21E-20	2.46E-16	-1.94241	5.92E-15	-2.07408
3623865	NM_032802 // SPPL2A // signal peptide peptidase-like 2A // 15q21.2 // 84888 ///	SPPL2A	7.70E-20	4.07E-16	-1.58212	5.03E-15	-1.67287

3768627	NM_007168 // ABCA8 // ATP-binding cassette, sub-family A (ABC1), member 8 // 17q	ABCA8	8.01E-20	9.93E-15	-3.54385	2.44E-16	-5.59519
3265224	NM_198496 // VWA2 // von Willebrand factor A domain containing 2 // 10q25.3 // 3	VWA2	8.42E-20	1.29E-15	2.81899	1.72E-15	3.47543
2952834	NM_003740 // KCNK5 // potassium channel, subfamily K, member 5 // 6p21 // 8645 /	KCNK5	9.63E-20	3.17E-16	-1.77378	1.04E-14	-1.86514
3745571	BC015790 // LOC400573 // hypothetical gene supported by BC015790; BC041634 // 17	LOC400573	1.16E-19	4.82E-17	-1.668	1.95E-13	-1.61257
3986346	NM_020384 // CLDN2 // claudin 2 // Xq22.3-q23 // 9075 /// ENST00000336803 // CLD	CLDN2	1.22E-19	8.39E-17	3.53132	9.59E-14	3.40982
3365203	NM_004179 // TPH1 // tryptophan hydroxylase 1 // 11p15.3-p14 // 7166 /// ENST000	TPH1	1.26E-19	3.98E-13	-4.95187	3.45E-17	-13.541
3396883	NM_032795 // RPUSD4 // RNA pseudouridylate synthase domain containing 4 // 11q24	RPUSD4	1.35E-19	1.87E-14	1.40888	3.43E-16	1.60175
3557851	NM_024658 // IPO4 // importin 4 // 14q12 // 79711 /// ENST00000354464 // IPO4 //	IPO4	1.40E-19	4.20E-11	1.35879	3.42E-18	1.8777
2709750	NM_001048 // SST // somatostatin // 3q28 // 6750 /// ENST00000287641 // SST // s	SST	1.47E-19	2.23E-12	-3.12595	1.56E-17	-7.50679
2345061	NM_012128 // CLCA4 // chloride channel, calcium activated, family member 4 // 1p	CLCA4	1.50E-19	1.60E-12	-8.41057	1.94E-17	-40.453
3871192	NM_002842 // PTPRH // protein tyrosine phosphatase, receptor type, H // 19q13.4	PTPRH	1.51E-19	2.68E-15	-1.75496	2.39E-15	-1.98273
3202224	NM_022901 // LRRC19 // leucine rich repeat containing 19 // 9p21.2 // 64922 ///	LRRC19	1.61E-19	1.85E-14	-2.57522	4.60E-16	-3.6252
2374126	NM_205860 // NR5A2 // nuclear receptor subfamily 5, group A, member 2 // 1q32.1	NR5A2	2.01E-19	1.93E-11	-2.03239	7.86E-18	-3.98378
3811000	NM_173557 // RNF152 // ring finger protein 152 // 18q21.33 // 220441 /// ENST000	RNF152	2.36E-19	4.55E-13	-2.68905	7.97E-17	-4.84713
3133345	NM_006749 // SLC20A2 // solute carrier family 20 (phosphate transporter), member	SLC20A2	3.43E-19	4.91E-15	-1.67612	5.72E-15	-1.86509
3835035	NM_020406 // CD177 // CD177 molecule // 19q13.2 // 57126 /// AF146747 // CD177 /	CD177	3.65E-19	1.42E-14	-4.21549	2.30E-15	-6.34905
3847873	NM_024103 // SLC25A23 // solute carrier family 25 (mitochondrial carrier; phosph	SLC25A23	3.95E-19	2.71E-15	-1.6352	1.38E-14	-1.76193
3705491	NM_024792 // FAM57A // family with sequence similarity 57, member A // 17p13.3 /	FAM57A	4.58E-19	6.92E-13	1.77331	1.62E-16	2.47785
3359448	BC030237 // SLC22A18AS // solute carrier family 22 (organic cation transporter),	SLC22A18AS	7.97E-19	3.28E-15	-2.35834	4.21E-14	-2.60909
3075531	NM_080660 // ZC3HAV1L // zinc finger CCCH-type, antiviral 1-like // 7q34 // 9209	ZC3HAV1L	8.35E-19	7.52E-14	1.70851	2.16E-15	2.07006
2708457	NM_004366 // CLCN2 // chloride channel 2 // 3q27-q28 // 1181 /// ENST00000265593	CLCN2	8.48E-19	2.70E-15	-1.98718	5.95E-14	-2.12637
2731986	NM_003943 // STBD1 // starch binding domain 1 // 4q24-q25 // 8987 /// ENST000002	STBD1	9.25E-19	4.13E-15	-2.11567	4.32E-14	-2.32334
3394356	NM_004205 // USP2 // ubiquitin specific peptidase 2 // 11q23.3 // 9099 /// NM_17	USP2	9.38E-19	1.83E-16	-3.0384	2.99E-12	-2.67681
3450655	NM_153634 // CPNE8 // copine VIII // 12q12 // 144402 /// ENST00000331366 // CPNE	CPNE8	1.04E-18	5.08E-12	-2.39744	1.55E-16	-4.42049
2458513	NM_014698 // TMEM63A // transmembrane protein 63A // 1q42.12 // 9725 /// ENST000	TMEM63A	1.08E-18	1.97E-16	1.83059	3.73E-12	1.70349
2463482	NM_014322 // OPN3 // opsin 3 // 1q43 // 23596 /// NM_001821 // CHML // choroider	OPN3	1.09E-18	1.98E-15	-1.60998	1.42E-13	-1.65452
3677752	NM_016292 // TRAP1 // TNF receptor-associated protein 1 // 16p13.3 // 10131 ///	TRAP1	1.43E-18	2.75E-09	1.36306	1.17E-17	2.06072
3758775	NM_004160 // PYY // peptide YY // 17q21.1 // 5697 /// ENST00000360085 // PYY //	PYY	1.46E-18	1.97E-11	-2.76827	1.14E-16	-6.25616
2998638	AK299133 // C7orf10 // chromosome 7 open reading frame 10 // 7p14.1 // 79783 ///	C7orf10	1.61E-18	9.52E-16	-3.08379	8.39E-13	-2.99347
3441849	NM_001065 // TNFRSF1A // tumor necrosis factor receptor superfamily, member 1A /	TNFRSF1A	1.63E-18	3.12E-16	-1.38092	4.60E-12	-1.33141
3332424	NM_017716 // MS4A12 // membrane-spanning 4-domains, subfamily A, member 12 // 11	MS4A12	1.74E-18	5.06E-13	-8.90193	1.55E-15	-24.4702
2679406	NM_003716 // CADPS // Ca++-dependent secretion activator // 3p14.2 // 8618 /// N	CADPS	1.80E-18	1.61E-15	3.01273	5.14E-13	3.03332
3974019	NM_004615 // TSPAN7 // tetraspanin 7 // Xp11.4 // 7102 /// ENST00000378482 // TS	TSPAN7	1.80E-18	9.21E-14	-3.04301	6.47E-15	-4.35017
2565246	NM_017849 // TMEM127 // transmembrane protein 127 // 2q11.2 // 55654 /// ENST000	TMEM127	1.85E-18	9.77E-14	-1.37484	6.45E-15	-1.52413
2562233	NM_017750 // RETSAT // retinol saturase (all-trans-retinol 13,14-reductase) // 2	RETSAT	1.89E-18	1.05E-14	-1.96061	5.93E-14	-2.16412
3886143	NM_016276 // SGK2 // serum/glucocorticoid regulated kinase 2 // 20q13.2 // 10110	SGK2	2.01E-18	1.41E-15	-1.94459	7.78E-13	-1.92912
3746845	NM_006470 // TRIM16 // tripartite motif-containing 16 // 17p11.2 // 10626 /// NM	TRIM16	2.14E-18	6.19E-13	1.62571	1.83E-15	2.03773
3816803	BC001528 // GNA11 // guanine nucleotide binding protein (G protein), alpha 11 (G	GNA11	2.31E-18	1.83E-16	-2.2005	2.67E-11	-1.90791
3710108	NM_004246 // GLP2R // glucagon-like peptide 2 receptor // 17p13.3 // 9340 /// EN	GLP2R	2.39E-18	2.58E-15	-2.01826	4.96E-13	-2.05009
3142967	NM_001128829 // CA1 // carbonic anhydrase I // 8q13-q22.1 // 759 /// NM_001738 /	CA1	2.39E-18	1.41E-12	-6.60221	1.20E-15	-17.8465
3064293	NM_004444 // EPHB4 // EPH receptor B4 // 7q22 // 2050 /// ENST00000358173 // EPH	EPHB4	2.48E-18	9.05E-14	1.61235	1.13E-14	1.85837
2699564	NM_182943 // PLOD2 // procollagen-lysine, 2-oxoglutarate 5-dioxygenase 2 // 3q23	PLOD2	2.56E-18	1.11E-13	-2.42375	9.87E-15	-3.19387

3655621	NM_152338 // ZG16 // zymogen granule protein 16 // 16p13.3 // 123887 /// ENST000	ZG16	2.57E-18	3.36E-14	-8.14808	3.07E-14	-12.8235
3544625	NM_017791 // FLVCR2 // feline leukemia virus subgroup C cellular receptor family	FLVCR2	2.69E-18	2.73E-15	-2.31361	5.90E-13	-2.3491
3914786	NR_003087 // ABCC13 // ATP-binding cassette, sub-family C (CFTR/MRP), member 13	ABCC13	2.99E-18	2.89E-13	-1.86401	5.67E-15	-2.35872
2611848	NM_003043 // SLC6A6 // solute carrier family 6 (neurotransmitter transporter, ta	SLC6A6	3.20E-18	4.99E-15	3.13709	3.85E-13	3.33189
3374890	NM_001062 // TCN1 // transcobalamin I (vitamin B12 binding protein, R binder fam	TCN1	3.35E-18	5.31E-14	12.4668	3.13E-14	22.4812
3592196	NM_207581 // DUOXA2 // dual oxidase maturation factor 2 // 15q15.1 // 405753 ///	DUOXA2	3.36E-18	1.16E-14	4.74527	1.56E-13	5.67225
3652902	NM_000336 // SCNN1B // sodium channel, nonvoltage-gated 1, beta // 16p12.2-p12.1	SCNN1B	3.38E-18	1.19E-11	-2.61999	4.98E-16	-5.09646
3662808	NM_201524 // GPR56 // G protein-coupled receptor 56 // 16q12.2-q21 // 9289 /// N	GPR56	3.68E-18	2.94E-14	1.68485	6.70E-14	1.85133
2955638	NM_001114086 // CLIC5 // chloride intracellular channel 5 // 6p21.1-p12.1 // 534	CLIC5	3.70E-18	1.18E-11	-2.23474	5.69E-16	-3.87173
2358320	NM_025150 // TARS2 // threonyl-tRNA synthetase 2, mitochondrial (putative) // 1q	TARS2	3.79E-18	1.31E-12	1.21229	2.55E-15	1.33159
2460325	BC066649 // C1orf198 // chromosome 1 open reading frame 198 // 1q42.13-q43 // 84	C1orf198	3.96E-18	1.07E-13	1.42476	2.14E-14	1.57219
2871617	NM_018700 // TRIM36 // tripartite motif-containing 36 // 5q22.3 // 55521 /// NM_	TRIM36	4.14E-18	6.07E-14	-2.10051	3.97E-14	-2.49064
4012299	NM_002637 // PHKA1 // phosphorylase kinase, alpha 1 (muscle) // Xq12-q13 // 5255	PHKA1	4.60E-18	1.44E-13	1.97292	2.11E-14	2.4041
2673773	NM_000387 // SLC25A20 // solute carrier family 25 (carnitine/acylcarnitine trans	SLC25A20	4.62E-18	2.11E-15	-1.9389	2.60E-12	-1.88794
3664982	NM_003869 // CES2 // carboxylesterase 2 (intestine, liver) // 16q22.1 // 8824 //	CES2	4.67E-18	1.03E-13	-2.13948	2.96E-14	-2.61288
3797032	NM_012307 // EPB41L3 // erythrocyte membrane protein band 4.1-like 3 // 18p11.32	EPB41L3	4.84E-18	2.61E-14	-2.32493	1.25E-13	-2.64319
3753966	NM_032962 // CCL14 // chemokine (C-C motif) ligand 14 // 17q11.2 // 6358 /// NM_	CCL14	4.90E-18	1.01E-13	-1.79876	3.27E-14	-2.09303
2381249	NM_024709 // C1orf115 // chromosome 1 open reading frame 115 // 1q41 // 79762 //	C1orf115	5.21E-18	1.09E-13	-1.63602	3.36E-14	-1.85975
2358949	NM_020770 // CGN // cingulin // 1q21 // 57530 /// ENST00000271636 // CGN // cing	CGN	5.54E-18	3.25E-14	-1.56303	1.27E-13	-1.67874
3830002	NM_020895 // GRAMD1A // GRAM domain containing 1A // 19q13.11 // 57655 /// ENST0	GRAMD1A	5.64E-18	2.78E-14	1.67728	1.55E-13	1.80905
3756566	NM_019010 // KRT20 // keratin 20 // 17q21.2 // 54474 /// ENST00000167588 // KRT2	KRT20	5.73E-18	8.41E-14	-2.98126	5.11E-14	-3.84374
3154317	NM_006096 // NDRG1 // N-myc downstream regulated gene 1 // 8q24.3 // 10397 /// E	NDRG1	5.77E-18	1.06E-14	-1.99527	4.95E-13	-2.09257
3767339	NM_006572 // GNA13 // guanine nucleotide binding protein (G protein), alpha 13 /	GNA13	5.91E-18	5.03E-13	-1.55948	1.08E-14	-1.8427
3960478	NM_001894 // CSNK1E // casein kinase 1, epsilon // 22q13.1 // 1454 /// NM_152221	CSNK1E	6.42E-18	4.21E-13	1.36492	1.43E-14	1.5243
2607923	NM_175607 // CNTN4 // contactin 4 // 3p26-p25 // 152330 /// NM_175613 // CNTN4 /	CNTN4	6.56E-18	4.02E-15	-2.09845	2.22E-12	-2.07487
3671076	NM_002153 // HSD17B2 // hydroxysteroid (17-beta) dehydrogenase 2 // 16q24.1-q24.	HSD17B2	6.79E-18	3.60E-13	-2.98048	1.80E-14	-4.3113
3023384	NM_015328 // AHCYL2 // S-adenosylhomocysteine hydrolase-like 2 // 7q32.1 // 2338	AHCYL2	6.89E-18	1.55E-14	-2.27651	4.41E-13	-2.44406
3886453	NM_000457 // HNF4A // hepatocyte nuclear factor 4, alpha // 20q12-q13.1 // 3172	HNF4A	8.00E-18	4.44E-13	-1.37019	1.96E-14	-1.52688
2910868	NM_014464 // TINAG // tubulointerstitial nephritis antigen // 6p11.2-p12 // 2728	TINAG	8.92E-18	1.76E-13	-2.3028	5.41E-14	-2.86204
3264948	NM_033338 // CASP7 // caspase 7, apoptosis-related cysteine peptidase // 10q25 /	CASP7	9.06E-18	2.79E-16	-1.61622	4.10E-10	-1.4321
2794408	NM_000860 // HPGD // hydroxyprostaglandin dehydrogenase 15-(NAD) // 4q34-q35 //	HPGD	9.12E-18	3.81E-13	-3.63251	2.78E-14	-5.50215
2584113	NM_002054 // GCG // glucagon // 2q36-q37 // 2641 /// ENST00000375497 // GCG // g	GCG	9.56E-18	8.47E-11	-5.92818	6.83E-16	-24.62
2411173	NM_005764 // PDZK1IP1 // PDZK1 interacting protein 1 // 1p33 // 10158 /// ENST00	PDZK1IP1	9.64E-18	8.45E-16	3.14585	5.93E-11	2.59914
3756262	NM_032865 // TNS4 // tensin 4 // 17q21.2 // 84951 /// ENST00000254051 // TNS4 //	TNS4	9.94E-18	4.46E-15	3.42481	4.63E-12	3.27186
3390641	NM_020809 // ARHGAP20 // Rho GTPase activating protein 20 // 11q22.3-q23.1 // 57	ARHGAP20	9.98E-18	1.78E-15	-1.64208	1.86E-11	-1.55492
2891556	NM_033260 // FOXQ1 // forkhead box Q1 // 6p25 // 94234 /// ENST00000296839 // FO	FOXQ1	1.01E-17	4.09E-15	2.08792	5.43E-12	2.01969
3767465	NM_004655 // AXIN2 // axin 2 // 17q23-q24 // 8313 /// ENST00000307078 // AXIN2 /	AXIN2	1.35E-17	4.03E-13	1.62933	5.09E-14	1.88516
2958172	NM_021073 // BMP5 // bone morphogenetic protein 5 // 6p12.1 // 653 /// ENST00000	BMP5	1.38E-17	2.36E-12	-2.04955	1.21E-14	-2.82044
2889486	NM_153373 // AGXT2L2 // alanine-glyoxylate aminotransferase 2-like 2 // 5q35.3 /	AGXT2L2	1.47E-17	8.40E-13	-1.38559	3.10E-14	-1.5547
3131563	XM_001718074 // LOC100128034 // hypothetical protein LOC100128034 // 8p12 // 100	LOC100128034	1.55E-17	3.42E-14	2.75304	8.19E-13	3.01961
3002420	NM_182546 // VSTM2A // V-set and transmembrane domain containing 2A // 7p11.2 //	VSTM2A	1.58E-17	6.68E-15	-1.87468	7.06E-12	-1.82903
2857733	NM_152622 // MIER3 // mesoderm induction early response 1, family member 3 // 5q	MIER3	1.65E-17	9.63E-14	-2.65729	2.93E-13	-3.13346

3461883	NM_002849 // PTPRR // protein tyrosine phosphatase, receptor type, R // 12q15 //	PTPRR	1.66E-17	3.85E-12	-2.82306	1.12E-14	-4.61663
3911767	NM_001336 // CTSZ // cathepsin Z // 20q13 // 1522 /// ENST00000217131 // CTSZ //	CTSZ	1.87E-17	1.57E-13	-1.48189	2.20E-13	-1.60254
2700244	NM_000096 // CP // ceruloplasmin (ferroxidase) // 3q23-q25 // 1356 /// ENST00000	CP	1.91E-17	5.54E-10	-2.19528	6.45E-16	-4.59291
3795733	NM_130386 // COLEC12 // collectin sub-family member 12 // 18pter-p11.3 // 81035	COLEC12	1.95E-17	1.76E-14	-1.99586	2.93E-12	-2.02665
2371346	NM_015149 // RGL1 // ral guanine nucleotide dissociation stimulator-like 1 // 1q	RGL1	1.99E-17	5.40E-12	-1.57257	1.15E-14	-1.96343
3325839	NM_018393 // TCP11L1 // t-complex 11 (mouse)-like 1 // 11p13 // 55346 /// ENST00	TCP11L1	2.07E-17	7.56E-11	-1.40212	2.13E-15	-1.79458
3439178	NM_018663 // PXMP2 // peroxisomal membrane protein 2, 22kDa // 12q24.33 // 5827	PXMP2	2.19E-17	6.56E-16	-1.77964	7.61E-10	-1.54021
2692447	NM_053025 // MYLK // myosin light chain kinase // 3q21 // 4638 /// NM_053026 //	MYLK	2.22E-17	9.24E-10	-1.64536	6.08E-16	-2.68367
2721087	NM_020973 // GBA3 // glucosidase, beta, acid 3 (cytosolic) // 4p15.31 // 57733 /	GBA3	2.23E-17	7.35E-14	-5.98194	6.83E-13	-7.49077
3338192	NM_053056 // CCND1 // cyclin D1 // 11q13 // 595 /// ENST00000227507 // CCND1 //	CCND1	2.40E-17	1.34E-11	1.44033	7.95E-15	1.76529
3174121	NM_153267 // MAMDC2 // MAM domain containing 2 // 9q21.11 // 256691 /// NM_00098	MAMDC2	2.60E-17	6.46E-12	-2.65618	1.51E-14	-4.273
3757630	NM_021078 // KAT2A // K(lysine) acetyltransferase 2A // 17q21 // 2648 /// ENST00	KAT2A	2.64E-17	3.64E-12	1.44903	2.39E-14	1.703
3299469	NM_144590 // ANKRD22 // ankyrin repeat domain 22 // 10q23.31 // 118932 /// ENST0	ANKRD22	2.71E-17	1.40E-10	2.02768	2.17E-15	3.49506
3340665	NM_032564 // DGAT2 // diacylglycerol O-acyltransferase homolog 2 (mouse) // 11q1	DGAT2	2.94E-17	1.78E-12	1.792	5.05E-14	2.21925
3980614	NM_017711 // GDPD2 // glycerophosphodiester phosphodiesterase domain containing	GDPD2	3.07E-17	1.49E-13	-2.45404	5.65E-13	-2.83245
3545311	NM_033426 // KIAA1737 // KIAA1737 // 14q24.3 // 85457 /// ENST00000361786 // KIA	KIAA1737	3.08E-17	3.13E-12	-1.38707	3.42E-14	-1.58703
3115504	NM_002467 // MYC // v-myc myelocytomatosis viral oncogene homolog (avian) // 8q2	MYC	3.20E-17	7.91E-13	1.85397	1.18E-13	2.22125
3734453	NM_004252 // SLC9A3R1 // solute carrier family 9 (sodium/hydrogen exchanger), me	SLC9A3R1	3.22E-17	1.95E-13	-1.93175	4.64E-13	-2.17181
3839346	NM_003121 // SPIB // Spi-B transcription factor (Spi-1/PU.1 related) // 19q13.3-	SPIB	3.26E-17	6.16E-11	-2.12415	4.57E-15	-3.53591
2621122	NM_015175 // NBEAL2 // neurobeachin-like 2 // 3p21.31 // 23218 /// AY358455 // N	NBEAL2	3.31E-17	8.41E-13	1.42156	1.18E-13	1.57722
2930007	NM_001030060 // SAMD5 // sterile alpha motif domain containing 5 // 6q24.3 // 38	SAMD5	3.41E-17	5.89E-14	1.97539	1.96E-12	2.08281
2865327	NM_001884 // HAPLN1 // hyaluronan and proteoglycan link protein 1 // 5q14.3 // 1	HAPLN1	3.67E-17	5.36E-12	-2.13696	2.95E-14	-2.99693
3067250	NM_000111 // SLC26A3 // solute carrier family 26, member 3 // 7q31 // 1811 /// E	SLC26A3	3.77E-17	3.98E-10	-5.16429	1.90E-15	-20.8777
3558418	NM_014178 // STXBP6 // syntaxin binding protein 6 (amisyn) // 14q12 // 29091 ///	STXBP6	3.78E-17	3.31E-14	1.6508	4.91E-12	1.67111
2829947	NM_000358 // TGFBI // transforming growth factor, beta-induced, 68kDa // 5q31 //	TGFBI	3.81E-17	1.36E-13	3.33429	9.29E-13	3.93117
3258772	NM_153226 // TMEM20 // transmembrane protein 20 // 10q23.33 // 159371 /// ENST00	TMEM20	3.94E-17	2.28E-15	-2.05802	3.17E-10	-1.78952
3557209	NM_012244 // SLC7A8 // solute carrier family 7 (cationic amino acid transporter,	SLC7A8	4.34E-17	2.05E-14	1.61413	1.23E-11	1.59595
3958658	NM_004737 // LARGE // like-glycosyltransferase // 22q12.3 // 9215 /// NM_133642	LARGE	4.35E-17	3.82E-14	-1.41715	5.40E-12	-1.42991
2474341	NM_004341 // CAD // carbamoyl-phosphate synthetase 2, aspartate transcarbamylase	CAD	4.69E-17	8.27E-11	1.36363	6.39E-15	1.68229
2619265	NM_004624 // VIPR1 // vasoactive intestinal peptide receptor 1 // 3p22 // 7433 /	VIPR1	4.70E-17	4.30E-10	-1.39589	2.45E-15	-1.84825
3144973	NM_012415 // RAD54B // RAD54 homolog B (S. cerevisiae) // 8q21.3-q22 // 25788 //	RAD54B	5.10E-17	2.61E-12	1.62136	8.88E-14	1.92911
2676671	NM_001064 // TKT // transketolase // 3p14.3 // 7086 /// ENST00000296289 // TKT /	TKT	5.56E-17	2.09E-11	1.51138	2.04E-14	1.88594
2865390	NM_005711 // EDIL3 // EGF-like repeats and discoidin I-like domains 3 // 5q14 //	EDIL3	5.88E-17	3.07E-10	-2.17733	4.01E-15	-4.02477
3445326	NM_000834 // GRIN2B // glutamate receptor, ionotropic, N-methyl D-aspartate 2B /	GRIN2B	6.19E-17	1.84E-13	2.24464	1.62E-12	2.4863
3907111	NM_006809 // TOMM34 // translocase of outer mitochondrial membrane 34 // --- //	TOMM34	6.33E-17	1.01E-07	1.23933	3.03E-16	1.70461
3663181	NM_014157 // CCDC113 // coiled-coil domain containing 113 // 16q21 // 29070 ///	CCDC113	6.45E-17	9.93E-12	1.71773	4.40E-14	2.20135
2669488	NM_006225 // PLCD1 // phospholipase C, delta 1 // 3p22-p21.3 // 5333 /// ENST000	PLCD1	6.80E-17	5.83E-13	-1.52152	5.70E-13	-1.66421
2910680	NM_018214 // LRRC1 // leucine rich repeat containing 1 // 6p12.1 // 55227 /// EN	LRRC1	6.80E-17	4.45E-12	-1.55496	9.03E-14	-1.84264
3740998	NM_018128 // TSR1 // TSR1, 20S rRNA accumulation, homolog (S. cerevisiae) // 17p	TSR1	6.94E-17	5.90E-11	1.37803	1.39E-14	1.67877
2580802	NM_005168 // RND3 // Rho family GTPase 3 // 2q23.3 // 390 /// ENST00000375734 //	RND3	7.47E-17	9.10E-14	-1.76668	5.28E-12	-1.8239
3356038	NM_138788 // TMEM45B // transmembrane protein 45B // 11q24.3 // 120224 /// ENST0	TMEM45B	8.23E-17	2.73E-13	-1.84561	1.77E-12	-2.00842
3466206	NM_020698 // TMCC3 // transmembrane and coiled-coil domain family 3 // 12q22 //	TMCC3	8.35E-17	1.68E-12	-1.68725	2.93E-13	-1.96051

2732844	NM_005139 // ANXA3 // annexin A3 // 4q13-q22 // 306 /// ENST00000264908 // ANXA3	ANXA3	8.41E-17	1.47E-13	2.73485	3.73E-12	2.98218
3864430	NM_014297 // ETHE1 // ethylmalonic encephalopathy 1 // 19q13.31 // 23474 /// ENS	ETHE1	8.63E-17	2.91E-14	-1.88412	3.18E-11	-1.82978
3358201	NM_021924 // MUPCDH // mucin-like protocadherin // 11p15.5 // 53841 /// NM_03126	MUPCDH	8.69E-17	2.94E-11	-1.69923	3.11E-14	-2.25565
2717078	NM_005980 // S100P // S100 calcium binding protein P // 4p16 // 6286 /// ENST000	S100P	8.73E-17	1.27E-13	2.8937	4.77E-12	3.12227
2734047	NM_032717 // AGPAT9 // 1-acylglycerol-3-phosphate O-acyltransferase 9 // 4q21.23	AGPAT9	8.83E-17	7.02E-14	-2.48539	1.02E-11	-2.53796
2400177	NM_018584 // CAMK2N1 // calcium/calmodulin-dependent protein kinase II inhibitor	CAMK2N1	9.09E-17	2.68E-11	-1.59321	3.55E-14	-2.03219
3863669	NM_001712 // CEACAM1 // carcinoembryonic antigen-related cell adhesion molecule	CEACAM1	9.18E-17	4.82E-14	-2.88839	1.80E-11	-2.85705
3150844	NM_021021 // SNTB1 // syntrophin, beta 1 (dystrophin-associated protein A1, 59kD	SNTB1	9.27E-17	3.64E-12	1.52544	1.76E-13	1.76463
3084950	NM_194284 // CLDN23 // claudin 23 // 8p23.1 // 137075 /// BC125148 // CLDN23 //	CLDN23	1.01E-16	4.93E-13	-1.81667	1.36E-12	-2.01234
3104489	NM_007029 // STMN2 // stathmin-like 2 // 8q21.13 // 11075 /// ENST00000220876 //	STMN2	1.02E-16	5.06E-14	-3.36563	2.10E-11	-3.30824
3274898	NM_024803 // TUBAL3 // tubulin, alpha-like 3 // 10p15.1 // 79861 /// ENST0000038	TUBAL3	1.04E-16	1.04E-13	-2.85884	8.51E-12	-2.99011
3946510	NM_022098 // XPNPEP3 // X-prolyl aminopeptidase (aminopeptidase P) 3, putative /	XPNPEP3	1.12E-16	2.00E-09	1.28182	3.46E-15	1.61798
2897899	NM_003107 // SOX4 // SRY (sex determining region Y)-box 4 // 6p22.3 // 6659 ///	SOX4	1.16E-16	9.06E-15	1.47197	3.81E-10	1.38156
3568603	NM_002083 // GPX2 // glutathione peroxidase 2 (gastrointestinal) // 14q24.1 // 2	GPX2	1.17E-16	4.93E-13	1.96158	1.78E-12	2.18565
3394660	NM_012101 // TRIM29 // tripartite motif-containing 29 // 11q22-q23 // 23650 ///	TRIM29	1.18E-16	6.15E-14	2.90077	2.17E-11	2.87299
2570193	NM_005434 // MALL // mal, T-cell differentiation protein-like // 2q13 // 7851 //	MALL	1.21E-16	1.12E-12	-3.09693	8.11E-13	-3.99988
3976341	NM_003254 // TIMP1 // TIMP metallopeptidase inhibitor 1 // Xp11.3-p11.23 // 7076	TIMP1	1.24E-16	8.17E-14	2.49606	1.64E-11	2.52015
3452818	NM_001017535 // VDR // vitamin D (1,25- dihydroxyvitamin D3) receptor // 12q13.1	VDR	1.25E-16	3.26E-13	-1.52086	3.14E-12	-1.60078
3786471	NM_015559 // SETBP1 // SET binding protein 1 // 18q21.1 // 26040 /// BC146776 //	SETBP1	1.34E-16	3.18E-11	-1.39868	5.61E-14	-1.65941
2579572	NM_014795 // ZEB2 // zinc finger E-box binding homeobox 2 // 2q22 // 9839 /// EN	ZEB2	1.36E-16	7.76E-11	-1.68786	3.07E-14	-2.30002
3208327	ENST00000377415 // LOC100132426 // similar to hCG1742442 // 9q12 // 100132426	LOC100132426	1.38E-16	4.36E-13	7.82385	2.74E-12	10.404
3222128	NM_005118 // TNFSF15 // tumor necrosis factor (ligand) superfamily, member 15 //	TNFSF15	1.39E-16	3.20E-13	2.21241	3.90E-12	2.41992
2670948	NM_001099668 // HIGD1A // HIG1 domain family, member 1A // 3p22.1 // 25994 /// N	HIGD1A	1.45E-16	1.02E-13	-1.88807	1.69E-11	-1.90823
3823410	DQ249310 // UCA1 // urothelial cancer associated 1 // 19p13 // 652995	UCA1	1.46E-16	2.51E-12	2.85402	5.18E-13	3.82869
2655845	NM_004443 // EPHB3 // EPH receptor B3 // 3q21-qter // 2049 /// ENST00000330394 /	EPHB3	1.49E-16	2.10E-12	2.23182	6.27E-13	2.75895
3622436	NM_013309 // SLC30A4 // solute carrier family 30 (zinc transporter), member 4 //	SLC30A4	1.55E-16	1.33E-11	-1.82339	1.37E-13	-2.34669
2924330	NM_001003395 // TPD52L1 // tumor protein D52-like 1 // 6q22-q23 // 7164 /// NM_0	TPD52L1	1.57E-16	1.79E-13	1.74361	9.68E-12	1.7996
3444252	NM_003651 // CSDA // cold shock domain protein A // 12p13.1 // 8531 /// ENST0000	CSDA	1.57E-16	3.09E-11	1.41226	7.30E-14	1.67537
3985717	NM_001128834 // PLP1 // proteolipid protein 1 // Xq22 // 5354 /// NM_000533 // P	PLP1	1.67E-16	1.08E-11	-2.44745	1.81E-13	-3.48953
3592109	NM_003104 // SORD // sorbitol dehydrogenase // 15q15.3 // 6652 /// ENST000002678	SORD	1.70E-16	2.39E-11	1.72552	9.96E-14	2.22489
2487549	NM_002357 // MXD1 // MAX dimerization protein 1 // 2p13-p12 // 4084 /// ENST0000	MXD1	1.80E-16	6.08E-12	-1.9204	3.31E-13	-2.39858
3015603	NM_006076 // HRBL // HIV-1 Rev binding protein-like // 7q22.1 // 3268 /// ENST00	HRBL	1.82E-16	5.03E-15	-1.59863	3.37E-09	-1.42252
3379644	NM_001876 // CPT1A // carnitine palmitoyltransferase 1A (liver) // 11q13.1-q13.2	CPT1A	1.83E-16	5.11E-14	-1.70197	6.95E-11	-1.65162
3317915	NM_003156 // STIM1 // stromal interaction molecule 1 // 11p15.5 // 6786 /// ENST	STIM1	1.87E-16	1.20E-10	-1.30844	3.66E-14	-1.54085
2404999	NM_023009 // MARCKSL1 // MARCKS-like 1 // 1p35.1 // 65108 /// ENST00000329421 //	MARCKSL1	1.88E-16	5.21E-15	1.33124	3.42E-09	1.23991
3771215	NM_004035 // ACOX1 // acyl-Coenzyme A oxidase 1, palmitoyl // 17q24-q25|17q25.1	ACOX1	2.08E-16	1.96E-14	-1.77432	4.03E-10	-1.63284
3556990	NM_032876 // JUB // jub, ajuba homolog (Xenopus laevis) // 14q11.2 // 84962 ///	JUB	2.12E-16	8.25E-12	1.72847	3.31E-13	2.09958
3204833	NM_020944 // GBA2 // glucosidase, beta (bile acid) 2 // 9p13.3 // 57704 /// ENST	GBA2	2.18E-16	2.31E-13	-1.48476	1.34E-11	-1.51645
3907473	NM_005469 // ACOT8 // acyl-CoA thioesterase 8 // 20q13.12 // 10005 /// NM_183386	ACOT8	2.32E-16	2.38E-14	-1.43677	3.75E-10	-1.36712
2955556	NM_001114086 // CLIC5 // chloride intracellular channel 5 // 6p21.1-p12.1 // 534	CLIC5	2.35E-16	5.31E-10	-1.64695	1.97E-14	-2.38046
2857204	NM_003711 // PPAP2A // phosphatidic acid phosphatase type 2A // 5q11 // 8611 ///	PPAP2A	2.43E-16	5.49E-12	-1.81201	5.90E-13	-2.17878
3864646	NM_002250 // KCNN4 // potassium intermediate/small conductance calcium-activated	KCNN4	2.58E-16	1.15E-12	1.65606	2.97E-12	1.80744

2965206	NM_004440 // EPHA7 // EPH receptor A7 // 6q16.1 // 2045 /// ENST00000369303 // E	EPHA7	2.85E-16	5.39E-10	-1.61893	2.54E-14	-2.29594
3507465	NM_181785 // SLC46A3 // solute carrier family 46, member 3 // 13q12.3 // 283537	SLC46A3	2.88E-16	9.21E-13	-2.37154	4.58E-12	-2.69246
3302240	NM_015179 // RRP12 // ribosomal RNA processing 12 homolog (S. cerevisiae) // 10q	RRP12	2.90E-16	4.91E-10	1.28091	2.77E-14	1.52864
2324919	NM_017449 // EPHB2 // EPH receptor B2 // 1p36.1-p35 // 2048 /// NM_004442 // EPH	EPHB2	3.21E-16	1.41E-12	1.83119	3.52E-12	2.03525
2842101	NM_022754 // SFXN1 // sideroflexin 1 // --- // 94081 /// ENST00000321442 // SFXN	SFXN1	3.42E-16	1.79E-14	-2.11867	1.50E-09	-1.83545
2835715	NM_002084 // GPX3 // glutathione peroxidase 3 (plasma) // 5q23 // 2878 /// ENST0	GPX3	3.43E-16	2.09E-13	-1.75721	3.67E-11	-1.76923
3868841	NM_144947 // KLK11 // kallikrein-related peptidase 11 // 19q13.3-q13.4 // 11012	KLK11	3.53E-16	2.67E-13	2.0969	2.85E-11	2.14401
4008275	NM_020717 // SHROOM4 // shroom family member 4 // Xp11.22 // 57477 /// ENST00000	SHROOM4	3.59E-16	2.58E-12	1.63694	2.31E-12	1.82205
3781654	NM_003831 // RIOK3 // RIO kinase 3 (yeast) // 18q11.2 // 8780 /// ENST0000033948	RIOK3	3.63E-16	3.02E-11	-1.62797	2.66E-13	-2.00847
2831350	NM_016463 // CXXC5 // CXXC finger 5 // 5q31.3 // 51523 /// ENST00000302517 // CX	CXXC5	3.67E-16	3.10E-14	1.60386	6.95E-10	1.49359
3606034	NM_002605 // PDE8A // phosphodiesterase 8A // 15q25.3 // 5151 /// NM_173454 // P	PDE8A	3.69E-16	2.45E-13	-1.68362	3.46E-11	-1.70099
2512790	NM_022058 // SLC4A10 // solute carrier family 4, sodium bicarbonate transporter-	SLC4A10	3.74E-16	1.01E-14	-2.82028	5.39E-09	-2.18328
3010503	NM_001001548 // CD36 // CD36 molecule (thrombospondin receptor) // 7q11.2 // 948	CD36	3.82E-16	4.00E-10	-2.0379	4.63E-14	-3.28857
3105600	NM_000067 // CA2 // carbonic anhydrase II // 8q22 // 760 /// ENST00000285379 //	CA2	3.97E-16	6.20E-11	-4.34241	1.76E-13	-8.9188
2923939	NM_006714 // SMPDL3A // sphingomyelin phosphodiesterase, acid-like 3A // 6q22.31	SMPDL3A	4.67E-16	6.94E-09	-1.77807	1.19E-14	-3.09695
3261971	NM_017649 // CNNM2 // cyclin M2 // 10q24.32 // 54805 /// NM_199076 // CNNM2 // c	CNNM2	4.68E-16	2.70E-09	-1.46666	1.97E-14	-2.03647
3930235	NM_004414 // RCAN1 // regulator of calcineurin 1 // 21q22.1-q22.2|21q22.12 // 18	RCAN1	4.70E-16	9.81E-14	-1.57703	2.00E-10	-1.52469
2533493	NM_014521 // SH3BP4 // SH3-domain binding protein 4 // 2q37.1-q37.2 // 23677 ///	SH3BP4	4.94E-16	3.06E-13	1.52406	4.64E-11	1.53448
3599758	NM_001104554 // PAQR5 // progestin and adipoQ receptor family member V // 15q23	PAQR5	5.39E-16	9.80E-14	-2.14706	2.68E-10	-2.01281
3707812	NM_015253 // WSCD1 // WSC domain containing 1 // 17p13.2 // 23302 /// ENST000003	WSCD1	5.55E-16	9.29E-14	-1.9179	3.09E-10	-1.80734
3407453	NM_000921 // PDE3A // phosphodiesterase 3A, cGMP-inhibited // 12p12 // 5139 ///	PDE3A	5.72E-16	6.09E-12	-3.39657	2.22E-12	-4.64774
3509842	NM_001127217 // SMAD9 // SMAD family member 9 // 13q12-q14 // 4093 /// NM_005905	SMAD9	6.36E-16	3.80E-10	1.68729	9.85E-14	2.34364
3687475	NM_024307 // GDPD3 // glycerophosphodiester phosphodiesterase domain containing	GDPD3	6.41E-16	4.73E-14	-2.42352	1.24E-09	-2.10583
3062082	NM_002612 // PDK4 // pyruvate dehydrogenase kinase, isozyme 4 // 7q21.3 // 5166	PDK4	6.42E-16	2.52E-10	-1.95483	1.32E-13	-2.8972
2931391	NM_015440 // MTHFD1L // methylenetetrahydrofolate dehydrogenase (NADP+ dependent	MTHFD1L	6.44E-16	2.99E-10	1.46554	1.18E-13	1.84578
3449760	NM_144973 // DENND5B // DENN/MADD domain containing 5B // 12p11.21 // 160518 ///	DENND5B	6.46E-16	8.62E-11	-1.75755	2.86E-13	-2.30954
3563861	NM_004196 // CDKL1 // cyclin-dependent kinase-like 1 (CDC2-related kinase) // 14	CDKL1	6.63E-16	4.95E-13	-1.37107	4.47E-11	-1.38595
2585476	NM_002976 // SCN7A // sodium channel, voltage-gated, type VII, alpha // 2q21-q23	SCN7A	6.90E-16	8.55E-11	-2.24178	3.18E-13	-3.29935
3571667	NM_001249 // ENTPD5 // ectonucleoside triphosphate diphosphohydrolase 5 // 14q24	ENTPD5	6.97E-16	1.94E-12	-1.95722	1.00E-11	-2.15671
3327057	NM_024841 // FLJ14213 // protor-2 // 11p13-p12 // 79899 /// ENST00000378867 // F	FLJ14213	7.06E-16	5.35E-14	-1.69346	1.26E-09	-1.55989
3665501	NM_000196 // HSD11B2 // hydroxysteroid (11-beta) dehydrogenase 2 // 16q22 // 329	HSD11B2	7.19E-16	1.00E-14	-2.00033	3.05E-08	-1.62194
3846709	NM_017720 // STAP2 // signal transducing adaptor family member 2 // 19p13.3 // 5	STAP2	7.45E-16	1.42E-13	-1.59135	3.10E-10	-1.53433
2954355	NM_014780 // CUL7 // cullin 7 // 6p21.1 // 9820 /// ENST00000265348 // CUL7 // c	CUL7	7.45E-16	4.31E-12	1.28116	4.87E-12	1.34874
3217361	NM_173551 // ANKS6 // ankyrin repeat and sterile alpha motif domain containing 6	ANKS6	7.85E-16	7.14E-12	1.39379	3.24E-12	1.51292
3470964	NM_016433 // GLTP // glycolipid transfer protein // 12q24.11 // 51228 /// ENST00	GLTP	8.22E-16	2.36E-13	-1.63843	1.83E-10	-1.60375
2635184	NM_007072 // HHLA2 // HERV-H LTR-associating 2 // 3q13.13 // 11148 /// ENST00000	HHLA2	8.33E-16	8.30E-11	-2.8921	4.33E-13	-4.72237
2673873	NM_000884 // IMPDH2 // IMP (inosine monophosphate) dehydrogenase 2 // 3p21.2 //	IMPDH2	8.62E-16	2.80E-11	1.78166	1.10E-12	2.19372
3595691	NM_000236 // LIPC // lipase, hepatic // 15q21-q23 // 3990 /// ENST00000356113 //	LIPC	8.72E-16	1.85E-13	-2.05875	2.92E-10	-1.95998
3890640	NM_002591 // PCK1 // phosphoenolpyruvate carboxykinase 1 (soluble) // 20q13.31 /	PCK1	9.13E-16	7.70E-09	-3.09548	2.71E-14	-8.76711
3783565	NM_000371 // TTR // transthyretin // 18q12.1 // 7276 /// ENST00000237014 // TTR	TTR	9.23E-16	1.38E-06	-1.38075	2.78E-15	-2.35275
2486178	NM_002398 // MEIS1 // Meis homeobox 1 // 2p14-p13 // 4211 /// BC036511 // MEIS1	MEIS1	9.31E-16	5.09E-10	-2.06967	1.40E-13	-3.26794
2845362	NM_004174 // SLC9A3 // solute carrier family 9 (sodium/hydrogen exchanger), memb	SLC9A3	9.87E-16	1.19E-13	-5.82096	7.41E-10	-4.75492

3649890	NM_004996 // ABCC1 // ATP-binding cassette, sub-family C (CFTR/MRP), member 1 //	ABCC1	1.01E-15	3.14E-10	1.39423	2.18E-13	1.68727
3824993	NM_004864 // GDF15 // growth differentiation factor 15 // 19p13.11 // 9518 /// E	GDF15	1.08E-15	2.38E-12	2.54824	1.74E-11	2.87763
2944491	NM_001080480 // MBOAT1 // membrane bound O-acyltransferase domain containing 1 /	MBOAT1	1.10E-15	2.09E-10	-1.56313	3.28E-13	-1.97925
2409275	NM_182517 // C1orf210 // chromosome 1 open reading frame 210 // 1p34.2 // 149466	C1orf210	1.12E-15	5.87E-13	-1.62478	1.00E-10	-1.632
2975014	NM_005627 // SGK1 // serum/glucocorticoid regulated kinase 1 // 6q23 // 6446 ///	SGK1	1.14E-15	2.32E-12	-2.70061	1.99E-11	-3.05284
3776583	BC137437 // FLJ35776 // hypothetical LOC649446 // 18p11.31 // 649446 /// NM_0010	FLJ35776	1.15E-15	1.62E-11	1.68129	2.83E-12	1.95496
2470470	NM_145175 // FAM84A // family with sequence similarity 84, member A // 2p24.3 //	FAM84A	1.17E-15	2.32E-11	1.37699	2.11E-12	1.52581
3472183	NM_004658 // RASAL1 // RAS protein activator like 1 (GAP1 like) // 12q23-q24 //	RASAL1	1.17E-15	5.77E-12	1.42772	7.93E-12	1.53259
2898934	NM_006998 // SCGN // secretagogin, EF-hand calcium binding protein // 6p22.3-p22	SCGN	1.19E-15	1.28E-10	-2.48147	5.30E-13	-3.82462
2590491	NM_002500 // NEUROD1 // neurogenic differentiation 1 // 2q32 // 4760 /// ENST000	NEUROD1	1.20E-15	3.34E-10	-2.67774	2.68E-13	-4.68067
2566414	NM_012214 // MGAT4A // mannosyl (alpha-1,3-)-glycoprotein beta-1,4-N-acetylgluco	MGAT4A	1.21E-15	1.14E-10	-2.20198	5.97E-13	-3.17424
3184710	NM_005592 // MUSK // muscle, skeletal, receptor tyrosine kinase // 9q31.3-q32 //	MUSK	1.22E-15	2.41E-10	-1.72075	3.44E-13	-2.29971
2809245	NM_002203 // ITGA2 // integrin, alpha 2 (CD49B, alpha 2 subunit of VLA-2 recepto	ITGA2	1.24E-15	3.44E-13	2.31059	2.52E-10	2.22852
3444216	NM_018423 // STYK1 // serine/threonine/tyrosine kinase 1 // 12p13.2 // 55359 ///	STYK1	1.30E-15	1.24E-10	-1.52976	6.26E-13	-1.86452
3768791	NM_080284 // ABCA6 // ATP-binding cassette, sub-family A (ABC1), member 6 // 17q	ABCA6	1.33E-15	7.11E-12	-1.85425	7.96E-12	-2.10814
2367086	NM_002022 // FMO4 // flavin containing monooxygenase 4 // 1q23-q25 // 2329 /// N	FMO4	1.36E-15	5.20E-12	-1.83029	1.14E-11	-2.03977
2558150	NM_014911 // AAK1 // AP2 associated kinase 1 // 2p14 // 22848 /// NR_003705 // S	AAK1	1.40E-15	7.12E-07	-1.29064	5.86E-15	-1.89257
2827057	NM_023927 // GRAMD3 // GRAM domain containing 3 // 5q23.2 // 65983 /// ENST00000	GRAMD3	1.41E-15	1.25E-12	-1.93989	6.06E-11	-2.01261
3472755	NM_016569 // TBX3 // T-box 3 // 12q24.1 // 6926 /// NM_005996 // TBX3 // T-box 3	TBX3	1.42E-15	9.85E-12	1.80085	6.46E-12	2.06301
3157385	NM_052963 // TOP1MT // topoisomerase (DNA) I, mitochondrial // 8q24.3 // 116447	TOP1MT	1.45E-15	3.24E-12	1.53748	2.11E-11	1.62883
2429235	NM_000036 // AMPD1 // adenosine monophosphate deaminase 1 (isoform M) // 1p13 //	AMPD1	1.45E-15	4.00E-11	-2.78392	1.85E-12	-3.99804
3210013	NM_017662 // TRPM6 // transient receptor potential cation channel, subfamily M,	TRPM6	1.46E-15	3.35E-08	-2.79135	2.34E-14	-8.29021
3212420	NM_022127 // SLC28A3 // solute carrier family 28 (sodium-coupled nucleoside tran	SLC28A3	1.46E-15	2.16E-13	2.60444	6.97E-10	2.37835
2740067	NM_001148 // ANK2 // ankyrin 2, neuronal // 4q25-q27 // 287 /// NM_001127493 //	ANK2	1.51E-15	7.16E-11	-1.5989	1.22E-12	-1.93216
2424524	NM_000110 // DPYD // dihydropyrimidine dehydrogenase // 1p22 // 1806 /// ENST000	DPYD	1.54E-15	7.41E-09	-1.68557	5.50E-14	-2.66114
2531589	NM_030926 // ITM2C // integral membrane protein 2C // 2q37 // 81618 /// NM_00101	ITM2C	1.57E-15	9.27E-11	-1.45714	1.04E-12	-1.70968
2367743	NM_004905 // PRDX6 // peroxiredoxin 6 // 1q25.1 // 9588 /// ENST00000340385 // P	PRDX6	1.59E-15	3.67E-11	-1.82802	2.32E-12	-2.24248
3091301	NM_173174 // PTK2B // PTK2B protein tyrosine kinase 2 beta // 8p21.1 // 2185 ///	PTK2B	1.65E-15	4.21E-10	-1.29511	3.63E-13	-1.49896
3219215	NM_004235 // KLF4 // Kruppel-like factor 4 (gut) // 9q31 // 9314 /// ENST0000037	KLF4	1.65E-15	1.12E-11	-2.07622	7.32E-12	-2.4585
3742130	NM_014520 // MYBBP1A // MYB binding protein (P160) 1a // 17p13.3 // 10514 /// NM	MYBBP1A	1.67E-15	5.33E-09	1.22981	7.39E-14	1.46035
2669052	NM_014831 // LBA1 // lupus brain antigen 1 // 3p22.2 // 9881	LBA1	1.69E-15	5.27E-08	-1.62476	2.27E-14	-2.77937
3376235	NM_018093 // WDR74 // WD repeat domain 74 // 11q12.3 // 54663 /// ENST0000027885	WDR74	1.70E-15	1.10E-08	1.32977	5.07E-14	1.72448
3540552	NM_178155 // FUT8 // fucosyltransferase 8 (alpha (1,6) fucosyltransferase) // 14	FUT8	1.73E-15	2.40E-12	1.8233	4.11E-11	1.93052
3892812	NM_016354 // SLCO4A1 // solute carrier organic anion transporter family, member	SLCO4A1	1.84E-15	9.95E-10	1.56228	2.36E-13	2.08159
2835300	NM_000112 // SLC26A2 // solute carrier family 26 (sulfate transporter), member 2	SLC26A2	1.84E-15	4.22E-10	-3.94644	4.26E-13	-8.47779
2453370	NM_025179 // PLXNA2 // plexin A2 // 1q32.2 // 5362 /// ENST00000367033 // PLXNA2	PLXNA2	1.86E-15	3.54E-09	-1.30569	1.08E-13	-1.60627
3739162	NM_005993 // TBCD // tubulin folding cofactor D // 17q25.3 // 6904 /// ENST00000	TBCD	1.86E-15	5.43E-09	1.23301	8.47E-14	1.46525
3815399	NM_004368 // CNN2 // calponin 2 // 19p13.3 // 1265 /// NM_201277 // CNN2 // calp	CNN2	1.88E-15	3.73E-12	1.57484	2.91E-11	1.66798
3987029	NM_032227 // TMEM164 // transmembrane protein 164 // Xq22.3 // 84187 /// ENST000	TMEM164	1.89E-15	1.11E-11	-1.45727	9.35E-12	-1.58318
3687277	NM_012410 // SEZ6L2 // seizure related 6 homolog (mouse)-like 2 // 16p11.2 // 26	SEZ6L2	1.90E-15	4.44E-13	1.62546	4.23E-10	1.58316
3375307	NM_153611 // CYBASC3 // cytochrome b, ascorbate dependent 3 // 11q12.2 // 220002	CYBASC3	1.98E-15	6.39E-15	-1.56246	1.65E-06	-1.28598
2822492	BC009203 // C5orf30 // chromosome 5 open reading frame 30 // 5q21.1 // 90355 ///	C5orf30	2.00E-15	4.35E-12	-1.98875	2.73E-11	-2.18267

3864352	XM_001724326 // LOC100131563 // hypothetical protein LOC100131563 // 19q13.31 //	LOC100131563	2.00E-15	7.54E-11	-1.85207	1.80E-12	-2.35138
3875423	NM_001200 // BMP2 // bone morphogenetic protein 2 // 20p12 // 650 /// ENST000003	BMP2	2.24E-15	7.71E-13	-1.63113	2.76E-10	-1.61509
2775909	NM_016619 // PLAC8 // placenta-specific 8 // 4q21.22 // 51316 /// ENST0000031150	PLAC8	2.45E-15	1.12E-09	-2.24619	3.28E-13	-3.74924
2854092	NM_002310 // LIFR // leukemia inhibitory factor receptor alpha // 5p13-p12 // 39	LIFR	2.58E-15	6.22E-09	-2.01201	1.22E-13	-3.55131
3808745	NM_025214 // CCDC68 // coiled-coil domain containing 68 // 18q21 // 80323 /// EN	CCDC68	2.59E-15	1.27E-09	-2.07949	3.27E-13	-3.32645
3758510	NM_001986 // ETV4 // ets variant gene 4 (E1A enhancer binding protein, E1AF) //	ETV4	2.59E-15	1.07E-11	3.06352	1.66E-11	3.80566
2401384	NM_017707 // DDEFL1 // development and differentiation enhancing factor-like 1 /	DDEFL1	2.59E-15	1.66E-13	-1.39966	3.74E-09	-1.32522
2693357	NM_017836 // SLC41A3 // solute carrier family 41, member 3 // 3q21.2 // 54946 //	SLC41A3	2.60E-15	1.79E-12	1.28638	1.25E-10	1.29938
2845351	AK023178 // LOC25845 // hypothetical LOC25845 // 5p15.33 // 25845 /// BC086861 /	LOC25845	2.63E-15	3.39E-13	-4.37695	1.25E-09	-3.76276
2766788	NM_001098634 // RBM47 // RNA binding motif protein 47 // 4p13-p12 // 54502 /// N	RBM47	2.64E-15	4.40E-12	-1.49649	4.44E-11	-1.56782
3949162	NM_015124 // GRAMD4 // GRAM domain containing 4 // 22q13.31 // 23151 /// ENST000	GRAMD4	2.69E-15	2.37E-12	-1.51226	9.44E-11	-1.551
3064501	NM_178176 // MOGAT3 // monoacylglycerol O-acyltransferase 3 // 7q22.1 // 346606	MOGAT3	2.80E-15	6.73E-13	-2.0024	5.24E-10	-1.93555
3945545	NM_004900 // APOBEC3B // apolipoprotein B mRNA editing enzyme, catalytic polypep	APOBEC3B	2.81E-15	1.71E-14	-2.29344	3.99E-07	-1.68288
2682088	NM_173359 // EIF4E3 // eukaryotic translation initiation factor 4E family member	EIF4E3	2.84E-15	3.98E-08	-1.3252	5.06E-14	-1.76889
2899012	BC109207 // SLC17A4 // solute carrier family 17 (sodium phosphate), member 4 //	SLC17A4	2.94E-15	2.17E-09	-2.06443	2.76E-13	-3.39848
3962678	NM_007229 // PACSIN2 // protein kinase C and casein kinase substrate in neurons	PACSIN2	3.18E-15	1.17E-11	-1.32941	2.15E-11	-1.40181
3674886	NM_001077350 // C16orf35 // chromosome 16 open reading frame 35 // 16p13.3 // 81	C16orf35	3.28E-15	5.59E-09	1.20437	1.79E-13	1.39277
3527935	XM_001716933 // C14orf176 // chromosome 14 open reading frame 176 // 14q11.2 //	C14orf176	3.39E-15	3.60E-11	-2.04602	8.00E-12	-2.50138
3716950	NM_018404 // CENTA2 // centaurin, alpha 2 // 17q11.2 // 55803 /// ENST0000033088	CENTA2	3.41E-15	3.39E-12	-1.56044	9.61E-11	-1.6126
2560076	NM_033046 // RTKN // rhotekin // 2p13.1 // 6242 /// NM_001015055 // RTKN // rhot	RTKN	3.76E-15	3.80E-09	1.23543	2.73E-13	1.44108
2334986	NM_178033 // CYP4X1 // cytochrome P450, family 4, subfamily X, polypeptide 1 //	CYP4X1	3.84E-15	4.62E-13	3.45601	1.75E-09	3.03242
3816815	NM_002068 // GNA15 // guanine nucleotide binding protein (G protein), alpha 15 (	GNA15	3.93E-15	5.62E-09	1.47792	2.28E-13	1.99463
2694123	NM_003707 // RUVBL1 // RuvB-like 1 (E. coli) // 3q21 // 8607 /// ENST00000322623	RUVBL1	4.14E-15	2.62E-10	1.45722	2.02E-12	1.72556
2827525	NM_001046 // SLC12A2 // solute carrier family 12 (sodium/potassium/chloride tran	SLC12A2	4.30E-15	2.45E-12	2.56241	2.21E-10	2.63174
2645764	NM_001679 // ATP1B3 // ATPase, Na+/K+ transporting, beta 3 polypeptide // 3q23 /	ATP1B3	4.44E-15	4.63E-12	-1.92205	1.08E-10	-2.02611
3422144	NM_003667 // LGR5 // leucine-rich repeat-containing G protein-coupled receptor 5	LGR5	4.45E-15	2.89E-13	6.25522	5.04E-09	4.68667
3787855	NM_006033 // LIPG // lipase, endothelial // 18q21.1 // 9388 /// ENST00000261292	LIPG	4.46E-15	2.90E-11	1.79937	1.54E-11	2.07291
2926447	NM_003206 // TCF21 // transcription factor 21 // 6pter-qter // 6943 /// NM_19839	TCF21	4.54E-15	7.81E-11	-2.01433	6.37E-12	-2.53609
3409127	NM_020183 // ARNTL2 // aryl hydrocarbon receptor nuclear translocator-like 2 //	ARNTL2	4.85E-15	1.96E-09	1.73446	5.95E-13	2.46398
3829751	NM_032346 // PDCD2L // programmed cell death 2-like // 19q13.11 // 84306 /// ENS	PDCD2L	4.97E-15	3.43E-09	1.37132	4.28E-13	1.70779
3341155	NM_004055 // CAPN5 // calpain 5 // 11q14 // 726 /// ENST00000278559 // CAPN5 //	CAPN5	5.02E-15	6.23E-12	-1.39714	9.62E-11	-1.44325
2414366	NM_003713 // PPAP2B // phosphatidic acid phosphatase type 2B // 1pter-p22.1 // 8	PPAP2B	5.04E-15	1.09E-11	-1.50068	5.22E-11	-1.59167
3972929	NM_001128127 // GK // glycerol kinase // Xp21.3 // 2710 /// NM_203391 // GK // g	GK	5.09E-15	4.96E-13	-1.86201	2.86E-09	-1.72667
3383130	NM_023930 // KCTD14 // potassium channel tetramerisation domain containing 14 //	KCTD14	5.13E-15	1.57E-11	1.77477	3.63E-11	1.96335
3091746	NM_017412 // FZD3 // frizzled homolog 3 (Drosophila) // 8p21 // 7976 /// ENST000	FZD3	5.16E-15	4.31E-12	2.09448	1.56E-10	2.19458
3375049	NM_014502 // PRPF19 // PRP19/PSO4 pre-mRNA processing factor 19 homolog (S. cere	PRPF19	5.16E-15	3.64E-09	1.23572	4.34E-13	1.43257
3115530	M34428 // PVT1 // Pvt1 oncogene (non-protein coding) // 8q24 // 5820 /// M34429	PVT1	5.33E-15	5.21E-13	1.66471	2.94E-09	1.56526
3450899	NM_052885 // SLC2A13 // solute carrier family 2 (facilitated glucose transporter	SLC2A13	5.38E-15	3.99E-10	-1.39953	2.16E-12	-1.63873
2675763	NM_004704 // RRP9 // ribosomal RNA processing 9, small subunit (SSU) processome	RRP9	5.76E-15	4.06E-06	1.18323	1.59E-14	1.56635
3237280	NM_001098844 // FAM23A // family with sequence similarity 23, member A // 10p12.	FAM23A	5.86E-15	1.17E-09	-3.69581	1.11E-12	-7.78262
2775994	NM_001098540 // HPSE // heparanase // 4q21.3 // 10855 /// NM_006665 // HPSE // h	HPSE	5.87E-15	1.25E-12	-1.4445	9.92E-10	-1.41665
3733590	NM_000346 // SOX9 // SRY (sex determining region Y)-box 9 // 17q24.3-q25.1 // 66	SOX9	5.88E-15	8.14E-10	1.47068	1.45E-12	1.80625

2879312	NM_000176 // NR3C1 // nuclear receptor subfamily 3, group C, member 1 (glucocort	NR3C1	6.19E-15	3.01E-08	-1.61006	1.60E-13	-2.50212
3458783	NM_000075 // CDK4 // cyclin-dependent kinase 4 // 12q14 // 1019 /// ENST00000257	CDK4	6.26E-15	2.36E-06	1.30762	2.16E-14	1.98685
3594031	NM_014548 // TMOD2 // tropomodulin 2 (neuronal) // 15q21.1-q21.2 // 29767 /// EN	TMOD2	6.49E-15	9.75E-10	-1.42568	1.47E-12	-1.72865
3318666	NM_000543 // SMPD1 // sphingomyelin phosphodiesterase 1, acid lysosomal // 11p15	SMPD1	6.53E-15	9.20E-13	-1.87047	1.92E-09	-1.77046
3430959	NM_001093 // ACACB // acetyl-Coenzyme A carboxylase beta // 12q24.11 // 32 /// E	ACACB	6.66E-15	3.91E-10	-1.42284	3.03E-12	-1.66829
2461037	NM_014801 // PCNXL2 // pecanex-like 2 (Drosophila) // 1q42.2 // 80003 /// ENST00	PCNXL2	6.69E-15	3.06E-14	1.60954	1.21E-06	1.3323
3973768	NM_198511 // LANCL3 // LanC lantibiotic synthetase component C-like 3 (bacterial	LANCL3	7.02E-15	6.54E-14	-1.63753	2.46E-07	-1.39236
3057955	NM_006682 // FGL2 // fibrinogen-like 2 // 7q11.23 // 10875 /// ENST00000248598 /	FGL2	7.04E-15	2.54E-08	-1.78782	2.08E-13	-3.00584
3723348	NM_006460 // HEXIM1 // hexamethylene bis-acetamide inducible 1 // 17q21.31 // 10	HEXIM1	7.14E-15	2.19E-11	-1.41792	4.56E-11	-1.51004
3517251	NM_080759 // DACH1 // dachshund homolog 1 (Drosophila) // 13q22 // 1602 /// NM_0	DACH1	7.17E-15	4.29E-11	1.78648	2.34E-11	2.05352
3168938	NM_022490 // POLR1E // polymerase (RNA) I polypeptide E, 53kDa // 9p13.2 // 6442	POLR1E	7.32E-15	5.59E-09	1.40921	5.37E-13	1.80224
3190061	NM_004957 // FPGS // folylpolyglutamate synthase // 9q34.1 // 2356 /// NM_001018	FPGS	7.37E-15	1.29E-07	1.20879	9.46E-14	1.48838
2976768	NM_006079 // CITED2 // Cbp/p300-interacting transactivator, with Glu/Asp-rich ca	CITED2	7.44E-15	1.59E-09	-1.44366	1.26E-12	-1.78789
2841964	NM_002449 // MSX2 // msh homeobox 2 // 5q34-q35 // 4488 /// NR_002307 // MSX2P1	MSX2	7.56E-15	2.37E-11	2.68766	4.64E-11	3.22071
3929076	NR_002996 // SNORA80 // small nucleolar RNA, H/ACA box 80 // 21q22.11 // 677846	SNORA80	7.58E-15	1.97E-09	1.38785	1.12E-12	1.69131
3417309	NM_006191 // PA2G4 // proliferation-associated 2G4, 38kDa // 12q13.2 // 5036 ///	PA2G4	7.59E-15	9.35E-06	1.24739	1.61E-14	1.85805
2945882	NR_002174 // CMAH // cytidine monophosphate-N-acetylneuraminic acid hydroxylase	CMAH	7.60E-15	8.87E-05	-1.4437	7.62E-15	-3.41036
3817116	NM_014428 // TJP3 // tight junction protein 3 (zona occludens 3) // 19p13.3 // 2	TJP3	8.15E-15	8.89E-12	-1.41507	1.54E-10	-1.46063
3903361	NM_000687 // AHCY // S-adenosylhomocysteine hydrolase // 20cen-q13.1 // 191 ///	AHCY	8.38E-15	1.27E-07	1.32438	1.12E-13	1.79608
2927604	NM_020340 // KIAA1244 // KIAA1244 // 6q23.3 // 57221 /// ENST00000251691 // KIAA	KIAA1244	8.44E-15	3.25E-12	1.87107	5.64E-10	1.87248
3129175	NM_173833 // SCARA5 // scavenger receptor class A, member 5 (putative) // 8p21.1	SCARA5	8.66E-15	1.03E-12	-1.74762	2.92E-09	-1.65284
3468345	NM_001111283 // IGF1 // insulin-like growth factor 1 (somatomedin C) // 12q22-q2	IGF1	8.68E-15	8.70E-10	-1.77638	2.44E-12	-2.38037
3202316	NM_024761 // MOBKL2B // MOB1, Mps One Binder kinase activator-like 2B (yeast) //	MOBKL2B	8.83E-15	2.07E-11	-1.47708	6.99E-11	-1.57179
2585400	NM_002977 // SCN9A // sodium channel, voltage-gated, type IX, alpha subunit // 2	SCN9A	8.88E-15	4.78E-09	-2.03233	7.75E-13	-3.30229
3127703	NM_003842 // TNFRSF10B // tumor necrosis factor receptor superfamily, member 10b	TNFRSF10B	9.39E-15	2.30E-10	1.53674	7.89E-12	1.80476
3142485	NM_005536 // IMPA1 // inositol(myo)-1(or 4)-monophosphatase 1 // 8q21.13-q21.3 /	IMPA1	9.82E-15	2.24E-10	-1.62851	8.64E-12	-1.94905
2854088	NM_001127671 // LIFR // leukemia inhibitory factor receptor alpha // 5p13-p12 //	LIFR	9.83E-15	1.23E-07	-1.95536	1.39E-13	-3.99792
2450668	NM_016456 // TMEM9 // transmembrane protein 9 // --- // 252839 /// ENST000003673	TMEM9	9.88E-15	2.41E-10	1.38228	8.20E-12	1.56066
3230697	NM_015392 // NPDC1 // neural proliferation, differentiation and control, 1 // 9q	NPDC1	9.98E-15	1.52E-08	1.42292	4.45E-13	1.88996
3535628	NM_053064 // GNG2 // guanine nucleotide binding protein (G protein), gamma 2 //	GNG2	1.00E-14	9.88E-11	-1.86905	1.84E-11	-2.24145
3540007	NM_005956 // MTHFD1 // methylenetetrahydrofolate dehydrogenase (NADP+ dependent)	MTHFD1	1.00E-14	6.41E-07	1.31914	6.56E-14	1.89129
3638607	NM_001150 // ANPEP // alanyl (membrane) aminopeptidase // 15q25-q26 // 290 /// E	ANPEP	1.01E-14	4.66E-11	-7.01314	3.82E-11	-10.8
2880679	NM_024577 // SH3TC2 // SH3 domain and tetratricopeptide repeats 2 // 5q32 // 796	SH3TC2	1.07E-14	1.02E-12	2.28499	4.68E-09	2.07268
2835531	NM_001543 // NDST1 // N-deacetylase/N-sulfotransferase (heparan glucosaminyl) 1	NDST1	1.07E-14	3.21E-12	-1.37261	9.17E-10	-1.36463
2841120	AK096661 // LOC54492 // hypothetical LOC54492 // 5q35.1 // 54492	LOC54492	1.09E-14	2.34E-12	-2.20018	1.45E-09	-2.12002
3718191	NM_005623 // CCL8 // chemokine (C-C motif) ligand 8 // 17q11.2 // 6355 /// ENST0	CCL8	1.11E-14	5.86E-12	-4.75041	4.54E-10	-4.9865
2763912	NM_173463 // CCDC149 // coiled-coil domain containing 149 // 4p15.2 // 91050 ///	CCDC149	1.13E-14	2.71E-12	1.38013	1.27E-09	1.36377
2735409	NM_016323 // HERC5 // hect domain and RLD 5 // 4q22.1 // 51191 /// ENST000002643	HERC5	1.14E-14	1.61E-10	-1.32058	1.47E-11	-1.44574
2463173	NM_022469 // GREM2 // gremlin 2, cysteine knot superfamily, homolog (Xenopus lae	GREM2	1.16E-14	2.46E-09	-2.21062	1.77E-12	-3.53723
3414739	NM_014033 // METTL7A // methyltransferase like 7A // 12q13.13 // 25840 /// ENST0	METTL7A	1.19E-14	7.05E-11	-2.041	3.33E-11	-2.43425
3442427	NM_005768 // LPCAT3 // lysophosphatidylcholine acyltransferase 3 // 12p13 // 101	LPCAT3	1.22E-14	1.59E-13	-1.74665	1.64E-07	-1.4816
2673270	NM_016479 // SHISA5 // shisa homolog 5 (Xenopus laevis) // 3p21.31 // 51246 ///	SHISA5	1.25E-14	6.44E-11	1.27547	3.99E-11	1.35033

3874636	NM_175839 // SMOX // spermine oxidase // 20p13 // 54498 /// NM_175842 // SMOX //	SMOX	1.28E-14	1.04E-11	1.52681	2.94E-10	1.57298
3933331	NM_015500 // C2CD2 // C2 calcium-dependent domain containing 2 // 21q22.3 // 259	C2CD2	1.31E-14	3.11E-12	1.29898	1.41E-09	1.28671
3496637	NM_005708 // GPC6 // glypican 6 // 13q32 // 10082 /// ENST00000377047 // GPC6 //	GPC6	1.33E-14	4.59E-09	-1.52922	1.39E-12	-2.01394
2990404	NM_001112706 // SCIN // scinderin // 7p21.3 // 85477 /// NM_033128 // SCIN // sc	SCIN	1.37E-14	2.16E-10	-2.63493	1.50E-11	-3.66164
2514304	NM_005771 // DHRS9 // dehydrogenase/reductase (SDR family) member 9 // 2q31.1 //	DHRS9	1.38E-14	7.72E-12	-3.53013	4.86E-10	-3.70537
4021433	NM_001421 // ELF4 // E74-like factor 4 (ets domain transcription factor) // Xq26	ELF4	1.39E-14	1.26E-11	-1.45405	2.73E-10	-1.49885
4000155	NM_001001995 // GPM6B // glycoprotein M6B // Xp22.2 // 2824 /// NM_001001996 //	GPM6B	1.43E-14	7.99E-11	-1.79037	4.01E-11	-2.06407
3346453	NM_006106 // YAP1 // Yes-associated protein 1, 65kDa // 11q13 // 10413 /// ENST0	YAP1	1.53E-14	1.48E-11	1.40308	2.69E-10	1.44551
2339872	NM_005012 // ROR1 // receptor tyrosine kinase-like orphan receptor 1 // 1p32-p31	ROR1	1.53E-14	2.63E-06	-1.30485	5.98E-14	-1.94085
3960722	ENST00000406767 // RP1-199H16.1 // hypothetical LOC388900 // 22q13.1 // 388900	RP1-199H16.1	1.59E-14	4.41E-12	1.42704	1.30E-09	1.4163
2374422	BC106877 // C1orf106 // chromosome 1 open reading frame 106 // 1q32.1 // 55765 /	C1orf106	1.61E-14	2.75E-08	-1.26149	5.94E-13	-1.53162
3596147	NM_004751 // GCNT3 // glucosaminyl (N-acetyl) transferase 3, mucin type // 15q21	GCNT3	1.67E-14	7.55E-11	-3.03652	5.49E-11	-3.9084
2515933	NM_016653 // ZAK // sterile alpha motif and leucine zipper containing kinase AZK	ZAK	1.75E-14	3.70E-10	1.56737	1.39E-11	1.85235
3940360	ENST00000406486 // CTA-221G9.4 // KIAA1671 protein // 22q11.23 // 85379 /// AL83	CTA-221G9.4	1.80E-14	2.68E-11	-1.25682	1.83E-10	-1.29421
2949524	NM_006709 // EHMT2 // euchromatic histone-lysine N-methyltransferase 2 // 6p21.3	EHMT2	1.88E-14	1.57E-09	1.18089	4.91E-12	1.28503
2459616	NM_033445 // HIST3H2A // histone cluster 3, H2a // 1q42.13 // 92815 /// ENST0000	HIST3H2A	1.90E-14	1.76E-10	1.52814	3.05E-11	1.732
3299463	NM_144590 // ANKRD22 // ankyrin repeat domain 22 // 10q23.31 // 118932 /// ENST0	ANKRD22	1.93E-14	2.55E-10	2.38637	2.23E-11	3.17721
3832114	NM_015073 // SIPA1L3 // signal-induced proliferation-associated 1 like 3 // 19q1	SIPA1L3	1.95E-14	9.09E-11	-1.34287	5.95E-11	-1.438
3800834	NM_138340 // ABHD3 // abhydrolase domain containing 3 // 18q11.2 // 171586 /// E	ABHD3	1.97E-14	2.65E-11	-1.48579	2.18E-10	-1.55831
3948259	NM_001017526 // ARHGAP8 // Rho GTPase activating protein 8 // 22q13.31 // 23779	ARHGAP8	1.97E-14	2.96E-11	1.29184	1.93E-10	1.33562
3256590	NM_004670 // PAPSS2 // 3'-phosphoadenosine 5'-phosphosulfate synthase 2 // 10q23	PAPSS2	2.12E-14	8.67E-11	-1.82895	7.12E-11	-2.09085
2612813	NM_015184 // PLCL2 // phospholipase C-like 2 // 3p24.3 // 23228 /// ENST00000285	PLCL2	2.12E-14	2.69E-09	-1.55746	3.93E-12	-1.99113
3868659	NM_199249 // C19orf48 // chromosome 19 open reading frame 48 // 19q13.33 // 8479	C19orf48	2.15E-14	5.64E-08	1.50148	5.77E-13	2.16341
2563536	NM_001443 // FABP1 // fatty acid binding protein 1, liver // 2p11 // 2168 /// EN	FABP1	2.16E-14	6.31E-11	-2.76414	1.02E-10	-3.35726
4011008	NM_007268 // VSIG4 // V-set and immunoglobulin domain containing 4 // Xq12-q13.3	VSIG4	2.25E-14	7.54E-10	-1.90028	1.13E-11	-2.49059
3029129	NM_003461 // ZYX // zyxin // 7q32 // 7791 /// NM_001010972 // ZYX // zyxin // 7q	ZYX	2.34E-14	8.46E-11	1.33546	8.63E-11	1.41984
3674659	NR_023348 // GAS8 // growth arrest-specific 8 // 16q24.3 // 2622 /// NM_001481 /	GAS8	2.35E-14	2.91E-10	1.29534	2.72E-11	1.40943
3189864	NM_138361 // LRSAM1 // leucine rich repeat and sterile alpha motif containing 1	LRSAM1	2.36E-14	1.09E-09	1.24174	9.05E-12	1.37006
2757427	NM_012318 // LETM1 // leucine zipper-EF-hand containing transmembrane protein 1	LETM1	2.45E-14	6.15E-14	-1.6283	9.76E-06	-1.30531
2488680	NM_006062 // SMYD5 // SMYD family member 5 // 2p13.2 // 10322 /// ENST0000038950	SMYD5	2.45E-14	3.05E-09	1.23703	4.42E-12	1.39236
3434760	NM_002560 // P2RX4 // purinergic receptor P2X, ligand-gated ion channel, 4 // 12	P2RX4	2.45E-14	4.33E-11	-1.50671	1.88E-10	-1.60059
3863060	NM_020158 // EXOSC5 // exosome component 5 // 19q13.1 // 56915 /// ENST000002212	EXOSC5	2.56E-14	4.32E-07	1.28719	2.50E-13	1.72369
3959918	NM_003312 // TST // thiosulfate sulfurtransferase (rhodanese) // 22q13.1 // 7263	TST	2.62E-14	2.48E-13	-1.96582	4.66E-07	-1.58238
3260937	NM_021830 // C10orf2 // chromosome 10 open reading frame 2 // 10q23.3-q24.3 // 5	C10orf2	2.65E-14	5.04E-08	1.29637	8.10E-13	1.62358
2945645	NM_016614 // TTRAP // TRAF and TNF receptor associated protein // 6p22.3-p22.1 /	TTRAP	2.68E-14	7.10E-11	-1.67215	1.29E-10	-1.83945
3975227	NM_000240 // MAOA // monoamine oxidase A // Xp11.3 // 4128 /// ENST00000338702 /	MAOA	2.72E-14	4.54E-11	-2.09478	2.13E-10	-2.32969
3964154	NM_022766 // CERK // ceramide kinase // 22q13.31 // 64781 /// ENST00000216264 //	CERK	2.77E-14	1.46E-08	-1.44048	1.82E-12	-1.87105
3590341	NM_007236 // CHP // calcium binding protein P22 // 15q13.3 // 11261 /// ENST0000	CHP	2.80E-14	5.63E-13	-1.52513	1.10E-07	-1.37235
3151883	NM_194291 // TMEM65 // transmembrane protein 65 // 8q24.13 // 157378 /// ENST000	TMEM65	2.81E-14	1.98E-11	-1.44817	5.78E-10	-1.48456
4015548	NM_212559 // XKRX // XK, Kell blood group complex subunit-related, X-linked // X	XKRX	2.81E-14	4.53E-10	1.74205	2.44E-11	2.1211
3688254	NM_002773 // PRSS8 // protease, serine, 8 // 16p11.2 // 5652 /// ENST00000317508	PRSS8	3.03E-14	3.48E-11	-1.61136	3.44E-10	-1.69958
2624291	NM_006254 // PRKCD // protein kinase C, delta // 3p21.31 // 5580 /// NM_212539 /	PRKCD	3.03E-14	5.01E-09	-1.31293	4.20E-12	-1.54248

2908052	NM_203290 // POLR1C // polymerase (RNA) I polypeptide C, 30kDa // 6p21.1 // 9533	POLR1C	3.07E-14	6.00E-09	1.33172	3.79E-12	1.58604
3743551	NM_001307 // CLDN7 // claudin 7 // 17p13 // 1366 /// ENST00000360325 // CLDN7 //	CLDN7	3.19E-14	4.25E-12	-1.52038	5.47E-09	-1.47067
3431376	NM_033121 // ANKRD13A // ankyrin repeat domain 13A // 12q24.11 // 88455 /// ENST	ANKRD13A	3.24E-14	1.14E-08	-1.36973	2.66E-12	-1.69417
3416921	NM_002905 // RDH5 // retinol dehydrogenase 5 (11-cis/9-cis) // 12q13-q14 // 5959	RDH5	3.33E-14	2.17E-12	-1.62664	1.64E-08	-1.51758
3761451	NM_024017 // HOXB9 // homeobox B9 // 17q21.3 // 3219 /// ENST00000311177 // HOXB	HOXB9	3.36E-14	3.96E-08	1.45556	1.28E-12	1.97848
4015312	NM_001105243 // PCDH19 // protocadherin 19 // Xq13.3 // 57526 /// NM_020766 // P	PCDH19	3.38E-14	5.81E-09	-1.40561	4.43E-12	-1.72361
2893895	NM_001718 // BMP6 // bone morphogenetic protein 6 // 6p24-p23 // 654 /// ENST000	BMP6	3.40E-14	3.76E-12	-1.72141	7.45E-09	-1.63456
3720817	NM_016339 // RAPGEFL1 // Rap guanine nucleotide exchange factor (GEF)-like 1 //	RAPGEFL1	3.48E-14	5.47E-10	-1.55469	2.89E-11	-1.81952
3535515	NM_001042481 // FRMD6 // FERM domain containing 6 // 14q22.1 // 122786 /// NM_15	FRMD6	3.51E-14	8.36E-11	-1.47999	1.73E-10	-1.58794
2659393	NM_152672 // OSTalpha // organic solute transporter alpha // 3q29 // 200931 ///	OSTalpha	3.55E-14	1.02E-13	-4.1584	8.21E-06	-2.22614
2787096	NM_015130 // TBC1D9 // TBC1 domain family, member 9 (with GRAM domain) // 4q31.2	TBC1D9	3.61E-14	1.29E-09	-1.6496	1.50E-11	-2.05372
3571553	NM_194278 // C14orf43 // chromosome 14 open reading frame 43 // 14q24.3 // 91748	C14orf43	3.67E-14	1.96E-10	-1.34091	8.00E-11	-1.44495
2909263	NM_005588 // MEP1A // meprin A, alpha (PABA peptide hydrolase) // 6p12-p11 // 42	MEP1A	3.69E-14	2.84E-09	-2.7035	8.43E-12	-4.51845
3957445	NM_014303 // PES1 // pescadillo homolog 1, containing BRCT domain (zebrafish) //	PES1	3.70E-14	7.36E-08	1.25617	1.01E-12	1.53742
3434594	NM_000017 // ACADS // acyl-Coenzyme A dehydrogenase, C-2 to C-3 short chain // 1	ACADS	3.70E-14	3.28E-13	-1.90256	6.35E-07	-1.54315
2427930	NM_024102 // WDR77 // WD repeat domain 77 // 1p13.2 // 79084 /// ENST00000235090	WDR77	3.71E-14	4.38E-08	1.46664	1.37E-12	2.00914
2728938	NM_015236 // LPHN3 // latrophilin 3 // 4q13.1 // 23284 /// ENST00000295349 // LP	LPHN3	3.77E-14	3.11E-09	-1.52565	8.13E-12	-1.90376
3941683	NM_032173 // ZNRF3 // zinc and ring finger 3 // 22q12.1 // 84133 /// ENST0000033	ZNRF3	3.81E-14	9.69E-11	1.75644	1.71E-10	1.95135
3978760	NM_014061 // MAGEH1 // melanoma antigen family H, 1 // Xp11.21 // 28986 /// ENST	MAGEH1	3.84E-14	1.09E-09	-1.50878	1.90E-11	-1.79015
3359224	NM_005170 // ASCL2 // achaete-scute complex homolog 2 (Drosophila) // 11p15.5 //	ASCL2	3.88E-14	1.74E-10	1.95848	9.81E-11	2.30041
2594627	BC039295 // FAM126B // family with sequence similarity 126, member B // 2q33.1 /	FAM126B	3.91E-14	1.71E-10	-1.52204	1.01E-10	-1.68163
3444086	NM_007360 // KLRK1 // killer cell lectin-like receptor subfamily K, member 1 //	KLRK1	3.96E-14	2.00E-06	-1.48848	2.09E-13	-2.55173
2371139	NM_005562 // LAMC2 // laminin, gamma 2 // 1q25-q31 // 3918 /// NM_018891 // LAMC	LAMC2	3.98E-14	4.72E-12	2.0111	7.42E-09	1.89131
2500919	NM_005415 // SLC20A1 // solute carrier family 20 (phosphate transporter), member	SLC20A1	4.00E-14	5.24E-13	-3.8984	3.00E-07	-2.63495
3347615	NM_000019 // ACAT1 // acetyl-Coenzyme A acetyltransferase 1 // 11q22.3-q23.1 //	ACAT1	4.03E-14	3.19E-11	-1.92768	6.35E-10	-2.03378
2619666	NM_017719 // SNRK // SNF related kinase // 3p22.1 // 54861 /// NM_001100594 // S	SNRK	4.16E-14	2.31E-09	-1.26009	1.17E-11	-1.40982
2615060	NM_001003793 // RBMS3 // RNA binding motif, single stranded interacting protein	RBMS3	4.23E-14	1.75E-09	-1.53787	1.49E-11	-1.87129
2445982	NM_004673 // ANGPTL1 // angiopoietin-like 1 // 1q25.2 // 9068 /// ENST0000023481	ANGPTL1	4.50E-14	9.45E-09	-1.73988	4.74E-12	-2.46485
2955761	NM_016593 // CYP39A1 // cytochrome P450, family 39, subfamily A, polypeptide 1 /	CYP39A1	4.55E-14	2.05E-10	1.68902	1.09E-10	1.91788
2866225	NM_002397 // MEF2C // myocyte enhancer factor 2C // 5q14 // 4208 /// ENST0000034	MEF2C	4.59E-14	7.56E-10	-1.86053	3.36E-11	-2.33569
2992814	NM_001005340 // GPNMB // glycoprotein (transmembrane) nmb // 7p15 // 10457 /// N	GPNMB	4.72E-14	5.06E-10	-2.30828	5.00E-11	-3.02984
3070712	NM_003941 // WASL // Wiskott-Aldrich syndrome-like // 7q31.3 // 8976 /// ENST000	WASL	4.82E-14	8.65E-10	-1.43973	3.24E-11	-1.65101
3960782	NM_014876 // JOSD1 // Josephin domain containing 1 // 22q13.1 // 9929 /// ENST00	JOSD1	4.86E-14	2.09E-12	-1.70088	3.98E-08	-1.54806
2778440	NM_003728 // UNC5C // unc-5 homolog C (C. elegans) // 4q21-q23 // 8633 /// ENST0	UNC5C	5.12E-14	5.76E-10	-1.44053	5.05E-11	-1.62578
3190659	NM_001122821 // SET // SET nuclear oncogene // 9q34 // 6418 /// NM_003011 // SET	SET	5.23E-14	3.54E-09	1.39024	1.19E-11	1.6456
3231846	NM_014023 // WDR37 // WD repeat domain 37 // 10p15.3 // 22884 /// ENST0000035822	WDR37	5.25E-14	3.00E-09	-1.16059	1.35E-11	-1.24925
2429914	NM_001542 // IGSF3 // immunoglobulin superfamily, member 3 // 1p13 // 3321 /// N	IGSF3	5.47E-14	1.42E-09	-1.39908	2.60E-11	-1.60818
3329649	NM_000107 // DDB2 // damage-specific DNA binding protein 2, 48kDa // 11p12-p11 /	DDB2	5.69E-14	1.77E-10	1.48256	1.82E-10	1.61123
3685610	NM_001006634 // ARHGAP17 // Rho GTPase activating protein 17 // 16p12.1 // 55114	ARHGAP17	5.92E-14	4.33E-09	-1.28637	1.22E-11	-1.46741
3337168	NM_000852 // GSTP1 // glutathione S-transferase pi 1 // 11q13 // 2950 /// ENST00	GSTP1	5.96E-14	3.26E-08	1.4156	3.11E-12	1.83523
3555340	NM_007110 // TEP1 // telomerase-associated protein 1 // 14q11.2 // 7011 /// ENST	TEP1	6.03E-14	6.83E-10	-1.29236	5.62E-11	-1.40835
2855285	NM_001093726 // SEPP1 // selenoprotein P, plasma, 1 // 5q31 // 6414 /// NM_00108	SEPP1	6.17E-14	1.92E-05	-1.72855	1.39E-13	-4.46719

3695699	NM_004691 // ATP6V0D1 // ATPase, H+ transporting, lysosomal 38kDa, V0 subunit d1	ATP6V0D1	6.47E-14	8.51E-14	-1.65064	8.38E-05	-1.27058
3783788	NM_005925 // MEP1B // meprin A, beta // 18q12.2-q12.3 // 4225 /// ENST0000026920	MEP1B	6.52E-14	2.29E-12	-8.89031	6.53E-08	-5.82649
3622282	NM_138356 // SHF // Src homology 2 domain containing F // 15q21.1 // 90525 /// E	SHF	6.55E-14	1.49E-10	1.67082	2.74E-10	1.83679
3442641	NM_174941 // CD163L1 // CD163 molecule-like 1 // 12p13.3 // 283316 /// ENST00000	CD163L1	6.59E-14	5.69E-10	-2.10647	7.61E-11	-2.65484
2502842	NM_183240 // TMEM37 // transmembrane protein 37 // 2q14.2 // 140738 /// ENST0000	TMEM37	6.70E-14	9.98E-10	-1.81068	4.75E-11	-2.24766
4021341	NM_016032 // ZDHHC9 // zinc finger, DHHC-type containing 9 // Xq26.1 // 51114 //	ZDHHC9	6.75E-14	5.98E-10	1.34826	7.54E-11	1.48072
2979111	NM_032832 // LRP11 // low density lipoprotein receptor-related protein 11 // 6q2	LRP11	6.84E-14	1.59E-07	1.1918	1.46E-12	1.40359
2348896	NM_003672 // CDC14A // CDC14 cell division cycle 14 homolog A (S. cerevisiae) //	CDC14A	6.91E-14	1.08E-07	-1.46834	1.85E-12	-2.0596
3742285	NM_022059 // CXCL16 // chemokine (C-X-C motif) ligand 16 // 17p13 // 58191 /// N	CXCL16	7.16E-14	4.57E-11	1.56965	1.18E-09	1.61936
2571217	NM_032494 // ZC3H8 // zinc finger CCCH-type containing 8 // 2q13 // 84524 /// EN	ZC3H8	7.24E-14	5.55E-10	1.34446	9.03E-11	1.46967
3228191	NM_022779 // DDX31 // DEAD (Asp-Glu-Ala-Asp) box polypeptide 31 // 9q34.13 // 64	DDX31	7.30E-14	2.63E-09	1.34399	2.44E-11	1.53725
3458248	NM_005379 // MYO1A // myosin IA // 12q13-q14 // 4640 /// ENST00000300119 // MYO1	MYO1A	7.41E-14	1.15E-09	-1.92402	4.93E-11	-2.45112
3823340	NM_023944 // CYP4F12 // cytochrome P450, family 4, subfamily F, polypeptide 12 /	CYP4F12	7.89E-14	2.63E-10	-1.92807	2.10E-10	-2.23244
2327482	NM_001048194 // RCC1 // regulator of chromosome condensation 1 // 1p36.1 // 1104	RCC1	7.91E-14	7.35E-08	1.2951	2.76E-12	1.60166
3961842	NM_002883 // RANGAP1 // Ran GTPase activating protein 1 // 22q13 // 5905 /// ENS	RANGAP1	7.96E-14	1.57E-06	1.26794	5.46E-13	1.70592
2907623	NM_201523 // KLC4 // kinesin light chain 4 // 6p21.1 // 89953 /// NM_201522 // K	KLC4	8.08E-14	8.99E-10	-1.2501	6.96E-11	-1.34844
3670918	NM_002661 // PLCG2 // phospholipase C, gamma 2 (phosphatidylinositol-specific) /	PLCG2	8.10E-14	1.72E-09	-1.46265	4.01E-11	-1.70518
3060300	NM_003130 // SRI // sorcin // 7q21.1 // 6717 /// NM_198901 // SRI // sorcin // 7	SRI	8.11E-14	5.89E-10	-1.70754	1.02E-10	-2.00246
3665410	NM_015432 // PLEKHG4 // pleckstrin homology domain containing, family G (with Rh	PLEKHG4	8.14E-14	6.25E-10	1.31673	9.77E-11	1.43125
2382117	NM_001748 // CAPN2 // calpain 2, (m/II) large subunit // 1q41-q42 // 824 /// ENS	CAPN2	8.36E-14	2.51E-09	-1.50357	3.10E-11	-1.79849
3333443	NM_001083926 // ASRGL1 // asparaginase like 1 // 11q12.3 // 80150 /// NM_025080	ASRGL1	8.49E-14	4.44E-08	1.62473	4.13E-12	2.34287
3332548	NM_024098 // CCDC86 // coiled-coil domain containing 86 // 11q12.2 // 79080 ///	CCDC86	8.49E-14	1.41E-06	1.20669	6.23E-13	1.51935
4004044	NM_000109 // DMD // dystrophin // Xp21.2 // 1756 /// NM_004010 // DMD // dystrop	DMD	8.60E-14	4.47E-09	-1.49058	2.06E-11	-1.81737
2995491	NM_032222 // FLJ22374 // hypothetical protein FLJ22374 // 7p15.1 // 84182 /// EN	FLJ22374	8.64E-14	5.90E-10	1.38312	1.13E-10	1.52102
3502156	NM_015205 // ATP11A // ATPase, class VI, type 11A // 13q34 // 23250 /// NM_03218	ATP11A	8.77E-14	1.11E-10	1.41687	6.17E-10	1.4849
2515627	NM_000210 // ITGA6 // integrin, alpha 6 // 2q31.1 // 3655 /// NM_001079818 // IT	ITGA6	8.85E-14	3.38E-10	1.9065	1.99E-10	2.22265
2398894	NM_018715 // RCC2 // regulator of chromosome condensation 2 // 1p36.13 // 55920	RCC2	8.85E-14	6.58E-10	1.40167	1.06E-10	1.55196
3865301	NM_000400 // ERCC2 // excision repair cross-complementing rodent repair deficien	ERCC2	8.97E-14	7.90E-06	1.14194	3.07E-13	1.39693
3717034	BC062632 // LOC400590 // hypothetical LOC400590 // 17q11.2 // 400590	LOC400590	9.06E-14	6.60E-10	-1.755	1.10E-10	-2.0778
3742727	NM_020162 // DHX33 // DEAH (Asp-Glu-Ala-His) box polypeptide 33 // 17p13.2 // 56	DHX33	9.13E-14	1.83E-07	1.24641	1.96E-12	1.52838
2594951	NM_001044385 // ALS2CR4 // amyotrophic lateral sclerosis 2 (juvenile) chromosome	ALS2CR4	9.19E-14	4.20E-08	1.28354	4.76E-12	1.54434
2323559	NM_016183 // MRTO4 // mRNA turnover 4 homolog (S. cerevisiae) // 1p36.13 // 5115	MRTO4	9.28E-14	7.46E-06	1.27303	3.27E-13	1.83044
3667652	NM_001017967 // MARVELD3 // MARVEL domain containing 3 // 16q22.3 // 91862 /// N	MARVELD3	9.78E-14	1.40E-11	-1.41745	9.70E-09	-1.38673
3820571	NM_032885 // ATG4D // ATG4 autophagy related 4 homolog D (S. cerevisiae) // 19p1	ATG4D	9.81E-14	8.72E-13	-1.48721	1.01E-06	-1.30991
2776670	NM_138980 // MAPK10 // mitogen-activated protein kinase 10 // 4q22.1-q23 // 5602	MAPK10	9.97E-14	2.61E-09	-1.3346	3.91E-11	-1.51066
2699623	NM_001128304 // PLSCR4 // phospholipid scramblase 4 // 3q24 // 57088 /// NM_0011	PLSCR4	1.01E-13	8.36E-06	-1.25648	3.46E-13	-1.77664
3377385	NM_005468 // NAALADL1 // N-acetylated alpha-linked acidic dipeptidase-like 1 //	NAALADL1	1.03E-13	2.64E-09	-2.07747	4.08E-11	-2.84021
3699581	NM_145254 // TMEM170A // transmembrane protein 170A // 16q23.1 // 124491 /// ENS	TMEM170A	1.04E-13	2.31E-11	-1.58093	5.52E-09	-1.56504
3364525	NM_175058 // PLEKHA7 // pleckstrin homology domain containing, family A member 7	PLEKHA7	1.05E-13	1.29E-09	-1.34006	7.64E-11	-1.48634
3676002	NM_014714 // IFT140 // intraflagellar transport 140 homolog (Chlamydomonas) // 1	IFT140	1.06E-13	2.42E-10	1.32921	3.74E-10	1.40401
2788926	NM_000901 // NR3C2 // nuclear receptor subfamily 3, group C, member 2 // 4q31.1	NR3C2	1.06E-13	8.13E-08	-1.45256	3.84E-12	-1.96481
3844238	NM_005762 // TRIM28 // tripartite motif-containing 28 // 19q13.4 // 10155 /// EN	TRIM28	1.10E-13	1.93E-07	1.28397	2.43E-12	1.61471

2439861	NM_020789 // IGSF9 // immunoglobulin superfamily, member 9 // 1q22-q23 // 57549	IGSF9	1.12E-13	1.00E-10	-1.52504	1.06E-09	-1.59472
2433371	NM_016361 // ACP6 // acid phosphatase 6, lysophosphatidic // 1q21 // 51205 /// E	ACP6	1.12E-13	8.88E-11	1.41343	1.22E-09	1.4604
3742182	NM_001122890 // GGT6 // gamma-glutamyltransferase 6 // 17p13.2 // 124975 /// NM_	GGT6	1.15E-13	8.56E-12	-1.46269	2.71E-08	-1.39736
2515240	NM_024843 // CYBRD1 // cytochrome b reductase 1 // 2q31.1 // 79901 /// NM_001127	CYBRD1	1.18E-13	5.20E-08	-1.97017	5.82E-12	-3.2671
3300242	NM_014912 // CPEB3 // cytoplasmic polyadenylation element binding protein 3 // 1	CPEB3	1.25E-13	4.20E-09	-1.35026	3.74E-11	-1.55046
2758076	NM_003703 // NOL14 // nucleolar protein 14 // 4p16.3 // 8602 /// ENST00000314262	NOL14	1.31E-13	1.16E-09	1.40427	1.18E-10	1.56893
3830166	NM_021910 // FXYD3 // FXYD domain containing ion transport regulator 3 // 19q13.	FXYD3	1.33E-13	2.42E-11	-1.83094	8.27E-09	-1.79025
3956781	NM_001127 // AP1B1 // adaptor-related protein complex 1, beta 1 subunit // 22q12	AP1B1	1.34E-13	2.61E-13	-1.4033	3.75E-05	-1.19477
2619761	NM_016006 // ABHD5 // abhydrolase domain containing 5 // 3p21 // 51099 /// ENST0	ABHD5	1.34E-13	3.37E-13	-1.6502	1.97E-05	-1.31911
2497301	NM_144632 // TMEM182 // transmembrane protein 182 // 2q12.1 // 130827 /// ENST00	TMEM182	1.35E-13	2.93E-08	1.28303	1.01E-11	1.51513
3959631	NM_003753 // EIF3D // eukaryotic translation initiation factor 3, subunit D // 2	EIF3D	1.37E-13	5.23E-10	1.3019	2.65E-10	1.38897
2699145	NM_173653 // SLC9A9 // solute carrier family 9 (sodium/hydrogen exchanger), memb	SLC9A9	1.38E-13	2.09E-09	-1.79942	7.70E-11	-2.25049
3190925	NM_020438 // DOLPP1 // dolichyl pyrophosphate phosphatase 1 // 9q34.1 // 57171 /	DOLPP1	1.41E-13	7.34E-13	-1.48825	3.70E-06	-1.28421
2971564	NM_001042475 // C6orf204 // chromosome 6 open reading frame 204 // 6q22 // 38711	C6orf204	1.44E-13	5.34E-07	-1.36388	1.96E-12	-1.87915
3815014	NM_001728 // BSG // basigin (Ok blood group) // 19p13.3 // 682 /// NM_198589 //	BSG	1.51E-13	3.60E-13	-1.59092	2.35E-05	-1.28964
3190463	NM_002540 // ODF2 // outer dense fiber of sperm tails 2 // 9q34.11 // 4957 /// N	ODF2	1.51E-13	9.19E-08	1.20306	5.70E-12	1.39339
3475324	NM_019034 // RHOF // ras homolog gene family, member F (in filopodia) // 12q24.3	RHOF	1.53E-13	2.05E-11	-2.74153	1.37E-08	-2.57021
2926969	NM_018945 // PDE7B // phosphodiesterase 7B // 6q23-q24 // 27115 /// ENST00000308	PDE7B	1.54E-13	2.90E-09	-1.54003	6.88E-11	-1.83472
3416895	NM_152637 // METTL7B // methyltransferase like 7B // 12q13.2 // 196410 /// ENST0	METTL7B	1.58E-13	7.55E-13	-1.78931	4.74E-06	-1.43495
2480383	NM_001430 // EPAS1 // endothelial PAS domain protein 1 // 2p21-p16 // 2034 /// E	EPAS1	1.62E-13	1.92E-09	-1.42244	1.06E-10	-1.61457
3470689	NM_001001655 // ALKBH2 // alkB, alkylation repair homolog 2 (E. coli) // 12q24.1	ALKBH2	1.63E-13	5.16E-09	1.39903	4.71E-11	1.633
3740651	ENST00000330676 // TLCD2 // TLC domain containing 2 // 17p13.3 // 727910	TLCD2	1.64E-13	8.07E-13	-1.56226	4.45E-06	-1.32123
3555300	NM_021178 // CCNB1IP1 // cyclin B1 interacting protein 1 // 14q11.2 // 57820 ///	CCNB1IP1	1.70E-13	1.20E-08	1.33769	2.63E-11	1.56882
3955815	NM_022081 // HPS4 // Hermansky-Pudlak syndrome 4 // 22cen-q12.3 // 89781 /// NM_	HPS4	1.82E-13	5.20E-11	1.31359	5.56E-09	1.31621
3602004	NM_138967 // SCAMP5 // secretory carrier membrane protein 5 // 15q24.1-q24.2 //	SCAMP5	1.85E-13	4.04E-11	-1.5724	7.97E-09	-1.56014
2447066	NM_002065 // GLUL // glutamate-ammonia ligase (glutamine synthetase) // 1q31 //	GLUL	1.87E-13	4.06E-11	1.32456	8.09E-09	1.31795
3876645	NM_014962 // BTBD3 // BTB (POZ) domain containing 3 // 20p12.2 // 22903 /// NM_1	BTBD3	1.90E-13	6.54E-11	-1.59489	4.53E-09	-1.61353
2731381	NM_001511 // CXCL1 // chemokine (C-X-C motif) ligand 1 (melanoma growth stimulat	CXCL1	1.91E-13	1.30E-09	2.15456	1.91E-10	2.72972
3411721	NM_001843 // CNTN1 // contactin 1 // 12q11-q12 // 1272 /// NM_175038 // CNTN1 //	CNTN1	1.91E-13	5.57E-09	-1.51991	5.61E-11	-1.83949
2601648	NM_014689 // DOCK10 // dedicator of cytokinesis 10 // 2q36.2 // 55619 /// ENST00	DOCK10	1.93E-13	3.60E-05	-1.41883	4.05E-13	-2.61861
3264997	NM_024889 // C10orf81 // chromosome 10 open reading frame 81 // 10q25.3 // 79949	C10orf81	1.94E-13	1.30E-11	2.99154	4.29E-08	2.60736
3575906	NM_145231 // C14orf143 // chromosome 14 open reading frame 143 // 14q32.11 // 90	C14orf143	1.95E-13	0.00766766	1.06996	7.10E-14	1.38595
3323052	NM_182964 // NAV2 // neuron navigator 2 // 11p15.1 // 89797 /// NM_145117 // NAV	NAV2	1.97E-13	2.27E-08	1.32265	2.04E-11	1.56726
3407629	NM_019844 // SLCO1B3 // solute carrier organic anion transporter family, member	SLCO1B3	2.03E-13	2.79E-11	5.66455	1.57E-08	5.11442
3739812	NM_015721 // GEMIN4 // gem (nuclear organelle) associated protein 4 // 17p13 //	GEMIN4	2.04E-13	1.72E-07	1.2889	5.83E-12	1.59847
3003228	NM_001042468 // SUMF2 // sulfatase modifying factor 2 // 7q11.1 // 25870 /// NM_	SUMF2	2.09E-13	3.95E-09	1.36301	8.44E-11	1.54901
3818732	NM_015318 // ARHGEF18 // rho/rac guanine nucleotide exchange factor (GEF) 18 //	ARHGEF18	2.09E-13	4.37E-10	-1.31484	6.35E-10	-1.38684
3120653	NM_005309 // GPT // glutamic-pyruvate transaminase (alanine aminotransferase) //	GPT	2.09E-13	1.69E-11	-1.81793	3.37E-08	-1.70514
2562932	NM_001768 // CD8A // CD8a molecule // 2p12 // 925 /// NM_171827 // CD8A // CD8a	CD8A	2.09E-13	7.36E-06	-1.20225	8.64E-13	-1.56207
3863214	L31792 // CEACAM7 // carcinoembryonic antigen-related cell adhesion molecule 7 /	CEACAM7	2.12E-13	1.34E-08	-4.00819	3.32E-11	-8.50563
3262198	NM_014976 // PDCD11 // programmed cell death 11 // 10q24.33 // 22984 /// ENST000	PDCD11	2.21E-13	2.79E-09	1.34384	1.23E-10	1.50033
2389718	BC036200 // C1orf71 // chromosome 1 open reading frame 71 // 1q44 // 163882 ///	C1orf71	2.22E-13	3.28E-08	-1.31102	1.88E-11	-1.55851

3257246	NM_001548 // IFIT1 // interferon-induced protein with tetratricopeptide repeats	IFIT1	2.24E-13	1.09E-07	-1.85346	8.69E-12	-3.0028
3464983	NM_001001323 // ATP2B1 // ATPase, Ca++ transporting, plasma membrane 1 // 12q21.	ATP2B1	2.31E-13	2.99E-09	-1.57709	1.24E-10	-1.87212
3678000	NM_003223 // TFAP4 // transcription factor AP-4 (activating enhancer binding pro	TFAP4	2.31E-13	7.95E-09	1.34065	5.59E-11	1.54253
2881083	NM_000440 // PDE6A // phosphodiesterase 6A, cGMP-specific, rod, alpha // 5q31.2-	PDE6A	2.31E-13	2.37E-11	-1.64721	2.54E-08	-1.5792
2403261	NM_002038 // IFI6 // interferon, alpha-inducible protein 6 // 1p35 // 2537 /// N	IFI6	2.35E-13	6.14E-08	1.74213	1.33E-11	2.58083
2477438	NM_012413 // QPCT // glutaminyl-peptide cyclotransferase // 2p22.2 // 25797 ///	QPCT	2.35E-13	3.38E-09	2.57363	1.15E-10	3.71226
2440586	NM_030916 // PVRL4 // poliovirus receptor-related 4 // 1q22-q23.2 // 81607 /// E	PVRL4	2.39E-13	3.63E-10	1.58611	9.65E-10	1.71273
2613293	NM_144633 // KCNH8 // potassium voltage-gated channel, subfamily H (eag-related)	KCNH8	2.53E-13	4.28E-12	2.08029	4.73E-07	1.72978
3946889	NM_001098 // ACO2 // aconitase 2, mitochondrial // 22q11.2-q13.31|22q13.2|22q13.	ACO2	2.56E-13	8.05E-12	-1.44246	1.65E-07	-1.34375
2410158	NM_007170 // TESK2 // testis-specific kinase 2 // 1p32 // 10420 /// ENST00000372	TESK2	2.57E-13	1.27E-05	-1.21933	8.66E-13	-1.64314
2572274	BC032913 // LOC389023 // hypothetical gene supported by BC032913; BC048425 // 2q	LOC389023	2.72E-13	1.02E-09	-2.65719	4.22E-10	-3.41305
3660075	NM_033119 // NKD1 // naked cuticle homolog 1 (Drosophila) // 16q12 // 85407 ///	NKD1	2.77E-13	1.80E-09	2.19965	2.57E-10	2.80964
3751042	NM_138463 // TLCD1 // TLC domain containing 1 // 17q11.2 // 116238 /// ENST00000	TLCD1	2.81E-13	0.021913	1.08317	7.95E-14	1.57201
3748798	NM_002404 // MFAP4 // microfibrillar-associated protein 4 // 17p11.2 // 4239 ///	MFAP4	2.88E-13	8.28E-08	-1.98913	1.44E-11	-3.27975
3837759	NM_000836 // GRIN2D // glutamate receptor, ionotropic, N-methyl D-aspartate 2D /	GRIN2D	2.89E-13	1.56E-10	1.71334	3.42E-09	1.78087
3975893	NM_014735 // PHF16 // PHD finger protein 16 // Xp11.3 // 9767 /// NM_001077445 /	PHF16	2.90E-13	1.51E-09	1.44417	3.25E-10	1.6062
3588658	ENST00000330188 // TPM3 // tropomyosin 3 // 1q21.2 // 7170 /// BC006254 // C15or	TPM3	2.92E-13	1.16E-08	1.31288	5.86E-11	1.50451
3773244	NM_019020 // TBC1D16 // TBC1 domain family, member 16 // 17q25.3 // 125058 /// E	TBC1D16	2.94E-13	1.09E-08	1.31163	6.21E-11	1.49937
2766419	NM_001024921 // RPL9 // ribosomal protein L9 // 4p13 // 6133 /// NM_000661 // RP	RPL9	2.99E-13	0.000127479	1.22334	4.11E-13	1.83606
3140920	NM_020647 // JPH1 // junctophilin 1 // 8q21 // 56704 /// ENST00000342232 // JPH1	JPH1	3.09E-13	2.58E-09	1.69361	2.20E-10	2.0239
2413886	NM_001114108 // TTC22 // tetratricopeptide repeat domain 22 // 1p32.3 // 55001 /	TTC22	3.11E-13	4.75E-09	-1.45931	1.31E-10	-1.69772
3937092	NM_000754 // COMT // catechol-O-methyltransferase // 22q11.21-q11.23|22q11.21 //	COMT	3.11E-13	4.73E-07	1.29711	5.59E-12	1.65959
3911217	NM_020182 // PMEPA1 // prostate transmembrane protein, androgen induced 1 // 20q	PMEPA1	3.11E-13	2.92E-12	2.02463	1.58E-06	1.62948
3168385	NM_022343 // GLIPR2 // GLI pathogenesis-related 2 // 9p13-p12 // 152007 /// ENST	GLIPR2	3.12E-13	4.88E-10	-1.95988	1.11E-09	-2.20259
3011409	NM_138290 // RUNDC3B // RUN domain containing 3B // 7q21.12 // 154661 /// ENST00	RUNDC3B	3.14E-13	4.98E-08	-1.59556	2.28E-11	-2.17079
3193900	NM_016034 // MRPS2 // mitochondrial ribosomal protein S2 // 9q34 // 51116 /// EN	MRPS2	3.14E-13	8.04E-05	1.16243	5.16E-13	1.54476
2890239	NM_054013 // MGAT4B // mannosyl (alpha-1,3-)-glycoprotein beta-1,4-N-acetylgluco	MGAT4B	3.17E-13	4.69E-11	-1.36196	1.83E-08	-1.3422
3355114	NM_014026 // DCPS // decapping enzyme, scavenger // 11q24.2 // 28960 /// ENST000	DCPS	3.18E-13	1.06E-08	1.29556	7.13E-11	1.46838
3326252	NM_024662 // NAT10 // N-acetyltransferase 10 // 11p13 // 55226 /// ENST000002578	NAT10	3.23E-13	6.81E-08	1.36987	1.92E-11	1.70406
3725035	NM_003204 // NFE2L1 // nuclear factor (erythroid-derived 2)-like 1 // 17q21.3 //	NFE2L1	3.29E-13	8.48E-11	-1.35207	9.09E-09	-1.3539
3666566	NM_032830 // CIRH1A // cirrhosis, autosomal recessive 1A (cirhin) // 16q22.1 //	CIRH1A	3.32E-13	2.88E-06	1.43117	2.34E-12	2.21167
3745525	NM_001004313 // TMEM220 // transmembrane protein 220 // 17p13.1 // 388335 /// EN	TMEM220	3.38E-13	8.14E-09	-1.7271	9.60E-11	-2.20882
3223687	NM_015651 // PHF19 // PHD finger protein 19 // 9q33.2 // 26147 /// NM_001009936	PHF19	3.43E-13	3.62E-07	1.32907	7.40E-12	1.71773
3455134	NM_182507 // KRT80 // keratin 80 // 12q13.13 // 144501 /// NM_001081492 // KRT80	KRT80	3.46E-13	1.99E-09	1.63542	3.32E-10	1.89819
3951768	AK292689 // CECR1 // cat eye syndrome chromosome region, candidate 1 // 22q11.2	CECR1	3.48E-13	8.30E-09	-1.60666	9.89E-11	-1.98859
3988165	NM_007231 // SLC6A14 // solute carrier family 6 (amino acid transporter), member	SLC6A14	3.52E-13	2.84E-11	5.02968	4.54E-08	4.2623
3855596	NM_176880 // NR2C2AP // nuclear receptor 2C2-associated protein // 19p13.11 // 1	NR2C2AP	3.55E-13	0.000101883	1.19996	5.43E-13	1.70765
2984616	NM_016098 // BRP44L // brain protein 44-like // 6q27 // 51660 /// ENST0000034175	BRP44L	3.56E-13	4.35E-11	-1.69509	2.54E-08	-1.63897
2427981	NM_020683 // ADORA3 // adenosine A3 receptor // 1p13.2 // 140 /// NM_001081976 /	ADORA3	3.56E-13	9.71E-11	-1.62488	8.87E-09	-1.63336
3874438	NM_021873 // CDC25B // cell division cycle 25 homolog B (S. pombe) // 20p13 // 9	CDC25B	3.57E-13	1.48E-06	1.37543	3.59E-12	1.95408
3996667	NM_001363 // DKC1 // dyskeratosis congenita 1, dyskerin // Xq28 // 1736 /// NR_0	DKC1	3.64E-13	3.40E-07	1.36624	8.27E-12	1.8027
2633737	NM_032787 // GPR128 // G protein-coupled receptor 128 // 3q12.2 // 84873 /// ENS	GPR128	3.67E-13	2.85E-08	-2.41319	4.18E-11	-4.02711

3464967	NM_003774 // GALNT4 // UDP-N-acetyl-alpha-D-galactosamine:polypeptide N-acetylga	GALNT4	3.68E-13	1.20E-10	1.74426	7.22E-09	1.77163
3762443	BC128165 // C17orf73 // chromosome 17 open reading frame 73 // 17q21.33 // 55018	C17orf73	3.83E-13	2.91E-10	-1.87647	2.75E-09	-2.00822
3203582	NM_022917 // NOL6 // nucleolar protein family 6 (RNA-associated) // 9p13.3 // 65	NOL6	3.85E-13	2.76E-06	1.2408	2.87E-12	1.60496
3875908	NM_000933 // PLCB4 // phospholipase C, beta 4 // 20p12 // 5332 /// NM_182797 //	PLCB4	3.93E-13	2.87E-10	2.9427	2.92E-09	3.29405
2485257	NM_001001521 // UGP2 // UDP-glucose pyrophosphorylase 2 // 2p14-p13 // 7360 ///	UGP2	3.94E-13	7.92E-10	-2.04606	9.91E-10	-2.3641
2634494	NM_001627 // ALCAM // activated leukocyte cell adhesion molecule // 3q13.1 // 21	ALCAM	3.98E-13	6.49E-11	1.94518	1.83E-08	1.8995
3263944	NM_145341 // PDCD4 // programmed cell death 4 (neoplastic transformation inhibit	PDCD4	4.01E-13	2.84E-07	-1.56441	1.05E-11	-2.29432
4018454	NM_133265 // AMOT // angiomotin // Xq23 // 154796 /// NM_001113490 // AMOT // an	AMOT	4.05E-13	2.85E-09	1.45617	3.07E-10	1.64627
2816494	NM_005242 // F2RL1 // coagulation factor II (thrombin) receptor-like 1 // 5q13 /	F2RL1	4.07E-13	1.40E-09	-1.43094	5.94E-10	-1.56806
3855506	NM_017814 // TMEM161A // transmembrane protein 161A // 19p13.11 // 54929 /// ENS	TMEM161A	4.07E-13	0.00043414	1.15112	3.75E-13	1.60082
3776504	NM_170695 // TGIF1 // TGFB-induced factor homeobox 1 // 18p11.3 // 7050 /// NM_1	TGIF1	4.08E-13	8.36E-09	1.26881	1.24E-10	1.40814
3204149	NM_147164 // CNTFR // ciliary neurotrophic factor receptor // 9p13 // 1271 /// N	CNTFR	4.12E-13	5.14E-12	-2.01777	1.06E-06	-1.65973
2616166	NM_006371 // CRTAP // cartilage associated protein // 3p22.3 // 10491 /// ENST00	CRTAP	4.16E-13	2.35E-08	1.18665	5.76E-11	1.30355
2379665	NM_002763 // PROX1 // prospero homeobox 1 // 1q32.2-q32.3 // 5629 /// ENST000003	PROX1	4.27E-13	1.19E-11	2.20547	2.64E-07	1.8813
3603199	NM_005530 // IDH3A // isocitrate dehydrogenase 3 (NAD+) alpha // 15q25.1-q25.2 /	IDH3A	4.42E-13	7.78E-12	-1.79301	5.84E-07	-1.55475
3203990	NM_020702 // KIAA1161 // KIAA1161 // 9p13.3 // 57462 /// ENST00000297625 // KIAA	KIAA1161	4.48E-13	5.47E-10	-1.68283	1.80E-09	-1.82492
3041875	NM_015550 // OSBPL3 // oxysterol binding protein-like 3 // 7p15 // 26031 /// NM_	OSBPL3	4.67E-13	1.15E-08	1.42597	1.18E-10	1.67929
3896524	NM_015939 // TRMT6 // tRNA methyltransferase 6 homolog (S. cerevisiae) // 20p12.	TRMT6	4.81E-13	1.73E-07	1.22917	1.80E-11	1.4425
2872047	NM_020796 // SEMA6A // sema domain, transmembrane domain (TM), and cytoplasmic d	SEMA6A	4.82E-13	1.30E-07	-1.84215	2.17E-11	-2.89285
3757399	NM_052935 // NT5C3L // 5'-nucleotidase, cytosolic III-like // 17q21.2 // 115024	NT5C3L	4.83E-13	8.36E-09	1.2735	1.60E-10	1.411
2326496	NM_024887 // DHDDS // dehydrodolichyl diphosphate synthase // 1p36.11 // 79947 /	DHDDS	4.88E-13	1.51E-10	-1.49707	9.12E-09	-1.51318
3244460	AB235418 // TMEM72 // transmembrane protein 72 // 10q11.21 // 643236 /// BC12779	TMEM72	4.88E-13	2.44E-08	-1.80257	7.00E-11	-2.47852
2985368	NM_024919 // FRMD1 // FERM domain containing 1 // 6q27 // 79981 /// NM_001122841	FRMD1	5.10E-13	6.89E-10	-1.48356	1.76E-09	-1.585
3699335	NM_153486 // LDHD // lactate dehydrogenase D // 16q23.1 // 197257 /// NM_194436	LDHD	5.12E-13	1.12E-10	-1.58566	1.45E-08	-1.5816
3027204	NM_001061 // TBXAS1 // thromboxane A synthase 1 (platelet) // 7q34-q35 // 6916 /	TBXAS1	5.23E-13	9.89E-09	1.41508	1.57E-10	1.64607
3712098	NR_002744 // SNORD49A // small nucleolar RNA, C/D box 49A // 17p11.2 // 26800 //	SNORD49A	5.38E-13	4.69E-09	1.26949	3.06E-10	1.38161
3645477	NM_152341 // PAQR4 // progestin and adipoQ receptor family member IV // 16p13.3	PAQR4	5.41E-13	3.46E-05	1.23199	1.35E-12	1.73227
3263624	NM_005962 // MXI1 // MAX interactor 1 // 10q24-q25 // 4601 /// NM_130439 // MXI1	MXI1	5.55E-13	2.21E-09	-1.49539	6.34E-10	-1.67078
2438657	NM_198236 // ARHGEF11 // Rho guanine nucleotide exchange factor (GEF) 11 // 1q21	ARHGEF11	5.59E-13	3.82E-08	-1.1588	6.13E-11	-1.2622
3414885	NM_001039960 // SLC4A8 // solute carrier family 4, sodium bicarbonate cotranspor	SLC4A8	5.62E-13	6.28E-10	1.67266	2.28E-09	1.80774
2793441	NM_016228 // AADAT // aminoadipate aminotransferase // 4q33 // 51166 /// NM_1826	AADAT	5.62E-13	5.06E-08	1.48265	5.05E-11	1.88682
3173673	NM_003558 // PIP5K1B // phosphatidylinositol-4-phosphate 5-kinase, type I, beta	PIP5K1B	5.65E-13	2.71E-08	-1.46081	8.02E-11	-1.79235
3461341	NM_001874 // CPM // carboxypeptidase M // 12q14.3 // 1368 /// NM_198320 // CPM /	CPM	5.72E-13	2.29E-07	-1.79156	1.90E-11	-2.85052
2375144	NM_001017403 // LGR6 // leucine-rich repeat-containing G protein-coupled recepto	LGR6	5.73E-13	2.63E-11	1.994	1.38E-07	1.79672
3134511	NM_003068 // SNAI2 // snail homolog 2 (Drosophila) // 8q11 // 6591 /// ENST00000	SNAI2	6.07E-13	1.52E-09	-2.22141	1.05E-09	-2.6712
3361116	NM_022061 // MRPL17 // mitochondrial ribosomal protein L17 // 11p15.5-p15.4 // 6	MRPL17	6.19E-13	7.15E-07	1.20287	1.07E-11	1.43203
3299465	NM_144590 // ANKRD22 // ankyrin repeat domain 22 // 10q23.31 // 118932 /// ENST0	ANKRD22	6.41E-13	4.15E-09	2.12475	4.46E-10	2.7208
3321150	NM_001178 // ARNTL // aryl hydrocarbon receptor nuclear translocator-like // 11p	ARNTL	6.50E-13	3.00E-10	-1.55829	6.70E-09	-1.60619
3057520	NM_031925 // TMEM120A // transmembrane protein 120A // 7q11.23 // 83862 /// ENST	TMEM120A	6.57E-13	7.78E-10	-1.48819	2.36E-09	-1.58532
3692516	AF275804 // hCG_1815491 // hCG1815491 // 16q12.2 // 643911	hCG_1815491	6.59E-13	2.21E-10	2.14577	9.87E-09	2.20928
3376512	NM_017878 // HRASLS2 // HRAS-like suppressor 2 // 11q12.3 // 54979 /// ENST00000	HRASLS2	6.64E-13	1.40E-10	-2.99987	1.76E-08	-2.98147
3382216	NM_004041 // ARRB1 // arrestin, beta 1 // 11q13 // 408 /// NM_020251 // ARRB1 //	ARRB1	6.65E-13	1.48E-07	-1.39222	3.07E-11	-1.77153

2991395	NM_178423 // HDAC9 // histone deacetylase 9 // 7p21.1 // 9734 /// NM_178425 // H	HDAC9	6.82E-13	8.63E-08	-1.37605	4.55E-11	-1.69845
3838624	NM_004107 // FCGRT // Fc fragment of IgG, receptor, transporter, alpha // 19q13.	FCGRT	6.86E-13	5.93E-10	-1.82022	3.40E-09	-1.96682
3276135	NM_001029880 // SFMBT2 // Scm-like with four mbt domains 2 // 10p14 // 57713 ///	SFMBT2	6.95E-13	8.44E-09	-1.40491	2.72E-10	-1.60712
2979267	NM_024518 // ULBP3 // UL16 binding protein 3 // 6q25 // 79465 /// ENST0000036733	ULBP3	7.00E-13	2.15E-09	1.61616	9.38E-10	1.82615
2727762	NM_024592 // SRD5A3 // steroid 5 alpha-reductase 3 // 4q12 // 79644 /// ENST0000	SRD5A3	7.07E-13	8.82E-10	1.54402	2.34E-09	1.65902
3875179	NM_001819 // CHGB // chromogranin B (secretogranin 1) // 20pter-p12 // 1114 ///	CHGB	7.25E-13	2.37E-09	-2.32433	9.09E-10	-2.89662
3077321	NM_005232 // EPHA1 // EPH receptor A1 // 7q34 // 2041 /// ENST00000275815 // EPH	EPHA1	7.33E-13	3.40E-09	1.3026	6.57E-10	1.40895
2976041	NM_014432 // IL20RA // interleukin 20 receptor, alpha // 6q22.33-q23.1 // 53832	IL20RA	7.39E-13	4.05E-08	1.50866	8.70E-11	1.90201
3286602	NM_000609 // CXCL12 // chemokine (C-X-C motif) ligand 12 (stromal cell-derived f	CXCL12	7.59E-13	1.46E-08	-1.95567	1.97E-10	-2.64036
3048749	NM_019082 // DDX56 // DEAD (Asp-Glu-Ala-Asp) box polypeptide 56 // 7p13 // 54606	DDX56	7.61E-13	6.36E-06	1.17679	4.37E-12	1.44678
3335697	NM_001335 // CTSW // cathepsin W // 11q13.1 // 1521 /// ENST00000307886 // CTSW	CTSW	7.68E-13	1.15E-09	-1.57771	2.04E-09	-1.71606
3191695	NM_014285 // EXOSC2 // exosome component 2 // 9q34 // 23404 /// ENST00000372358	EXOSC2	7.87E-13	0.00011332	1.21903	1.29E-12	1.76664
3726934	NM_198175 // NME1 // non-metastatic cells 1, protein (NM23A) expressed in // 17q	NME1	7.94E-13	3.77E-05	1.29798	2.04E-12	1.97612
3550307	NM_000710 // BDKRB1 // bradykinin receptor B1 // 14q32.1-q32.2 // 623 /// ENST00	BDKRB1	8.00E-13	4.10E-11	-2.22031	1.39E-07	-1.99009
2500275	NM_138621 // BCL2L11 // BCL2-like 11 (apoptosis facilitator) // 2q13 // 10018 //	BCL2L11	8.09E-13	1.95E-07	-1.3343	3.34E-11	-1.65445
2886130	NM_024594 // PANK3 // pantothenate kinase 3 // 5q34 // 79646 /// ENST00000239231	PANK3	8.37E-13	9.51E-10	-1.29154	2.86E-09	-1.34522
2531908	NM_145236 // B3GNT7 // UDP-GlcNAc:betaGal beta-1,3-N-acetylglucosaminyltransfera	B3GNT7	8.71E-13	0.000548577	-1.68415	8.02E-13	-5.66427
3970307	NM_004726 // REPS2 // RALBP1 associated Eps domain containing 2 // Xp22.2 // 918	REPS2	8.71E-13	1.39E-09	1.6782	2.06E-09	1.85488
4012511	NM_021963 // NAP1L2 // nucleosome assembly protein 1-like 2 // Xq13 // 4674 ///	NAP1L2	9.16E-13	2.52E-07	-1.73804	3.34E-11	-2.65778
2417016	NM_024763 // WDR78 // WD repeat domain 78 // 1p31.3 // 79819 /// NM_207014 // WD	WDR78	9.47E-13	1.04E-10	-1.92727	5.11E-08	-1.84898
3557614	NM_080545 // AP1G2 // adaptor-related protein complex 1, gamma 2 subunit // 14q1	AP1G2	9.59E-13	4.91E-08	1.20753	1.09E-10	1.34307
2840393	NM_014211 // GABRP // gamma-aminobutyric acid (GABA) A receptor, pi // 5q33-q34	GABRP	9.61E-13	2.17E-11	2.83205	5.63E-07	2.26596
3462816	NM_007350 // PHLDA1 // pleckstrin homology-like domain, family A, member 1 // 12	PHLDA1	9.66E-13	3.12E-08	1.69163	1.55E-10	2.21346
4006594	AK098783 // FLJ25917 // hypothetical gene supported by AK098783 // Xp11.3 // 401	FLJ25917	9.78E-13	6.38E-11	1.94934	1.08E-07	1.8087
3453252	NM_015270 // ADCY6 // adenylate cyclase 6 // 12q12-q13 // 112 /// NM_020983 // A	ADCY6	1.03E-12	3.69E-10	-1.32424	1.19E-08	-1.34316
3226661	NM_006336 // ZER1 // zer-1 homolog (C. elegans) // 9q34.11 // 10444 /// ENST0000	ZER1	1.04E-12	7.15E-08	-1.25111	9.25E-11	-1.43165
3601955	NM_002435 // MPI // mannose phosphate isomerase // 15q22-qter // 4351 /// ENST00	MPI	1.05E-12	4.97E-12	-1.47774	1.10E-05	-1.27866
2749560	NM_004453 // ETFDH // electron-transferring-flavoprotein dehydrogenase // 4q32-q	ETFDH	1.06E-12	9.05E-11	-2.02636	7.65E-08	-1.90762
3168309	NM_021111 // RECK // reversion-inducing-cysteine-rich protein with kazal motifs	RECK	1.07E-12	5.26E-09	-1.3719	8.00E-10	-1.51348
3339382	NM_000803 // FOLR2 // folate receptor 2 (fetal) // 11q13.3-q13.5 // 2350 /// NM_	FOLR2	1.08E-12	1.21E-09	-1.98388	3.38E-09	-2.21744
2835213	NM_133263 // PPARGC1B // peroxisome proliferator-activated receptor gamma, coact	PPARGC1B	1.08E-12	1.39E-09	-1.28694	2.95E-09	-1.34521
3255220	NM_014394 // GHITM // growth hormone inducible transmembrane protein // 10q23.1	GHITM	1.10E-12	8.56E-12	-1.58852	4.10E-06	-1.37067
2987632	NM_025250 // TTYH3 // tweety homolog 3 (Drosophila) // 7p22 // 80727 /// ENST000	TTYH3	1.11E-12	3.87E-08	1.34514	1.60E-10	1.57138
3895381	NM_001009984 // C20orf194 // chromosome 20 open reading frame 194 // 20p13 // 25	C20orf194	1.16E-12	3.73E-09	-1.46747	1.24E-09	-1.62709
3861557	NM_006149 // LGALS4 // lectin, galactoside-binding, soluble, 4 // 19q13.2 // 396	LGALS4	1.20E-12	1.31E-11	-1.31842	2.23E-06	-1.21895
3332334	NM_032597 // MS4A14 // membrane-spanning 4-domains, subfamily A, member 14 // 11	MS4A14	1.23E-12	3.04E-10	-1.62377	2.07E-08	-1.63754
2976448	AK299585 // NHSL1 // NHS-like 1 // 6q23.3 // 57224 /// ENST00000343505 // NHSL1	NHSL1	1.26E-12	8.10E-07	-1.36694	2.47E-11	-1.81018
3090209	NM_014265 // ADAM28 // ADAM metallopeptidase domain 28 // 8p21.2 // 10863 /// NM	ADAM28	1.27E-12	1.44E-07	-1.76814	7.50E-11	-2.58886
3430552	NM_007062 // PWP1 // PWP1 homolog (S. cerevisiae) // 12q23.3 // 11137 /// ENST00	PWP1	1.27E-12	1.28E-07	1.27206	8.15E-11	1.48903
3191074	NM_014064 // METTL11A // methyltransferase like 11A // 9q34.11 // 28989 /// ENST	METTL11A	1.27E-12	8.74E-07	1.28255	2.40E-11	1.60779
3600212	NM_017691 // LRRC49 // leucine rich repeat containing 49 // 15q23 // 54839 /// E	LRRC49	1.27E-12	2.69E-10	1.56098	2.56E-08	1.56305
2409970	NM_024602 // HECTD3 // HECT domain containing 3 // 1p34.1 // 79654 /// ENST00000	HECTD3	1.28E-12	3.26E-08	-1.30707	2.25E-10	-1.49141

3258477	NM_016341 // PLCE1 // phospholipase C, epsilon 1 // 10q23 // 51196 /// ENST00000	PLCE1	1.30E-12	1.91E-08	-1.73698	3.50E-10	-2.20548
3375648	NM_002032 // FTH1 // ferritin, heavy polypeptide 1 // 11q13 // 2495 /// NM_00203	FTH1	1.30E-12	6.65E-09	-2.11467	8.68E-10	-2.68644
2337716	NM_006252 // PRKAA2 // protein kinase, AMP-activated, alpha 2 catalytic subunit	PRKAA2	1.31E-12	1.84E-07	-1.84203	6.65E-11	-2.81934
2905391	ENST00000406939 // LOC646875 // similar to ribosomal protein L12 // 6p21.2 // 64	LOC646875	1.32E-12	2.28E-08	1.31577	3.10E-10	1.489
3929721	NM_000819 // GART // phosphoribosylglycinamide formyltransferase, phosphoribosyl	GART	1.33E-12	1.14E-07	1.43015	9.38E-11	1.79616
3648391	NM_001192 // TNFRSF17 // tumor necrosis factor receptor superfamily, member 17 /	TNFRSF17	1.33E-12	6.97E-10	-2.43944	8.89E-09	-2.64562
2334602	NM_005727 // TSPAN1 // tetraspanin 1 // 1p34.1 // 10103 /// ENST00000372003 // T	TSPAN1	1.38E-12	2.51E-08	-1.60142	3.06E-10	-1.98674
2354433	NM_000198 // HSD3B2 // hydroxy-delta-5-steroid dehydrogenase, 3 beta- and steroi	HSD3B2	1.39E-12	3.11E-11	-5.95578	6.87E-07	-4.08007
3948640	NM_006486 // FBLN1 // fibulin 1 // 22q13.31 // 2192 /// NM_006485 // FBLN1 // fi	FBLN1	1.43E-12	2.79E-08	-1.68872	2.97E-10	-2.15632
4018080	NM_145234 // CHRDL1 // chordin-like 1 // Xq22.3 // 91851 /// ENST00000372045 //	CHRDL1	1.43E-12	1.50E-07	-1.84919	8.61E-11	-2.78127
2779231	NM_000668 // ADH1B // alcohol dehydrogenase 1B (class I), beta polypeptide // 4q	ADH1B	1.47E-12	6.07E-05	-1.77628	3.40E-12	-4.59149
3834046	NM_021913 // AXL // AXL receptor tyrosine kinase // 19q13.1 // 558 /// NM_001699	AXL	1.47E-12	9.44E-09	-1.38526	7.67E-10	-1.55073
2880552	NM_001040172 // HTR4 // 5-hydroxytryptamine (serotonin) receptor 4 // 5q31-q33 /	HTR4	1.48E-12	7.36E-10	-1.7997	1.00E-08	-1.8948
3850725	NM_020812 // DOCK6 // dedicator of cytokinesis 6 // 19p13.2 // 57572 /// ENST000	DOCK6	1.49E-12	2.57E-09	1.26696	2.66E-09	1.33177
2544484	NM_004036 // ADCY3 // adenylate cyclase 3 // 2p23.3 // 109 /// ENST00000260600 /	ADCY3	1.50E-12	3.33E-08	1.29834	2.77E-10	1.47259
3025740	NM_018295 // TMEM140 // transmembrane protein 140 // 7q33 // 55281 /// ENST00000	TMEM140	1.50E-12	3.01E-06	-1.43955	1.48E-11	-2.13302
3753452	NM_001014445 // NLE1 // notchless homolog 1 (Drosophila) // 17q12 // 54475 /// N	NLE1	1.53E-12	1.45E-05	1.23399	6.80E-12	1.63916
3480885	NM_002010 // FGF9 // fibroblast growth factor 9 (glia-activating factor) // 13q1	FGF9	1.60E-12	1.39E-08	-1.5496	6.26E-10	-1.83054
3687494	NM_001040056 // MAPK3 // mitogen-activated protein kinase 3 // 16p11.2 // 5595 /	MAPK3	1.62E-12	1.18E-10	-1.55727	1.21E-07	-1.49234
3279313	NM_003638 // ITGA8 // integrin, alpha 8 // 10p13 // 8516 /// ENST00000378076 //	ITGA8	1.63E-12	1.14E-09	-1.78117	7.24E-09	-1.91185
3018309	NM_002649 // PIK3CG // phosphoinositide-3-kinase, catalytic, gamma polypeptide /	PIK3CG	1.65E-12	1.18E-06	-1.49362	2.81E-11	-2.16695
3802980	NM_004949 // DSC2 // desmocollin 2 // 18q12.1 // 1824 /// NM_024422 // DSC2 // d	DSC2	1.66E-12	1.75E-08	-1.4031	5.39E-10	-1.6083
2409507	NM_201649 // SLC6A9 // solute carrier family 6 (neurotransmitter transporter, gl	SLC6A9	1.66E-12	1.13E-11	-1.75541	6.29E-06	-1.45873
3026834	NM_024926 // TTC26 // tetratricopeptide repeat domain 26 // 7q34 // 79989 /// EN	TTC26	1.70E-12	3.09E-08	1.4192	3.53E-10	1.66923
3922793	NM_002606 // PDE9A // phosphodiesterase 9A // 21q22.3 // 5152 /// NM_001001582 /	PDE9A	1.77E-12	5.53E-10	-1.66045	1.92E-08	-1.69871
2534252	NM_024101 // MLPH // melanophilin // 2q37.3 // 79083 /// NM_001042467 // MLPH //	MLPH	1.81E-12	2.60E-11	1.66959	1.65E-06	1.46639
2387606	NM_000740 // CHRM3 // cholinergic receptor, muscarinic 3 // 1q43 // 1131 /// ENS	CHRM3	1.84E-12	8.92E-12	1.76856	1.31E-05	1.43697
3556924	NM_001039619 // PRMT5 // protein arginine methyltransferase 5 // 14q11.2-q21 //	PRMT5	1.85E-12	1.69E-06	1.31031	2.64E-11	1.70351
2600689	NM_004438 // EPHA4 // EPH receptor A4 // 2q36.1 // 2043 /// ENST00000281821 // E	EPHA4	1.85E-12	2.03E-11	1.99601	2.70E-06	1.64477
3682028	NM_022844 // MYH11 // myosin, heavy chain 11, smooth muscle // 16p13.11 // 4629	MYH11	1.86E-12	7.86E-07	-1.69638	4.19E-11	-2.67103
3942502	NM_001001479 // SLC35E4 // solute carrier family 35, member E4 // 22q12.2 // 339	SLC35E4	1.90E-12	6.07E-06	1.32932	1.37E-11	1.85596
3426502	NM_005761 // PLXNC1 // plexin C1 // 12q23.3 // 10154 /// ENST00000258526 // PLXN	PLXNC1	1.92E-12	1.53E-06	-1.33473	2.93E-11	-1.75719
3203753	NM_018449 // UBAP2 // ubiquitin associated protein 2 // 9p13.3 // 55833 /// ENST	UBAP2	1.93E-12	2.04E-08	1.25773	5.97E-10	1.38067
3296386	NM_004747 // DLG5 // discs, large homolog 5 (Drosophila) // 10q23 // 9231 /// EN	DLG5	1.96E-12	1.08E-09	1.17909	1.05E-08	1.19917
3957486	NM_152511 // DUSP18 // dual specificity phosphatase 18 // 22q12.2 // 150290 ///	DUSP18	1.98E-12	1.14E-09	1.62129	1.01E-08	1.70707
2754073	NM_020225 // STOX2 // storkhead box 2 // 4q35.1 // 56977 /// ENST00000308497 //	STOX2	1.98E-12	9.64E-11	-1.38655	2.43E-07	-1.32748
3160658	NM_004170 // SLC1A1 // solute carrier family 1 (neuronal/epithelial high affinit	SLC1A1	2.00E-12	3.76E-08	-2.03619	3.82E-10	-2.84802
2546054	NM_022128 // RBKS // ribokinase // 2p23.3 // 64080 /// ENST00000302188 // RBKS /	RBKS	2.09E-12	5.74E-10	-1.62107	2.47E-08	-1.64859
3057514	NM_002991 // CCL24 // chemokine (C-C motif) ligand 24 // 7q11.23 // 6369 /// ENS	CCL24	2.10E-12	5.95E-08	2.33765	2.87E-10	3.63702
3815143	BC052236 // C19orf21 // chromosome 19 open reading frame 21 // 19p13.3 // 126353	C19orf21	2.11E-12	2.15E-10	-1.5787	8.78E-08	-1.53541
3471300	NM_139283 // PPTC7 // PTC7 protein phosphatase homolog (S. cerevisiae) // 12q24.	PPTC7	2.14E-12	3.72E-11	-1.34745	1.29E-06	-1.25696
2950590	NM_004761 // RGL2 // ral guanine nucleotide dissociation stimulator-like 2 // 6p	RGL2	2.14E-12	8.87E-08	1.2212	2.18E-10	1.36739

2842624	NM_017675 // PCDH24 // protocadherin 24 // 5q35.2 // 54825 /// ENST00000261944 /	PCDH24	2.15E-12	1.02E-09	-2.23769	1.31E-08	-2.40431
2635741	NM_198196 // CD96 // CD96 molecule // 3q13.13-q13.2 // 10225 /// NM_005816 // CD	CD96	2.16E-12	0.0049556	-1.22715	1.04E-12	-2.34565
3592401	NM_032413 // C15orf48 // chromosome 15 open reading frame 48 // 15q21.1 // 84419	C15orf48	2.17E-12	4.77E-08	-1.61925	3.55E-10	-2.053
3589857	BC061640 // LOC644844 // hypothetical LOC644844 // 15q15.1 // 644844	LOC644844	2.17E-12	7.12E-11	-2.61301	4.63E-07	-2.21815
2974935	NM_145176 // SLC2A12 // solute carrier family 2 (facilitated glucose transporter	SLC2A12	2.20E-12	4.86E-12	2.158	7.88E-05	1.52756
3465409	NM_001731 // BTG1 // B-cell translocation gene 1, anti-proliferative // 12q22 //	BTG1	2.22E-12	2.38E-07	-1.28871	1.14E-10	-1.53287
3655723	NM_017458 // MVP // major vault protein // 16p13.1-p11.2 // 9961 /// NM_005115 /	MVP	2.27E-12	7.15E-12	-1.44229	3.59E-05	-1.24139
2528020	NM_014640 // TTLL4 // tubulin tyrosine ligase-like family, member 4 // 2p24.3-p2	TTLL4	2.31E-12	2.61E-08	1.27314	6.34E-10	1.4087
3185498	NM_001860 // SLC31A2 // solute carrier family 31 (copper transporters), member 2	SLC31A2	2.39E-12	2.16E-08	-1.46344	7.82E-10	-1.7011
2735459	NM_014606 // HERC3 // hect domain and RLD 3 // 4q21 // 8916 /// ENST00000402738	HERC3	2.44E-12	7.65E-07	-1.39402	6.05E-11	-1.83729
3746574	NM_000304 // PMP22 // peripheral myelin protein 22 // 17p12-p11.2 // 5376 /// NM	PMP22	2.45E-12	3.30E-06	-1.56448	2.59E-11	-2.50087
2360506	NM_015872 // ZBTB7B // zinc finger and BTB domain containing 7B // 1q21.3 // 510	ZBTB7B	2.46E-12	2.18E-10	-1.42858	1.15E-07	-1.39207
3848540	NM_021155 // CD209 // CD209 molecule // 19p13 // 30835 /// ENST00000315599 // CD	CD209	2.48E-12	1.76E-09	-1.90824	9.13E-09	-2.0773
3442024	NM_001033714 // NOL1 // nucleolar protein 1, 120kDa // 12p13 // 4839 /// NM_0061	NOL1	2.49E-12	7.68E-05	1.25736	5.68E-12	1.83478
3762380	NM_001267 // CHAD // chondroadherin // 17q21.33 // 1101 /// ENST00000258969 // C	CHAD	2.49E-12	2.04E-07	-1.49322	1.48E-10	-1.9415
2505501	NM_033416 // IMP4 // IMP4, U3 small nucleolar ribonucleoprotein, homolog (yeast)	IMP4	2.53E-12	0.000117894	1.13332	4.81E-12	1.41128
3127156	NM_001495 // GFRA2 // GDNF family receptor alpha 2 // 8p21.3 // 2675 /// ENST000	GFRA2	2.54E-12	9.90E-10	-1.51625	1.81E-08	-1.56264
2657250	NM_005578 // LPP // LIM domain containing preferred translocation partner in lip	LPP	2.57E-12	1.86E-05	-1.19733	1.13E-11	-1.52576
3665116	NM_001755 // CBFB // core-binding factor, beta subunit // 16q22.1 // 865 /// NM_	CBFB	2.65E-12	9.47E-09	1.38595	1.89E-09	1.52761
3302360	NM_022362 // MMS19 // MMS19 nucleotide excision repair homolog (S. cerevisiae) /	MMS19	2.65E-12	3.15E-07	1.18974	1.20E-10	1.34465
3244488	NM_032023 // RASSF4 // Ras association (RalGDS/AF-6) domain family member 4 // 1	RASSF4	2.67E-12	1.13E-08	-1.47425	1.63E-09	-1.66658
2773387	NM_002090 // CXCL3 // chemokine (C-X-C motif) ligand 3 // 4q21 // 2921 /// ENST0	CXCL3	2.70E-12	5.71E-09	1.63327	3.15E-09	1.84056
3921068	NM_005239 // ETS2 // v-ets erythroblastosis virus E26 oncogene homolog 2 (avian)	ETS2	2.71E-12	8.14E-10	1.81267	2.55E-08	1.86485
3734966	NR_003587 // MYO15B // myosin XVB pseudogene // 17q25.1 // 80022 /// AF418286 //	MYO15B	2.73E-12	1.41E-08	-1.59763	1.38E-09	-1.87176
2656379	---		2.76E-12	9.28E-11	-2.91561	5.04E-07	-2.44136
3944826	NM_018957 // SH3BP1 // SH3-domain binding protein 1 // 22q13.1 // 23616 /// ENST	SH3BP1	2.78E-12	5.54E-12	-1.48182	0.000109245	-1.23663
3613725	NM_002487 // NDN // necdin homolog (mouse) // 15q11.2-q12 // 4692 /// ENST000003	NDN	2.79E-12	2.76E-07	-1.51847	1.40E-10	-2.0202
3401259	NM_003213 // TEAD4 // TEA domain family member 4 // 12p13.3-p13.2 // 7004 /// NM	TEAD4	2.85E-12	6.89E-07	1.36899	7.93E-11	1.76154
2423422	NM_003567 // BCAR3 // breast cancer anti-estrogen resistance 3 // 1p22.1 // 8412	BCAR3	2.93E-12	1.39E-09	-1.35734	1.58E-08	-1.39676
2440354	NM_001778 // CD48 // CD48 molecule // 1q21.3-q22 // 962 /// ENST00000368046 // C	CD48	2.94E-12	1.83E-05	-1.46423	1.33E-11	-2.4306
3425108	NM_001009894 // C12orf29 // chromosome 12 open reading frame 29 // 12q21.32 // 9	C12orf29	3.05E-12	8.83E-06	1.21173	2.00E-11	1.52333
2648305	NM_002563 // P2RY1 // purinergic receptor P2Y, G-protein coupled, 1 // 3q25.2 //	P2RY1	3.06E-12	4.79E-08	-1.42991	5.82E-10	-1.688
2351854	BC017973 // C1orf162 // chromosome 1 open reading frame 162 // 1p13.2 // 128346	C1orf162	3.07E-12	1.28E-07	-1.60884	2.75E-10	-2.11914
3933039	NM_005656 // TMPRSS2 // transmembrane protease, serine 2 // 21q22.3 // 7113 ///	TMPRSS2	3.10E-12	3.17E-10	-1.63467	1.08E-07	-1.59029
2735598	NM_145715 // TIGD2 // tigger transposable element derived 2 // 4q22.1 // 166815	TIGD2	3.18E-12	3.68E-08	1.42184	7.65E-10	1.65451
2824089	NR_002922 // SNORA13 // small nucleolar RNA, H/ACA box 13 // 5q22.2 // 654322 //	SNORA13	3.23E-12	6.06E-11	1.44107	1.38E-06	1.32879
2479433	NM_172069 // PLEKHH2 // pleckstrin homology domain containing, family H (with My	PLEKHH2	3.28E-12	4.01E-10	-1.51731	8.77E-08	-1.49362
3653123	NM_002738 // PRKCB // protein kinase C, beta // 16p11.2 // 5579 /// NM_212535 //	PRKCB	3.29E-12	2.62E-08	-1.60434	1.07E-09	-1.92913
3263743	NM_004419 // DUSP5 // dual specificity phosphatase 5 // 10q25 // 1847 /// ENST00	DUSP5	3.29E-12	3.70E-10	-1.82043	9.81E-08	-1.77102
3864445	NM_006297 // XRCC1 // X-ray repair complementing defective repair in Chinese ham	XRCC1	3.45E-12	8.07E-07	1.20073	9.21E-11	1.3919
3633148	NM_005697 // SCAMP2 // secretory carrier membrane protein 2 // 15q23-q25 // 1006	SCAMP2	3.54E-12	1.20E-09	-1.27076	2.60E-08	-1.2902
2351063	NM_000757 // CSF1 // colony stimulating factor 1 (macrophage) // 1p21-p13 // 143	CSF1	3.55E-12	1.04E-08	-1.39375	2.73E-09	-1.53129

3577612	NM_001002236 // SERPINA1 // serpin peptidase inhibitor, clade A (alpha-1 antipro	SERPINA1	3.58E-12	1.85E-08	1.8123	1.64E-09	2.22467
2961177	NM_004370 // COL12A1 // collagen, type XII, alpha 1 // 6q12-q13 // 1303 /// NM_0	COL12A1	3.65E-12	1.58E-10	1.97862	3.97E-07	1.8003
2514566	NM_003142 // SSB // Sjogren syndrome antigen B (autoantigen La) // 2q31.1 // 674	SSB	3.65E-12	6.43E-10	1.5326	5.83E-08	1.53218
2447877	NM_052966 // FAM129A // family with sequence similarity 129, member A // 1q25 //	FAM129A	3.69E-12	1.33E-07	-1.45401	3.47E-10	-1.79849
3132782	NM_003012 // SFRP1 // secreted frizzled-related protein 1 // 8p12-p11.1 // 6422	SFRP1	3.71E-12	3.71E-08	-1.52268	9.51E-10	-1.81576
3667281	NM_012426 // SF3B3 // splicing factor 3b, subunit 3, 130kDa // 16q22.1 // 23450	SF3B3	3.73E-12	2.09E-08	1.40506	1.56E-09	1.5852
3572443	BC001448 // FLVCR2 // feline leukemia virus subgroup C cellular receptor family,	FLVCR2	3.74E-12	1.04E-10	-2.23928	7.92E-07	-1.93384
4015709	NM_000061 // BTK // Bruton agammaglobulinemia tyrosine kinase // Xq21.33-q22 //	BTK	3.76E-12	1.14E-07	-1.52942	3.98E-10	-1.93058
3050462	NM_001001555 // GRB10 // growth factor receptor-bound protein 10 // 7p12-p11.2 /	GRB10	3.80E-12	4.92E-10	1.49627	8.79E-08	1.47819
3795466	BC014195 // C18orf22 // chromosome 18 open reading frame 22 // 18q23 // 79863 //	C18orf22	3.83E-12	7.73E-08	1.26213	5.50E-10	1.4181
3391149	NM_138378 // hCG_2033039 // hypothetical protein BC006136 // 11q23.1 // 91893 //	hCG_2033039	3.87E-12	1.37E-08	-1.95959	2.42E-09	-2.40716
2338487	NM_001113411 // FGGY // FGGY carbohydrate kinase domain containing // 1p32.1 //	FGGY	3.88E-12	8.01E-09	1.57035	4.00E-09	1.75718
3118818	NM_032611 // PTP4A3 // protein tyrosine phosphatase type IVA, member 3 // 8q24.3	PTP4A3	3.88E-12	4.62E-07	1.6028	1.54E-10	2.25278
3599709	NM_015554 // GLCE // glucuronic acid epimerase // 15q23 // 26035 /// ENST0000026	GLCE	3.89E-12	5.07E-09	1.50472	6.32E-09	1.63375
2980516	NM_173515 // CNKSR3 // CNKSR family member 3 // 6q25.2 // 154043 /// ENST0000036	CNKSR3	3.90E-12	3.51E-06	-1.42117	4.48E-11	-2.02992
3680583	NM_015659 // RSL1D1 // ribosomal L1 domain containing 1 // 16p13.13 // 26156 ///	RSL1D1	3.91E-12	5.63E-08	1.44041	7.27E-10	1.70492
3824775	NM_015016 // MAST3 // microtubule associated serine/threonine kinase 3 // 19p13.	MAST3	3.93E-12	1.40E-08	-1.23256	2.42E-09	-1.31429
3554523	NM_174891 // C14orf79 // chromosome 14 open reading frame 79 // 14q32.33 // 1226	C14orf79	3.95E-12	8.31E-08	1.36864	5.44E-10	1.60429
3859622	NM_175872 // ZNF792 // zinc finger protein 792 // 19q13.11 // 126375 /// ENST000	ZNF792	4.04E-12	1.53E-09	1.43475	2.45E-08	1.4751
2673830	NM_001009996 // DALRD3 // DALR anticodon binding domain containing 3 // 3p21.31	DALRD3	4.05E-12	4.58E-07	1.12992	1.65E-10	1.23327
3753860	NM_002985 // CCL5 // chemokine (C-C motif) ligand 5 // 17q11.2-q12 // 6352 /// E	CCL5	4.11E-12	7.25E-06	-1.34684	3.21E-11	-1.88473
3761551	NM_173623 // TTLL6 // tubulin tyrosine ligase-like family, member 6 // 17q21.32	TTLL6	4.12E-12	1.76E-07	-1.47774	3.29E-10	-1.86285
3970338	NM_198270 // NHS // Nance-Horan syndrome (congenital cataracts and dental anomal	NHS	4.22E-12	3.22E-11	1.48924	7.67E-06	1.31558
3059667	NM_152754 // SEMA3D // sema domain, immunoglobulin domain (Ig), short basic doma	SEMA3D	4.26E-12	0.000246605	-1.63608	6.42E-12	-4.14544
3658980	NM_133443 // GPT2 // glutamic pyruvate transaminase (alanine aminotransferase) 2	GPT2	4.26E-12	0.00038987	1.27399	5.34E-12	2.07883
3775425	NM_001009905 // B3GNTL1 // UDP-GlcNAc:betaGal beta-1,3-N-acetylglucosaminyltrans	B3GNTL1	4.29E-12	2.03E-07	1.30743	3.12E-10	1.53869
3642815	NM_005009 // NME4 // non-metastatic cells 4, protein expressed in // 16p13.3 //	NME4	4.47E-12	1.52E-05	1.22694	2.42E-11	1.58499
2363248	NM_002348 // LY9 // lymphocyte antigen 9 // 1q21.3-q22 // 4063 /// NM_001033667	LY9	4.62E-12	6.30E-08	-1.43185	8.47E-10	-1.68939
3843180	NM_020657 // ZNF304 // zinc finger protein 304 // 19q13.4 // 57343 /// ENST00000	ZNF304	4.72E-12	3.11E-10	-1.59039	2.47E-07	-1.52245
2643901	NM_002718 // PPP2R3A // protein phosphatase 2 (formerly 2A), regulatory subunit	PPP2R3A	4.78E-12	6.43E-08	-1.56724	8.76E-10	-1.92723
3260895	NM_017893 // SEMA4G // sema domain, immunoglobulin domain (Ig), transmembrane do	SEMA4G	4.85E-12	3.73E-06	-1.27729	5.69E-11	-1.63281
3518455	NM_012158 // FBXL3 // F-box and leucine-rich repeat protein 3 // 13q22 // 26224	FBXL3	4.87E-12	1.80E-07	-1.34965	4.06E-10	-1.60687
2826343	NM_014035 // SNX24 // sorting nexin 24 // 5q23.2 // 28966 /// ENST00000261369 //	SNX24	4.92E-12	4.84E-09	-1.5658	9.70E-09	-1.69515
3210457	NM_018339 // RFK // riboflavin kinase // 9q21.13 // 55312 /// ENST00000257452 //	RFK	4.93E-12	1.19E-10	-1.31886	1.13E-06	-1.25024
3743906	NM_000546 // TP53 // tumor protein p53 // 17p13.1 // 7157 /// NM_001126112 // TP	TP53	5.01E-12	3.55E-08	1.48743	1.53E-09	1.73565
3293724	NM_022153 // C10orf54 // chromosome 10 open reading frame 54 // 10q22.1 // 64115	C10orf54	5.06E-12	4.20E-09	-1.41835	1.18E-08	-1.50001
3389330	NM_004347 // CASP5 // caspase 5, apoptosis-related cysteine peptidase // 11q22.2	CASP5	5.06E-12	1.06E-11	-2.23137	0.000119562	-1.55364
3103818	NM_004133 // HNF4G // hepatocyte nuclear factor 4, gamma // 8q21.11 // 3174 ///	HNF4G	5.07E-12	2.48E-08	-1.86288	2.13E-09	-2.31307
2955061	NM_178148 // SLC35B2 // solute carrier family 35, member B2 // 6p12.1-p11.2 // 3	SLC35B2	5.07E-12	1.67E-05	1.20184	2.68E-11	1.51445
3891278	NM_198976 // TH1L // TH1-like (Drosophila) // 20q13 // 51497 /// ENST00000344018	TH1L	5.08E-12	4.44E-06	1.219	5.47E-11	1.49386
2896545	NM_006877 // GMPR // guanosine monophosphate reductase // 6p23 // 2766 /// ENST0	GMPR	5.20E-12	2.39E-10	1.6642	4.34E-07	1.55869
2318656	NM_016831 // PER3 // period homolog 3 (Drosophila) // 1p36.23 // 8863 /// ENST00	PER3	5.24E-12	1.33E-07	-1.45072	5.65E-10	-1.77246

2680046	NM_182920 // ADAMTS9 // ADAM metallopeptidase with thrombospondin type 1 motif,	ADAMTS9	5.33E-12	4.62E-09	1.44582	1.16E-08	1.53685
2786322	NM_014331 // SLC7A11 // solute carrier family 7, (cationic amino acid transporte	SLC7A11	5.38E-12	1.24E-08	1.95347	4.40E-09	2.33744
3543481	NM_000021 // PSEN1 // presenilin 1 // 14q24.3 // 5663 /// ENST00000324501 // PSE	PSEN1	5.46E-12	1.10E-09	-1.29908	6.11E-08	-1.30556
3286343	NM_001099282 // ZNF239 // zinc finger protein 239 // 10q11.22-q11.23 // 8187 ///	ZNF239	5.46E-12	7.20E-09	1.43689	7.65E-09	1.55027
3168136	NM_001080496 // RGP1 // RGP1 retrograde golgi transport homolog (S. cerevisiae)	RGP1	5.47E-12	4.71E-11	-1.31344	6.86E-06	-1.21133
3624607	NM_000259 // MYO5A // myosin VA (heavy chain 12, myoxin) // 15q21 // 4644 /// EN	MYO5A	5.47E-12	8.39E-08	-1.50345	8.61E-10	-1.82816
3916527	NM_021219 // JAM2 // junctional adhesion molecule 2 // 21q21.2 // 58494 /// ENST	JAM2	5.62E-12	8.08E-05	-1.29739	1.43E-11	-1.95456
3521816	NM_080818 // OXGR1 // oxoglutarate (alpha-ketoglutarate) receptor 1 // 13q32.1 /	OXGR1	5.66E-12	5.19E-07	1.60658	2.37E-10	2.2427
2364231	NM_001014796 // DDR2 // discoidin domain receptor tyrosine kinase 2 // 1q23.3 //	DDR2	5.71E-12	6.86E-08	-1.66955	1.07E-09	-2.10541
2864849	NM_012446 // SSBP2 // single-stranded DNA binding protein 2 // 5q14.1 // 23635 /	SSBP2	5.75E-12	1.28E-07	-1.55308	6.64E-10	-1.95727
3178583	NM_001827 // CKS2 // CDC28 protein kinase regulatory subunit 2 // 9q22 // 1164 /	CKS2	5.78E-12	0.000106336	1.36334	1.30E-11	2.26343
3357397	NM_138342 // GLB1L2 // galactosidase, beta 1-like 2 // 11q25 // 89944 /// ENST00	GLB1L2	5.78E-12	0.738773	-1.01318	8.57E-13	1.62598
3251023	NM_018344 // SLC29A3 // solute carrier family 29 (nucleoside transporters), memb	SLC29A3	5.81E-12	2.32E-06	1.24004	9.45E-11	1.50911
2448710	NM_199051 // FAM5C // family with sequence similarity 5, member C // 1q31.1 // 3	FAM5C	5.86E-12	1.14E-06	-1.99363	1.48E-10	-3.48145
3665857	NM_005796 // NUTF2 // nuclear transport factor 2 // 16q22.1 // 10204 /// ENST000	NUTF2	5.96E-12	1.07E-05	1.23719	4.13E-11	1.58346
2590582	NM_005019 // PDE1A // phosphodiesterase 1A, calmodulin-dependent // 2q32.1 // 51	PDE1A	5.97E-12	3.19E-08	-1.38112	2.18E-09	-1.55236
3249533	BT006794 // AKR1B10 // aldo-keto reductase family 1, member B10 (aldose reductas	AKR1B10	6.00E-12	1.66E-11	-3.07458	6.83E-05	-1.92168
2433232	NM_001461 // FMO5 // flavin containing monooxygenase 5 // 1q21.1 // 2330 /// ENS	FMO5	6.08E-12	9.77E-07	-1.49298	1.72E-10	-2.04359
3473436	NM_017899 // TESC // tescalcin // 12q24.22 // 54997 /// ENST00000392545 // TESC	TESC	6.13E-12	3.99E-10	1.98262	2.88E-07	1.86136
2414958	NM_002353 // TACSTD2 // tumor-associated calcium signal transducer 2 // 1p32-p31	TACSTD2	6.24E-12	4.20E-08	1.69744	1.84E-09	2.08528
2908474	NM_007355 // HSP90AB1 // heat shock protein 90kDa alpha (cytosolic), class B mem	HSP90AB1	6.28E-12	7.54E-08	1.46928	1.14E-09	1.75075
2418078	NM_173808 // NEGR1 // neuronal growth regulator 1 // 1p31.1 // 257194 /// ENST00	NEGR1	6.28E-12	7.11E-09	-1.50387	9.72E-09	-1.62937
2438125	NM_005998 // CCT3 // chaperonin containing TCP1, subunit 3 (gamma) // 1q23 // 72	CCT3	6.32E-12	8.68E-08	1.37001	1.03E-09	1.58918
2623922	NM_015136 // STAB1 // stabilin 1 // 3p21.1 // 23166 /// ENST00000321725 // STAB1	STAB1	6.33E-12	1.62E-09	-1.71604	4.99E-08	-1.75816
3472225	NM_001111322 // DDX54 // DEAD (Asp-Glu-Ala-Asp) box polypeptide 54 // 12q24.13 /	DDX54	6.36E-12	1.94E-05	1.14454	3.27E-11	1.35731
2939298	NM_015482 // SLC22A23 // solute carrier family 22, member 23 // 6p25.2 // 63027	SLC22A23	6.44E-12	3.20E-07	-1.25773	3.95E-10	-1.45301
2516023	NM_031942 // CDCA7 // cell division cycle associated 7 // 2q31 // 83879 /// NM_1	CDCA7	6.47E-12	2.10E-08	1.54297	3.58E-09	1.76451
2807686	NM_032587 // CARD6 // caspase recruitment domain family, member 6 // 5p13.1 // 8	CARD6	6.53E-12	1.59E-09	1.62111	5.39E-08	1.65303
3598758	NM_005585 // SMAD6 // SMAD family member 6 // 15q21-q22 // 4091 /// ENST00000288	SMAD6	6.59E-12	3.27E-08	1.26792	2.47E-09	1.37992
3741769	NM_002558 // P2RX1 // purinergic receptor P2X, ligand-gated ion channel, 1 // 17	P2RX1	6.70E-12	1.17E-09	-1.46666	8.20E-08	-1.47083
3770390	NM_015654 // NAT9 // N-acetyltransferase 9 // 17q25.1 // 26151 /// ENST000003578	NAT9	6.71E-12	8.41E-05	1.15813	1.72E-11	1.457
2734629	NM_080683 // PTPN13 // protein tyrosine phosphatase, non-receptor type 13 (APO-1	PTPN13	6.72E-12	1.66E-09	2.41171	5.39E-08	2.50298
2343823	NM_012302 // LPHN2 // latrophilin 2 // 1p31.1 // 23266 /// ENST00000359929 // LP	LPHN2	6.88E-12	1.79E-06	-1.64646	1.38E-10	-2.52602
3851651	NM_013433 // TNPO2 // transportin 2 (importin 3, karyopherin beta 2b) // 19p13.1	TNPO2	6.93E-12	0.000462715	1.1272	8.62E-12	1.43494
2461891	NM_152490 // B3GALNT2 // beta-1,3-N-acetylgalactosaminyltransferase 2 // 1q42.3	B3GALNT2	7.00E-12	1.14E-09	1.25322	9.20E-08	1.25343
2378662	NM_145759 // TRAF5 // TNF receptor-associated factor 5 // 1q32 // 7188 /// NM_00	TRAF5	7.00E-12	6.43E-10	1.88003	1.92E-07	1.81443
3820921	NM_001128844 // SMARCA4 // SWI/SNF related, matrix associated, actin dependent r	SMARCA4	7.01E-12	1.48E-08	1.18357	5.63E-09	1.23753
2388794	NM_205768 // ZNF238 // zinc finger protein 238 // 1q44-qter // 10472 /// NM_0063	ZNF238	7.02E-12	3.32E-11	1.35939	2.39E-05	1.2177
3405748	NM_001423 // EMP1 // epithelial membrane protein 1 // 12p12.3 // 2012 /// ENST00	EMP1	7.06E-12	1.21E-08	-2.12247	6.88E-09	-2.54838
2547114	NM_000379 // XDH // xanthine dehydrogenase // 2p23.1 // 7498 /// ENST00000379416	XDH	7.11E-12	7.52E-06	-1.50723	6.19E-11	-2.34938
2585972	NM_003742 // ABCB11 // ATP-binding cassette, sub-family B (MDR/TAP), member 11 /	ABCB11	7.20E-12	1.30E-11	-1.82513	0.000191323	-1.37806
3374934	NM_152852 // MS4A6A // membrane-spanning 4-domains, subfamily A, member 6A // 11	MS4A6A	7.20E-12	3.08E-07	-1.6815	4.73E-10	-2.31415

3995392	NM_007150 // ZNF185 // zinc finger protein 185 (LIM domain) // Xq28 // 7739 ///	ZNF185	7.34E-12	8.20E-08	1.37254	1.34E-09	1.58372
2778273	NM_014485 // PGDS // prostaglandin D2 synthase, hematopoietic // 4q22.3 // 27306	PGDS	7.35E-12	1.28E-08	-2.2895	6.97E-09	-2.80459
2371547	NM_030806 // C1orf21 // chromosome 1 open reading frame 21 // 1q25 // 81563 ///	C1orf21	7.50E-12	1.53E-05	-1.29939	4.52E-11	-1.78013
2815488	NM_001080479 // RGNEF // Rho-guanine nucleotide exchange factor // 5q13.2 // 642	RGNEF	7.51E-12	1.36E-10	1.75074	2.18E-06	1.54976
2809810	NM_006144 // GZMA // granzyme A (granzyme 1, cytotoxic T-lymphocyte-associated s	GZMA	7.52E-12	7.46E-07	-1.65084	2.71E-10	-2.37687
3576749	NM_006329 // FBLN5 // fibulin 5 // 14q32.1 // 10516 /// ENST00000342058 // FBLN5	FBLN5	7.69E-12	6.69E-07	-1.44122	3.00E-10	-1.86851
2400518	NM_001113349 // ECE1 // endothelin converting enzyme 1 // 1p36.1 // 1889 /// NM_	ECE1	7.93E-12	3.48E-07	-1.3786	4.94E-10	-1.68333
3726406	NM_025149 // ACSF2 // acyl-CoA synthetase family member 2 // 17q21.33 // 80221 /	ACSF2	7.95E-12	1.07E-09	-1.96431	1.25E-07	-1.94258
2778856	NM_005723 // TSPAN5 // tetraspanin 5 // 4q23 // 10098 /// ENST00000305798 // TSP	TSPAN5	7.98E-12	2.41E-09	1.76868	4.70E-08	1.83547
3239380	NM_024838 // THNSL1 // threonine synthase-like 1 (S. cerevisiae) // 10p12.1 // 7	THNSL1	8.04E-12	4.84E-08	1.56033	2.37E-09	1.85065
3746040	NM_018127 // ELAC2 // elaC homolog 2 (E. coli) // 17p11.2 // 60528 /// ENST00000	ELAC2	8.06E-12	6.44E-06	1.17229	7.90E-11	1.38383
2320411	NM_001040196 // AGTRAP // angiotensin II receptor-associated protein // 1p36.22	AGTRAP	8.19E-12	2.29E-06	1.21075	1.48E-10	1.43255
2599153	NM_022648 // TNS1 // tensin 1 // 2q35-q36 // 7145 /// ENST00000171887 // TNS1 //	TNS1	8.22E-12	6.52E-08	-1.54795	1.90E-09	-1.85626
3317071	NM_002339 // LSP1 // lymphocyte-specific protein 1 // 11p15.5 // 4046 /// NM_001	LSP1	8.49E-12	2.81E-06	-1.3929	1.37E-10	-1.88104
3381063	NM_030813 // CLPB // ClpB caseinolytic peptidase B homolog (E. coli) // 11q13.4	CLPB	8.60E-12	0.0309109	1.06492	2.59E-12	1.40146
3182199	AY598327 // C9orf30 // chromosome 9 open reading frame 30 // 9q31.1 // 91283 ///	C9orf30	8.64E-12	3.57E-09	1.49087	3.42E-08	1.55072
3735151	NM_000213 // ITGB4 // integrin, beta 4 // 17q25 // 3691 /// NM_001005731 // ITGB	ITGB4	8.70E-12	9.96E-11	1.47401	5.06E-06	1.3307
2828716	NM_001039780 // CCNI2 // cyclin I family, member 2 // 5q31.1 // 645121 /// ENST0	CCNI2	8.71E-12	4.88E-07	1.58626	4.41E-10	2.14843
3041294	NM_032581 // FAM126A // family with sequence similarity 126, member A // 7p15.3	FAM126A	8.72E-12	2.10E-06	-1.45166	1.69E-10	-2.00074
3842675	NR_003127 // ZNF542 // zinc finger protein 542 // 19q13.43 // 147947 /// BC08941	ZNF542	8.74E-12	1.20E-07	-1.48519	1.27E-09	-1.79704
2645951	NM_003304 // TRPC1 // transient receptor potential cation channel, subfamily C,	TRPC1	8.77E-12	8.76E-09	-1.42496	1.34E-08	-1.52428
3329886	NM_175732 // PTPMT1 // protein tyrosine phosphatase, mitochondrial 1 // 11p11.2	PTPMT1	8.80E-12	0.00662752	1.09859	4.26E-12	1.47292
3284302	NM_003873 // NRP1 // neuropilin 1 // 10p12 // 8829 /// NM_001024628 // NRP1 // n	NRP1	8.91E-12	1.22E-08	-1.4586	9.86E-09	-1.58739
3753500	NM_001104587 // SLFN11 // schlafen family member 11 // 17q12 // 91607 /// NM_001	SLFN11	9.12E-12	4.47E-07	-1.37408	5.00E-10	-1.68504
3940001	NM_015330 // SPECC1L // SPECC1-like // 22q11.23 // 23384 /// ENST00000314328 //	SPECC1L	9.12E-12	4.80E-06	-1.29397	1.09E-10	-1.66749
2677723	NM_001128615 // ARHGEF3 // Rho guanine nucleotide exchange factor (GEF) 3 // 3p2	ARHGEF3	9.23E-12	1.08E-11	1.65925	0.000586828	1.27592
3454576	NM_000617 // SLC11A2 // solute carrier family 11 (proton-coupled divalent metal	SLC11A2	9.25E-12	1.61E-08	1.57834	7.98E-09	1.7696
3740664	NM_032895 // C17orf91 // chromosome 17 open reading frame 91 // 17p13.3 // 84981	C17orf91	9.26E-12	4.49E-10	-1.85172	5.37E-07	-1.72337
2622547	NM_004186 // SEMA3F // sema domain, immunoglobulin domain (Ig), short basic doma	SEMA3F	9.43E-12	2.83E-08	1.52732	4.85E-09	1.74163
3205659	NM_003028 // SHB // Src homology 2 domain containing adaptor protein B // 9p13.2	SHB	9.83E-12	7.78E-08	1.28521	2.13E-09	1.42841
2485406	NM_014181 // HSPC159 // galectin-related protein // 2p14 // 29094 /// ENST000002	HSPC159	9.92E-12	4.24E-09	-1.5915	3.57E-08	-1.67061
2878437	NM_001040021 // CD14 // CD14 molecule // 5q22-q32|5q31.1 // 929 /// NM_000591 //	CD14	9.97E-12	4.75E-08	-1.71331	3.31E-09	-2.08346
3226369	NM_012127 // CIZ1 // CDKN1A interacting zinc finger protein 1 // 9q34.1 // 25792	CIZ1	1.01E-11	2.31E-06	1.15702	1.92E-10	1.3119
3631964	NM_182470 // PKM2 // pyruvate kinase, muscle // 15q22 // 5315 /// NM_002654 // P	PKM2	1.01E-11	4.61E-06	1.23213	1.27E-10	1.50793
3101629	NM_144650 // ADHFE1 // alcohol dehydrogenase, iron containing, 1 // 8q13.1 // 13	ADHFE1	1.01E-11	9.24E-08	-1.56273	1.92E-09	-1.90072
2954678	NM_020750 // XPO5 // exportin 5 // 6p21.1 // 57510 /// ENST00000398799 // XPO5 /	XPO5	1.01E-11	7.52E-07	1.33815	4.02E-10	1.64158
3205506	NM_012166 // FBXO10 // F-box protein 10 // 9p13.2 // 26267 /// NM_001001790 // T	FBXO10	1.02E-11	0.00804936	1.09507	4.68E-12	1.46637
2518272	NM_000885 // ITGA4 // integrin, alpha 4 (antigen CD49D, alpha 4 subunit of VLA-4	ITGA4	1.04E-11	2.35E-05	-1.45038	5.38E-11	-2.30827
3701000	NM_001031804 // MAF // v-maf musculoaponeurotic fibrosarcoma oncogene homolog (a	MAF	1.06E-11	1.37E-07	-1.42081	1.50E-09	-1.68249
3752258	NM_006495 // EVI2B // ecotropic viral integration site 2B // 17q11.2 // 2124 ///	EVI2B	1.07E-11	1.22E-06	-1.78451	3.11E-10	-2.77751
3706659	NM_000049 // ASPA // aspartoacylase (Canavan disease) // 17pter-p13 // 443 /// N	ASPA	1.08E-11	2.04E-08	-2.2789	8.11E-09	-2.82961
3239760	NM_019043 // APBB1IP // amyloid beta (A4) precursor protein-binding, family B, m	APBB1IP	1.12E-11	0.00412936	-1.18803	6.46E-12	-1.9313

2445643	NM_033127 // SEC16B // SEC16 homolog B (S. cerevisiae) // 1q25.2 // 89866 /// EN	SEC16B	1.13E-11	7.65E-10	1.65634	3.69E-07	1.5907
3821908	NM_006397 // RNASEH2A // ribonuclease H2, subunit A // 19p13.13 // 10535 /// ENS	RNASEH2A	1.14E-11	0.0334334	1.11116	3.39E-12	1.76651
3332465	NM_031457 // MS4A8B // membrane-spanning 4-domains, subfamily A, member 8B // 11	MS4A8B	1.14E-11	1.51E-05	-1.74274	7.57E-11	-3.31589
2640855	NM_004526 // MCM2 // minichromosome maintenance complex component 2 // 3q21 // 4	MCM2	1.15E-11	0.029654	1.08938	3.54E-12	1.56944
3346147	NM_032021 // TMEM133 // transmembrane protein 133 // 11q22.1 // 83935 /// ENST00	TMEM133	1.16E-11	1.48E-05	-1.40048	7.85E-11	-2.06482
3349293	NM_181351 // NCAM1 // neural cell adhesion molecule 1 // 11q23.1 // 4684 /// NM_	NCAM1	1.17E-11	2.40E-08	-1.42751	7.87E-09	-1.57359
4015440	NM_080737 // SYTL4 // synaptotagmin-like 4 // Xq21.33 // 94121 /// NM_001129896	SYTL4	1.19E-11	1.92E-08	-1.35668	9.95E-09	-1.46348
3553389	NM_030943 // AMN // amnionless homolog (mouse) // 14q32.3 // 81693 /// ENST00000	AMN	1.20E-11	2.26E-09	-1.4822	1.03E-07	-1.49606
3063589	NM_001185 // AZGP1 // alpha-2-glycoprotein 1, zinc-binding // 7q22.1 // 563 ///	AZGP1	1.21E-11	1.22E-08	2.2719	1.60E-08	2.67357
4021508	NM_017666 // ZNF280C // zinc finger protein 280C // Xq25 // 55609 /// ENST000003	ZNF280C	1.23E-11	1.33E-09	1.50499	2.08E-07	1.48551
3334025	NM_017490 // MARK2 // MAP/microtubule affinity-regulating kinase 2 // 11q12-q13	MARK2	1.24E-11	6.89E-10	-1.30859	5.15E-07	-1.27405
4055661	NM_000240 // MAOA // monoamine oxidase A // Xp11.3 // 4128 /// ENST00000338702 /	MAOA	1.25E-11	9.34E-09	-2.34764	2.23E-08	-2.70742
4011889	NM_201599 // ZMYM3 // zinc finger, MYM-type 3 // Xq13.1 // 9203 /// NM_005096 //	ZMYM3	1.27E-11	1.49E-09	1.29775	1.91E-07	1.28992
3069082	NM_012252 // TFEC // transcription factor EC // 7q31.2 // 22797 /// NM_001018058	TFEC	1.28E-11	1.22E-08	-1.42619	1.76E-08	-1.52746
3071063	NM_001127323 // GRM8 // glutamate receptor, metabotropic 8 // 7q31.3-q32.1 // 29	GRM8	1.30E-11	2.56E-09	2.71388	1.01E-07	2.79653
3918535	NM_000628 // IL10RB // interleukin 10 receptor, beta // 21q22.1-q22.2|21q22.11 /	IL10RB	1.30E-11	2.58E-08	-1.33602	8.61E-09	-1.44597
2405152	NM_030786 // SYNC1 // syncoilin, intermediate filament 1 // 1p34.3-p33 // 81493	SYNC1	1.33E-11	2.24E-08	-1.49628	1.03E-08	-1.6583
4022106	NM_018388 // MBNL3 // muscleblind-like 3 (Drosophila) // Xq26.2 // 55796 /// NM_	MBNL3	1.37E-11	2.31E-07	-1.27573	1.42E-09	-1.44899
3272736	NM_145806 // ZNF511 // zinc finger protein 511 // 10q26.3 // 118472 /// ENST0000	ZNF511	1.37E-11	1.10E-05	1.28073	1.13E-10	1.67426
2339786	NM_002633 // PGM1 // phosphoglucomutase 1 // 1p31 // 5236 /// ENST00000371084 //	PGM1	1.37E-11	1.70E-09	-1.43242	1.85E-07	-1.42393
3704376	D87071 // FAM38A // family with sequence similarity 38, member A // 16q24.3 // 9	FAM38A	1.40E-11	1.09E-06	1.24618	4.79E-10	1.46121
2703902	NM_000055 // BCHE // butyrylcholinesterase // 3q26.1-q26.2 // 590 /// ENST000002	BCHE	1.42E-11	1.91E-09	-1.7021	1.70E-07	-1.69524
3185593	NM_017688 // BSPRY // B-box and SPRY domain containing // 9q32 // 54836 /// ENST	BSPRY	1.42E-11	3.04E-07	1.31409	1.22E-09	1.52873
3666189	NM_019023 // PRMT7 // protein arginine methyltransferase 7 // 16q22.1 // 54496 /	PRMT7	1.43E-11	0.000168906	1.13238	3.02E-11	1.3901
3127775	NM_003844 // TNFRSF10A // tumor necrosis factor receptor superfamily, member 10a	TNFRSF10A	1.44E-11	1.44E-06	1.27335	4.12E-10	1.5302
2438207	NM_005920 // MEF2D // myocyte enhancer factor 2D // 1q12-q23 // 4209 /// ENST000	MEF2D	1.44E-11	2.38E-08	-1.31716	1.10E-08	-1.41305
3656223	NM_002209 // ITGAL // integrin, alpha L (antigen CD11A (p180), lymphocyte functi	ITGAL	1.44E-11	1.02E-05	-1.32959	1.26E-10	-1.80095
3320819	NM_032867 // MICALCL // MICAL C-terminal like // 11p15.3 // 84953 /// ENST000002	MICALCL	1.44E-11	2.65E-08	-1.5468	9.92E-09	-1.73751
3290649	NM_198215 // FAM13C1 // family with sequence similarity 13, member C1 // 10q21.1	FAM13C1	1.46E-11	1.11E-07	-1.34448	2.80E-09	-1.52652
3215245	NM_198841 // FAM120AOS // family with sequence similarity 120A opposite strand /	FAM120AOS	1.47E-11	3.00E-09	-1.33446	1.04E-07	-1.34811
4027769	NM_001289 // CLIC2 // chloride intracellular channel 2 // Xq28 // 1193 /// ENST0	CLIC2	1.50E-11	6.54E-08	-1.63545	4.61E-09	-1.9567
3351166	NM_001558 // IL10RA // interleukin 10 receptor, alpha // 11q23 // 3587 /// ENST0	IL10RA	1.52E-11	2.04E-07	-1.55278	1.83E-09	-1.93334
3909553	NM_012340 // NFATC2 // nuclear factor of activated T-cells, cytoplasmic, calcine	NFATC2	1.53E-11	0.000437861	-1.14968	2.16E-11	-1.4993
3804195	NM_012319 // SLC39A6 // solute carrier family 39 (zinc transporter), member 6 //	SLC39A6	1.53E-11	1.07E-07	1.39925	3.12E-09	1.61135
3718204	NM_005408 // CCL13 // chemokine (C-C motif) ligand 13 // 17q11.2 // 6357 /// ENS	CCL13	1.55E-11	1.76E-09	-2.47036	2.21E-07	-2.41778
3276337	NM_030569 // ITIH5 // inter-alpha (globulin) inhibitor H5 // 10p14 // 80760 ///	ITIH5	1.56E-11	1.13E-06	-1.43587	5.41E-10	-1.86192
3994795	NM_000252 // MTM1 // myotubularin 1 // Xq28 // 4534 /// ENST00000306167 // MTM1	MTM1	1.61E-11	2.51E-07	-1.51537	1.69E-09	-1.87994
3726298	NM_153229 // TMEM92 // transmembrane protein 92 // 17q21.33 // 162461 /// ENST00	TMEM92	1.62E-11	2.22E-10	1.99735	4.92E-06	1.69247
3250990	NM_170744 // UNC5B // unc-5 homolog B (C. elegans) // 10q22.1 // 219699 /// ENST	UNC5B	1.63E-11	5.64E-11	-1.38946	6.22E-05	-1.22316
3221598	NM_001012361 // WDR31 // WD repeat domain 31 // 9q32 // 114987 /// NM_145241 //	WDR31	1.65E-11	2.36E-07	1.36245	1.83E-09	1.59454
2979246	NM_130900 // RAET1L // retinoic acid early transcript 1L // 6q25.1 // 154064 ///	RAET1L	1.72E-11	1.67E-07	2.64886	2.56E-09	4.1582
3957816	NM_014323 // PATZ1 // POZ (BTB) and AT hook containing zinc finger 1 // 22q12.2	PATZ1	1.73E-11	1.13E-08	1.31796	3.09E-08	1.3773

3169331	NM_000692 // ALDH1B1 // aldehyde dehydrogenase 1 family, member B1 // 9p11.1 //	ALDH1B1	1.75E-11	2.27E-06	1.49466	3.96E-10	2.06826
3507710	NM_003045 // SLC7A1 // solute carrier family 7 (cationic amino acid transporter,	SLC7A1	1.75E-11	0.000235042	1.1934	3.30E-11	1.61524
2562271	NM_001747 // CAPG // capping protein (actin filament), gelsolin-like // 2p11.2 /	CAPG	1.76E-11	4.48E-06	1.28747	2.61E-10	1.62074
3278813	BC064407 // FAM107B // family with sequence similarity 107, member B // 10p13 //	FAM107B	1.77E-11	3.85E-09	-1.60473	1.07E-07	-1.6392
2733498	NM_001201 // BMP3 // bone morphogenetic protein 3 // 4q21 // 651 /// ENST0000028	BMP3	1.79E-11	5.67E-08	-3.54516	6.79E-09	-5.40599
3017080	NM_031905 // ARMC10 // armadillo repeat containing 10 // 7q22.1 // 83787 /// ENS	ARMC10	1.81E-11	3.15E-08	1.2817	1.19E-08	1.36931
2434233	NM_020205 // OTUD7B // OTU domain containing 7B // 1q21.2 // 56957 /// ENST00000	OTUD7B	1.82E-11	3.59E-08	-1.27933	1.06E-08	-1.37079
3355733	NM_002017 // FLI1 // Friend leukemia virus integration 1 // 11q24.1-q24.3 // 231	FLI1	1.83E-11	4.23E-07	-1.49279	1.35E-09	-1.8784
3469180	NM_032148 // SLC41A2 // solute carrier family 41, member 2 // 12q23.3 // 84102 /	SLC41A2	1.83E-11	1.66E-07	-1.65438	2.80E-09	-2.08247
3246888	NM_001098512 // PRKG1 // protein kinase, cGMP-dependent, type I // 10q11.2 // 55	PRKG1	1.84E-11	7.30E-10	-1.51265	1.00E-06	-1.43431
3289445	NM_138933 // A1CF // APOBEC1 complementation factor // 10q11.23 // 29974 /// NM_	A1CF	1.88E-11	1.06E-08	-1.55359	3.77E-08	-1.65671
2324097	NM_032409 // PINK1 // PTEN induced putative kinase 1 // 1p36 // 65018 /// ENST00	PINK1	1.88E-11	2.29E-06	-1.2133	4.32E-10	-1.41699
3870692	NM_001081442 // LILRB5 // leukocyte immunoglobulin-like receptor, subfamily B (w	LILRB5	1.91E-11	2.98E-10	-1.78145	4.28E-06	-1.56501
3388830	NM_002422 // MMP3 // matrix metallopeptidase 3 (stromelysin 1, progelatinase) //	MMP3	1.92E-11	1.63E-06	2.79735	5.56E-10	6.06084
2398287	NM_001102663 // NBPF16 // neuroblastoma breakpoint family, member 16 // 1q21.1 /	NBPF16	1.93E-11	2.56E-05	-1.27429	1.09E-10	-1.70592
3689880	NM_024745 // SHCBP1 // SHC SH2-domain binding protein 1 // 16q11.2 // 79801 ///	SHCBP1	1.94E-11	0.0095606	1.17049	8.79E-12	1.94427
3875108	AK292708 // C20orf196 // chromosome 20 open reading frame 196 // 20p12.3 // 1498	C20orf196	1.96E-11	6.91E-06	1.26045	2.30E-10	1.57791
2633256	NM_006100 // ST3GAL6 // ST3 beta-galactoside alpha-2,3-sialyltransferase 6 // 3q	ST3GAL6	2.01E-11	4.11E-08	-1.37787	1.09E-08	-1.51068
3696666	NM_000903 // NQO1 // NAD(P)H dehydrogenase, quinone 1 // 16q22.1 // 1728 /// NM_	NQO1	2.02E-11	7.69E-05	1.46334	6.55E-11	2.5171
2555830	NM_198276 // TMEM17 // transmembrane protein 17 // 2p15 // 200728 /// ENST000003	TMEM17	2.02E-11	6.77E-08	1.39177	6.97E-09	1.55887
2558612	NM_003236 // TGFA // transforming growth factor, alpha // 2p13 // 7039 /// NM_00	TGFA	2.03E-11	2.34E-09	-1.48749	2.50E-07	-1.47677
3252534	NM_144660 // SAMD8 // sterile alpha motif domain containing 8 // 10q22.2 // 1428	SAMD8	2.06E-11	8.10E-08	-1.32334	6.10E-09	-1.46464
2431886	NM_014644 // PDE4DIP // phosphodiesterase 4D interacting protein // 1q12 // 9659	PDE4DIP	2.06E-11	2.51E-08	-1.264	1.82E-08	-1.33409
2940202	NM_000129 // F13A1 // coagulation factor XIII, A1 polypeptide // 6p25.3-p24.3 //	F13A1	2.07E-11	9.60E-07	-2.61462	8.82E-10	-4.98177
2673181	NM_002673 // PLXNB1 // plexin B1 // 3p21.31 // 5364 /// ENST00000296440 // PLXNB	PLXNB1	2.07E-11	3.44E-09	1.23596	1.61E-07	1.24111
3709327	NM_001037144 // CNTROB // centrobin, centrosomal BRCA2 interacting protein // 17	CNTROB	2.08E-11	3.35E-06	1.11892	3.87E-10	1.23108
2840036	NM_004946 // DOCK2 // dedicator of cytokinesis 2 // 5q35.1 // 1794 /// ENST00000	DOCK2	2.11E-11	1.92E-05	-1.41552	1.41E-10	-2.10397
2934521	NM_021977 // SLC22A3 // solute carrier family 22 (extraneuronal monoamine transp	SLC22A3	2.12E-11	1.10E-08	2.16672	4.41E-08	2.41343
2708066	NM_130446 // KLHL6 // kelch-like 6 (Drosophila) // --- // 89857 /// ENST00000341	KLHL6	2.13E-11	3.40E-08	-1.58562	1.42E-08	-1.78843
2777564	NM_014883 // FAM13A1 // family with sequence similarity 13, member A1 // 4q22.1	FAM13A1	2.15E-11	8.61E-08	1.33142	6.15E-09	1.4783
3435980	NM_024809 // TCTN2 // tectonic family member 2 // 12q24.31 // 79867 /// ENST0000	TCTN2	2.15E-11	2.70E-08	1.32827	1.80E-08	1.41986
3014159	NM_014916 // LMTK2 // lemur tyrosine kinase 2 // 7q21.3 // 22853 /// ENST0000029	LMTK2	2.17E-11	4.21E-08	-1.31184	1.20E-08	-1.41663
2405284	NM_033504 // TMEM54 // transmembrane protein 54 // 1p35-p34 // 113452 /// ENST00	TMEM54	2.18E-11	1.34E-11	-1.70131	0.00403508	-1.23438
4010461	NM_001012968 // SPIN4 // spindlin family, member 4 // Xq11.1 // 139886 /// ENST0	SPIN4	2.18E-11	6.79E-08	1.34704	7.77E-09	1.48925
3817464	NM_032868 // MPND // MPN domain containing // 19p13.3 // 84954 /// ENST000002629	MPND	2.24E-11	4.40E-10	-1.29925	3.17E-06	-1.23341
2396781	NM_001127325 // MAD2L2 // MAD2 mitotic arrest deficient-like 2 (yeast) // 1p36 /	MAD2L2	2.27E-11	1.38E-06	1.28735	7.79E-10	1.54104
2953139	NM_005943 // MOCS1 // molybdenum cofactor synthesis 1 // 6p21.3 // 4337 /// NM_0	MOCS1	2.28E-11	1.10E-10	-1.54585	3.63E-05	-1.32856
2955673	NM_021572 // ENPP5 // ectonucleotide pyrophosphatase/phosphodiesterase 5 (putati	ENPP5	2.35E-11	6.81E-10	1.83948	1.79E-06	1.67066
2645387	NM_152282 // ACPL2 // acid phosphatase-like 2 // 3q23 // 92370 /// NM_001037172	ACPL2	2.36E-11	2.68E-06	1.20086	5.25E-10	1.39152
3992408	NM_001449 // FHL1 // four and a half LIM domains 1 // Xq26 // 2273 /// ENST00000	FHL1	2.38E-11	2.84E-08	-1.76117	2.01E-08	-2.0078
2922215	NM_002356 // MARCKS // myristoylated alanine-rich protein kinase C substrate //	MARCKS	2.43E-11	1.48E-05	-1.28108	1.94E-10	-1.67386
3884044	BC127688 // C20orf118 // chromosome 20 open reading frame 118 // 20q11.23 // 140	C20orf118	2.43E-11	2.97E-10	-1.67125	7.12E-06	-1.47171

2460296	NM_000029 // AGT // angiotensinogen (serpin peptidase inhibitor, clade A, member	AGT	2.44E-11	5.49E-09	1.57894	1.22E-07	1.61837
3839920	NM_002030 // FPR3 // formyl peptide receptor 3 // 19q13.3-q13.4 // 2359 /// ENST	FPR3	2.45E-11	1.67E-08	-1.89131	3.62E-08	-2.10917
3129731	NM_057158 // DUSP4 // dual specificity phosphatase 4 // 8p12-p11 // 1846 /// NM_	DUSP4	2.47E-11	8.76E-10	1.85954	1.36E-06	1.70853
2519480	NM_016315 // GULP1 // GULP, engulfment adaptor PTB domain containing 1 // 2q32.3	GULP1	2.47E-11	4.05E-05	-1.47939	1.15E-10	-2.43094
3744965	NM_201433 // GAS7 // growth arrest-specific 7 // 17p13.1 // 8522 /// NM_201432 /	GAS7	2.50E-11	5.57E-08	-1.44566	1.14E-08	-1.6163
3651509	NM_030941 // LOC81691 // exonuclease NEF-sp // 16p12.2 // 81691 /// ENST00000261	LOC81691	2.53E-11	0.0775343	1.06066	6.14E-12	1.46012
3590498	NM_006293 // TYRO3 // TYRO3 protein tyrosine kinase // 15q15.1-q21.1 // 7301 ///	TYRO3	2.54E-11	6.60E-08	1.44978	1.00E-08	1.63306
2777070	NM_016245 // HSD17B11 // hydroxysteroid (17-beta) dehydrogenase 11 // 4q22.1 //	HSD17B11	2.57E-11	1.23E-06	-1.51956	9.93E-10	-2.02374
3388631	NM_052932 // TMEM123 // transmembrane protein 123 // 11q22.1 // 114908 /// ENST0	TMEM123	2.58E-11	5.74E-09	1.57831	1.27E-07	1.61763
3031466	NM_175571 // GIMAP8 // GTPase, IMAP family member 8 // 7q36.1 // 155038 /// ENST	GIMAP8	2.60E-11	1.67E-05	-1.27919	1.97E-10	-1.67495
3191352	NM_014286 // FREQ // frequenin homolog (Drosophila) // 9q34 // 23413 /// NM_0011	FREQ	2.61E-11	0.000875934	1.20889	2.95E-11	1.78668
2360206	NM_020452 // ATP8B2 // ATPase, class I, type 8B, member 2 // 1q21.3 // 57198 ///	ATP8B2	2.61E-11	9.79E-08	-1.40334	7.35E-09	-1.58727
2607568	NM_006614 // CHL1 // cell adhesion molecule with homology to L1CAM (close homolo	CHL1	2.62E-11	2.75E-06	-1.4859	5.91E-10	-2.03892
3957160	NM_002309 // LIF // leukemia inhibitory factor (cholinergic differentiation fact	LIF	2.68E-11	1.10E-09	1.74348	1.14E-06	1.63093
3833093	NM_001001563 // TIMM50 // translocase of inner mitochondrial membrane 50 homolog	TIMM50	2.71E-11	0.00483033	1.1301	1.59E-11	1.5861
3418007	NM_005412 // SHMT2 // serine hydroxymethyltransferase 2 (mitochondrial) // 12q12	SHMT2	2.72E-11	0.00145339	1.20812	2.51E-11	1.84379
3435902	NM_020936 // DDX55 // DEAD (Asp-Glu-Ala-Asp) box polypeptide 55 // 12q24.31 // 5	DDX55	2.73E-11	5.59E-07	1.24334	1.90E-09	1.40885
2798915	NM_004237 // TRIP13 // thyroid hormone receptor interactor 13 // 5p15.33 // 9319	TRIP13	2.73E-11	5.39E-05	1.43345	1.12E-10	2.30281
2700365	NM_014220 // TM4SF1 // transmembrane 4 L six family member 1 // 3q21-q25 // 4071	TM4SF1	2.74E-11	1.07E-07	1.75999	7.26E-09	2.16947
3956342	BC016465 // TTC28 // tetratricopeptide repeat domain 28 // 22q12.1 // 23331 ///	TTC28	2.74E-11	4.46E-07	-1.26288	2.27E-09	-1.43396
3706992	NM_001124758 // SPNS2 // spinster homolog 2 (Drosophila) // 17p13.2 // 124976 //	SPNS2	2.74E-11	1.88E-06	1.38057	8.08E-10	1.75232
3167187	NM_007343 // PRSS3 // protease, serine, 3 // 9p11.2 // 5646 /// NM_002771 // PRS	PRSS3	2.75E-11	2.48E-08	-1.48573	2.90E-08	-1.61083
3722304	NM_000988 // RPL27 // ribosomal protein L27 // 17q21.1-q21.2 // 6155 /// ENST000	RPL27	2.76E-11	0.00041076	1.18712	4.33E-11	1.6205
2353988	NM_017709 // FAM46C // family with sequence similarity 46, member C // 1p12 // 5	FAM46C	2.77E-11	1.86E-08	-1.69235	3.92E-08	-1.85299
3997780	NM_000047 // ARSE // arylsulfatase E (chondrodysplasia punctata 1) // Xp22.3 //	ARSE	2.79E-11	1.28E-07	1.45666	6.41E-09	1.68648
2997272	NM_030636 // EEPD1 // endonuclease/exonuclease/phosphatase family domain contain	EEPD1	2.80E-11	4.75E-09	1.33671	1.83E-07	1.34721
3381925	NM_173582 // PGM2L1 // phosphoglucomutase 2-like 1 // 11q13.4 // 283209 /// ENST	PGM2L1	2.83E-11	2.71E-09	1.81677	3.77E-07	1.78194
2797393	NM_005245 // FAT // FAT tumor suppressor homolog 1 (Drosophila) // 4q35 // 2195	FAT	2.84E-11	5.84E-10	1.48046	3.30E-06	1.3733
2987441	NM_001037283 // EIF3B // eukaryotic translation initiation factor 3, subunit B /	EIF3B	2.85E-11	3.99E-06	1.27379	5.19E-10	1.56379
3061805	NM_001099401 // SGCE // sarcoglycan, epsilon // 7q21-q22 // 8910 /// NM_003919 /	SGCE	2.87E-11	1.99E-07	-1.48569	4.58E-09	-1.76843
2378180	NM_014388 // C1orf107 // chromosome 1 open reading frame 107 // 1q32.2 // 27042	C1orf107	2.87E-11	5.27E-08	1.43443	1.48E-08	1.58945
3680434	NM_004862 // LITAF // lipopolysaccharide-induced TNF factor // 16p13.13 // 9516	LITAF	2.88E-11	3.03E-09	-1.35468	3.36E-07	-1.3456
2812359	NM_020726 // NLN // neurolysin (metallopeptidase M3 family) // 5q12.3 // 57486 /	NLN	2.88E-11	3.00E-05	1.27842	1.62E-10	1.71367
3667811	NM_001361 // DHODH // dihydroorotate dehydrogenase // 16q22 // 1723 /// ENST0000	DHODH	2.89E-11	5.20E-05	1.16284	1.22E-10	1.41544
3323748	NM_213599 // ANO5 // anoctamin 5 // 11p14.3 // 203859 /// ENST00000324559 // ANO	ANO5	2.90E-11	0.000264379	-1.66409	5.57E-11	-3.92653
3258444	NM_018131 // CEP55 // centrosomal protein 55kDa // 10q23.33 // 55165 /// NM_0011	CEP55	2.93E-11	1.22E-05	1.52243	2.74E-10	2.3439
2426676	NM_144584 // C1orf59 // chromosome 1 open reading frame 59 // 1p13.3 // 113802 /	C1orf59	2.94E-11	5.17E-07	1.44682	2.23E-09	1.77745
3709540	NM_012393 // PFAS // phosphoribosylformylglycinamidine synthase // 17p13.1 // 51	PFAS	2.98E-11	8.09E-06	1.18064	3.56E-10	1.38376
3867223	NM_000979 // RPL18 // ribosomal protein L18 // 19q13 // 6141 /// ENST00000084795	RPL18	3.03E-11	1.59E-07	1.21373	6.01E-09	1.31349
3962023	CR456458 // FAM152B // family with sequence similarity 152, member B // 22q13.2	FAM152B	3.07E-11	0.000448009	1.14264	4.69E-11	1.45794
3998247	NM_020742 // NLGN4X // neuroligin 4, X-linked // Xp22.32-p22.31 // 57502 /// NM_	NLGN4X	3.10E-11	1.09E-07	-1.4684	8.62E-09	-1.68678
3474256	NM_006836 // GCN1L1 // GCN1 general control of amino-acid synthesis 1-like 1 (ye	GCN1L1	3.13E-11	5.15E-06	1.21425	4.99E-10	1.43999

3047660	NM_000168 // GLI3 // GLI-Kruppel family member GLI3 // 7p13 // 2737 /// ENST0000	GLI3	3.14E-11	6.98E-08	-1.43982	1.31E-08	-1.61129
3340410	NM_006656 // NEU3 // sialidase 3 (membrane sialidase) // 11q13.5 // 10825 /// EN	NEU3	3.15E-11	3.26E-07	1.19937	3.52E-09	1.3117
3031573	NM_018384 // GIMAP5 // GTPase, IMAP family member 5 // 7q36.1 // 55340 /// ENST0	GIMAP5	3.18E-11	0.000550518	-1.28587	4.47E-11	-2.0656
2373336	NM_000186 // CFH // complement factor H // 1q32 // 3075 /// NM_001014975 // CFH	CFH	3.23E-11	0.000157794	-1.57428	8.02E-11	-3.16825
3438027	NM_006325 // RAN // RAN, member RAS oncogene family // 12q24.3 // 5901 /// ENST0	RAN	3.32E-11	3.15E-06	1.18228	7.38E-10	1.35112
2601414	NM_006216 // SERPINE2 // serpin peptidase inhibitor, clade E (nexin, plasminogen	SERPINE2	3.41E-11	5.95E-10	2.51339	4.63E-06	2.07755
2356818	NM_004326 // BCL9 // B-cell CLL/lymphoma 9 // 1q21 // 607 /// ENST00000234739 //	BCL9	3.41E-11	5.77E-10	1.28112	4.87E-06	1.2162
3888263	NR_003605 // C20orf199 // chromosome 20 open reading frame 199 // 20q13.13 // 44	C20orf199	3.42E-11	3.15E-08	1.50244	3.20E-08	1.63776
3193339	NM_002957 // RXRA // retinoid X receptor, alpha // 9q34.3 // 6256 /// ENST000003	RXRA	3.45E-11	3.63E-10	-1.36285	1.06E-05	-1.25744
3317352	NM_000218 // KCNQ1 // potassium voltage-gated channel, KQT-like subfamily, membe	KCNQ1	3.45E-11	3.54E-07	1.27167	3.75E-09	1.43215
3692033	NM_015272 // RPGRIP1L // RPGRIP1-like // 16q12.2 // 23322 /// NM_001127897 // RP	RPGRIP1L	3.50E-11	7.72E-07	1.3978	2.10E-09	1.70557
3955483	NM_001001663 // TMEM211 // transmembrane protein 211 // 22q11.23 // 255349 /// E	TMEM211	3.50E-11	3.80E-08	2.58707	2.76E-08	3.22031
3402398	NM_018173 // PLEKHG6 // pleckstrin homology domain containing, family G (with Rh	PLEKHG6	3.51E-11	2.38E-10	-1.31498	2.30E-05	-1.20885
3299467	NM_144590 // ANKRD22 // ankyrin repeat domain 22 // 10q23.31 // 118932 /// ENST0	ANKRD22	3.52E-11	2.16E-06	1.9542	1.02E-09	3.20006
2868904	NM_005668 // ST8SIA4 // ST8 alpha-N-acetyl-neuraminide alpha-2,8-sialyltransfera	ST8SIA4	3.55E-11	3.28E-06	-1.39596	7.84E-10	-1.82114
2476671	NM_170672 // RASGRP3 // RAS guanyl releasing protein 3 (calcium and DAG-regulate	RASGRP3	3.56E-11	3.04E-08	-1.65292	3.52E-08	-1.83197
2893392	NM_004271 // LY86 // lymphocyte antigen 86 // 6p25.1 // 9450 /// ENST00000379953	LY86	3.63E-11	7.33E-06	-1.37187	4.84E-10	-1.83556
3374874	NM_005142 // GIF // gastric intrinsic factor (vitamin B synthesis) // 11q13 // 2	GIF	3.68E-11	7.64E-09	2.14699	1.67E-07	2.23525
3625052	NM_182758 // WDR72 // WD repeat domain 72 // 15q21.3 // 256764 /// ENST000003963	WDR72	3.69E-11	1.30E-07	1.36569	9.53E-09	1.53103
2728056	NM_020722 // KIAA1211 // KIAA1211 protein // 4q12 // 57482 /// ENST00000264229 /	KIAA1211	3.70E-11	4.84E-06	-1.36047	6.42E-10	-1.7689
3021158	NM_024913 // C7orf58 // chromosome 7 open reading frame 58 // 7q31.31 // 79974 /	C7orf58	3.74E-11	4.48E-06	-1.48656	6.84E-10	-2.07387
2844888	NM_197975 // BTNL3 // butyrophilin-like 3 // 5q35.3 // 10917 /// ENST00000342868	BTNL3	3.76E-11	1.09E-06	-2.32208	1.81E-09	-3.95989
3064638	NM_022777 // RABL5 // RAB, member RAS oncogene family-like 5 // 7q22.1 // 64792	RABL5	3.79E-11	1.28E-07	1.53422	1.01E-08	1.79168
3261859	NM_178858 // SFXN2 // sideroflexin 2 // 10q24.32 // 118980 /// ENST00000369893 /	SFXN2	3.79E-11	0.000482706	1.16244	5.78E-11	1.52975
3747812	NM_148172 // PEMT // phosphatidylethanolamine N-methyltransferase // 17p11.2 //	PEMT	3.85E-11	6.39E-05	1.21288	1.54E-10	1.56366
3358950	NM_001909 // CTSD // cathepsin D // 11p15.5 // 1509 /// ENST00000236671 // CTSD	CTSD	3.90E-11	2.82E-08	-1.39195	4.41E-08	-1.48137
2728189	NM_001079525 // PAICS // phosphoribosylaminoimidazole carboxylase, phosphoribosy	PAICS	3.97E-11	1.84E-05	1.3205	3.15E-10	1.77771
2562605	NM_015425 // POLR1A // polymerase (RNA) I polypeptide A, 194kDa // 2p11.2 // 258	POLR1A	3.98E-11	3.25E-07	1.24867	4.90E-09	1.38648
2431066	NM_032044 // REG4 // regenerating islet-derived family, member 4 // 1p13.1-p12 /	REG4	4.01E-11	9.56E-09	3.5859	1.49E-07	3.91654
3969081	NM_016562 // TLR7 // toll-like receptor 7 // Xp22.3 // 51284 /// ENST00000380659	TLR7	4.01E-11	1.02E-07	-1.60261	1.34E-08	-1.87304
2973232	NM_014702 // KIAA0408 // KIAA0408 // 6q22.33 // 9729 /// NM_001012279 // C6orf17	KIAA0408	4.03E-11	3.16E-08	-1.57974	4.13E-08	-1.72942
3229529	NM_015447 // CAMSAP1 // calmodulin regulated spectrin-associated protein 1 // 9q	CAMSAP1	4.04E-11	3.92E-09	1.32512	4.44E-07	1.31559
2976360	NM_022121 // PERP // PERP, TP53 apoptosis effector // 6q24 // 64065 /// ENST0000	PERP	4.09E-11	3.10E-09	1.54899	6.13E-07	1.51475
3923218	NM_015056 // RRP1B // ribosomal RNA processing 1 homolog B (S. cerevisiae) // 21	RRP1B	4.11E-11	5.25E-06	1.25913	7.00E-10	1.53344
2351004	NM_000851 // GSTM5 // glutathione S-transferase M5 // 1p13.3 // 2949 /// ENST000	GSTM5	4.12E-11	2.18E-08	-1.87039	6.27E-08	-2.06159
3820727	NM_031209 // QTRT1 // queuine tRNA-ribosyltransferase 1 // 19p13.3 // 81890 ///	QTRT1	4.12E-11	1.83E-05	1.18733	3.30E-10	1.42563
2775214	NM_006259 // PRKG2 // protein kinase, cGMP-dependent, type II // 4q13.1-q21.1 //	PRKG2	4.14E-11	2.35E-08	-2.2074	5.86E-08	-2.51142
3946351	NM_000026 // ADSL // adenylosuccinate lyase // 22q13.1|22q13.2 // 158 /// NM_001	ADSL	4.16E-11	5.38E-05	1.20653	1.85E-10	1.53201
2807716	NM_000587 // C7 // complement component 7 // 5p13 // 730 /// ENST00000313164 //	C7	4.23E-11	2.26E-07	-2.13613	7.23E-09	-2.9406
2705164	NM_020390 // EIF5A2 // eukaryotic translation initiation factor 5A2 // 3q26.2 //	EIF5A2	4.28E-11	1.64E-07	1.38807	9.70E-09	1.5728
2645906	NM_002670 // PLS1 // plastin 1 (I isoform) // 3q23 // 5357 /// ENST00000337777 /	PLS1	4.33E-11	6.84E-08	-1.67758	2.17E-08	-1.9374
2427469	NM_004696 // SLC16A4 // solute carrier family 16, member 4 (monocarboxylic acid	SLC16A4	4.39E-11	2.48E-09	3.11251	9.41E-07	2.83907

2620410	NR_023353 // EXOSC7 // exosome component 7 // 3p21.31 // 23016 /// NM_015004 //	EXOSC7	4.45E-11	3.66E-07	1.25634	5.23E-09	1.4006
3601387	NM_033240 // PML // promyelocytic leukemia // 15q22 // 5371 /// NM_033244 // PML	PML	4.45E-11	2.83E-08	1.26764	5.41E-08	1.32205
3226844	NM_000755 // CRAT // carnitine acetyltransferase // 9q34.1 // 1384 /// NM_004003	CRAT	4.47E-11	6.07E-10	-1.45291	7.81E-06	-1.33307
2621917	NM_018031 // WDR6 // WD repeat domain 6 // 3p21.31 // 11180 /// ENST00000395474	WDR6	4.48E-11	2.99E-07	1.22653	6.21E-09	1.3447
2325479	NM_013441 // RCAN3 // RCAN family member 3 // 1p35.3-p33 // 11123 /// ENST000003	RCAN3	4.48E-11	5.34E-10	1.43247	9.69E-06	1.31198
3390542	NM_002906 // RDX // radixin // 11q23 // 5962 /// ENST00000343115 // RDX // radix	RDX	4.49E-11	2.00E-07	-1.77916	8.74E-09	-2.24168
2872848	NM_002317 // LOX // lysyl oxidase // 5q23.2 // 4015 /// ENST00000231004 // LOX /	LOX	4.50E-11	1.74E-09	-1.857	1.60E-06	-1.7241
2908100	NM_006502 // POLH // polymerase (DNA directed), eta // 6p21.1 // 5429 /// ENST00	POLH	4.52E-11	1.67E-08	1.46296	9.70E-08	1.53049
2324873	NM_001114101 // C1QC // complement component 1, q subcomponent, C chain // 1p36.	C1QC	4.57E-11	5.33E-09	-1.85118	3.75E-07	-1.84628
2407314	NM_001099439 // EPHA10 // EPH receptor A10 // 1p34.3 // 284656 /// ENST000003730	EPHA10	4.85E-11	2.21E-06	-1.2151	1.54E-09	-1.39534
2770039	NM_006681 // NMU // neuromedin U // 4q12 // 10874 /// ENST00000264218 // NMU //	NMU	4.92E-11	2.75E-09	1.60566	1.01E-06	1.54565
3148545	NM_178565 // RSPO2 // R-spondin 2 homolog (Xenopus laevis) // 8q23.1 // 340419 /	RSPO2	4.97E-11	1.02E-07	-1.55934	1.85E-08	-1.79122
3107342	NM_018444 // PPM2C // protein phosphatase 2C, magnesium-dependent, catalytic sub	PPM2C	5.07E-11	3.49E-10	1.56069	2.60E-05	1.36407
3645901	NM_024845 // FLJ14154 // hypothetical protein FLJ14154 // 16p13.3 // 79903 /// N	FLJ14154	5.26E-11	7.17E-09	-1.25851	3.32E-07	-1.26276
2903401	NM_002121 // HLA-DPB1 // major histocompatibility complex, class II, DP beta 1 /	HLA-DPB1	5.26E-11	4.30E-05	-1.48538	2.76E-10	-2.38987
3417371	NM_015292 // FAM62A // family with sequence similarity 62 (C2 domain containing)	FAM62A	5.27E-11	2.77E-06	1.28206	1.47E-09	1.53897
2949380	NM_006295 // VARS // valyl-tRNA synthetase // 6p21.3 // 7407 /// ENST00000211402	VARS	5.31E-11	5.35E-05	1.17645	2.48E-10	1.44031
3474104	NM_007174 // CIT // citron (rho-interacting, serine/threonine kinase 21) // 12q2	CIT	5.35E-11	1.37E-05	1.32395	5.41E-10	1.74684
2994981	NM_175887 // PRR15 // proline rich 15 // 7p15.1 // 222171 /// ENST00000319694 //	PRR15	5.36E-11	4.17E-10	-1.28407	2.14E-05	-1.19469
3860137	NM_003332 // TYROBP // TYRO protein tyrosine kinase binding protein // 19q13.1 /	TYROBP	5.40E-11	1.15E-08	-1.58654	1.99E-07	-1.63301
3319840	NM_006391 // IPO7 // importin 7 // 11p15.4 // 10527 /// NR_002962 // SNORA23 //	IPO7	5.41E-11	7.40E-08	1.59808	2.83E-08	1.81182
3939183	NM_004327 // BCR // breakpoint cluster region // 22q11|22q11.23 // 613 /// NM_02	BCR	5.44E-11	6.42E-08	1.18481	3.26E-08	1.23636
3601741	NM_003992 // CLK3 // CDC-like kinase 3 // 15q24 // 1198 /// ENST00000345005 // C	CLK3	5.50E-11	3.71E-08	-1.18891	5.72E-08	-1.22837
3527493	NM_001641 // APEX1 // APEX nuclease (multifunctional DNA repair enzyme) 1 // 14q	APEX1	5.61E-11	9.08E-09	1.42048	2.80E-07	1.43751
2322004	NM_207348 // SLC25A34 // solute carrier family 25, member 34 // 1p36.21 // 28472	SLC25A34	5.66E-11	7.12E-09	-1.57788	3.80E-07	-1.58326
2328713	NM_175852 // TXLNA // taxilin alpha // 1p35.1 // 200081 /// ENST00000373610 // T	TXLNA	5.67E-11	2.29E-06	1.14277	1.85E-09	1.25477
3936913	NM_003504 // CDC45L // CDC45 cell division cycle 45-like (S. cerevisiae) // 22q1	CDC45L	5.70E-11	0.0720972	1.10364	1.46E-11	1.82696
3630668	NM_033429 // CALML4 // calmodulin-like 4 // 15q23 // 91860 /// NM_001031733 // C	CALML4	5.76E-11	1.69E-08	-1.28853	1.43E-07	-1.32113
3303870	NM_013274 // POLL // polymerase (DNA directed), lambda // 10q23 // 27343 /// ENS	POLL	5.98E-11	1.85E-07	1.19814	1.42E-08	1.28023
2577700	NM_032143 // ZRANB3 // zinc finger, RAN-binding domain containing 3 // 2q21.3 //	ZRANB3	5.99E-11	5.59E-07	1.24086	5.66E-09	1.38332
2910352	AK091117 // LOC730101 // hypothetical LOC730101 // 6p12.1 // 730101 /// BC003416	LOC730101	6.06E-11	6.40E-08	1.57143	3.87E-08	1.75248
3579501	NM_001039355 // SLC25A29 // solute carrier family 25, member 29 // 14q32.2 // 12	SLC25A29	6.08E-11	8.36E-09	1.35014	3.55E-07	1.35747
3939545	NM_002415 // MIF // macrophage migration inhibitory factor (glycosylation-inhibi	MIF	6.11E-11	0.000876893	1.23071	7.64E-11	1.84607
2964231	NM_021244 // RRAGD // Ras-related GTP binding D // 6q15-q16 // 58528 /// ENST000	RRAGD	6.13E-11	2.82E-08	-1.59295	9.06E-08	-1.70718
3345427	NM_015036 // ENDOD1 // endonuclease domain containing 1 // 11q21 // 23052 /// EN	ENDOD1	6.18E-11	6.88E-06	-1.26882	9.91E-10	-1.55696
2588487	BC030713 // LOC401022 // hypothetical LOC401022 // 2q31.2 // 401022	LOC401022	6.19E-11	0.000185751	-1.27897	1.58E-10	-1.85393
3548346	NM_006888 // CALM1 // calmodulin 1 (phosphorylase kinase, delta) // 14q24-q31 //	CALM1	6.20E-11	6.24E-08	-1.27724	4.11E-08	-1.35328
2679917	NM_198859 // PRICKLE2 // prickle homolog 2 (Drosophila) // 3p14.1 // 166336 ///	PRICKLE2	6.25E-11	2.79E-08	-1.31361	9.44E-08	-1.367
3674249	NM_004413 // DPEP1 // dipeptidase 1 (renal) // 16q24.3 // 1800 /// NM_001128141	DPEP1	6.36E-11	4.66E-08	2.61399	5.71E-08	3.17179
3192117	NM_013318 // KIAA0515 // KIAA0515 // 9q34.13 // 84726 /// NR_002914 // SNORD62A	KIAA0515	6.40E-11	9.60E-08	1.24505	2.85E-08	1.32474
3250055	NM_004728 // DDX21 // DEAD (Asp-Glu-Ala-Asp) box polypeptide 21 // 10q21 // 9188	DDX21	6.41E-11	1.82E-06	1.5052	2.55E-09	1.96886
3431426	NM_014055 // IFT81 // intraflagellar transport 81 homolog (Chlamydomonas) // 12q	IFT81	6.43E-11	3.25E-07	1.24468	9.73E-09	1.36715

2324884	NM_000491 // C1QB // complement component 1, q subcomponent, B chain // 1p36.12	C1QB	6.44E-11	7.13E-09	-1.71157	4.75E-07	-1.70799
4010860	NM_031206 // LAS1L // LAS1-like (S. cerevisiae) // Xq12-q13 // 81887 /// ENST000	LAS1L	6.47E-11	0.000102022	1.13426	2.24E-10	1.34674
3231774	NM_012341 // GTPBP4 // GTP binding protein 4 // 10p15-p14 // 23560 /// ENST00000	GTPBP4	6.50E-11	4.84E-06	1.29638	1.33E-09	1.59529
2845973	NM_024830 // LPCAT1 // lysophosphatidylcholine acyltransferase 1 // 5p15.33 // 7	LPCAT1	6.53E-11	8.91E-07	1.27347	4.44E-09	1.45699
3920003	NM_005441 // CHAF1B // chromatin assembly factor 1, subunit B (p60) // 21q22.13	CHAF1B	6.54E-11	0.00229698	1.14388	5.52E-11	1.55847
2686458	NM_015429 // ABI3BP // ABI gene family, member 3 (NESH) binding protein // 3q12	ABI3BP	6.59E-11	4.37E-05	-1.57814	3.60E-10	-2.706
2715634	NM_176801 // ADD1 // adducin 1 (alpha) // 4p16.3 // 118 /// NM_014189 // ADD1 //	ADD1	6.63E-11	0.00108599	-1.08295	7.64E-11	-1.27161
3185558	NM_004697 // PRPF4 // PRP4 pre-mRNA processing factor 4 homolog (yeast) // 9q31-	PRPF4	6.64E-11	5.48E-05	1.23775	3.21E-10	1.60801
3482888	NM_002097 // GTF3A // general transcription factor IIIA // 13q12.3-q13.1 // 2971	GTF3A	6.65E-11	3.77E-07	1.43601	9.02E-09	1.68651
2792800	NM_017631 // DDX60 // DEAD (Asp-Glu-Ala-Asp) box polypeptide 60 // 4q32.3 // 556	DDX60	6.74E-11	5.53E-07	-1.80139	6.74E-09	-2.40591
3403299	NM_000319 // PEX5 // peroxisomal biogenesis factor 5 // 12p13.31 // 5830 /// ENS	PEX5	6.84E-11	1.58E-06	1.25812	3.09E-09	1.45406
3163982	NM_001040272 // ADAMTSL1 // ADAMTS-like 1 // 9p22.2-p22.1 // 92949 /// NM_052866	ADAMTSL1	6.85E-11	8.09E-09	-1.48243	4.54E-07	-1.4847
2828757	NM_175873 // ANKRD43 // ankyrin repeat domain 43 // 5q31.1 // 134548 /// ENST000	ANKRD43	7.04E-11	6.71E-08	-1.31118	4.65E-08	-1.39681
3392871	NM_003904 // ZNF259 // zinc finger protein 259 // 11q23.3 // 8882 /// ENST000002	ZNF259	7.08E-11	1.67E-06	1.18303	3.10E-09	1.31641
3308619	NM_173791 // PDZD8 // PDZ domain containing 8 // 10q25.3-q26.11 // 118987 /// EN	PDZD8	7.15E-11	6.34E-09	1.47302	6.61E-07	1.45839
2783493	NM_000134 // FABP2 // fatty acid binding protein 2, intestinal // 4q28-q31 // 21	FABP2	7.31E-11	3.56E-09	-2.66621	1.47E-06	-2.44332
3663228	NM_001126129 // GINS3 // GINS complex subunit 3 (Psf3 homolog) // 16q21 // 64785	GINS3	7.35E-11	0.572164	1.02493	1.16E-11	1.63593
3164601	NM_017794 // KIAA1797 // KIAA1797 // 9p21 // 54914 /// ENST00000380249 // KIAA17	KIAA1797	7.38E-11	2.30E-07	1.48685	1.59E-08	1.7248
2950329	NM_033554 // HLA-DPA1 // major histocompatibility complex, class II, DP alpha 1	HLA-DPA1	7.39E-11	3.51E-05	-1.50672	4.67E-10	-2.39187
3865715	NM_004819 // SYMPK // symplekin // 19q13.3 // 8189 /// ENST00000245934 // SYMPK	SYMPK	7.49E-11	4.16E-07	1.19001	9.85E-09	1.28603
3452743	NM_015401 // HDAC7 // histone deacetylase 7 // 12q13.1 // 51564 /// NM_001098416	HDAC7	7.70E-11	9.91E-09	1.25406	4.33E-07	1.25839
3874498	NM_020746 // VISA // virus-induced signaling adapter // 20p13 // 57506 /// ENST0	VISA	7.78E-11	3.91E-09	-1.31904	1.45E-06	-1.28833
3049025	NM_004749 // TBRG4 // transforming growth factor beta regulator 4 // 7p14-p13 //	TBRG4	7.83E-11	0.117648	1.06326	1.76E-11	1.53741
3197231	NM_001039395 // C9orf68 // chromosome 9 open reading frame 68 // 9p24.2-p24.1 //	C9orf68	7.93E-11	3.01E-10	1.8071	9.22E-05	1.45546
3913926	NM_005975 // PTK6 // PTK6 protein tyrosine kinase 6 // 20q13.3 // 5753 /// ENST0	PTK6	7.96E-11	3.52E-10	-1.36549	6.91E-05	-1.22514
3279915	NM_001004470 // ST8SIA6 // ST8 alpha-N-acetyl-neuraminide alpha-2,8-sialyltransf	ST8SIA6	8.04E-11	7.71E-08	-1.52123	4.99E-08	-1.6807
4000839	NM_175859 // CTPS2 // CTP synthase II // Xp22 // 56474 /// NM_019857 // CTPS2 //	CTPS2	8.46E-11	9.38E-08	1.31984	4.46E-08	1.41692
3985490	NM_001080425 // BEX4 // BEX family member 4 // Xq22.1-q22.3 // 56271 /// NM_0011	BEX4	8.54E-11	3.73E-06	-1.76022	2.26E-09	-2.66592
2704763	NM_153353 // LRRC34 // leucine rich repeat containing 34 // 3q26.2 // 151827 ///	LRRC34	8.64E-11	7.91E-08	1.51041	5.42E-08	1.66366
3457824	NM_003920 // TIMELESS // timeless homolog (Drosophila) // 12q12-q13 // 8914 ///	TIMELESS	8.69E-11	0.0626845	1.09073	2.35E-11	1.65407
3043264	NM_175061 // JAZF1 // JAZF zinc finger 1 // 7p15.2-p15.1 // 221895 /// ENST00000	JAZF1	8.71E-11	0.000136454	-1.167	2.75E-10	-1.448
3649811	NM_017668 // NDE1 // nudE nuclear distribution gene E homolog 1 (A. nidulans) //	NDE1	8.89E-11	2.19E-07	1.33698	2.19E-08	1.4806
3845296	NM_203304 // MEX3D // mex-3 homolog D (C. elegans) // 19p13.3 // 399664 /// ENST	MEX3D	8.89E-11	3.00E-08	1.28727	1.55E-07	1.3278
2783207	NM_003619 // PRSS12 // protease, serine, 12 (neurotrypsin, motopsin) // 4q28.1 /	PRSS12	8.97E-11	1.05E-06	-1.48404	6.05E-09	-1.84412
2939892	NM_020408 // LYRM4 // LYR motif containing 4 // 6p25.1 // 57128 /// ENST00000330	LYRM4	9.04E-11	1.03E-07	1.46391	4.51E-08	1.61674
3821263	NM_001299 // CNN1 // calponin 1, basic, smooth muscle // 19p13.2-p13.1 // 1264 /	CNN1	9.12E-11	1.09E-07	-1.64871	4.34E-08	-1.88331
3261544	NM_004193 // GBF1 // golgi-specific brefeldin A resistance factor 1 // 10q24 //	GBF1	9.28E-11	1.17E-07	-1.19155	4.15E-08	-1.25002
3468743	NM_016575 // NT5DC3 // 5'-nucleotidase domain containing 3 // 12q22-q23.1 // 515	NT5DC3	9.29E-11	1.03E-10	1.81817	0.00130799	1.33564
3970214	NM_004726 // REPS2 // RALBP1 associated Eps domain containing 2 // Xp22.2 // 918	REPS2	9.32E-11	5.47E-08	1.5181	8.84E-08	1.64041
2796790	NM_020827 // KIAA1430 // KIAA1430 // 4q35.1 // 57587 /// BC030535 // KIAA1430 //	KIAA1430	9.41E-11	2.07E-08	1.44632	2.56E-07	1.48797
3443348	NM_000014 // A2M // alpha-2-macroglobulin // 12p13.3-p12.3 // 2 /// ENST00000404	A2M	9.42E-11	0.00085229	-1.31179	1.26E-10	-2.19097
3186966	NM_138554 // TLR4 // toll-like receptor 4 // 9q32-q33 // 7099 /// ENST0000035562	TLR4	9.53E-11	1.54E-07	1.80357	3.33E-08	2.15695

2471364	NM_001105569 // MSGN1 // mesogenin 1 // 2p24.2 // 343930 /// ENST00000281047 //	MSGN1	9.56E-11	1.77E-09	3.23428	6.69E-06	2.59086
3536706	NR_003225 // LGALS3 // lectin, galactoside-binding, soluble, 3 // 14q21-q22 // 3	LGALS3	9.63E-11	1.24E-07	-1.38881	4.15E-08	-1.52097
3351300	NM_000073 // CD3G // CD3g molecule, gamma (CD3-TCR complex) // 11q23 // 917 ///	CD3G	9.70E-11	0.0116957	-1.23559	4.58E-11	-2.37921
2447124	NM_021133 // RNASEL // ribonuclease L (2',5'-oligoisoadenylate synthetase-depend	RNASEL	9.74E-11	4.64E-07	-1.43935	1.31E-08	-1.68707
2738378	NM_001033047 // NPNT // nephronectin // 4q24 // 255743 /// ENST00000379987 // NP	NPNT	1.01E-10	2.71E-08	1.45223	2.11E-07	1.50787
2677853	NM_017563 // IL17RD // interleukin 17 receptor D // 3p14.3 // 54756 /// ENST0000	IL17RD	1.01E-10	7.95E-08	1.5493	6.86E-08	1.70677
3504226	NM_015974 // CRYL1 // crystallin, lambda 1 // 13q12.11 // 51084 /// ENST00000298	CRYL1	1.01E-10	1.06E-10	-1.66682	0.00153839	-1.27569
3747236	NM_001113567 // C17orf76 // chromosome 17 open reading frame 76 // 17p11.2 // 38	C17orf76	1.02E-10	3.69E-08	-1.33108	1.55E-07	-1.38273
4004853	NM_006307 // SRPX // sushi-repeat-containing protein, X-linked // Xp21.1 // 8406	SRPX	1.02E-10	2.45E-09	-1.69811	4.70E-06	-1.55969
3181600	NM_024642 // GALNT12 // UDP-N-acetyl-alpha-D-galactosamine:polypeptide N-acetylg	GALNT12	1.03E-10	9.84E-07	-1.45088	7.74E-09	-1.76622
3319119	NM_198474 // OLFML1 // olfactomedin-like 1 // 11p15.4 // 283298 /// ENST00000329	OLFML1	1.05E-10	1.47E-06	-1.57557	5.84E-09	-2.05189
3003193	NM_001762 // CCT6A // chaperonin containing TCP1, subunit 6A (zeta 1) // 7p11.2	CCT6A	1.06E-10	2.59E-06	1.40092	3.87E-09	1.75022
2613441	NM_003884 // KAT2B // K(lysine) acetyltransferase 2B // 3p24 // 8850 /// ENST000	KAT2B	1.06E-10	0.000103946	-1.32029	4.00E-10	-1.90186
3175971	NM_058179 // PSAT1 // phosphoserine aminotransferase 1 // 9q21.2 // 29968 /// NM	PSAT1	1.06E-10	0.000622496	1.64946	1.66E-10	4.01335
2363202	NM_021181 // SLAMF7 // SLAM family member 7 // 1q23.1-q24.1 // 57823 /// ENST000	SLAMF7	1.06E-10	3.58E-07	-1.77102	1.84E-08	-2.22067
2427619	NM_002232 // KCNA3 // potassium voltage-gated channel, shaker-related subfamily,	KCNA3	1.07E-10	4.17E-07	-1.89101	1.63E-08	-2.46287
3190822	NM_015354 // NUP188 // nucleoporin 188kDa // 9q34.11 // 23511 /// ENST0000037257	NUP188	1.08E-10	0.000716272	1.18185	1.59E-10	1.60135
3102096	NM_024870 // DEPDC2 // DEP domain containing 2 // 8q13.2 // 80243 /// NM_025170	DEPDC2	1.08E-10	1.76E-07	-1.39143	3.57E-08	-1.54023
2322036	NM_017556 // FBLIM1 // filamin binding LIM protein 1 // 1p36.21 // 54751 /// NM_	FBLIM1	1.09E-10	3.32E-08	-1.31081	1.94E-07	-1.35242
3072368	NM_016478 // ZC3HC1 // zinc finger, C3HC-type containing 1 // 7q32.2 // 51530 //	ZC3HC1	1.11E-10	0.00240649	1.08487	9.72E-11	1.30288
3031650	NM_001091 // ABP1 // amiloride binding protein 1 (amine oxidase (copper-containi	ABP1	1.12E-10	4.77E-07	-1.46718	1.56E-08	-1.72813
3300597	NM_013451 // FER1L3 // fer-1-like 3, myoferlin (C. elegans) // 10q24 // 26509 //	FER1L3	1.13E-10	2.15E-10	2.13841	0.000420114	1.5237
3850040	NM_003755 // EIF3G // eukaryotic translation initiation factor 3, subunit G // 1	EIF3G	1.14E-10	3.85E-07	1.25431	1.92E-08	1.37283
3822122	NM_002501 // NFIX // nuclear factor I/X (CCAAT-binding transcription factor) //	NFIX	1.15E-10	6.00E-09	1.29444	1.65E-06	1.26971
2651711	NM_001080460 // LRRIQ4 // leucine-rich repeats and IQ motif containing 4 // 3q26	LRRIQ4	1.15E-10	2.70E-06	1.3802	4.20E-09	1.70654
3372097	NM_001610 // ACP2 // acid phosphatase 2, lysosomal // 11p11.2-p11.11|11p12-p11 /	ACP2	1.15E-10	2.19E-08	-1.30491	3.35E-07	-1.32776
3333899	NM_004585 // RARRES3 // retinoic acid receptor responder (tazarotene induced) 3	RARRES3	1.15E-10	0.0146815	-1.27434	5.08E-11	-2.78705
3402506	NM_001242 // CD27 // CD27 molecule // 12p13 // 939 /// ENST00000266557 // CD27 /	CD27	1.16E-10	2.60E-06	-1.48816	4.35E-09	-1.92895
3102372	NM_001128205 // SULF1 // sulfatase 1 // 8q13.2-q13.3 // 23213 /// NM_015170 // S	SULF1	1.16E-10	8.83E-11	1.7134	0.0034332	1.26264
2772167	NR_024010 // UGT2A3 // UDP glucuronosyltransferase 2 family, polypeptide A3 // 4	UGT2A3	1.17E-10	1.52E-07	-3.27454	4.59E-08	-4.58248
2491661	NM_003761 // VAMP8 // vesicle-associated membrane protein 8 (endobrevin) // 2p12	VAMP8	1.18E-10	3.08E-07	-1.36476	2.44E-08	-1.53028
3136229	NM_138969 // RDHE2 // epidermal retinal dehydrogenase 2 // 8q12.1 // 195814 ///	RDHE2	1.19E-10	2.35E-09	2.16415	6.62E-06	1.88503
3774635	NM_004104 // FASN // fatty acid synthase // 17q25 // 2194 /// ENST00000306749 //	FASN	1.19E-10	1.11E-05	1.30862	1.70E-09	1.65511
2688955	NM_138806 // CD200R1 // CD200 receptor 1 // 3q13.2 // 131450 /// NM_170780 // CD	CD200R1	1.20E-10	0.00015261	-1.26087	3.77E-10	-1.73954
2508611	NM_018460 // ARHGAP15 // Rho GTPase activating protein 15 // 2q22.2 // 55843 ///	ARHGAP15	1.20E-10	0.000182698	-1.46204	3.45E-10	-2.51761
2427898	NM_002557 // OVGP1 // oviductal glycoprotein 1, 120kDa // 1p13 // 5016 /// ENST0	OVGP1	1.20E-10	2.09E-08	1.3812	3.79E-07	1.40658
2384401	NM_021205 // RHOU // ras homolog gene family, member U // 1q42.11-q42.3 // 58480	RHOU	1.21E-10	4.86E-07	-1.29787	1.71E-08	-1.44902
2745547	NM_207123 // GAB1 // GRB2-associated binding protein 1 // 4q31.21 // 2549 /// NM	GAB1	1.24E-10	8.29E-06	-1.32343	2.15E-09	-1.66634
2950561	NM_005452 // WDR46 // WD repeat domain 46 // 6p21.3 // 9277 /// ENST00000383074	WDR46	1.25E-10	2.48E-05	1.17579	1.09E-09	1.38457
3237282	NM_001098844 // FAM23A // family with sequence similarity 23, member A // 10p12.	FAM23A	1.25E-10	3.23E-05	-2.6037	9.33E-10	-7.16439
2336706	NM_000098 // CPT2 // carnitine palmitoyltransferase II // 1p32 // 1376 /// ENST0	CPT2	1.25E-10	2.78E-10	-1.46525	0.00031212	-1.24522
3453370	NM_001659 // ARF3 // ADP-ribosylation factor 3 // 12q13 // 377 /// ENST000002566	ARF3	1.26E-10	3.37E-10	-1.35344	0.000214349	-1.19791

3373724	NM_003146 // SSRP1 // structure specific recognition protein 1 // 11q12 // 6749	SSRP1	1.26E-10	1.14E-05	1.24429	1.79E-09	1.50553
2891341	NM_002460 // IRF4 // interferon regulatory factor 4 // 6p25-p23 // 3662 /// ENST	IRF4	1.28E-10	1.70E-08	-1.78415	5.39E-07	-1.81321
3001479	NM_006060 // IKZF1 // IKAROS family zinc finger 1 (Ikaros) // 7p13-p11.1 // 1032	IKZF1	1.29E-10	0.000120276	-1.29127	4.68E-10	-1.81177
2410522	NM_017739 // POMGNT1 // protein O-linked mannose beta1,2-N-acetylglucosaminyltra	POMGNT1	1.32E-10	1.38E-06	1.19497	8.31E-09	1.31848
3302495	NM_021732 // AVPI1 // arginine vasopressin-induced 1 // 10q24.2 // 60370 /// ENS	AVPI1	1.33E-10	1.48E-09	-1.59052	1.71E-05	-1.42247
3764199	NM_017777 // MKS1 // Meckel syndrome, type 1 // 17q22 // 54903 /// ENST000003931	MKS1	1.34E-10	8.31E-07	1.18334	1.27E-08	1.28348
3736259	NM_001010982 // AFMID // arylformamidase // 17q25.3 // 125061 /// ENST0000032789	AFMID	1.34E-10	3.26E-07	1.2177	2.81E-08	1.30801
2935475	NM_206855 // QKI // quaking homolog, KH domain RNA binding (mouse) // 6q26|6q26-	QKI	1.35E-10	1.74E-06	-1.46554	7.25E-09	-1.82985
3048413	NM_001127218 // POLD2 // polymerase (DNA directed), delta 2, regulatory subunit	POLD2	1.37E-10	0.000200817	1.18351	3.85E-10	1.50817
3355956	NM_003658 // BARX2 // BARX homeobox 2 // 11q25 // 8538 /// ENST00000281437 // BA	BARX2	1.38E-10	1.03E-07	-1.43351	8.60E-08	-1.55337
3845944	NM_052847 // GNG7 // guanine nucleotide binding protein (G protein), gamma 7 //	GNG7	1.38E-10	2.21E-08	-1.50277	4.50E-07	-1.53348
3873629	NM_001040022 // SIRPA // signal-regulatory protein alpha // 20p13 // 140885 ///	SIRPA	1.38E-10	1.80E-06	-1.39042	7.24E-09	-1.68561
3837866	NM_004605 // SULT2B1 // sulfotransferase family, cytosolic, 2B, member 1 // 19q1	SULT2B1	1.41E-10	0.000221057	1.36418	3.77E-10	2.14666
3079103	NM_024711 // GIMAP6 // GTPase, IMAP family member 6 // --- // 474344 /// NM_0010	GIMAP6	1.43E-10	3.18E-05	-1.33494	1.11E-09	-1.80313
3646542	NM_019109 // ALG1 // asparagine-linked glycosylation 1 homolog (S. cerevisiae, b	ALG1	1.46E-10	5.74E-06	1.19168	3.39E-09	1.35891
3288518	NM_001031746 // C10orf72 // chromosome 10 open reading frame 72 // 10q11.22 // 1	C10orf72	1.48E-10	3.26E-07	-1.44165	3.24E-08	-1.64123
3159040	NM_000973 // RPL8 // ribosomal protein L8 // 8q24.3 // 6132 /// NM_033301 // RPL	RPL8	1.49E-10	0.000275078	1.17143	3.61E-10	1.48733
3555675	NM_198232 // RNASE1 // ribonuclease, RNase A family, 1 (pancreatic) // 14q11.2 /	RNASE1	1.53E-10	1.61E-09	-1.74084	1.97E-05	-1.51978
2384705	AK291013 // KIAA0133 // KIAA0133 // 1q42.13 // 9816 /// BC114559 // KIAA0133 //	KIAA0133	1.53E-10	0.0001034	1.22067	6.21E-10	1.57331
3672059	NM_014732 // KIAA0513 // KIAA0513 // 16q24.1 // 9764 /// ENST00000258180 // KIAA	KIAA0513	1.54E-10	2.94E-08	-1.2705	3.90E-07	-1.29233
3261492	NM_004741 // NOLC1 // nucleolar and coiled-body phosphoprotein 1 // 10q24.32 //	NOLC1	1.57E-10	2.71E-05	1.40318	1.38E-09	1.97006
3350908	NM_014956 // CEP164 // centrosomal protein 164kDa // 11q23.3 // 22897 /// ENST00	CEP164	1.58E-10	3.27E-09	1.19807	7.02E-06	1.16173
3394488	NM_002855 // PVRL1 // poliovirus receptor-related 1 (herpesvirus entry mediator	PVRL1	1.60E-10	0.000109923	1.22456	6.33E-10	1.58758
3217167	NM_003389 // CORO2A // coronin, actin binding protein, 2A // 9q22.3 // 7464 ///	CORO2A	1.62E-10	3.75E-10	-1.60113	0.000311219	-1.31454
3715489	NM_014573 // TMEM97 // transmembrane protein 97 // 17q11.2 // 27346 /// ENST0000	TMEM97	1.62E-10	0.000761523	1.22539	2.45E-10	1.76213
2599869	NM_144712 // SLC23A3 // solute carrier family 23 (nucleobase transporters), memb	SLC23A3	1.63E-10	6.70E-10	-2.14741	0.000102681	-1.64259
2669533	NM_001607 // ACAA1 // acetyl-Coenzyme A acyltransferase 1 // 3p23-p22 // 30 ///	ACAA1	1.64E-10	1.01E-09	-1.37333	5.00E-05	-1.24694
3331730	NM_053023 // ZFP91 // zinc finger protein 91 homolog (mouse) // 11q12 // 80829 /	ZFP91	1.68E-10	1.80E-08	-1.24544	7.99E-07	-1.24802
3837001	NM_004491 // GRLF1 // glucocorticoid receptor DNA binding factor 1 // 19q13.3 //	GRLF1	1.68E-10	2.35E-06	-1.20473	7.72E-09	-1.34809
3960440	NM_012264 // TMEM184B // transmembrane protein 184B // 22q12 // 25829 /// ENST00	TMEM184B	1.69E-10	2.70E-07	1.2968	4.66E-08	1.40909
3756546	NM_000223 // KRT12 // keratin 12 // 17q12 // 3859 /// ENST00000251643 // KRT12 /	KRT12	1.71E-10	1.63E-10	-1.773	0.0021738	-1.30659
2401849	BC063891 // C1orf201 // chromosome 1 open reading frame 201 // 1p36.11 // 90529	C1orf201	1.71E-10	2.14E-08	-1.59613	6.72E-07	-1.6161
3018375	NM_002736 // PRKAR2B // protein kinase, cAMP-dependent, regulatory, type II, bet	PRKAR2B	1.71E-10	2.58E-07	-1.77009	4.97E-08	-2.11591
3338293	NM_018043 // ANO1 // anoctamin 1, calcium activated chloride channel // 11q13.3	ANO1	1.72E-10	5.57E-08	1.42617	2.30E-07	1.49503
3846538	NM_001961 // EEF2 // eukaryotic translation elongation factor 2 // 19pter-q12 //	EEF2	1.73E-10	3.31E-06	1.24969	6.25E-09	1.44448
2354082	NM_006784 // WDR3 // WD repeat domain 3 // 1p13-p12 // 10885 /// ENST00000349139	WDR3	1.74E-10	3.34E-07	1.46226	4.01E-08	1.66587
2877028	NM_017415 // KLHL3 // kelch-like 3 (Drosophila) // 5q31 // 26249 /// ENST0000030	KLHL3	1.75E-10	1.70E-08	1.42234	9.21E-07	1.422
3838118	NM_006666 // RUVBL2 // RuvB-like 2 (E. coli) // 19q13.3 // 10856 /// ENST0000022	RUVBL2	1.76E-10	0.00262127	1.14014	1.56E-10	1.52571
3512449	NM_012345 // NUFIP1 // nuclear fragile X mental retardation protein interacting	NUFIP1	1.76E-10	5.35E-06	1.31241	4.54E-09	1.59619
3778772	NM_153000 // APCDD1 // adenomatosis polyposis coli down-regulated 1 // 18p11.22	APCDD1	1.78E-10	1.90E-06	1.76006	9.83E-09	2.42667
2501835	NM_020868 // DPP10 // dipeptidyl-peptidase 10 // 2q14.1 // 57628 /// NM_00100436	DPP10	1.80E-10	9.10E-07	-2.0955	1.78E-08	-2.96139
2379068	NM_013349 // NENF // neuron derived neurotrophic factor // 1q32.3 // 29937 /// E	NENF	1.82E-10	1.50E-05	1.18506	2.38E-09	1.37676

2511820	NM_003628 // PKP4 // plakophilin 4 // 2q23-q31 // 8502 /// NM_001005476 // PKP4	PKP4	1.82E-10	1.13E-08	1.51786	1.64E-06	1.48732
3000984	NM_152701 // ABCA13 // ATP-binding cassette, sub-family A (ABC1), member 13 // 7	ABCA13	1.84E-10	2.28E-09	1.45603	1.65E-05	1.33793
3389077	NM_025208 // PDGFD // platelet derived growth factor D // 11q22.3 // 80310 /// N	PDGFD	1.86E-10	3.76E-07	-1.47647	3.97E-08	-1.6934
3204692	NM_032818 // C9orf100 // chromosome 9 open reading frame 100 // 9p13.3 // 84904	C9orf100	1.86E-10	0.0425766	1.09193	5.86E-11	1.56893
3877892	NM_002594 // PCSK2 // proprotein convertase subtilisin/kexin type 2 // 20p11.2 /	PCSK2	1.86E-10	6.29E-09	-1.48323	3.75E-06	-1.41759
2713095	NM_025163 // PIGZ // phosphatidylinositol glycan anchor biosynthesis, class Z //	PIGZ	1.88E-10	1.71E-07	-1.37814	8.40E-08	-1.49547
3726211	NM_002611 // PDK2 // pyruvate dehydrogenase kinase, isozyme 2 // 17q21.33 // 516	PDK2	1.89E-10	1.27E-06	-1.34713	1.45E-08	-1.56719
3774593	NM_022156 // DUS1L // dihydrouridine synthase 1-like (S. cerevisiae) // 17q25.3	DUS1L	1.90E-10	0.00272776	1.10526	1.67E-10	1.38124
3831620	NM_198539 // ZNF568 // zinc finger protein 568 // 19q13.12 // 374900 /// ENST000	ZNF568	1.90E-10	5.93E-07	-1.51302	2.77E-08	-1.79054
2530713	NM_004591 // CCL20 // chemokine (C-C motif) ligand 20 // 2q33-q37 // 6364 /// EN	CCL20	1.91E-10	7.60E-06	1.94848	3.96E-09	3.25005
3852034	NM_017722 // TRMT1 // TRM1 tRNA methyltransferase 1 homolog (S. cerevisiae) // 1	TRMT1	1.92E-10	2.23E-05	1.22942	1.98E-09	1.495
2706938	NM_021629 // GNB4 // guanine nucleotide binding protein (G protein), beta polype	GNB4	1.93E-10	2.94E-07	-1.4055	5.26E-08	-1.56605
2593159	NM_004226 // STK17B // serine/threonine kinase 17b // 2q32.3 // 9262 /// ENST000	STK17B	1.94E-10	2.17E-06	-1.58949	1.00E-08	-2.07806
2925237	NM_000426 // LAMA2 // laminin, alpha 2 // 6q22-q23 // 3908 /// NM_001079823 // L	LAMA2	1.95E-10	8.92E-08	-1.51159	1.70E-07	-1.62527
2477598	NM_144713 // FAM82A1 // family with sequence similarity 82, member A1 // 2p22.2	FAM82A1	1.96E-10	7.70E-08	-1.62662	2.00E-07	-1.75653
2545478	NM_006569 // CGREF1 // cell growth regulator with EF-hand domain 1 // 2p23.3 //	CGREF1	1.97E-10	2.12E-07	1.57137	7.33E-08	1.78052
3008376	NM_032999 // GTF2I // general transcription factor II, i // 7q11.23 // 2969 ///	GTF2I	1.97E-10	1.28E-09	1.39662	4.93E-05	1.2647
3434413	NM_014868 // RNF10 // ring finger protein 10 // 12q24.31 // 9921 /// ENST0000032	RNF10	1.99E-10	2.63E-08	-1.20433	6.74E-07	-1.21244
2402942	NM_003047 // SLC9A1 // solute carrier family 9 (sodium/hydrogen exchanger), memb	SLC9A1	2.01E-10	4.93E-08	-1.45948	3.37E-07	-1.51856
3902764	NM_080616 // C20orf112 // chromosome 20 open reading frame 112 // 20q11.1-q11.23	C20orf112	2.02E-10	4.55E-07	-1.20501	3.79E-08	-1.29056
3108226	NM_016134 // PGCP // plasma glutamate carboxypeptidase // 8q22.2 // 10404 /// EN	PGCP	2.02E-10	9.75E-07	-1.40028	1.98E-08	-1.63814
3150455	NM_002546 // TNFRSF11B // tumor necrosis factor receptor superfamily, member 11b	TNFRSF11B	2.03E-10	1.78E-07	1.66432	9.06E-08	1.89304
3333169	NM_001127392 // C11orf9 // chromosome 11 open reading frame 9 // 11q12-q13.1 //	C11orf9	2.04E-10	7.15E-09	1.42097	3.73E-06	1.36723
2848265	NM_138809 // CMBL // carboxymethylenebutenolidase homolog (Pseudomonas) // 5p15.	CMBL	2.05E-10	2.08E-07	-1.80103	7.93E-08	-2.11172
3731142	NM_001085423 // C17orf60 // chromosome 17 open reading frame 60 // 17q23.3 // 28	C17orf60	2.05E-10	1.19E-06	-1.24302	1.73E-08	-1.38308
3227159	NM_015033 // FNBP1 // formin binding protein 1 // 9q34 // 23048 /// ENST00000372	FNBP1	2.06E-10	3.86E-06	-1.3988	7.04E-09	-1.74342
3757970	NM_013290 // PSMC3IP // PSMC3 interacting protein // 17q12-q21 // 29893 /// NM_0	PSMC3IP	2.08E-10	0.151765	1.0697	4.49E-11	1.64803
2403793	NM_001024732 // MECR // mitochondrial trans-2-enoyl-CoA reductase // 1p36.1-p35.	MECR	2.13E-10	3.38E-05	1.17905	1.75E-09	1.39289
2464005	NM_181690 // AKT3 // v-akt murine thymoma viral oncogene homolog 3 (protein kina	AKT3	2.15E-10	1.14E-05	-1.58609	3.51E-09	-2.31621
3987996	NM_005032 // PLS3 // plastin 3 (T isoform) // Xq23 // 5358 /// ENST00000289290 /	PLS3	2.16E-10	1.58E-08	1.88305	1.45E-06	1.84996
2466039	NM_017865 // ZNF692 // zinc finger protein 692 // 1q44 // 55657 /// ENST00000306	ZNF692	2.19E-10	2.79E-07	1.26013	6.65E-08	1.35063
2881187	NM_005211 // CSF1R // colony stimulating factor 1 receptor // 5q33-q35 // 1436 /	CSF1R	2.20E-10	2.42E-07	-1.50321	7.62E-08	-1.68674
3243708	NM_014753 // BMS1 // BMS1 homolog, ribosome assembly protein (yeast) // 10q11.21	BMS1	2.21E-10	1.78E-08	1.36721	1.30E-06	1.36002
3272205	NM_005539 // INPP5A // inositol polyphosphate-5-phosphatase, 40kDa // 10q26.3 //	INPP5A	2.24E-10	2.58E-09	-1.25783	2.00E-05	-1.19296
3204463	NM_004629 // FANCG // Fanconi anemia, complementation group G // 9p13 // 2189 //	FANCG	2.24E-10	0.0377917	1.07727	7.42E-11	1.44539
3125571	NM_002445 // MSR1 // macrophage scavenger receptor 1 // 8p22 // 4481 /// NM_1387	MSR1	2.25E-10	9.40E-08	-1.65704	2.02E-07	-1.80436
2633460	BC006512 // C3orf26 // chromosome 3 open reading frame 26 // 3q12.1 // 84319 ///	C3orf26	2.28E-10	2.57E-06	1.26818	1.09E-08	1.45809
3687803	NM_012248 // SEPHS2 // selenophosphate synthetase 2 // 16p11.2 // 22928 /// ENST	SEPHS2	2.29E-10	1.52E-09	-1.28821	4.99E-05	-1.1962
3374606	NM_001039396 // MPEG1 // macrophage expressed gene 1 // 11q12.1 // 219972 /// EN	MPEG1	2.29E-10	2.43E-06	-1.7636	1.15E-08	-2.4498
3408505	NM_006152 // LRMP // lymphoid-restricted membrane protein // 12p12.1 // 4033 ///	LRMP	2.30E-10	4.91E-07	-1.59659	4.29E-08	-1.89426
3824963	NM_017712 // PGPEP1 // pyroglutamyl-peptidase I // 19p13.11 // 54858 /// ENST000	PGPEP1	2.33E-10	4.76E-08	-1.25926	4.46E-07	-1.28494
2908323	NM_018426 // TMEM63B // transmembrane protein 63B // 6p21.1 // 55362 /// ENST000	TMEM63B	2.34E-10	3.29E-07	-1.2626	6.28E-08	-1.35863

3761441	NM_024016 // HOXB8 // homeobox B8 // 17q21.3 // 3218 /// ENST00000239144 // HOXB	HOXB8	2.34E-10	2.67E-06	1.58422	1.10E-08	2.07892
3703885	NM_003486 // SLC7A5 // solute carrier family 7 (cationic amino acid transporter,	SLC7A5	2.36E-10	0.000407404	1.46557	5.09E-10	2.66004
3548152	NM_018319 // TDP1 // tyrosyl-DNA phosphodiesterase 1 // 14q32.11 // 55775 /// NM	TDP1	2.36E-10	5.20E-06	1.22589	6.83E-09	1.41021
2632225	NM_005233 // EPHA3 // EPH receptor A3 // 3p11.2 // 2042 /// NM_182644 // EPHA3 /	EPHA3	2.37E-10	0.0529195	-1.14087	7.06E-11	-2.02141
3755976	NM_014815 // MED24 // mediator complex subunit 24 // 17q21.1 // 9862 /// NM_0010	MED24	2.38E-10	0.00257539	1.07898	2.20E-10	1.27273
2615808	NM_015141 // GPD1L // glycerol-3-phosphate dehydrogenase 1-like // 3p22.3 // 231	GPD1L	2.41E-10	2.67E-09	-1.55227	2.20E-05	-1.40019
3456049	NM_000889 // ITGB7 // integrin, beta 7 // 12q13.13 // 3695 /// ENST00000267082 /	ITGB7	2.43E-10	4.15E-06	-1.32594	8.34E-09	-1.59327
2855614	BC036867 // C5orf34 // chromosome 5 open reading frame 34 // 5p12 // 375444 ///	C5orf34	2.43E-10	0.0153848	1.12227	1.11E-10	1.61159
3638566	NM_003847 // PEX11A // peroxisomal biogenesis factor 11 alpha // 15q26.1 // 8800	PEX11A	2.44E-10	6.08E-10	-1.37328	0.000306533	-1.20693
2882897	NM_015465 // GEMIN5 // gem (nuclear organelle) associated protein 5 // 5q33.2 //	GEMIN5	2.46E-10	5.51E-07	1.35839	4.27E-08	1.52323
2610241	NM_033084 // FANCD2 // Fanconi anemia, complementation group D2 // 3p26 // 2177	FANCD2	2.47E-10	0.00253891	1.1381	2.31E-10	1.50528
3771642	NM_134268 // CYGB // cytoglobin // 17q25.3 // 114757 /// ENST00000293230 // CYGB	CYGB	2.48E-10	3.71E-09	-1.66143	1.38E-05	-1.50077
3621194	NM_005657 // TP53BP1 // tumor protein p53 binding protein 1 // 15q15-q21 // 7158	TP53BP1	2.49E-10	1.31E-09	1.39534	7.73E-05	1.25476
2413203	NM_004631 // LRP8 // low density lipoprotein receptor-related protein 8, apolipo	LRP8	2.51E-10	2.10E-06	1.52337	1.45E-08	1.92038
2896958	NM_016255 // FAM8A1 // family with sequence similarity 8, member A1 // 6p22-p23	FAM8A1	2.53E-10	5.37E-05	-1.15737	1.64E-09	-1.35586
3404567	NM_207345 // CLEC9A // C-type lectin domain family 9, member A // 12p13.2 // 283	CLEC9A	2.54E-10	4.39E-07	-1.36723	5.46E-08	-1.52181
3581386	NM_017955 // CDCA4 // cell division cycle associated 4 // 14q32.33 // 55038 ///	CDCA4	2.58E-10	0.0255613	1.1086	9.85E-11	1.59614
2955691	NM_005822 // RCAN2 // regulator of calcineurin 2 // 6p12.3 // 10231 /// ENST0000	RCAN2	2.60E-10	6.23E-07	-1.49093	4.13E-08	-1.73856
3332276	NM_000139 // MS4A2 // membrane-spanning 4-domains, subfamily A, member 2 (Fc fra	MS4A2	2.63E-10	8.80E-05	-1.27329	1.30E-09	-1.69326
3261447	NM_015062 // PPRC1 // peroxisome proliferator-activated receptor gamma, coactiva	PPRC1	2.64E-10	0.000138747	1.18211	1.01E-09	1.46428
3443891	NM_005127 // CLEC2B // C-type lectin domain family 2, member B // 12p13-p12 // 9	CLEC2B	2.65E-10	1.55E-05	-1.40199	3.77E-09	-1.86912
3861738	NM_017827 // SARS2 // seryl-tRNA synthetase 2, mitochondrial // 19q13.2 // 54938	SARS2	2.66E-10	0.000438906	1.14306	5.61E-10	1.40934
3815328	NM_024100 // WDR18 // WD repeat domain 18 // 19p13.3 // 57418 /// ENST0000025128	WDR18	2.66E-10	0.130547	1.05499	6.04E-11	1.45003
3442706	NM_004244 // CD163 // CD163 molecule // 12p13.3 // 9332 /// NM_203416 // CD163 /	CD163	2.66E-10	1.26E-08	-1.79715	2.79E-06	-1.7229
3703665	NM_015144 // ZCCHC14 // zinc finger, CCHC domain containing 14 // 16q24.2 // 231	ZCCHC14	2.70E-10	1.39E-06	-1.16993	2.22E-08	-1.26285
3416577	NM_005337 // NCKAP1L // NCK-associated protein 1-like // 12q13.1 // 3071 /// ENS	NCKAP1L	2.71E-10	3.61E-06	-1.53042	1.07E-08	-1.99277
3850576	NM_024029 // YIPF2 // Yip1 domain family, member 2 // 19p13.2 // 78992 /// ENST0	YIPF2	2.76E-10	0.00066292	1.11656	4.79E-10	1.3438
2332144	NM_001905 // CTPS // CTP synthase // 1p34.1 // 1503 /// ENST00000372621 // CTPS	CTPS	2.77E-10	0.000444485	1.34403	5.86E-10	2.13465
3601229	NM_001024736 // CD276 // CD276 molecule // 15q23-q24 // 80381 /// NM_025240 // C	CD276	2.78E-10	8.64E-07	1.23572	3.44E-08	1.35082
3223967	NR_003191 // GGTA1 // glycoprotein, alpha-galactosyltransferase 1 // 9q33.2-q34.	GGTA1	2.79E-10	8.54E-07	-1.82263	3.50E-08	-2.34361
3046020	NM_001100425 // KIAA0895 // KIAA0895 protein // 7p14.2 // 23366 /// NM_015314 //	KIAA0895	2.80E-10	4.65E-07	1.29318	5.99E-08	1.41155
3628498	NM_001218 // CA12 // carbonic anhydrase XII // 15q22 // 771 /// NM_206925 // CA1	CA12	2.81E-10	5.93E-07	-1.65171	4.83E-08	-1.99004
3459956	NM_152440 // C12orf66 // chromosome 12 open reading frame 66 // 12q14.2 // 14457	C12orf66	2.82E-10	4.01E-06	1.25727	1.04E-08	1.453
2532894	NM_152879 // DGKD // diacylglycerol kinase, delta 130kDa // 2q37.1 // 8527 /// N	DGKD	2.83E-10	2.63E-07	-1.16173	1.03E-07	-1.20965
3349453	NM_017868 // TTC12 // tetratricopeptide repeat domain 12 // 11q23.1 // 54970 ///	TTC12	2.90E-10	6.38E-08	1.23423	4.59E-07	1.26072
3538555	NM_021003 // PPM1A // protein phosphatase 1A (formerly 2C), magnesium-dependent,	PPM1A	2.91E-10	7.26E-07	-1.33373	4.26E-08	-1.49395
3652424	NM_013302 // EEF2K // eukaryotic elongation factor-2 kinase // 16p12.1 // 29904	EEF2K	2.92E-10	6.85E-07	-1.21321	4.50E-08	-1.30725
3742627	AY358809 // C17orf87 // chromosome 17 open reading frame 87 // 17p13.2 // 388325	C17orf87	2.92E-10	2.63E-05	-1.52122	3.02E-09	-2.25116
3378433	NM_006946 // SPTBN2 // spectrin, beta, non-erythrocytic 2 // 11q13 // 6712 /// E	SPTBN2	2.92E-10	2.51E-07	1.38359	1.13E-07	1.50593
3342426	ENST00000329143 // C11orf82 // chromosome 11 open reading frame 82 // 11q14.1 //	C11orf82	2.97E-10	0.00435394	1.22189	2.25E-10	1.96554
2953408	NM_173561 // UNC5CL // unc-5 homolog C (C. elegans)-like // 6p21.1 // 222643 ///	UNC5CL	2.99E-10	1.49E-07	1.68391	1.95E-07	1.86573
3429406	NM_013320 // HCFC2 // host cell factor C2 // 12q23.3 // 29915 /// ENST0000022933	HCFC2	2.99E-10	1.69E-06	-1.28188	2.19E-08	-1.45272

3590460	NM_002220 // ITPKA // inositol 1,4,5-trisphosphate 3-kinase A // 15q14-q21 // 37	ITPKA	3.01E-10	3.93E-09	-1.49763	1.86E-05	-1.37395
2622912	NM_004635 // MAPKAPK3 // mitogen-activated protein kinase-activated protein kina	MAPKAPK3	3.01E-10	1.24E-05	1.14478	5.11E-09	1.27593
3379597	NM_004923 // MTL5 // metallothionein-like 5, testis-specific (tesmin) // 11q13.2	MTL5	3.04E-10	2.00E-07	1.25646	1.50E-07	1.32411
2525182	NM_152523 // CCNYL1 // cyclin Y-like 1 // 2q33.3 // 151195 /// ENST00000295414 /	CCNYL1	3.06E-10	4.59E-08	-1.38445	7.26E-07	-1.4111
2902844	NM_001710 // CFB // complement factor B // 6p21.3 // 629 /// ENST00000375443 //	CFB	3.08E-10	2.25E-07	1.89548	1.36E-07	2.21386
3665949	NM_006742 // PSKH1 // protein serine kinase H1 // 16q22.1 // 5681 /// ENST000002	PSKH1	3.08E-10	1.92E-10	-1.30844	0.00714346	-1.11549
2955282	NM_181356 // SUPT3H // suppressor of Ty 3 homolog (S. cerevisiae) // 6p21.1-p21.	SUPT3H	3.14E-10	3.98E-09	1.38339	1.98E-05	1.28962
3095002	NM_003816 // ADAM9 // ADAM metallopeptidase domain 9 (meltrin gamma) // 8p11.23	ADAM9	3.17E-10	8.20E-09	1.36392	6.91E-06	1.30734
3712675	NM_030665 // RAI1 // retinoic acid induced 1 // 17p11.2 // 10743 /// ENST0000035	RAI1	3.19E-10	3.75E-07	1.23649	8.80E-08	1.31841
2541699	NM_030797 // FAM49A // family with sequence similarity 49, member A // 2p24.3 //	FAM49A	3.20E-10	3.60E-07	-1.45976	9.19E-08	-1.63323
3140478	BC042877 // RPESP // RPE-spondin // 8q21.11 // 157869 /// AK292970 // RPESP // R	RPESP	3.20E-10	1.70E-07	2.24785	1.90E-07	2.65606
2528308	NM_138802 // ZFAND2B // zinc finger, AN1-type domain 2B // 2q35 // 130617 /// EN	ZFAND2B	3.22E-10	1.90E-09	-1.28511	6.93E-05	-1.19114
3577256	NM_032490 // C14orf142 // chromosome 14 open reading frame 142 // 14q32.12 // 84	C14orf142	3.23E-10	4.99E-10	-1.84832	0.00088465	-1.38893
3098756	NM_052898 // XKR4 // XK, Kell blood group complex subunit-related family, member	XKR4	3.23E-10	2.41E-09	-1.4563	4.68E-05	-1.31282
2627390	NM_001128149 // ATXN7 // ataxin 7 // 3p21.1-p12 // 6314 /// NM_000333 // ATXN7 /	ATXN7	3.23E-10	0.000660507	-1.12348	5.75E-10	-1.363
3815278	NM_005224 // ARID3A // AT rich interactive domain 3A (BRIGHT-like) // 19p13.3 //	ARID3A	3.26E-10	1.24E-06	1.25807	3.18E-08	1.39625
3219788	NM_019114 // EPB41L4B // erythrocyte membrane protein band 4.1 like 4B // 9q31-q	EPB41L4B	3.30E-10	3.25E-08	-1.19399	1.23E-06	-1.19675
3719980	NM_006148 // LASP1 // LIM and SH3 protein 1 // 17q11-q21.3 // 3927 /// ENST00000	LASP1	3.30E-10	4.45E-07	-1.24074	7.93E-08	-1.32945
2906333	NM_015345 // DAAM2 // dishevelled associated activator of morphogenesis 2 // 6p2	DAAM2	3.32E-10	2.36E-09	-1.45681	5.13E-05	-1.31054
2931569	NM_005100 // AKAP12 // A kinase (PRKA) anchor protein 12 // 6q24-q25 // 9590 ///	AKAP12	3.33E-10	1.85E-06	-1.27151	2.36E-08	-1.43589
3952825	NM_024627 // C22orf29 // chromosome 22 open reading frame 29 // 22q11.21 // 7968	C22orf29	3.34E-10	2.79E-06	1.20941	1.72E-08	1.34608
3671935	NM_031476 // CRISPLD2 // cysteine-rich secretory protein LCCL domain containing	CRISPLD2	3.36E-10	1.38E-08	-1.34931	3.76E-06	-1.3157
3320717	NM_014632 // MICAL2 // microtubule associated monoxygenase, calponin and LIM dom	MICAL2	3.43E-10	4.29E-07	-1.32825	8.66E-08	-1.45129
3652489	NM_018119 // POLR3E // polymerase (RNA) III (DNA directed) polypeptide E (80kD)	POLR3E	3.44E-10	2.25E-05	1.12766	4.11E-09	1.2549
2374501	DQ983818 // C1orf81 // chromosome 1 open reading frame 81 // 1q32.1 // 647215	C1orf81	3.45E-10	2.74E-08	-1.55904	1.64E-06	-1.55171
2593407	NM_024989 // PGAP1 // post-GPI attachment to proteins 1 // 2q33.1 // 80055 /// E	PGAP1	3.53E-10	1.35E-09	2.45645	0.000154116	1.78942
2962683	NM_198920 // UBE2CBP // ubiquitin-conjugating enzyme E2C binding protein // 6q14	UBE2CBP	3.57E-10	4.96E-07	1.26487	8.04E-08	1.36575
3839142	NM_015428 // ZNF473 // zinc finger protein 473 // 19q13.33 // 25888 /// NM_00100	ZNF473	3.59E-10	0.000146369	1.16083	1.42E-09	1.40033
3572782	NM_015305 // ANGEL1 // angel homolog 1 (Drosophila) // 14q24.3 // 23357 /// ENST	ANGEL1	3.60E-10	0.000861019	1.15397	5.73E-10	1.4779
3217123	NM_014788 // TRIM14 // tripartite motif-containing 14 // 9q22.33 // 9830 /// NM_	TRIM14	3.60E-10	8.61E-10	-1.26995	0.000377909	-1.15158
2759582	NM_198595 // AFAP1 // actin filament associated protein 1 // 4p16 // 60312 /// N	AFAP1	3.61E-10	1.18E-07	1.29225	3.34E-07	1.34359
3465274	NM_001920 // DCN // decorin // 12q21.33 // 1634 /// NM_133503 // DCN // decorin	DCN	3.62E-10	1.63E-05	-1.74497	5.41E-09	-2.76802
3986672	NM_052936 // ATG4A // ATG4 autophagy related 4 homolog A (S. cerevisiae) // Xq22	ATG4A	3.64E-10	3.12E-08	-1.55472	1.53E-06	-1.55424
2340845	NM_020948 // MIER1 // mesoderm induction early response 1 homolog (Xenopus laevi	MIER1	3.65E-10	7.71E-07	-1.51177	5.59E-08	-1.7695
3189932	NM_003165 // STXBP1 // syntaxin binding protein 1 // 9q34.1 // 6812 /// NM_00103	STXBP1	3.65E-10	3.36E-09	1.77122	3.48E-05	1.53491
3050609	NM_015198 // COBL // cordon-bleu homolog (mouse) // 7p12.1 // 23242 /// ENST0000	COBL	3.66E-10	1.16E-07	-1.32615	3.46E-07	-1.38316
3185063	NM_003358 // UGCG // UDP-glucose ceramide glucosyltransferase // 9q31 // 7357 //	UGCG	3.70E-10	5.67E-08	-1.56037	7.77E-07	-1.60633
3006572	NM_015570 // AUTS2 // autism susceptibility candidate 2 // 7q11.22 // 26053 ///	AUTS2	3.71E-10	8.49E-09	1.28679	8.80E-06	1.23969
3377423	NM_080668 // CDCA5 // cell division cycle associated 5 // 11q12.1 // 113130 ///	CDCA5	3.73E-10	0.139335	1.08754	8.40E-11	1.80186
3457667	NM_014255 // CNPY2 // canopy 2 homolog (zebrafish) // 12q15 // 10330 /// ENST000	CNPY2	3.73E-10	1.85E-05	1.16863	5.17E-09	1.33368
3260338	NM_145285 // NKX2-3 // NK2 transcription factor related, locus 3 (Drosophila) //	NKX2-3	3.75E-10	2.99E-07	-1.3204	1.39E-07	-1.41919
3431620	NM_001082538 // TCTN1 // tectonic family member 1 // 12q24.11 // 79600 /// NM_00	TCTN1	3.76E-10	1.40E-06	1.32201	3.51E-08	1.50189

3599873	BC029061 // LOC145837 // hypothetical protein LOC145837 // 15q23 // 145837 /// B	LOC145837	3.77E-10	8.15E-09	-1.88452	9.65E-06	-1.70912
3148871	NM_001099744 // GOLSYN // Golgi-localized protein // 8q23.2 // 55638 /// NM_0010	GOLSYN	3.80E-10	2.06E-08	1.42367	2.78E-06	1.39796
3962338	NM_005650 // TCF20 // transcription factor 20 (AR1) // 22q13.3|22q13.3 // 6942 /	TCF20	3.81E-10	7.60E-08	1.25944	5.86E-07	1.28764
3781980	NM_153211 // TTC39C // tetratricopeptide repeat domain 39C // 18q11.2 // 125488	TTC39C	3.82E-10	3.13E-09	1.54469	4.27E-05	1.37763
2887633	NM_138369 // FAM44B // family with sequence similarity 44, member B // 5q35.2 //	FAM44B	3.83E-10	9.40E-07	1.21342	5.04E-08	1.31161
2536625	NM_032515 // BOK // BCL2-related ovarian killer // 2q37.3 // 666 /// ENST0000031	BOK	3.86E-10	1.72E-07	1.35289	2.50E-07	1.43312
3286921	NM_001002265 // MARCH8 // membrane-associated ring finger (C3HC4) 8 // 10q11.21	MARCH8	3.88E-10	6.95E-07	-1.37485	6.70E-08	-1.54268
2766492	BC008502 // C4orf34 // chromosome 4 open reading frame 34 // 4p14 // 201895 ///	C4orf34	3.88E-10	3.85E-06	-1.36854	1.65E-08	-1.64979
2746693	NM_024605 // ARHGAP10 // Rho GTPase activating protein 10 // 4q31.23 // 79658 //	ARHGAP10	3.92E-10	6.15E-06	-1.36639	1.18E-08	-1.68149
2611779	NM_024334 // TMEM43 // transmembrane protein 43 // 3p25.1 // 79188 /// ENST00000	TMEM43	3.95E-10	3.65E-09	1.31052	3.57E-05	1.22507
3073013	NM_001018111 // PODXL // podocalyxin-like // 7q32-q33 // 5420 /// NM_005397 // P	PODXL	3.96E-10	1.20E-09	1.44009	0.000248561	1.25372
3962781	NM_173467 // MCAT // malonyl CoA:ACP acyltransferase (mitochondrial) // 22q13.31	MCAT	3.98E-10	0.014987	1.07169	1.90E-10	1.32238
3792656	NM_024781 // CCDC102B // coiled-coil domain containing 102B // 18q22.1 // 79839	CCDC102B	4.01E-10	8.32E-08	-1.52252	5.77E-07	-1.58901
2527971	NM_015690 // STK36 // serine/threonine kinase 36, fused homolog (Drosophila) //	STK36	4.10E-10	1.29E-07	1.20498	3.72E-07	1.23927
3022465	NM_014390 // SND1 // staphylococcal nuclease and tudor domain containing 1 // 7q	SND1	4.11E-10	6.26E-07	1.35553	7.99E-08	1.50469
3381965	NM_005472 // KCNE3 // potassium voltage-gated channel, Isk-related family, membe	KCNE3	4.13E-10	1.24E-08	1.82813	6.32E-06	1.70446
2997376	NM_018685 // ANLN // anillin, actin binding protein // 7p15-p14 // 54443 /// ENS	ANLN	4.20E-10	0.000154859	1.50767	1.66E-09	2.52234
2766456	NM_003359 // UGDH // UDP-glucose dehydrogenase // 4p15.1 // 7358 /// ENST0000031	UGDH	4.27E-10	2.08E-08	-2.05747	3.36E-06	-1.96841
2835576	NM_007286 // SYNPO // synaptopodin // 5q33.1 // 11346 /// NM_001109974 // SYNPO	SYNPO	4.34E-10	8.13E-08	-1.32402	6.71E-07	-1.35857
3942681	NM_134269 // SMTN // smoothelin // 22q12.2 // 6525 /// NM_134270 // SMTN // smoo	SMTN	4.35E-10	2.97E-06	1.20183	2.35E-08	1.3291
2625907	NM_001457 // FLNB // filamin B, beta (actin binding protein 278) // 3p14.3 // 23	FLNB	4.38E-10	8.33E-08	-1.36922	6.64E-07	-1.41014
3915936	NM_004540 // NCAM2 // neural cell adhesion molecule 2 // 21q21.1 // 4685 /// ENS	NCAM2	4.39E-10	5.55E-08	-1.31647	1.05E-06	-1.33359
3931112	NM_000411 // HLCS // holocarboxylase synthetase (biotin-(proprionyl-Coenzyme A-c	HLCS	4.40E-10	3.23E-07	1.30895	1.64E-07	1.40166
3139580	NM_030958 // SLCO5A1 // solute carrier organic anion transporter family, member	SLCO5A1	4.42E-10	1.08E-09	1.47548	0.000387872	1.26022
3458133	NM_000946 // PRIM1 // primase, DNA, polypeptide 1 (49kDa) // 12q13 // 5557 /// E	PRIM1	4.42E-10	0.0632723	1.10365	1.28E-10	1.7122
2770242	NM_002703 // PPAT // phosphoribosyl pyrophosphate amidotransferase // 4q12 // 54	PPAT	4.49E-10	1.61E-06	1.53193	4.02E-08	1.86294
2981912	NM_003379 // EZR // ezrin // 6q25.2-q26 // 7430 /// NM_001111077 // EZR // ezrin	EZR	4.52E-10	4.68E-07	-1.38697	1.20E-07	-1.52887
3521372	NM_198968 // DZIP1 // DAZ interacting protein 1 // 13q32.1 // 22873 /// NM_01493	DZIP1	4.52E-10	1.10E-07	-1.25031	5.15E-07	-1.28511
2903703	NM_006772 // SYNGAP1 // synaptic Ras GTPase activating protein 1 homolog (rat) /	SYNGAP1	4.53E-10	0.00261894	1.10835	4.45E-10	1.3745
3509473	NM_004734 // DCLK1 // doublecortin-like kinase 1 // 13q13 // 9201 /// ENST000002	DCLK1	4.53E-10	1.90E-07	-1.36379	2.90E-07	-1.44548
3063685	NM_005916 // MCM7 // minichromosome maintenance complex component 7 // 7q21.3-q2	MCM7	4.54E-10	0.000909113	1.21689	7.26E-10	1.70434
3201120	NM_001010915 // PTPLAD2 // protein tyrosine phosphatase-like A domain containing	PTPLAD2	4.58E-10	3.21E-05	-1.41827	4.69E-09	-1.95893
3643703	NM_194259 // UBE2I // ubiquitin-conjugating enzyme E2I (UBC9 homolog, yeast) //	UBE2I	4.58E-10	1.90E-05	1.10603	6.59E-09	1.20269
2365119	NM_004528 // MGST3 // microsomal glutathione S-transferase 3 // 1q23 // 4259 ///	MGST3	4.58E-10	1.74E-07	-1.52012	3.23E-07	-1.63632
2901879	NM_001109938 // C6orf136 // chromosome 6 open reading frame 136 // 6p21.33 // 22	C6orf136	4.59E-10	3.09E-08	-1.29639	2.30E-06	-1.28842
3541073	NM_022474 // MPP5 // membrane protein, palmitoylated 5 (MAGUK p55 subfamily memb	MPP5	4.59E-10	2.26E-07	-1.44798	2.48E-07	-1.56332
3442941	NM_004054 // C3AR1 // complement component 3a receptor 1 // 12p13.31 // 719 ///	C3AR1	4.69E-10	6.91E-08	-1.68393	9.14E-07	-1.74279
3421630	NM_006431 // CCT2 // chaperonin containing TCP1, subunit 2 (beta) // 12q15 // 10	CCT2	4.75E-10	4.74E-05	1.36967	3.84E-09	1.87213
3989448	NM_007325 // GRIA3 // glutamate receptor, ionotrophic, AMPA 3 // Xq25-q26 // 289	GRIA3	4.78E-10	4.05E-09	-1.44959	4.40E-05	-1.3178
3923312	NM_003683 // RRP1 // ribosomal RNA processing 1 homolog (S. cerevisiae) // 21q22	RRP1	4.85E-10	4.06E-06	1.18818	2.13E-08	1.31367
3181193	NM_014290 // TDRD7 // tudor domain containing 7 // 9q22.33 // 23424 /// ENST0000	TDRD7	4.88E-10	1.63E-07	-1.32081	3.82E-07	-1.38176
2635391	AK026416 // FLJ22763 // hypothetical gene supported by AK026416 // 3q13.13 // 40	FLJ22763	4.88E-10	5.31E-07	-2.12553	1.19E-07	-2.6781

3040518	NM_182762 // 7A5 // putative binding protein 7a5 // 7p15.3 // 346389 /// ENST000	7A5	4.90E-10	3.16E-07	1.73634	1.97E-07	1.98401
3190893	BC009114 // FAM73B // family with sequence similarity 73, member B // 9q34.11 //	FAM73B	4.93E-10	6.71E-10	-1.36642	0.00130901	-1.17648
3404660	NM_002262 // KLRD1 // killer cell lectin-like receptor subfamily D, member 1 //	KLRD1	4.94E-10	0.000181059	-1.31833	1.84E-09	-1.8734
2881860	NM_015621 // CCDC69 // coiled-coil domain containing 69 // 5q33.1 // 26112 /// E	CCDC69	5.04E-10	4.02E-05	-1.35226	4.59E-09	-1.80448
3025433	NM_020299 // AKR1B10 // aldo-keto reductase family 1, member B10 (aldose reducta	AKR1B10	5.10E-10	9.20E-09	-3.05691	1.42E-05	-2.52775
2779199	NM_000667 // ADH1A // alcohol dehydrogenase 1A (class I), alpha polypeptide // 4	ADH1A	5.12E-10	4.92E-05	-1.67448	4.12E-09	-2.79334
3445820	NM_032918 // RERG // RAS-like, estrogen-regulated, growth inhibitor // 12p12.3 /	RERG	5.12E-10	1.44E-06	-1.38059	5.31E-08	-1.58659
2695295	NM_014065 // ASTE1 // asteroid homolog 1 (Drosophila) // 3q22.1 // 28990 /// ENS	ASTE1	5.14E-10	4.96E-08	-1.39263	1.57E-06	-1.40158
3015911	NM_003302 // TRIP6 // thyroid hormone receptor interactor 6 // 7q22 // 7205 ///	TRIP6	5.16E-10	1.52E-06	1.38155	5.10E-08	1.592
4026263	NM_004344 // CETN2 // centrin, EF-hand protein, 2 // Xq28 // 1069 /// ENST000003	CETN2	5.29E-10	1.16E-05	1.29702	1.11E-08	1.57035
3428447	NM_014503 // UTP20 // UTP20, small subunit (SSU) processome component, homolog (	UTP20	5.30E-10	3.76E-07	1.51619	1.87E-07	1.68645
4011683	NM_001003811 // TEX11 // testis expressed 11 // Xq13.1 // 56159 /// NM_031276 //	TEX11	5.38E-10	2.93E-08	-1.23256	3.24E-06	-1.22104
4015481	NM_007052 // NOX1 // NADPH oxidase 1 // Xq22 // 27035 /// NM_013955 // NOX1 // N	NOX1	5.39E-10	1.53E-07	2.14458	4.76E-07	2.39674
3486096	NM_207361 // FREM2 // FRAS1 related extracellular matrix protein 2 // 13q13.3 //	FREM2	5.41E-10	6.13E-06	1.67309	1.81E-08	2.31765
3697015	NM_001605 // AARS // alanyl-tRNA synthetase // 16q22 // 16 /// ENST00000261772 /	AARS	5.42E-10	0.0119614	1.13685	2.88E-10	1.63513
2505957	NM_017958 // PLEKHB2 // pleckstrin homology domain containing, family B (evectin	PLEKHB2	5.44E-10	6.53E-09	-1.35552	2.68E-05	-1.26956
3725572	NM_153446 // B4GALNT2 // beta-1,4-N-acetyl-galactosaminyl transferase 2 // 17q21	B4GALNT2	5.46E-10	8.42E-10	-2.69086	0.00103713	-1.70278
2726542	NM_025087 // FLJ21511 // hypothetical protein FLJ21511 // 4p12-p11 // 80157 ///	FLJ21511	5.50E-10	1.16E-08	-3.38716	1.18E-05	-2.81481
3895795	NM_007219 // RNF24 // ring finger protein 24 // 20p13-p12.1 // 11237 /// ENST000	RNF24	5.51E-10	4.09E-06	1.19764	2.52E-08	1.32761
3704980	NM_000135 // FANCA // Fanconi anemia, complementation group A // 16q24.3 // 2175	FANCA	5.52E-10	0.217764	1.05877	1.11E-10	1.61207
3396003	NM_170601 // SIAE // sialic acid acetylesterase // 11q24 // 54414 /// ENST000002	SIAE	5.59E-10	1.04E-07	-1.32275	7.65E-07	-1.35921
3942766	NM_001002837 // PIB5PA // phosphatidylinositol (4,5) bisphosphate 5-phosphatase,	PIB5PA	5.66E-10	1.62E-09	-1.52468	0.000308539	-1.29698
3417500	NM_173596 // SLC39A5 // solute carrier family 39 (metal ion transporter), member	SLC39A5	5.67E-10	6.17E-09	-1.86391	3.17E-05	-1.61915
3474831	NM_003733 // OASL // 2'-5'-oligoadenylate synthetase-like // 12q24.2 // 8638 ///	OASL	5.70E-10	5.21E-10	-2.2169	0.00326292	-1.44987
2351572	NM_000560 // CD53 // CD53 molecule // 1p13 // 963 /// NM_001040033 // CD53 // CD	CD53	5.76E-10	9.27E-05	-1.49915	3.25E-09	-2.34718
3719515	NM_007026 // DUSP14 // dual specificity phosphatase 14 // 17q12 // 11072 /// ENS	DUSP14	5.80E-10	6.23E-06	1.38202	1.96E-08	1.69393
3451375	NM_153026 // PRICKLE1 // prickle homolog 1 (Drosophila) // 12q12 // 144165 /// E	PRICKLE1	5.92E-10	9.63E-07	-1.30361	9.22E-08	-1.43599
2669184	NM_006309 // LRRFIP2 // leucine rich repeat (in FLII) interacting protein 2 // 3	LRRFIP2	5.94E-10	1.00E-05	-1.32716	1.43E-08	-1.61801
2672857	NM_003074 // SMARCC1 // SWI/SNF related, matrix associated, actin dependent regu	SMARCC1	5.99E-10	3.62E-08	1.47091	2.99E-06	1.45335
3413212	AK294075 // FLJ20489 // hypothetical protein FLJ20489 // 12q13.11 // 55652 /// B	FLJ20489	6.01E-10	0.0100911	1.08129	3.44E-10	1.33657
2352609	NM_152900 // MAGI3 // membrane associated guanylate kinase, WW and PDZ domain co	MAGI3	6.03E-10	0.000149244	-1.19776	2.61E-09	-1.48875
3990566	NM_006649 // UTP14A // UTP14, U3 small nucleolar ribonucleoprotein, homolog A (y	UTP14A	6.04E-10	1.38E-05	1.31682	1.17E-08	1.61895
3928415	NM_199328 // CLDN8 // claudin 8 // 21q22.11 // 9073 /// ENST00000399899 // CLDN8	CLDN8	6.18E-10	0.000177156	-2.50043	2.44E-09	-7.80063
3444117	NM_007333 // KLRC3 // killer cell lectin-like receptor subfamily C, member 3 //	KLRC3	6.18E-10	1.06E-06	-1.37524	9.03E-08	-1.54878
3362124	NM_020644 // TMEM9B // TMEM9 domain family, member B // 11p15.3 // 56674 /// ENS	TMEM9B	6.29E-10	2.25E-06	-1.26273	4.86E-08	-1.41015
3944147	NM_006739 // MCM5 // minichromosome maintenance complex component 5 // 22q13.1 /	MCM5	6.30E-10	0.0652635	1.08454	1.83E-10	1.55253
3752271	NM_001003927 // EVI2A // ecotropic viral integration site 2A // 17q11.2 // 2123	EVI2A	6.31E-10	3.03E-07	-1.53171	3.01E-07	-1.67738
3644764	NM_001761 // CCNF // cyclin F // 16p13.3 // 899 /// NR_003574 // ABCA17P // ATP-	CCNF	6.40E-10	0.02706	1.12012	2.53E-10	1.65125
3419471	ENST00000338970 // RPL14 // ribosomal protein L14 // 3p22-p21.2 // 9045 /// U167	RPL14	6.41E-10	2.02E-05	1.31359	9.71E-09	1.63776
3740479	NM_006445 // PRPF8 // PRP8 pre-mRNA processing factor 8 homolog (S. cerevisiae)	PRPF8	6.48E-10	1.76E-07	1.17811	5.49E-07	1.20643
3662150	NM_176870 // MT1M // metallothionein 1M // 16q13 // 4499 /// ENST00000379818 //	MT1M	6.51E-10	1.31E-05	-2.99125	1.34E-08	-6.68863
3113352	NM_021110 // COL14A1 // collagen, type XIV, alpha 1 // 8q23 // 7373 /// ENST0000	COL14A1	6.52E-10	0.000198447	-1.36271	2.44E-09	-2.01378

3395416	NM_006597 // HSPA8 // heat shock 70kDa protein 8 // 11q24.1 // 3312 /// NM_15320	HSPA8	6.58E-10	0.00111548	1.13942	1.01E-09	1.42901
3830216	NM_144779 // FXYD5 // FXYD domain containing ion transport regulator 5 // 19q12-	FXYD5	6.59E-10	5.25E-07	1.43553	1.88E-07	1.58692
3837796	NM_031485 // GRWD1 // glutamate-rich WD repeat containing 1 // 19q13.32 // 83743	GRWD1	6.61E-10	0.00429141	1.11144	5.45E-10	1.4099
3321361	NM_006108 // SPON1 // spondin 1, extracellular matrix protein // 11p15.2 // 1041	SPON1	6.61E-10	0.000364056	-1.64226	1.78E-09	-3.30508
3578069	BC008299 // C14orf139 // chromosome 14 open reading frame 139 // 14q32.13 // 796	C14orf139	6.64E-10	2.04E-05	-1.40181	1.01E-08	-1.84104
3000953	NM_003364 // UPP1 // uridine phosphorylase 1 // 7p12.3 // 7378 /// NM_181597 //	UPP1	6.72E-10	3.78E-09	-1.51818	9.86E-05	-1.33895
2347732	NM_152487 // TMEM56 // transmembrane protein 56 // 1p21.3 // 148534 /// ENST0000	TMEM56	6.76E-10	1.15E-09	-1.5978	0.000902464	-1.29517
3335952	NM_018026 // PACS1 // phosphofurin acidic cluster sorting protein 1 // 11q13.1 /	PACS1	6.76E-10	5.51E-09	1.29232	5.36E-05	1.20976
3844567	NM_012435 // SHC2 // SHC (Src homology 2 domain containing) transforming protein	SHC2	6.79E-10	2.22E-06	1.26865	5.45E-08	1.41695
3685329	NM_024675 // PALB2 // partner and localizer of BRCA2 // 16p12.1 // 79728 /// ENS	PALB2	6.80E-10	6.78E-05	1.23624	4.80E-09	1.53666
2701018	NM_013308 // GPR171 // G protein-coupled receptor 171 // 3q25.1 // 29909 /// ENS	GPR171	6.87E-10	0.000163223	-1.30262	2.90E-09	-1.79415
2599955	NM_001077198 // ATG9A // ATG9 autophagy related 9 homolog A (S. cerevisiae) // 2	ATG9A	6.95E-10	4.73E-08	-1.14809	2.75E-06	-1.14581
4004575	NM_031442 // TMEM47 // transmembrane protein 47 // Xp11.4 // 83604 /// ENST00000	TMEM47	6.97E-10	7.15E-06	-1.4729	2.26E-08	-1.88138
2533019	NM_021027 // UGT1A9 // UDP glucuronosyltransferase 1 family, polypeptide A9 // 2	UGT1A9	7.02E-10	8.12E-09	-1.59704	3.15E-05	-1.44307
2841699	NM_030627 // CPEB4 // cytoplasmic polyadenylation element binding protein 4 // 5	CPEB4	7.08E-10	6.45E-08	-1.44495	1.95E-06	-1.45528
2741139	NM_001128933 // SYNPO2 // synaptopodin 2 // 4q26 // 171024 /// NM_133477 // SYNP	SYNPO2	7.09E-10	2.23E-06	-1.80701	5.78E-08	-2.37363
3662265	NM_014669 // NUP93 // nucleoporin 93kDa // 16q13 // 9688 /// ENST00000308159 //	NUP93	7.09E-10	0.00942113	1.1321	4.24E-10	1.57194
3216319	NM_153695 // ZNF367 // zinc finger protein 367 // 9q22|9q22.32 // 195828 /// ENS	ZNF367	7.11E-10	0.22244	1.04212	1.43E-10	1.41232
2468351	NM_080657 // RSAD2 // radical S-adenosyl methionine domain containing 2 // 2p25.	RSAD2	7.18E-10	2.60E-08	-1.98716	6.25E-06	-1.87342
3369442	NM_015430 // DKFZP586H2123 // regeneration associated muscle protease // 11p13 /	DKFZP586H2123	7.26E-10	1.00E-09	-1.55916	0.00141235	-1.26259
2738244	BC105695 // FLJ20184 // hypothetical protein FLJ20184 // 4q24 // 54848 /// NM_01	FLJ20184	7.33E-10	3.73E-09	1.79885	0.000120417	1.49798
3638819	NM_006384 // CIB1 // calcium and integrin binding 1 (calmyrin) // 15q25.3-q26 //	CIB1	7.39E-10	2.85E-08	-1.32735	5.85E-06	-1.29817
2952065	NM_016059 // PPIL1 // peptidylprolyl isomerase (cyclophilin)-like 1 // 6p21.1 //	PPIL1	7.40E-10	0.000842754	1.19773	1.32E-09	1.60795
3577938	AB007969 // CLMN // calmin (calponin-like, transmembrane) // 14q32.13 // 79789	CLMN	7.49E-10	0.000236296	-1.29566	2.61E-09	-1.80858
2644702	NM_001033030 // FAIM // Fas apoptotic inhibitory molecule // 3q22.3 // 55179 ///	FAIM	7.52E-10	2.39E-06	1.39088	5.94E-08	1.62129
3590164	NM_181642 // SPINT1 // serine peptidase inhibitor, Kunitz type 1 // 15q15.1 // 6	SPINT1	7.57E-10	3.98E-06	-1.22011	3.96E-08	-1.3576
3838809	NM_198319 // PRMT1 // protein arginine methyltransferase 1 // 19q13.3 // 3276 //	PRMT1	7.60E-10	3.20E-05	1.23979	8.86E-09	1.49547
2329041	NM_020888 // KIAA1522 // KIAA1522 // 1p35.1 // 57648 /// ENST00000401073 // KIAA	KIAA1522	7.63E-10	8.88E-07	-1.18725	1.43E-07	-1.25659
3258966	NM_000772 // CYP2C18 // cytochrome P450, family 2, subfamily C, polypeptide 18 /	CYP2C18	7.64E-10	1.06E-09	-2.99916	0.00141015	-1.78258
3619690	NM_017726 // PPP1R14D // protein phosphatase 1, regulatory (inhibitor) subunit 1	PPP1R14D	7.69E-10	1.61E-08	-1.55713	1.37E-05	-1.45873
2495758	BC021264 // C2orf15 // chromosome 2 open reading frame 15 // 2q11.2 // 150590 //	C2orf15	7.77E-10	1.26E-07	1.56131	1.05E-06	1.62402
2902633	NM_025259 // MSH5 // mutS homolog 5 (E. coli) // 6p21.3 // 4439 /// NM_002441 //	MSH5	7.80E-10	1.12E-06	1.24721	1.20E-07	1.35014
3136129	NM_001023 // RPS20 // ribosomal protein S20 // 8q12 // 6224 /// NR_002437 // SNO	RPS20	7.83E-10	2.35E-06	1.23439	6.36E-08	1.35953
2714644	NM_052861 // C4orf42 // chromosome 4 open reading frame 42 // 4p16.3 // 92070 //	C4orf42	7.83E-10	0.00164418	1.10852	1.02E-09	1.34049
2867443	NM_024717 // MCTP1 // multiple C2 domains, transmembrane 1 // 5q15 // 79772 ///	MCTP1	7.88E-10	0.000136744	-1.23168	3.78E-09	-1.56733
3549517	NM_023112 // OTUB2 // OTU domain, ubiquitin aldehyde binding 2 // 14q32.13 // 78	OTUB2	7.88E-10	1.57E-06	1.44399	9.02E-08	1.67452
3854297	NM_005234 // NR2F6 // nuclear receptor subfamily 2, group F, member 6 // 19p13.1	NR2F6	7.97E-10	1.86E-09	-1.31896	0.000509022	-1.1786
3497790	NM_002271 // IPO5 // importin 5 // 13q32.2 // 3843 /// ENST00000357602 // IPO5 /	IPO5	8.00E-10	1.99E-05	1.30602	1.30E-08	1.60995
3408018	NM_018638 // ETNK1 // ethanolamine kinase 1 // 12p12.1 // 55500 /// NM_001039481	ETNK1	8.00E-10	1.10E-09	-2.19041	0.0014701	-1.50899
3485074	NM_002915 // RFC3 // replication factor C (activator 1) 3, 38kDa // 13q12.3-q13	RFC3	8.07E-10	0.0628008	1.13956	2.41E-10	2.00161
3351841	NM_000190 // HMBS // hydroxymethylbilane synthase // 11q23.3 // 3145 /// NM_0010	HMBS	8.25E-10	0.541537	1.02326	1.36E-10	1.47419
3654614	NM_177536 // SULT1A1 // sulfotransferase family, cytosolic, 1A, phenol-preferrin	SULT1A1	8.26E-10	4.11E-08	-1.44086	4.42E-06	-1.41622

3356115	NM_001642 // APLP2 // amyloid beta (A4) precursor-like protein 2 // 11q23-q25|11	APLP2	8.42E-10	7.69E-08	-1.33558	2.12E-06	-1.34461
2545549	NM_021095 // SLC5A6 // solute carrier family 5 (sodium-dependent vitamin transpo	SLC5A6	8.45E-10	0.038091	1.11854	3.00E-10	1.69296
2451043	NM_012134 // LMOD1 // leiomodin 1 (smooth muscle) // 1q32 // 25802 /// ENST00000	LMOD1	8.48E-10	1.88E-06	-1.48191	8.56E-08	-1.74855
3726960	NM_001018137 // NME2 // non-metastatic cells 2, protein (NM23B) expressed in //	NME2	8.51E-10	4.37E-05	1.28137	8.34E-09	1.60877
3734575	NM_001545 // ICT1 // immature colon carcinoma transcript 1 // 17q25.1 // 3396 //	ICT1	8.55E-10	0.00422401	1.12187	7.29E-10	1.44608
2925953	NM_006208 // ENPP1 // ectonucleotide pyrophosphatase/phosphodiesterase 1 // 6q22	ENPP1	8.59E-10	3.27E-06	-1.55971	5.51E-08	-1.94473
2442493	NM_005814 // GPA33 // glycoprotein A33 (transmembrane) // 1q24.1 // 10223 /// EN	GPA33	8.64E-10	1.52E-07	-1.33724	1.01E-06	-1.37701
3058991	NM_000722 // CACNA2D1 // calcium channel, voltage-dependent, alpha 2/delta subun	CACNA2D1	8.71E-10	0.000117449	-1.26313	4.66E-09	-1.63804
3634071	NM_005724 // TSPAN3 // tetraspanin 3 // 15q24.3 // 10099 /// NM_198902 // TSPAN3	TSPAN3	8.82E-10	7.82E-06	-1.24226	2.89E-08	-1.42198
3973839	NM_000397 // CYBB // cytochrome b-245, beta polypeptide // Xp21.1 // 1536 /// EN	CYBB	8.83E-10	1.93E-05	-1.38055	1.51E-08	-1.76879
3367036	NM_030771 // CCDC34 // coiled-coil domain containing 34 // 11p14.1 // 91057 ///	CCDC34	8.88E-10	0.0291207	1.07775	3.48E-10	1.39312
2554018	NM_004105 // EFEMP1 // EGF-containing fibulin-like extracellular matrix protein	EFEMP1	8.90E-10	0.0297377	-1.20763	3.47E-10	-2.31382
2324084	NM_001785 // CDA // cytidine deaminase // 1p36.2-p35 // 978 /// ENST00000375071	CDA	8.95E-10	1.84E-06	-2.24611	9.42E-08	-3.13584
3554728	NM_004689 // MTA1 // metastasis associated 1 // 14q32.3 // 9112 /// ENST00000331	MTA1	9.05E-10	8.18E-07	1.17867	1.98E-07	1.23906
3470193	NM_004072 // CMKLR1 // chemokine-like receptor 1 // 12q24.1 // 1240 /// ENST0000	CMKLR1	9.12E-10	1.46E-08	-1.61415	2.16E-05	-1.4837
3160773	NM_005772 // RCL1 // RNA terminal phosphate cyclase-like 1 // 9p24.1-p23 // 1017	RCL1	9.19E-10	2.80E-06	1.34302	6.85E-08	1.54187
2526759	NM_004044 // ATIC // 5-aminoimidazole-4-carboxamide ribonucleotide formyltransfe	ATIC	9.22E-10	2.26E-05	1.37031	1.43E-08	1.75818
2326749	NM_032283 // ZDHHC18 // zinc finger, DHHC-type containing 18 // 1p36.11 // 84243	ZDHHC18	9.24E-10	1.14E-07	-1.1976	1.56E-06	-1.2107
2691668	NM_005335 // HCLS1 // hematopoietic cell-specific Lyn substrate 1 // 3q13 // 305	HCLS1	9.26E-10	0.000177483	-1.27034	3.94E-09	-1.6917
2641083	NM_021937 // EEFSEC // eukaryotic elongation factor, selenocysteine-tRNA-specifi	EEFSEC	9.27E-10	0.00180971	1.09487	1.17E-09	1.29552
3803120	NM_004775 // B4GALT6 // UDP-Gal:betaGlcNAc beta 1,4- galactosyltransferase, poly	B4GALT6	9.36E-10	9.53E-08	1.37884	1.96E-06	1.3959
3525538	NM_024537 // CARS2 // cysteinyl-tRNA synthetase 2, mitochondrial (putative) // 1	CARS2	9.41E-10	0.00562892	1.11415	7.16E-10	1.433
2621881	NM_177938 // PH-4 // hypoxia-inducible factor prolyl 4-hydroxylase // 3p21.31 //	PH-4	9.46E-10	3.60E-06	1.14477	5.83E-08	1.22494
2828146	NM_020240 // CDC42SE2 // CDC42 small effector 2 // 5q31.1 // 56990 /// NM_001038	CDC42SE2	9.53E-10	2.52E-06	-1.30263	7.89E-08	-1.46706
3942531	NM_030758 // OSBP2 // oxysterol binding protein 2 // 22q12.2 // 23762 /// ENST00	OSBP2	9.62E-10	6.69E-07	1.26439	2.61E-07	1.34785
2395564	NM_003039 // SLC2A5 // solute carrier family 2 (facilitated glucose/fructose tra	SLC2A5	9.73E-10	2.74E-07	-1.51877	6.48E-07	-1.62405
3974948	NM_001097579 // GPR34 // G protein-coupled receptor 34 // Xp11.4-p11.3 // 2857 /	GPR34	9.79E-10	3.80E-06	-1.54431	5.84E-08	-1.92345
2938636	NM_001500 // GMDS // GDP-mannose 4,6-dehydratase // 6p25 // 2762 /// ENST0000038	GMDS	9.83E-10	4.09E-05	1.30064	1.04E-08	1.64351
3944129	NM_002133 // HMOX1 // heme oxygenase (decycling) 1 // 22q12|22q13.1 // 3162 ///	HMOX1	9.84E-10	3.91E-10	-2.06767	0.0285507	-1.27543
3095815	NM_178819 // AGPAT6 // 1-acylglycerol-3-phosphate O-acyltransferase 6 (lysophosp	AGPAT6	9.85E-10	3.51E-05	1.14842	1.16E-08	1.29399
2461531	NM_182972 // IRF2BP2 // interferon regulatory factor 2 binding protein 2 // 1q42	IRF2BP2	9.85E-10	1.06E-08	1.28888	4.02E-05	1.21867
3293537	NM_000281 // PCBD1 // pterin-4 alpha-carbinolamine dehydratase/dimerization cofa	PCBD1	9.89E-10	4.78E-06	1.21973	4.93E-08	1.35717
4012142	NM_017669 // ERCC6L // excision repair cross-complementing rodent repair deficie	ERCC6L	9.91E-10	0.0126461	1.168	5.40E-10	1.79641
3526325	BC080517 // hCG_1774568 // similar to hCG1774568 // 13q34 // 100134018	hCG_1774568	9.91E-10	9.70E-07	1.22458	1.93E-07	1.30592
4054639	NM_015658 // NOC2L // nucleolar complex associated 2 homolog (S. cerevisiae) //	NOC2L	1.01E-09	0.0209019	1.10413	4.51E-10	1.50474
2363579	NM_032174 // TOMM40L // translocase of outer mitochondrial membrane 40 homolog (	TOMM40L	1.01E-09	5.22E-08	-1.28407	4.64E-06	-1.2715
2951567	NM_004117 // FKBP5 // FK506 binding protein 5 // 6p21.3-p21.2 // 2289 /// ENST00	FKBP5	1.02E-09	3.89E-07	-1.54493	4.88E-07	-1.68435
2596763	NM_003468 // FZD5 // frizzled homolog 5 (Drosophila) // 2q33-q34 // 7855 /// ENS	FZD5	1.03E-09	3.24E-06	-1.41222	7.10E-08	-1.6654
3636522	NM_016073 // HDGFRP3 // hepatoma-derived growth factor, related protein 3 // 15q	HDGFRP3	1.04E-09	1.17E-06	-1.41478	1.74E-07	-1.59072
2435195	NM_031420 // MRPL9 // mitochondrial ribosomal protein L9 // 1q21 // 65005 /// EN	MRPL9	1.04E-09	8.74E-07	1.22576	2.29E-07	1.3027
3861948	NM_004877 // GMFG // glia maturation factor, gamma // 19q13.2 // 9535 /// ENST00	GMFG	1.04E-09	0.000247196	-1.32848	3.77E-09	-1.90065
2559494	NM_032319 // C2orf7 // chromosome 2 open reading frame 7 // 2p13.2 // 84279 ///	C2orf7	1.05E-09	6.40E-10	-1.69502	0.00980157	-1.24004

3678147	NM_020677 // NMRAL1 // NmrA-like family domain containing 1 // 16p13.3 // 57407	NMRAL1	1.05E-09	0.0257937	1.06368	4.37E-10	1.30318
3896370	NM_019593 // RP5-1022P6.2 // hypothetical protein KIAA1434 // 20p12.3 // 56261 /	RP5-1022P6.2	1.06E-09	2.87E-08	1.66281	1.09E-05	1.57053
3645555	NM_016639 // TNFRSF12A // tumor necrosis factor receptor superfamily, member 12A	TNFRSF12A	1.06E-09	2.15E-05	1.3853	1.77E-08	1.77946
3844470	NM_003712 // PPAP2C // phosphatidic acid phosphatase type 2C // 19p13 // 8612 //	PPAP2C	1.07E-09	0.000292634	1.15112	3.52E-09	1.38216
2836518	NM_198321 // GALNT10 // UDP-N-acetyl-alpha-D-galactosamine:polypeptide N-acetylg	GALNT10	1.08E-09	5.07E-08	1.2727	5.37E-06	1.25778
3157660	NM_003313 // TSTA3 // tissue specific transplantation antigen P35B // 8q24.3 //	TSTA3	1.09E-09	1.30E-05	1.42676	2.64E-08	1.81796
3773241	AL512709 // TBC1D16 // TBC1 domain family, member 16 // 17q25.3 // 125058	TBC1D16	1.10E-09	7.47E-07	1.55819	2.86E-07	1.75968
3279108	NM_004808 // NMT2 // N-myristoyltransferase 2 // 10p13 // 9397 /// ENST000003781	NMT2	1.12E-09	8.33E-06	-1.33789	3.80E-08	-1.59738
3850261	NM_002162 // ICAM3 // intercellular adhesion molecule 3 // 19p13.3-p13.2 // 3385	ICAM3	1.13E-09	6.20E-07	-1.39001	3.57E-07	-1.50812
3244061	NM_145312 // ZNF485 // zinc finger protein 485 // 10q11.21 // 220992 /// ENST000	ZNF485	1.14E-09	2.87E-06	1.38756	9.08E-08	1.60827
4023467	NM_004840 // ARHGEF6 // Rac/Cdc42 guanine nucleotide exchange factor (GEF) 6 //	ARHGEF6	1.15E-09	0.00106077	-1.29596	1.94E-09	-1.98758
3160175	NM_003383 // VLDLR // very low density lipoprotein receptor // 9p24 // 7436 ///	VLDLR	1.15E-09	3.96E-08	-1.6087	8.25E-06	-1.54594
2954207	NM_003192 // TBCC // tubulin folding cofactor C // 6pter-p12.1 // 6903 /// ENST0	TBCC	1.16E-09	5.99E-10	-1.28518	0.0148263	-1.10053
2957126	NM_002388 // MCM3 // minichromosome maintenance complex component 3 // 6p12 // 4	MCM3	1.16E-09	0.000727083	1.25247	2.38E-09	1.76896
3859668	NM_139284 // LGI4 // leucine-rich repeat LGI family, member 4 // 19q13.12|19q13.	LGI4	1.17E-09	2.98E-08	-1.46138	1.24E-05	-1.39734
3434048	NM_178499 // CCDC60 // coiled-coil domain containing 60 // 12q24.23 // 160777 //	CCDC60	1.17E-09	1.33E-06	1.47766	1.84E-07	1.68958
2524602	NM_020923 // ZDBF2 // zinc finger, DBF-type containing 2 // 2q33.3 // 57683 ///	ZDBF2	1.17E-09	1.39E-06	-1.46095	1.77E-07	-1.66748
3830530	NM_032635 // TMEM147 // transmembrane protein 147 // 19q13.1 // 10430 /// ENST00	TMEM147	1.18E-09	0.0166593	1.13983	5.84E-10	1.67239
3214845	NM_017680 // ASPN // asporin // 9q22 // 54829 /// ENST00000375544 // ASPN // asp	ASPN	1.19E-09	6.62E-06	-1.82568	4.88E-08	-2.57055
2346625	NM_173567 // ABHD7 // abhydrolase domain containing 7 // 1p22.1 // 253152 /// EN	ABHD7	1.20E-09	5.20E-09	1.88445	0.000186785	1.5332
3880827	BC012542 // GINS1 // GINS complex subunit 1 (Psf1 homolog) // 20p11.21 // 9837 /	GINS1	1.20E-09	0.490395	1.04399	2.02E-10	1.88336
3698919	NM_012201 // GLG1 // golgi apparatus protein 1 // 16q22-q23 // 2734 /// ENST0000	GLG1	1.21E-09	7.72E-09	1.38306	9.93E-05	1.26314
3149528	NM_014112 // TRPS1 // trichorhinophalangeal syndrome I // 8q24.12 // 7227 /// EN	TRPS1	1.21E-09	4.92E-05	-1.27922	1.21E-08	-1.5977
3956433	NM_001005735 // CHEK2 // CHK2 checkpoint homolog (S. pombe) // 22q11|22q12.1 //	CHEK2	1.21E-09	0.00642022	1.10141	8.94E-10	1.38288
2909167	NM_001010870 // TDRD6 // tudor domain containing 6 // 6p12.3 // 221400 /// NM_00	TDRD6	1.23E-09	4.78E-09	1.67967	0.000229485	1.40883
2407729	NM_022157 // RRAGC // Ras-related GTP binding C // 1p34 // 64121 /// ENST0000037	RRAGC	1.23E-09	1.10E-06	-1.24352	2.36E-07	-1.33133
3415937	NM_021640 // C12orf10 // chromosome 12 open reading frame 10 // 12q13 // 60314 /	C12orf10	1.24E-09	0.000333864	1.11341	3.90E-09	1.28239
2886174	NM_003062 // SLIT3 // slit homolog 3 (Drosophila) // 5q35 // 6586 /// ENST000003	SLIT3	1.24E-09	4.80E-07	-1.36512	5.28E-07	-1.45583
3923436	NM_003274 // TRAPPC10 // trafficking protein particle complex 10 // 21q22.3 // 7	TRAPPC10	1.24E-09	1.98E-07	-1.24026	1.35E-06	-1.26677
2496962	NM_000877 // IL1R1 // interleukin 1 receptor, type I // 2q12 // 3554 /// ENST000	IL1R1	1.25E-09	4.76E-06	-1.42716	6.81E-08	-1.71362
3660213	NM_015247 // CYLD // cylindromatosis (turban tumor syndrome) // 16q12.1 // 1540	CYLD	1.26E-09	0.00443524	-1.17471	1.10E-09	-1.66717
3696317	NM_018667 // SMPD3 // sphingomyelin phosphodiesterase 3, neutral membrane (neutr	SMPD3	1.27E-09	4.42E-06	-1.4077	7.34E-08	-1.67155
3984907	NM_016608 // ARMCX1 // armadillo repeat containing, X-linked 1 // Xq21.33-q22.2	ARMCX1	1.27E-09	5.47E-08	-1.41848	6.44E-06	-1.39102
3748957	NM_000691 // ALDH3A1 // aldehyde dehydrogenase 3 family, memberA1 // 17p11.2 //	ALDH3A1	1.28E-09	0.0189773	1.14234	6.07E-10	1.70507
2731332	NM_000584 // IL8 // interleukin 8 // 4q13-q21 // 3576 /// ENST00000307407 // IL8	IL8	1.30E-09	2.68E-06	2.38543	1.16E-07	3.46199
2636626	NM_017577 // GRAMD1C // GRAM domain containing 1C // 3q13.31 // 54762 /// NM_015	GRAMD1C	1.31E-09	5.89E-06	-1.35455	6.08E-08	-1.59658
4017212	NM_024657 // MORC4 // MORC family CW-type zinc finger 4 // Xq22.3 // 79710 /// N	MORC4	1.31E-09	4.13E-07	1.84215	6.66E-07	2.06022
3362191	NM_020974 // SCUBE2 // signal peptide, CUB domain, EGF-like 2 // 11p15.3 // 5775	SCUBE2	1.33E-09	6.80E-08	-1.64308	5.31E-06	-1.61462
3743306	NM_182906 // CLEC10A // C-type lectin domain family 10, member A // 17p13.1 // 1	CLEC10A	1.34E-09	9.80E-07	-1.46521	2.97E-07	-1.63694
2633631	NM_020202 // NIT2 // nitrilase family, member 2 // 3q12.2 // 56954 /// ENST00000	NIT2	1.35E-09	1.28E-05	1.28549	3.51E-08	1.5167
3960827	NM_015374 // UNC84B // unc-84 homolog B (C. elegans) // 22q13.1 // 25777 /// ENS	UNC84B	1.36E-09	6.50E-07	-1.17655	4.50E-07	-1.22258
3351280	NM_000733 // CD3E // CD3e molecule, epsilon (CD3-TCR complex) // 11q23 // 916 //	CD3E	1.37E-09	0.138989	-1.11965	3.24E-10	-2.12199

2720584	NM_004787 // SLIT2 // slit homolog 2 (Drosophila) // 4p15.2 // 9353 /// ENST0000	SLIT2	1.39E-09	2.64E-06	-1.58089	1.28E-07	-1.91652
3838067	NM_138764 // BAX // BCL2-associated X protein // 19q13.3-q13.4 // 581 /// NM_138	BAX	1.40E-09	0.00351377	1.13895	1.36E-09	1.48885
3858794	NM_032816 // CCDC123 // coiled-coil domain containing 123 // 19q13.11 // 84902 /	CCDC123	1.40E-09	2.25E-05	1.13891	2.44E-08	1.25538
3676300	NM_002952 // RPS2 // ribosomal protein S2 // 16p13.3 // 6187 /// NR_002327 // SN	RPS2	1.40E-09	4.16E-05	1.28527	1.62E-08	1.59346
3296981	NM_153367 // ZCCHC24 // zinc finger, CCHC domain containing 24 // 10q22.3 // 219	ZCCHC24	1.43E-09	1.27E-07	-1.31144	2.78E-06	-1.3229
3848118	NM_001080452 // GPR108 // G protein-coupled receptor 108 // 19p13.3 // 56927 ///	GPR108	1.45E-09	2.19E-08	-1.24772	2.85E-05	-1.20002
2454378	NM_021194 // SLC30A1 // solute carrier family 30 (zinc transporter), member 1 //	SLC30A1	1.45E-09	2.39E-08	-1.24243	2.51E-05	-1.1985
2726910	NM_145263 // SPATA18 // spermatogenesis associated 18 homolog (rat) // 4q12 // 1	SPATA18	1.46E-09	1.11E-06	1.58542	2.99E-07	1.81891
2835290	BX648997 // LOC153346 // hypothetical protein LOC153346 // 5q33.1 // 153346	LOC153346	1.46E-09	2.39E-07	-1.60449	1.41E-06	-1.68648
2473149	NM_147223 // NCOA1 // nuclear receptor coactivator 1 // 2p23 // 8648 /// NM_0037	NCOA1	1.46E-09	0.0142241	-1.14044	7.83E-10	-1.64464
2404209	NM_014654 // SDC3 // syndecan 3 // 1pter-p22.3 // 9672 /// ENST00000339394 // SD	SDC3	1.47E-09	2.06E-06	1.29162	1.72E-07	1.42382
3978518	NM_014599 // MAGED2 // melanoma antigen family D, 2 // Xp11.2 // 10916 /// NM_17	MAGED2	1.48E-09	2.04E-06	1.25253	1.76E-07	1.36391
2369680	NM_173533 // TDRD5 // tudor domain containing 5 // 1q25.2 // 163589 /// ENST0000	TDRD5	1.49E-09	6.59E-06	1.36019	6.65E-08	1.60876
2814756	NM_005909 // MAP1B // microtubule-associated protein 1B // 5q13 // 4131 /// ENST	MAP1B	1.50E-09	3.39E-07	-1.40863	1.01E-06	-1.48066
3188697	NM_014397 // NEK6 // NIMA (never in mitosis gene a)-related kinase 6 // 9q33.3-q	NEK6	1.52E-09	0.000289673	1.13373	5.38E-09	1.32745
2350952	NM_000848 // GSTM2 // glutathione S-transferase M2 (muscle) // 1p13.3 // 2946 //	GSTM2	1.52E-09	8.11E-06	-1.47328	5.83E-08	-1.84092
3473750	BC034471 // FLJ20674 // hypothetical protein FLJ20674 // 12q24.23 // 54621 /// B	FLJ20674	1.54E-09	0.000245644	-1.14989	6.00E-09	-1.36272
3957507	ENST00000377087 // DUSP18 // dual specificity phosphatase 18 // 22q12.2 // 15029	DUSP18	1.54E-09	8.50E-07	1.23218	4.16E-07	1.30056
2906824	NM_001012426 // FOXP4 // forkhead box P4 // 6p21.1 // 116113 /// NM_001012427 //	FOXP4	1.54E-09	5.84E-09	1.29046	0.000258651	1.18332
3868857	NM_145894 // KLK12 // kallikrein-related peptidase 12 // 19q13.3-q13.4 // 43849	KLK12	1.55E-09	3.09E-07	1.84643	1.17E-06	2.00121
3305801	NM_052918 // SORCS1 // sortilin-related VPS10 domain containing receptor 1 // 10	SORCS1	1.55E-09	2.82E-08	-1.32098	2.23E-05	-1.26598
2460817	NM_020808 // SIPA1L2 // signal-induced proliferation-associated 1 like 2 // 1q42	SIPA1L2	1.55E-09	1.84E-06	-1.38849	2.06E-07	-1.5624
2745899	NM_022475 // HHIP // hedgehog interacting protein // 4q28-q32 // 64399 /// ENST0	HHIP	1.56E-09	4.00E-05	-1.43205	1.90E-08	-1.93504
2406735	NM_145047 // C1orf102 // chromosome 1 open reading frame 102 // 1p34.3 // 127700	C1orf102	1.56E-09	3.07E-05	1.16349	2.27E-08	1.31154
2592356	NM_003151 // STAT4 // signal transducer and activator of transcription 4 // 2q32	STAT4	1.57E-09	0.000958412	-1.16873	2.92E-09	-1.49506
2777113	NM_001128310 // SPARCL1 // SPARC-like 1 (hevin) // 4q22.1 // 8404 /// NM_004684	SPARCL1	1.57E-09	1.54E-05	-1.74502	3.75E-08	-2.53807
2780999	NM_005443 // PAPSS1 // 3'-phosphoadenosine 5'-phosphosulfate synthase 1 // 4q24	PAPSS1	1.57E-09	8.99E-09	1.45149	0.000130241	1.30298
2783596	NM_001083 // PDE5A // phosphodiesterase 5A, cGMP-specific // 4q25-q27 // 8654 //	PDE5A	1.59E-09	0.000227965	-1.35555	6.50E-09	-1.94965
2457261	NM_007207 // DUSP10 // dual specificity phosphatase 10 // 1q41 // 11221 /// NM_1	DUSP10	1.59E-09	5.00E-08	1.45238	1.06E-05	1.40532
3475838	NM_024667 // VPS37B // vacuolar protein sorting 37 homolog B (S. cerevisiae) //	VPS37B	1.59E-09	8.98E-07	-1.20534	4.16E-07	-1.26589
3778601	NM_003574 // VAPA // VAMP (vesicle-associated membrane protein)-associated prote	VAPA	1.60E-09	8.00E-07	-1.2935	4.68E-07	-1.3784
3400730	NM_199460 // CACNA1C // calcium channel, voltage-dependent, L type, alpha 1C sub	CACNA1C	1.61E-09	6.48E-06	1.24714	7.48E-08	1.40372
2485688	NM_015147 // CEP68 // centrosomal protein 68kDa // 2p14 // 23177 /// ENST0000037	CEP68	1.62E-09	2.33E-07	1.28581	1.71E-06	1.31613
3290368	NM_152230 // IPMK // inositol polyphosphate multikinase // 10q21.1 // 253430 ///	IPMK	1.62E-09	3.83E-07	-1.33061	1.00E-06	-1.3902
4025339	NM_000202 // IDS // iduronate 2-sulfatase // Xq28 // 3423 /// NM_006123 // IDS /	IDS	1.62E-09	0.278682	-1.04384	3.14E-10	-1.48155
2417095	NM_015139 // SLC35D1 // solute carrier family 35 (UDP-glucuronic acid/UDP-N-acet	SLC35D1	1.63E-09	5.26E-07	-1.62185	7.29E-07	-1.77981
3567556	NM_001017970 // TMEM30B // transmembrane protein 30B // 14q23.1 // 161291 /// EN	TMEM30B	1.66E-09	2.14E-08	-1.27679	3.76E-05	-1.21816
3642137	NM_203472 // SELS // selenoprotein S // 15q26.3 // 55829 /// NM_018445 // SELS /	SELS	1.68E-09	2.19E-05	-1.28773	3.17E-08	-1.54675
2495121	NM_001862 // COX5B // cytochrome c oxidase subunit Vb // 2cen-q13 // 1329 /// EN	COX5B	1.70E-09	2.48E-09	-1.35716	0.00159919	-1.17851
2561955	NM_003849 // SUCLG1 // succinate-CoA ligase, alpha subunit // 2p11.2 // 8802 ///	SUCLG1	1.74E-09	8.27E-09	-1.52914	0.000182837	-1.34004
3742236	NM_014389 // PELP1 // proline, glutamate and leucine rich protein 1 // 17p13.2 /	PELP1	1.74E-09	0.00132839	1.11059	2.80E-09	1.32311
2378121	NM_025228 // TRAF3IP3 // TRAF3 interacting protein 3 // 1q32.3-q41 // 80342 ///	TRAF3IP3	1.75E-09	0.000289314	-1.32299	6.35E-09	-1.8723

3816699	NM_173480 // ZNF57 // zinc finger protein 57 // 19p13.3 // 126295 /// ENST000003	ZNF57	1.75E-09	1.66E-08	-1.48063	6.05E-05	-1.35416
2701033	NM_001081455 // P2RY14 // purinergic receptor P2Y, G-protein coupled, 14 // 3q24	P2RY14	1.75E-09	8.30E-07	-1.58481	5.16E-07	-1.77265
2479693	XR_038049 // LOC100129982 // similar to ribosomal protein L12 // 2p21 // 1001299	LOC100129982	1.76E-09	6.23E-06	1.38675	8.73E-08	1.64414
3558745	NM_002515 // NOVA1 // neuro-oncological ventral antigen 1 // 14q // 4857 /// NM_	NOVA1	1.77E-09	1.06E-05	-1.28469	5.81E-08	-1.49353
3598430	NM_004727 // SLC24A1 // solute carrier family 24 (sodium/potassium/calcium excha	SLC24A1	1.78E-09	1.38E-06	1.2618	3.26E-07	1.35543
3887479	NM_172111 // EYA2 // eyes absent homolog 2 (Drosophila) // 20q13.1 // 2139 /// N	EYA2	1.78E-09	1.80E-08	-1.8239	5.55E-05	-1.59795
3899111	NM_001195 // BFSP1 // beaded filament structural protein 1, filensin // 20p11.23	BFSP1	1.81E-09	7.02E-06	1.37584	8.22E-08	1.6325
3340449	NM_007256 // SLCO2B1 // solute carrier organic anion transporter family, member	SLCO2B1	1.81E-09	3.93E-08	-1.47979	1.86E-05	-1.40646
3949017	NM_017931 // TTC38 // tetratricopeptide repeat domain 38 // 22q13 // 55020 /// E	TTC38	1.81E-09	1.92E-09	-1.34486	0.00314468	-1.1576
2904597	NM_006238 // PPARD // peroxisome proliferator-activated receptor delta // 6p21.2	PPARD	1.82E-09	3.57E-08	-1.39101	2.14E-05	-1.32758
3352404	NM_178507 // OAF // OAF homolog (Drosophila) // 11q23.3 // 220323 /// ENST000003	OAF	1.83E-09	4.08E-07	-1.33282	1.14E-06	-1.39115
2363389	NM_005600 // NIT1 // nitrilase 1 // 1q21-q22 // 4817 /// ENST00000368009 // NIT1	NIT1	1.86E-09	1.51E-07	-1.31867	3.51E-06	-1.32851
3825201	NM_001033930 // UBA52 // ubiquitin A-52 residue ribosomal protein fusion product	UBA52	1.86E-09	7.18E-05	1.18688	1.61E-08	1.39199
3336640	AK026328 // C11orf86 // chromosome 11 open reading frame 86 // 11q13.1 // 254439	C11orf86	1.87E-09	3.22E-07	-1.72604	1.50E-06	-1.8414
2815331	NM_001037637 // BTF3 // basic transcription factor 3 // 5q13.2 // 689 /// NM_001	BTF3	1.87E-09	2.64E-06	1.27954	1.95E-07	1.40913
2677850	NM_017563 // IL17RD // interleukin 17 receptor D // 3p14.3 // 54756 /// ENST0000	IL17RD	1.95E-09	1.89E-07	2.1531	2.91E-06	2.23641
2544781	NM_021907 // DTNB // dystrobrevin, beta // 2p24 // 1838 /// NM_033147 // DTNB //	DTNB	1.95E-09	7.66E-06	1.19559	8.49E-08	1.31711
3732885	NM_212472 // PRKAR1A // protein kinase, cAMP-dependent, regulatory, type I, alph	PRKAR1A	1.96E-09	2.67E-07	1.25667	1.99E-06	1.28303
2475407	NM_024692 // CLIP4 // CAP-GLY domain containing linker protein family, member 4	CLIP4	1.98E-09	6.27E-06	-1.34918	1.01E-07	-1.57208
3417075	NM_201444 // DGKA // diacylglycerol kinase, alpha 80kDa // 12q13.3 // 1606 /// N	DGKA	1.98E-09	2.43E-06	-1.33052	2.28E-07	-1.48065
3718682	NM_001030006 // AP2B1 // adaptor-related protein complex 2, beta 1 subunit // 17	AP2B1	2.02E-09	1.03E-06	1.32023	5.19E-07	1.41795
3068097	NM_014705 // DOCK4 // dedicator of cytokinesis 4 // 7q31.1 // 9732 /// ENST00000	DOCK4	2.02E-09	1.50E-06	-1.37461	3.62E-07	-1.51573
3401197	NM_031465 // C12orf32 // chromosome 12 open reading frame 32 // 12p13.33 // 8369	C12orf32	2.02E-09	0.00192048	1.11131	2.75E-09	1.34037
3955327	NM_031444 // C22orf13 // chromosome 22 open reading frame 13 // 22q11.2 // 83606	C22orf13	2.02E-09	1.32E-08	-1.30435	0.000115137	-1.21377
3335029	NM_002689 // POLA2 // polymerase (DNA directed), alpha 2 (70kD subunit) // 11q13	POLA2	2.03E-09	0.452612	1.03526	3.51E-10	1.58053
3708798	NM_015670 // SENP3 // SUMO1/sentrin/SMT3 specific peptidase 3 // 17p13 // 26168	SENP3	2.04E-09	0.137154	1.04585	4.89E-10	1.33943
2887164	NM_001017995 // SH3PXD2B // SH3 and PX domains 2B // 5q35.1 // 285590 /// ENST00	SH3PXD2B	2.05E-09	4.26E-06	1.38183	1.47E-07	1.59841
2550175	NM_133329 // KCNG3 // potassium voltage-gated channel, subfamily G, member 3 //	KCNG3	2.07E-09	1.62E-09	-1.51699	0.00630103	-1.20626
3421523	NM_006530 // YEATS4 // YEATS domain containing 4 // 12q13-q15 // 8089 /// ENST00	YEATS4	2.08E-09	4.28E-06	1.38467	1.49E-07	1.60289
2327391	NM_031459 // SESN2 // sestrin 2 // 1p35.3 // 83667 /// ENST00000253063 // SESN2	SESN2	2.08E-09	1.46E-07	-1.19587	4.37E-06	-1.19853
3812074	NM_032160 // DSEL // dermatan sulfate epimerase-like // 18q22.1 // 92126 /// ENS	DSEL	2.08E-09	3.16E-07	-1.37623	1.82E-06	-1.42346
3666146	NM_003983 // SLC7A6 // solute carrier family 7 (cationic amino acid transporter,	SLC7A6	2.09E-09	5.72E-05	1.28457	2.16E-08	1.59897
3105749	NM_152565 // ATP6V0D2 // ATPase, H+ transporting, lysosomal 38kDa, V0 subunit d2	ATP6V0D2	2.12E-09	4.01E-07	-1.70727	1.44E-06	-1.83346
3984468	NM_014467 // SRPX2 // sushi-repeat-containing protein, X-linked 2 // Xq21.33-q23	SRPX2	2.13E-09	6.96E-05	1.61165	1.93E-08	2.48842
3067302	NM_002291 // LAMB1 // laminin, beta 1 // 7q22 // 3912 /// ENST00000222399 // LAM	LAMB1	2.15E-09	1.05E-08	1.46325	0.000187637	1.30279
3204301	NM_002989 // CCL21 // chemokine (C-C motif) ligand 21 // 9p13 // 6366 /// ENST00	CCL21	2.20E-09	0.00154791	-1.75467	3.37E-09	-4.53913
3362826	NM_006691 // LYVE1 // lymphatic vessel endothelial hyaluronan receptor 1 // 11p1	LYVE1	2.23E-09	8.28E-06	-1.70255	9.56E-08	-2.26988
3944404	NM_145343 // APOL1 // apolipoprotein L, 1 // 22q13.1 // 8542 /// NM_003661 // AP	APOL1	2.26E-09	3.21E-07	1.62858	2.03E-06	1.70972
2545869	NM_015662 // IFT172 // intraflagellar transport 172 homolog (Chlamydomonas) // 2	IFT172	2.27E-09	4.79E-08	1.23115	2.12E-05	1.19849
3216671	NM_001333 // CTSL2 // cathepsin L2 // 9q22.2 // 1515 /// ENST00000259470 // CTSL	CTSL2	2.27E-09	0.0157635	1.19793	1.21E-09	1.97968
3970642	NM_001037343 // CDKL5 // cyclin-dependent kinase-like 5 // Xp22 // 6792 /// NM_0	CDKL5	2.29E-09	0.000119206	1.17329	1.50E-08	1.37905
2527253	NM_000597 // IGFBP2 // insulin-like growth factor binding protein 2, 36kDa // 2q	IGFBP2	2.30E-09	0.00646668	1.27291	1.80E-09	2.19876

3592511	NM_021199 // SQRDL // sulfide quinone reductase-like (yeast) // 15q15 // 58472 /	SQRDL	2.32E-09	2.59E-08	-1.51763	5.28E-05	-1.39362
3755820	NM_033419 // PERLD1 // per1-like domain containing 1 // 17q12 // 93210 /// ENST0	PERLD1	2.33E-09	5.41E-09	-1.23655	0.000709171	-1.13639
3214668	NM_013417 // IARS // isoleucyl-tRNA synthetase // 9q21 // 3376 /// NM_002161 //	IARS	2.35E-09	9.62E-05	1.4012	1.77E-08	1.93959
2348992	NM_001078 // VCAM1 // vascular cell adhesion molecule 1 // 1p32-p31 // 7412 ///	VCAM1	2.35E-09	0.000249763	-1.45789	9.87E-09	-2.26758
2855542	NM_148672 // CCL28 // chemokine (C-C motif) ligand 28 // 5p12 // 56477 /// ENST0	CCL28	2.36E-09	8.72E-06	-1.50432	9.88E-08	-1.87776
2334098	NM_006845 // KIF2C // kinesin family member 2C // 1p34.1 // 11004 /// ENST000003	KIF2C	2.36E-09	0.00150433	1.23374	3.71E-09	1.75272
2458338	NM_001008493 // ENAH // enabled homolog (Drosophila) // 1q42.12 // 55740 /// NM_	ENAH	2.37E-09	2.99E-07	1.53861	2.38E-06	1.59671
2334706	NM_199044 // NSUN4 // NOL1/NOP2/Sun domain family, member 4 // 1p34 // 387338 //	NSUN4	2.38E-09	0.000118923	1.18283	1.58E-08	1.40051
2793137	NM_020870 // SH3RF1 // SH3 domain containing ring finger 1 // 4q32.3-q33 // 5763	SH3RF1	2.39E-09	1.27E-05	-1.18825	7.50E-08	-1.31791
3590086	NM_002875 // RAD51 // RAD51 homolog (RecA homolog, E. coli) (S. cerevisiae) // 1	RAD51	2.39E-09	0.979804	1.00124	3.73E-10	1.62563
3110789	NM_012082 // ZFPM2 // zinc finger protein, multitype 2 // 8q23 // 23414 /// ENST	ZFPM2	2.40E-09	1.14E-06	-1.42505	6.03E-07	-1.55936
2404158	NM_006762 // LAPTM5 // lysosomal multispanning membrane protein 5 // 1p34 // 780	LAPTM5	2.42E-09	1.63E-05	-1.48294	6.31E-08	-1.90791
3851868	NM_004461 // FARSA // phenylalanyl-tRNA synthetase, alpha subunit // 19p13.2 //	FARSA	2.43E-09	0.0672742	1.05882	7.45E-10	1.34376
3866898	NM_000234 // LIG1 // ligase I, DNA, ATP-dependent // 19q13.2-q13.3 // 3978 /// E	LIG1	2.45E-09	0.00167815	1.11279	3.65E-09	1.33507
3962054	NM_005008 // NHP2L1 // NHP2 non-histone chromosome protein 2-like 1 (S. cerevisi	NHP2L1	2.51E-09	0.00873935	1.12809	1.73E-09	1.50801
3420854	NM_006482 // DYRK2 // dual-specificity tyrosine-(Y)-phosphorylation regulated ki	DYRK2	2.55E-09	9.91E-07	-1.25602	7.58E-07	-1.32365
3712949	NM_001388 // DRG2 // developmentally regulated GTP binding protein 2 // 17p11.2	DRG2	2.61E-09	0.0171114	1.07287	1.36E-09	1.30777
3736290	NM_001168 // BIRC5 // baculoviral IAP repeat-containing 5 // 17q25 // 332 /// NM	BIRC5	2.62E-09	0.0310736	1.1429	1.07E-09	1.7731
3509719	NM_015087 // SPG20 // spastic paraplegia 20 (Troyer syndrome) // 13q13.3 // 2311	SPG20	2.62E-09	7.67E-06	-1.42117	1.26E-07	-1.70192
2500803	NM_153712 // TTL // tubulin tyrosine ligase // 2q13 // 150465 /// ENST0000023333	TTL	2.62E-09	5.56E-06	1.24637	1.65E-07	1.38073
3969047	NM_001039091 // PRPS2 // phosphoribosyl pyrophosphate synthetase 2 // Xp22.3-p22	PRPS2	2.64E-09	0.00237871	1.1568	3.35E-09	1.50762
2723605	NM_001104629 // C4orf19 // chromosome 4 open reading frame 19 // 4p14 // 55286 /	C4orf19	2.64E-09	8.39E-07	-1.37466	9.42E-07	-1.46743
2796951	NM_014476 // PDLIM3 // PDZ and LIM domain 3 // 4q35 // 27295 /// NM_001114107 //	PDLIM3	2.64E-09	6.56E-05	-1.32937	2.64E-08	-1.70578
2877861	NM_005847 // SLC23A1 // solute carrier family 23 (nucleobase transporters), memb	SLC23A1	2.66E-09	7.71E-08	-1.74266	1.48E-05	-1.65901
2721633	NM_003102 // SOD3 // superoxide dismutase 3, extracellular // 4p15.3-p15.1 // 66	SOD3	2.66E-09	1.00E-08	1.62395	0.000313112	1.38044
3066436	NM_019042 // PUS7 // pseudouridylate synthase 7 homolog (S. cerevisiae) // 7q22.	PUS7	2.67E-09	1.17E-05	1.56744	9.27E-08	2.03049
3568616	NM_198686 // RAB15 // RAB15, member RAS onocogene family // 14q23.3 // 376267 //	RAB15	2.67E-09	3.30E-06	1.41058	2.65E-07	1.61198
2359817	NM_023015 // INTS3 // integrator complex subunit 3 // 1q21.3 // 65123 /// ENST00	INTS3	2.70E-09	7.22E-08	1.24395	1.65E-05	1.21764
3340589	NM_001235 // SERPINH1 // serpin peptidase inhibitor, clade H (heat shock protein	SERPINH1	2.70E-09	0.000610401	1.16355	6.98E-09	1.43457
2617433	NM_015873 // VILL // villin-like // 3p21.3 // 50853 /// ENST00000283713 // VILL	VILL	2.73E-09	3.99E-05	-1.29131	3.85E-08	-1.57632
2656146	NM_004721 // MAP3K13 // mitogen-activated protein kinase kinase kinase 13 // 3q2	MAP3K13	2.76E-09	0.000239168	-1.26402	1.23E-08	-1.65244
4026956	NM_005334 // HCFC1 // host cell factor C1 (VP16-accessory protein) // Xq28 // 30	HCFC1	2.76E-09	0.000291908	1.0906	1.09E-08	1.20922
2474977	NM_005253 // FOSL2 // FOS-like antigen 2 // 2p23.3 // 2355 /// ENST00000264716 /	FOSL2	2.79E-09	6.47E-07	-1.28126	1.33E-06	-1.33532
3986585	NM_012216 // MID2 // midline 2 // Xq22 // 11043 /// NM_052817 // MID2 // midline	MID2	2.79E-09	2.44E-06	1.30012	3.69E-07	1.42211
2615892	NM_178868 // CMTM8 // CKLF-like MARVEL transmembrane domain containing 8 // 3p22	CMTM8	2.84E-09	1.18E-07	1.34698	9.52E-06	1.32953
3064574	NM_014343 // CLDN15 // claudin 15 // 7q11.22 // 24146 /// ENST00000401528 // CLD	CLDN15	2.85E-09	2.86E-07	-1.45736	3.36E-06	-1.49201
3886223	NM_002466 // MYBL2 // v-myb myeloblastosis viral oncogene homolog (avian)-like 2	MYBL2	2.86E-09	0.0304954	1.16167	1.19E-09	1.89198
3738224	NM_012140 // SLC25A10 // solute carrier family 25 (mitochondrial carrier; dicarb	SLC25A10	2.90E-09	0.00864059	-1.10451	2.04E-09	1.39936
2675315	NM_001005505 // CACNA2D2 // calcium channel, voltage-dependent, alpha 2/delta su	CACNA2D2	2.91E-09	2.65E-06	1.58458	3.63E-07	1.8607
2383356	NM_020247 // CABC1 // chaperone, ABC1 activity of bc1 complex homolog (S. pombe)	CABC1	2.93E-09	1.99E-06	1.20341	4.76E-07	1.27433
2555174	NM_144709 // PUS10 // pseudouridylate synthase 10 // 2p16.1 // 150962 /// ENST00	PUS10	2.95E-09	2.81E-06	-1.37141	3.50E-07	-1.53474
3290875	NM_020987 // ANK3 // ankyrin 3, node of Ranvier (ankyrin G) // 10q21 // 288 ///	ANK3	2.95E-09	0.000236633	-1.25746	1.34E-08	-1.63036

3032446	NM_020445 // ACTR3B // ARP3 actin-related protein 3 homolog B (yeast) // 7q36.1	ACTR3B	2.97E-09	9.45E-05	1.26783	2.40E-08	1.58272
3007894	NM_017528 // WBSCR22 // Williams Beuren syndrome chromosome region 22 // --- //	WBSCR22	2.98E-09	8.18E-05	1.21035	2.64E-08	1.43889
2456805	NM_006085 // BPNT1 // 3'(2'), 5'-bisphosphate nucleotidase 1 // 1q41 // 10380 //	BPNT1	2.98E-09	1.20E-06	-1.36135	7.91E-07	-1.46598
3108526	NM_002380 // MATN2 // matrilin 2 // 8q22 // 4147 /// NM_030583 // MATN2 // matri	MATN2	3.01E-09	0.000211645	-1.40164	1.47E-08	-2.03587
3736232	NM_004710 // SYNGR2 // synaptogyrin 2 // 17q25.3 // 9144 /// ENST00000225777 //	SYNGR2	3.02E-09	4.58E-05	1.23499	3.99E-08	1.46047
3870824	NM_002287 // LAIR1 // leukocyte-associated immunoglobulin-like receptor 1 // 19q	LAIR1	3.04E-09	5.60E-06	-1.35544	2.01E-07	-1.55486
2408111	NM_017646 // TRIT1 // tRNA isopentenyltransferase 1 // 1p35.3-p34.1 // 54802 ///	TRIT1	3.06E-09	6.05E-07	1.37452	1.65E-06	1.44138
3589697	NM_001211 // BUB1B // BUB1 budding uninhibited by benzimidazoles 1 homolog beta	BUB1B	3.09E-09	0.00436792	1.21895	2.98E-09	1.82587
3192062	NM_013318 // KIAA0515 // KIAA0515 // 9q34.13 // 84726 /// ENST00000357304 // KIA	KIAA0515	3.10E-09	3.18E-07	1.24653	3.40E-06	1.2652
2770427	NM_032313 // C4orf14 // chromosome 4 open reading frame 14 // 4q12 // 84273 ///	C4orf14	3.13E-09	1.22E-06	1.235	8.38E-07	1.2984
4053550	NM_198576 // AGRN // agrin // 1p36.33 // 375790 /// ENST00000379370 // AGRN // a	AGRN	3.14E-09	4.02E-07	1.23427	2.67E-06	1.25926
3572235	NM_001040108 // MLH3 // mutL homolog 3 (E. coli) // 14q24.3 // 27030 /// NM_0143	MLH3	3.15E-09	1.55E-07	1.32217	8.12E-06	1.31417
2870964	NM_022140 // EPB41L4A // erythrocyte membrane protein band 4.1 like 4A // 5q22.2	EPB41L4A	3.17E-09	0.0256553	-1.23019	1.42E-09	-2.33236
2605735	NM_018645 // HES6 // hairy and enhancer of split 6 (Drosophila) // 2q37.3 // 555	HES6	3.17E-09	0.000170818	1.33435	1.78E-08	1.80747
3881786	NM_015352 // POFUT1 // protein O-fucosyltransferase 1 // 20q11 // 23509 /// NM_1	POFUT1	3.18E-09	6.42E-07	1.30537	1.65E-06	1.35965
3864597	NM_019108 // C19orf61 // chromosome 19 open reading frame 61 // 19q13.31 // 5600	C19orf61	3.22E-09	0.000569222	1.11559	8.90E-09	1.29207
3469844	NM_001033050 // MTERFD3 // MTERF domain containing 3 // 12q24.1 // 80298 /// NM_	MTERFD3	3.27E-09	0.00027764	1.24117	1.37E-08	1.5945
4000269	NM_017856 // GEMIN8 // gem (nuclear organelle) associated protein 8 // Xp22.2 //	GEMIN8	3.27E-09	1.17E-06	1.26249	9.30E-07	1.33128
3884830	NM_015568 // PPP1R16B // protein phosphatase 1, regulatory (inhibitor) subunit 1	PPP1R16B	3.28E-09	6.86E-06	-1.27195	1.88E-07	-1.42558
3982612	NM_032553 // GPR174 // G protein-coupled receptor 174 // Xq21.1 // 84636 /// ENS	GPR174	3.33E-09	0.0409329	-1.29605	1.25E-09	-3.21942
2883349	NM_032782 // HAVCR2 // hepatitis A virus cellular receptor 2 // 5q33.3 // 84868	HAVCR2	3.41E-09	1.73E-06	-1.28289	6.77E-07	-1.37403
3401704	NM_001759 // CCND2 // cyclin D2 // 12p13 // 894 /// ENST00000261254 // CCND2 //	CCND2	3.42E-09	5.25E-06	1.4979	2.50E-07	1.78233
3561952	NM_006364 // SEC23A // Sec23 homolog A (S. cerevisiae) // 14q21.1 // 10484 /// E	SEC23A	3.42E-09	2.79E-08	-1.50993	9.80E-05	-1.36953
3150715	NM_024094 // DSCC1 // defective in sister chromatid cohesion 1 homolog (S. cerev	DSCC1	3.43E-09	0.0126088	1.19091	2.08E-09	1.8662
3302990	NM_002079 // GOT1 // glutamic-oxaloacetic transaminase 1, soluble (aspartate ami	GOT1	3.47E-09	3.00E-09	-1.62732	0.00566399	-1.25599
2420642	NM_153259 // MCOLN2 // mucolipin 2 // 1p22 // 255231 /// ENST00000370608 // MCOL	MCOLN2	3.48E-09	8.37E-06	-1.88582	1.73E-07	-2.58641
2420511	BC137361 // C1orf180 // chromosome 1 open reading frame 180 // 1p22.3 // 439927	C1orf180	3.51E-09	2.89E-08	2.05528	9.75E-05	1.7347
2918037	NM_052904 // KLHL32 // kelch-like 32 (Drosophila) // 6q16.1 // 114792 /// ENST00	KLHL32	3.59E-09	6.16E-07	1.695	2.07E-06	1.82105
4002741	NM_001037171 // ACOT9 // acyl-CoA thioesterase 9 // Xp22.11 // 23597 /// NM_0010	ACOT9	3.60E-09	4.54E-05	1.19229	5.01E-08	1.36627
2362469	NM_021189 // CADM3 // cell adhesion molecule 3 // 1q21.2-q22 // 57863 /// NM_001	CADM3	3.62E-09	1.04E-06	-1.36949	1.22E-06	-1.4592
3430868	NM_001917 // DAO // D-amino-acid oxidase // 12q24 // 1610 /// ENST00000228476 //	DAO	3.64E-09	3.28E-08	-1.83225	8.60E-05	-1.60008
3454223	NM_013277 // RACGAP1 // Rac GTPase activating protein 1 // 12q13.13 // 29127 ///	RACGAP1	3.69E-09	0.00953745	1.16806	2.54E-09	1.69507
3089535	NM_176871 // PDLIM2 // PDZ and LIM domain 2 (mystique) // 8p21.2 // 64236 /// NM	PDLIM2	3.70E-09	4.30E-07	-1.40974	3.21E-06	-1.45285
2432714	NM_007053 // CD160 // CD160 molecule // 1q21.1 // 11126 /// ENST00000369288 // C	CD160	3.72E-09	1.32E-05	-1.33301	1.31E-07	-1.56682
3705539	NM_018146 // RNMTL1 // RNA methyltransferase like 1 // 17p13.3 // 55178 /// ENST	RNMTL1	3.73E-09	0.0491639	1.06927	1.31E-09	1.36856
3862273	NM_018457 // PRR13 // proline rich 13 // 12q12 // 54458 /// ENST00000379786 // P	PRR13	3.75E-09	1.17E-07	-1.58864	1.55E-05	-1.53586
3878533	NM_080820 // DTD1 // D-tyrosyl-tRNA deacylase 1 homolog (S. cerevisiae) // 20p11	DTD1	3.77E-09	1.36E-05	1.23242	1.30E-07	1.38698
3409211	NM_003622 // PPFIBP1 // PTPRF interacting protein, binding protein 1 (liprin bet	PPFIBP1	3.77E-09	5.49E-07	1.28785	2.53E-06	1.32638
3323443	NM_005788 // PRMT3 // protein arginine methyltransferase 3 // 11p15.1 // 10196 /	PRMT3	3.79E-09	0.00011664	1.31939	2.82E-08	1.71756
3974098	NM_021242 // MID1IP1 // MID1 interacting protein 1 (gastrulation specific G12 ho	MID1IP1	3.83E-09	2.93E-06	1.24859	4.89E-07	1.34536
2888284	AF151875 // HSPC111 // hypothetical protein HSPC111 // 5q35.2 // 51491 /// AK300	HSPC111	3.85E-09	7.65E-05	1.22152	3.81E-08	1.45243
3951732	NM_033070 // CECR5 // cat eye syndrome chromosome region, candidate 5 // --- //	CECR5	3.86E-09	0.00777734	1.10009	2.92E-09	1.36757

3150060	NM_000127 // EXT1 // exostoses (multiple) 1 // 8q24.11-q24.13 // 2131 /// ENST00	EXT1	3.86E-09	1.56E-06	-1.34286	8.95E-07	-1.44548
3428225	NM_005123 // NR1H4 // nuclear receptor subfamily 1, group H, member 4 // 12q23.1	NR1H4	3.89E-09	2.04E-08	-2.68101	0.000205684	-2.01469
2971801	NM_005907 // MAN1A1 // mannosidase, alpha, class 1A, member 1 // 6q22 // 4121 //	MAN1A1	3.89E-09	5.77E-08	-1.47485	4.28E-05	-1.38467
3921490	NM_033171 // B3GALT5 // UDP-Gal:betaGlcNAc beta 1,3-galactosyltransferase, polyp	B3GALT5	3.90E-09	0.00232302	-1.66679	5.26E-09	-4.09176
3067890	NM_032549 // IMMP2L // IMP2 inner mitochondrial membrane peptidase-like (S. cere	IMMP2L	3.93E-09	4.28E-06	1.32198	3.62E-07	1.47274
3938384	BC071804 // IGL@ // immunoglobulin lambda locus // 22q11.1-q11.2 // 3535 /// BC0	IGL@	3.94E-09	7.62E-07	-1.68346	1.91E-06	-1.82386
3985218	NM_022838 // ARMCX5 // armadillo repeat containing, X-linked 5 // Xq22.1-q22.3 /	ARMCX5	3.97E-09	0.000191579	1.10631	2.18E-08	1.2304
3607232	NM_022767 // AEN // apoptosis enhancing nuclease // 15q26.1 // 64782 /// ENST000	AEN	3.98E-09	3.44E-05	1.34323	6.95E-08	1.65843
2989112	NM_018106 // ZDHHC4 // zinc finger, DHHC-type containing 4 // 7p22.1 // 55146 //	ZDHHC4	3.98E-09	0.000178201	1.14209	2.29E-08	1.31064
3107242	NM_153704 // TMEM67 // transmembrane protein 67 // 8q22.1 // 91147 /// ENST00000	TMEM67	4.02E-09	5.47E-07	1.43798	2.81E-06	1.49641
2950263	NM_002118 // HLA-DMB // major histocompatibility complex, class II, DM beta // 6	HLA-DMB	4.03E-09	2.84E-05	-1.59051	8.13E-08	-2.18048
3591704	NM_024908 // WDR76 // WD repeat domain 76 // 15q15.3 // 79968 /// ENST0000026379	WDR76	4.05E-09	0.00263253	1.15601	5.15E-09	1.50054
2787266	NM_020724 // RNF150 // ring finger protein 150 // 4q31.21 // 57484 /// ENST00000	RNF150	4.08E-09	2.71E-07	-1.26827	6.36E-06	-1.27449
3543714	NM_152331 // ACOT4 // acyl-CoA thioesterase 4 // 14q24.3 // 122970 /// ENST00000	ACOT4	4.11E-09	1.04E-09	-1.40046	0.127052	-1.08376
3352040	NM_024791 // PDZD3 // PDZ domain containing 3 // 11q23.3 // 79849 /// ENST000003	PDZD3	4.12E-09	2.67E-05	-1.43575	8.75E-08	-1.82763
2443120	NM_001937 // DPT // dermatopontin // 1q12-q23 // 1805 /// ENST00000367817 // DPT	DPT	4.12E-09	3.98E-06	-1.78258	4.13E-07	-2.21009
3763390	NM_001099640 // TMEM100 // transmembrane protein 100 // 17q22 // 55273 /// NM_01	TMEM100	4.13E-09	7.95E-08	-1.81552	3.05E-05	-1.6803
2904683	NM_007104 // RPL10A // ribosomal protein L10a // 6p21.3-p21.2 // 4736 /// ENST00	RPL10A	4.14E-09	2.12E-05	1.22587	1.05E-07	1.39315
3413344	NM_000289 // PFKM // phosphofructokinase, muscle // 12q13.3 // 5213 /// ENST0000	PFKM	4.16E-09	0.00140284	1.20003	7.34E-09	1.59974
3711700	NM_020652 // ZNF286A // zinc finger protein 286A // 17p11.2 // 57335 /// ENST000	ZNF286A	4.25E-09	2.59E-07	1.31292	7.15E-06	1.31691
3855633	NM_001001524 // TM6SF2 // transmembrane 6 superfamily member 2 // 19p13.3-p12 //	TM6SF2	4.27E-09	2.76E-07	-1.95335	6.69E-06	-1.97764
2464909	NM_022743 // SMYD3 // SET and MYND domain containing 3 // 1q44 // 64754 /// ENST	SMYD3	4.29E-09	3.42E-06	1.20485	5.00E-07	1.28523
3947036	NM_152513 // MEI1 // meiosis inhibitor 1 // 22q13.2 // 150365 /// BC070111 // ME	MEI1	4.30E-09	3.03E-07	-1.46608	6.06E-06	-1.48268
3625234	NM_016304 // C15orf15 // chromosome 15 open reading frame 15 // 15q21 // 51187 /	C15orf15	4.31E-09	6.38E-07	1.38864	2.64E-06	1.44564
3513794	NM_018191 // RCBTB1 // regulator of chromosome condensation (RCC1) and BTB (POZ)	RCBTB1	4.33E-09	3.48E-06	1.3193	4.99E-07	1.45294
3833793	NM_016154 // RAB4B // RAB4B, member RAS oncogene family // 19q13.2 // 53916 ///	RAB4B	4.34E-09	9.37E-07	-1.25526	1.78E-06	-1.30509
2905327	NM_173558 // FGD2 // FYVE, RhoGEF and PH domain containing 2 // 6p21.2 // 221472	FGD2	4.34E-09	1.33E-06	-1.2926	1.25E-06	-1.36655
3217807	NM_017746 // TEX10 // testis expressed 10 // 9q31.1 // 54881 /// ENST00000374902	TEX10	4.38E-09	1.80E-06	1.40917	9.36E-07	1.5389
3168066	NM_001216 // CA9 // carbonic anhydrase IX // 9p13-p12 // 768 /// ENST00000378357	CA9	4.38E-09	9.04E-08	2.0515	2.84E-05	1.88169
3644375	NM_000548 // TSC2 // tuberous sclerosis 2 // 16p13.3 // 7249 /// NM_001114382 //	TSC2	4.41E-09	5.51E-07	1.15133	3.20E-06	1.16795
3326183	NM_005898 // CAPRIN1 // cell cycle associated protein 1 // 11p13 // 4076 /// NM_	CAPRIN1	4.42E-09	1.35E-06	1.27416	1.26E-06	1.34315
2887309	NM_004417 // DUSP1 // dual specificity phosphatase 1 // 5q34 // 1843 /// ENST000	DUSP1	4.43E-09	0.000263071	-1.70319	2.04E-08	-3.07935
2920803	AK094715 // FLJ37396 // hypothetical protein FLJ37396 // 6q21 // 285754	FLJ37396	4.46E-09	2.36E-08	1.60644	0.000212053	1.40223
2884578	NM_024565 // CCNJL // cyclin J-like // 5q33.3 // 79616 /// ENST00000393977 // CC	CCNJL	4.46E-09	6.47E-09	-1.38911	0.00208889	-1.19588
3835879	NM_000041 // APOE // apolipoprotein E // 19q13.2 // 348 /// ENST00000252486 // A	APOE	4.47E-09	3.80E-08	-1.62718	0.000101074	-1.45635
3031517	NM_153236 // GIMAP7 // GTPase, IMAP family member 7 // 7q36.1 // 168537 /// ENST	GIMAP7	4.47E-09	0.0103102	-1.31369	3.02E-09	-2.53632
2468376	NM_014746 // RNF144A // ring finger protein 144A // 2p25.2-p25.1 // 9781 /// ENS	RNF144A	4.51E-09	0.000220255	-1.17489	2.33E-08	-1.39589
3951927	NM_197966 // BID // BH3 interacting domain death agonist // 22q11.1 // 637 /// N	BID	4.52E-09	8.13E-05	1.12989	4.46E-08	1.25504
3607510	NM_001113378 // FANCI // Fanconi anemia, complementation group I // 15q26.1 // 5	FANCI	4.54E-09	0.0729553	1.15204	1.40E-09	2.07226
3768880	NM_080282 // ABCA10 // ATP-binding cassette, sub-family A (ABC1), member 10 // 1	ABCA10	4.57E-09	0.000103917	-1.2888	3.84E-08	-1.62253
3862167	NM_001436 // FBL // fibrillarin // 19q13.1 // 2091 /// ENST00000221801 // FBL //	FBL	4.57E-09	2.94E-06	1.30786	6.29E-07	1.42485
3976609	NM_177439 // FTSJ1 // FtsJ homolog 1 (E. coli) // Xp11.23 // 24140 /// NM_012280	FTSJ1	4.61E-09	0.00828872	1.11065	3.45E-09	1.41202

3214800	NM_033014 // OGN // osteoglycin // 9q22 // 4969 /// NM_014057 // OGN // osteogly	OGN	4.66E-09	6.25E-05	-1.66535	5.55E-08	-2.51276
3354443	NM_198277 // SLC37A2 // solute carrier family 37 (glycerol-3-phosphate transport	SLC37A2	4.72E-09	1.36E-07	-4.01585	1.88E-05	-3.60268
3834502	NM_001783 // CD79A // CD79a molecule, immunoglobulin-associated alpha // 19q13.2	CD79A	4.74E-09	9.04E-06	-1.63788	2.47E-07	-2.07426
2532699	NM_001017915 // INPP5D // inositol polyphosphate-5-phosphatase, 145kDa // 2q37.1	INPP5D	4.79E-09	9.49E-08	1.48582	3.11E-05	1.41488
3264059	NM_000681 // ADRA2A // adrenergic, alpha-2A-, receptor // 10q24-q26 // 150 /// E	ADRA2A	4.80E-09	9.68E-09	-1.64135	0.00113514	-1.33964
3684486	NM_005849 // IGSF6 // immunoglobulin superfamily, member 6 // 16p12-p13 // 10261	IGSF6	4.83E-09	1.96E-07	-1.44415	1.24E-05	-1.42519
2568687	NM_201555 // FHL2 // four and a half LIM domains 2 // 2q12-q14 // 2274 /// NM_00	FHL2	4.83E-09	1.26E-05	1.24645	1.93E-07	1.40029
3166815	NM_014471 // SPINK4 // serine peptidase inhibitor, Kazal type 4 // 9p13.3 // 272	SPINK4	4.89E-09	3.74E-05	2.60301	8.50E-08	5.12492
3846667	NM_016539 // SIRT6 // sirtuin (silent mating type information regulation 2 homol	SIRT6	4.89E-09	2.47E-08	-1.35734	0.000234549	-1.24183
3724969	NM_018129 // PNPO // pyridoxamine 5'-phosphate oxidase // 17q21.32 // 55163 ///	PNPO	4.91E-09	0.25439	1.05231	1.00E-09	1.52757
3508898	NM_178006 // STARD13 // StAR-related lipid transfer (START) domain containing 13	STARD13	4.92E-09	1.68E-07	-1.23518	1.55E-05	-1.22047
2333635	NM_001384 // DPH2 // DPH2 homolog (S. cerevisiae) // 1p34 // 1802 /// NM_0010395	DPH2	4.94E-09	0.0325123	1.08898	2.07E-09	1.43192
3307680	NM_014881 // DCLRE1A // DNA cross-link repair 1A (PSO2 homolog, S. cerevisiae) /	DCLRE1A	4.95E-09	2.03E-05	1.26773	1.37E-07	1.4624
3532935	NM_138731 // MIPOL1 // mirror-image polydactyly 1 // 14q13.3-q21.1 // 145282 ///	MIPOL1	4.96E-09	3.33E-07	1.6092	6.82E-06	1.62998
3189080	NM_005833 // RABEPK // Rab9 effector protein with kelch motifs // 9q33.3 // 1024	RABEPK	5.00E-09	0.00818551	1.10991	3.79E-09	1.40621
2871801	NM_020177 // FEM1C // fem-1 homolog c (C. elegans) // 5q22 // 56929 /// ENST0000	FEM1C	5.04E-09	5.69E-07	-1.22717	3.81E-06	-1.25063
2544201	NM_004881 // TP53I3 // tumor protein p53 inducible protein 3 // 2p23.3 // 9540 /	TP53I3	5.07E-09	4.11E-07	-1.33235	5.55E-06	-1.35197
2650357	NM_025047 // ARL14 // ADP-ribosylation factor-like 14 // 3q26.1 // 80117 /// ENS	ARL14	5.10E-09	3.45E-06	-1.86757	6.33E-07	-2.29644
2952497	NM_052893 // BTBD9 // BTB (POZ) domain containing 9 // 6p21 // 114781 /// NM_001	BTBD9	5.15E-09	1.26E-05	-1.24992	2.11E-07	-1.40414
3031533	NM_018326 // GIMAP4 // GTPase, IMAP family member 4 // 7q36.1 // 55303 /// ENST0	GIMAP4	5.20E-09	0.00118739	-1.32452	1.04E-08	-2.01666
3676395	NM_002528 // NTHL1 // nth endonuclease III-like 1 (E. coli) // 16p13.3 // 4913 /	NTHL1	5.21E-09	0.000516602	1.16826	1.66E-08	1.42102
3890109	NM_080821 // C20orf108 // chromosome 20 open reading frame 108 // 20q13.2 // 116	C20orf108	5.22E-09	1.37E-06	1.18869	1.59E-06	1.23106
3708201	BC040148 // RNASEK // ribonuclease, RNase K // 17p13.1 // 440400 /// AK295795 //	RNASEK	5.25E-09	0.000155583	1.18653	3.50E-08	1.40208
3894047	NM_018257 // PCMTD2 // protein-L-isoaspartate (D-aspartate) O-methyltransferase	PCMTD2	5.28E-09	3.56E-08	1.41468	0.000152905	1.29527
3016380	NM_181552 // CUX1 // cut-like homeobox 1 // 7q22.1 // 1523 /// NM_001913 // CUX1	CUX1	5.29E-09	2.88E-05	1.14124	1.15E-07	1.24426
3301914	NM_152309 // PIK3AP1 // phosphoinositide-3-kinase adaptor protein 1 // 10q24.1 /	PIK3AP1	5.32E-09	0.000162736	-1.17599	3.45E-08	-1.37942
3838385	NM_001774 // CD37 // CD37 molecule // 19q13.3 // 951 /// NM_001040031 // CD37 //	CD37	5.38E-09	0.000241142	-1.51771	2.73E-08	-2.37175
3071636	NM_018077 // RBM28 // RNA binding motif protein 28 // 7q32.1 // 55131 /// ENST00	RBM28	5.39E-09	1.15E-06	1.24323	1.99E-06	1.29203
3382061	NM_182969 // XRRA1 // X-ray radiation resistance associated 1 // 11q13.4 // 1435	XRRA1	5.40E-09	5.17E-05	1.08951	7.67E-08	1.1624
2795819	NM_001012732 // DCTD // dCMP deaminase // 4q35.1 // 1635 /// NM_001921 // DCTD /	DCTD	5.43E-09	6.79E-06	1.34445	3.79E-07	1.52348
3645947	NM_015041 // CLUAP1 // clusterin associated protein 1 // 16p13.3 // 23059 /// NM	CLUAP1	5.44E-09	7.97E-07	1.40988	2.98E-06	1.47319
3699044	NM_018124 // RFWD3 // ring finger and WD repeat domain 3 // 16q22.3 // 55159 ///	RFWD3	5.45E-09	0.00602897	1.15355	4.81E-09	1.55822
2780388	NM_025212 // CXXC4 // CXXC finger 4 // 4q22-q24 // 80319 /// ENST00000394767 //	CXXC4	5.45E-09	1.56E-07	1.77727	2.02E-05	1.70123
2537171	NM_001002919 // FAM150B // family with sequence similarity 150, member B // 2p25	FAM150B	5.47E-09	3.47E-08	-1.78776	0.000170067	-1.53602
3850832	NM_198536 // TMEM205 // transmembrane protein 205 // 19p13.2 // 374882 /// ENST0	TMEM205	5.47E-09	9.85E-06	1.23147	2.80E-07	1.36015
3755862	NM_012481 // IKZF3 // IKAROS family zinc finger 3 (Aiolos) // 17q21 // 22806 ///	IKZF3	5.48E-09	0.00105283	-1.3146	1.18E-08	-1.95598
3888217	NM_017895 // DDX27 // DEAD (Asp-Glu-Ala-Asp) box polypeptide 27 // 20q13.13 // 5	DDX27	5.49E-09	8.29E-05	1.17401	5.62E-08	1.34401
3301011	NM_022451 // NOC3L // nucleolar complex associated 3 homolog (S. cerevisiae) //	NOC3L	5.53E-09	5.61E-05	1.39496	7.45E-08	1.80129
3479438	NM_018223 // CHFR // checkpoint with forkhead and ring finger domains // 12q24.3	CHFR	5.59E-09	1.72E-07	-1.40647	1.86E-05	-1.37478
3390852	NM_207429 // FLJ45803 // FLJ45803 protein // 11q23.1 // 399948 /// ENST000003554	FLJ45803	5.62E-09	7.83E-08	2.26903	5.38E-05	1.98397
2328465	NM_006559 // KHDRBS1 // KH domain containing, RNA binding, signal transduction a	KHDRBS1	5.65E-09	1.90E-06	1.2134	1.30E-06	1.27066
3956854	NM_001002878 // THOC5 // THO complex 5 // 22q12.2 // 8563 /// NM_001002877 // TH	THOC5	5.67E-09	0.000206179	1.14075	3.21E-08	1.30624

2766289	NM_024943 // TMEM156 // transmembrane protein 156 // 4p14 // 80008 /// ENST00000	TMEM156	5.69E-09	2.49E-05	-1.54369	1.41E-07	-2.02224
2768273	NM_152995 // NFXL1 // nuclear transcription factor, X-box binding-like 1 // 4p12	NFXL1	5.71E-09	4.81E-07	1.34355	5.61E-06	1.36705
2863885	NM_005779 // LHFPL2 // lipoma HMGIC fusion partner-like 2 // 5q14.1 // 10184 ///	LHFPL2	5.79E-09	1.63E-07	-1.32418	2.13E-05	-1.29572
2429556	NM_001232 // CASQ2 // calsequestrin 2 (cardiac muscle) // 1p13.3-p11 // 845 ///	CASQ2	5.83E-09	3.57E-06	-1.41373	7.42E-07	-1.58069
3046520	NM_001003799 // TARP // TCR gamma alternate reading frame protein // 7p15-p14 //	TARP	5.84E-09	0.00182973	-1.19871	9.40E-09	-1.6081
3662041	NM_018233 // OGFOD1 // 2-oxoglutarate and iron-dependent oxygenase domain contai	OGFOD1	6.02E-09	0.000193451	1.16236	3.59E-08	1.35271
3473727	NM_018639 // WSB2 // WD repeat and SOCS box-containing 2 // 12q24.23 // 55884 //	WSB2	6.02E-09	4.35E-09	-1.34557	0.00944822	-1.14066
3758317	NM_007296 // BRCA1 // breast cancer 1, early onset // 17q21 // 672 /// NM_007294	BRCA1	6.02E-09	0.143348	1.09496	1.48E-09	1.77675
2589929	NM_178123 // SESTD1 // SEC14 and spectrin domains 1 // 2q31.2 // 91404 /// ENST0	SESTD1	6.08E-09	7.41E-09	1.6254	0.00317668	1.28874
3514348	NR_003923 // GUCY1B2 // guanylate cyclase 1, soluble, beta 2 // 13q14.2-q14.3 //	GUCY1B2	6.11E-09	3.17E-08	1.42846	0.000243162	1.2903
3854877	NM_005354 // JUND // jun D proto-oncogene // 19p13.2 // 3727 /// ENST00000252818	JUND	6.17E-09	2.99E-07	-1.28242	1.11E-05	-1.27966
2503200	NM_002881 // RALB // v-ral simian leukemia viral oncogene homolog B (ras related	RALB	6.18E-09	4.48E-08	-1.42316	0.000144388	-1.30627
3035135	NM_182491 // ZFAND2A // zinc finger, AN1-type domain 2A // 7p22.3 // 90637 /// E	ZFAND2A	6.19E-09	9.03E-07	-1.42175	3.18E-06	-1.48896
3304355	NM_024040 // CUEDC2 // CUE domain containing 2 // 10q24.32 // 79004 /// ENST0000	CUEDC2	6.20E-09	0.000117464	1.19048	5.17E-08	1.39253
3741715	NM_032294 // CAMKK1 // calcium/calmodulin-dependent protein kinase kinase 1, alp	CAMKK1	6.31E-09	6.42E-05	1.19726	8.00E-08	1.37758
3945014	NM_014291 // GCAT // glycine C-acetyltransferase (2-amino-3-ketobutyrate coenzym	GCAT	6.31E-09	0.000958518	1.17302	1.46E-08	1.46838
2531522	NM_016289 // CAB39 // calcium binding protein 39 // 2q37.1 // 51719 /// ENST0000	CAB39	6.32E-09	1.99E-05	-1.28763	1.92E-07	-1.48865
3040454	NM_001002926 // TWISTNB // TWIST neighbor // 7p15.3 // 221830 /// ENST0000022256	TWISTNB	6.37E-09	1.13E-05	1.26204	3.05E-07	1.41251
2843283	NM_007255 // B4GALT7 // xylosylprotein beta 1,4-galactosyltransferase, polypepti	B4GALT7	6.40E-09	0.000960306	1.0951	1.48E-08	1.24432
2714955	NM_006342 // TACC3 // transforming, acidic coiled-coil containing protein 3 // 4	TACC3	6.40E-09	0.00361576	1.16076	7.36E-09	1.53173
2401643	NM_000147 // FUCA1 // fucosidase, alpha-L- 1, tissue // 1p34 // 2517 /// ENST000	FUCA1	6.53E-09	5.06E-07	-1.81278	6.55E-06	-1.86934
2333678	NM_003780 // B4GALT2 // UDP-Gal:betaGlcNAc beta 1,4- galactosyltransferase, poly	B4GALT2	6.59E-09	0.000313458	1.12671	2.96E-08	1.28592
3833992	NM_030622 // CYP2S1 // cytochrome P450, family 2, subfamily S, polypeptide 1 //	CYP2S1	6.59E-09	3.47E-08	1.52596	0.000243461	1.35431
3417485	NM_024068 // OBFC2B // oligonucleotide/oligosaccharide-binding fold containing 2	OBFC2B	6.63E-09	0.00814764	1.12203	5.18E-09	1.44951
3944873	NM_020315 // PDXP // pyridoxal (pyridoxine, vitamin B6) phosphatase // 22cen-q12	PDXP	6.66E-09	1.63E-07	-1.33642	2.69E-05	-1.30141
3418534	NM_206914 // FAM119B // family with sequence similarity 119, member B // 12q14.1	FAM119B	6.67E-09	3.75E-06	1.20346	8.60E-07	1.27598
2462456	NM_018072 // HEATR1 // HEAT repeat containing 1 // 1q43 // 55127 /// ENST0000036	HEATR1	6.68E-09	2.63E-07	1.46651	1.47E-05	1.44845
3417146	NM_001798 // CDK2 // cyclin-dependent kinase 2 // 12q13 // 1017 /// NM_052827 //	CDK2	6.69E-09	0.0896569	1.09406	1.94E-09	1.6216
3744229	NM_032354 // TMEM107 // transmembrane protein 107 // 17p13.1 // 84314 /// NM_183	TMEM107	6.81E-09	0.480013	1.02314	1.19E-09	1.35829
2779271	NM_000669 // ADH1C // alcohol dehydrogenase 1C (class I), gamma polypeptide // 4	ADH1C	6.82E-09	0.000201084	-1.9574	4.09E-08	-3.83767
3378732	NM_021173 // POLD4 // polymerase (DNA-directed), delta 4 // 11q13 // 57804 /// E	POLD4	6.83E-09	2.62E-07	-1.33406	1.54E-05	-1.32054
3012064	NM_012395 // PFTK1 // PFTAIRE protein kinase 1 // 7q21-q22 // 5218 /// ENST00000	PFTK1	6.85E-09	8.13E-06	-1.322	4.47E-07	-1.48885
3730784	NM_016360 // CCDC44 // coiled-coil domain containing 44 // 17q23.3 // 51204 ///	CCDC44	6.86E-09	4.15E-09	-1.29468	0.0144605	-1.11311
3695107	NM_004614 // TK2 // thymidine kinase 2, mitochondrial // 16q22-q23.1 // 7084 ///	TK2	6.87E-09	0.000236066	1.12095	3.72E-08	1.2619
3456130	NM_015665 // AAAS // achalasia, adrenocortical insufficiency, alacrimia (Allgrov	AAAS	6.97E-09	0.0406141	1.06988	2.74E-09	1.34227
3869097	NM_001245 // SIGLEC6 // sialic acid binding Ig-like lectin 6 // 19q13.3 // 946 /	SIGLEC6	7.02E-09	1.41E-05	-1.25293	2.91E-07	-1.4051
3235789	NM_182751 // MCM10 // minichromosome maintenance complex component 10 // 10p13 /	MCM10	7.02E-09	0.224494	1.06464	1.51E-09	1.61584
3226331	AL833509 // LOC286208 // hypothetical protein LOC286208 // 9q34.11 // 286208 ///	LOC286208	7.05E-09	2.07E-08	-1.3029	0.000652869	-1.18558
3210497	NM_015225 // PRUNE2 // prune homolog 2 (Drosophila) // 9q21.13 // 158471 /// AB0	PRUNE2	7.07E-09	2.24E-06	1.71405	1.53E-06	1.94905
3985665	NM_004780 // TCEAL1 // transcription elongation factor A (SII)-like 1 // Xq22.1	TCEAL1	7.13E-09	8.34E-07	1.31328	4.30E-06	1.35209
2914444	NM_001010844 // IRAK1BP1 // interleukin-1 receptor-associated kinase 1 binding p	IRAK1BP1	7.13E-09	1.31E-06	1.21441	2.67E-06	1.25405
3151607	NM_058229 // FBXO32 // F-box protein 32 // 8q24.13 // 114907 /// NM_148177 // FB	FBXO32	7.15E-09	0.00654286	-1.26976	6.24E-09	-2.09884

2481379	NM_172311 // STON1-GTF2A1L // STON1-GTF2A1L // 2p16.3 // 286749 /// NM_006872 //	STON1-GTF2A1L	7.23E-09	2.89E-05	-1.25651	1.72E-07	-1.44837
3960174	NM_006498 // LGALS2 // lectin, galactoside-binding, soluble, 2 // 22q12-q13|22q1	LGALS2	7.28E-09	0.000878199	-1.71903	1.81E-08	-3.59992
2470838	NM_005378 // MYCN // v-myc myelocytomatosis viral related oncogene, neuroblastom	MYCN	7.36E-09	1.74E-06	1.40183	2.08E-06	1.50013
3878836	NM_018993 // RIN2 // Ras and Rab interactor 2 // 20p11.22 // 54453 /// ENST00000	RIN2	7.39E-09	0.00172831	-1.16352	1.27E-08	-1.47613
3335327	NM_006396 // SSSCA1 // Sjogren syndrome/scleroderma autoantigen 1 // 11q13.1 //	SSSCA1	7.39E-09	0.0330416	1.10121	3.17E-09	1.49214
2587790	NM_001033045 // GPR155 // G protein-coupled receptor 155 // 2q31.1 // 151556 ///	GPR155	7.41E-09	2.01E-05	-1.43527	2.35E-07	-1.75703
2880422	NM_003122 // SPINK1 // serine peptidase inhibitor, Kazal type 1 // 5q32 // 6690	SPINK1	7.42E-09	1.26E-06	2.10226	2.94E-06	2.36212
3709107	NM_020877 // DNAH2 // dynein, axonemal, heavy chain 2 // 17p13.1 // 146754 /// E	DNAH2	7.42E-09	1.66E-06	1.36422	2.22E-06	1.44864
3995804	NM_005629 // SLC6A8 // solute carrier family 6 (neurotransmitter transporter, cr	SLC6A8	7.46E-09	9.05E-07	-1.41292	4.22E-06	-1.46913
2528476	NM_001927 // DES // desmin // 2q35 // 1674 /// ENST00000373960 // DES // desmin	DES	7.48E-09	8.76E-06	-1.39884	4.74E-07	-1.61497
2620842	NM_000648 // CCR2 // chemokine (C-C motif) receptor 2 // 3p21.31 // 1231 /// NM_	CCR2	7.50E-09	2.63E-05	-1.7851	1.94E-07	-2.53099
3751541	NM_001085454 // GIT1 // G protein-coupled receptor kinase interactor 1 // 17p11.	GIT1	7.53E-09	0.000253799	1.10184	3.97E-08	1.2192
3304004	NM_006993 // NPM3 // nucleophosmin/nucleoplasmin, 3 // 10q24.31 // 10360 /// ENS	NPM3	7.57E-09	0.00479983	1.13679	7.73E-09	1.46062
3661940	NM_020988 // GNAO1 // guanine nucleotide binding protein (G protein), alpha acti	GNAO1	7.64E-09	2.93E-05	-1.3147	1.83E-07	-1.55725
2977471	NM_182503 // ADAT2 // adenosine deaminase, tRNA-specific 2, TAD2 homolog (S. cer	ADAT2	7.72E-09	9.16E-06	1.33608	4.76E-07	1.5141
3630099	NM_017858 // TIPIN // TIMELESS interacting protein // 15q22.31 // 54962 /// NR_0	TIPIN	7.79E-09	0.00567049	1.17581	7.35E-09	1.63219
3817698	NM_001048201 // UHRF1 // ubiquitin-like with PHD and ring finger domains 1 // 19	UHRF1	7.79E-09	0.000613429	1.25591	2.41E-08	1.6724
3720921	NM_000964 // RARA // retinoic acid receptor, alpha // 17q21 // 5914 /// NM_00102	RARA	7.80E-09	2.38E-07	-1.2384	2.16E-05	-1.22243
3294142	NM_032562 // PLA2G12B // phospholipase A2, group XIIB // 10q22.1 // 84647 /// EN	PLA2G12B	7.82E-09	1.84E-06	-2.09258	2.16E-06	-2.42932
3636956	NM_032856 // WDR73 // WD repeat domain 73 // 15q25.2 // 84942 /// ENST0000039852	WDR73	7.85E-09	0.000674173	1.12157	2.30E-08	1.29918
3302886	NM_021828 // HPSE2 // heparanase 2 // 10q23-q24 // 60495 /// ENST00000370552 //	HPSE2	7.86E-09	3.18E-08	-1.506	0.000393549	-1.32453
2587841	NM_003387 // WIPF1 // WAS/WASL interacting protein family, member 1 // 2q31.1 //	WIPF1	7.90E-09	0.00128648	-1.3211	1.61E-08	-1.98823
3038065	NM_004968 // ICA1 // islet cell autoantigen 1, 69kDa // 7p22 // 3382 /// NM_0223	ICA1	7.91E-09	1.62E-07	1.63111	3.63E-05	1.54569
2827709	NM_016048 // ISOC1 // isochorismatase domain containing 1 // 5q22.1-q33.3 // 510	ISOC1	8.07E-09	2.22E-08	-1.30371	0.000759482	-1.18386
2608725	NM_003670 // BHLHB2 // basic helix-loop-helix domain containing, class B, 2 // 3	BHLHB2	8.08E-09	7.38E-09	1.55586	0.00610406	1.23722
3424218	NM_024560 // ACSS3 // acyl-CoA synthetase short-chain family member 3 // 12q21.3	ACSS3	8.17E-09	1.59E-05	-1.27644	3.24E-07	-1.4461
3458837	NM_005371 // METTL1 // methyltransferase like 1 // 12q13 // 4234 /// NM_023033 /	METTL1	8.28E-09	0.0320382	1.0921	3.62E-09	1.43542
3639031	NM_003981 // PRC1 // protein regulator of cytokinesis 1 // 15q26.1 // 9055 /// N	PRC1	8.30E-09	0.00458266	1.25541	8.75E-09	1.9439
3510858	NM_002015 // FOXO1 // forkhead box O1 // 13q14.1 // 2308 /// ENST00000379561 //	FOXO1	8.31E-09	0.000557793	-1.14081	2.76E-08	-1.34045
3630701	NM_017882 // CLN6 // ceroid-lipofuscinosis, neuronal 6, late infantile, variant	CLN6	8.32E-09	0.934554	-1.00308	1.32E-09	1.42487
2324856	NM_015991 // C1QA // complement component 1, q subcomponent, A chain // 1p36.12	C1QA	8.45E-09	1.69E-07	-1.84641	3.84E-05	-1.7244
2513827	---		8.49E-09	0.00154805	-1.1614	1.58E-08	-1.4574
3908631	NM_020820 // PREX1 // phosphatidylinositol 3,4,5-trisphosphate-dependent RAC exc	PREX1	8.53E-09	5.79E-05	-1.23832	1.27E-07	-1.44677
3208995	NM_001206 // KLF9 // Kruppel-like factor 9 // 9q13 // 687 /// ENST00000377126 //	KLF9	8.55E-09	4.35E-07	-1.30086	1.20E-05	-1.30272
3971877	NM_001415 // EIF2S3 // eukaryotic translation initiation factor 2, subunit 3 gam	EIF2S3	8.58E-09	2.42E-06	1.33181	1.88E-06	1.42249
2949488	NM_025257 // SLC44A4 // solute carrier family 44, member 4 // 6p21.3 // 80736 //	SLC44A4	8.60E-09	2.73E-06	-1.23456	1.68E-06	-1.30022
3735623	NM_024311 // MFSD11 // major facilitator superfamily domain containing 11 // 17q	MFSD11	8.61E-09	7.63E-07	-1.25163	6.36E-06	-1.27327
3946817	NM_003216 // TEF // thyrotrophic embryonic factor // 22q13|22q13.2 // 7008 /// E	TEF	8.71E-09	3.46E-06	-1.21556	1.36E-06	-1.28326
2453365	NM_025179 // PLXNA2 // plexin A2 // 1q32.2 // 5362 /// ENST00000367033 // PLXNA2	PLXNA2	8.73E-09	4.14E-06	-1.44753	1.15E-06	-1.61924
3634811	NM_004390 // CTSH // cathepsin H // 15q24-q25 // 1512 /// NM_148979 // CTSH // c	CTSH	8.82E-09	3.07E-07	1.62072	1.92E-05	1.58854
3589822	NM_033510 // DISP2 // dispatched homolog 2 (Drosophila) // 15q15.1 // 85455 ///	DISP2	8.91E-09	7.44E-08	-1.58038	0.000133175	-1.42908
2773641	XM_001716699 // LOC643100 // hypothetical LOC643100 // 4q13.3 // 643100	LOC643100	8.91E-09	5.14E-05	-1.39919	1.46E-07	-1.7709

3802602	NM_001792 // CDH2 // cadherin 2, type 1, N-cadherin (neuronal) // 18q11.2 // 100	CDH2	8.91E-09	4.68E-06	-1.24336	1.06E-06	-1.33262
2640579	NM_032242 // PLXNA1 // plexin A1 // 3q21.3 // 5361 /// ENST00000251772 // PLXNA1	PLXNA1	8.92E-09	5.94E-05	1.19018	1.31E-07	1.35099
3474815	BC014661 // C12orf43 // chromosome 12 open reading frame 43 // 12q // 64897 ///	C12orf43	8.93E-09	0.00760393	1.07826	7.43E-09	1.26735
3448428	NM_018164 // C12orf11 // chromosome 12 open reading frame 11 // 12p11.23 // 5572	C12orf11	9.01E-09	3.20E-05	1.40513	2.12E-07	1.73322
3434907	NM_001080825 // TMEM120B // transmembrane protein 120B // 12q24.31 // 144404 ///	TMEM120B	9.03E-09	0.00209994	1.14747	1.44E-08	1.43219
3424442	NM_152588 // TMTC2 // transmembrane and tetratricopeptide repeat containing 2 //	TMTC2	9.05E-09	3.33E-07	1.46269	1.82E-05	1.44381
3828112	NM_001238 // CCNE1 // cyclin E1 // 19q12 // 898 /// NM_057182 // CCNE1 // cyclin	CCNE1	9.05E-09	0.152541	1.07763	2.22E-09	1.6111
2604254	NM_018410 // HJURP // Holliday junction recognition protein // 2q37.1 // 55355 /	HJURP	9.06E-09	0.00407937	1.17983	1.02E-08	1.60503
3518418	NM_138444 // KCTD12 // potassium channel tetramerisation domain containing 12 //	KCTD12	9.09E-09	0.00034447	-1.2424	4.11E-08	-1.5751
3674199	NM_014427 // CPNE7 // copine VII // 16q24.3 // 27132 /// NM_153636 // CPNE7 // c	CPNE7	9.10E-09	5.29E-07	1.41021	1.06E-05	1.4218
2772088	NM_001077 // UGT2B17 // UDP glucuronosyltransferase 2 family, polypeptide B17 //	UGT2B17	9.12E-09	0.000112483	-2.21135	8.60E-08	-4.33515
3811949	NM_021153 // CDH19 // cadherin 19, type 2 // 18q22-q23 // 28513 /// ENST00000262	CDH19	9.13E-09	8.54E-07	-1.37396	6.15E-06	-1.4116
3603687	NM_007364 // TMED3 // transmembrane emp24 protein transport domain containing 3	TMED3	9.13E-09	2.35E-06	1.29725	2.12E-06	1.37358
3768703	NM_080283 // ABCA9 // ATP-binding cassette, sub-family A (ABC1), member 9 // 17q	ABCA9	9.15E-09	2.34E-07	-1.46383	2.88E-05	-1.42027
2369110	NM_170692 // RASAL2 // RAS protein activator like 2 // 1q24 // 9462 /// NM_00484	RASAL2	9.21E-09	2.64E-07	1.33005	2.50E-05	1.30561
3725392	NM_005831 // CALCOCO2 // calcium binding and coiled-coil domain 2 // 17q21.32 //	CALCOCO2	9.32E-09	2.25E-06	-1.39105	2.29E-06	-1.49164
3633109	NM_001099436 // ULK3 // unc-51-like kinase 3 (C. elegans) // 15q24.1 // 25989 //	ULK3	9.38E-09	1.93E-06	-1.21174	2.69E-06	-1.25683
2633191	NM_005290 // GPR15 // G protein-coupled receptor 15 // 3q11.2-q13.1 // 2838 ///	GPR15	9.40E-09	4.11E-05	-1.91344	1.85E-07	-2.92872
3658925	NM_014321 // ORC6L // origin recognition complex, subunit 6 like (yeast) // 16q1	ORC6L	9.46E-09	0.502204	1.03308	1.65E-09	1.57233
3384321	NM_014488 // RAB30 // RAB30, member RAS oncogene family // 11q12-q14 // 27314 //	RAB30	9.48E-09	1.98E-07	-1.57486	3.80E-05	-1.50223
3148796	NM_001128211 // NUDCD1 // NudC domain containing 1 // 8q23 // 84955 /// NM_03286	NUDCD1	9.62E-09	6.31E-05	1.25102	1.39E-07	1.47346
3275042	NM_024701 // ASB13 // ankyrin repeat and SOCS box-containing 13 // 10p15.1 // 79	ASB13	9.64E-09	7.56E-08	-1.2765	0.000150387	-1.2078
3442054	NM_001273 // CHD4 // chromodomain helicase DNA binding protein 4 // 12p13 // 110	CHD4	9.68E-09	5.40E-07	1.31847	1.14E-05	1.32585
3896034	NM_014737 // RASSF2 // Ras association (RalGDS/AF-6) domain family member 2 // 2	RASSF2	9.74E-09	2.78E-05	-1.33907	2.62E-07	-1.58841
2326463	NM_001803 // CD52 // CD52 molecule // 1p36 // 1043 /// ENST00000374213 // CD52 /	CD52	9.78E-09	0.00674393	-1.29987	8.70E-09	-2.23856
3347831	NM_004398 // DDX10 // DEAD (Asp-Glu-Ala-Asp) box polypeptide 10 // 11q22-q23 //	DDX10	9.78E-09	1.74E-06	1.48008	3.20E-06	1.58314
2886595	NM_005565 // LCP2 // lymphocyte cytosolic protein 2 (SH2 domain containing leuko	LCP2	9.88E-09	0.00315604	-1.20435	1.29E-08	-1.66672
3587015	NM_015995 // KLF13 // Kruppel-like factor 13 // 15q12 // 51621 /// ENST000003071	KLF13	1.00E-08	7.63E-07	-1.16656	8.09E-06	-1.17754
3056131	NM_012453 // TBL2 // transducin (beta)-like 2 // 7q11.23 // 26608 /// ENST000003	TBL2	1.01E-08	7.97E-05	1.13185	1.25E-07	1.24499
3089285	NM_001722 // POLR3D // polymerase (RNA) III (DNA directed) polypeptide D, 44kDa	POLR3D	1.01E-08	1.56E-05	1.13524	4.39E-07	1.20754
2571075	NM_022662 // ANAPC1 // anaphase promoting complex subunit 1 // 2q12.1 // 64682 /	ANAPC1	1.03E-08	0.000662278	1.16589	3.19E-08	1.41127
2652675	NM_018098 // ECT2 // epithelial cell transforming sequence 2 oncogene // 3q26.1-	ECT2	1.03E-08	1.05E-05	1.74525	6.25E-07	2.21007
3183364	NM_018112 // TMEM38B // transmembrane protein 38B // 9q31.2 // 55151 /// ENST000	TMEM38B	1.03E-08	2.17E-09	-1.68527	0.25195	-1.10055
3942161	NM_001003684 // UCRC // ubiquinol-cytochrome c reductase complex (7.2 kD) // 22c	UCRC	1.04E-08	1.27E-08	-1.35237	0.00358531	-1.17245
2325002	NM_015013 // AOF2 // amine oxidase (flavin containing) domain 2 // 1p36.12 // 23	AOF2	1.06E-08	1.82E-06	1.44406	3.42E-06	1.53727
3842768	NM_020813 // ZNF471 // zinc finger protein 471 // 19q13.43 // 57573 /// ENST0000	ZNF471	1.06E-08	1.17E-06	-1.29387	5.48E-06	-1.3315
3778504	NM_006868 // RAB31 // RAB31, member RAS oncogene family // 18p11.3 // 11031 ///	RAB31	1.06E-08	5.31E-07	-1.39754	1.35E-05	-1.40141
3329904	NM_004551 // NDUFS3 // NADH dehydrogenase (ubiquinone) Fe-S protein 3, 30kDa (NA	NDUFS3	1.07E-08	2.25E-08	-1.31954	0.00133271	-1.18187
4013460	NM_006639 // CYSLTR1 // cysteinyl leukotriene receptor 1 // Xq13.2-q21.1 // 1080	CYSLTR1	1.08E-08	8.19E-05	-1.49877	1.32E-07	-2.04491
3168255	NM_001039792 // UNQ338 // hypothetical protein LOC646962 // 9p13.3 // 646962 ///	UNQ338	1.09E-08	5.16E-06	-1.87198	1.28E-06	-2.27694
3818515	NM_004240 // TRIP10 // thyroid hormone receptor interactor 10 // 19p13.3 // 9322	TRIP10	1.09E-08	3.90E-09	-1.37846	0.0548293	-1.10823
3474935	NM_016237 // ANAPC5 // anaphase promoting complex subunit 5 // 12q24.31 // 51433	ANAPC5	1.09E-08	2.13E-06	1.2259	3.04E-06	1.27386

3753760	NM_024302 // MMP28 // matrix metallopeptidase 28 // 17q11-q21.1 // 79148 /// NM_	MMP28	1.09E-08	0.000425067	-1.32747	4.50E-08	-1.82455
3290210	NM_032997 // ZWINT // ZW10 interactor // 10q21-q22 // 11130 /// NM_007057 // ZWI	ZWINT	1.09E-08	0.370992	1.05054	2.06E-09	1.66284
3833757	NM_004596 // SNRPA // small nuclear ribonucleoprotein polypeptide A // 19q13.1 /	SNRPA	1.11E-08	0.0294115	1.08944	5.14E-09	1.40577
3850069	NM_001379 // DNMT1 // DNA (cytosine-5-)-methyltransferase 1 // 19p13.2 // 1786 /	DNMT1	1.11E-08	0.0346989	1.07608	4.81E-09	1.35258
3190366	NM_005094 // SLC27A4 // solute carrier family 27 (fatty acid transporter), membe	SLC27A4	1.13E-08	2.20E-09	-1.47657	0.326135	-1.06313
2327283	NM_001105556 // C1orf38 // chromosome 1 open reading frame 38 // 1p35.3 // 9473	C1orf38	1.13E-08	1.78E-07	-1.34411	5.91E-05	-1.29123
3808854	NM_001083962 // TCF4 // transcription factor 4 // 18q21.1 // 6925 /// NM_003199	TCF4	1.13E-08	2.56E-05	-1.41719	3.40E-07	-1.72021
2835614	ENST00000394243 // SYNPO // synaptopodin // 5q33.1 // 11346 /// AK095279 // SYNP	SYNPO	1.13E-08	2.56E-07	-1.41658	3.69E-05	-1.37249
3061319	NM_001259 // CDK6 // cyclin-dependent kinase 6 // 7q21-q22 // 1021 /// ENST00000	CDK6	1.14E-08	8.58E-08	1.70267	0.000168924	1.50724
3192525	NM_012204 // GTF3C4 // general transcription factor IIIC, polypeptide 4, 90kDa /	GTF3C4	1.14E-08	5.42E-05	1.23058	1.93E-07	1.41837
2326561	NM_002953 // RPS6KA1 // ribosomal protein S6 kinase, 90kDa, polypeptide 1 // 1p	RPS6KA1	1.15E-08	3.32E-07	-1.24996	2.70E-05	-1.23358
2420521	NM_014021 // SSX2IP // synovial sarcoma, X breakpoint 2 interacting protein // 1	SSX2IP	1.15E-08	2.29E-06	1.35944	3.07E-06	1.44232
3734413	NM_175738 // RAB37 // RAB37, member RAS oncogene family // 17q25.1 // 326624 ///	RAB37	1.16E-08	8.86E-05	-1.25786	1.37E-07	-1.50264
3022814	NM_013332 // HIG2 // hypoxia-inducible protein 2 // 7q32.1 // 29923 /// NM_00109	HIG2	1.17E-08	6.57E-05	1.31722	1.73E-07	1.60505
2730281	NM_017855 // ODAM // odontogenic, ameloblast asssociated // 4q13.3 // 54959 ///	ODAM	1.17E-08	5.09E-08	2.17764	0.000400767	1.72462
3687752	NM_052838 // SEPT1 // septin 1 // 16p11.1 // 1731 /// ENST00000321367 // SEPT1 /	SEPT1	1.18E-08	0.00328264	-1.2034	1.54E-08	-1.66028
3918779	NM_003024 // ITSN1 // intersectin 1 (SH3 domain protein) // 21q22.1-q22.2 // 645	ITSN1	1.18E-08	9.16E-05	-1.17396	1.37E-07	-1.33029
3080283	NM_005431 // XRCC2 // X-ray repair complementing defective repair in Chinese ham	XRCC2	1.18E-08	0.172543	1.07007	2.81E-09	1.56694
3874249	NM_033453 // ITPA // inosine triphosphatase (nucleoside triphosphate pyrophospha	ITPA	1.19E-08	0.000164708	1.16269	9.22E-08	1.33106
3881874	NM_015338 // ASXL1 // additional sex combs like 1 (Drosophila) // 20q11.1 // 171	ASXL1	1.19E-08	4.13E-08	1.22955	0.00057871	1.14881
2491788	NM_032827 // ATOH8 // atonal homolog 8 (Drosophila) // 2p11.2 // 84913 /// ENST0	ATOH8	1.20E-08	0.000667084	1.2509	3.84E-08	1.64634
2363852	NM_032738 // FCRLA // Fc receptor-like A // 1q23.3 // 84824 /// ENST00000236938	FCRLA	1.21E-08	0.000125457	-1.38322	1.13E-07	-1.81626
2819779	NM_032119 // GPR98 // G protein-coupled receptor 98 // 5q13 // 84059 /// NR_0031	GPR98	1.21E-08	7.74E-07	-1.31947	1.06E-05	-1.33568
2500838	NM_019014 // POLR1B // polymerase (RNA) I polypeptide B, 128kDa // 2q13 // 84172	POLR1B	1.21E-08	7.35E-06	1.35349	1.07E-06	1.50632
3320944	NM_021961 // TEAD1 // TEA domain family member 1 (SV40 transcriptional enhancer	TEAD1	1.21E-08	4.40E-07	1.45672	2.08E-05	1.44094
3471819	NM_024953 // C12orf30 // chromosome 12 open reading frame 30 // 12q24.13 // 8001	C12orf30	1.22E-08	6.14E-06	1.39281	1.29E-06	1.55144
2620937	NM_003212 // TDGF1 // teratocarcinoma-derived growth factor 1 // 3p21.31 // 6997	TDGF1	1.23E-08	8.14E-07	4.65759	1.03E-05	5.02208
2542651	NM_001006657 // WDR35 // WD repeat domain 35 // 2p24.1 // 57539 /// NM_020779 //	WDR35	1.23E-08	2.26E-07	1.46081	4.95E-05	1.39875
2911903	NM_003463 // PTP4A1 // protein tyrosine phosphatase type IVA, member 1 // 6q12 /	PTP4A1	1.23E-08	1.20E-05	-1.58626	7.14E-07	-1.9305
3925473	NM_022136 // SAMSN1 // SAM domain, SH3 domain and nuclear localization signals 1	SAMSN1	1.24E-08	5.88E-05	-1.31313	2.03E-07	-1.58484
2489172	NM_001040409 // MTHFD2 // methylenetetrahydrofolate dehydrogenase (NADP+ depende	MTHFD2	1.26E-08	0.000377945	1.29742	5.72E-08	1.7178
3012213	NM_003505 // FZD1 // frizzled homolog 1 (Drosophila) // 7q21 // 8321 /// ENST000	FZD1	1.26E-08	1.37E-06	-1.21205	6.03E-06	-1.23895
2488732	NM_006429 // CCT7 // chaperonin containing TCP1, subunit 7 (eta) // 2p13.2 // 10	CCT7	1.26E-08	0.00213193	1.19793	2.09E-08	1.59136
3896200	NM_002592 // PCNA // proliferating cell nuclear antigen // 20pter-p12 // 5111 //	PCNA	1.26E-08	0.112639	1.09332	3.48E-09	1.65223
2352804	NM_020190 // OLFML3 // olfactomedin-like 3 // 1p13.2 // 56944 /// ENST0000032033	OLFML3	1.27E-08	4.05E-06	-1.37471	2.02E-06	-1.4941
3743701	NM_020360 // PLSCR3 // phospholipid scramblase 3 // 17p13.1 // 57048 /// ENST000	PLSCR3	1.27E-08	6.02E-06	1.24745	1.39E-06	1.33845
3723264	NM_021079 // NMT1 // N-myristoyltransferase 1 // 17q21.31 // 4836 /// ENST000002	NMT1	1.27E-08	1.11E-06	1.19181	7.73E-06	1.20975
3931250	NM_153681 // PIGP // phosphatidylinositol glycan anchor biosynthesis, class P //	PIGP	1.28E-08	1.92E-05	1.25174	5.06E-07	1.39904
3845365	NM_003200 // TCF3 // transcription factor 3 (E2A immunoglobulin enhancer binding	TCF3	1.29E-08	0.000258259	1.1175	7.56E-08	1.24686
2612175	NM_003298 // NR2C2 // nuclear receptor subfamily 2, group C, member 2 // 3p25 //	NR2C2	1.30E-08	0.313098	1.02281	2.57E-09	-1.22649
2678526	BC132815 // C3orf67 // chromosome 3 open reading frame 67 // 3p14.2 // 200844 //	C3orf67	1.31E-08	1.52E-05	1.36329	6.36E-07	1.57024
3528172	BC110354 // TRA@ // T cell receptor alpha locus // 14q11.2 // 6955 /// BC035680	TRA@	1.31E-08	0.00916678	-1.12832	1.04E-08	-1.46828

3872928	NM_003433 // ZNF132 // zinc finger protein 132 // 19q13.4 // 7691 /// ENST000002	ZNF132	1.31E-08	3.34E-07	-1.44764	3.36E-05	-1.40937
3830993	NM_014266 // HCST // hematopoietic cell signal transducer // 19q13.1 // 10870 //	HCST	1.32E-08	2.00E-05	-1.43632	5.09E-07	-1.72097
2352743	NM_022836 // DCLRE1B // DNA cross-link repair 1B (PSO2 homolog, S. cerevisiae) /	DCLRE1B	1.32E-08	0.42155	1.03561	2.42E-09	1.49088
4017281	NM_017681 // NUP62CL // nucleoporin 62kDa C-terminal like // Xq22.3 // 54830 ///	NUP62CL	1.33E-08	0.000431905	1.21715	5.64E-08	1.51192
2854327	NM_001465 // FYB // FYN binding protein (FYB-120/130) // 5p13.1 // 2533 /// NM_1	FYB	1.34E-08	0.0108379	-1.27484	9.83E-09	-2.2111
2420229	NM_024686 // TTLL7 // tubulin tyrosine ligase-like family, member 7 // 1p31.1 //	TTLL7	1.34E-08	6.17E-07	-1.36048	1.64E-05	-1.36199
3075932	NM_022750 // PARP12 // poly (ADP-ribose) polymerase family, member 12 // 7q34 //	PARP12	1.35E-08	1.89E-05	-1.22705	5.52E-07	-1.35573
3665029	NM_024922 // CES3 // carboxylesterase 3 // 16q22.1 // 23491 /// ENST00000303334	CES3	1.36E-08	1.92E-06	-1.40889	4.71E-06	-1.48422
3696454	NM_001039690 // CTF8 // chromosome transmission fidelity factor 8 homolog (S. ce	CTF8	1.36E-08	0.00174797	1.11746	2.55E-08	1.3194
2434746	NM_018379 // FAM63A // family with sequence similarity 63, member A // 1q21.2 //	FAM63A	1.36E-08	8.08E-05	-1.14999	1.81E-07	-1.27522
3821869	NM_017682 // BEST2 // bestrophin 2 // 19p13.13 // 54831 /// ENST00000042931 // B	BEST2	1.37E-08	4.43E-06	-1.79987	2.06E-06	-2.10572
3602497	NM_173469 // UBE2Q2 // ubiquitin-conjugating enzyme E2Q family member 2 // 15q24	UBE2Q2	1.37E-08	7.92E-06	1.32649	1.20E-06	1.46496
3094286	NM_007198 // PROSC // proline synthetase co-transcribed homolog (bacterial) // 8	PROSC	1.38E-08	9.18E-06	-1.1937	1.06E-06	-1.2752
3274173	NM_014889 // PITRM1 // pitrilysin metallopeptidase 1 // 10p15.2 // 10531 /// ENS	PITRM1	1.38E-08	1.44E-06	1.24169	6.54E-06	1.27212
3759356	NM_004247 // EFTUD2 // elongation factor Tu GTP binding domain containing 2 // 1	EFTUD2	1.38E-08	0.00523607	1.1445	1.45E-08	1.48044
3727583	NM_002126 // HLF // hepatic leukemia factor // 17q22 // 3131 /// ENST00000226067	HLF	1.39E-08	1.91E-07	-1.46162	7.72E-05	-1.381
2573232	NR_000034 // TMEM185B // transmembrane protein 185B (pseudogene) // 2q14.2 // 79	TMEM185B	1.39E-08	0.0029044	1.12758	1.98E-08	1.37787
3433591	NM_153348 // FBXW8 // F-box and WD repeat domain containing 8 // 12q24.22|tdb993	FBXW8	1.39E-08	0.000443485	1.10276	5.87E-08	1.22858
2816459	NM_001992 // F2R // coagulation factor II (thrombin) receptor // 5q13 // 2149 //	F2R	1.40E-08	2.05E-07	1.41189	7.05E-05	1.34496
3607537	NM_001113378 // FANCI // Fanconi anemia, complementation group I // 15q26.1 // 5	FANCI	1.40E-08	0.00514714	1.28501	1.48E-08	2.06818
2531233	NM_007237 // SP140 // SP140 nuclear body protein // 2q37.1 // 11262 /// NM_00100	SP140	1.41E-08	0.000274291	-1.26052	8.06E-08	-1.58522
3502710	NM_007111 // TFDP1 // transcription factor Dp-1 // 13q34 // 7027 /// ENST0000037	TFDP1	1.41E-08	0.0143163	1.09511	9.13E-09	1.36457
2678448	NM_007177 // FAM107A // family with sequence similarity 107, member A // 3p21.1	FAM107A	1.43E-08	1.44E-06	-1.40846	6.93E-06	-1.46147
2593464	NM_153697 // ANKRD44 // ankyrin repeat domain 44 // 2q33.1 // 91526 /// ENST0000	ANKRD44	1.43E-08	0.000865498	-1.26029	4.04E-08	-1.69341
3055999	NM_018044 // NSUN5 // NOL1/NOP2/Sun domain family, member 5 // 7q11.23 // 55695	NSUN5	1.45E-08	0.0376287	1.09801	6.14E-09	1.47334
3399545	NM_015261 // NCAPD3 // non-SMC condensin II complex, subunit D3 // 11q25 // 2331	NCAPD3	1.45E-08	0.0116788	1.14673	1.03E-08	1.57062
3722195	NM_003734 // AOC3 // amine oxidase, copper containing 3 (vascular adhesion prote	AOC3	1.45E-08	2.59E-05	-1.46822	4.68E-07	-1.80073
3159483	NM_153186 // KANK1 // KN motif and ankyrin repeat domains 1 // 9p24.3 // 23189 /	KANK1	1.46E-08	3.57E-07	1.32687	3.68E-05	1.29892
3939707	NM_012295 // CABIN1 // calcineurin binding protein 1 // 22q11.23 // 23523 /// EN	CABIN1	1.46E-08	0.000883265	1.07841	4.09E-08	1.18783
3173831	NM_000144 // FXN // frataxin // 9q13-q21.1 // 2395 /// NM_181425 // FXN // frata	FXN	1.47E-08	0.0425424	1.0963	5.92E-09	1.47953
3856594	NM_003423 // ZNF43 // zinc finger protein 43 // 19p13.1-p12 // 7594 /// ENST0000	ZNF43	1.48E-08	4.35E-05	-1.7358	3.18E-07	-2.44093
2768954	NM_001024611 // LRRC66 // leucine rich repeat containing 66 // 4q12 // 339977 //	LRRC66	1.48E-08	1.70E-06	-1.91639	6.09E-06	-2.08143
2870397	NM_014819 // PJA2 // praja 2, RING-H2 motif containing // 5q21.3 // 9867 /// ENS	PJA2	1.48E-08	0.000198818	-1.356	1.07E-07	-1.79039
2451593	NM_001276 // CHI3L1 // chitinase 3-like 1 (cartilage glycoprotein-39) // 1q32.1	CHI3L1	1.49E-08	0.000126102	1.73482	1.46E-07	2.72178
2613880	NM_152653 // UBE2E2 // ubiquitin-conjugating enzyme E2E 2 (UBC4/5 homolog, yeast	UBE2E2	1.49E-08	9.63E-06	-1.34889	1.13E-06	-1.50792
2681278	NM_015123 // FRMD4B // FERM domain containing 4B // 3p14.1 // 23150 /// ENST0000	FRMD4B	1.49E-08	1.08E-05	-1.33089	1.02E-06	-1.48751
3145564	NM_006294 // UQCRB // ubiquinol-cytochrome c reductase binding protein // 8q22 /	UQCRB	1.49E-08	3.60E-07	-1.49887	3.77E-05	-1.45327
3051868	NM_004577 // PSPH // phosphoserine phosphatase // 7p15.2-p15.1 // 5723 /// ENST0	PSPH	1.50E-08	0.00113731	1.18177	3.63E-08	1.48066
2748163	NM_032117 // MND1 // meiotic nuclear divisions 1 homolog (S. cerevisiae) // 4q31	MND1	1.52E-08	0.000941681	1.26155	4.11E-08	1.7039
3320169	NM_001025390 // AMPD3 // adenosine monophosphate deaminase (isoform E) // 11p15	AMPD3	1.52E-08	5.07E-07	1.15464	2.54E-05	1.14892
3526761	XM_001721602 // LOC100134226 // hypothetical protein LOC100134226 // --- // 1001	LOC100134226	1.54E-08	1.75E-07	1.47316	0.000103771	1.37844
3490655	NM_018204 // CKAP2 // cytoskeleton associated protein 2 // 13q14 // 26586 /// NM	CKAP2	1.54E-08	6.23E-05	1.41697	2.55E-07	1.79485

2905069	NM_173562 // KCTD20 // potassium channel tetramerisation domain containing 20 //	KCTD20	1.54E-08	3.07E-05	1.25026	4.43E-07	1.41478
3845681	NM_130807 // MOBKL2A // MOB1, Mps One Binder kinase activator-like 2A (yeast) //	MOBKL2A	1.55E-08	3.18E-06	-1.21806	3.41E-06	-1.26902
3129234	NM_001010906 // C8orf80 // chromosome 8 open reading frame 80 // 8p21.1 // 38964	C8orf80	1.56E-08	7.06E-07	-1.3176	1.77E-05	-1.31966
3394192	NM_001382 // DPAGT1 // dolichyl-phosphate (UDP-N-acetylglucosamine) N-acetylgluc	DPAGT1	1.56E-08	0.152952	1.06394	3.91E-09	1.47182
3864893	NM_014518 // ZNF229 // zinc finger protein 229 // 19q13.31 // 7772 /// ENST00000	ZNF229	1.57E-08	4.98E-06	-1.27287	2.24E-06	-1.3585
3699080	NM_152649 // MLKL // mixed lineage kinase domain-like // 16q22.3 // 197259 /// E	MLKL	1.57E-08	5.00E-06	1.3051	2.24E-06	1.40244
3845782	NM_018049 // PLEKHJ1 // pleckstrin homology domain containing, family J member 1	PLEKHJ1	1.57E-08	2.02E-08	-1.26958	0.00365088	-1.13668
3129588	NM_015254 // KIF13B // kinesin family member 13B // 8p21.1 // 23303 /// ENST0000	KIF13B	1.58E-08	0.0237987	-1.10035	8.20E-09	-1.43078
3023483	AK290165 // FAM40B // family with sequence similarity 40, member B // 7q32.1 //	FAM40B	1.58E-08	0.00042245	1.31901	7.02E-08	1.77788
3901361	NM_001898 // CST1 // cystatin SN // 20p11.21 // 1469 /// NM_001899 // CST4 // cy	CST1	1.60E-08	1.10E-05	2.06305	1.11E-06	2.72613
3815710	NM_001405 // EFNA2 // ephrin-A2 // 19p13.3 // 1943 /// ENST00000215368 // EFNA2	EFNA2	1.60E-08	2.53E-06	-1.53286	4.53E-06	-1.65015
2970532	NM_001527 // HDAC2 // histone deacetylase 2 // 6q21 // 3066 /// ENST00000398283	HDAC2	1.60E-08	1.61E-06	1.46474	7.32E-06	1.52818
3395464	NM_024769 // ASAM // adipocyte-specific adhesion molecule // 11q24.1 // 79827 //	ASAM	1.61E-08	1.25E-05	-1.36952	9.96E-07	-1.55519
2438282	NM_178229 // IQGAP3 // IQ motif containing GTPase activating protein 3 // 1q22-q	IQGAP3	1.63E-08	0.000407778	1.25398	7.47E-08	1.59601
3728037	NM_021626 // SCPEP1 // serine carboxypeptidase 1 // 17q22 // 59342 /// ENST00000	SCPEP1	1.65E-08	2.17E-06	-1.34877	5.54E-06	-1.41019
3719702	NM_032351 // MRPL45 // mitochondrial ribosomal protein L45 // 17q21.2 // 84311 /	MRPL45	1.65E-08	4.44E-05	1.25643	3.62E-07	1.44412
3450861	NM_005164 // ABCD2 // ATP-binding cassette, sub-family D (ALD), member 2 // 12q1	ABCD2	1.66E-08	2.72E-05	-1.26102	5.38E-07	-1.42444
3281068	NM_005028 // PIP4K2A // phosphatidylinositol-5-phosphate 4-kinase, type II, alph	PIP4K2A	1.66E-08	0.0166544	-1.11276	1.02E-08	-1.45181
2513925	NM_020981 // B3GALT1 // UDP-Gal:betaGlcNAc beta 1,3-galactosyltransferase, polyp	B3GALT1	1.67E-08	0.000366959	-1.5696	8.22E-08	-2.5059
3354799	NM_001114122 // CHEK1 // CHK1 checkpoint homolog (S. pombe) // 11q24-q24 // 1111	CHEK1	1.67E-08	0.00313032	1.2926	2.34E-08	1.98563
3037839	NM_001037763 // COL28A1 // collagen, type XXVIII, alpha 1 // 7p21.3 // 340267 //	COL28A1	1.68E-08	1.96E-06	-1.35527	6.37E-06	-1.41105
3154136	NM_012472 // LRRC6 // leucine rich repeat containing 6 // 8q24.22 // 23639 /// E	LRRC6	1.72E-08	1.11E-05	1.733	1.21E-06	2.13507
4000704	NM_003916 // AP1S2 // adaptor-related protein complex 1, sigma 2 subunit // Xp22	AP1S2	1.72E-08	4.91E-05	-1.2195	3.52E-07	-1.38013
3721886	NM_170607 // MLX // MAX-like protein X // 17q21.1 // 6945 /// NM_198204 // MLX /	MLX	1.72E-08	1.11E-06	-1.26601	1.24E-05	-1.28226
2569649	NM_022336 // EDAR // ectodysplasin A receptor // 2q11-q13 // 10913 /// ENST00000	EDAR	1.72E-08	7.01E-08	1.61887	0.000501435	1.39896
3191391	AL834139 // HMCN2 // hemicentin 2 // 9q34.11 // 256158 /// AK093583 // HMCN2 //	HMCN2	1.73E-08	9.79E-08	-1.32218	0.000299081	-1.22974
3542145	BC064697 // KIAA0247 // KIAA0247 // 14q24.1 // 9766 /// ENST00000342745 // KIAA0	KIAA0247	1.73E-08	4.26E-05	-1.19757	3.99E-07	-1.33377
3438617	NM_015409 // EP400 // E1A binding protein p400 // 12q24.33 // 57634 /// NR_00297	EP400	1.76E-08	7.68E-08	1.1555	0.00045098	1.10752
3129361	NM_172366 // FBXO16 // F-box protein 16 // 8p21.1 // 157574 /// ENST00000380254	FBXO16	1.76E-08	2.69E-05	1.39447	5.90E-07	1.65605
2835021	NM_024028 // PCYOX1L // prenylcysteine oxidase 1 like // 5q33.1 // 78991 /// ENS	PCYOX1L	1.76E-08	2.48E-05	1.19092	6.30E-07	1.30053
3442579	NM_031491 // RBP5 // retinol binding protein 5, cellular // 12p13.31 // 83758 //	RBP5	1.77E-08	0.000560059	-1.25	6.74E-08	-1.61032
3402899	NM_001098536 // USP5 // ubiquitin specific peptidase 5 (isopeptidase T) // 12p13	USP5	1.78E-08	0.290743	1.04118	3.63E-09	1.40985
2621451	NM_138615 // DHX30 // DEAH (Asp-Glu-Ala-His) box polypeptide 30 // 3p21.31 // 22	DHX30	1.78E-08	9.17E-05	1.10772	2.31E-07	1.19421
3046062	NM_001637 // AOAH // acyloxyacyl hydrolase (neutrophil) // 7p14-p12 // 313 /// E	AOAH	1.79E-08	3.00E-06	-1.58924	4.48E-06	-1.73129
3539499	NM_020663 // RHOJ // ras homolog gene family, member J // 14q23.2 // 57381 /// E	RHOJ	1.79E-08	9.28E-06	-1.38795	1.51E-06	-1.55547
3607503	NM_007011 // ABHD2 // abhydrolase domain containing 2 // 15q26.1 // 11057 /// NM	ABHD2	1.79E-08	1.06E-06	1.34447	1.39E-05	1.36203
3142381	NM_001442 // FABP4 // fatty acid binding protein 4, adipocyte // 8q21 // 2167 //	FABP4	1.80E-08	1.36E-05	-1.70019	1.08E-06	-2.10881
2484520	BC014578 // C2orf74 // chromosome 2 open reading frame 74 // 2p15 // 339804	C2orf74	1.81E-08	7.85E-05	-1.2915	2.64E-07	-1.54622
3468261	NM_024057 // NUP37 // nucleoporin 37kDa // 12q23.2 // 79023 /// ENST00000251074	NUP37	1.81E-08	0.000111354	1.31793	2.04E-07	1.63057
2732508	NM_006419 // CXCL13 // chemokine (C-X-C motif) ligand 13 // 4q21 // 10563 /// EN	CXCL13	1.81E-08	0.00348723	-1.81405	2.43E-08	-5.00003
2881672	NM_006058 // TNIP1 // TNFAIP3 interacting protein 1 // 5q32-q33.1 // 10318 /// E	TNIP1	1.82E-08	6.56E-06	-1.17567	2.13E-06	-1.23305
3369249	NM_015957 // APIP // APAF1 interacting protein // 11p13 // 51074 /// ENST0000027	APIP	1.84E-08	0.000176937	1.55684	1.50E-07	2.28181

3569257	NM_016445 // PLEK2 // pleckstrin 2 // 14q23.3 // 26499 /// ENST00000216446 // PL	PLEK2	1.85E-08	0.00480452	1.23722	2.10E-08	1.82585
3212848	NM_016548 // GOLM1 // golgi membrane protein 1 // 9q21.33 // 51280 /// NM_177937	GOLM1	1.87E-08	8.77E-05	-1.37315	2.53E-07	-1.72598
2522094	NM_001100422 // LOC26010 // viral DNA polymerase-transactivated protein 6 // 2q3	LOC26010	1.87E-08	2.42E-06	-1.34201	6.00E-06	-1.40265
3947123	NM_004599 // SREBF2 // sterol regulatory element binding transcription factor 2	SREBF2	1.89E-08	7.84E-08	-1.26303	0.000499286	-1.17782
3033531	AK124321 // tcag7.1275 // hypothetical LOC389602 // 7q36.3 // 389602 /// ENST000	tcag7.1275	1.89E-08	0.000119929	1.88783	2.05E-07	3.10033
2995254	NM_152793 // C7orf41 // chromosome 7 open reading frame 41 // 7p15.1 // 222166 /	C7orf41	1.89E-08	1.40E-07	1.57681	0.000206407	1.42443
3902743	NM_080616 // C20orf112 // chromosome 20 open reading frame 112 // 20q11.1-q11.23	C20orf112	1.90E-08	4.82E-06	-1.58356	3.04E-06	-1.77268
3824540	NM_015122 // FCHO1 // FCH domain only 1 // 19p13.11 // 23149 /// ENST00000252771	FCHO1	1.92E-08	9.03E-07	1.46024	1.85E-05	1.46916
2863363	NM_004101 // F2RL2 // coagulation factor II (thrombin) receptor-like 2 // 5q13 /	F2RL2	1.92E-08	5.62E-05	1.44347	3.67E-07	1.82278
3943101	NM_014662 // DEPDC5 // DEP domain containing 5 // 22q12.3 // 9681 /// NM_0010071	DEPDC5	1.93E-08	3.79E-07	-1.19894	5.42E-05	-1.178
3333226	NM_004111 // FEN1 // flap structure-specific endonuclease 1 // 11q12 // 2237 ///	FEN1	1.94E-08	0.325489	1.05063	3.84E-09	1.57007
2449711	NM_144977 // DENND1B // DENN/MADD domain containing 1B // 1q31.3 // 163486 /// E	DENND1B	1.95E-08	0.000329757	-1.26884	1.07E-07	-1.60774
3775157	NM_019613 // WDR45L // WDR45-like // 17q25.3 // 56270 /// ENST00000392325 // WDR	WDR45L	1.96E-08	0.00623852	1.09867	1.96E-08	1.31801
2676854	NM_018397 // CHDH // choline dehydrogenase // 3p21.1 // 55349 /// ENST0000031525	CHDH	1.97E-08	3.88E-06	1.24989	3.99E-06	1.31004
2327219	NM_177424 // STX12 // syntaxin 12 // 1p35-p34.1 // 23673 /// ENST00000373943 //	STX12	1.98E-08	7.38E-07	-1.43564	2.46E-05	-1.42872
2855578	BC013351 // C5orf28 // chromosome 5 open reading frame 28 // 5p12 // 64417 /// B	C5orf28	1.98E-08	9.50E-06	1.29034	1.70E-06	1.4075
2493858	NM_002371 // MAL // mal, T-cell differentiation protein // 2cen-q13 // 4118 ///	MAL	1.98E-08	5.56E-06	-1.38531	2.80E-06	-1.5088
3255491	AK056561 // LOC170425 // hypothetical protein LOC170425 // 10q23.1 // 170425	LOC170425	1.98E-08	6.21E-07	2.27441	3.05E-05	2.20772
2869096	NM_180991 // SLCO4C1 // solute carrier organic anion transporter family, member	SLCO4C1	1.99E-08	0.00560576	-1.21577	2.10E-08	-1.75687
3693214	NM_018110 // DOK4 // docking protein 4 // 16q13 // 55715 /// ENST00000340099 //	DOK4	2.00E-08	4.55E-07	-1.3226	4.58E-05	-1.29419
3662387	NM_014685 // HERPUD1 // homocysteine-inducible, endoplasmic reticulum stress-ind	HERPUD1	2.01E-08	1.19E-06	-1.4439	1.44E-05	-1.4697
3420151	NM_001031679 // MSRB3 // methionine sulfoxide reductase B3 // 12q14.3 // 253827	MSRB3	2.01E-08	1.89E-06	-1.34926	8.65E-06	-1.3944
3315607	NM_025092 // ATHL1 // ATH1, acid trehalase-like 1 (yeast) // 11p15.5 // 80162 //	ATHL1	2.02E-08	1.74E-06	1.52604	9.56E-06	1.59047
3423002	AK074510 // LOC652993 // hypothetical LOC652993 // 12q21 // 652993	LOC652993	2.03E-08	0.000208525	1.28001	1.52E-07	1.59342
3415668	NM_170754 // TENC1 // tensin like C1 domain containing phosphatase (tensin 2) //	TENC1	2.04E-08	5.49E-06	-1.18858	2.97E-06	-1.24252
2481142	NM_000179 // MSH6 // mutS homolog 6 (E. coli) // 2p16 // 2956 /// ENST0000023442	MSH6	2.04E-08	0.00063424	1.16455	7.39E-08	1.38756
2358360	NM_004425 // ECM1 // extracellular matrix protein 1 // 1q21 // 1893 /// NM_02266	ECM1	2.06E-08	5.38E-05	1.50249	4.15E-07	1.9342
3831143	NM_001281 // TBCB // tubulin folding cofactor B // 19q13.11-q13.12 // 1155 /// E	TBCB	2.07E-08	0.00209848	1.12189	3.72E-08	1.33343
2379754	NM_020197 // SMYD2 // SET and MYND domain containing 2 // 1q41 // 56950 /// ENST	SMYD2	2.08E-08	5.15E-06	1.35295	3.26E-06	1.45721
2438344	NM_182679 // GPATCH4 // G patch domain containing 4 // 1q22 // 54865 /// NM_0155	GPATCH4	2.09E-08	5.07E-06	1.22725	3.32E-06	1.28984
3042012	NM_138811 // C7orf31 // chromosome 7 open reading frame 31 // 7p15.2 // 136895 /	C7orf31	2.09E-08	1.92E-06	-1.42706	9.06E-06	-1.4827
3683018	NM_001019 // RPS15A // ribosomal protein S15a // 16p // 6210 /// NM_001030009 //	RPS15A	2.10E-08	0.00270744	1.22875	3.29E-08	1.70434
3874751	NM_000311 // PRNP // prion protein // 20p13 // 5621 /// NM_183079 // PRNP // pri	PRNP	2.11E-08	0.000404658	-1.36127	1.03E-07	-1.87228
3373893	NM_003627 // SLC43A1 // solute carrier family 43, member 1 // 11p11.2-p11.1 // 8	SLC43A1	2.11E-08	1.58E-05	1.25557	1.18E-06	1.37892
3734379	NM_007261 // CD300A // CD300a molecule // 17q25.1 // 11314 /// ENST00000360141 /	CD300A	2.17E-08	6.34E-07	-1.40174	3.44E-05	-1.3815
2742935	NM_014278 // HSPA4L // heat shock 70kDa protein 4-like // 4q28 // 22824 /// ENST	HSPA4L	2.17E-08	3.83E-06	1.82275	4.64E-06	2.05423
3294576	NM_152586 // USP54 // ubiquitin specific peptidase 54 // 10q22.2 // 159195 /// E	USP54	2.18E-08	2.86E-07	1.40516	9.77E-05	1.3365
3933817	NM_018669 // WDR4 // WD repeat domain 4 // 21q22.3 // 10785 /// NM_033661 // WDR	WDR4	2.20E-08	0.080062	1.07872	7.08E-09	1.4532
2407439	NM_006802 // SF3A3 // splicing factor 3a, subunit 3, 60kDa // 1p34.3 // 10946 //	SF3A3	2.22E-08	7.73E-07	1.30119	2.81E-05	1.29443
2832459	NM_018934 // PCDHB14 // protocadherin beta 14 // 5q31 // 56122 /// ENST000002394	PCDHB14	2.23E-08	8.86E-08	1.81087	0.00056118	1.51323
3329029	NM_021117 // CRY2 // cryptochrome 2 (photolyase-like) // 11p11.2 // 1408 /// NM_	CRY2	2.24E-08	4.55E-06	-1.14863	4.08E-06	-1.18427
2317434	NM_182752 // TPRG1L // tumor protein p63 regulated 1-like // 1p36.32 // 127262 /	TPRG1L	2.26E-08	5.20E-07	-1.2738	4.71E-05	-1.25143

3076882	NM_176817 // TAS2R38 // taste receptor, type 2, member 38 // 7q34 // 5726 /// EN	TAS2R38	2.26E-08	3.09E-06	1.72665	6.13E-06	1.8895
3355021	NM_024556 // FAM118B // family with sequence similarity 118, member B // 11q24.2	FAM118B	2.26E-08	6.83E-07	-1.30989	3.36E-05	-1.2966
3556816	NM_003982 // SLC7A7 // solute carrier family 7 (cationic amino acid transporter,	SLC7A7	2.29E-08	9.75E-07	-1.59676	2.24E-05	-1.60247
3402522	NM_018009 // TAPBPL // TAP binding protein-like // 12p13.31 // 55080 /// ENST000	TAPBPL	2.31E-08	9.22E-08	-1.27683	0.000563195	-1.18619
3203524	NM_001170 // AQP7 // aquaporin 7 // 9p13 // 364 /// NR_002817 // AQP7P1 // aquap	AQP7	2.33E-08	6.57E-07	-1.62919	3.71E-05	-1.59294
3300115	NM_005398 // PPP1R3C // protein phosphatase 1, regulatory (inhibitor) subunit 3C	PPP1R3C	2.34E-08	3.43E-07	-1.64606	8.58E-05	-1.54196
3329099	NM_152312 // GYLTL1B // glycosyltransferase-like 1B // 11p11.2 // 120071 /// ENS	GYLTL1B	2.34E-08	1.07E-06	1.41198	2.07E-05	1.42069
3204243	NM_005866 // OPRS1 // opioid receptor, sigma 1 // 9p13.3 // 10280 /// NM_147157	OPRS1	2.34E-08	0.163236	1.05657	5.81E-09	1.41354
3504617	NM_145061 // C13orf3 // chromosome 13 open reading frame 3 // 13q12.11 // 221150	C13orf3	2.34E-08	0.0340147	1.16937	1.07E-08	1.8591
2967769	BC131628 // KIAA1553 // KIAA1553 // 6q21 // 57673 /// NM_001080450 // KIAA1553 /	KIAA1553	2.37E-08	2.65E-05	1.17822	8.83E-07	1.2755
2486927	NM_014882 // ARHGAP25 // Rho GTPase activating protein 25 // 2p14 // 9938 /// NM	ARHGAP25	2.39E-08	0.000915009	-1.21081	7.12E-08	-1.53191
2328320	NM_022164 // TINAGL1 // tubulointerstitial nephritis antigen-like 1 // 1p35.2 //	TINAGL1	2.39E-08	3.28E-07	1.29147	9.44E-05	1.24632
2452977	NM_005449 // FAIM3 // Fas apoptotic inhibitory molecule 3 // 1q32.1 // 9214 ///	FAIM3	2.41E-08	0.000252045	-1.46841	1.65E-07	-2.08222
3944690	NM_013385 // CYTH4 // cytohesin 4 // 22q12.3-q13.1 // 27128 /// ENST00000248901	CYTH4	2.46E-08	1.49E-05	-1.32609	1.53E-06	-1.4793
2829171	NM_003202 // TCF7 // transcription factor 7 (T-cell specific, HMG-box) // 5q31.1	TCF7	2.46E-08	2.87E-07	1.42145	0.000119504	1.34364
3726569	NM_022827 // SPATA20 // spermatogenesis associated 20 // 17q21.33 // 64847 /// E	SPATA20	2.46E-08	0.0029783	1.11753	3.74E-08	1.33519
2862274	BC043557 // LOC340090 // hypothetical protein LOC340090 // 5q13.3 // 340090	LOC340090	2.48E-08	9.66E-07	-1.47398	2.58E-05	-1.47269
3842301	NM_016535 // ZNF581 // zinc finger protein 581 // 19q13.42 // 51545 /// ENST0000	ZNF581	2.53E-08	3.64E-05	1.20511	7.42E-07	1.33039
3301512	NM_002860 // ALDH18A1 // aldehyde dehydrogenase 18 family, member A1 // 10q24.3	ALDH18A1	2.54E-08	4.32E-08	-1.27981	0.00243711	-1.15446
3435154	NM_020993 // BCL7A // B-cell CLL/lymphoma 7A // 12q24.13 // 605 /// NM_001024808	BCL7A	2.55E-08	0.0415193	1.0529	1.08E-08	1.23729
3624145	NM_015263 // DMXL2 // Dmx-like 2 // 15q21.2 // 23312 /// ENST00000251076 // DMXL	DMXL2	2.55E-08	0.00147149	-1.26161	5.79E-08	-1.73081
3230282	NM_006412 // AGPAT2 // 1-acylglycerol-3-phosphate O-acyltransferase 2 (lysophosp	AGPAT2	2.60E-08	1.60E-08	-1.45777	0.0179082	-1.17364
2407191	NM_013285 // GNL2 // guanine nucleotide binding protein-like 2 (nucleolar) // 1p	GNL2	2.60E-08	8.86E-05	1.25643	3.84E-07	1.46965
2747961	NM_033393 // FHDC1 // FH2 domain containing 1 // 4q31.3 // 85462 /// ENST0000026	FHDC1	2.63E-08	7.11E-06	1.28774	3.34E-06	1.37806
2426385	NM_006113 // VAV3 // vav 3 guanine nucleotide exchange factor // 1p13.3 // 10451	VAV3	2.66E-08	0.00337997	-1.17507	3.80E-08	-1.53047
2693217	NM_022776 // OSBPL11 // oxysterol binding protein-like 11 // 3q21 // 114885 ///	OSBPL11	2.67E-08	2.24E-07	-1.52067	0.000194715	-1.39756
3325680	NM_006360 // EIF3M // eukaryotic translation initiation factor 3, subunit M // 1	EIF3M	2.70E-08	1.06E-05	1.4035	2.36E-06	1.56726
4017381	NM_198057 // TSC22D3 // TSC22 domain family, member 3 // Xq22.3 // 1831 /// NM_0	TSC22D3	2.70E-08	2.11E-05	-1.36617	1.28E-06	-1.56366
3464912	NM_172240 // WDR51B // WD repeat domain 51B // 12q21.33 // 282809 /// ENST000003	WDR51B	2.72E-08	4.10E-06	1.69711	6.02E-06	1.87207
3565571	NM_007086 // WDHD1 // WD repeat and HMG-box DNA binding protein 1 // 14q22.3 //	WDHD1	2.72E-08	0.0389983	1.15496	1.19E-08	1.79434
3212008	NM_174938 // FRMD3 // FERM domain containing 3 // 9q21.32 // 257019 /// ENST0000	FRMD3	2.75E-08	4.10E-06	-1.51357	6.12E-06	-1.6337
3598721	NR_003105 // ZWILCH // Zwilch, kinetochore associated, homolog (Drosophila) // 1	ZWILCH	2.75E-08	0.247113	1.06829	5.97E-09	1.65185
3339971	NM_021200 // PLEKHB1 // pleckstrin homology domain containing, family B (evectin	PLEKHB1	2.76E-08	1.08E-05	1.41408	2.40E-06	1.5829
2428501	NM_003051 // SLC16A1 // solute carrier family 16, member 1 (monocarboxylic acid	SLC16A1	2.79E-08	1.94E-07	-1.99823	0.000258512	-1.70987
4001850	NM_031892 // SH3KBP1 // SH3-domain kinase binding protein 1 // Xp22.1-p21.3 // 3	SH3KBP1	2.80E-08	1.79E-05	-1.24261	1.55E-06	-1.35618
3360772	NM_032127 // FAM160A2 // family with sequence similarity 160, member A2 // 11p15	FAM160A2	2.80E-08	4.80E-06	-1.22382	5.37E-06	-1.27545
2859195	NM_014473 // DIMT1L // DIM1 dimethyladenosine transferase 1-like (S. cerevisiae)	DIMT1L	2.82E-08	1.75E-05	1.30875	1.60E-06	1.45679
2774365	NM_006835 // CCNI // cyclin I // 4q21.1 // 10983 /// ENST00000237654 // CCNI //	CCNI	2.82E-08	6.88E-08	1.27198	0.00133907	1.1648
3476796	NM_032656 // DHX37 // DEAH (Asp-Glu-Ala-His) box polypeptide 37 // 12q24.31 // 5	DHX37	2.83E-08	0.000694074	1.12458	1.03E-07	1.28471
2409220	NM_006824 // EBNA1BP2 // EBNA1 binding protein 2 // 1p35-p33 // 10969 /// ENST00	EBNA1BP2	2.84E-08	0.000181477	1.25255	2.54E-07	1.50646
3721926	NM_001070 // TUBG1 // tubulin, gamma 1 // 17q21 // 7283 /// ENST00000251413 // T	TUBG1	2.86E-08	0.786106	1.01671	4.70E-09	1.72796
3367096	NM_018490 // LGR4 // leucine-rich repeat-containing G protein-coupled receptor 4	LGR4	2.87E-08	9.12E-05	-1.2947	4.26E-07	-1.54381

3235726	NM_001008211 // OPTN // optineurin // 10p13 // 10133 /// NM_001008213 // OPTN //	OPTN	2.88E-08	0.00136603	-1.22776	6.97E-08	-1.61049
3009399	NM_001540 // HSPB1 // heat shock 27kDa protein 1 // 7q11.23 // 3315 /// ENST0000	HSPB1	2.89E-08	1.98E-08	-1.45952	0.014572	-1.18256
2462329	NM_019891 // ERO1LB // ERO1-like beta (S. cerevisiae) // 1q42.2-q43 // 56605 ///	ERO1LB	2.89E-08	0.000796961	-1.20679	9.72E-08	-1.50311
3638760	NM_002168 // IDH2 // isocitrate dehydrogenase 2 (NADP+), mitochondrial // 15q26.	IDH2	2.90E-08	0.00691406	1.15728	2.87E-08	1.53283
3645359	NM_145252 // LOC124220 // similar to common salivary protein 1 // 16p13.3 // 124	LOC124220	2.90E-08	2.98E-05	1.34067	1.05E-06	1.54386
2700404	NM_015472 // WWTR1 // WW domain containing transcription regulator 1 // 3q23-q24	WWTR1	2.92E-08	0.000106537	-1.27584	3.87E-07	-1.51655
3031544	NM_130759 // GIMAP1 // GTPase, IMAP family member 1 // 7q36.1 // 170575 /// ENST	GIMAP1	2.92E-08	0.000689697	-1.16122	1.08E-07	-1.37456
3310041	NM_000141 // FGFR2 // fibroblast growth factor receptor 2 // 10q26 // 2263 /// N	FGFR2	2.93E-08	1.05E-06	-1.54969	3.04E-05	-1.54357
2688717	NM_181780 // BTLA // B and T lymphocyte associated // 3q13.2 // 151888 /// NM_00	BTLA	2.94E-08	0.000492696	-1.42702	1.34E-07	-2.0673
3815243	NM_001928 // CFD // complement factor D (adipsin) // 19p13.3 // 1675 /// ENST000	CFD	2.94E-08	4.77E-08	-1.61957	0.00276102	-1.32054
3072546	NM_018718 // TSGA14 // testis specific, 14 // 7q32 // 95681 /// ENST00000223208	TSGA14	2.95E-08	0.000340291	1.11314	1.72E-07	1.23293
3262535	NM_183239 // GSTO2 // glutathione S-transferase omega 2 // 10q25.1 // 119391 ///	GSTO2	2.95E-08	2.08E-05	1.22367	1.47E-06	1.33202
3331903	AY457926 // FAM111B // family with sequence similarity 111, member B // 11q12.1	FAM111B	2.99E-08	0.0124532	1.28604	2.22E-08	2.24745
3627422	NM_134260 // RORA // RAR-related orphan receptor A // 15q21-q22 // 6095 /// NM_0	RORA	3.00E-08	0.0147288	-1.13619	2.05E-08	-1.52722
2891052	NM_006098 // GNB2L1 // guanine nucleotide binding protein (G protein), beta poly	GNB2L1	3.00E-08	1.47E-05	1.2402	2.04E-06	1.34136
3155489	NM_015912 // FAM135B // family with sequence similarity 135, member B // 8q24.23	FAM135B	3.02E-08	2.35E-07	-1.45071	0.000225679	-1.34215
2326993	NM_032872 // SYTL1 // synaptotagmin-like 1 // 1p36.11 // 84958 /// ENST000003180	SYTL1	3.02E-08	3.01E-06	1.38461	9.74E-06	1.44485
3307939	NM_002313 // ABLIM1 // actin binding LIM protein 1 // 10q25 // 3983 /// NM_00100	ABLIM1	3.04E-08	3.88E-06	1.24217	7.55E-06	1.28759
2343289	NM_007034 // DNAJB4 // DnaJ (Hsp40) homolog, subfamily B, member 4 // 1p31.1 //	DNAJB4	3.05E-08	2.00E-05	-1.61677	1.58E-06	-1.96985
2995589	NM_198098 // AQP1 // aquaporin 1 (Colton blood group) // 7p14 // 358 /// ENST000	AQP1	3.05E-08	0.00136151	-1.30749	7.48E-08	-1.85968
3707214	NM_002663 // PLD2 // phospholipase D2 // 17p13.1 // 5338 /// ENST00000263088 //	PLD2	3.05E-08	5.89E-07	1.19891	6.63E-05	1.17958
2672016	NM_024513 // FYCO1 // FYVE and coiled-coil domain containing 1 // 3p21.31 // 794	FYCO1	3.07E-08	1.01E-07	1.21688	0.0008331	1.14207
3940185	NM_004175 // SNRPD3 // small nuclear ribonucleoprotein D3 polypeptide 18kDa // 2	SNRPD3	3.10E-08	0.000852662	1.12756	1.01E-07	1.29884
3772661	NM_003255 // TIMP2 // TIMP metallopeptidase inhibitor 2 // 17q25 // 7077 /// ENS	TIMP2	3.11E-08	0.00394995	-1.29962	4.17E-08	-2.01646
2738314	NM_001031720 // GSTCD // glutathione S-transferase, C-terminal domain containing	GSTCD	3.13E-08	0.000315568	1.17054	1.95E-07	1.35501
3048631	NM_015332 // NUDCD3 // NudC domain containing 3 // 7p13-p12 // 23386 /// ENST000	NUDCD3	3.14E-08	9.95E-05	1.14922	4.47E-07	1.26468
3421985	NM_014505 // KCNMB4 // potassium large conductance calcium-activated channel, su	KCNMB4	3.16E-08	4.56E-07	-1.32699	9.78E-05	-1.2802
3959613	NM_024955 // FOXRED2 // FAD-dependent oxidoreductase domain containing 2 // 22q1	FOXRED2	3.17E-08	0.0417177	1.07856	1.36E-08	1.36273
3822074	NM_005053 // RAD23A // RAD23 homolog A (S. cerevisiae) // 19p13.2 // 5886 /// EN	RAD23A	3.17E-08	0.00315365	1.10149	4.83E-08	1.28425
3449910	NR_004854 // AMN1 // antagonist of mitotic exit network 1 homolog (S. cerevisiae	AMN1	3.18E-08	0.000125817	1.23093	3.81E-07	1.43331
3532793	NM_006194 // PAX9 // paired box 9 // 14q12-q13 // 5083 /// ENST00000402703 // PA	PAX9	3.20E-08	2.30E-06	1.57048	1.42E-05	1.63381
2621705	NM_130384 // ATRIP // ATR interacting protein // 3p21.31 // 84126 /// NM_032166	ATRIP	3.21E-08	0.00150921	1.08776	7.47E-08	1.21742
3145953	NM_000989 // RPL30 // ribosomal protein L30 // 8q22 // 6156 /// NR_002581 // SNO	RPL30	3.22E-08	3.55E-05	1.23501	1.04E-06	1.37248
3905875	NM_005461 // MAFB // v-maf musculoaponeurotic fibrosarcoma oncogene homolog B (a	MAFB	3.26E-08	5.44E-06	-1.25587	5.91E-06	-1.31639
3699757	NM_005548 // KARS // lysyl-tRNA synthetase // 16q23-q24 // 3735 /// ENST00000319	KARS	3.28E-08	0.00013734	1.22514	3.72E-07	1.42569
3638660	NR_023361 // AP3S2 // adaptor-related protein complex 3, sigma 2 subunit // 15q2	AP3S2	3.33E-08	3.48E-07	-1.48079	0.000154267	-1.38605
2439052	NM_030764 // FCRL2 // Fc receptor-like 2 // 1q21 // 79368 /// NM_138738 // FCRL2	FCRL2	3.36E-08	3.09E-05	-1.30936	1.24E-06	-1.48697
3771543	NM_022066 // UBE2O // ubiquitin-conjugating enzyme E2O // 17q25.1 // 63893 /// E	UBE2O	3.37E-08	5.26E-05	1.13177	8.05E-07	1.21346
3845909	NM_032737 // LMNB2 // lamin B2 // 19p13.3 // 84823 /// ENST00000325327 // LMNB2	LMNB2	3.38E-08	0.0771338	1.06905	1.13E-08	1.37641
2725013	NM_004181 // UCHL1 // ubiquitin carboxyl-terminal esterase L1 (ubiquitin thioles	UCHL1	3.42E-08	1.17E-07	-1.46197	0.000810046	-1.29631
4019784	NM_017938 // FAM70A // family with sequence similarity 70, member A // Xq24 // 5	FAM70A	3.42E-08	1.36E-05	-1.30038	2.63E-06	-1.42101
3799542	NM_024899 // CEP76 // centrosomal protein 76kDa // 18p11.21 // 79959 /// ENST000	CEP76	3.44E-08	1.41E-05	1.21537	2.56E-06	1.29951

3565663	NM_014750 // DLGAP5 // discs, large (Drosophila) homolog-associated protein 5 //	DLGAP5	3.44E-08	0.00387267	1.33273	4.74E-08	2.14335
3824874	NM_006332 // IFI30 // interferon, gamma-inducible protein 30 // 19p13.1 // 10437	IFI30	3.48E-08	7.93E-06	-1.42569	4.47E-06	-1.56059
2420808	NM_003921 // BCL10 // B-cell CLL/lymphoma 10 // 1p22 // 8915 /// ENST00000394761	BCL10	3.48E-08	7.18E-06	-1.29621	4.93E-06	-1.37955
3513953	NM_020456 // C13orf1 // chromosome 13 open reading frame 1 // 13q14 // 57213 ///	C13orf1	3.52E-08	3.59E-08	-1.25555	0.00682424	-1.12279
3992148	NM_182540 // DDX26B // DEAD/H (Asp-Glu-Ala-Asp/His) box polypeptide 26B // Xq26.	DDX26B	3.53E-08	0.00113413	-1.30377	9.89E-08	-1.8124
3395735	NM_003455 // ZNF202 // zinc finger protein 202 // 11q23.3 // 7753 /// ENST000003	ZNF202	3.54E-08	2.44E-05	1.20081	1.63E-06	1.29845
3227696	NM_198679 // RAPGEF1 // Rap guanine nucleotide exchange factor (GEF) 1 // 9q34.3	RAPGEF1	3.55E-08	3.49E-06	-1.17625	1.06E-05	-1.20227
3722084	NM_032387 // WNK4 // WNK lysine deficient protein kinase 4 // 17q21-q22 // 65266	WNK4	3.57E-08	1.41E-06	1.40074	2.92E-05	1.40538
2792166	NM_017923 // MARCH1 // membrane-associated ring finger (C3HC4) 1 // 4q32.3 // 55	MARCH1	3.59E-08	0.000149191	-1.50333	3.93E-07	-2.04346
3595096	NM_207036 // TCF12 // transcription factor 12 // 15q21 // 6938 /// NM_207037 //	TCF12	3.62E-08	4.81E-06	1.46005	7.82E-06	1.5617
3687241	BC150579 // C16orf53 // chromosome 16 open reading frame 53 // 16p11.2 // 79447	C16orf53	3.63E-08	4.24E-07	-1.48717	0.00013683	-1.40009
3129258	NM_001010906 // C8orf80 // chromosome 8 open reading frame 80 // 8p21.1 // 38964	C8orf80	3.64E-08	8.38E-07	-1.64117	5.68E-05	-1.5914
4047607	NM_024850 // BTNL8 // butyrophilin-like 8 // 5q35.3 // 79908 /// NM_001040462 //	BTNL8	3.66E-08	2.41E-06	-1.92196	1.66E-05	-2.02487
2476510	NM_206943 // LTBP1 // latent transforming growth factor beta binding protein 1 /	LTBP1	3.67E-08	2.32E-07	1.31266	0.000324905	1.232
3822593	BC011002 // LOC113230 // hypothetical protein LOC113230 // 19p13.12 // 113230	LOC113230	3.67E-08	0.00181525	1.14126	7.81E-08	1.36944
3105033	NM_152284 // CHMP4C // chromatin modifying protein 4C // 8q21.13 // 92421 /// EN	CHMP4C	3.67E-08	3.18E-06	1.26258	1.23E-05	1.29776
2877990	NM_198282 // TMEM173 // transmembrane protein 173 // 5q31.2 // 340061 /// ENST00	TMEM173	3.72E-08	4.12E-07	1.27972	0.000148681	1.23056
3032243	NM_022087 // GALNT11 // UDP-N-acetyl-alpha-D-galactosamine:polypeptide N-acetylg	GALNT11	3.72E-08	0.00233619	1.13131	6.87E-08	1.35468
2993639	NM_016587 // CBX3 // chromobox homolog 3 (HP1 gamma homolog, Drosophila) // 7p15	CBX3	3.73E-08	0.000591784	1.15455	1.59E-07	1.3444
3214749	NM_017948 // NOL8 // nucleolar protein 8 // 9q22.31 // 55035 /// ENST00000358855	NOL8	3.76E-08	1.13E-05	1.33023	3.56E-06	1.44905
3490892	NM_006418 // OLFM4 // olfactomedin 4 // 13q21.1 // 10562 /// ENST00000219022 //	OLFM4	3.77E-08	0.000619204	2.22941	1.56E-07	5.25604
3226493	NM_015679 // TRUB2 // TruB pseudouridine (psi) synthase homolog 2 (E. coli) // 9	TRUB2	3.78E-08	0.255664	1.05818	8.21E-09	1.53975
2830638	NM_005733 // KIF20A // kinesin family member 20A // 5q31 // 10112 /// ENST000003	KIF20A	3.80E-08	0.000990759	1.38341	1.17E-07	2.03841
2638676	NM_018456 // EAF2 // ELL associated factor 2 // 3q13.33 // 55840 /// ENST0000027	EAF2	3.80E-08	0.000300222	-1.35138	2.56E-07	-1.76972
2334314	NM_032756 // HPDL // 4-hydroxyphenylpyruvate dioxygenase-like // 1p34.1 // 84842	HPDL	3.83E-08	9.60E-05	1.33332	5.93E-07	1.61177
3121054	NR_003572 // FLJ45055 // 60S ribosomal pseudogene // 8p23.3 // 644128 /// NM_001	FLJ45055	3.84E-08	0.000110806	1.25431	5.33E-07	1.46546
3241316	NM_030751 // ZEB1 // zinc finger E-box binding homeobox 1 // 10p11.2 // 6935 ///	ZEB1	3.84E-08	2.58E-05	-1.31392	1.74E-06	-1.47652
3019793	NM_148898 // FOXP2 // forkhead box P2 // 7q31 // 93986 /// NM_148899 // FOXP2 //	FOXP2	3.87E-08	5.25E-05	-1.52011	9.65E-07	-1.91206
2628785	NM_006722 // MITF // microphthalmia-associated transcription factor // 3p14.2-p1	MITF	3.88E-08	5.62E-06	-1.24654	7.36E-06	-1.30077
3108146	NM_002998 // SDC2 // syndecan 2 // 8q22-q23 // 6383 /// ENST00000302190 // SDC2	SDC2	3.89E-08	5.89E-06	-1.26976	7.05E-06	-1.33179
3061438	NM_017654 // SAMD9 // sterile alpha motif domain containing 9 // 7q21.2 // 54809	SAMD9	3.92E-08	0.0294699	-1.26443	1.99E-08	-2.41021
3317868	NM_014489 // FRAG1 // FGF receptor activating protein 1 // 11p15.5 // 27315 ///	FRAG1	3.94E-08	0.0425345	1.0773	1.70E-08	1.35388
2877257	NM_139199 // BRD8 // bromodomain containing 8 // 5q31 // 10902 /// NM_006696 //	BRD8	3.96E-08	2.00E-08	1.2307	0.0295987	1.08478
3224650	NM_020946 // DENND1A // DENN/MADD domain containing 1A // 9q33.2 // 57706 /// NM	DENND1A	3.96E-08	4.43E-06	-1.1957	9.69E-06	-1.22972
3064541	NM_001084 // PLOD3 // procollagen-lysine, 2-oxoglutarate 5-dioxygenase 3 // 7q22	PLOD3	3.97E-08	0.0196787	1.08954	2.43E-08	1.34463
2340186	NM_018211 // RAVER2 // ribonucleoprotein, PTB-binding 2 // 1p31.3 // 55225 /// E	RAVER2	3.99E-08	3.83E-05	-1.2847	1.30E-06	-1.45238
3047581	NM_002192 // INHBA // inhibin, beta A // 7p15-p13 // 3624 /// ENST00000242208 //	INHBA	4.00E-08	1.58E-06	1.51617	3.06E-05	1.52449
3230811	NM_013379 // DPP7 // dipeptidyl-peptidase 7 // 9q34.3 // 29952 /// ENST000003715	DPP7	4.04E-08	0.00110591	1.13023	1.18E-07	1.31189
3152558	NM_174911 // FAM84B // family with sequence similarity 84, member B // 8q24.21 /	FAM84B	4.06E-08	0.0106863	1.08335	3.35E-08	1.28046
3134034	NM_006904 // PRKDC // protein kinase, DNA-activated, catalytic polypeptide // 8q	PRKDC	4.08E-08	8.27E-06	1.45163	5.39E-06	1.59006
2726234	NM_207330 // NPAL1 // NIPA-like domain containing 1 // 4p12 // 152519 /// ENST00	NPAL1	4.08E-08	1.72E-05	-1.17329	2.70E-06	-1.24202
3815165	NM_002819 // PTBP1 // polypyrimidine tract binding protein 1 // 19p13.3 // 5725	PTBP1	4.12E-08	0.0068835	1.08766	4.26E-08	1.27273

3547696	NM_144596 // TTC8 // tetratricopeptide repeat domain 8 // 14q31.3 // 123016 ///	TTC8	4.15E-08	1.09E-05	1.25826	4.23E-06	1.34311
2430762	NM_201263 // WARS2 // tryptophanyl tRNA synthetase 2, mitochondrial // 1p13.3-p1	WARS2	4.17E-08	6.56E-05	1.26693	8.92E-07	1.45301
3848871	NM_016579 // CD320 // CD320 molecule // 19p13.3-p13.2 // 51293 /// ENST000003014	CD320	4.18E-08	0.0562752	1.09693	1.61E-08	1.49518
2549007	NM_198963 // DHX57 // DEAH (Asp-Glu-Ala-Asp/His) box polypeptide 57 // 2p22.1 //	DHX57	4.21E-08	2.26E-07	1.20538	0.000432442	1.1498
2376849	NM_182663 // RASSF5 // Ras association (RalGDS/AF-6) domain family member 5 // 1	RASSF5	4.22E-08	0.00291875	-1.17623	6.99E-08	-1.50563
2417272	NM_018841 // GNG12 // guanine nucleotide binding protein (G protein), gamma 12 /	GNG12	4.22E-08	0.000226038	-1.26957	3.56E-07	-1.54444
2862784	NM_015566 // FAM169A // family with sequence similarity 169, member A // 5q13.3	FAM169A	4.24E-08	0.000200244	1.47966	3.90E-07	2.02039
3388785	NM_002425 // MMP10 // matrix metallopeptidase 10 (stromelysin 2) // 11q22.3 // 4	MMP10	4.29E-08	0.00112255	1.64556	1.25E-07	3.01298
3185354	NM_001012994 // SNX30 // sorting nexin family member 30 // 9q32 // 401548 /// EN	SNX30	4.29E-08	8.37E-06	-1.24051	5.73E-06	-1.30656
3149754	NM_003756 // EIF3H // eukaryotic translation initiation factor 3, subunit H // 8	EIF3H	4.39E-08	1.01E-05	1.29498	4.93E-06	1.38734
3443804	NM_002258 // KLRB1 // killer cell lectin-like receptor subfamily B, member 1 //	KLRB1	4.42E-08	0.0666161	-1.13991	1.59E-08	-1.81091
3025545	NM_033138 // CALD1 // caldesmon 1 // 7q33 // 800 /// NM_033157 // CALD1 // calde	CALD1	4.46E-08	0.00016618	-1.34111	4.77E-07	-1.67152
3947302	NM_001002034 // FAM109B // family with sequence similarity 109, member B // 22q1	FAM109B	4.46E-08	0.000103119	1.19255	6.82E-07	1.33857
2724671	NM_004310 // RHOH // ras homolog gene family, member H // 4p13 // 399 /// ENST00	RHOH	4.47E-08	0.00369113	-1.2798	6.54E-08	-1.89902
2626097	NM_020676 // ABHD6 // abhydrolase domain containing 6 // 3p14.3 // 57406 /// ENS	ABHD6	4.47E-08	6.30E-07	-1.36035	0.000114824	-1.30989
2428796	NM_015967 // PTPN22 // protein tyrosine phosphatase, non-receptor type 22 (lymph	PTPN22	4.54E-08	0.00360665	-1.24275	6.74E-08	-1.75522
3085403	NM_012331 // MSRA // methionine sulfoxide reductase A // 8p23.1 // 4482 /// ENST	MSRA	4.55E-08	1.99E-06	-1.21738	2.87E-05	-1.22471
3293280	NM_021129 // PPA1 // pyrophosphatase (inorganic) 1 // 10q11.1-q24 // 5464 /// EN	PPA1	4.59E-08	1.93E-05	1.66352	2.87E-06	1.99952
3488985	NM_021999 // ITM2B // integral membrane protein 2B // 13q14.3 // 9445 /// ENST00	ITM2B	4.60E-08	0.0182475	-1.10577	2.95E-08	-1.40459
3393670	NM_001098526 // AMICA1 // adhesion molecule, interacts with CXADR antigen 1 // 1	AMICA1	4.64E-08	0.00745096	-1.28336	4.67E-08	-2.05596
3695648	NM_013304 // ZDHHC1 // zinc finger, DHHC-type containing 1 // 16q22.1 // 29800 /	ZDHHC1	4.65E-08	1.60E-05	1.25492	3.48E-06	1.35271
2329196	NM_052998 // ADC // arginine decarboxylase // 1p33-p34.3 // 113451 /// ENST00000	ADC	4.67E-08	2.57E-08	-1.4244	0.0255865	-1.15503
3631517	NM_020147 // THAP10 // THAP domain containing 10 // 15q23 // 56906 /// ENST00000	THAP10	4.72E-08	0.000104594	1.19875	7.24E-07	1.3493
3261009	NM_030929 // KAZALD1 // Kazal-type serine peptidase inhibitor domain 1 // 10q24.	KAZALD1	4.73E-08	6.92E-05	1.23241	1.01E-06	1.38979
3374538	AK091446 // LOC283194 // hypothetical protein LOC283194 // 11q12.2 // 283194	LOC283194	4.73E-08	4.66E-07	1.47071	0.000189755	1.37754
2705706	NM_003810 // TNFSF10 // tumor necrosis factor (ligand) superfamily, member 10 //	TNFSF10	4.76E-08	0.01517	-1.19337	3.35E-08	-1.77912
2619480	ENST00000396102 // CCBP2 // chemokine binding protein 2 // 3p21.3 // 1238 /// BC	CCBP2	4.76E-08	1.05E-05	-1.46328	5.32E-06	-1.61804
3035682	NM_013393 // FTSJ2 // FtsJ homolog 2 (E. coli) // 7p22 // 29960 /// ENST00000242	FTSJ2	4.76E-08	0.172562	1.04568	1.19E-08	1.32119
3846594	NM_015898 // ZBTB7A // zinc finger and BTB domain containing 7A // 19p13.3 // 51	ZBTB7A	4.78E-08	4.01E-06	-1.16607	1.42E-05	-1.18825
3250699	NM_004096 // EIF4EBP2 // eukaryotic translation initiation factor 4E binding pro	EIF4EBP2	4.78E-08	0.000706102	-1.16134	1.91E-07	-1.36382
3484641	NM_000059 // BRCA2 // breast cancer 2, early onset // 13q12.3 // 675 /// ENST000	BRCA2	4.82E-08	0.050284	1.14539	1.96E-08	1.76782
3592214	NM_017434 // DUOX1 // dual oxidase 1 // 15q15.3 // 53905 /// NM_175940 // DUOX1	DUOX1	4.86E-08	8.40E-06	1.32512	6.83E-06	1.413
3402786	NM_000616 // CD4 // CD4 molecule // 12pter-p12 // 920 /// ENST00000011653 // CD4	CD4	4.89E-08	0.000240641	-1.37158	4.08E-07	-1.77593
3236958	NM_003380 // VIM // vimentin // 10p13 // 7431 /// ENST00000224237 // VIM // vime	VIM	4.89E-08	4.75E-05	-1.47453	1.43E-06	-1.79381
3043648	NM_019029 // CPVL // carboxypeptidase, vitellogenic-like // 7p15-p14 // 54504 //	CPVL	4.96E-08	8.50E-05	-1.35347	9.10E-07	-1.62674
3088213	NM_022071 // SH2D4A // SH2 domain containing 4A // 8p21.2 // 63898 /// ENST00000	SH2D4A	5.02E-08	1.83E-06	1.36403	3.69E-05	1.36759
3430926	NM_003362 // UNG // uracil-DNA glycosylase // 12q23-q24.1 // 7374 /// NM_080911	UNG	5.11E-08	0.121605	1.05764	1.46E-08	1.35548
2947572	NM_006510 // TRIM27 // tripartite motif-containing 27 // 6p22 // 5987 /// ENST00	TRIM27	5.11E-08	1.62E-05	1.23711	3.92E-06	1.32495
3948047	NM_022141 // PARVG // parvin, gamma // 22q13.2-q13 // 64098 /// ENST00000356909	PARVG	5.14E-08	0.000600498	-1.21811	2.31E-07	-1.49097
3945614	NM_145298 // APOBEC3F // apolipoprotein B mRNA editing enzyme, catalytic polypep	APOBEC3F	5.14E-08	8.96E-06	-1.24228	6.94E-06	-1.30632

Supplementary table 4.

GeneGo MetaCore pathways, process and metabolic networks significantly overrepresented in the set of genes differentially expressed in nonpolypoid (*vs* normal mucosa) and polypoid (*vs* normal mucosa) precancerous lesions.

	Pathway name	min (p Value)
1	Cytoskeleton remodeling_TGF, WNT and cytoskeletal remodeling	2.798e-14
2	Cytoskeleton remodeling_Cytoskeleton remodeling	3.743e-11
3	Immune response_BCR pathway	5.686e-11
4	Cell adhesion_Chemokines and adhesion	5.990e-11
5	Signal transduction_AKT signaling	1.403e-10
6	DNA damage_ATM/ATR regulation of G1/S checkpoint	6.172e-10
7	Development_WNT signaling pathway. Part 2	9.584e-10
8	Immune response_Classical complement pathway	2.642e-9
9	Development_GM-CSF signaling	3.464e-9
10	Development_IGF-1 receptor signaling	6.506e-9
	Process Network name	
1	Cell cycle_G2-M	1.183e-16
2	Cell cycle_S phase	1.076e-15
3	Cell cycle_Core	4.337e-14
4	Cytoskeleton_Actin filaments	1.117e-9
5	Cytoskeleton_Regulation of cytoskeleton rearrangement	6.350e-9
6	Cell adhesion_Attractive and repulsive receptors	7.805e-8
7	Translation_Regulation of initiation	3.251e-7
8	Cell cycle_G1-S Growth factor regulation	5.445e-7
9	Cell adhesion_Integrin-mediated cell-matrix adhesion	5.601e-7
10	Immune_Phagocytosis	6.331e-7
	Metabolic Network name	
1	Phosphatidylinositol-4,5-diphosphate pathway	2.238e-14
2	Phosphatidylinositol-3,4,5-triphosphate pathway	3.532e-13
3	1,2-dioleoyl-sn-glycerol_3-phosphate pathway	8.820e-11
4	1,2-didocosapentaenoyl-sn-glycerol_3-phosphate pathway	1.064e-10
5	N-acyl-sphingosine phosphate pathway	1.143e-10
6	1,2-didocosahexaenoyl-sn-glycerol_3-phosphate pathway	1.633e-10
7	1-oleoyl-glycerol_3-phosphate pathway	2.111e-8
8	1-linoleoyl-glycerol_3-phosphate pathway	1.087e-7
9	Sphingomyelin pathway	1.385e-6
10	2-oleoyl-glycerol_3-phosphate pathway	6.222e-6

11.2 Publications

Here included:

- Sabates-Bellver J., Cattaneo E., Heinimann K., Jiricny J., and Marra G. "Getting familiar with familial colon cancer." Chapter in the Falk Symposium 158 book "Intestinal Inflammation and colorectal Cancer", 2007

- Elisa Cattaneo, Michael Baudis, Federico Buffoli, Maria Antonia Bianco, Fausto Zorzi, and Giancarlo Marra. "Pathways and crossroads to colorectal cancer". In *Advances in understanding the basic pathogenesis and clinical management of pre-invasive disease*. Edited by Fitzegerald R., 2009, in press

Getting familiar with familial colon cancer

Jacob Sabates-Bellver*, Elisa Cattaneo*, Karl Heinimann^, Josef Jiricny*, and Giancarlo Marra*[¥].

* Institute of Molecular Cancer Research, University of Zurich, Switzerland

^ Division of Medical Genetics, University of Basel, Switzerland

[¥] Corresponding author:

Giancarlo Marra, M.D., Ph.D.

Institute of Molecular Cancer Research

University of Zurich

Winterthurerstrasse 190

8057 Zurich, Switzerland

Tel. 0041 044 635 3472

Fax. 0041 044 635 3484

marra@imcr.unizh.ch

INTRODUCTION

Based on cancer incidence rates estimated in the United States, colorectal cancer is the fourth most frequent cancer in humans (after prostate, breast, and lung) [1]. This estimation is very similar in most of the countries offering reliable cancer statistics. In these countries, approximately one out of eighteen persons develop colorectal cancer (more than twice more frequently in the colon than in the rectum). This ~5% lifetime probability of developing colorectal cancer increases to 10-15% in individuals with one first-degree relative affected by colorectal cancer [2(and references herein)]. The percentage increases considerably if more than one relative are affected by colorectal cancer or other cancers often diagnosed in familial aggregations of colorectal cancer. The cumulative lifetime probability reaches 60-100% in carriers of a mutation in a highly-penetrant allele, such as in one of the DNA mismatch repair (MMR) genes [3] in hereditary non-polyposis colon cancer (HNPCC, also known as Lynch syndrome) or in the *adenomatous polyposis coli (APC*) gene in familial adenomatous polyposis (FAP) [4]. MMR-defective HNPCC, which will be the main subject of this article, represents the most frequent colorectal cancer predisposition syndrome of known etiology, and adenocarcinomas of MMR(-) HNPCC account for ~3% of all cancers in the colon.

FAP is responsible for ~0.5% of all colorectal cancers, and an additional ~0.5% arise in the colorectum of individuals affected by one of the *hamartomatous polyposis syndromes* or by *hyperplastic polyposis*, whose underlying genetic alterations are the subject of intensive search. The latter three conditions will be discussed solely in the light of some interesting aspects that emerged recently from basic and clinical research studies.

A genetic susceptibility underlies an additional ~15% of all colorectal cancers [5], also referred to as familial or hereditary, but the underlying genetic disorder is unknown. In this large portion of familial colon cancers, the cumulative lifetime risk is very variable, ranging

from very high in familial aggregations that are clinically indistinguishable from HNPCC, but not associated with MMR defects, to conditions with only a slightly higher predisposition to colorectal cancer as compared to the general population. At this latter end of the spectrum lies a blurred border between familial and non-familial (hereafter called sporadic) colorectal cancers. In this group lie many apparently sporadic cases that could be familial (i.e. in small families where only one case has been detected so far, in cases of poor diagnosis or where medical records are incomplete, in families where a *de novo* mutation arose for the first time, non-paternity, etc), or apparently familial that could be sporadic (i.e., two sporadic colorectal cancers in the same family). Thus, the challenge for the years to come is to unravel novel high-penetrance predisposition alleles responsible for familial aggregations of colorectal cancer clinically similar to HNPCC but with intact MMR, and low-penetrance alleles responsible for the remainder of familial colorectal cancers. Theoretically, all the remaining sporadic colorectal cancers might also be associated with very-low penetrance mutations or polymorphisms whose degree of penetrance may be modulated by environmental factors, mainly dietary ones.

Importantly, the genetic alterations detected in rare inherited syndromes can have roles also in the initiation and progression of a large portion of sporadic cases when these alterations occur somatically, as for those in *APC* or the MMR gene *MLH1*.

The discovery rate in the field of cancer genetics has dramatically increased due to the implementation of genomics, with which an enormous number of identified genetic variants and their combinations can be used in studies aimed at verifying their association with the predisposition to colorectal cancer. Transcriptomics, another tool for molecular global screening of tumours, has been instrumental in the classification of tumours, and is helping to unravel the molecular mechanisms underlying their origin and to identify the genes

responsible for the epithelial cell transformation (an example of application of this approach is reported in the last section of this article). A paradigm of this type of search was the discovery, in 1992, of the involvement of the MMR defect in HNPCC by using a molecular, yet pre-omics, screening technique, the arbitrarily-primed polymerase chain reaction, which helped identify a specific tumour phenotype, *microasatellite instability* [6]. Since this phenotype was already known to be caused by a defect of the MMR system in bacteria and yeast, the mutated MMR alleles were easily identified in members of HNPCC families [7].

MMR(-) HNPCC (Lynch syndrome)

The recent advancements in the MMR field have been propelled by the discovery in the early nineties of a causal link between inherited mutations in *MMR* genes and the colon cancer predisposition syndrome HNPCC [7]. As mentioned, this was possible only after the identification of microsatellite instability (MSI) in a subset of colorectal cancers by using arbitrarily-primed PCR [6]. Later on, about 10% of sporadic colon cancers were also found to be defective in MMR as a result of somatic transcriptional silencing of the *MMR* gene *MLH1* [8 9]. Thus, there was an urgent need to identify tools that could be easily deployed in the diagnosis of this type of tumours, which would facilitate more effective clinical management. One tool was of course the analysis of tumour DNA for the presence of MSI. This test is today performed routinely by many molecular biology or genetic laboratories. Later, when antibodies able to reliably recognize MMR proteins in tissue samples became available, immunohistochemistry started to be used extensively in research laboratories and in pathology departments. In order to appreciate the prowess of these diagnostic procedures, it is essential to understand the basics of MMR. The brief excursion into MMR biochemistry

that follows will also help the reader to understand some of the phenotypic differences underlying defects in different *MMR* genes.

MMR is often referred to as post-replicative MMR, as its primary function is the correction of errors occurring during DNA replication. This editing function is necessary, since the fidelity of replicating DNA polymerases is insufficient to generate an error-free copy of genomic DNA. Single-base substitutions arise once in every 10^4-10^6 nucleotides incorporated. The intrinsic exonucleolytic proofreading activity of the replicative polymerases increases the fidelity of DNA synthesis by a further two orders of magnitude, i.e. to one error in 10^7 to 10^8 [ref.10]. MMR reduces the error rate to a range of 10^{-9} to 10^{-10}, which ensures that the human genome of 6.6×10^9 nucleotides can be duplicated without mutations. When MMR is defective, the mutation rate increases considerably and mutations are accumulated in the genome (i.e. a *mutator phenotype* arises).

In addition to base-base mismatches, slippage of the newly synthesized strand with respect to the template can give rise to misalignments, often referred to as insertion/deletion loops (IDLs) (**FIGURE 1**). These structures arise more often in repetitive DNA sequences, such as mono- and di-nucleotide repeats, also called microsatellites, where replicative DNA polymerases are more prone to "slippage" than on non-repetitive templates. The frequency of IDLs rises substantially with increasing length of the repeat. When not repaired by the MMR, extrahelical nucleotides in the primer strand give rise to insertions in the progeny DNA, while their presence in the template strand leads to deletions (Figure 1). The term MSI refers to the length variation of these sequences in the tumour DNA, when compared with their normal length in the DNA from normal tissue. Interestingly, deletions predominate over insertions in microsatellites of MMR(-) tumours, which suggests either that the formation of

extrahelical loops in the template strand is more frequent than in the newly-synthesized strand, and/or that the latter lesions are repaired by a system distinct from MMR.

The process of mismatch correction is initiated by the binding of one of two mismatch recognition complexes, MSH2/MSH6 (also termed MutSα) or MSH2/MSH3 (MutSβ), to base/base mismatches or strand misalignments (IDLs) that were generated by the replicating DNA polymerase, but that escaped its proofreading activity (**FIGURE 2**) (refer to [11] for a detailed description of the MMR reaction). The mismatch-bound MutS heterodimer then undergoes an ATP-driven conformational change that enables its interaction with the MLH1/PMS2 heterodimer (MutLα). This interaction stimulates an endonucleolytic function of MutLα, which nicks the newly synthesized strand both on the 3' and the 5' side of the mismatch [12]. The nick 5' from the mismatch is then utilized by exonuclease 1 (EXO1) to degrade the newly synthesized strand up to and a short distance beyond the mispaired nucleotide, which is thus removed. Finally, the degraded tract is filled-in by the replicating DNA polymerase δ.

In vitro MMR repair assays showed that MutSα supports the correction of G/T, A/C, G/G and A/A mispairs, and of IDLs of 1 to 4 extrahelical nucleotides with high efficiency. The remaining mismatches were repaired with intermediate efficiency, while C/C and larger IDLs were poor substrates for the MMR system (reviewed in [13]). *In vivo*, MSH6 and MSH3 compete for MSH2. The MSH2/MSH3 heterodimer, termed MutSβ, has been shown to address IDLs of 1-8 extrahelical nucleotides, but not mismatches. It has been suggested that MutSα might have a prominent role in the repair of IDLs *in vivo*, given that MutSα is around 10 times more abundant than MutSβ in cultured human cells [14-16]. The reverse is true in cells overexpressing MSH3 as a result of amplification of the *DHFR/MSH3* locus through exposure to methotrexate. These cells have extremely low levels of MutSα, because the

abundant MSH3 sequesters all available MSH2, and the partnerless MSH6 is degraded [14 17]. As anticipated, these cells are proficient in IDL repair, but deficient in the repair of base-base mismatches, thus they would display no MSI, in spite of having a mutator phenotype. Indeed, MSI is in general not detectable in MMR(-) tumours in which the mutated *MMR* gene is *MSH6*, and MutSβ is normally expressed. As we will see later, the clinical phenotype of MSH6-defective HNPCC families also differs from that of MSH2-defective ones.

At this point it is important to introduce another biochemical feature of the MMR MutS heterodimers that has also implication in diagnostics. MSH3 and MSH6 compete for the same region of MSH2 [18], and several studies showed that molecules of the former polypeptides that fail to form heterodimers with MSH2 are destabilized. Thus, when *MSH2* is mutated and its protein product is not expressed (germline mutation in one allele and somatic second-hit in the wild type allele, see below), MSH6 and MSH3 are degraded and both MutSα and MutSβ are absent. The cells are consequently unable to repair mismatches and IDL, and MSI is clearly evident. This should be taken into consideration during immunohistochemical analysis of tumours for MMR protein expression. MSH2-defective tumours lack MSH2, MSH6 and MSH3, whereas MSH6- or MSH3-defective tumours normally express MSH2, since this latter protein is stabilized by its interaction with MSH3 or MSH6, respectively. As in the case of the MutS homologs, the stabilities of the MLH1 and PMS2 polypeptides are also different. Thus, when MLH1 is not expressed, or when it is mutated such that it is either destabilized or that it cannot interact with PMS2, the latter protein is degraded. In contrast, MLH1 remains stable in the absence of PMS2 [15 19] through interactions with other MutL homologs such as PMS1 or MLH3, whose involvement in MMR however appears to be marginal [19 20]. Translating this biochemical knowledge to clinical pathology, a MLH1-defective tumour lacks both MLH1 and PMS2, whereas a

tumour with a primary alteration in the *PMS2* gene lacks only PMS2, but contains normal levels of MLH1.

The role of the MLH1/PMS2 heterodimer in MMR is only partially known. Its most probable role is to link the mismatch- or IDL-recognition event by one of the two MutS heterodimers to the excision function of EXO1 (**FIGURE 2**). The endonucleolytic activity of MutLα that has been only recently described [12] and that is essential for the 5' to 3' exonucleolytic activity of EXO1, relies on an endonuclease active site localized in PMS2 [12]. Both of these proteins are thus essential for MMR and an alteration of either *MLH1* or *PMS2* leads to MSI.

The biochemical mechanism of MMR discussed above implies that inactivating mutations in the *MMR* genes *MSH2*, *MLH1* and *PMS2* should have the most severe phenotypes, whereas those in *MSH6* would have reduced MSI and thus also a weaker MMR defect. Indeed, analysis of HNPCC families shows that germline mutations in *MSH2* and *MLH1* are substantially more often associated with this syndrome than mutations in the other two genes (HNPCC mutation database at http://www.insight-group.org/). Germline mutations in *MSH3* have not been reported yet, and it makes little sense to search for them in tumours with classical MSI, because of the redundant function of the two MutS heterodimers in the repair of short IDLs. The role of missense *EXO1* variants in predisposition to colorectal cancer is still under investigation [21(and references herein)], however these variants might represent low-penetrance alleles due to the possible redundancy of EXO1 with other, as yet unidentified, exonucleases during MMR.

Today, MSI analysis and immunohistochemistry are the most common tools used in the diagnosis of MMR(-) tumours. Immunohistochemistry for the four most frequently involved MMR proteins (MSH2, MSH6, MLH1 and PMS2) has the advantage that it is rapid

and economical, and it allows to compare tumour with normal tissue in the same histological section. It also identifies the defective *MMR* gene, and should thus be carried out prior to DNA sequence analysis in search for germline mutations. In contrast, MSI analysis only detects a defect in the MMR, not in a specific *MMR* gene. However, there are occasions when MMR(-) tumours will not be identified by these methods: *i*) in MSH6-defective cases, the level of MSI is often low, such that it is not detected with the standard panel of microsatellite primers, and *ii*) in cases of missense germline mutations that do not affect the stability of the protein but only its function. However, most of the genetic changes in *MMR* genes, including missense mutations, lead to decay or degradation of the corresponding RNA or protein. This situation is very different from that resulting from alterations in the *APC* gene (see below). Since only ~3% of colorectal cancers are associated with an inherited mutation in one of the *MMR* genes, today only cases fulfilling the Bethesda guidelines [22] are included in the diagnostic screening using MSI analysis and immunohistochemistry. These guidelines consider the age of the patient (younger than the average age of onset of sporadic colorectal cancers), the presence of synchronous or metachronous HNPCC-related carcinomas (MMR defects predispose individuals to colorectal and endometrial cancers, but to a lesser extent also to carcinoma of the small bowel, transitional cell carcinoma of the upper urinary tract, stomach cancer and ovarian cancer), cases carrying tumours with pathological features more often found in MMR-deficient tumours (conspicuous, peritumoural and intratumoural, lymphocytic infiltration, and mucinous differentiation), and the presence in the family of first or second-degree relatives with HNPCC-related tumours.

It has been often the case that genes whose alterations were found to cause inherited forms of cancer were also found somatically altered in a portion of sporadic tumours. Thus, a few years ago, we initiated an immunohistochemical screening of consecutive, unselected

colorectal cancers (not selected for family history or other parameters) for the four main MMR proteins. Using this approach, we identified aberrant patterns of MMR protein expression in 13.2% of 1048 colorectal cancers in Switzerland. Loss of expression of MSH2, MSH6, MLH1 and PMS2 was found in 1.4%, 0.5%, 9.8% and 1.5%, respectively [9]. Most of the MLH1-defective cases were sporadic, and the expression of this gene was silenced by somatic, bi-allelic methylation of its promoter. Thus, sporadic, MLH1-defective tumours are the most frequent MMR(-) colorectal cancers; they occur more often in old persons (even older than in the rest of the sporadic cases), slightly more frequently in women, and almost exclusively in the proximal colon. Several other studies have reported that ~10% of all colorectal cancers are MLH1-defective, sporadic tumours. This large subset of colorectal cancers could be detected by routinely applying immunohistochemistry for MLH1 in all sporadic cancers of the proximal colon (~ 25% of the tumours in this tract).

A considerable proportion of inherited forms of MMR(-) colorectal cancers fulfill the Amsterdam criteria for diagnosis of HNPCC [23]: 1) at least 3 colon or endometrial cancers in a family; 2) one case should be a first-degree relative of the other two, and 3) at least one of them should be diagnosed before the age of 50. Most persons carrying germline mutations in *MSH2* or *MLH1* do belong to classical HNPCC families, but germline mutations in *MMR* genes have been found also in families with a lower burden of cancers and even in individuals without a family history of colorectal cancers. Germline mutations in *MSH6* for example, result in an attenuated phenotype, the families often not fulfilling the above-mentioned criteria [24(and references herein)]. The risk of colorectal cancer is lower in women and, in both genders, the mean age of diagnosis of colorectal cancer is around 12 years later than in those with *MSH2* or *MLH1* mutations. However, by the age of 70, men with *MSH6* mutations have the same risk of colorectal cancer as those with *MSH2* or *MLH1* mutations.

In addition, the risk of endometrial cancer, although delayed in onset, is significantly greater than in women carriers of *MSH2* or *MLH1* mutations. These phenotypic differences can be explained by the biochemical role of MSH6 in MMR, in particular its partial functional redundancy with MSH3. Correspondingly, the MSI phenotype in MSH6-negative tumours is attenuated, as the MSH2/MSH3 heterodimer partially compensates for the absence of MSH2/MSH6 in the IDL repair, but the mutator phenotype due to uncorrected base/base mismatches remains extremely high.

Since the discovery of the etiologic association between MMR deficiency and hereditary colorectal cancer, only a few cases with germline mutations in *PMS2* have been described [25-30]. The mutation carriers did not belong to classical HNPCC families, rather, they presented with colorectal cancers and brain tumours in their first two decades of life, a condition also called Turcot's syndrome (reviewed in [31] and [29]). In most of these cases, both *PMS2* alleles were mutated in the germline, and MSI was detectable even in non-neoplastic tissues, suggesting a recessive way of inheritance. These findings resemble the childhood cancer syndromes characterized by gastrointestinal, haematological and brain cancers in subjects with compound heterozygous germline mutations in *MLH1* [32(and references herein)]. The severity of this syndrome is attributed to the fact that both alleles of a *MMR* gene are affected in the germline. Besides the rare cases of a *PMS2*-associated childhood cancer syndrome, the absence of involvement of *PMS2* in HNPCC was unexpected. Despite the existence of PMS1 and MLH3, both of which have been shown to interact with MLH1, the participation of the former proteins in MMR appears to be only marginal [19 20 33]. These two polypeptides are therefore unlikely to compensate for the lack of PMS2 to a substantial extent. Correspondingly, cell lines lacking PMS2 display MSI and their extracts are MMR deficient to an extent similar to that observed in cells mutated in *MLH1* or *MSH2*. It might therefore

be anticipated that, similarly to *MSH2* and *MLH1*, germline mutations in a single *PMS2* allele would predispose to colorectal cancer. Indeed, loss of expression of PMS2 has been recently identified [9 34-39]. In our immunohistochemical study [9], tumours lacking PMS2 expression were identified with a frequency similar to that of MSH2-defective colorectal cancers. As the 1048 tumours were collected consecutively and without any selection bias, this frequency represents the true occurrence of PMS2 deficiency. Individuals carrying PMS2-deficient colon cancers did not belong to HNPCC families as defined by Amsterdam criteria, however, a closer examination of the clinical and pathological data showed several features of inheritance. Indeed, we identified heterozygous germline mutations in *PMS2* in many of these subjects. Thus, the inheritance pattern of *PMS2* mutations apparently differs from the autosomal dominant trait characteristic of *MSH2* and *MLH1* mutations in HNPCC kindred, and is most likely the main reason why PMS2-negative tumours escaped detection to date. The mechanisms underlying the limited penetrance of *PMS2* germline mutations are under investigation.

HNPCC is inherited in an autosomal dominant way, but MMR deficiency arises only when also the wild-type *MMR* allele is mutated or lost. Thus, the disease is recessive at the somatic level. Indeed, the tumour cells do not express the MMR protein, whereas cells in the normal tissue, which is almost always present in the same histological section (normal colonic crypt epithelium, germinal centers of lymphocytic folliculi, and dividing stromal cells), express the protein because they retain heterozygosity. When do the cells of the colonic epithelium acquire the second hit and thus become fully MMR deficient ? The carcinogenic process in MMR(-) HNPCC seems to follow the *adenoma-carcinoma* histological pathway, i.e., cancer arises in precancerous adenomatous polyps, which represent also the most frequent precancerous lesions leading to sporadic colorectal cancers and the

characteristic lesions in FAP. These lesions are believed to arise from the normal colorectal epithelial crypts, because of a dysregulation of the Wnt signalling pathway (see below), but the temporal relationship between alterations in this or other signalling pathways and the onset of MMR deficiency in adenomas remains obscure. It has been reported that MSI and lack of immunostaining for MMR proteins might not be a very early event, being detectable more often in adenomas of large size and tubulo-villous architecture with high degree of dysplasia [40 41]. In HNPCC, adenomas also develop at a younger age (early forties) than in the control population, and it is commonly believed that HNPCC adenomas transform into cancer very frequently and in a short period of time. Indeed, the acquisition of the MMR deficiency and consequently of the mutator phenotype and MSI, should markedly accelerate the transformation process. In spite of a germline mutation in a *MMR* gene present in all the epithelial cells of the colonic mucosa, it is still surprising and unexplained why the number of adenomatous polyps in HNPCC patients is not as high as in FAP. Actually, the index adenoma in HNPCC cases is often isolated or almost never accompanied by more than five other adenomas.

In conclusion, MMR(-) colorectal cancers in HNPCC arise from isolated, early-onset adenomas along a fast transformation process driven by a high rate of mutations in the DNA, often in tumour suppressor genes [42 43]. This pathway is probably dominant to another frequent pathway in carcinogensis, that of chromosomal instability, since MMR-deficient tumours show only a limited number of chromosomal gains and losses and are often near-diploid. Fortunately, later on in carcinogenesis, their aggressiveness and invasiveness is restrained by a conspicuous anti-tumour immune response, whose molecular components have only recently started to be investigated [44], and which is believed to be triggered by the presentation of novel antigens produced by highly mutable, MMR(-) tumour cells. Unfortunately, the

defect in MMR makes these tumours more tolerant to some drugs, in particular alkylating agents [45], and probably less responsive to the standard treatment with 5FU [46 47]. Due to the peculiar histological and molecular characteristics of MMR(-) tumours, more studies and clinical trials should aim to identify drugs that specifically kill this type of neoplastic cells.

Serrated adenomatous polyposis as a model of the serrated pathway of transformation.

A large number of familial colon cancer aggregations are not linked to germ-line alterations in *MMR* genes. The intense study being dedicated to these kindreds has produced (among other things) compelling evidence for the existence of a familial CRC syndrome that is distinct from HNPCC and does not appear to evolve through the traditional adenoma-carcinoma sequence. The pathway involved in the development of these is known as the *serrated pathway* of colorectal carcinogenesis, which is thought to be responsible for approximately 20% of the *sporadic* cancers affecting this organ [48 49].

The precursor lesions in the serrated pathway are characterized histologically by a saw-toothed pattern of glandular architecture (**FIGURE 3**)[50]. Formerly referred to as *hyperplastic polyps* (a term that has gradually been abandoned over the past decade), these lesions are now known as *serrated polyps*. For many years, they were considered innocuous with a negligible risk for progression to cancer. It is becoming increasingly clear, however, that this morphologically and molecularly heterogeneous set of lesions includes certain subtypes that are indeed likely to undergo malignant transformation [48 51 52]. A recently proposed classification scheme [53] divides serrated polyps into two broad categories. Those with "normal proliferation" (in which the proliferative compartment is confined to the lower portion of the crypts) generally develop as protruding lesions located in the distal colon and rectum – features traditionally attributed to the so-called *hyperplastic polyp*. Those with

"abnormal proliferation" (reflected by an upward shift of the proliferative compartment) [54 55] can be further divided into two subgroups (**FIGURE 3A and B**): *traditional serrated adenomas* (TSA), which are quite rare (accounting for ~1% of all serrated polyps) and generally present as sessile or pedunculated polyps, and *sessile serrated adenomas* (SSA), which are much more common. SSAs are sessile or non-polypoid lesions (i.e., usually slightly elevated) [56]. They are distinguished from TSAs (and from classical adenomas) by the absence of cytological dysplasia. Nevertheless, an increasingly compelling body of evidence suggests that SSAs (especially those arising in the proximal colon) are precursors to adenocarcinomas with serrated features [57].

Recent studies have also demonstrated molecular differences between classic adenomas and serrated polyps. For instance, the latter are often characterized by DNA methylation of the promoter regions of multiple gene [48 51 58 (and references herein)]. This phenomenon, which is known as the CpG-island methylator phenotype (CIMP), is found in approximately 20% of all sporadic colorectal cancers. These cancers are encountered mainly in the proximal colon, and this pattern is consistent with previous reports of the increased risk for malignant transformation associated with serrated lesions in the left colon [59]. CpG-island methylation can result in the epigenetic silencing of various genes, including those with tumour suppressor function, and it is thus a potential driver of carcinogenesis. In roughly half of all CIMP-positive cancers, the promoter of the MMR gene *MLH1* is hypermethylated and this gene is not expressed (This mechanism accounts for those MLH1-deficient cancers mentioned in the previous section, which represent 10% of all sporadic CRCs.). Hypermethylation of *MLH1* is considered by many to be a relatively late event associated with the transition to malignancy [58 60] .

Sporadic CIMP-positive cancers are also frequently characterized by somatic mutations of the *BRAF* gene, which encodes a serine/threonine kinase [48 61-63]. The *BRAF* mutation most frequently identified in sporadic serrated tumours [64] involves a glutamate-for-valine substitution (V600E) in the regulatory domain of the gene, which results in a constitutively activated kinase with increased (~ 500-fold) activity [65]. Like RAS mutation (which is encountered more frequently in the adenoma-carcinoma pathway), BRAF V600E causes aberrant, growth factor-independent signaling through the RAS/RAF/MEK/ERK signalling pathway, which is crucial for the response of cells to growth signals.

However, BRAFV600E is also a frequent finding in tumours from patients with familial colon cancer, particularly those that are CIMP(+) and MLH1-deficient. In fact, some investigators have suggested that screening for BRAFV600E should be used to differentiate these tumours from HNPCCs caused by a germ-line mutation of an MMR gene [66 67]. Young et al. [68] recently analyzed 11 non-FAP, non-HNPCC CRC families characterized by interindividual (and sometimes intraindividual) variability in the MSI-status of colorectal tumours (MSI-H, MSI-L, or MSS), that they called MSI-V (variable) kindreds. Seventy percent of the CRCs tested for *BRAF* mutation were positive (vs. 15.2% of an unselected CRC reference series and 0% of the reference HNPCCs), including all of those that were MSI-H, half of those that were MSI-L, and 67% of the MSS cancers. All six of the tumours classified as MSI-H were cancers that presented immunohistochemical negativity for MLH1 protein expression and hypermethylation of *MINT31*, a marker of the CIMP. Compared with their sporadic counterparts, the CIMP-positive CRCs in these MSI-V families had clearly earlier onsets (by about 10 years) although they occurred approximately two decades later than HNPCCs [68].

In the MSI-V kindreds, *BRAF* mutations were also found in 63% of the precancerous lesions of different histologic subtype. Unlike the CRCs in this study, the polyps were all normal in immunohistochemical studies of the mismatch repair proteins. This finding is consistent with the view that MLH1 silencing is a relatively late event associated with the transition to malignancy [58 60] (although it has also been detected in some early precancerous lesions [69]).

The picture that emerges from these findings is that of a familial condition characterized by somatic methylation of the *MLH1* promoter caused by an unidentified genetic predisposition to CIMP. The possibility that CRC-related hypermethylation of gene promoters is genetically determined has also emerged from previous studies, which revealed associations between CIMP and family histories of colon cancer [70 71] (although in one case this association was not statistically significant [72]).

BRAFV600E and CIMP are also associated with the apparently rare condition known as *hyperplastic polyposis* [68 71 73-79], which is diagnosed when the patient presents [80]: *i*) at least five histologically diagnosed, hyperplastic polyps proximal to the sigmoid colon, including two with diameters exceeding 10 mm; *ii*) any number of hyperplastic polyps proximal to the sigmoid colon and first-degree kinship with a patient already diagnosed with hyperplastic polyposis; or *iii*) over 30 hyperplastic polyps distributed throughout the colon. Hyperplastic polyposis is known to carry an increased risk for malignant transformation, although the magnitude of the risk varies to some extent from family to family [81-83]. Colorectal cancers complicating hyperplastic polyposis have been associated with a predilection for the proximal colon and onset age that is roughly 10 years earlier than that of sporadic CRCs but two decades later than that of HNPCC – both of which were also documented in the familial CIMP-positive, MLH1-deficient CRCs examined by Young et al. [68]. In patients with this

condition, the normal mucosa has a significantly higher frequency of methylated alleles than that of individuals with sporadic serrated lesions [84 85], which is also consistent with the possibility of genetically determined CIMP. Indeed, it seems likely that hyperplastic polyposis arises as a result of an inherited predisposition. However, fewer than 150 cases have been reported to date, and only a small percentage of these are characterized by familial aggregation. Those that are seem to have dominant inheritance patterns [77 81 83 85 86].

One of the peculiarities of hyperplastic polyposis is that it is manifested by a variety of polyp types, including hyperplastic polyps, larger SSA, and even classical adenomas. Torlakovic and Snover [59] suggest that this condition includes two different phenotypes, which must be distinguished from each other. They reserve the term "hyperplastic polyposis" for cases characterized by multiple, small, pancolonic hyperplastic polyps. The second phenotype, which is manifested by smaller numbers of relatively large, proximal hyperplastic polyps with features of SSA, should in their opinion be referred to as "serrated adenomatous polyposis". Their review of the literature indicates that this phenotype accounts for a large portion of the cases reported as *hyperplastic polyposis*.

Serrated adenomatous polyposis is likely to be diagnosed with increasing frequency thanks to the introduction of innovative colonoscopy technologies and greater awareness of these lesions among pathologists. If its inherited nature is confirmed, it might someday provide a model for the identification of the initial molecular alterations that trigger the *serrated pathway* of colorectal carcinogenesis.

FAP and *APC*

FAP is an inheritable colon cancer predisposition syndrome that is transmitted in an autosomal dominant way, although almost 30% of the patients represent new cases in the

family (i.e., *de novo* mutations). FAP is characterized by the presence of hundreds (classical FAP) to thousands (severe FAP) colorectal *adenomatous* polyps developing during the first, second, and third decades of life. In a milder form, called attenuated FAP (AFAP), patients show a later disease onset and develop less than 100 colorectal polyps [87]. Because around 5% of the polyps transform to cancer, the probability of colorectal cancer at the age of 40-50 years is 100% in these patients. In addition to colorectal adenomas, FAP and AFAP patients show extracolonic manifestations such as congenital hypertrophy of the retinal pigment epithelium (CHRPE), desmoid tumours of the abdomen, upper gastrointestinal adenomas and carcinomas, and, less frequently, osteomas, dental abnormalities, lipomas, and epidermoid cysts. Malignant tumours of the brain, thyroid and hepatobiliary tract have also been associated with FAP.

Germline mutations in the *APC* gene have been directly linked to FAP and AFAP [88-90]. To date, more than 1000 mutations throughout the *APC* gene have been compiled in databases [91] (and http://www.hgmd.cf.ac.uk/ac/index.php). However, mutations in the *APC* gene have not been identified with the current methods in 30-50% of FAP and AFAP [92 93]. In a portion of these cases, bi-allelic germline mutations have instead been detected in the base excision repair gene *MYH*. This group is represented by recessively-inherited FAP or AFAP, in which the development of adenomatous polyposis is believed to occur through somatic mutations in the *APC* gene because of defective processing of DNA oxidative damage by the base excision repair system [94-98].

APC mutations have been detected also in most of the sporadic adenomatous polyps (that is, somatic mutations). Since these mutations have been found in the early stages of adenoma formation, the effects of the malfunction or inactivation of APC on the Wnt signalling (**FIGURE 4A**) are believed to be, similarly to FAP, an early event in sporadic

colorectal cancers arising from adenomas. The canonical Wnt signalling cascade plays a crucial role in driving the division of epithelial cells within the lower third of the intestinal crypt, which represents one of the simplest self-renewing biological entities in humans. In this proliferative crypt compartment, secreted proteins of the Wnt family bind to serpentine receptors of the frizzled family (FZD) and to low-density lipid receptors (LRP) on the crypt epithelial cells (**FIGURE 4A**). The signal transduction pathway activated by this binding (formation of disheveled –DVL-/FZD complexes, phosphorylation of LRP by CK1γ, and relocation of Axin to the membrane) inhibits the formation of a cytoplasmic protein complex, which includes, among others, APC, glycogen synthase kinase-3β (GSK-3β), axin, and casein kinase 1α (CK1α). This complex catalyzes the phosphorylation of β-catenin, targeting the protein for ubiquitin-mediated destruction. In its absence, β-catenin accumulates in the cytoplasm and enters the nucleus, where it associates with DNA-binding proteins of the T-cell factor (TCF)/lymphoid enhancer factor (LEF1) family. The formation of a β-catenin/TCF/LEF1 complex converts the latter polypeptides from transcription repressors into transcription activators, which activate the expression of genes encoding the transcription factors *MYC, c-Jun,* and *PEA3*, the cell cycle kinase activator *cyclin D1* and the matrix metalloproteinase *MMP-7*. Some of these genes are essential for the maintenance and proliferation of stem and cycling cells in the lower third of the colorectal crypts. In contrast, cells in the upper two-thirds of the crypts are not stimulated by Wnt signalling proteins. Here, the key player in the Wnt pathway, β-catenin, is recruited to the destruction complex and degraded. In this manner, cells of the upper crypts are allowed to differentiate as they migrate upward toward the intestinal lumen, where they undergo a form of apoptosis known as *anoikis*.

In sporadic and FAP adenomas, the inappropriate signalling reflects abnormal stabilization of β-catenin as a result of *APC* mutations. *APC* encodes a 2843 amino acids protein containing several functional domains (briefly described in the legend to **FIGURE 4B**). Interestingly, nonsense *germline APC* mutations are predicted to give rise to N-terminal APC fragments with diverse number and type of domains (for instance, the number of the 20-aa repeat domains for β-catenin binding and degradation, or the number of axin-binding domains SAMP that persist in a truncated APC polypeptide) that may lead to different degree of Wnt signalling dysregulation and/or may have various deleterious effects on cell-cell adhesion, cell migration, cell division and chromosomal stability [99]. This phenomenon is believed to be associated with different levels of severity of the disease (the so-called genotype-phenotype association). The frequency of mutations between codons 1250 and 1464 (**FIGURE 4B**) is significantly higher than in the rest of the gene (mutation cluster region) [92 100]. Two clear mutational hotspots have been identified at codons 1309 and 1061, which account for approximately 17% and 11% of all germline *APC* mutations, respectively [91] (although it should be considered that the general use of mutational analyses restricted to the mutation cluster region might mischaracterize the mutational spectrum). Mutations in the cluster region are generally found in patients with *profuse* or *severe FAP*, which is characterized by the presence of thousands of polyps at very early age (first and second decades) and an average onset of colorectal cancer at 30-35 years [101 102]. However, mutations in the cluster region were also found in a patient without a profuse polyposis [103]. Furthermore, large genomic deletions leading to absence of truncated APC were detected in 10-15% of mutation-negative cases carrying profuse or classical FAP. [104 105]. Individuals with profuse FAP usually present extracolonic manifestations. Patients with *classical* or *intermediate FAP* develop hundreds of adenomas during their second and third decades of

life [101 106]. The average onset of cancer in untreated patients is 42 years [101]. CHRPE is the most common extracolonic manifestation of the intermediate polyposis, although desmoid tumours also appear in some patients [101]. It has been shown that codons 1249 and 1250 might form the boundary between the profuse and intermediate phenotypes [101 107 108] (**FIGURE 4B**). Most of the *APC* germline mutations were located between codons 157 and 1595, not including the mutation cluster region 1250-1464 [100 101 103 108-110]. Finally, AFAP patients develop less than 100 adenomas, and the onset of cancer is delayed compared with the more severe FAP syndromes [111]. Extracolonic manifestations seem to be rare, but desmoid tumours and upper gastrointestinal tumours are frequently reported in AFAP patients. The causative germline mutations of AFAP were mostly found in the 5' or 3' ends of the *APC* gene, as well as in the border between exons 4 and 5 and within exon 9 gene, a region that undergoes physiological alternative splicing[93 100 103 107 108 112-120]. Among the extracolonic manifestations, CHRPE has often been linked to mutations between codons 311 and 1465 [103 107-109 113 121 122], desmoid tumours to mutations in the 3' end of *APC*, particularly beyond codon 1400 [123-125], and upper gastrointestinal tumours to mutations in the 3' end [108 121 123], exon 4 [114] and between codons 564 and 1465 [107 108].

However, many studies have provided inconsistencies and contradictions of the genotype-phenotype correlation in FAP [103 118 119 126 127]. For instance, similar phenotypes have been described for germline mutations in very different sites of *APC*, and phenotype variability has been reported between families carrying the same mutation, or even within a family. In addition, the stability of truncated APC proteins have been investigated in clinical samples only in few studies, and in some, the truncated polypeptide was not detected [116 119 128 129]. Thus, although most of the germline *APC* mutations can be identified with *in vitro* transcription/translation assays (a reliable mutation detection method in the genetic diagnosis

of FAP), and the biological role of truncated APC has been investigated in cell lines [130-133] and mouse models [134 135], the *in vivo* situation (i.e. in human colorectal lesions) might be different. The severity of the disease might also be dictated, at the somatic level, by the type of the second mutation occurring in the wild type *APC* allele, and even by a third hit in the mutated allele that may further diminish or abolish the partial function of the truncated APC protein encoded by the germline mutation [136-139]. However, during adenoma progression, the Wnt signalling dysregulation might be also modulated or reinforced by alterations in other components of this signalling pathway, such as the epigenetic silencing of the negative regulator of Wnt *SFRP1* (secreted frizzled-related protein 1) [140]. Finally, alterations in as yet unknown modifier genes might contribute to the phenotype heterogeneity. In conclusion, although genotype-phenotype correlation can be used to focus the initial mutation detection effort on a restricted region of the long *APC* gene, its use as guidance for the clinical surveillance of FAP patients should be discouraged.

Hamartomatous polyposis syndromes

Although they account for less than 1% of all colorectal cancers, the hamartomatous polyposis syndromes represent an interesting example of the importance of integrating clinical and molecular knowledge for a better disease definition, classification and treatment. In these rare syndromes, colorectal hamartomas are one of a large list of clinical features in different organs, and colorectal cancer is not the only neoplasia to which individuals with these syndromes are predisposed (see ref. [141] for a more detailed description of clinical phenotypes). Reports of previously-unreported clinical findings and scrupulous diagnostic re-evaluations of known series of cases and/or families affected by these syndromes lead to frequent revisions of the list of common manifestations that should be used as diagnostic

criteria. As for FAP, the number of first cases in families (probable *de novo* mutations) is rather high (30-50%), and consequently a family history of colorectal cancer is often absent. However, in all the described kindred, inheritance appears to be autosomal dominant. Germline mutations in a number of genes have been found associated with a portion of cases in every syndrome, but other genes, still to be identified, are believed to be altered in the remainder of the cases. The hamartomatous nature of the polyps (disproportionate growth and distribution of cellular lineages that are normal constituents of gastrointestinal mucosa and submucosa) may be explained by the fact that the mutated genes encode proteins involved in signalling pathways regulating the stromal/epithelial homeostasis, i.e., the cross-talk between epithelium and the extracellular matrix, fibroblasts, inflammatory cells and blood vasculature.

Hamartomatous polyposis syndromes fall into three categories: 1) *Juvenile polyposis*, characterized by the presence of multiple juvenile polyps (hamartomas with abundant *lamina propria* that lacks smooth muscle and may contain cystically dilated glands lined by normal-appearing epithelium) in the colorectum and other gastrointestinal tracts, and predisposition to colorectal, gastric, duodenal and pancreatic cancers (atypical juvenile colonic polyps have been also reported in kindred with hereditary mixed polyposis syndrome, along with hyperplastic polyps, serrated and classical adenomas, and colon carcinomas – details on this rare syndrome in [142] –). Juvenile polyposis can be associated with hereditary hemorrhagic telangiectasia; 2) *Peutz-Jeghers syndrome*, with hamartomatous polyps (hamartomas with bands of smooth muscle in the *lamina propria*, similar to those occurring in the colon of patients with tuberous sclerosis) occurring most frequently in the small intestine, characteristic mucocutanous pigmentation (most commonly around the mouth) and high risk for breast, colorectal, pancreatic, gastric, ovarian and other cancers; 3) *Cowden's disease*, in

which the gastrointestinal hamartomas (often juvenile-like polyps that contain some neural elements with no increased risk of cancer) are not the defining feature as in the previous two syndromes, but in which the affected individuals display distinctive mucocutaneous manifestations (the trichilemmomas are patognomonic), benign and malignant breast and thyroid tumours, endometrial and renal cell carcinomas, and central nervous system features such as macrocephaly and adult-onset Lhermitte-Duclos disease, which is characterized by enlarged cerebellar folia containing abnormal ganglion cells. Macrocephaly and gastrointestinal hamartomas similar to those found in Cowden's disease are also manifestations of the developmental disorder *Bannayan-Riley-Rulvalcaba syndrome*.

Colorectal hamartomas in juvenile polyposis and Peutz-Jeghers syndrome are considered neoplastic, and transformation is thought to initiate in the stroma, although adenomatous changes of the epithelium also occur during carcinogenesis. Multiple adenomas, which have been detected concurrently with hamartomas in these conditions, might represent the precancerous lesions in some cases. The genetic evidence accumulated to date indicates that in juvenile polyposis, the primary alteration might deregulate the stroma/epithelium interaction. Indeed, germline mutations in three components (*SMAD4*, *BMPR1A* and *ENG*) of the TGFβ and BMP signalling pathways have been detected in ~50% of juvenile polyposis [143 144]. These two cross-talking signalling pathways are considered important regulators of the interaction between stromal and epithelial cells [145], however, whether the germline alteration in these genes is followed by their somatic inactivation (i.e., second hit in the wild-type allele) in the stromal or the epithelial cells (or both) of the juvenile polyps [146 147] is subject to discussion.

Most of the Peutz-Jegers syndrome cases carry a germline alteration in the *STK11* gene (also called *LKB1*) [148-151], which encodes a nuclear and cytoplasmic serine/threonine

kinase. STK11 is a tumour suppressor with growth-inhibitory effects mediated through induction of the cell-cycle regulators p21 and p27 expression [152 153] and negative regulation of the TSC2/mTOR signalling [154 155]. As shown in **FIGURE 5**, STK11 is activated in situations of energy deprivation, i.e., in conditions that are adverse to cell proliferation such as in the absence of nutrients or growth factors. Activated STK11 phosphorylates and activates AMPK (AMP-activated protein kinase), another serine/threonine kinase, which in turn phosphorylates many substrates involved in energy conservation pathways. One of these substrates is tuberin (TSC2), which, when phosphorylated and activated by AMPK, binds hamartin (TSC1). Activated TSC1/2 inhibits mTOR (target of rapamycin), a critical regulator of protein translation. Indeed, protein synthesis is one of the major energy-consuming processes. Thus, inactivating mutations or loss of *STK11*, as found in Peutz-Jeghers cases, lead to decreased activation of AMPK, downregulation of TSC1/2 function, activation of mTOR and increased translation of proteins that might fuel tumour progression. Independently of this pathway, STK11 inactivation might also favour tumour formation by deregulation of cell polarity [156]. Mutations in either the *TSC1* or *TSC2* tumour suppressor genes also result in a complex hamartomatous syndrome, tuberous sclerosis, with hamartomas in several organs, but only rarely in the colon. It is has been hypothesized that activation of mTOR may initiate hamartomatous tumours through the up-regulation of translation factors (such as eIF4E) and the hypoxia-inducible transcription factor (HIF), which in turn increases the expression of growth factors such as TGFα, PDGFβ and VEGF. For Peutz-Jeghers hamartomas, as for juvenile polyps, the sequence of somatic carcinogenic events in heterozygous *STK11* cells (in particular whether STK11 haploinsufficiency is sufficient or LOH is necessary for transformation), and the cell lineages of the

gastrointestinal mucosa that are primarily involved in transformation, remain to be fully elucidated [157-160].

Interestingly, another molecule, the lipid phosphatase PTEN (phosphatase with tensin homology), whose gene is mutated in the germline of individuals with a variety of clinical syndromes, including Cowden's disease (in ~80% of cases) and Bannayan-Riley-Rulvalcaba syndrome (in ~50% of cases), also impinges on the TSC2/mTOR signalling (**FIGURE 5**). PTEN negatively regulates PI3K (phosphatidylinositol 3-kinase), which is normally activated in response to growth factors. PI3K activates protein kinase B (PKB, also known as AKT), which in turn phosphorylates and inactivates TSC2, leading to increased mTOR activity. Thus, the loss of PTEN function derepresses the mTOR pathway and thus favours cell transformation. It will be important to understand why mTOR signalling is associated with malignant transformation in the breast, the thyroid gland and the endometrium, but not of gastrointestinal hamartomas of patients with Cowden's disease.

Clinical manifestations in the hamartomatous syndromes are complex and clinicians are often unable to assign them to one or the other syndrome. Although in some cases this is the result of poor diagnostics, most of the cases will be clarified by a better understanding of the functional consequences of genetic alterations. For instance, very early onset juvenile polyposes have been reported to be associated with a deletion of a region of 10q encompassing both *PTEN* and *BMPR1A* [144 161 162], a situation in which both the mTOR and the TGFβ signalling are abnormal. Different mutations could also affect the cellular localization of these proteins and mediate different phenotypes. For example, although PTEN acts as a plasma-membrane lipid phosphatase, it is also found in the nucleus. The Cowden's disease associated K289E PTEN mutant was recently found to be defective in nuclear import, yet enzymatically functional, ascribing thus a tumour-suppressive function of

PTEN to its function(s) in the nucleus [163]. Cytoplasmic localization of STK11 is favoured by its interaction with LIP (LKB-interacting protein), and this could favour the formation of STK11-LIP1-SMAD4 ternary complex linking STK11 to the TGFβ pathway [164]. Even more intriguingly, STK11 also interacts with and phosphorylates PTEN, and also this interaction leads to cytoplasmic relocalization of STK11 [165]. The dissection of the extensive cross-talk among pathways involved in different hamartomatoses will eventually help us understand the phenotype and predict the outcome of these diseases.

In conclusion, the diagnosis and classification of hamartomatous syndromes appear much more difficult than those of HNPCC and FAP, due to the complex and variable phenotypes and to the absence of reliable diagnostic tests. These tests will become available when the steps of the carcinogenic process at the somatic level are elucidated. Tests aimed at the identification of abnormalities in the mTOR, TGFβ and BMP pathways in clinical samples should also be developed. It is probable that alterations in other genes involved in these pathways might explain the cases where *PTEN*, *STK11*, *SMAD4* and *BMPR1A* are found normal.

Inflammatory factors in familial and sporadic colorectal neoplastic lesions.

The involvement of inflammation in the development of colorectal cancer is documented by the high incidence of this cancer in patients with long-term ulcerative colitis. However, that inflammation may play a role in the formation of a much larger proportion of colorectal neoplasias was first suggested by epidemiological studies showing that long-term users of aspirin or other NSAID have a reduced risk of developing adenomas and carcinomas [166 167]. Furthermore, the NSAID Sulindac was found to reduce the number and size of adenomas in FAP patients [168 169]. Sulindac showed only an anti-tumour promotion effect

since it was not effective to prevent the onset of adenomas in *APC*-mutation carriers who had not yet developed polyps [170]. In addition, the adenomas relapsed after the Sulindac treatment was stopped. A worldwide chemopreventive trial with aspirin (CAPP2 study) has been initiated also in HNPCC mutation carriers, and the results are expected in 2007. Evidence for an anti tumour initiation effect of NSAIDs came when these drugs (mainly aspirin and COX-2 inhibitors) were used to verify the possibility of reducing the interval between colonoscopies in subjects with a previously-excised, sporadic adenoma [171 (and references herein)]. In these trials, long-term treatment reduced the risk of metachronous adenomas, but the relatively short period of treatment (less than 10 years) was not sufficient to provide evidence of a reduced risk of colorectal cancer. Unfortunately, treatment with the COX-2 inhibitor Celecoxib has been recently found associated with an increased risk of cardiovascular events [171 172]. These two latter observations, together with the obvious benefit of colonoscopy in preventing colon cancer through polypectomy, have recently reduced the enthusiasm in the field of chemoprevention of sporadic adenomas by NSAID, but the use of these substances in inherited polyposis may still be appropriate to reduce the risk of colonic and extra-colonic malignancies. Neverthless, the considerable amount of information gathered from basic and clinical research during the last 15 years clearly indicates that alterations in inflammatory genes and pathways are important mediators of adenoma formation and progression [167 173].

More attention should be focused on the complexity of alterations in factors involved in inflammation in colorectal neoplasms of different type and stage. The finding of an increased expression of only one such factors might not be sufficient to embark on chemopreventive trials. For instance, an increase of *COX-2* expression has been detected not only in adenomatous polyps (more frequently in those of larger size) [174-177], but also in Peutz-Jeghers polyps [178], familial juvenile polyps [179], serrated adenomas [180] and mixed lesions [181],

and Celecoxib has even been used in a small number of Peutz-Jeghers patients [182]. In such histologically different lesions, it is possible that the increased expression of *COX-2* is limited to a particular cell type or subtype, or that it is associated with different patterns of expression of other inflammatory factors. Inflammatory genes and pathways should also be investigated in non-colonic lesions of polyposis syndromes, since their location in organs less accessible than colon make them more difficult to detect and remove in early phase of development and for which a chemopreventive approach might be more justified.

Genomic, transcriptomic and proteomic studies have opened new avenues to investigate the complexity of this phenomenon. As an example of this complexity, we describe here results of a recent study in which we have studied the transcriptome of sporadic adenomatous polyps (≥1cm) compared with that of normal colonic mucosa and colorectal cancers [this latter group included both MMR(+) and MMR(-) tumours]. Although we have not used tissue microdissection to isolate RNA from different cell types (in our experience, this approach reduces RNA quality), our sampling procedure allowed us to enrich for epithelial cell RNA. When we focused on the expression levels of genes included in the "*prostaglandin*" category by Gene Ontology [183], sporadic adenomas could be easily distinguished from normal mucosa and from colon cancers (**FIGURE 6**) (similar results were obtained using a larger series of genes classified in the Gene Ontology category "*inflammatory response*" – data not shown). These data indicate that arachidonic acid metabolism might be considerably remodelled in colorectal tumours and that the remodelling is different in adenomas and carcinomas. For a few genes, mainly those involved in the metabolism of prostaglandin E_2 (PGE2), which has been associated with tumour progression in the colon [173] [167], we show in **FIGURE 6** the average values of expression in a series of colorectal tissues. Interestingly, *PTGS2* (*COX-2*) mRNA was not significantly upregulated in

the adenomas compared with the normal mucosa, but the gene was more than 10 times more expressed in adenocarcinomas, suggesting that upregulation of *PTGS2* is not an early event in colorectal transformation. Thus, while the beneficial effects of COX-2 inhibitors in the treatment of fully-developed adenomas in FAP patients might be explained by our finding, it is difficult to understand the mechanism by which these drugs may prevent or delay the appearance of sporadic adenomas. A second gene encoding the PGE_2 synthesizing enzyme *PTGES*, was also significantly upregulated in carcinomas, whereas *HPGD*, which encodes the key enzyme of the PGE_2 (and other PGs) biological inactivation, was downregulated to the same extent in both adenomas and carcinomas, confirming previous observations [184] [185]. The expression levels of *IL1B*, which plays a role in the regulation of *HPGD* and *PTGS2* [186], and of the four PGE_2 receptors [187] in colorectal tissues are also reported in **FIGURE 6** . Although these gene expression data need to be validated by the analysis of the corresponding proteins in colorectal tissues, they suggest that alternative approaches, such as inhibition of the PGE_2 synthesis acting downstream of PTGS2 (on PTGES [188]) or restoration of an efficient degradation of PGE_2, should be considered to overcome some of the side effects of COX-2 inhibitors.

Global molecular screening analyses should be extended to non-adenomatous colorectal precancerous lesions, inherited or sporadic, and to extracolonic tumours of different familial polyposis. The level and cellular localization of proteins whose genes have been found differentially expressed in these lesions will have to be analyzed with procedures that preserve tissue architecture. The ultimate goal is to identify agents able to modulate molecular pathways, such as inflammation, Wnt, TGFβ, or TSC/mTOR signalling, in a specific way for effective and safe treatment or chemoprevention of colorectal tumours.

Conclusions

Molecular genetics has made tremendous advances during the past decade. This progress was driven on the one hand by technological developments that accompanied the human genome sequencing project and on the other by an increased understanding of the molecular pathways that control the rate of proliferation of cells of different tissues. The latter discoveries were often made in model organisms ranging from yeast through nematodes to fruit flies, and their validity was tested in transgenic mice, which have become an indispensable tool of cancer research. However, it would be wrong to ignore the painstaking efforts of numerous groups that searched for chromosomal aberrations in human cancer cells and that succeeded in identifying the loci, which were later shown to harbour key oncogenes and tumour suppressor genes that have since become household names.

In the specific case of colorectal cancer, the characterization of the Wnt signalling pathway helped us understand at the molecular level how the proliferation of colonic epithelial cells is controlled and why a perturbation of this machinery results in the appearance of polyps in both sporadic and familial colorectal cancer. A better understanding of the biochemistry of DNA metabolism has also been of key importance. Thus, intimate knowledge of mismatch repair helped explain the differences in penetrance of mutations in different *MMR* genes and understanding of the base excision repair of oxidative damage was of key importance in the identification of a link between somatic G to T transversion mutations in the *APC* gene of patients with multiple colonic adenomas and germline mutations in *MYH*. The number of similar examples is getting larger, such that most familial cancers have in the past decade been linked to at least one genetic locus.

With this invaluable genetic information in hand, we have to ask ourselves how to use it most effectively. At this time, it is inconceivable that an inherited mutation could be

corrected, such that the cancer predisposition might be eliminated. What remains are three avenues: diagnosis, prevention and personalized therapy. Identification of at-risk individuals by molecular genetic screening has gained broad acceptance, in spite of the ethical and psychological issues that such diagnosis carries with it. This is particularly true for HNPCC, where the benefits are clear: on the one hand, mutation carriers can be enrolled in endoscopic surveillance programs that are extremely effective in preventing cancer onset by removing colonic polyps during their benign stage. On the other hand, unaffected family members are relieved of the threat of cancer hanging over their heads like the sword of Damocles.

In other cancer predisposition syndromes, such as breast cancer associated with mutations in the *BRCA1* and *BRCA2* genes, cancer onset cannot be prevented, but frequent surveillance ensure that the tumours are detected at a very early stage, which significantly increases the chances of complete remission.

Cancer prevention has met with little success to date. The use of NSAIDs in the prevention of colorectal cancer has suffered some serious setbacks, but this should not mean that attempts at curbing the growth of polyps should cease. It may, however, be necessary to identify better intervention targets based on our latest knowledge of the mechanisms controlling epithelial cell growth. Pathways leading to mutation should also be targeted, Thus, given that *APC* somatic mutations in homozygous *MYH* mutation carriers are linked to oxidative damage, it would be interesting to test the effects of antioxidants on polyp incidence.

In cases where cancer onset could not be prevented, we need to develop new therapeutic criteria that are tailor-made to the affected person. We need to gather as much information as possible about the genetic background of the patient and of the tumour prior to initiating treatment. In many cases, the side effects of chemo- and/or radiotherapy outweigh

their benefits, and it is imperative that we learn to predict these scenarios in the future. If a clinical study reveals that a particular therapeutic regimen had 80% responders, this should not be taken as a justification to treat 100% of the patients with that regimen. Rather, it should bring up the question why 20% failed to respond and, having identified the reason, avoid treating them.

When cancer statistics of the past 30 years are examined, it transpires that we have made very little progress in treating advanced disease. The successes lie in early diagnosis and thus in earlier intervention, as well as in advances in radio-oncology and tumour surgery. It is imperative that advances made in cancer genetics and in our understanding of the molecular mechanisms of cancer make their way into the clinic. Familial cancer predisposition syndromes represent a patient pool, where a substantial wealth of knowledge is already available. What is needed is for basic researchers and clinicians to join forces and develop novel therapeutic approaches based on these foundations.

Acknowledgements

J.S.-B. and E.C. are supported by grants to G.M. of the Zurich Cancer League and the Swiss National Science Foundation, respectively. The generous financial support of the Bonizzi-Theler Foundation, the European Community and the Swiss National Science Foundation to J.J. is also gratefully acknowledged. We thank Jeremy R. Jass for critical reading of the section regarding the serrated pathway of colorectal carcinogenesis.

References

1. Jemal A, Siegel R, Ward E, Murray T, Xu J, Smigal C, et al. Cancer statistics, 2006. *CA Cancer J Clin* 2006;56(2):106-30.
2. Fuchs CS, Giovannucci EL, Colditz GA, Hunter DJ, Speizer FE, Willett WC. A prospective study of family history and the risk of colorectal cancer. *N Engl J Med* 1994;331(25):1669-74.
3. Hendriks YM, de Jong AE, Morreau H, Tops CM, Vasen HF, Wijnen JT, et al. Diagnostic approach and management of Lynch syndrome (hereditary nonpolyposis colorectal carcinoma): a guide for clinicians. *CA Cancer J Clin* 2006;56(4):213-25.
4. Bussey H. Familial polyposis coli. *Baltimore: Johns Hopkins University Press* 1975.
5. Cannon-Albright LA, Skolnick MH, Bishop DT, Lee RG, Burt RW. Common inheritance of susceptibility to colonic adenomatous polyps and associated colorectal cancers. *N Engl J Med* 1988;319(9):533-7.
6. Peinado MA, Malkhosyan S, Velazquez A, Perucho M. Isolation and characterization of allelic losses and gains in colorectal tumours by arbitrarily primed polymerase chain reaction. *Proc Natl Acad Sci U S A* 1992;89(21):10065-9.
7. Marra G, Boland CR. Hereditary nonpolyposis colorectal cancer: the syndrome, the genes, and historical perspectives. *J Natl Cancer Inst* 1995;87(15):1114-25.
8. Herman JG, Umar A, Polyak K, Graff JR, Ahuja N, Issa JP, et al. Incidence and functional consequences of hMLH1 promoter hypermethylation in colorectal carcinoma. *Proc Natl Acad Sci U S A* 1998;95(12):6870-5.
9. Truninger K, Menigatti M, Luz J, Russell A, Haider R, Gebbers JO, et al. Immunohistochemical analysis reveals high frequency of PMS2 defects in colorectal cancer. *Gastroenterology* 2005;128(5):1160-71.
10. Kunkel TA, Bebenek K. DNA replication fidelity. *Annu Rev Biochem* 2000;69:497-529.
11. Jiricny J. The multifaceted mismatch-repair system. *Nat Rev Mol Cell Biol* 2006;7(5):335-46.
12. Kadyrov FA, Dzantiev L, Constantin N, Modrich P. Endonucleolytic function of MutLalpha in human mismatch repair. *Cell* 2006;126(2):297-308.
13. Marra G, Schär P. Recognition of DNA alterations by the mismatch repair system. *Biochem J* 1999;338 (Pt 1):1-13.
14. Drummond JT, Genschel J, Wolf E, Modrich P. DHFR/MSH3 amplification in methotrexate-resistant cells alters the hMutSalpha/hMutSbeta ratio and reduces the efficiency of base-base mismatch repair. *Proc Natl Acad Sci U S A* 1997;94(19):10144-9.
15. Chang DK, Ricciardiello L, Goel A, Chang CL, Boland CR. Steady-state regulation of the human DNA mismatch repair system. *J Biol Chem* 2000;275(24):18424-31.
16. Genschel J, Littman SJ, Drummond JT, Modrich P. Isolation of MutSbeta from human cells and comparison of the mismatch repair specificities of MutSbeta and MutSalpha. *J Biol Chem* 1998;273(31):19895-901.
17. Marra G, Iaccarino I, Lettieri T, Roscilli G, Delmastro P, Jiricny J. Mismatch repair deficiency associated with overexpression of the MSH3 gene. *Proc Natl Acad Sci U S A* 1998;95(15):8568-73.
18. Guerrette S, Wilson T, Gradia S, Fishel R. Interactions of human hMSH2 with hMSH3 and hMSH2 with hMSH6: examination of mutations found in hereditary nonpolyposis colorectal cancer. *Mol Cell Biol* 1998;18(11):6616-23.

19. Räschle M, Marra G, Nyström-Lahti M, Schär P, Jiricny J. Identification of hMutLbeta, a heterodimer of hMLH1 and hPMS1. *J Biol Chem* 1999;274(45):32368-75.
20. Cannavo E, Marra G, Sabates-Bellver J, Menigatti M, Lipkin SM, Fischer F, et al. Expression of the MutL homologue hMLH3 in human cells and its role in DNA mismatch repair. *Cancer Res* 2005;65(23):10759-66.
21. Alam NA, Gorman P, Jaeger EE, Kelsell D, Leigh IM, Ratnavel R, et al. Germline deletions of EXO1 do not cause colorectal tumours and lesions which are null for EXO1 do not have microsatellite instability. *Cancer Genet Cytogenet* 2003;147(2):121-7.
22. Umar A, Boland CR, Terdiman JP, Syngal S, de la Chapelle A, Ruschoff J, et al. Revised Bethesda Guidelines for hereditary nonpolyposis colorectal cancer (Lynch syndrome) and microsatellite instability. *J Natl Cancer Inst* 2004;96(4):261-8.
23. Vasen HF, Watson P, Mecklin JP, Lynch HT. New clinical criteria for hereditary nonpolyposis colorectal cancer (HNPCC, Lynch syndrome) proposed by the International Collaborative group on HNPCC. *Gastroenterology* 1999;116(6):1453-6.
24. Hendriks YM, Wagner A, Morreau H, Menko F, Stormorken A, Quehenberger F, et al. Cancer risk in hereditary nonpolyposis colorectal cancer due to MSH6 mutations: impact on counseling and surveillance. *Gastroenterology* 2004;127(1):17-25.
25. Nicolaides NC, Papadopoulos N, Liu B, Wei YF, Carter KC, Ruben SM, et al. Mutations of two PMS homologues in hereditary nonpolyposis colon cancer. *Nature* 1994;371(6492):75-80.
26. Hamilton SR, Liu B, Parsons RE, Papadopoulos N, Jen J, Powell SM, et al. The molecular basis of Turcot's syndrome. *N Engl J Med* 1995;332(13):839-47.
27. Miyaki M, Nishio J, Konishi M, Kikuchi-Yanoshita R, Tanaka K, Muraoka M, et al. Drastic genetic instability of tumours and normal tissues in Turcot syndrome. *Oncogene* 1997;15(23):2877-81.
28. De Rosa M, Fasano C, Panariello L, Scarano MI, Belli G, Iannelli A, et al. Evidence for a recessive inheritance of Turcot's syndrome caused by compound heterozygous mutations within the PMS2 gene. *Oncogene* 2000;19(13):1719-23.
29. De Vos M, Hayward BE, Picton S, Sheridan E, Bonthron DT. Novel PMS2 pseudogenes can conceal recessive mutations causing a distinctive childhood cancer syndrome. *Am J Hum Genet* 2004;74(5):954-64.
30. Trimbath JD, Petersen GM, Erdman SH, Ferre M, Luce MC, Giardiello FM. Cafe-au-lait spots and early onset colorectal neoplasia: a variant of HNPCC? *Fam Cancer* 2001;1(2):101-5.
31. Paraf F, Jothy S, Van Meir EG. Brain tumour-polyposis syndrome: two genetic diseases? *J Clin Oncol* 1997;15(7):2744-58.
32. Gallinger S, Aronson M, Shayan K, Ratcliffe EM, Gerstle JT, Parkin PC, et al. Gastrointestinal cancers and neurofibromatosis type 1 features in children with a germline homozygous MLH1 mutation. *Gastroenterology* 2004;126(2):576-85.
33. Lipkin SM, Wang V, Jacoby R, Banerjee-Basu S, Baxevanis AD, Lynch HT, et al. MLH3: a DNA mismatch repair gene associated with mammalian microsatellite instability. *Nat Genet* 2000;24(1):27-35.
34. Young J, Simms LA, Biden KG, Wynter C, Whitehall V, Karamatic R, et al. Features of colorectal cancers with high-level microsatellite instability occurring in familial and sporadic settings: parallel pathways of tumourigenesis. *Am J Pathol* 2001;159(6):2107-16.

35. Plaschke J, Kruger S, Pistorius S, Theissig F, Saeger HD, Schackert HK. Involvement of hMSH6 in the development of hereditary and sporadic colorectal cancer revealed by immunostaining is based on germline mutations, but rarely on somatic inactivation. *Int J Cancer* 2002;97(5):643-8.
36. Rigau V, Sebbagh N, Olschwang S, Paraf F, Mourra N, Parc Y, et al. Microsatellite instability in colorectal carcinoma. The comparison of immunohistochemistry and molecular biology suggests a role for hMSH6 [correction of hMLH6] immunostaining. *Arch Pathol Lab Med* 2003;127(6):694-700.
37. de Jong AE, van Puijenbroek M, Hendriks Y, Tops C, Wijnen J, Ausems MG, et al. Microsatellite instability, immunohistochemistry, and additional PMS2 staining in suspected hereditary nonpolyposis colorectal cancer. *Clin Cancer Res* 2004;10(3):972-80.
38. Nakagawa H, Lockman JC, Frankel WL, Hampel H, Steenblock K, Burgart LJ, et al. Mismatch repair gene PMS2: disease-causing germline mutations are frequent in patients whose tumours stain negative for PMS2 protein, but paralogous genes obscure mutation detection and interpretation. *Cancer Res* 2004;64(14):4721-7.
39. Hendriks YM, Jagmohan-Changur S, van der Klift HM, Morreau H, van Puijenbroek M, Tops C, et al. Heterozygous mutations in PMS2 cause hereditary nonpolyposis colorectal carcinoma (Lynch syndrome). *Gastroenterology* 2006;130(2):312-22.
40. Jacoby RF, Marshall DJ, Kailas S, Schlack S, Harms B, Love R. Genetic instability associated with adenoma to carcinoma progression in hereditary nonpolyposis colon cancer. *Gastroenterology* 1995;109(1):73-82.
41. de Jong AE, Morreau H, Van Puijenbroek M, Eilers PH, Wijnen J, Nagengast FM, et al. The role of mismatch repair gene defects in the development of adenomas in patients with HNPCC. *Gastroenterology* 2004;126(1):42-8.
42. Markowitz S, Wang J, Myeroff L, Parsons R, Sun L, Lutterbaugh J, et al. Inactivation of the type II TGF-beta receptor in colon cancer cells with microsatellite instability. *Science* 1995;268(5215):1336-8.
43. Rampino N, Yamamoto H, Ionov Y, Li Y, Sawai H, Reed JC, et al. Somatic frameshift mutations in the BAX gene in colon cancers of the microsatellite mutator phenotype. *Science* 1997;275(5302):967-9.
44. di Pietro M, Sabates Bellver J, Menigatti M, Bannwart F, Schnider A, Russell A, et al. Defective DNA mismatch repair determines a characteristic transcriptional profile in proximal colon cancers. *Gastroenterology* 2005;129(3):1047-59.
45. Stojic L, Brun R, Jiricny J. Mismatch repair and DNA damage signalling. *DNA Repair (Amst)* 2004;3(8-9):1091-101.
46. Carethers JM, Smith EJ, Behling CA, Nguyen L, Tajima A, Doctolero RT, et al. Use of 5-fluorouracil and survival in patients with microsatellite-unstable colorectal cancer. *Gastroenterology* 2004;126(2):394-401.
47. Ribic CM, Sargent DJ, Moore MJ, Thibodeau SN, French AJ, Goldberg RM, et al. Tumour microsatellite-instability status as a predictor of benefit from fluorouracil-based adjuvant chemotherapy for colon cancer. *N Engl J Med* 2003;349(3):247-57.
48. Jass JR. Classification of colorectal cancer based on correlation of clinical, morphological and molecular features. *Histopathology* 2007;50(1):113-30.
49. Jass JR, Whitehall VL, Young J, Leggett BA. Emerging concepts in colorectal neoplasia. *Gastroenterology* 2002;123(3):862-76.

50. Goldstein NS, Bhanot P, Odish E, Hunter S. Hyperplastic-like colon polyps that preceded microsatellite-unstable adenocarcinomas. *Am J Clin Pathol* 2003;119(6):778-96.
51. Jass JR, Baker K, Zlobec I, Higuchi T, Barker M, Buchanan D, et al. Advanced colorectal polyps with the molecular and morphological features of serrated polyps and adenomas: concept of a 'fusion' pathway to colorectal cancer. *Histopathology* 2006;49(2):121-31.
52. Liljegren A, Lindblom A, Rotstein S, Nilsson B, Rubio C, Jaramillo E. Prevalence and incidence of hyperplastic polyps and adenomas in familial colorectal cancer: correlation between the two types of colon polyps. *Gut* 2003;52(8):1140-7.
53. Snover DC. Serrated polyps of the large intestine. *Semin Diagn Pathol* 2005;22(4):301-8.
54. Torlakovic E, Skovlund E, Snover DC, Torlakovic G, Nesland JM. Morphologic reappraisal of serrated colorectal polyps. *Am J Surg Pathol* 2003;27(1):65-81.
55. Snover DC, Jass JR, Fenoglio-Preiser C, Batts KP. Serrated polyps of the large intestine: a morphologic and molecular review of an evolving concept. *Am J Clin Pathol* 2005;124(3):380-91.
56. Soetikno R, Friedland S, Kaltenbach T, Chayama K, Tanaka S. Nonpolypoid (flat and depressed) colorectal neoplasms. *Gastroenterology* 2006;130(2):566-76; quiz 588-9.
57. Makinen MJ. Colorectal serrated adenocarcinoma. *Histopathology* 2007;50(1):131-50.
58. O'Brien MJ, Yang S, Mack C, Xu H, Huang CS, Mulcahy E, et al. Comparison of microsatellite instability, CpG island methylation phenotype, BRAF and KRAS status in serrated polyps and traditional adenomas indicates separate pathways to distinct colorectal carcinoma end points. *Am J Surg Pathol* 2006;30(12):1491-501.
59. Torlakovic E, Snover DC. Sessile serrated adenoma: a brief history and current status. *Crit Rev Oncog* 2006;12(1-2):27-39.
60. Oh K, Redston M, Odze RD. Support for hMLH1 and MGMT silencing as a mechanism of tumourigenesis in the hyperplastic-adenoma-carcinoma (serrated) carcinogenic pathway in the colon. *Hum Pathol* 2005;36(1):101-11.
61. Davies H, Bignell GR, Cox C, Stephens P, Edkins S, Clegg S, et al. Mutations of the BRAF gene in human cancer. *Nature* 2002;417(6892):949-54.
62. Weisenberger DJ, Siegmund KD, Campan M, Young J, Long TI, Faasse MA, et al. CpG island methylator phenotype underlies sporadic microsatellite instability and is tightly associated with BRAF mutation in colorectal cancer. *Nat Genet* 2006;38(7):787-93.
63. Kambara T, Simms LA, Whitehall VL, Spring KJ, Wynter CV, Walsh MD, et al. BRAF mutation is associated with DNA methylation in serrated polyps and cancers of the colorectum. *Gut* 2004;53(8):1137-44.
64. Deng G, Bell I, Crawley S, Gum J, Terdiman JP, Allen BA, et al. BRAF mutation is frequently present in sporadic colorectal cancer with methylated hMLH1, but not in hereditary nonpolyposis colorectal cancer. *Clin Cancer Res* 2004;10(1 Pt 1):191-5.
65. Wan PT, Garnett MJ, Roe SM, Lee S, Niculescu-Duvaz D, Good VM, et al. Mechanism of activation of the RAF-ERK signaling pathway by oncogenic mutations of B-RAF. *Cell* 2004;116(6):855-67.
66. Lubomierski N, Plotz G, Wormek M, Engels K, Kriener S, Trojan J, et al. BRAF mutations in colorectal carcinoma suggest two entities of microsatellite-unstable tumours. *Cancer* 2005;104(5):952-61.
67. Vandrovcova J, Lagerstedt-Robinsson K, Pahlman L, Lindblom A. Somatic BRAF-V600E mutations in familial colorectal cancer. *Cancer Epidemiol Biomarkers Prev* 2006;15(11):2270-3.

68. Young J, Barker MA, Simms LA, Walsh MD, Biden KG, Buchanan D, et al. Evidence for BRAF mutation and variable levels of microsatellite instability in a syndrome of familial colorectal cancer. *Clin Gastroenterol Hepatol* 2005;3(3):254-63.
69. Hawkins NJ, Ward RL. Sporadic colorectal cancers with microsatellite instability and their possible origin in hyperplastic polyps and serrated adenomas. *J Natl Cancer Inst* 2001;93(17):1307-13.
70. Frazier ML, Xi L, Zong J, Viscofsky N, Rashid A, Wu EF, et al. Association of the CpG island methylator phenotype with family history of cancer in patients with colorectal cancer. *Cancer Res* 2003;63(16):4805-8.
71. Wynter CV, Walsh MD, Higuchi T, Leggett BA, Young J, Jass JR. Methylation patterns define two types of hyperplastic polyp associated with colorectal cancer. *Gut* 2004;53(4):573-80.
72. Ward RL, Williams R, Law M, Hawkins NJ. The CpG island methylator phenotype is not associated with a personal or family history of cancer. *Cancer Res* 2004;64(20):7618-21.
73. Chan TL, Zhao W, Leung SY, Yuen ST. BRAF and KRAS mutations in colorectal hyperplastic polyps and serrated adenomas. *Cancer Res* 2003;63(16):4878-81.
74. Beach R, Chan AO, Wu TT, White JA, Morris JS, Lunagomez S, et al. BRAF mutations in aberrant crypt foci and hyperplastic polyposis. *Am J Pathol* 2005;166(4):1069-75.
75. Spring KJ, Zhao ZZ, Karamatic R, Walsh MD, Whitehall VL, Pike T, et al. High prevalence of sessile serrated adenomas with BRAF mutations: a prospective study of patients undergoing colonoscopy. *Gastroenterology* 2006;131(5):1400-7.
76. Chan AO, Issa JP, Morris JS, Hamilton SR, Rashid A. Concordant CpG island methylation in hyperplastic polyposis. *Am J Pathol* 2002;160(2):529-36.
77. Rubio CA, Stemme S, Jaramillo E, Lindblom A. Hyperplastic polyposis coli syndrome and colorectal carcinoma. *Endoscopy* 2006;38(3):266-70.
78. Lauwers GY, Chung DC. The serrated polyp comes of age. *Gastroenterology* 2006;131(5):1631-4.
79. Goswami RS, Minoo P, Baker K, Chong G, Foulkes WD, Jass JR. Hyperplastic polyposis and cancer of the colon with gastrinoma of the duodenum. *Nat Clin Pract Oncol* 2006;3(5):281-4; quiz 285.
80. Burt RW JJ. *World Health Organization classification of tumours. Pathology & genetics. Tumours of the digestive system.*, 2000.
81. Jass JR. Familial colorectal cancer: pathology and molecular characteristics. *Lancet Oncol* 2000;1:220-6.
82. Ferrandez A, Samowitz W, DiSario JA, Burt RW. Phenotypic characteristics and risk of cancer development in hyperplastic polyposis: case series and literature review. *Am J Gastroenterol* 2004;99(10):2012-8.
83. Lage P, Cravo M, Sousa R, Chaves P, Salazar M, Fonseca R, et al. Management of Portuguese patients with hyperplastic polyposis and screening of at-risk first-degree relatives: a contribution for future guidelines based on a clinical study. *Am J Gastroenterol* 2004;99(9):1779-84.
84. Minoo P, Baker K, Goswami R, Chong G, Foulkes WD, Ruszkiewicz AR, et al. Extensive DNA methylation in normal colorectal mucosa in hyperplastic polyposis. *Gut* 2006;55(10):1467-74.

85. Young J, Jass JR. The case for a genetic predisposition to serrated neoplasia in the colorectum: hypothesis and review of the literature. *Cancer Epidemiol Biomarkers Prev* 2006;15(10):1778-84.
86. Chow E, Lipton L, Lynch E, D'Souza R, Aragona C, Hodgkin L, et al. Hyperplastic polyposis syndrome: phenotypic presentations and the role of MBD4 and MYH. *Gastroenterology* 2006;131(1):30-9.
87. Knudsen AL, Bisgaard ML, Bulow S. Attenuated familial adenomatous polyposis (AFAP). A review of the literature. *Fam Cancer* 2003;2(1):43-55.
88. Groden J, Thliveris A, Samowitz W, Carlson M, Gelbert L, Albertsen H, et al. Identification and characterization of the familial adenomatous polyposis coli gene. *Cell* 1991;66(3):589-600.
89. Kinzler KW, Nilbert MC, Su LK, Vogelstein B, Bryan TM, Levy DB, et al. Identification of FAP locus genes from chromosome 5q21. *Science* 1991;253(5020):661-5.
90. Nishisho I, Nakamura Y, Miyoshi Y, Miki Y, Ando H, Horii A, et al. Mutations of chromosome 5q21 genes in FAP and colorectal cancer patients. *Science* 1991;253(5020):665-9.
91. Laurent-Puig P, Beroud C, Soussi T. APC gene: database of germline and somatic mutations in human tumours and cell lines. *Nucleic Acids Res* 1998;26(1):269-70.
92. Bertario L, Russo A, Sala P, Varesco L, Giarola M, Mondini P, et al. Multiple approach to the exploration of genotype-phenotype correlations in familial adenomatous polyposis. *J Clin Oncol* 2003;21(9):1698-707.
93. Moisio AL, Jarvinen H, Peltomaki P. Genetic and clinical characterisation of familial adenomatous polyposis: a population based study. *Gut* 2002;50(6):845-50.
94. Al-Tassan N, Chmiel NH, Maynard J, Fleming N, Livingston AL, Williams GT, et al. Inherited variants of MYH associated with somatic G:C-->T:A mutations in colorectal tumours. *Nat Genet* 2002;30(2):227-32.
95. Kairupan CF, Meldrum CJ, Crooks R, Milward EA, Spigelman AD, Burgess B, et al. Mutation analysis of the MYH gene in an Australian series of colorectal polyposis patients with or without germline APC mutations. *Int J Cancer* 2005;116(1):73-7.
96. Leite JS, Isidro G, Martins M, Regateiro F, Albuquerque O, Amaro P, et al. Is prophylactic colectomy indicated in patients with MYH-associated polyposis? *Colorectal Dis* 2005;7(4):327-31.
97. Sieber OM, Lipton L, Crabtree M, Heinimann K, Fidalgo P, Phillips RK, et al. Multiple colorectal adenomas, classic adenomatous polyposis, and germ-line mutations in MYH. *N Engl J Med* 2003;348(9):791-9.
98. Marra G, Jiricny J. Multiple colorectal adenomas--is their number up? *N Engl J Med* 2003;348(9):845-7.
99. Schneikert J, Behrens J. The canonical Wnt signalling pathway and its APC partner in colon cancer development. *Gut* 2007;56(3):417-25.
100. Friedl W, Caspari R, Sengteller M, Uhlhaas S, Lamberti C, Jungck M, et al. Can APC mutation analysis contribute to therapeutic decisions in familial adenomatous polyposis? Experience from 680 FAP families. *Gut* 2001;48(4):515-21.
101. Miyoshi Y, Ando H, Nagase H, Nishisho I, Horii A, Miki Y, et al. Germ-line mutations of the APC gene in 53 familial adenomatous polyposis patients. *Proc Natl Acad Sci U S A* 1992;89(10):4452-6.

102. Caspari R, Friedl W, Mandl M, Moslein G, Kadmon M, Knapp M, et al. Familial adenomatous polyposis: mutation at codon 1309 and early onset of colon cancer. *Lancet* 1994;343(8898):629-32.
103. Walon C, Kartheuser A, Michils G, Smaers M, Lannoy N, Ngounou P, et al. Novel germline mutations in the APC gene and their phenotypic spectrum in familial adenomatous polyposis kindreds. *Hum Genet* 1997;100(5-6):601-5.
104. Michils G, Tejpar S, Thoelen R, van Cutsem E, Vermeesch JR, Fryns JP, et al. Large deletions of the APC gene in 15% of mutation-negative patients with classical polyposis (FAP): a Belgian study. *Hum Mutat* 2005;25(2):125-34.
105. Sieber OM, Lamlum H, Crabtree MD, Rowan AJ, Barclay E, Lipton L, et al. Whole-gene APC deletions cause classical familial adenomatous polyposis, but not attenuated polyposis or "multiple" colorectal adenomas. *Proc Natl Acad Sci U S A* 2002;99(5):2954-8.
106. Goss KH, Groden J. Biology of the adenomatous polyposis coli tumour suppressor. *J Clin Oncol* 2000;18(9):1967-79.
107. Enomoto M, Konishi M, Iwama T, Utsunomiya J, Sugihara KI, Miyaki M. The relationship between frequencies of extracolonic manifestations and the position of APC germline mutation in patients with familial adenomatous polyposis. *Jpn J Clin Oncol* 2000;30(2):82-8.
108. Ficari F, Cama A, Valanzano R, Curia MC, Palmirotta R, Aceto G, et al. APC gene mutations and colorectal adenomatosis in familial adenomatous polyposis. *Br J Cancer* 2000;82(2):348-53.
109. Dihlmann S, Gebert J, Siermann A, Herfarth C, von Knebel Doeberitz M. Dominant negative effect of the APC1309 mutation: a possible explanation for genotype-phenotype correlations in familial adenomatous polyposis. *Cancer Res* 1999;59(8):1857-60.
110. Michils G, Tejpar S, Fryns JP, Legius E, Van Cutsem E, Cassiman JJ, et al. Pathogenic mutations and rare variants of the APC gene identified in 75 Belgian patients with familial adenomatous polyposis by fluorescent enzymatic mutation detection (EMD). *Eur J Hum Genet* 2002;10(9):505-10.
111. Groden J, Gelbert L, Thliveris A, Nelson L, Robertson M, Joslyn G, et al. Mutational analysis of patients with adenomatous polyposis: identical inactivating mutations in unrelated individuals. *Am J Hum Genet* 1993;52(2):263-72.
112. Fearnhead NS, Britton MP, Bodmer WF. The ABC of APC. *Hum Mol Genet* 2001;10(7):721-33.
113. Giardiello FM, Petersen GM, Piantadosi S, Gruber SB, Traboulsi EI, Offerhaus GJ, et al. APC gene mutations and extraintestinal phenotype of familial adenomatous polyposis. *Gut* 1997;40(4):521-5.
114. Soravia C, Berk T, Madlensky L, Mitri A, Cheng H, Gallinger S, et al. Genotype-phenotype correlations in attenuated adenomatous polyposis coli. *Am J Hum Genet* 1998;62(6):1290-301.
115. Spirio L, Olschwang S, Groden J, Robertson M, Samowitz W, Joslyn G, et al. Alleles of the APC gene: an attenuated form of familial polyposis. *Cell* 1993;75(5):951-7.
116. van der Luijt RB, Meera Khan P, Vasen HF, Breukel C, Tops CM, Scott RJ, et al. Germline mutations in the 3' part of APC exon 15 do not result in truncated proteins and are associated with attenuated adenomatous polyposis coli. *Hum Genet* 1996;98(6):727-34.

117. Gebert JF, Dupon C, Kadmon M, Hahn M, Herfarth C, von Knebel Doeberitz M, et al. Combined molecular and clinical approaches for the identification of families with familial adenomatous polyposis coli. *Ann Surg* 1999;229(3):350-61.
118. Rozen P, Samuel Z, Shomrat R, Legum C. Notable intrafamilial phenotypic variability in a kindred with familial adenomatous polyposis and an APC mutation in exon 9. *Gut* 1999;45(6):829-33.
119. van der Luijt RB, Vasen HF, Tops CM, Breukel C, Fodde R, Meera Khan P. APC mutation in the alternatively spliced region of exon 9 associated with late onset familial adenomatous polyposis. *Hum Genet* 1995;96(6):705-10.
120. Young J, Simms LA, Tarish J, Buttenshaw R, Knight N, Anderson GJ, et al. A family with attenuated familial adenomatous polyposis due to a mutation in the alternatively spliced region of APC exon 9. *Hum Mutat* 1998;11(6):450-5.
121. Caspari R, Olschwang S, Friedl W, Mandl M, Boisson C, Boker T, et al. Familial adenomatous polyposis: desmoid tumours and lack of ophthalmic lesions (CHRPE) associated with APC mutations beyond codon 1444. *Hum Mol Genet* 1995;4(3):337-40.
122. Davies DR, Armstrong JG, Thakker N, Horner K, Guy SP, Clancy T, et al. Severe Gardner syndrome in families with mutations restricted to a specific region of the APC gene. *Am J Hum Genet* 1995;57(5):1151-8.
123. Dobbie Z, Spycher M, Mary JL, Haner M, Guldenschuh I, Hurliman R, et al. Correlation between the development of extracolonic manifestations in FAP patients and mutations beyond codon 1403 in the APC gene. *J Med Genet* 1996;33(4):274-80.
124. Eccles DM, van der Luijt R, Breukel C, Bullman H, Bunyan D, Fisher A, et al. Hereditary desmoid disease due to a frameshift mutation at codon 1924 of the APC gene. *Am J Hum Genet* 1996;59(6):1193-201.
125. Scott RJ, Froggatt NJ, Trembath RC, Evans DG, Hodgson SV, Maher ER. Familial infiltrative fibromatosis (desmoid tumours) (MIM135290) caused by a recurrent 3' APC gene mutation. *Hum Mol Genet* 1996;5(12):1921-4.
126. Burt RW, Leppert MF, Slattery ML, Samowitz WS, Spirio LN, Kerber RA, et al. Genetic testing and phenotype in a large kindred with attenuated familial adenomatous polyposis. *Gastroenterology* 2004;127(2):444-51.
127. Su LK, Kohlmann W, Ward PA, Lynch PM. Different familial adenomatous polyposis phenotypes resulting from deletions of the entire APC exon 15. *Hum Genet* 2002;111(1):88-95.
128. Smith KJ, Johnson KA, Bryan TM, Hill DE, Markowitz S, Willson JK, et al. The APC gene product in normal and tumour cells. *Proc Natl Acad Sci U S A* 1993;90(7):2846-50.
129. Akehi S, Murao S, Ueda N, Okujima M, Magaribuchi T, Saheki S, et al. Immunohistochemical detection of truncated APC protein in sporadic human colorectal adenomas and adenocarcinomas. *Virchows Arch* 1996;429(1):21-6.
130. Schneikert J, Grohmann A, Behrens J. Truncated APC regulates the transcriptional activity of beta-catenin in a cell cycle dependent manner. *Hum Mol Genet* 2007;16(2):199-209.
131. Kawasaki Y, Sato R, Akiyama T. Mutated APC and Asef are involved in the migration of colorectal tumour cells. *Nat Cell Biol* 2003;5(3):211-5.

132. Tighe A, Johnson VL, Taylor SS. Truncating APC mutations have dominant effects on proliferation, spindle checkpoint control, survival and chromosome stability. *J Cell Sci* 2004;117(Pt 26):6339-53.
133. Heppner Goss K, Trzepacz C, Tuohy TM, Groden J. Attenuated APC alleles produce functional protein from internal translation initiation. *Proc Natl Acad Sci U S A* 2002;99(12):8161-6.
134. Smits R, Kielman MF, Breukel C, Zurcher C, Neufeld K, Jagmohan-Changur S, et al. Apc1638T: a mouse model delineating critical domains of the adenomatous polyposis coli protein involved in tumourigenesis and development. *Genes Dev* 1999;13(10):1309-21.
135. Li Q, Ishikawa TO, Oshima M, Taketo MM. The threshold level of adenomatous polyposis coli protein for mouse intestinal tumourigenesis. *Cancer Res* 2005;65(19):8622-7.
136. Lamlum H, Ilyas M, Rowan A, Clark S, Johnson V, Bell J, et al. The type of somatic mutation at APC in familial adenomatous polyposis is determined by the site of the germline mutation: a new facet to Knudson's 'two-hit' hypothesis. *Nat Med* 1999;5(9):1071-5.
137. Spirio LN, Samowitz W, Robertson J, Robertson M, Burt RW, Leppert M, et al. Alleles of APC modulate the frequency and classes of mutations that lead to colon polyps. *Nat Genet* 1998;20(4):385-8.
138. Rowan AJ, Lamlum H, Ilyas M, Wheeler J, Straub J, Papadopoulou A, et al. APC mutations in sporadic colorectal tumours: A mutational "hotspot" and interdependence of the "two hits". *Proc Natl Acad Sci U S A* 2000;97(7):3352-7.
139. Sieber OM, Segditsas S, Knudsen AL, Zhang J, Luz J, Rowan AJ, et al. Disease severity and genetic pathways in attenuated familial adenomatous polyposis vary greatly but depend on the site of the germline mutation. *Gut* 2006;55(10):1440-1448.
140. Suzuki H, Gabrielson E, Chen W, Anbazhagan R, van Engeland M, Weijenberg MP, et al. A genomic screen for genes upregulated by demethylation and histone deacetylase inhibition in human colorectal cancer. *Nat Genet* 2002;31(2):141-9.
141. Doxey BW, Kuwada SK, Burt RW. Inherited polyposis syndromes: molecular mechanisms, clinicopathology, and genetic testing. *Clin Gastroenterol Hepatol* 2005;3(7):633-41.
142. Jaeger EE, Woodford-Richens KL, Lockett M, Rowan AJ, Sawyer EJ, Heinimann K, et al. An ancestral Ashkenazi haplotype at the HMPS/CRAC1 locus on 15q13-q14 is associated with hereditary mixed polyposis syndrome. *Am J Hum Genet* 2003;72(5):1261-7.
143. Howe JR, Sayed MG, Ahmed AF, Ringold J, Larsen-Haidle J, Merg A, et al. The prevalence of MADH4 and BMPR1A mutations in juvenile polyposis and absence of BMPR2, BMPR1B, and ACVR1 mutations. *J Med Genet* 2004;41(7):484-91.
144. Sweet K, Willis J, Zhou XP, Gallione C, Sawada T, Alhopuro P, et al. Molecular classification of patients with unexplained hamartomatous and hyperplastic polyposis. *Jama* 2005;294(19):2465-73.
145. Bhowmick NA, Chytil A, Plieth D, Gorska AE, Dumont N, Shappell S, et al. TGF-beta signaling in fibroblasts modulates the oncogenic potential of adjacent epithelia. *Science* 2004;303(5659):848-51.
146. Woodford-Richens K, Williamson J, Bevan S, Young J, Leggett B, Frayling I, et al. Allelic loss at SMAD4 in polyps from juvenile polyposis patients and use of

fluorescence in situ hybridization to demonstrate clonal origin of the epithelium. *Cancer Res* 2000;60(9):2477-82.
147. Kim BG, Li C, Qiao W, Mamura M, Kasprzak B, Anver M, et al. Smad4 signalling in T cells is required for suppression of gastrointestinal cancer. *Nature* 2006;441(7096):1015-9.
148. Hemminki A, Markie D, Tomlinson I, Avizienyte E, Roth S, Loukola A, et al. A serine/threonine kinase gene defective in Peutz-Jeghers syndrome. *Nature* 1998;391(6663):184-7.
149. Hearle N, Schumacher V, Menko FH, Olschwang S, Boardman LA, Gille JJ, et al. Frequency and spectrum of cancers in the Peutz-Jeghers syndrome. *Clin Cancer Res* 2006;12(10):3209-15.
150. Jenne DE, Reimann H, Nezu J, Friedel W, Loff S, Jeschke R, et al. Peutz-Jeghers syndrome is caused by mutations in a novel serine threonine kinase. *Nat Genet* 1998;18(1):38-43.
151. Aretz S, Stienen D, Uhlhaas S, Loff S, Back W, Pagenstecher C, et al. High proportion of large genomic STK11 deletions in Peutz-Jeghers syndrome. *Hum Mutat* 2005;26(6):513-9.
152. Tiainen M, Vaahtomeri K, Ylikorkala A, Makela TP. Growth arrest by the LKB1 tumour suppressor: induction of p21(WAF1/CIP1). *Hum Mol Genet* 2002;11(13):1497-504.
153. Xie X, Wang Z, Chen Y. Association of LKB1 with a WD-repeat protein WDR6 is implicated in cell growth arrest and p27(Kip1) induction. *Mol Cell Biochem* 2007.
154. Corradetti MN, Inoki K, Bardeesy N, DePinho RA, Guan KL. Regulation of the TSC pathway by LKB1: evidence of a molecular link between tuberous sclerosis complex and Peutz-Jeghers syndrome. *Genes Dev* 2004;18(13):1533-8.
155. Shaw RJ, Bardeesy N, Manning BD, Lopez L, Kosmatka M, DePinho RA, et al. The LKB1 tumour suppressor negatively regulates mTOR signaling. *Cancer Cell* 2004;6(1):91-9.
156. Baas AF, Smit L, Clevers H. LKB1 tumour suppressor protein: PARtaker in cell polarity. *Trends Cell Biol* 2004;14(6):312-9.
157. Wang ZJ, Ellis I, Zauber P, Iwama T, Marchese C, Talbot I, et al. Allelic imbalance at the LKB1 (STK11) locus in tumours from patients with Peutz-Jeghers' syndrome provides evidence for a hamartoma-(adenoma)-carcinoma sequence. *J Pathol* 1999;188(1):9-13.
158. Bardeesy N, Sinha M, Hezel AF, Signoretti S, Hathaway NA, Sharpless NE, et al. Loss of the Lkb1 tumour suppressor provokes intestinal polyposis but resistance to transformation. *Nature* 2002;419(6903):162-7.
159. Miyoshi H, Nakau M, Ishikawa TO, Seldin MF, Oshima M, Taketo MM. Gastrointestinal hamartomatous polyposis in Lkb1 heterozygous knockout mice. *Cancer Res* 2002;62(8):2261-6.
160. Katajisto P, Vallenius T, Vaahtomeri K, Ekman N, Udd L, Tiainen M, et al. The LKB1 tumour suppressor kinase in human disease. *Biochim Biophys Acta* 2007;1775(1):63-75.
161. Delnatte C, Sanlaville D, Mougenot JF, Vermeesch JR, Houdayer C, Blois MC, et al. Contiguous gene deletion within chromosome arm 10q is associated with juvenile polyposis of infancy, reflecting cooperation between the BMPR1A and PTEN tumour-suppressor genes. *Am J Hum Genet* 2006;78(6):1066-74.

162. Salviati L, Patricelli M, Guariso G, Sturniolo GC, Alaggio R, Bernardi F, et al. Deletion of PTEN and BMPR1A on chromosome 10q23 is not always associated with juvenile polyposis of infancy. *Am J Hum Genet* 2006;79(3):593-6; author reply 596-7.
163. Trotman LC, Wang X, Alimonti A, Chen Z, Teruya-Feldstein J, Yang H, et al. Ubiquitination Regulates PTEN Nuclear Import and Tumour Suppression. *Cell* 2007;128(1):141-56.
164. Smith DP, Rayter SI, Niederlander C, Spicer J, Jones CM, Ashworth A. LIP1, a cytoplasmic protein functionally linked to the Peutz-Jeghers syndrome kinase LKB1. *Hum Mol Genet* 2001;10(25):2869-77.
165. Mehenni H, Lin-Marq N, Buchet-Poyau K, Reymond A, Collart MA, Picard D, et al. LKB1 interacts with and phosphorylates PTEN: a functional link between two proteins involved in cancer predisposing syndromes. *Hum Mol Genet* 2005;14(15):2209-19.
166. Giovannucci E, Egan KM, Hunter DJ, Stampfer MJ, Colditz GA, Willett WC, et al. Aspirin and the risk of colorectal cancer in women. *N Engl J Med* 1995;333(10):609-14.
167. Dannenberg AJ, Subbaramaiah K. Targeting cyclooxygenase-2 in human neoplasia: rationale and promise. *Cancer Cell* 2003;4(6):431-6.
168. Giardiello FM, Hamilton SR, Krush AJ, Piantadosi S, Hylind LM, Celano P, et al. Treatment of colonic and rectal adenomas with sulindac in familial adenomatous polyposis. *N Engl J Med* 1993;328(18):1313-6.
169. Cruz-Correa M, Hylind LM, Romans KE, Booker SV, Giardiello FM. Long-term treatment with sulindac in familial adenomatous polyposis: a prospective cohort study. *Gastroenterology* 2002;122(3):641-5.
170. Giardiello FM, Yang VW, Hylind LM, Krush AJ, Petersen GM, Trimbath JD, et al. Primary chemoprevention of familial adenomatous polyposis with sulindac. *N Engl J Med* 2002;346(14):1054-9.
171. Psaty BM, Potter JD. Risks and benefits of celecoxib to prevent recurrent adenomas. *N Engl J Med* 2006;355(9):950-2.
172. Kearney PM, Baigent C, Godwin J, Halls H, Emberson JR, Patrono C. Do selective cyclo-oxygenase-2 inhibitors and traditional non-steroidal anti-inflammatory drugs increase the risk of atherothrombosis? Meta-analysis of randomised trials. *Bmj* 2006;332(7553):1302-8.
173. Buchanan FG, DuBois RN. Connecting COX-2 and Wnt in cancer. *Cancer Cell* 2006;9(1):6-8.
174. Elder DJ, Baker JA, Banu NA, Moorghen M, Paraskeva C. Human colorectal adenomas demonstrate a size-dependent increase in epithelial cyclooxygenase-2 expression. *J Pathol* 2002;198(4):428-34.
175. Chapple KS, Cartwright EJ, Hawcroft G, Tisbury A, Bonifer C, Scott N, et al. Localization of cyclooxygenase-2 in human sporadic colorectal adenomas. *Am J Pathol* 2000;156(2):545-53.
176. Hao X, Bishop AE, Wallace M, Wang H, Willcocks TC, Maclouf J, et al. Early expression of cyclo-oxygenase-2 during sporadic colorectal carcinogenesis. *J Pathol* 1999;187(3):295-301.
177. Eberhart CE, Coffey RJ, Radhika A, Giardiello FM, Ferrenbach S, DuBois RN. Up-regulation of cyclooxygenase 2 gene expression in human colorectal adenomas and adenocarcinomas. *Gastroenterology* 1994;107(4):1183-8.

178. McGarrity TJ, Peiffer LP, Amos CI, Frazier ML, Ward MG, Howett MK. Overexpression of cyclooxygenase 2 in hamartomatous polyps of Peutz-Jeghers syndrome. *Am J Gastroenterol* 2003;98(3):671-8.
179. Brazowski E, Rozen P, Misonzhnick-Bedny F, Gitstein G. Characteristics of familial juvenile polyps expressing cyclooxygenase-2. *Am J Gastroenterol* 2005;100(1):130-8.
180. Takeuchi M, Kobayashi M, Ajioka Y, Honma T, Suzuki Y, Azumaya M, et al. Comparison of cyclo-oxygenase 2 expression in colorectal serrated adenomas to expression in tubular adenomas and hyperplastic polyps. *Int J Colorectal Dis* 2002;17(3):144-9.
181. Brazowski E, Misonzhnick-Bedny F, Rozen P. Cyclooxygenase-2 expression in the hereditary mixed polyposis syndrome. *Dig Dis Sci* 2004;49(11-12):1906-11.
182. Udd L, Katajisto P, Rossi DJ, Lepisto A, Lahesmaa AM, Ylikorkala A, et al. Suppression of Peutz-Jeghers polyposis by inhibition of cyclooxygenase-2. *Gastroenterology* 2004;127(4):1030-7.
183. Ashburner M, Ball CA, Blake JA, Botstein D, Butler H, Cherry JM, et al. Gene ontology: tool for the unification of biology. The Gene Ontology Consortium. *Nat Genet* 2000;25(1):25-9.
184. Myung SJ, Rerko RM, Yan M, Platzer P, Guda K, Dotson A, et al. 15-Hydroxyprostaglandin dehydrogenase is an in vivo suppressor of colon tumourigenesis. *Proc Natl Acad Sci U S A* 2006;103(32):12098-102.
185. Backlund MG, Mann JR, Holla VR, Buchanan FG, Tai HH, Musiek ES, et al. 15-Hydroxyprostaglandin dehydrogenase is down-regulated in colorectal cancer. *J Biol Chem* 2005;280(5):3217-23.
186. Tong M, Ding Y, Tai HH. Reciprocal regulation of cyclooxygenase-2 and 15-hydroxyprostaglandin dehydrogenase expression in A549 human lung adenocarcinoma cells. *Carcinogenesis* 2006;27(11):2170-9.
187. Hull MA, Ko SC, Hawcroft G. Prostaglandin EP receptors: targets for treatment and prevention of colorectal cancer? *Mol Cancer Ther* 2004;3(8):1031-9.
188. Kamei D, Murakami M, Nakatani Y, Ishikawa Y, Ishii T, Kudo I. Potential role of microsomal prostaglandin E synthase-1 in tumourigenesis. *J Biol Chem* 2003;278(21):19396-405.

Figure Legends

Figure 1. **Mechanism with which microsatellite instability occurs in the DNA of mismatch repair deficient cells**. The DNA polymerase δ holonzyme can slip during replication of the DNA primer strand (white) on a template (black) containing a mononucleotide (i.e., a poly$(A)_n$) or dinucleotide (i.e., poly$(CA)_n$) microsatellite repeat. Insertion/deletion loops (IDLs) will form and if not repaired by the MMR, extrahelical

nucleotides in the primer strand give rise to insertions, while extrahelical nucleotides in the template strand lead to deletions in the progeny DNA.

Figure 2. **Mismatch repair at the replication fork**. This model is based on biochemical evidence from *in vitro* experiments using recombinant human proteins and DNA substrates carrying a base/base mismatch or IDLs. Details on the steps of the MMR reaction depicted in this figure are provided in the text.

Figure 3. Colorectal lesions with serrated (i.e., saw-tooth contour) morphology. In both panels, the serrated shape of the epithelium is evident in crypts cut longitudinally. (**A**) A *traditional serrated adenoma* (TSA) showing cytoplasmic eosinophilia (not appreciable in this black & white picture), and nuclear crowding and stratification extending up to the surface of the epithelium. This cytological abnormality is equivalent to mild dysplasia in a classical adenoma. (**B**) A *sessile serrated adenoma* (SSA) with atypical crypt architecture including exaggerated serration, crypt branching and horizontally spreading crypts. Noteworthy, the architectural dysplasia of the serrated crypts, which is believed to emanate from abnormal proliferation and/or decreased apoptosis, is not associated with cytologic dysplasia. Pictures kindly provided by Jeremy R. Jass (McGill University, Montreal)

Figure 4. The Wnt signalling and the APC protein. **A**) the Wnt signalling pathway is represented in its inactive (left) or active (right) state. This latter can be achieved in several ways, for instance by production of Wnt ligands by epithelial or non-epithelial cells at the bottom of normal colorectal crypts, or by mutations in the *APC* gene (details are reported in the text). **B**) In this panel, the protein APC domains are shown in the top bar representing the

primary structure of the protein, whereas the associations between the site of germline *APC* mutations and the FAP phenotype are graphically represented by the rest of bars of different length. Truncated proteins start at the N-terminal part of APC and terminates at the site of the mutation or beyond it, retaining thus only a limited number of functional domains. The Armadillo repeats domain functions as a protein-protein intraction site (between APC and a variety of proteins), whereas binding of β-catenin to APC occurs through three 15-aa repeats and seven 20-aa repeats, the latter being also important for β-catenin degradation. The three SAMP repeats mediate binding to Axin. The C-terminal region of APC binds to several different proteins, such as EB1 and HDLG, for normal cell division and chromosome segregation to occur. (Nuclear export sequences and nuclear localization signal domains of APC are not shown). SAMP repeats: Serine Alanine Methionine Proline repeats; EB1: End binding protein 1; HDLG: human disc large homolog; CHRPE: Congenital hypertrophy of the retinal pigment epithelium.

Figure 5. **The mTOR signalling**. Model describing the upstream regulation of this signalling cascade by tumours suppressors (STK11, PTEN, and TSC1/TSC2) mutated in hamartoma syndromes. Details on this pathway are provided in the text.

Figure 6. **Expression profile of genes encoding proteins involved in the prostaglandin pathway**. A) Hierarchical clustering analysis of microarray data obtained with an Affymetrix gene expression platform: The 89 tissue samples represented on the *x*-axis include 32 adenomas, each with matched samples of normal mucosa, and 25 colon adenocarcinomas from a different group of patients. Each probe (135 genes, whose expression levels changed significantly in adenomas and/or carcinomas compared with

normal mucosa with a minimal fold difference of 1.9) plotted on the *y*-axis is grayscale-coded to indicate the gene's level of expression relative to its median expression level across the entire tissue-sample set (white: low; black: high). Based on the expression of these set of genes, the three groups of samples were perfectly segragated (also most of the MMR(+) colorectal cancers clustered differently from most of those MMR(-)). B) The expression levels (normalized intensity on *y*-axes; average with confidence intervals) of genes involved in the PGE_2 pathway are shown in the three group of samples (white columns: normal colonic mucosa; light gray columns: colorectal adenomas; dark gray columns: colon adenocarcinomas). (*): changes statistically significant when compared with the basal levels of expression in the normal mucosa. *PTGS2*: prostaglandin-endoperoxide synthase 2; *PTGES*: prostaglandin E synthase; *HPGD*: hydroxyprostaglandin dehydrogenase 15-(NAD); *IL1B*: interleukin 1, beta; *PTGER3*: prostaglandin E receptor 3 (subtype EP3) ; *PTGER4*: prostaglandin E receptor 4 (subtype EP4). (The expression of the *PTGER1* and *2* was similar in the three tissue groups.)

Sabates-Bellver et al., Figure 1

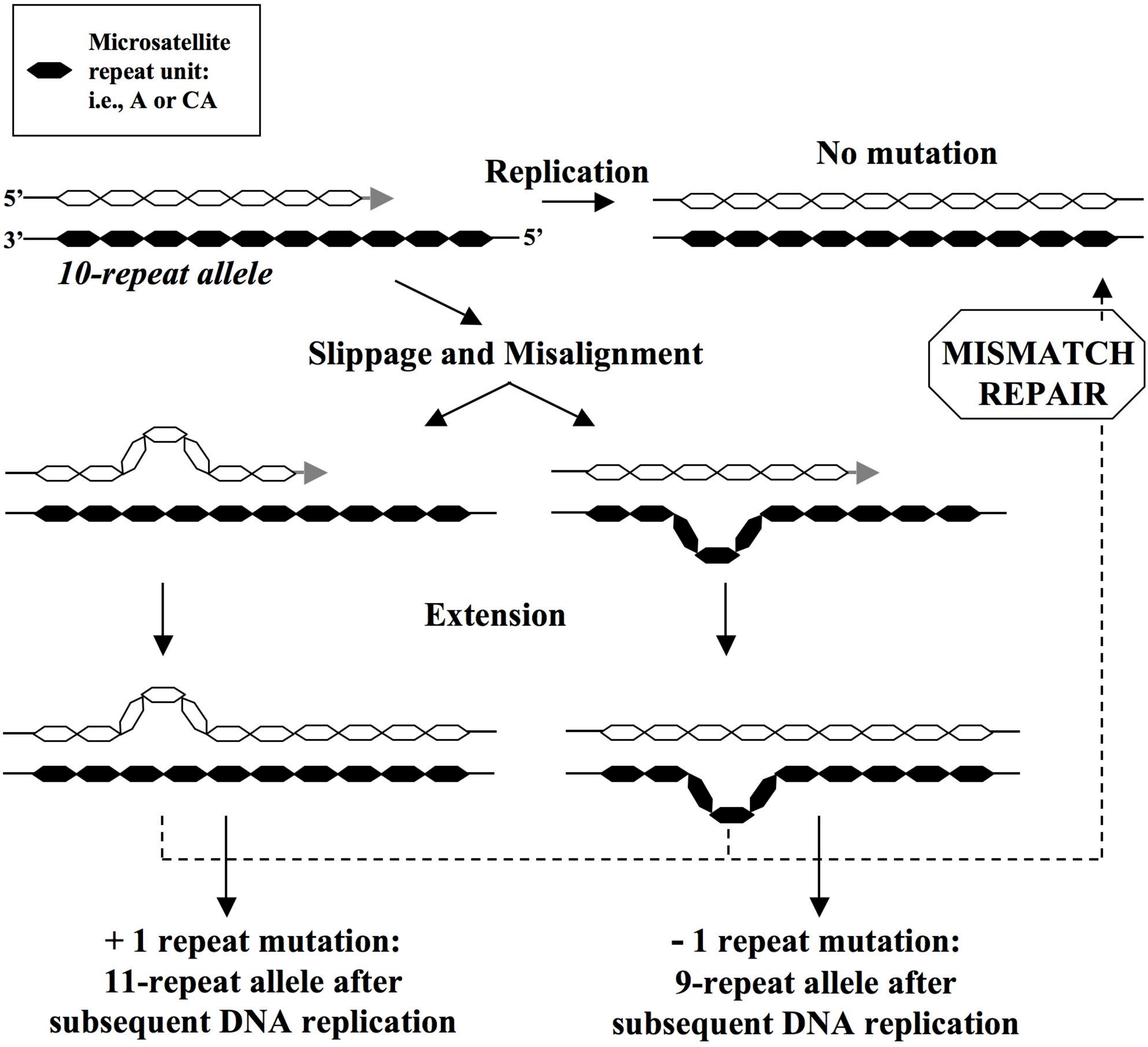

Sabates-Bellver et al., Figure 2

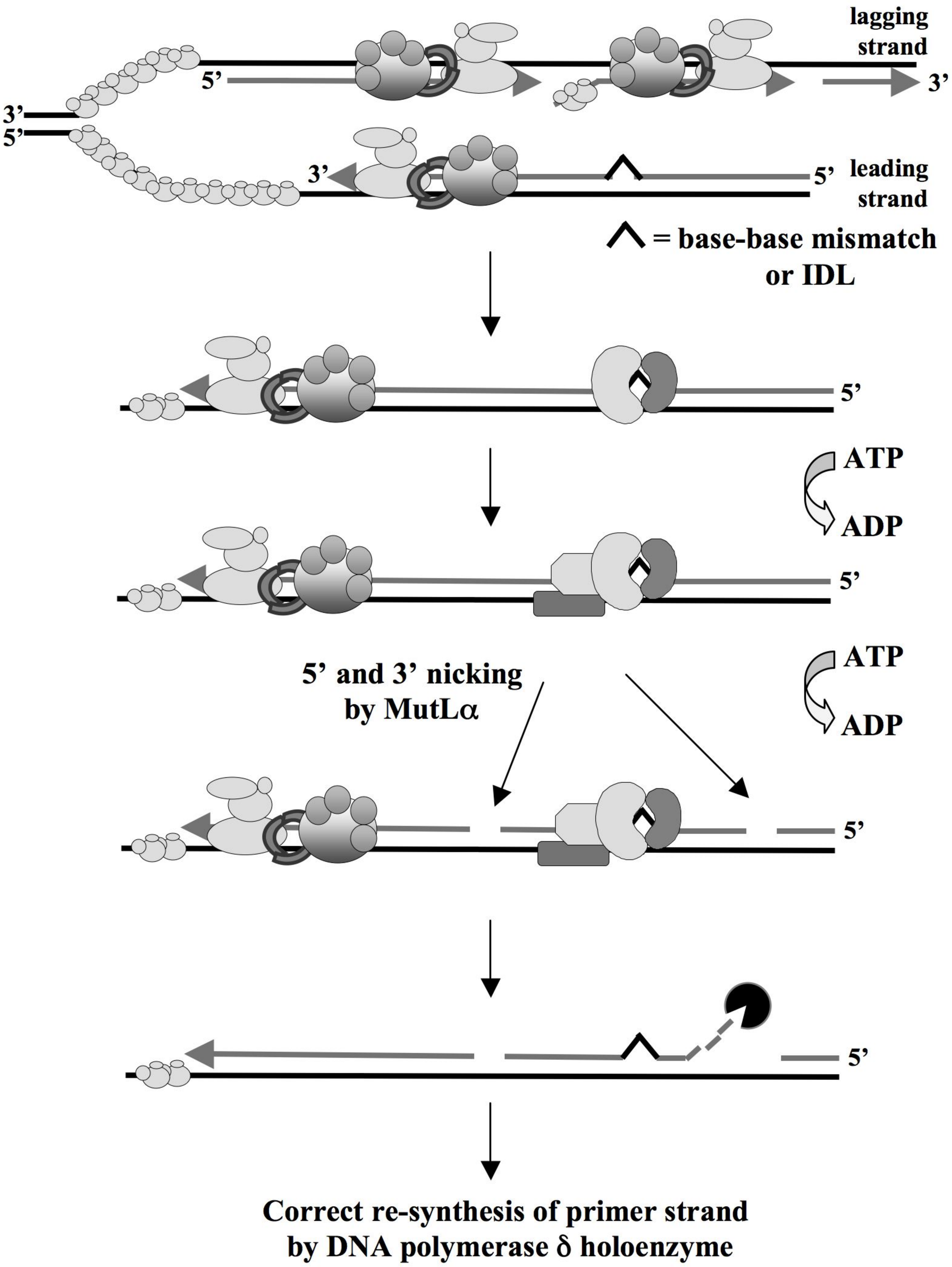

Sabates-Bellver et al., Figure 3

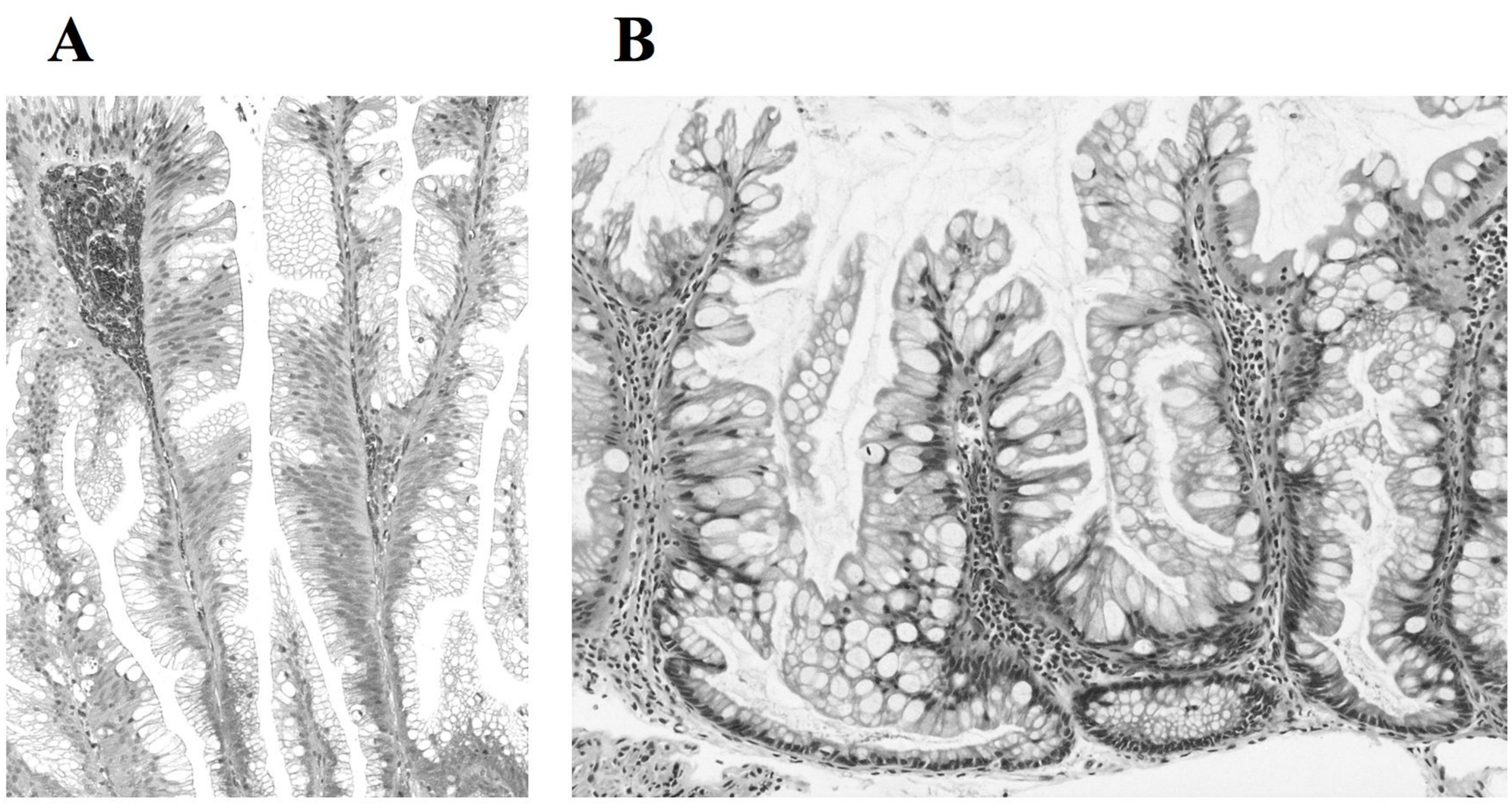

A

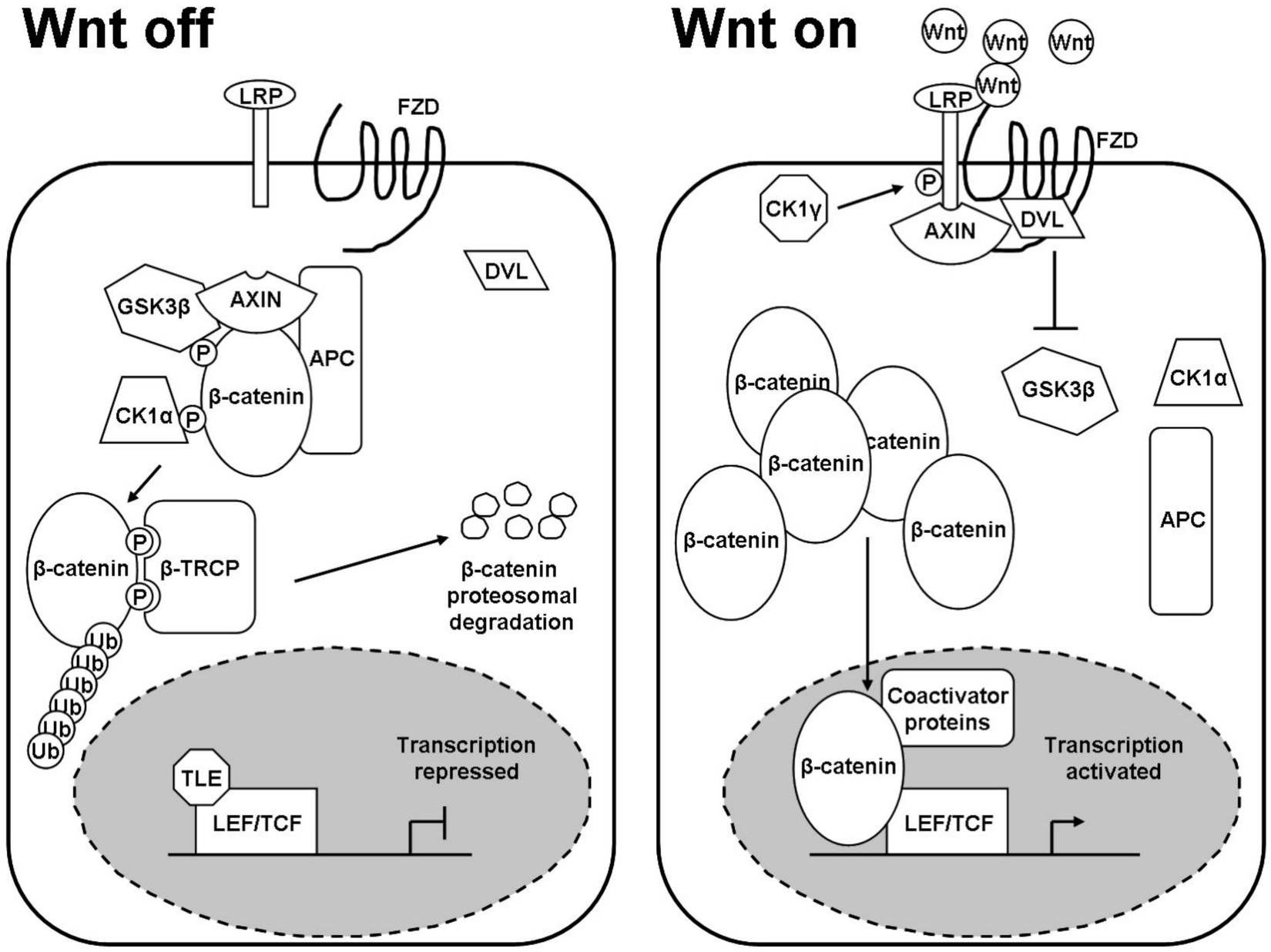
Wnt off
LRP
FZD
DVL
GSK3β
AXIN
APC
P
β-catenin
CK1α
β-catenin
β-TRCP
Ub
β-catenin proteosomal degradation
TLE
LEF/TCF
Transcription repressed
Wnt on
Wnt
LRP
FZD
CK1γ
AXIN
DVL
GSK3β
CK1α
β-catenin
APC
Coactivator proteins
Transcription activated

B

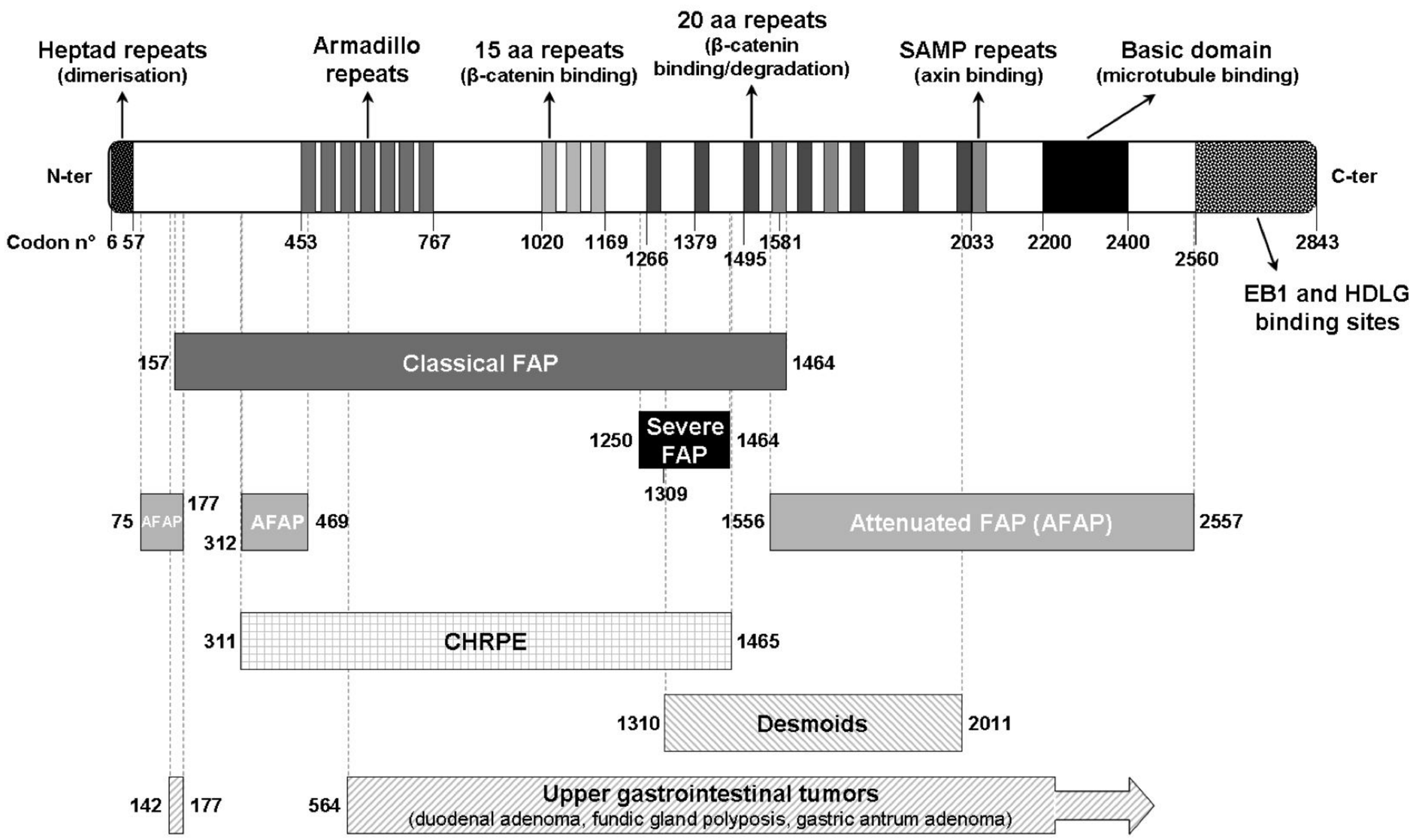
Heptad repeats (dimerisation)
Armadillo repeats
15 aa repeats (β-catenin binding)
20 aa repeats (β-catenin binding/degradation)
SAMP repeats (axin binding)
Basic domain (microtubule binding)
N-ter
C-ter
Codon n° 6 57 453 767 1020 1169 1266 1379 1495 1581 2033 2200 2400 2560 2843
EB1 and HDLG binding sites
157 Classical FAP 1464
1250 Severe FAP 1464
1309
75 AFAP 177
312 AFAP 469
1556 Attenuated FAP (AFAP) 2557
311 CHRPE 1465
1310 Desmoids 2011
142 177
564 Upper gastrointestinal tumors
(duodenal adenoma, fundic gland polyposis, gastric antrum adenoma)

Sabates-Bellver et al., Figure 5

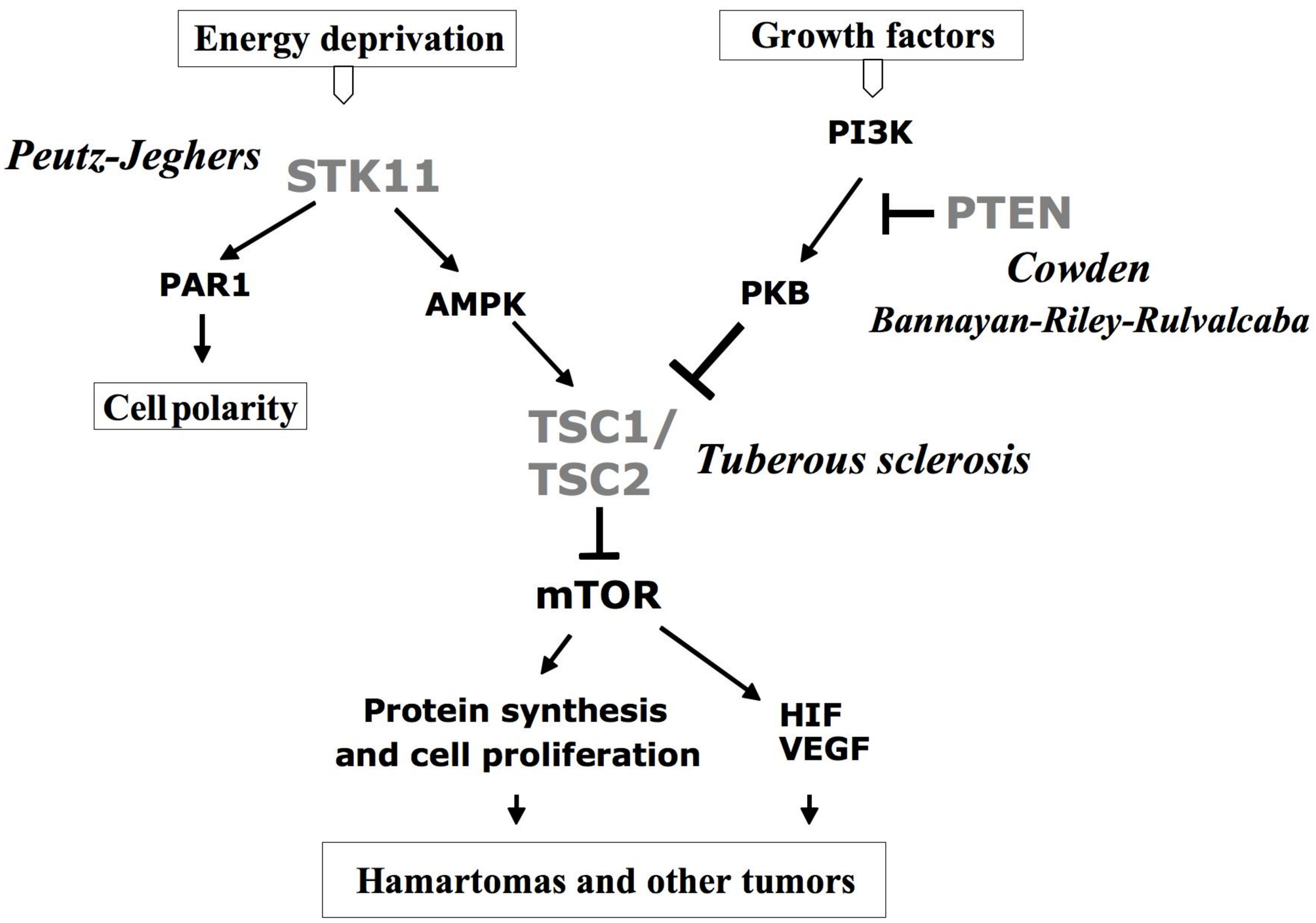

Sabates-Bellver et al., Figure 6

A

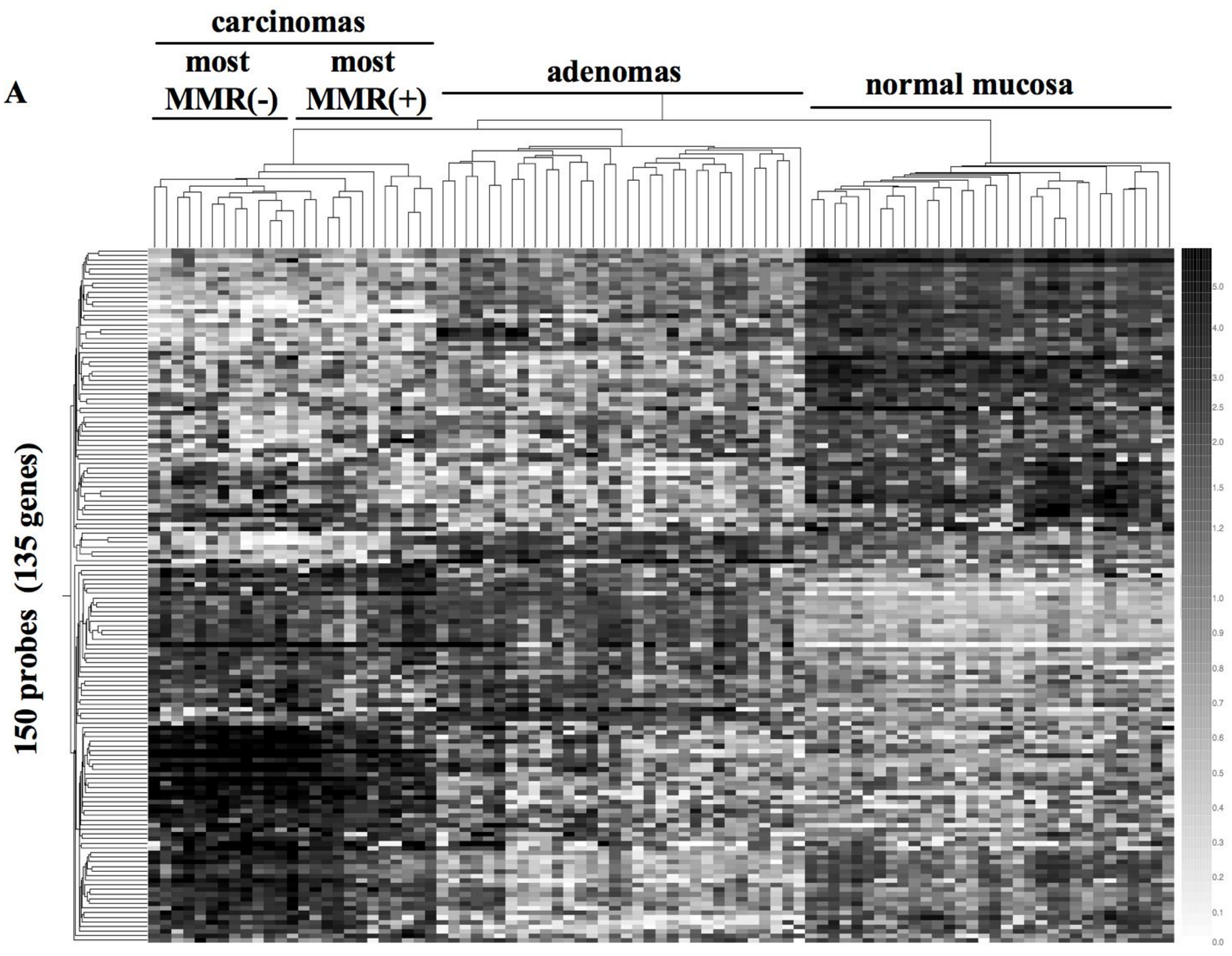

B

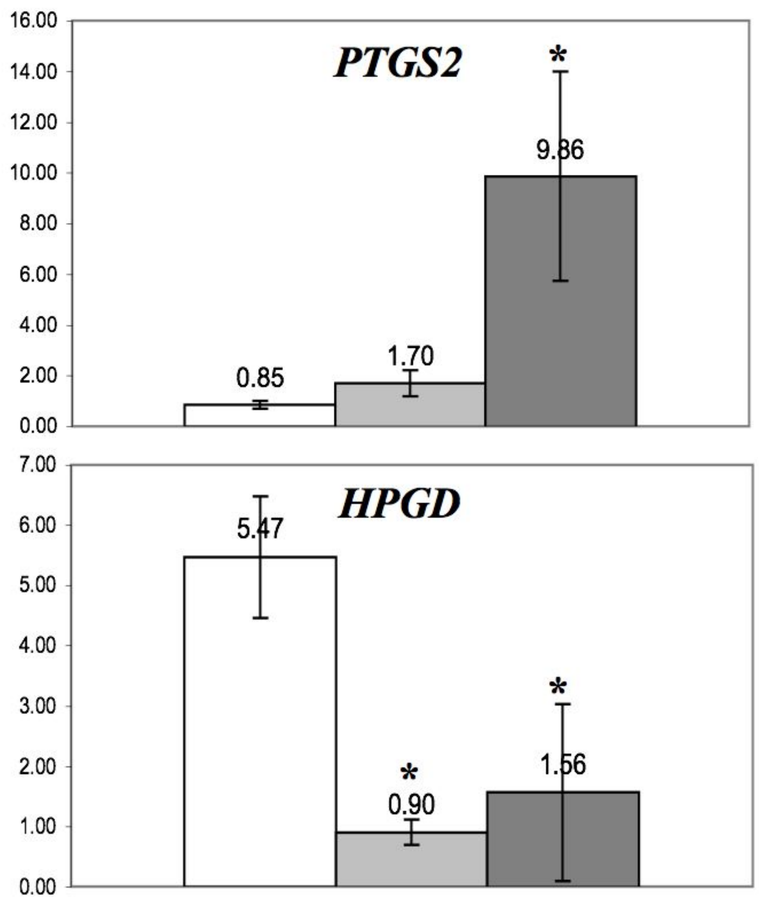

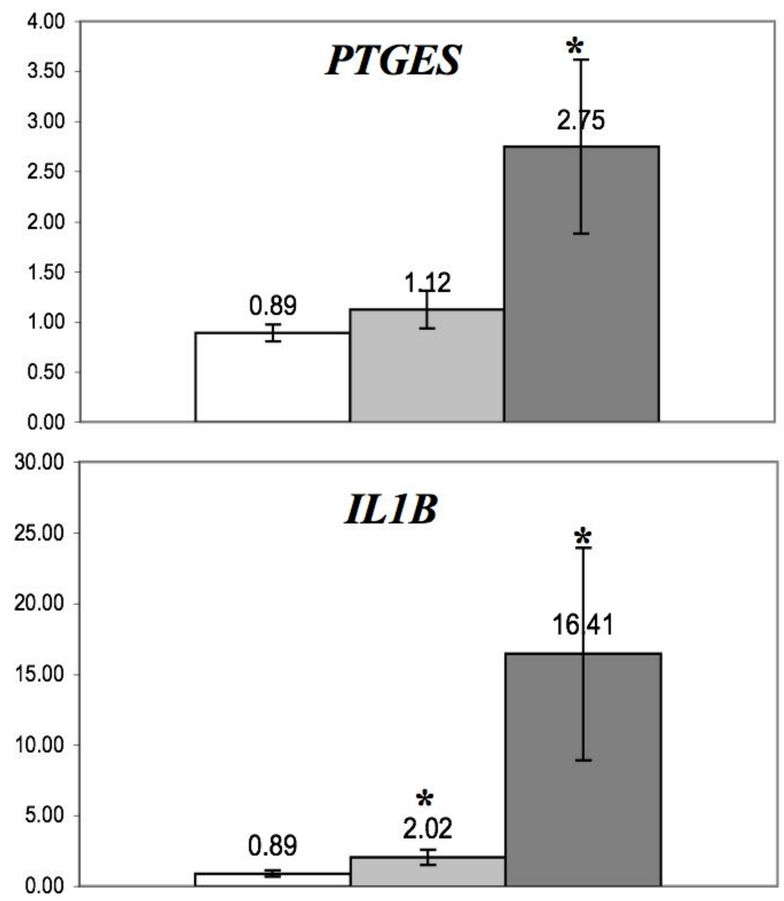

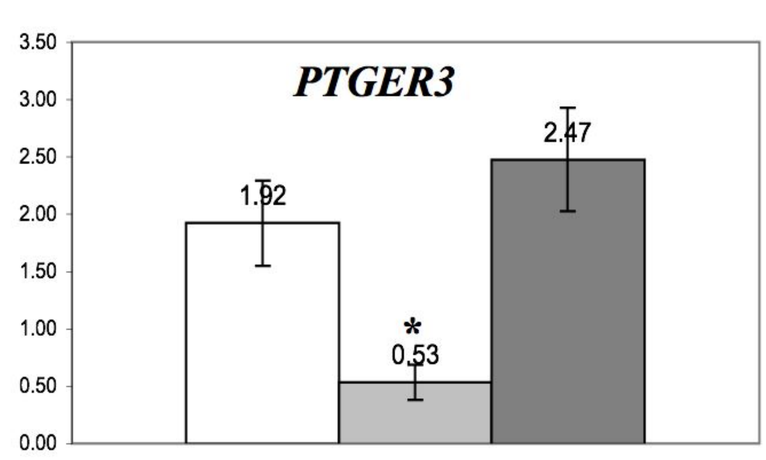

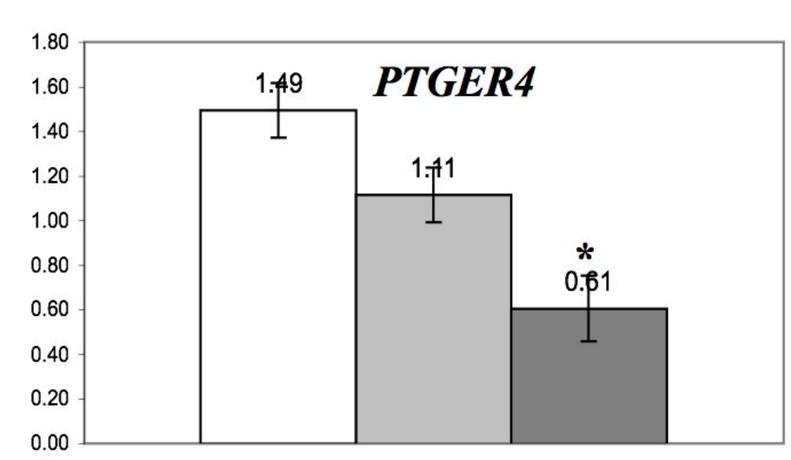

Book title: *Advances in understanding the basic pathogenesis and clinical management of pre-invasive disease.* Editor: Rebecca Fitzgerald.

Colon

Pathways and crossroads to colorectal cancer.

Elisa Cattaneo, M.D.[¶], Michael Baudis, M.D.[#], Federico Buffoli, M.D.[*], Maria Antonia Bianco, M.D.[§], Fausto Zorzi, M.D.[^], and Giancarlo Marra, M.D., Ph.D.[¶]

Institutes of [¶]Molecular Cancer Research and [#]Molecular Biology, University of Zurich, Switzerland

Gastroenterology Units, [*]Hospital of Cremona and [§]Hospital A. Maresca of Torre del Greco, Italy

[^] Department of Pathology, Poliambulanza Hospital, Brescia, Italy

Corresponding author:

Giancarlo Marra, M.D., Ph.D.
Institute of Molecular Cancer Research
University of Zurich
Winterthurerstrasse 190
(building 17, room K68)
8057 Zurich (Switzerland)

tel ++41 044 635 3472
fax ++41 044 635 3484
marra@imcr.uzh.ch

Index

Abbreviations: Aberrant crypt foci (ACFs); Adenomatous polyposis coli (APC); Chromosomal instability (CIN); CpG island methylator phenotype (CIMP); DNA mismatch repair (MMR); Familial adenomatous polyposis (FAP); Goblet-cell serrated polyps (GCSPs); Hyperplastic polyposis (HP); Inflammatory bowel disease (IBD); Microsatellite instability (MSI); Microvesicular serrated polyps (MVSPs); Serrated adenomas (SAs); Sessile serrated adenomas (SSAs).

Introduction

Colorectal tumorigenesis is one of the best known processes of cellular transformation in humans. Its characterization has moved ahead by leaps and bounds during the last three decades thanks to major advances in the fields of endoscopy, histology and molecular pathology. And as often happens when a human disease is subjected to in-depth investigation, what originally appeared to be a single entity turns out to include several distinct clinical, histologic, and molecular phenotypes. Among other things, tumor phenotypes can tell us a great deal about the route taken by the tumor cells on their journey toward malignancy. Not surprisingly, some tumors develop along pathways that are "heavily trafficked" (and for this reason, relatively well known); others follow the "roads less traveled." But if obstacles arise along the way, tumor cells are adept at exploiting alternative routes that permit them to continue their journey toward cancer, and these deviations can give rise to mixed phenotypes. These phenotypes are nonetheless consistent with the concept of carcinogenesis as a nonrandom – and therefore, predictable --process. Each pathway, each crossroads is the result of a specific set of genetic or epigenetic alterations. Many are already well defined, others are only partially characterized, and some are still in the realm of hypothesis. Thus far, we have fairly reliable maps of at least two of the major pathways to colorectal cancer, but with increasingly sophisticated molecular analysis of preinvasive lesions, there is little doubt that we will eventually identify variants of these pathways and uncover others whose existence was not even suspected.

In this chapter, we have attempted to provide an overview of the enormous amount of work and progress that has characterized this field over the past 30 years or so – a challenging task that has involved a number of difficult choices. Some aspects

undeniably deserved much more attention than they have received, and important references have regrettably been omitted. We have kept our focus on the basic pathogenesis of preinvasive lesions of the colorectum; as for their clinical management, there are several excellent articles that can and should be consulted [1-10].

On the way to cancer

Preinvasive lesions of the human colorectum are small areas of tissue that alter the surface contour of the gut mucosa. They are conventionally referred to as "polyps," which indicates growth protruding into the intestinal lumen, and this is indeed a fair description of most premalignant colorectal lesions. But we now know that there are also others, which are only slightly raised above the mucosal surface, or flat, or even depressed. Standard colonoscopy is performed to identify and resect these benign lesions in the belief that some of them will progress to cancer. **Figure 1** illustrates the conventional pathway by which this progression is thought to occur. The first step is the development of early morphologic changes in discrete clusters of epithelial crypts. The benign polypoid lesion in panel C is believed to represent an intermediate stage between these aberrant crypt foci (ACFs) and invasive adenocarcinoma. The transformation process summarized in the figure has never been directly documented — when a preinvasive neoplasm is found at endoscopy, it has to be removed, so its natural history can never be monitored — but it is consistent with the findings of innumerable endoscopic and histologic studies performed over the last three decades.

In mucosal biopsies stained with methylene blue, ACFs appear darker than the normal mucosa surrounding them [11]. In situ, these minute lesions are invisible during standard colonoscopy, but they are easily identified when magnifying endoscopes are used with dyes (e.g., indigo carmine or methylene blue) that enhance mucosal detail, a process known as high-magnification-chromoscopic-colonoscopy or, more simply, magnifying chromoendoscopy [12]. The aberrant crypts are usually larger than normal and have thicker epithelial linings and dilated or slit-like openings that are raised slightly above the adjacent mucosa.

ACFs are classified histologically as dysplastic and nondysplastic. Apart from their size, nondysplastic crypts are not remarkably abnormal, and their proliferative compartments are confined to the lower portion of the glands, as they should be. However, they often display signs of hyperplasia and infolding of the epithelium into the crypt lumen, a phenomenon referred to as *serration,* which is discussed in greater detail below. Dysplastic crypts, in contrast, present signs of cellular atypia (mucin depletion, nuclear enlargement, stratification, and loss of polarity) and upward expansion of the proliferative compartment toward the mouth of the crypts.

Around 60% of all healthy adults have a few ACFs in their colons, but these lesions are rarely dysplastic. ACFs are encountered much more frequently in colons harboring adenomatous polyps or adenocarcinomas (80%-100% of all cases), and 20%-50% of these show signs of dysplasia [13]. Dysplastic ACFs are also frequently detected in the colons of patients with familial adenomatous polyposis (FAP) [14], a high-penetrance genetic condition that causes a clear predisposition to colorectal cancer. And in ulcerative colitis (a chronic inflammatory disease that also increases the risk for colorectal cancer), the number of ACFs increases when the colon also presents signs of epithelial dysplasia or cancer [15]. The view of ACFs as probable precursors of preinvasive colorectal neoplasms is supported by findings of identical molecular changes in both types of lesions. Indeed, although they are more common features of premalignant neoplasms, mutations involving the *KRAS* or *BRAF* oncogene or the adenomatous polyposis coli (*APC*) tumor-suppressor gene, nuclear accumulation of β-catenin, aberrant DNA methylation, and low-level genomic instability have also been reported in some ACFs.

It is widely acknowledged that, while a few ACFs will progress to the preinvasive and, later, invasive stages (adenocarcinomas), others will not, and some

might actually regress spontaneously [16]. These lesions are so small and so numerous that it is virtually impossible to eliminate them by endoscopic resection (which is no problem with larger preinvasive lesions), but they do seem to respond to chemoprevention [13]. The weight that should be assigned to ACFs — their presence, number, and type — in planning surveillance colonoscopy is currently unclear, but the increasing use of magnifying chromoendoscopy is expected to provide important information on this question.

Preinvasive neoplasms — the next stage — are also a frequent finding. They are identified in roughly one third of all asymptomatic adults undergoing standard colonoscopy, but, like ACFs, some may regress on their own, and only a fraction will be transformed into cancers. The progression process generally involves increases in size and in the degree of cellular atypia. Lesions over 1 cm in diameter with high-grade dysplasia (referred to as *advanced adenomas*) are the ones farthest along on the road toward malignancy. (The term *adenoma* is used hereafter to refer to neoplasms -- regardless of their macroscopic appearance -- that display epithelial dysplasia.)

Several lines of evidence indicate that some of these preinvasive lesions will indeed give rise to colorectal cancers. For one thing, the frequency of these benign neoplasms and that of colorectal cancers both increase with age, but the age/prevalence curve for the former is shifted to the left by ~10 years. The regional distribution of cancers within the colon also parallels that of large adenomas. In addition, the expected incidence of colorectal cancer is substantially reduced by colonoscopy with polypectomy (even though 10-20% of all premalignant lesions, mainly those with diameters <5 mm, are likely to be missed on standard endoscopy) [17]. And finally, there is the impressive frequency at which invasive adenocarcinomas are detected within an advanced adenoma, especially those

displaying villous growth patterns and particularly severe dysplasia. About half of all adenocarcinomas are elevated above the surrounding mucosa, and in the other half growth occurs at or below the surface of the normal tissue, so it seems that both polypoid and nonpolypoid benign lesions give rise to cancer.

Breaking convention: The contributions of modern endoscopy and histology

For decades, all preinvasive colorectal lesions were referred to as polyps. Pre-neoplastic growth that did not protrude into the gut lumen was first detected in the eighties by Japanese endoscopists [18]. Once these nonprojecting lesions were recognized, they were reported with increasing frequency in other countries as well, where they represented 10-40% of all the preinvasive neoplasms encountered during screening colonoscopy [19].

Since then, attempts have been made to reclassify preinvasive lesions of the digestive tract. These efforts have been more or less successful, but older terms are still encountered, and they can be a source of considerable confusion. When possible, we will give preference in this chapter to the newer, more precise terminology, which refers to all protruding lesions as *polypoid* and sub-classifies them as *pedunculated* (attached with a pedicle or stalk) or *sessile* (attached by a broad base). At the other end of the spectrum are the *nonpolypoid* lesions. They are still widely referred to as "flat" although most are actually slightly elevated (< 2.5 mm above the surface of the gut mucosa); those that are completely flat or slightly depressed are rare, but even when they are small, they are generally farther along on the road to cancer (**Figure 2**) [20]. O'Brien et al. highlighted the impact of the new terminology in their recent reassessment of 1505 superficial neoplasms classified as polyps in the United States' National Polyp Study. Around 30% — specifically, two-thirds of those originally considered *sessile polyps* — met the new criteria for *nonpolypoid* neoplasms [21].

These lesions had all been detected in the 1980s with standard colonoscopy. In a more recent study based on high-magnification chromoendoscopy, 38% of the adenomatous lesions were nonpolypoid [22]. This approach also allows accurate in vivo classification of lesions based on surface morphology. The shape of the colon

crypt lumen in particular (the so-called pit pattern) has proved to be a very reliable predictor of a lesion's histologic features [23]. These newer techniques are becoming increasingly popular, and their use will undoubtedly improve the accuracy of endoscopic diagnoses. Nevertheless, high-quality standard colonoscopy — that is, *complete* examination of a clean colon, all the way to the cecum, with slow, careful withdrawal and re-examination of potential blind spots — is still widely regarded as a reliable tool for detecting preinvasive lesions and preventing colorectal cancer.

The more accurate endoscopic classification of preinvasive colorectal lesions led to some important observations. While true polypoid lesions were more frequently detected in the left colon (from the splenic flexure to rectum), nonpolypoid neoplasms were more common in the right colon (from the cecum to the splenic flexure). Even more important was the discovery that, while most of the latter lesions had classic adenomatous features, others presented a peculiar histologic pattern characterized by infolding of the glandular epithelium. As noted earlier, this phenomenon is referred to as *serration*, because it produces a saw-toothed (or serrated) pattern in longitudinally sectioned crypts [24] (Figure 2E-F). On cross-section, the serrated crypt has a star-shaped appearance, and this feature can also be discerned in vivo by careful examination of crypt mouths with magnification chromoendoscopy.

Serrated crypt architecture proved to be typical of lesions that were then (and sometimes still are) being referred to as *hyperplastic polyps*. They had long been considered innocuous with a negligible risk for progression to cancer, mainly because, in spite of their architectural abnormality, they showed no clear signs of epithelial dysplasia. The term *hyperplastic polyp* is gradually being abandoned in favor of *nondysplastic serrated polyp* (although in both cases, the term "polyp" is a misnomer

since many of these lesions are nonpolypoid). It is also becoming increasingly clear that this category includes morphologically and molecularly distinct subsets with different propensities for malignant transformation.

Three major histologic subtypes have been identified thus far (see [25] for details). *Goblet-cell serrated polyps* (GCSPs) have the fewest architectural anomalies, and it is generally agreed that they are unlikely to progress to cancer. These lesions are found primarily in the left colon, and most are small rectal lesions. They contain enlarged, nonbranching crypts displaying little or no epithelial infolding. Their main abnormality consists in an increased goblet cell / columnar cell ratio that affects the entire length of the gland. *Microvesicular serrated polyps* (MVSPs) are more common than GCSPs. They are found throughout the colon, although their frequency is also highest in the left colon and rectum. The crypts are elongated and funnel-shaped, but the proliferative compartment is normally confined to the bottom of the gland. The upper crypts contain numerous microvacuolated columnar cells. The upper 2/3 of the crypt (and less commonly the crypt base as well) typically presents epithelial serration. The third subset comprises lesions that are still widely referred to as *sessile serrated adenomas* (SSAs). The term is imprecise: first, because the group includes both sessile polyps and nonpolypoid lesions, and second, because the dysplasia that is the hallmark of an adenoma is absent in these lesions. SSAs are generally found in the right colon. They are characterized by L-shaped or inverted-T shaped crypts lined with infolded epithelium from base to mouth. The proliferative compartment is sometimes expanded, but as noted, there is no real cytologic dysplasia.

Histologic and molecular findings (detailed in the next section) suggest that SSAs evolve from MVSPs and that some do eventually become dysplastic. But at

this point, they are usually referred to as *serrated adenomas* (SAs). The histologic definition of this term is still a matter of debate among pathologists so their diagnosis displays substantial interobserver variation. Because cellular dysplasia is an essential feature of SAs, some are likely to be classified as conventional adenomas. Mixed lesions containing serrated areas interspersed with areas displaying conventional adenomatous changes can also be found [26].

In a recent study [27], 65% of the premalignant lesions resected during standard colonoscopy were conventional adenomas. The other 35% displayed serrated architecture and were generally classified as "hyperplastic polyps." Most of the latter were MVSPs or GCSPs (30%), a few were SSAs (~4%), and less than 2% were dysplastic. Similar figures (~60% conventional adenomas, ~40% serrated lesions) emerged from another study based on magnifying chromoendoscopy [28]. Nine percent of all lesions removed in this study were SSAs, and 2.4% were dysplastic (SAs). The coexistence of adenomatous and serrated lesions in the same patient is a common finding.

Therefore, alongside the conventional adenoma-carcinoma pathway illustrated in Figure 1, there seems to be a second, less-frequented route, the serrated pathway, which also leads to the development of colorectal adenocarcinoma (**Figure 3**). There is evidence of its existence at both ends of the transformation process. Serrated / stellate crypt morphology has, in fact, been described in some nondysplastic (or hyperplastic) ACFs [29], and ~10% of all colorectal cancers have predominantly serrated histologic patterns (the serrated adenocarcinomas) [30] or contain peripheral remnants of serrated adenoma [31]. The mixed (serrated and conventionally adenomatous) histology observed in some preinvasive lesions suggests that the two pathways have somehow intersected or merged during tumorigenesis.

In summary, 2 out of 3 preinvasive colorectal lesions discovered at endoscopy are classic adenomas with tubular and/or villous architecture and some degree of dysplasia (Figures 1 and 2E). The third will present a serrated histological pattern, in rare cases combined with dysplastic changes (Figure 2F). The classic adenomas are usually pedunculated (or less frequently, sessile) polyps, but around 1/3 are nonpolypoid [22,27,28] (Figure 2A-D). Among serrated lesions, polypoid and nonpolypoid growth patterns are more or less equally represented. Small serrated polyps (<5 mm in diameter) with microvesicular or goblet-cell features are likely to be encountered in the left colon and rectum. Larger MVSPs (which are usually sessile polyps or nonpolypoid lesions) and SSAs are more frequently found in the right colon. As for the dysplastic serrated lesions (SA), over two thirds are polypoid, and most are located in the left colon [32]. However, there is compelling molecular evidence (see next section) that their less common, right-colon counterparts are far more important: these proximal SAs seem to be the ones that evolve along the serrated pathway, presumably giving rise to ~ 20% of adenocarcinomas found in the colorectum.

Advances in the fields of endoscopy and pathology have provided us with a more accurate classification of preinvasive lesions that better reflects their relevance in colorectal tumorigenesis. In the next section, we will review the results of studies aimed at defining the molecular features of these lesions.

Convention-breaking findings from molecular biology

The availability of tissue samples of preinvasive lesions removed during endoscopy or surgery fuelled attempts to identify the crucial molecular events that allow these lesions to form and progress toward cancer. In general, increases in lesion size — from tiny ACFs to advanced adenomas over 1 cm in diameter — are paralleled by increasingly bizarre architectural and cytologic atypia, and the larger lesions (polypoid or nonpolypoid) are the ones most likely to become malignant. Analyzing lesions of different sizes thus reveals distinct stages or steps in the transformation process. And when molecular changes are discovered in malignant tumors (adenocarcinomas), we can backtrack along the various steps of the pathway to find out when (and perhaps why) the alteration appeared. Some abnormalities can even be traced back to the normal mucosa, where they reflect a genetically- and/or environmentally-determined field defect.

Interestingly, molecular alterations considered highly relevant to the transformation process in the colon are often found in some but not all premalignant lesions, and when they are present, their prevalence frequently correlates poorly with the size or severity of lesions. Some well known examples are oncogene mutations (*KRAS* and *BRAF*) and more extensive genetic or epigenetic alterations, such as microsatellite instability or the methylator phenotype (see below). The fact that some of these changes appear to be mutually exclusive suggests that pre-cancerous cells can be transformed into invasive cancer cells by different sequences of mutations.

Nevertheless, there does seem to be a common denominator in the onset and progression of most, if not all, pre-cancerous lesions of the colorectum: aberrant activation of the Wnt signaling cascade. Canonical Wnt signaling is a crucial driver of epithelial-cell division within the lower third of the intestinal crypt, which

represents one of the simplest self-renewing biological entities in mammals [33]. In this proliferative compartment of the gland, secreted Wnt proteins interact with serpentine receptors of the frizzled family and low-density lipid receptors 5 or 6 expressed by the dividing epithelial cells. Signal transduction activated by this binding inhibits the formation of a cytoplasmic complex whose core components include APC (a multidomain protein encoded by the adenomatous polyposis coli gene), glycogen synthase kinase-3ß, the scaffolding protein axin, and casein kinase 1. This so-called destruction complex catalyzes the phosphorylation of ß-catenin, thereby targeting it for ubiquitin-mediated degradation. In its absence, ß-catenin accumulates in the cytoplasm and eventually translocates into nucleus, where it encounters DNA-binding proteins of the T-cell factor (TCF)/lymphoid enhancer factor (LEF) family. ß-catenin binding converts the TCF and LEF1 proteins from transcription repressors to transcription activators. Among their targets are genes whose products play fundamental roles in maintaining stem- and cycling-cell populations at the bases of colon crypts (other transcription factors like CMYC, the cell cycle kinase activator cyclin D, and matrix metalloproteinase 7, to name a few). Cells in the upper two-thirds of the crypt are not stimulated by Wnt signaling proteins, so the ß-catenin in these cells is recruited to the destruction complex and promptly degraded. This leaves the upper-crypt cells free to differentiate as they migrate upward toward the intestinal lumen.

Constitutive Wnt signaling leads to an expansion of the proliferative compartment of the crypt, destroying the equilibrium between proliferation and differentiation, and this loss generally coincides with the development of precancerous lesions. In virtually all colorectal tumors (preinvasive and invasive), this inappropriate signaling reflects abnormal stabilization of ß-catenin, and in 60%-

80%, the cause is homozygous mutation of the well-known tumor suppressor gene *APC* [34-37] (**Figure 4**), which presumably occurs in the progenitor stem cells at the crypt base [38,39]. *APC* mutation is therefore a frequent event in the initial stages of colon tumorigenesis, but it is not the only cause of the altered stability and distribution of ß-catenin that characterize colorectal tumors. Wnt signaling can also be constitutively activated by somatic changes affecting other crucial pathway components. They can be genetic (e.g., mutations involving the gene that encodes ß-catenin, which generally result in substitution of serine or threonine residues whose phosphorylation allows the protein to be degraded by the destruction complex [40-42]) or epigenetic (transcriptional silencing of the *SFRP1* gene [43], which encodes a receptor that normally inhibits Wnt signaling).

APC and ß-catenin mutations are mutually exclusive in colorectal neoplasms, but other genetic and epigenetic changes in Wnt-pathway components are often found together in the same tumor. Many human tumors develop and evolve as a result of the deregulation of multiple signaling pathways, and this is undoubtedly true of colorectal tumors as well, but colorectal tumorigenesis also seems to be characterized by the selection of repeated alterations (or "hits") involving the Wnt pathway. These observations suggest that Wnt signalling dysregulation itself may be modulated during transformation to meet the specific needs of the tumor at various points in its journey.

Changes of this type can naturally have an impact on the tumor phenotype. For example, biallelic mutation of tumor suppressor genes is generally envisioned as causing loss of protein function, but in the case of *APC*, the mutant gene products are usually stable, truncated proteins that may well retain some ability to interact with ß-catenin, for example [44]). The mutant alleles (i.e., the first and second hits) seem to

be co-selected to achieve a level of aberrant Wnt signaling that is "optimal" for tumor cell proliferation and DNA replication. During tumor progression, however, one of the two *APC* alleles may develop a second mutation – a "third hit" that readjusts the level or characteristics of the dysregulated signaling to meet the tumor's current needs [45].

The quality of the dysregulated signaling also changes when one pathway component instead of another is altered. For instance, compared with tumors bearing ß-catenin mutations, those with abnormal APC function are thought to be more prone to DNA ploidy changes, because APC is also involved in mitotic spindle formation and chromosome segregation, processes that are essential for the maintenance of chromosomal stability [46]. Low-level chromosomal instability has in fact been detected in adenomatous polyps (mainly gains of chromosome 7 and 20, as well as deletions in multiple regions) and in dysplastic ACFs of patients with APC mutations [47,48], although no genomic imbalances were found when a small series of adenomas with biallelic *APC* mutations were recently subjected to comparative genomic hybridization analysis [49]

The RAS/RAF/MEK/ERK (or MAPK/ERK) cascade is another signaling pathway that is frequently dysregulated in colorectal carcinogenesis, and it, too, transforms extracellular signals into transcriptional regulation. The MAPK/ERK cascade is a classical "survival" pathway, in that it promotes cell proliferation and prevents apoptosis. Two of its gene components, *KRAS* and *BRAF,* are known oncogenes that often present gain-of-function mutations in preinvasive colorectal lesions. The hyperactive mutant kinases they encode ($KRAS^{G12D}$ and $BRAF^{V600E}$, for example) maintain a state of chronically activated "survival signaling" in premalignant cells.

The level of this aberrant MAPK/ERK activity has yet to be well defined, but the balance between cellular proliferation and apoptosis undoubtedly differs from that observed in the normal mucosa. Loss of this normal homeostatic equilibrium seems to be associated with a substantial increase in DNA replication stress. Unlike the proliferating cells of normal colorectal crypts, premalignant epithelial cells with oncogene-activated survival signaling display classic examples of cellular responses to DNA damage, including phosphorylation of checkpoint kinase CHK2 and the histone protein H2AX, or signs of telomere attrition [50,51]. These events halt the cells at a specific stage of the cell cycle so that the DNA damage can be repaired. This checkpoint repair system is probably one of several mechanisms that put a brake on the progression of tumorigenesis and allow lesions to remain in the preinvasive stage for years (Figure 4).

BRAF and *KRAS* oncogene mutations are early mutually exclusive events that can already be detected in ACFs [29]. The former is more frequent in serrated ACFs, and the latter is more common in ACFs that lack serration. Interestingly enough, this difference is maintained as transformation progresses. In fact, *BRAF* mutations are found in over two thirds of all MVSPs, SSAs, and dysplastic SAs, and they are also present in ~15% of all adenocarcinomas, mainly those right-colon cancers that develop along the serrated pathway. *KRAS* mutations are detected in 30-40% of conventional adenomas and in ~1/3 of all adenocarcinomas [31,52] (Figure 4).

Therefore, although KRAS is located immediately upstream to BRAF in the MAPK/ERK signaling pathway and each intermediate is frequently mutated in preinvasive colorectal lesions, the phenotypic consequences of these mutations are quite different. (We saw the same thing above, when we looked at mutations of APC and β-catenin in the Wnt pathway.) The distinctive effects of mutations involving

two components of a given pathway, even those that are adjacent to one another in the signaling cascade, are not surprising, because each component is transduced differently downstream and each interacts in its own way with factors of other signaling pathways (e.g., cross-talk between components of the MAPK/ERK and PTEN/PI3K/AKT/mTOR pathways [53]).

While activating mutation of *KRAS* or *BRAF* seems to be an early event in the process of colorectal transformation, 50-60% of all colorectal adenocarcinomas show no sign of either mutation (Figure 4). If, as it seems, oncogene activation of survival signaling allows preinvasive lesions to avoid cell death for many years, it seems reasonable to expect that benign lesions without *KRAS* or *BRAF* mutation would have mutations/alterations involving other oncogenes. To date, however, none have been identified.

The end of this more or less lengthy preinvasive stage and the onset of true malignancy is believed to be caused by the addition of one or more new genetic or epigenetic alterations. The "brake-releasing" events are nonrandom, but they may differ, depending on the nature of the preinvasive neoplasm. Some lesions are set in motion by mutation of the tumor-suppressor gene *TP53*, which is often altered in advanced colorectal tumors; in others, the crucial event affects another survival signaling pathway (e.g., mutation of *PIK3CA* or *PTEN* in the PTEN/PI3K/AKT/mTOR pathway [54]) or another Wnt signaling protein; and in others, the brake-releasing hit targets a gene needed for genomic stability (the DNA mismatch repair gene, *MLH1*, for example). The type of event(s) necessary to provoke the transition to invasiveness seems to be dictated at least in part by the original genetic features of the premalignant lesion. (Somatic *MLH1* silencing, for

instance, seems to be the most common trigger for progression of *BRAF*-mutated serrated lesions.)

Analysis of a dozen or more different genetic and epigenetic alterations in a substantial number of colorectal neoplasms has revealed at least 2 clearly discernable paths toward the invasive stage (Figure 4). Each includes a number of molecular crossroads, however, and the tumor-in-motion can thus be deviated toward a different pathway by biological obstacles encountered during progression (most of which have yet to be characterized). Route changes of this type can result in mixed phenotypes [55-58].

The serrated pathway shown in Figure 4 generates colorectal neoplasms that are phenotypically distinct from those that develop through the conventional, APC-driven, adenoma-carcinoma sequence. *BRAF*-mutated, serrated lesions give rise to sporadic *MLH1*-deficient cancers of the right colon, which are more frequent in women and occur later than other sporadic colorectal cancers (peak prevalence between the ages of 70 and 80 years). A frequent feature of these neoplasms is the CpG island methylator phenotype (CIMP), which is characterized by nonrandom transcriptional silencing of several cancer-relevant gene promoters, like those of *p16* and *MLH1* [31,59-66]. Relatively rare in conventional adenomas, the CIMP is found in 70%-80% of all dysplastic serrated lesions of the right colon, and it is closely associated with *BRAF* mutations. The basis of this association is unknown, and it is also unclear why CIMP-positive tumors prefer the right colon of women. The latter aspect presumably highlights roles played by hormonal and environmental factors (including cigarette smoking [67] and hypoxia [68,69]).

High-throughput sequencing technology and system biology studies (based on genomics, transcriptomics, and proteomics, and other more specific –omics) will

certainly improve mutation detection, providing us with a more precise picture of the colorectal oncogenetic tree [70,71] than the one represented in Figure 4. These advances will bring us several steps closer to the goal of type-specific treatment for colorectal cancers. The different phenotypes might also have specific mechanisms for developing resistance to treatment regimens, so detailed knowledge of a given phenotype might also facilitate the early detection and prompt treatment of tumors that are no longer responding to treatment.

Fast-track transformation models: Inherited syndromes and inflammatory bowel disease

The adenomatous and serrated pathways of colorectal transformation can be discerned within three inherited syndromes that are major risk factors for the development of colon cancer. Because the susceptibility to cancer is inherited, tumorigenesis generally begins earlier and proceeds more rapidly than it does in sporadic disease, and mutation carriers frequently develop adenocarcinomas between the third and fifth decades of life.

Familial adenomatous polyposis – Less than 1% of all colorectal cancers are related to familial adenomatous polyposis (FAP), but this syndrome provides us with an invaluable "fast-forward" view of mutant APC-driven transformation through the adenomatous pathway. Individuals with FAP are born with a heterozygous germ-line mutation in *APC*, and by adolescence or early adulthood, their colons are filled with hundreds or thousands of classical adenomatous polyps. They also develop extracolonic disease, such as congenital hypertrophy of the retinal pigment epithelium, desmoid tumors of the abdomen, upper gastrointestinal adenomas and carcinomas, and, less frequently, osteomas, dental abnormalities, lipomas, and epidermoid cysts. Malignant tumors of the brain, thyroid, and hepatobiliary tract have also been associated with FAP.

FAP is transmitted in an autosomal dominant fashion, although ~30% of all patients represent new cases in the family (i.e., *de novo* mutations). There is also a milder variant, attenuated FAP, characterized by later disease onset and a smaller number of colorectal polyps (conventionally, fewer than 100) [72]. But since approximately 5% of all adenomas eventually become cancers, the probability of colorectal cancer by the age of 40-50 years is 100% even in these patients. FAP

adenomas do not seem to be more prone to transformation than their sporadic counterparts. The accelerated tumorigenesis associated with this syndrome appears to be related primarily to the prodigious numbers of polyps that form and the early age at which they appear.

APC encodes a 2843-amino-acid protein with several functional domains, including several that bind with β-catenin and others that interacts with axin. As mentioned in the previous section, nonsense germ-line *APC* mutations usually generate partially functional N-terminal APC fragments lacking one or more of these domains. Variability in the domain make-up of these truncated proteins is reflected by different degrees of Wnt signaling dysregulation, which produce different effects on cell-cell adhesion, cell migration, cell division, and chromosomal stability [73]. This is the basis for the genotype-phenotype association model of FAP (reviewed in [74]), which holds that the severity of the disease — in terms of number and onset of colorectal adenomas and extracolonic manifestations — depends on the location of the germ-line mutation within the *APC* gene.

The model has some obvious shortcomings. For one thing, past analyses have been largely restricted to the mutation cluster region of *APC,* and this may have provided a skewed picture of the mutational spectrum in this gene. Furthermore, the transformation process within single lesions can also be influenced by the characteristics of second and (in some cases) third hits involving *APC* at the somatic level (as discussed in the previous section). Numerous studies have revealed inconsistencies and contradictions in the genotype-phenotype association model, the most striking of which is the fact that, in 30%-50% of patients with FAP or attenuated FAP phenotypes, current testing methods reveal no *APC* mutations at all! In some of these cases, bi-allelic germ-line mutations involving the base excision repair gene

MYH have been detected. They represent a recessively inherited variant of FAP (or attenuated FAP), in which the development of adenomatous polyposis is believed to be triggered by *somatic APC* mutations resulting from defective processing of oxidative DNA damage by the base excision repair system [75-77].

Lynch syndrome – This is the most common colorectal cancer predisposition syndrome of known etiology and the cause of ~3% of all adenocarcinomas of the colon. Like FAP, Lynch syndrome is a model of accelerated transformation along the conventional adenomatous pathway, but the driving force here is completely different. Lynch syndrome patients generally harbor a heterozygous germ-line mutation involving one of four genes that are essential for DNA mismatch repair (MMR): *MSH2*, *MSH6*, *MLH1,* and *PMS2*. As a result, base/base mismatches and strand misalignments generated during DNA replication by polymerase δ or ε go unrepaired, and the rate of mutations rises markedly (reviewed in [78]). This defect results in what is known as a *mutator phenotype* characterized by the accumulation of large numbers of mutations in the genome.

MMR is normally initiated when a mispair or misalignment is bound by the mismatch recognition complex, MSH2/MSH6. The heterodimer then undergoes an ATP-driven conformational change, which allows it to interact with another MMR protein heterodimer, MLH1/PMS2. This interaction activates the endonucleolytic function of PMS2, which nicks the newly synthesized DNA strand on the 3′ and 5′ sides of the mismatch. Exonuclease 1 then degrades the mispair-containing segment, beginning at the 5′ nick, and the resulting gap is then filled in with the correct sequence by replicating DNA polymerase δ or ε.

Genes whose germ-line mutations cause inherited forms of cancer are often found to be somatically altered in certain sporadic tumors, and the MMR genes are no

exception [79]. This is especially true of *MLH1*. Loss of MLH1 expression is found in approximately 10% of all colorectal carcinomas, and the vast majority are unrelated to Lynch syndrome. Sporadic, MLH1-defective tumors are in fact the most common MMR-defective colorectal cancers. These are the cancers discussed in the previous section, the ones that are almost always found in the right colon. They arise through the serrated pathway and are often characterized by *BRAF* mutations and CIMP-positivity, which leads to somatic silencing of *MLH1* via bi-allelic methylation of its promoter.

In contrast, the inherited MMR-defective colorectal cancers associated with Lynch syndrome develop along the conventional adenomatous pathway. The first hit -- heterozygous germ-line mutation of one of the MMR genes – predisposes the carrier to MMR deficiency, but the system remains proficient until some somatic event leads to the mutation or loss of the wild-type allele of this gene. So, the disease is inherited as an autosomal dominant predisposition, but it is recessive at the somatic level. Consequently, the affected MMR protein is fully expressed in normal tissue, where heterozygosity has been maintained, but absent in tumor cells, where the wild-type allele has been lost.

When does this second hit occur in the epithelial cells of the colon? Heterozygosity is generally believed to be lost fairly early in the pre-cancerous adenomatous polyp stage [80]. Failure of the MMR system gives rise to a mutator phenotype and microsatellite instability, which should markedly accelerate the adenoma's transformation, and Lynch syndrome adenomas do indeed progress to adenocarcinoma more rapidly (within 2-5 years) and at a higher frequency than their sporadic counterparts. As noted above, adenoma formation itself seems to be triggered by dysregulation of Wnt signaling, which is a very early event in colorectal

tumorigenesis (Figure 4). In fact, although the temporal relationships between the various events are still fairly obscure, aberrant Wnt signaling almost certainly precedes the loss of the wild type *MMR* allele. The adenomatous polyps associated with Lynch syndrome are by no means as numerous as those seen in FAP. In most cases, the patient presents with a single adenoma, and there are rarely more than five or six. It seems then that these early dysplastic lesions somehow favor the loss of MMR in heterozygous cells.

In summary, the MMR-defective colorectal cancers associated with the Lynch syndrome arise from isolated adenomatous lesions, which undergo "fast-track" transformation driven by high-rate mutation that often targets tumor suppressor genes [81,82]. This mechanism probably predominates over chromosomal instability (another frequent driver of carcinogenesis), since MMR-deficient tumors have few chromosomal gains and losses and are often near-diploid (Figue 4). Later on, their aggressiveness and invasiveness are fortunately curbed by a strong antitumor immune response. The molecular components of this response are now under investigation [70], but the trigger seems to consist in the presentation of novel antigens produced by highly mutable, MMR-defective tumor cells.

Hyperplastic polyposis – The paradigm of "fast-track transformation" along the serrated pathway is the syndrome known as *hyperplastic polyposis* (HP), a rare (and underdiagnosed) condition that is often associated with $BRAF^{V600E}$ and the CIMP. HP is diagnosed when there are [83]: *i*) at least five histologically diagnosed hyperplastic polyps proximal to the sigmoid colon, including two with diameters exceeding 10 mm; *ii*) any number of hyperplastic polyps proximal to the sigmoid colon plus first-degree kinship with a patient known to have HP; or *iii*) over 30 hyperplastic polyps distributed throughout the colon. HP presents with a variety of preinvasive lesions,

which include not only hyperplastic polyps but also larger SSAs and even classical adenomas. The syndrome is now known to confer an increased risk for malignant transformation, although the reported magnitude of this risk varies to some extent from study to study [84-86]. HP-related colorectal cancers show a predilection for the proximal colon, and their onset occurs roughly 10 years earlier than that of sporadic colorectal cancers and about two decades later than those related to the Lynch syndrome.

Fewer than 150 cases of HP have been reported to date, and the picture that is emerging is that of a heterogeneous entity. Some authors have suggested [87] that there are actually two different phenotypes. They advocate reserving the term "hyperplastic polyposis" for cases characterized by multiple, small, pancolonic hyperplastic polyps and using "serrated adenomatous polyposis" when there are smaller numbers of relatively large, proximal, hyperplastic polyps with features of SSA. Familial aggregation has been documented in relatively few cases. When present, it seems to reflect dominant transmission of an unidentified genetic predisposition to CIMP, which frequently leads to somatic methylation of the *MLH1* promoter [88,89]. Compared with patients harboring sporadic serrated lesions, those with HP have a significantly higher frequency of methylated alleles in the normal colon mucosa [90,91], and this finding is also consistent with the possibility of genetically determined CIMP.

Inflammatory bowel disease - Third on the list of conditions conferring high risk for colorectal cancer – after the Lynch syndrome and FAP – is inflammatory bowel disease (IBD). Ulcerative colitis and Crohn's disease are chronic disorders with an onset peak between the second and fourth decades of life. They are caused by the combined effects of genetic, immune, and environmental factors – most of which are

still poorly characterized. Strong evidence supports the view that both involve a dysregulated immune response to commensal bacteria in genetically susceptible individuals [92,93]. The risk for IBD has been linked to variations in numerous genes [94].

Both ulcerative colitis and Crohn's disease confer an increased risk for colorectal cancer, but this risk varies with disease duration, the extent of colonic involvement, age at diagnosis, the severity of inflammation, family history of colon cancer, and the presence or absence of primary sclerosing cholangitis. The cumulative risk in patients with ulcerative colitis was recently estimated to be 8% at 20 years and 18% at 30 years; similar figures have been reported for Crohn's disease [95,96]. Most of what we know about colitis-associated carcinogenesis comes from studies of ulcerative colitis, so the rest of this section will focus mainly on this IBD.

The mechanism that links chronic inflammation to carcinogenesis has never been precisely defined. However, persistent inflammation is believed to trigger and sustain oxidative stress that increases proliferation and eventually leads to dysplasia [97]. Two important features of colitis-associated dysplasia are macroscopic heterogeneity and multifocality [98]. Elevated lesions (sometimes referred to as DALM [dysplasia-associated lesion or mass]) range from circumscribed, pedunculated or sessile polyps that resemble noncolitic adenomas to nonadenoma-like lesions that are irregular, broad-based, or poorly circumscribed. These latter lesions often contain ulcerated or hemorrhagic foci, and the flat mucosa surrounding them is also frequently dysplastic. They have often been referred to as "invisible dysplasia," because they are usually undetectable with standard colonoscopy. The only way to demonstrate their existence was to collect large numbers of biopsies from randomly selected sites throughout the colon, and this approach is still used today. However,

thanks to the introduction of magnifying chromoendoscopy, these flat lesions can be identified and biopsied, and this advance has greatly facilitated the demonstration of IBD-related dysplasia [99].

The finding of flat or elevated areas of high-grade dysplasia in a patient with ulcerative colitis is an indication for proctocolectomy because these lesions are likely to be multifocal, and their presence is associated with a high risk (~50%) for concurrent or imminent colorectal cancer [100]. Prophylactic surgery for low-grade dysplasia is more controversial [101], in part because there is no real consensus on the criteria for a pathologic diagnosis of this type. Endoscopic detection of preinvasive lesions and histologic assessment of dysplasia are problematic in settings of chronic inflammation, but thus far colorectal carcinogenesis in ulcerative colitis also seems to involve the development of dysplastic ACFs followed by low-grade and then high-grade dysplastic lesions that are eventually transformed into cancers. The identification of molecular markers of these stages will undoubtedly improve the quality of the clinical choices during the follow up of these patients.

Numerous studies have analyzed the molecular profiles of colitis-associated preinvasive lesions and the nonlesional inflamed mucosa. The typical approach involves the search for molecular abnormalities found in noncolitic carcinogenesis -- the chromosomal and microsatellite instability, epigenetic alterations, and oncogene and tumor-suppressor-gene mutations mentioned in the previous sections. As expected, most have also been detectable in colitis-associated mucosal lesions, but in many cases it is still unclear how their frequency and timing differ from those observed in the absence of chronic inflammation.

The discrepancies that have arisen were to be expected for several reasons. The availability of tissue samples of colitis-associated lesions is limited, and the linear

correlation between lesion size and disease severity observed in noncolitic tumorigenesis tends to break down in IBD, where small lesions are often advanced and molecular changes can also be found in the inflamed, nonneoplastic mucosa. The molecular analyses were also marred by selection biases related to the difficulties mentioned above in the endoscopic detection and histologic classification of colitis-associated lesions, as well as other methodologic flaws that had hampered the molecular investigation of noncolitic lesions (analysis restricted to the most frequently mutated regions of genes, the use of different -- sometimes incomplete – marker panels for the detection of specific phenotypes, suboptimal diagnostic reliability of most of the methods used).

Nevertheless, certain differences with respect to noncolitic carcinogenesis have emerged from these studies. *KRAS* and *APC* mutations, for example, are rare in IBD-related carcinogenesis, whereas *TP53* mutations are frequently encountered in the early stages and are sometimes found even in nondysplastic mucosa [15,102-104]. DNA methylation [105] and microsatellite instability [106] seem to play less important roles, but chromosomal instability is very common and appears to be an early event that probably stems from *TP53* mutations and inflammation-triggered DNA damage [107]. Genome-wide screening with comparative genomic hybridization has revealed several recurrent genomic imbalances. Losses of chromosome 5q and 18q, for example, were found in nondysplastic colitis tissue [108] (**Figure 5**), but their frequency was higher in dysplastic colitis tissue and higher still in colitis-associated colorectal cancer. Progression was also associated with the accumulation of other genomic imbalances typical of colorectal cancer such as -4, +7, +8q, +13q, +20q and +X. Changes detected in premalignant colitis tissue were encountered more often in colitis-associated colorectal cancers than in their sporadic

counterparts (for example: -5q: 53% vs. 10%; -18q: 76% vs. 49%; Figure 5) (data through www.progenetix.net; [109]). The presence of specific genomic changes in colon tissues from patients with ulcerative colitis is evidence of preinvasive clonal expansion, and it might someday serve as an additional marker for disease monitoring in these patients.

In conclusion, magnifying chromoendoscopy and the analysis of *TP53* mutations and chromosomal abnormalities in endoscopic biopsies are important tools that can substantially improve early diagnosis of colorectal cancer in patients with ulcerative colitis. The challenge is to implement these adjunctive diagnostic modalities in the surveillance of all patients with long-standing ulcerative in a way that optimizes the cost-benefit ratio.

Acknowledgements

E.C. is supported by grants received by G.M. from the Swiss National Science Foundation. G.M. also gratefully acknowledges the generous financial support of the Zurich Cancer League. The authors wish to thank Luca Roncucci for photos illustrating the histologic features of ACFs, Jana Rojickova for editing the figures, and Marian Kent for editing the text.

References

1. Winawer SJ, Zauber AG, Fletcher RH, et al. Guidelines for colonoscopy surveillance after polypectomy: a consensus update by the US Multi-Society Task Force on Colorectal Cancer and the American Cancer Society. Gastroenterology 2006;130:1872-1885
2. Levine JS, Ahnen DJ. Clinical practice. Adenomatous polyps of the colon. N Engl J Med 2006;355:2551-2557
3. Gupta S. Colorectal polyps: the scope and management of the problem. Am J Med Sci 2008;336:407-417
4. Young GP, Cole SR. Which fecal occult blood test is best to screen for colorectal cancer? Nat Clin Pract Gastroenterol Hepatol 2009
5. Psaty BM, Potter JD. Risks and benefits of celecoxib to prevent recurrent adenomas. N Engl J Med 2006;355:950-952
6. Schoenfeld P, Cash B, Flood A, et al. Colonoscopic screening of average-risk women for colorectal neoplasia. N Engl J Med 2005;352:2061-2068
7. Neklason DW, Thorpe BL, Ferrandez A, et al. Colonic adenoma risk in familial colorectal cancer--a study of six extended kindreds. Am J Gastroenterol 2008;103:2577-2584
8. Hendriks YM, de Jong AE, Morreau H, et al. Diagnostic approach and management of Lynch syndrome (hereditary nonpolyposis colorectal carcinoma): a guide for clinicians. CA Cancer J Clin 2006;56:213-225
9. Vasen HF, Moslein G, Alonso A, et al. Guidelines for the clinical management of familial adenomatous polyposis (FAP). Gut 2008;57:704-713
10. Ahmadi A, Polyak S, Draganov PV. Colorectal cancer surveillance in inflammatory bowel disease: The search continues. World J Gastroenterol 2009;15:61-66
11. Roncucci L, Stamp D, Medline A, Cullen JB, Bruce WR. Identification and quantification of aberrant crypt foci and microadenomas in the human colon. Hum Pathol 1991;22:287-294
12. Hurlstone DP, Karajeh M, Sanders DS, Drew SK, Cross SS. Rectal aberrant crypt foci identified using high-magnification-chromoscopic colonoscopy: biomarkers for flat and depressed neoplasia. Am J Gastroenterol 2005;100:1283-1289
13. Takayama T, Katsuki S, Takahashi Y, et al. Aberrant crypt foci of the colon as precursors of adenoma and cancer. N Engl J Med 1998;339:1277-1284
14. Takayama T, Ohi M, Hayashi T, et al. Analysis of K-ras, APC, and beta-catenin in aberrant crypt foci in sporadic adenoma, cancer, and familial adenomatous polyposis. Gastroenterology 2001;121:599-611
15. Kukitsu T, Takayama T, Miyanishi K, et al. Aberrant crypt foci as precursors of the dysplasia-carcinoma sequence in patients with ulcerative colitis. Clin Cancer Res 2008;14:48-54
16. Schoen RE, Mutch M, Rall C, et al. The natural history of aberrant crypt foci. Gastrointest Endosc 2008;67:1097-1102
17. Winawer SJ. The multidisciplinary management of gastrointestinal cancer. Colorectal cancer screening. Best Pract Res Clin Gastroenterol 2007;21:1031-1048
18. Muto T, Kamiya J, Sawada T, et al. Small "flat adenoma" of the large bowel with special reference to its clinicopathologic features. Dis Colon Rectum 1985;28:847-851

19. Kudo S, Lambert R, Allen JI, et al. Nonpolypoid neoplastic lesions of the colorectal mucosa. Gastrointest Endosc 2008;68:S3-47
20. Update on the Paris classification of superficial neoplastic lesions in the digestive tract. Endoscopy 2005;37:570-578
21. O'Brien M J, Winawer SJ, Zauber AG, et al. Flat adenomas in the National Polyp Study: is there increased risk for high-grade dysplasia initially or during surveillance? Clin Gastroenterol Hepatol 2004;2:905-911
22. Hurlstone DP, Cross SS, Adam I, et al. A prospective clinicopathological and endoscopic evaluation of flat and depressed colorectal lesions in the United Kingdom. Am J Gastroenterol 2003;98:2543-2549
23. Kudo S, Rubio CA, Teixeira CR, Kashida H, Kogure E. Pit pattern in colorectal neoplasia: endoscopic magnifying view. Endoscopy 2001;33:367-373
24. Snover DC, Jass JR, Fenoglio-Preiser C, Batts KP. Serrated polyps of the large intestine: a morphologic and molecular review of an evolving concept. Am J Clin Pathol 2005;124:380-391
25. O'Brien MJ. Hyperplastic and serrated polyps of the colorectum. Gastroenterol Clin North Am 2007;36:947-968, viii
26. Jass JR, Baker K, Zlobec I, et al. Advanced colorectal polyps with the molecular and morphological features of serrated polyps and adenomas: concept of a 'fusion' pathway to colorectal cancer. Histopathology 2006;49:121-131
27. Carr NJ, Mahajan H, Tan KL, Hawkins NJ, Ward RL. Serrated and non-serrated polyps of the colorectum: their prevalence in an unselected case series and correlation of BRAF mutation analysis with the diagnosis of sessile serrated adenoma. J Clin Pathol 2009
28. Spring KJ, Zhao ZZ, Karamatic R, et al. High prevalence of sessile serrated adenomas with BRAF mutations: a prospective study of patients undergoing colonoscopy. Gastroenterology 2006;131:1400-1407
29. Rosenberg DW, Yang S, Pleau DC, et al. Mutations in BRAF and KRAS differentially distinguish serrated versus non-serrated hyperplastic aberrant crypt foci in humans. Cancer Res 2007;67:3551-3554
30. Makinen MJ. Colorectal serrated adenocarcinoma. Histopathology 2007;50:131-150
31. O'Brien MJ, Yang S, Mack C, et al. Comparison of microsatellite instability, CpG island methylation phenotype, BRAF and KRAS status in serrated polyps and traditional adenomas indicates separate pathways to distinct colorectal carcinoma end points. Am J Surg Pathol 2006;30:1491-1501
32. Oka S, Tanaka S, Hiyama T, et al. Clinicopathologic and endoscopic features of colorectal serrated adenoma: differences between polypoid and superficial types. Gastrointest Endosc 2004;59:213-219
33. Clevers H. Wnt/beta-catenin signaling in development and disease. Cell 2006;127:469-480
34. Powell SM, Zilz N, Beazer-Barclay Y, et al. APC mutations occur early during colorectal tumorigenesis. Nature 1992;359:235-237
35. Groden J, Thliveris A, Samowitz W, et al. Identification and characterization of the familial adenomatous polyposis coli gene. Cell 1991;66:589-600
36. Su LK, Kinzler KW, Vogelstein B, et al. Multiple intestinal neoplasia caused by a mutation in the murine homolog of the APC gene. Science 1992;256:668-670

37. Iwamoto M, Ahnen DJ, Franklin WA, Maltzman TH. Expression of beta-catenin and full-length APC protein in normal and neoplastic colonic tissues. Carcinogenesis 2000;21:1935-1940
38. Barker N, Ridgway RA, van Es JH, et al. Crypt stem cells as the cells-of-origin of intestinal cancer. Nature 2009;457:608-611
39. Zhu L, Gibson P, Currle DS, et al. Prominin 1 marks intestinal stem cells that are susceptible to neoplastic transformation. Nature 2009;457:603-607
40. Ilyas M, Tomlinson IP, Rowan A, Pignatelli M, Bodmer WF. Beta-catenin mutations in cell lines established from human colorectal cancers. Proc Natl Acad Sci U S A 1997;94:10330-10334
41. Morin PJ, Sparks AB, Korinek V, et al. Activation of beta-catenin-Tcf signaling in colon cancer by mutations in beta-catenin or APC. Science 1997;275:1787-1790
42. Samowitz WS, Powers MD, Spirio LN, et al. Beta-catenin mutations are more frequent in small colorectal adenomas than in larger adenomas and invasive carcinomas. Cancer Res 1999;59:1442-1444
43. Suzuki H, Watkins DN, Jair KW, et al. Epigenetic inactivation of SFRP genes allows constitutive WNT signaling in colorectal cancer. Nat Genet 2004;36:417-422
44. Schneikert J, Grohmann A, Behrens J. Truncated APC regulates the transcriptional activity of beta-catenin in a cell cycle dependent manner. Hum Mol Genet 2007;16:199-209
45. Segditsas S, Rowan AJ, Howarth K, et al. APC and the three-hit hypothesis. Oncogene 2009;28:146-155
46. Alberici P, Fodde R. The role of the APC tumor suppressor in chromosomal instability. Genome Dyn 2006;1:149-170
47. Cardoso J, Molenaar L, de Menezes RX, et al. Chromosomal instability in MYH- and APC-mutant adenomatous polyps. Cancer Res 2006;66:2514-2519
48. Luo L, Li B, Pretlow TP. DNA alterations in human aberrant crypt foci and colon cancers by random primed polymerase chain reaction. Cancer Res 2003;63:6166-6169
49. Sieber OM, Heinimann K, Gorman P, et al. Analysis of chromosomal instability in human colorectal adenomas with two mutational hits at APC. Proc Natl Acad Sci U S A 2002;99:16910-16915
50. Bartkova J, Rezaei N, Liontos M, et al. Oncogene-induced senescence is part of the tumorigenesis barrier imposed by DNA damage checkpoints. Nature 2006;444:633-637
51. Raynaud CM, Jang SJ, Nuciforo P, et al. Telomere shortening is correlated with the DNA damage response and telomeric protein down-regulation in colorectal preneoplastic lesions. Ann Oncol 2008;19:1875-1881
52. Vogelstein B, Fearon ER, Hamilton SR, et al. Genetic alterations during colorectal-tumor development. N Engl J Med 1988;319:525-532
53. Grant S. Cotargeting survival signaling pathways in cancer. J Clin Invest 2008;118:3003-3006
54. Wood LD, Parsons DW, Jones S, et al. The genomic landscapes of human breast and colorectal cancers. Science 2007;318:1108-1113
55. Sweeney C, Boucher KM, Samowitz WS, et al. Oncogenetic tree model of somatic mutations and DNA methylation in colon tumors. Genes Chromosomes Cancer 2009;48:1-9

56. Shen L, Toyota M, Kondo Y, et al. Integrated genetic and epigenetic analysis identifies three different subclasses of colon cancer. Proc Natl Acad Sci U S A 2007;104:18654-18659
57. Samowitz WS, Slattery ML, Sweeney C, et al. APC Mutations and Other Genetic and Epigenetic Changes in Colon Cancer. Mol Cancer Res 2007;5:165-170
58. Goel A, Arnold CN, Niedzwiecki D, et al. Characterization of sporadic colon cancer by patterns of genomic instability. Cancer Res 2003;63:1608-1614
59. Toyota M, Ahuja N, Ohe-Toyota M, et al. CpG island methylator phenotype in colorectal cancer. Proc Natl Acad Sci U S A 1999;96:8681-8686
60. O'Brien MJ, Yang S, Clebanoff JL, et al. Hyperplastic (serrated) polyps of the colorectum: relationship of CpG island methylator phenotype and K-ras mutation to location and histologic subtype. Am J Surg Pathol 2004;28:423-434
61. Chan TL, Zhao W, Leung SY, Yuen ST. BRAF and KRAS mutations in colorectal hyperplastic polyps and serrated adenomas. Cancer Res 2003;63:4878-4881
62. Nosho K, Irahara N, Shima K, et al. Comprehensive biostatistical analysis of CpG island methylator phenotype in colorectal cancer using a large population-based sample. PLoS ONE 2008;3:e3698
63. Kambara T, Simms LA, Whitehall VL, et al. BRAF mutation is associated with DNA methylation in serrated polyps and cancers of the colorectum. Gut 2004;53:1137-1144
64. Weisenberger DJ, Siegmund KD, Campan M, et al. CpG island methylator phenotype underlies sporadic microsatellite instability and is tightly associated with BRAF mutation in colorectal cancer. Nat Genet 2006;38:787-793
65. Goel A, Nagasaka T, Arnold CN, et al. The CpG island methylator phenotype and chromosomal instability are inversely correlated in sporadic colorectal cancer. Gastroenterology 2007;132:127-138
66. Menigatti M, Truninger K, Gebbers JO, et al. Normal colorectal mucosa exhibits sex- and segment-specific susceptibility to DNA methylation at the hMLH1 and MGMT promoters. Oncogene 2009;28:899-909
67. Samowitz WS, Albertsen H, Sweeney C, et al. Association of smoking, CpG island methylator phenotype, and V600E BRAF mutations in colon cancer. J Natl Cancer Inst 2006;98:1731-1738
68. Laiho P, Kokko A, Vanharanta S, et al. Serrated carcinomas form a subclass of colorectal cancer with distinct molecular basis. Oncogene 2007;26:312-320
69. Lee SH, Kim J, Kim WH, Lee YM. Hypoxic silencing of tumor suppressor RUNX3 by histone modification in gastric cancer cells. Oncogene 2009;28:184-194
70. di Pietro M, Sabates Bellver J, Menigatti M, et al. Defective DNA mismatch repair determines a characteristic transcriptional profile in proximal colon cancers. Gastroenterology 2005;129:1047-1059
71. Sabates-Bellver J, Van der Flier LG, de Palo M, et al. Transcriptome profile of human colorectal adenomas. Mol Cancer Res 2007;5:1263-1275
72. Knudsen AL, Bisgaard ML, Bulow S. Attenuated familial adenomatous polyposis (AFAP). A review of the literature. Fam Cancer 2003;2:43-55
73. Schneikert J, Behrens J. The canonical Wnt signalling pathway and its APC partner in colon cancer development. Gut 2007;56:417-425

74. Sabates Bellver J, Cattaneo E, Heinimann K, Jiricny J, Marra G. Getting familiar with familial colon cancer. In: Gasche C ed, Intestinal Inflammation and Colorectal Cancer (FALK Symposium 158): Springer; 2007:27-60
75. Al-Tassan N, Chmiel NH, Maynard J, et al. Inherited variants of MYH associated with somatic G:C-->T:A mutations in colorectal tumors. Nat Genet 2002;30:227-232
76. Sieber OM, Lipton L, Crabtree M, et al. Multiple colorectal adenomas, classic adenomatous polyposis, and germ-line mutations in MYH. N Engl J Med 2003;348:791-799
77. Marra G, Jiricny J. Multiple colorectal adenomas--is their number up? N Engl J Med 2003;348:845-847
78. Marra G, Jiricny J. DNA mismatch repair and colon cancer. In: Nigg E ed, Genome Instability in Cancer Development (Advances in Experimental Medicine and Biology): Springer; 2005:85-123
79. Truninger K, Menigatti M, Luz J, et al. Immunohistochemical analysis reveals high frequency of PMS2 defects in colorectal cancer. Gastroenterology 2005;128:1160-1171
80. de Jong AE, Morreau H, Van Puijenbroek M, et al. The role of mismatch repair gene defects in the development of adenomas in patients with HNPCC. Gastroenterology 2004;126:42-48
81. Markowitz S, Wang J, Myeroff L, et al. Inactivation of the type II TGF-beta receptor in colon cancer cells with microsatellite instability. Science 1995;268:1336-1338
82. Rampino N, Yamamoto H, Ionov Y, et al. Somatic frameshift mutations in the BAX gene in colon cancers of the microsatellite mutator phenotype. Science 1997;275:967-969
83. Burt RW JJ. World Health Organization classification of tumors. Pathology & genetics. Tumors of the digestive system.; 2000:135-136
84. Jass JR. Familial colorectal cancer: pathology and molecular characteristics. Lancet Oncol 2000;1:220-226
85. Ferrandez A, Samowitz W, DiSario JA, Burt RW. Phenotypic characteristics and risk of cancer development in hyperplastic polyposis: case series and literature review. Am J Gastroenterol 2004;99:2012-2018
86. Lage P, Cravo M, Sousa R, et al. Management of Portuguese patients with hyperplastic polyposis and screening of at-risk first-degree relatives: a contribution for future guidelines based on a clinical study. Am J Gastroenterol 2004;99:1779-1784
87. Torlakovic E, Snover DC. Sessile serrated adenoma: a brief history and current status. Crit Rev Oncog 2006;12:27-39
88. Jass JR. Colorectal polyposes: from phenotype to diagnosis. Pathol Res Pract 2008;204:431-447
89. Beach R, Chan AO, Wu TT, et al. BRAF mutations in aberrant crypt foci and hyperplastic polyposis. Am J Pathol 2005;166:1069-1075
90. Minoo P, Baker K, Goswami R, et al. Extensive DNA methylation in normal colorectal mucosa in hyperplastic polyposis. Gut 2006;55:1467-1474
91. Young J, Jass JR. The case for a genetic predisposition to serrated neoplasia in the colorectum: hypothesis and review of the literature. Cancer Epidemiol Biomarkers Prev 2006;15:1778-1784
92. Cho JH. The genetics and immunopathogenesis of inflammatory bowel disease. Nat Rev Immunol 2008;8:458-466

93. Xavier RJ, Podolsky DK. Unravelling the pathogenesis of inflammatory bowel disease. Nature 2007;448:427-434
94. Budarf ML, Labbe C, David G, Rioux JD. GWA studies: rewriting the story of IBD. Trends Genet 2009
95. Eaden JA, Abrams KR, Mayberry JF. The risk of colorectal cancer in ulcerative colitis: a meta-analysis. Gut 2001;48:526-535
96. Canavan C, Abrams KR, Mayberry J. Meta-analysis: colorectal and small bowel cancer risk in patients with Crohn's disease. Aliment Pharmacol Ther 2006;23:1097-1104
97. Itzkowitz SH, Yio X. Inflammation and cancer IV. Colorectal cancer in inflammatory bowel disease: the role of inflammation. Am J Physiol Gastrointest Liver Physiol 2004;287:G7-17
98. Itzkowitz SH, Harpaz N. Diagnosis and management of dysplasia in patients with inflammatory bowel diseases. Gastroenterology 2004;126:1634-1648
99. Kiesslich R, Goetz M, Lammersdorf K, et al. Chromoscopy-guided endomicroscopy increases the diagnostic yield of intraepithelial neoplasia in ulcerative colitis. Gastroenterology 2007;132:874-882
100. Kornbluth A, Sachar DB. Ulcerative colitis practice guidelines in adults. American College of Gastroenterology, Practice Parameters Committee. Am J Gastroenterol 1997;92:204-211
101. Lewis JD. The many faces of low-grade dysplasia. Gastroenterology 2003;125:1531-1533
102. Yin J, Harpaz N, Tong Y, et al. p53 point mutations in dysplastic and cancerous ulcerative colitis lesions. Gastroenterology 1993;104:1633-1639
103. Brentnall TA, Crispin DA, Rabinovitch PS, et al. Mutations in the p53 gene: an early marker of neoplastic progression in ulcerative colitis. Gastroenterology 1994;107:369-378
104. Fujii S, Fujimori T, Chiba T. Usefulness of analysis of p53 alteration and observation of surface microstructure for diagnosis of ulcerative colitis-associated colorectal neoplasia. J Exp Clin Cancer Res 2003;22:107-115
105. Konishi K, Shen L, Wang S, et al. Rare CpG island methylator phenotype in ulcerative colitis-associated neoplasias. Gastroenterology 2007;132:1254-1260
106. Risques RA, Rabinovitch PS, Brentnall TA. Cancer surveillance in inflammatory bowel disease: new molecular approaches. Curr Opin Gastroenterol 2006;22:382-390
107. Risques RA, Lai LA, Brentnall TA, et al. Ulcerative colitis is a disease of accelerated colon aging: evidence from telomere attrition and DNA damage. Gastroenterology 2008;135:410-418
108. Willenbucher RF, Aust DE, Chang CG, et al. Genomic instability is an early event during the progression pathway of ulcerative-colitis-related neoplasia. Am J Pathol 1999;154:1825-1830
109. Baudis M, Cleary ML. Progenetix.net: an online repository for molecular cytogenetic aberration data. Bioinformatics 2001;17:1228-1229

Legends to Figures

Figure 1: A simplified 4-stage model of the transformation of normal colorectal mucosa into adenocarcinoma. The figure shows the histologic features of the four stages of the adenoma-carcinoma pathway to colorectal cancer: **A**: normal mucosa; **B**: aberrant crypt focus (ACF); **C**: tubulo-villous adenoma with epithelial dysplasia; and **D**: invasive adenocarcinoma. The dysplastic ACF shown in panel B came from the colon of a patient with colon cancer (H&E staining, 25x magnification). The photomicrogram shows approximately 12 of the 50 or so aberrant crypts included in the ACF, which is slightly raised above (≈ 500 μm) the surface of the gut mucosa. Compared with the surrounding normal crypts (right, upper corner), the aberrant crypts are larger and longer with initial signs of branching and infolding of the epithelium. The epithelial lining presents low-grade dysplasia (mild mucin depletion, hyperchromatic nuclei, initial signs of nuclear enlargement, occasional areas of stratification). In the lower left corner, the crypt lumens are enlarged – a frequent finding at the borders of ACFs. **C**: the adenomatous polypoid lesion shows a prevalent tubular growth pattern with some villous projections. The degree of dysplasia varies from low-grade (left half of the lesion) to high-grade (right half, superficial). In the lower left corner is present a portion of normal mucosa of the stalk. **D** (adenocarcinoma): irregular branching of glands showing atypical epithelium. They are surrounded by stroma composed of dense fibrous tissue comprising spindle cells in a collagenuos and inflammatory background (desmoplastic reaction). (Magnification: Normal mucosa, 10 X; ACF, 10X; Adenoma, 2X; Adenocarcinoma, 10X)

Figure 2: Polypoid and nonpolypoid preinvasive lesions of the colorectum. **A** and **B**, Types of tumor growth associated with the development of colorectal neoplasia (Paris classification, ref. [20]). Polypoid (**A**) lesions can be pedunculated *(Type Ip*) or sessile (*Type Is*); most nonpolypoid (**B**) lesions are slightly elevated (*Type IIa*), but some are completely flat (*Type IIb*) or depressed (*Type IIc*). Mixed growth patterns can also be found. The endoscopic appearances of polypoid (pedunculated) and nonpolypoid (slightly elevated) lesions are shown in panel **C** and **D**, respectively. Histological examination shows conventional adenomatous features (tubular proliferation with low-grade epithelial dysplasia) in a pedunculated polyp (**E**; magnification, 10X) and the serrated pattern (irregular shape of the crypts with serration of glandular lumens) in a nonpolypoid lesion (**F**; magnification, 10X). (See text for description of the histotypes.) Either of these histological patterns can be found in polypoid and nonpolypoid lesions.

Figure 3: The best characterized pathways to colorectal adenocarcinoma. The conventional adenomatous pathway is the most common route to adenocarcinoma. The cancers that arise through this pathway can be located anywhere in the colorectum, but they are more frequent in the left colon and rectum. Progressively severe cellular and architectural dysplasia (shaded region) is the hallmark of this pathway. It can already be found in the earliest-stage lesions, such as ACFs. The putative stations in the "less traveled" serrated pathway are shown on the right. Architectural abnormalities are an early feature of this pathway, whereas cellular dysplasia appears late (details in the text). Among the lesions that develop through this pathway, those most likely to develop into cancer are located in the right colon.

Figure 4: Molecular pathways and crossroads in colorectal transformation. The conventional adenomatous pathway and the serrated pathway are currently the best characterized stepwise models of colorectal carcinogenesis. In both, dysregulation of Wnt signaling (β-catenin stabilization and nuclear translocation) is an early event. It can be caused by different (epi)mutations. (In the conventional adenomatous pathway, the most frequent cause is *APC* mutation). Other early events have also been documented, including mutations affecting components of the MAPK/ERK cascades (i.e., *KRAS* or *BRAF* mutations, which are mutually exclusive) and chromosomal changes, like CIN (lower-level compared to that seen in advanced adenocarcinomas) or CIMP. And there are undoubtedly others that have yet to be discovered. They account for roughly half of all adenocarcinomas, i.e., those with no evidence of the early alterations listed above (far right column – light blue segment). Mutations involving "survival signaling" cascades (e.g., MAPK/ERK) alter the normal homeostatic equilibrium between proliferation, checkpoint repair of DNA damage, and apoptosis, allowing preinvasive lesions to survive for years. Additional mutations are necessary to allow the tumor to move on into the advanced stage, where malignancy is imminent. The nature of these "brake-releasing" events differs, depending on which pathway the tumor is moving along. Crossroad warning sign: Examples from the literature [26,55-58,64] of "molecular deviation" from the original pathway, a phenomenon that can occur at almost any stage of carcinogenesis. Accelerators: Colon cancer predisposition syndromes - each represents high-speed transformation along one of the pathways shown in this figure: the adenomatous pathway in Lynch syndrome and familial adenomatous polyposis; the serrated pathway in hyperplastic polyposis.

The information reported in this figure is based on rates of detection of a dozen or so genetic and epigenetic alterations in preinvasive colorectal lesions and their persistence in advanced adenocarcinomas. The relative frequency of a given alteration or combination of alterations can vary considerably from study to study owing to differences in inclusion criteria (i.e., types of lesion studied), in the number and type of molecular changes investigated, and in the method(s) employed to detect these changes. Abbreviations: CIN (chromosomal instability); CIMP (CpG island methylator phenotype); MIN: microsatellite instability.

Figure 5. Chromosomal instability in preinvasive and invasive colorectal lesions from patients with and without ulcerative colitis. Histograms show the frequency of genomic imbalances in selected colorectal tissue samples (gains appear in green above the baseline; losses appear below in red). In ulcerative colitis (upper panel), chromosomal aberrations leading to clonal imbalances can already be observed in nondysplastic tissues. Examples are the recurring deletions involving the long arms of chromosomes 5 and 18, which increase in frequency as malignancy progresses. Interestingly, both aberrations are earlier and more frequent events in tumorigenesis associated with ulcerative colitis than in sporadic adenomatous tumorigenesis (two lower panels) or FAP-related tumorigenesis, where 5q deletions are rarely detected (data not shown). During progression, colitis-associated lesions accumulate most of the other genomic imbalances observed in sporadic tumors, namely gains of chromosomes 7, 8q, 13q, 20 and X, as well as deletions of chromosomes 4 and 8p. The data was extracted from the Progenetix database (www.progenetix.net; [109]).

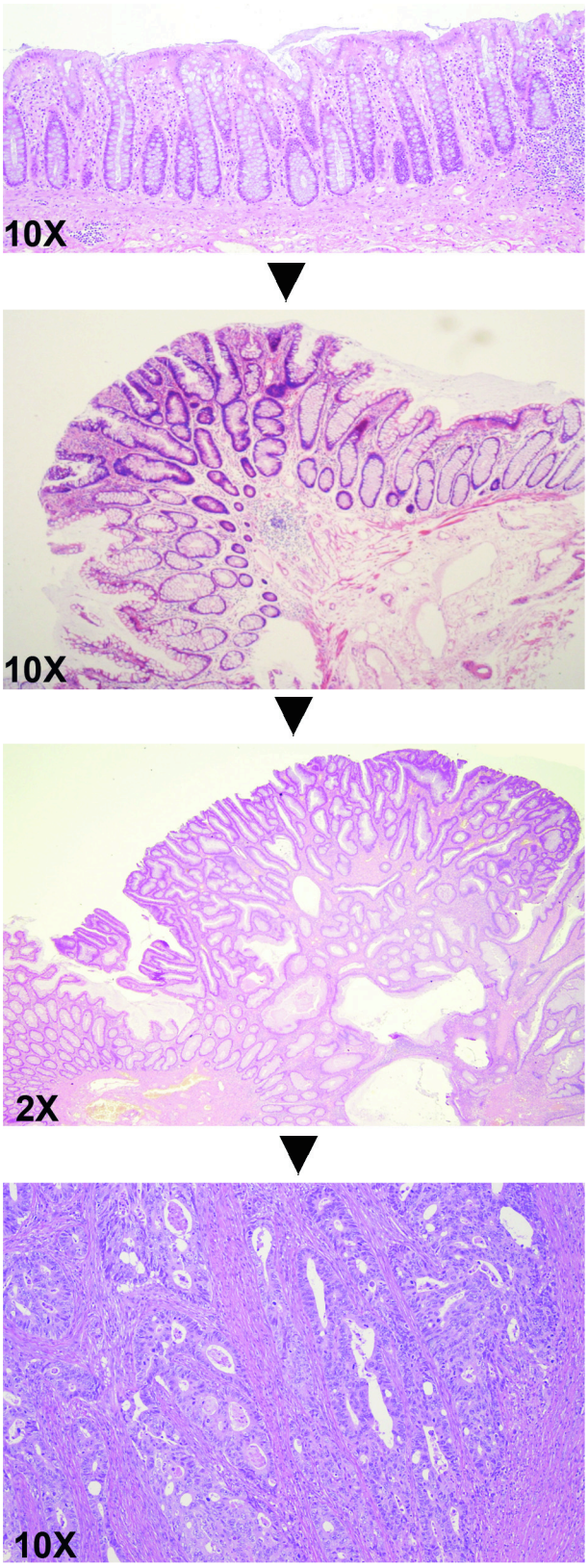
10X
Normal mucosa
10X
ACF
2X
Adenomatous polypoid lesion
10X
Adeno-carcinoma

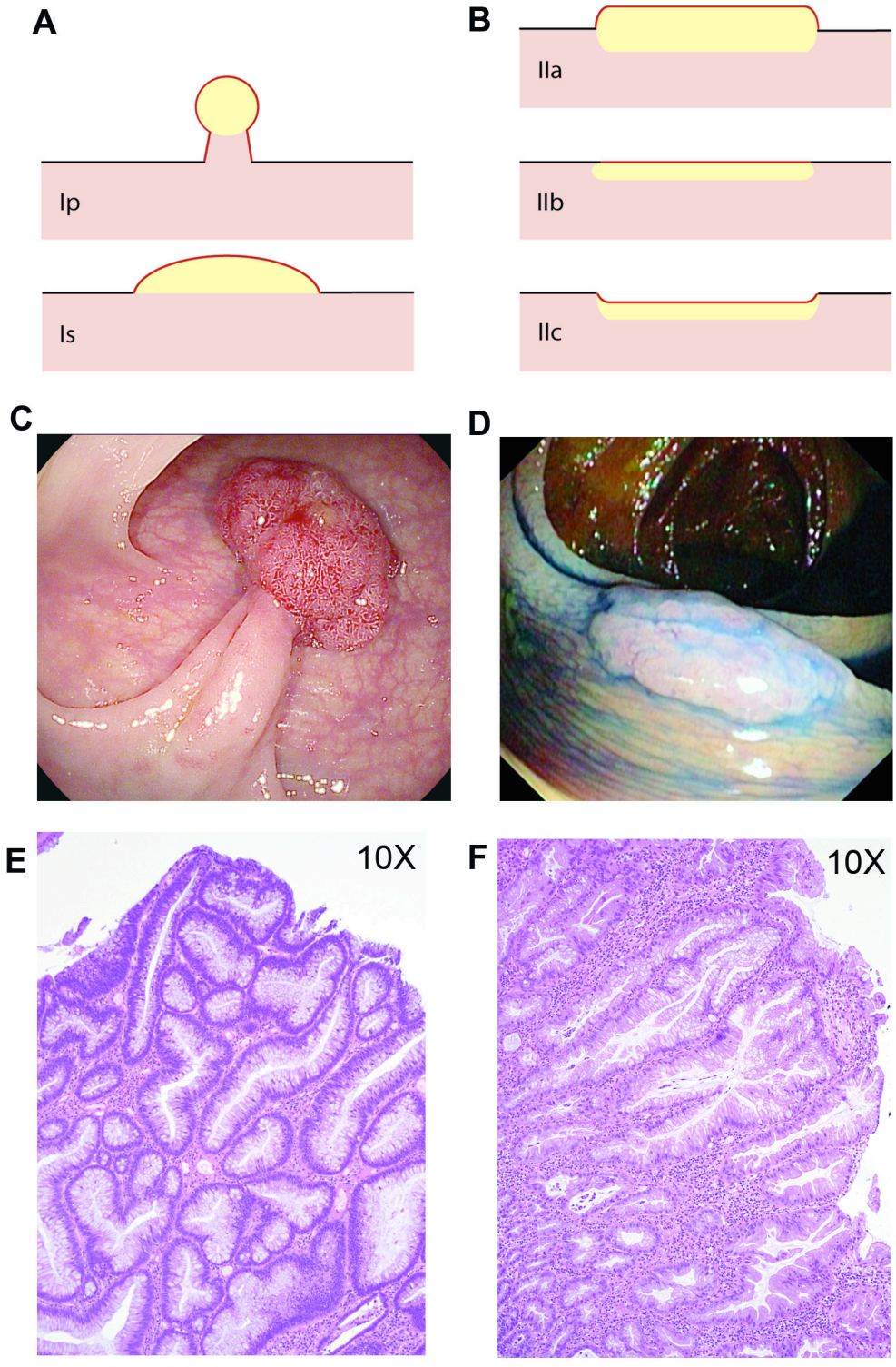
A
Ip
Is
B
IIa
IIb
IIc
C
D
E
10X
F
10X

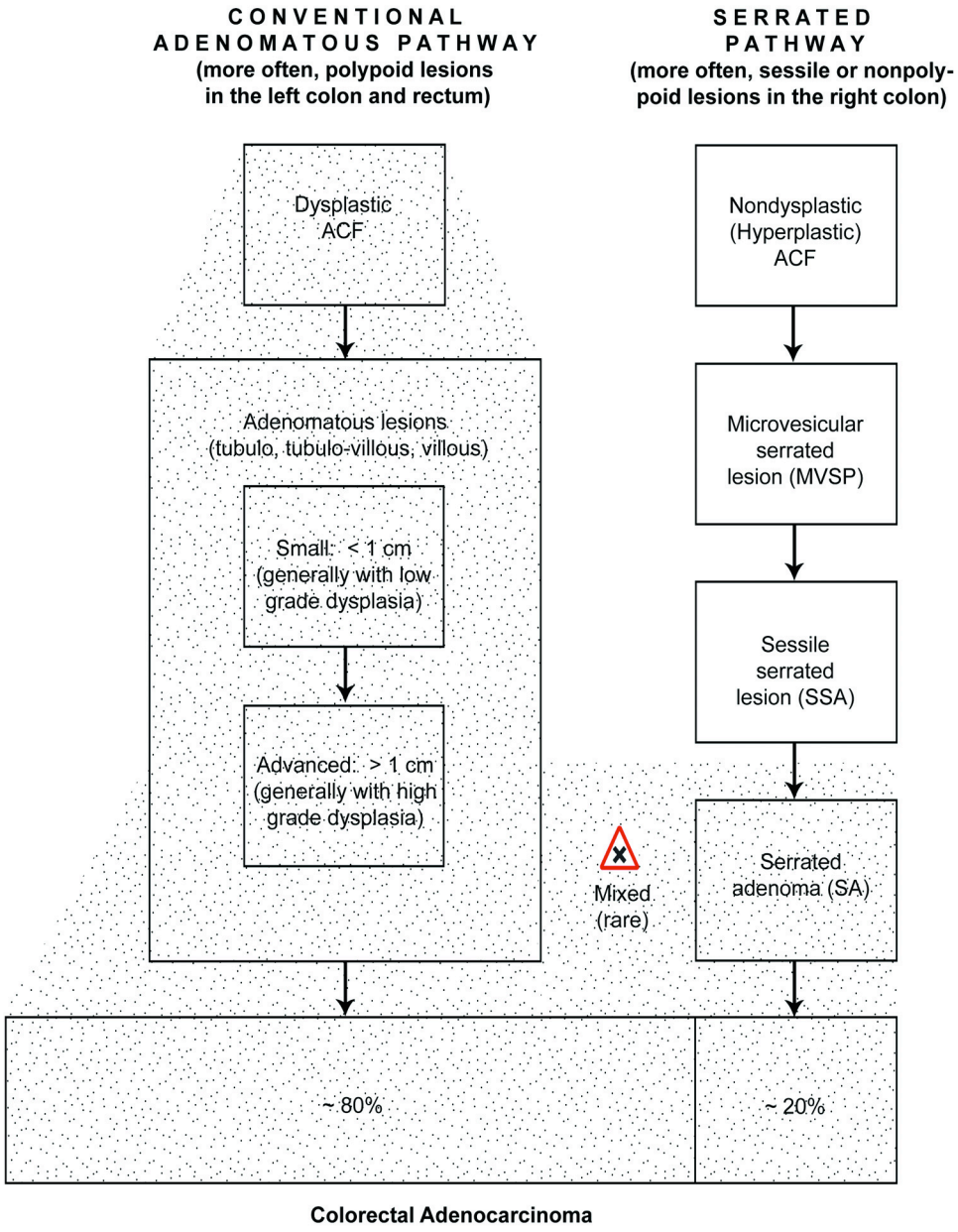

Colorectal Adenocarcinoma

Colorectal neoplasms in motion

Altered signal transduction (e.g.,Wnt, MAPK) and chromosomal (DNA, chromatin) changes	Altered survival signaling maintains lesions in preinvasive stage for years	"Brake-releasing" events (5-10% of preinvasive lesions enter advanced stage)	Early-stage (epi)genotypes that are still discernible in invasive adenocarcinomas
"Accelerators": Lynch Syndrome, Familial Adenomatous Polyposis			
Stabilization and nuclear translocation of β-catenin Unidentified genetic or epigenetic events CIN	**CONVENTIONAL ADENOMATOUS PATHWAY**	Mutations of *p53*, *PI3K*, *PTEN* and/or others	Unidentified genetic or epigenetic events ~ 50%
KRAS mutation		Epigenetic silencing of *p16*, *MLH1* and/or others	*KRAS* mutation ~ 30%
BRAF mutation CIMP	**SERRATED PATHWAY**	MSI	CIMP Low, *KRAS* mut. ~ 5% CIMP(+), *BRAF* mut. [~75% MSI(+)] ~ 15%
"Accelerator": Hyperplastic Polyposis			

- Mixed (serrated & conventional) adenomas
- Adenocarcinomas with various combinations of CIMP, BRAF or KRAS mutation, and MSI
- Low levels of MSI (MSI-Low) and CIMP (CIMP-Low)
- Adenocarcinomas that are CIN+/MSI+ or CIN-/MSI-

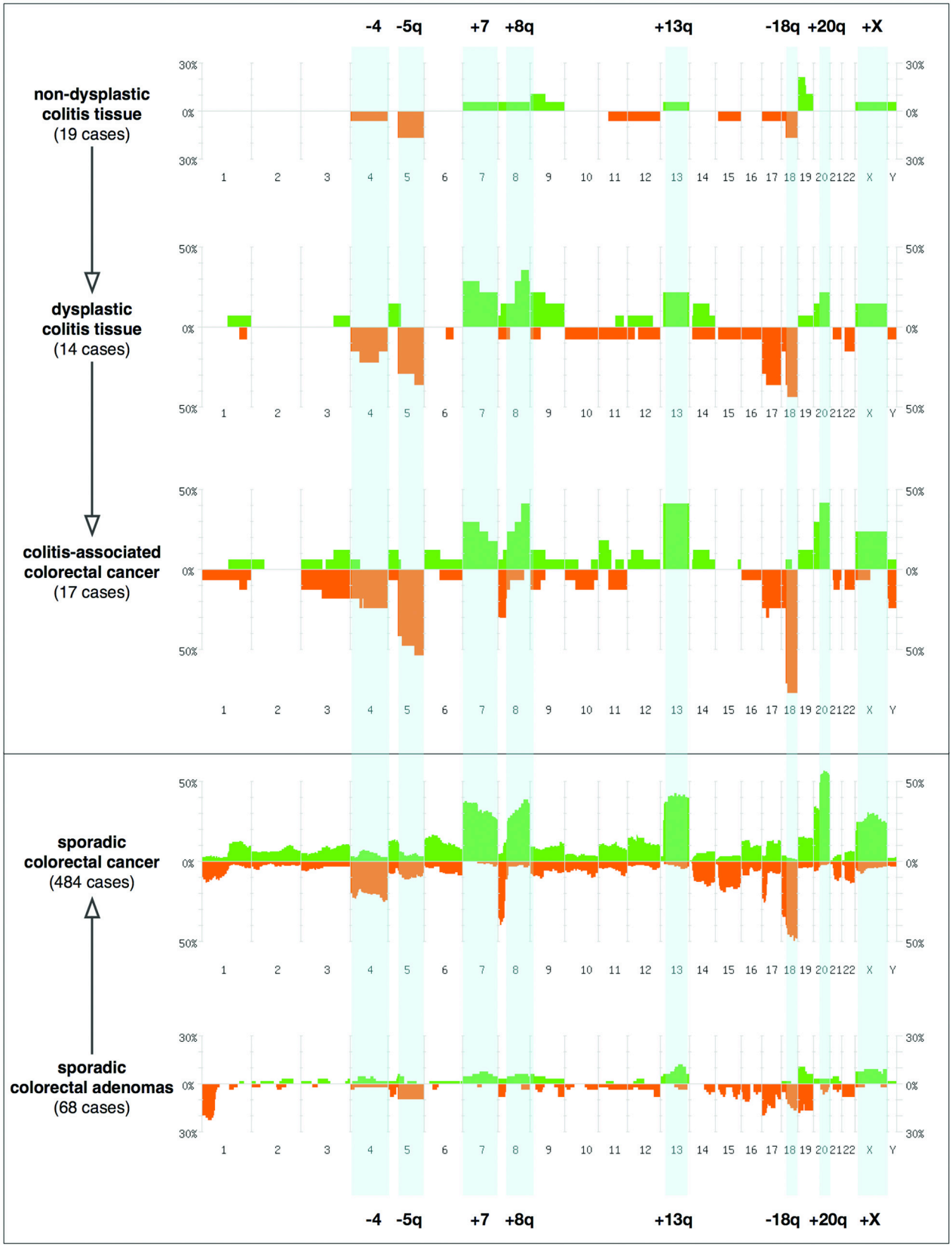
-4
-5q
+7
+8q
+13q
-18q
+20q
+X
non-dysplastic colitis tissue (19 cases)
dysplastic colitis tissue (14 cases)
colitis-associated colorectal cancer (17 cases)
sporadic colorectal cancer (484 cases)
sporadic colorectal adenomas (68 cases)
30%
0%
50%
1 2 3 4 5 6 7 8 9 10 11 12 13 14 15 16 17 18 19 20 21 22 X Y